Thermodynamic modelling of hydrocarbon-chains and light-weight supercritical solvents

by

James Edward Lombard

Thesis presented in partial fulfilment
of the requirements for the Degree

of

MASTER OF ENGINEERING
(CHEMICAL ENGINEERING)

in the Faculty of Engineering
at Stellenbosch University

Supervisor
Prof. J.H. Knoetze

Co-Supervisor/s
Dr. C.E. Schwarz

March 2015

Stellenbosch University https://scholar.sun.ac.za

DECLARATION

By submitting this thesis electronically, I declare that the entirety of the work contained therein is my own, original work, that I am the sole author thereof (save to the extent explicitly otherwise stated), that reproduction and publication thereof by Stellenbosch University will not infringe any third party rights and that I have not previously in its entirety or in part submitted it for obtaining any qualification.

James Lombard February 2015

……. …….

Signature *Date*

Copyright © 2015 Stellenbosch University
All rights reserved

Stellenbosch University https://scholar.sun.ac.za

ABSTRACT

Long-chain hydrocarbons are of value to numerous lucrative industries. Due to the low volatility and close melting and boiling points of these solutes, traditional fractionation methods lack the required selectivity for separation and cause thermal degradation of the product.

This project investigates the feasibility of Supercritical Fluid Extraction (SFE) for processing these systems, with the primary objective of modelling the high-pressure vapour-liquid equilibrium (VLE) properties of hydrocarbon solutes with a light-weight solvent using a semi-empirical equation of state (EOS). Pure component vapour pressures and saturated liquid volumes are also investigated.

A thorough investigation into the phase behaviour of the n-alkanes, 1-alcohols, carboxylic acids and esters in light weight supercritical solvents CO_2, ethane and propane revealed that the solute structure and temperature largely influence the solute solubility and process feasibility. Good selectivity amongst the various solutes was observed for all three solvents, but very high pressures were required for complete miscibility using CO_2 (exceeding 30 MPa). The quadrapole moment of CO_2 further leads to complexities in phase behaviour such as temperature and density inversions (CO_2/alkanes and CO_2/alcohols) and 3-phase regions within the operating range. Simple linear trends in pressure vs. carbon number and temperature were observed for all the considered series using ethane and propane and these solvents were thus selected for conducting the modelling for this study.

A thorough review of semi-emperical EOS models from literature revealed that the simple cubic equations of state (CEOSs) provide a promising modelling approach for SFE applications due to their simplicity, flexibility and reliability.

The simple Peng-Robinson (PR) and Soave-Redlich-Kwong (SRK) EOSs provide good correlation of vapour pressure (%AAD below 5 %) for all the series over a large carbon number range (up to nC20), provided a two parameter alpha function is used. A 3rd parameter in the volume dependence for Patel-Teja (PT) EOS provides considerable improvement over the PR and SRK EOSs for satureate liquid volume correlations of the non-polar solutes (alkanes and esters), but offers virtually no advantage for the more polar alcohols and acids. The CEOSs therefore suffer clear limitations in simultaneous representation of these saturation properties (vapour pressure and liquid molar volume) for the systems of interest.

Good correlations of high pressure binary VLE data were obtained using CEOSs available in the Aspen Plus ® simulator (% AAD in P, T and X_2 generally below 1 % and ranging from 4

Stellenbosch University https://scholar.sun.ac.za

to 12 % for Y_2 for all series) provided that two binary interaction parameters (BIPs) are used in the model mixing rules, irrespective of the model used. Aspen Plus ® was further validated as a reliable thermodynamic tool by comparing model fits using the RK-ASPEN model with parameters obtained from the Aspen Plus ® data regression routine and computational methods used in self-developed MATLAB software. Very similar results were obtained for both computational methods, which encourages the use of Aspen Plus ® for process modelling in SFE applications.

A statistical sensitivity analysis into the relative effect and interactions between 6 modelling factors in applying the CEOSs revealed that the mixing rules, temperature and solute structure had the largest effect on the correlation of the high pressure VLE, with the pure component limit having negligible effect once BIPs are fitted to data. A significant interaction was, however, observed between the pure component model and the solute structure and temperature, which suggest that accurate correlation of mixture VLE does not solely rely on appropriate mixing rule selection, but also the pure model.

Binary interaction parameters (BIPs) in model mixing rules were found to become intercorrelated when more than one are used, greatly impeding the development of generalized correlations. BIPs were also found to be sensitive to the pure component limit (alpha function and pure constants used), the temperature, the combining rules used and possibly the fluid density. These factors should all be taken into account systematically for developing generalized correlations which therefore fell outside the scope of this study. Recommendations were, however, made on how the MATLAB software developed in this study can be used to both expand the size of the statistical analysis already conducted into relevant modelling factors and to develop new generalized correlations for BIPs and new mixing rules.

Stellenbosch University https://scholar.sun.ac.za

OPSOMMING

Lang-ketting koolwaterstowwe is van waarde in talle winsgewende industriële toepassings. Vanweë die lae vlugbaarheiden ooreenstemmende kook- en smeltpunte van hierdie molekules, toon tradisionele fraktioneringsmetodes nie die nodige selektiwiteit vir ekstraksie nie en veroorsaak bonop termiese degradering van die produk.

Hierdie projek ondersoek dus die lewensvatbaarheid van superkritiese ekstraksie vir die prosesering van hierdie sisteme, met primêre fokus op die modellering van die hoë-druk damp-vloeistof ewewig eienskappe van koolwaterstowwe opgelos in ‘n lae-massa oplosmiddel met gebruik van ‘n semi-empiriese toestandsvergelyking. Suiwer-komponent dampdrukke en versadigde vloeistof volumes word ook ondersoek.

‘n Deeglike ondersoek na die fasegedrag van die n-alkane, 1-alkohole, korboksiel-sure asook esters in lae-massa superkritiese oplosmidds CO_2, etaan en propaan toon dat die struktuur van die opgeloste stof en die temperatuur ‘n groot invloed het op die oplosbaarheid en proses lewensvatbaarheid. Goeie selektiwiteit tussen die verskillende koolwaterstowwe was waargeneem vir al drie oplosmiddels, alhoewel baie hoë drukke nodig was vir totale vermenging van die fases in CO_2 (hoër as 30 MPa). Die quadrupool moment van CO_2 veroorsaak verder ongewenste kompleksiteite in fase gedrag soos temperatuuren digtheid inversies (CO_2/alkane en CO_2/alkohole) en 3-fase-gebiede in die bedryfs-kondisies. Eenvoudige lineêre tendense in druk tenoor die koolstofnommer van die opgeloste stof asook die temperatuur was waargeneem vir al die ondersoekte koolwaterstof reekse in etaan en propaan en hierdie oplosmiddels was dus gekies vir die modellering vir hierdie studie.

n’ Deeglike oorsig van semi-empiriese toestandsvergelykings uit die literatuur het getoon dat die eenvoudige kubiese toestandsvergelykings ‘n belowende modelleringsbenadering bied vir superkritiese ekstraksie toepassings vanweë hul eenvoudigeid, buigsaamheid enbetroubaarheid.

Die eenvoudige Peng-Robinson (PR) en Soave-Redlich-Kwong (SRK) toestandsvergelykings bied goeie korrelasie van suiwer dampdruk (foute laer as 5 %) vir alle koolwaterstowwe oor ‘n groot koolstofnommer gebied (tot by nC20), met die voorwaarde dat ‘n 2 parameter alpha funksie gebruik word. ‘n 3rde parameter in die volume afhanklikheid van die Patel-Teja (PT) toestandsvergelyking bied ‘n beduidende verbetering in die passing van die versadigde vloeistof volume vir die nie-polêre koolwaterstowwe (n-alkane en die esters), maar bied geen voordeel vir die meer polêre alkohole en karkoksiel sure nie. Die kubiese modelle toon dus duidelike beperkings vir die gelyktydige voorstelling van hierdie versadigingde eienskappe (dampdruk en vloeistof volume) vir die sisteme van belang.

Stellenbosch University https://scholar.sun.ac.za

Goeie korrelasie van hoë druk binêre damp-vloeistof ewewig data was verkry deur gebruik van die kubiese toestandsvergelykings beskikbaar inAspen Plus ® (fout in P, T en X_2 tipies laer as 1 % en van 4 tot 12 % vir Y_2 vir alle sisteme), met die voorwaarde dat 2 binêre interaksie parameters gebuik word in die model mengreëls, onafhanklik van die model. Aspen Plus ® was verder bekraktig as ‘n betroubare termodinamiese hulpmiddel deur model passings te vergelyk met die RK-ASPEN model tussen gevalle waar parameters verkry is deur die beskikbare regressie metode in Aspen Plus ® en metodes gebruik in self-ontwikkelde MATLAB sagteware. Eenderse resultate was verkry vir beide berekeningsmetodes, wat die gebruik van Aspen Plus ® vir prosesmodellering in superkritiese ekstrasie toepassings aanmoedig.

‘n Satistiese sensitiwiteits analise op die relatiewe effek en interaksies tussen 6 modelleringsfaktore in die toepassing van die kubiese toestandsvergelykings het gevind dat die mengreëls, temperatuur en die stuktuur van die opgeloste stof die grootste effek op die korrelasie van hoë druk binêre damp-vloeistof ewewig het, met ‘n weglaatbare effek vandie suiwerkomponent limiet waargeneem sodra binêre interaksie parameters gepas is aan data. ‘n Beduidende interaksie was wel waargeneem tussen die suiwerkomponent model en die struktuur van die opgeloste stof asook die temperatuur, wat daarop dui dat akurate korrelasie van mengsel damp-vloeistof ewewig nie slegs afhanklink is van ‘n gepaste keuse van mengreëls nie, maar ook die suiwer-komponent model.

Binêre interaksie parameters in die model mengreëls ondergaan *inter-korrelasie* wanneer meer as een interaksie parameter gebruik word, wat die ontwikkeling van algemeen toepaslike korrelasies grotendeels belemmer. Binêre interaksie parameters was ook bevind om sensitief te wees tot die suiwer component limiet (alpha funksie en suiwer konstantes wat gebruik is), die temperatuur, die kombineringsreëls en moontlik die vloeistof digtheid. Hierdie faktore moet dus almal sistematies in ag geneem word wanneer algemeen toepaslike korrelasies ontwikkel word, wat dus buite die omvang van die huidge studie val. Aanbevelings was wel gemaak vir hoe die MATLAB sagteware ontwikkel vir hierdie studie gebruik kan word om beide die betaande statistiese analise uit te brei, asook nuwe korrelasies vir binêre interaksies parameters en nuwe mengreëls te ontwikkel.

Stellenbosch University https://scholar.sun.ac.za

ACKNOWLEDGEMENTS

The financial assistance of the National Research Foundation (DAAD-NRF) towards this research is hereby acknowledged. Opinions expressed and conclusions arrived at, are those of the author and are not necessarily to be attributed to the DAAD-NRF.

Aspen Plus ® is a registered trademark of Aspen Technology Inc.

A special word of gratitude is conveyed to the following people, without whom the completion of this project would not have been possible:

- My supervisors Dr. C.E. Schwarz and Prof. J.H. Knoetze for their continued support and encouragement in pursuing my ideas throughout the duration of the study

- Dr. Christo Crause at SASOL for providing useful tips regarding the binary VLE calculations performed in the developed MATLAB software

- My parents and brother for their unconditional love, encouragement and patience

- Fellow researchers at the Separations Technology group at Stellenbosch University for providing a stimulating working environment

Stellenbosch University https://scholar.sun.ac.za

TABLE OF CONTENTS

Stellenbosch University https://scholar.sun.ac.za

Stellenbosch University https://scholar.sun.ac.za

Stellenbosch University https://scholar.sun.ac.za

Stellenbosch University https://scholar.sun.ac.za

Stellenbosch University https://scholar.sun.ac.za

Stellenbosch University https://scholar.sun.ac.za

Stellenbosch University https://scholar.sun.ac.za

Stellenbosch University https://scholar.sun.ac.za

1. INTRODUCTION

This project involves thethermodynamic modelling of the high-pressure binary vapour-liquid equilibrium (VLE) properties of long-chain hydrocarbon solutes (carbon number greater than 10) from different homologous series in solution with a supercritical solvent. This property information is crucial in the design of a super-critical fluid extraction (SFE) process, which aims to fractionate certain ranges of hydrocarbon-chain molecules into narrow cuts of similar structural features from a complex mixture. The data for this study has been measured using the facilities at Stellenbosch University and include the n-alkane, 1-alcohol, methyl and ethyl ester, as well as the carboxylic acid family in light-weight solvents, ethane, propane and CO_2 [1-17].

1.1 The feasibility of SFE

This section briefly overviews the feasibility of SFE for fractionating the systems investigated for this study. The value of the systems, the shortfalls of traditional methods and the viability of SFE is discussed.

1.1.1 Systems

Complex hydrocarbon-chain mixtures are encountered in a wide range of both naturally and synthetically occurring matrices and their processing is of interest to numerous lucrative industries [18]. Synthetic paraffin waxes in the carbon number range 30 – 300, for example, are present in crude oil reserves and are also the primary constituents of the Fischer Tropsch petro-chemical process effluent stream [19]. Fractionation of these mixtures into narrower cuts of similar carbon backbone lengths are of interest, amongst others, to the manufacture of candles, coatings in the printing, paper and food industries as well as additives to improve insulation properties of construction materials [20]. Long-chain alcohols play an important role in the production of cosmetic and detergent range (carbon number 12 to 16) products and are typically naturally sourced, converted from natural products or synthesized from the oxidation of other long-chain hydrocarbons [3, 21, 22]. The processing of fats and oils as found naturally in plant and animal materials is also of considerable commercial value to the food, cosmetic, pharmaceutical and oleo-chemical industries [23]. These oils and fats are comprised of complex mixtures of lipids such as triglycerides, free fatty acids, phospholipids, glycolipids, sterols and other fat soluble components [23]. Often in processing the fatty acids from a feedstock, they are converted to their corresponding methyl or ethyl ester and subsequently fractionated [6].

Stellenbosch University https://scholar.sun.ac.za

1.1.2 Traditional methods

Traditional fractionation methods for the mentioned systems include distillation, liquid-liquid extraction, adsorption, fractional crystallization and membrane technologies. These technologies are well-established in industry, require lower operating pressures, and have few safety concerns [24]. Due to the low-volatility of the long-chain solutes, these technologies require high operation temperatures which lead to thermal degradation of the product [18]. They also have insufficient selectivity for the close melting and boiling points of these solutes. Organic solvents such as hexane and toluene, as typically used in the liquid-liquid extraction of fats and oils, are furthermore facing government restrictions due to safety and environmental concerns [23].

1.1.3 SFE as alternative

The use of supercritical solvents is emerging as a feasible alternative for treating such systems. Close to the solvent critical temperature, the fluid shows large variations in density with small changes in temperature and pressure. Solubility is a strong function of density, which allows solvents to be selectively tuned for fractionation of certain solute ranges with small changes in the operating conditions and enables dissolving capabilities approaching those of liquids. Low weight super-critical solvents are volatile gases at atmospheric conditions, which further leads to simple separation from the final extract by either pressure reduction or temperature rise, with virtually negligible solvent residue in the product [19, 23].

The most common method for fractionating synthetic waxes is currently short path distillation (SPD) [19]. Operating pressures in the 0.1 – 10 Pa range can be reached, which is much lower than standard vacuum distillation units and low enough to prevent thermal degradation of most solutes [19]. Nieuwoudt et al. [25] compared the technical feasibility of SFE with SPD for wax fractionation and found that SFE gave much narrower cuts and that SPD gave a yellow colouration of the product. Crause et al. [19] found that static crystallisation had higher up-front capital costs than both SFE and SPD and that through efficient heat integration, SFE was technically and financially the more viable technology for fractionating long chain paraffins with carbon backbone exceeding nC45. Most petro-chemical plants also have ethane and propane available on site as cracker feedstock, as well as low pressure steam utilities, which improves the feasibility of integrating SFE with existing process units and possible re-processing of effluent streams [19].

In addition to providing solutions for the inadequacy of traditional methods, the unique properties of supercritical solvents also allow for new niche-markets to be exploited [24].

Stellenbosch University https://scholar.sun.ac.za

Recent developments include removing pesticides from phytochemicals and neutraceuticals, dry cleaning and degreasing of precision parts in electronics, dying of textiles and use as mobile phases in chromatography. Due to the high solvent selectivity, novel products in the extraction and purification of nutraceuticals, food supplements, active ingredients of pharmaceuticals, as well as application as a polymerization media are also being developed [24].

1.1.4 Summary

The unique characteristics of supercritical fluids (SCFs) have spurred immense research activity over the last two decades, but this activity is currently not proportional to the number of industrial applications [24, 25]. The general process complexities lead to case specificdesign for large scale applications, requiring substantial R&D efforts [18, 27]. This situation makes reliable cost estimates difficult, but recent reviews suggest that process economics improve substantially as the throughput of the process increases [18, 26]. Continuous operation or long-duration batches further allows for substantial savings on manpower [26].

It is believed that the immense research efforts in this field over the last 25 years will be able to accommodate the flurry of new applications currently waiting in the pipe-line, while simultaneously soothing growing environmental concerns regarding traditional solvents. With realistic capital cost and maintenance estimation, as well as optimized design and operation, SFE has the full potential to emerge as a prominent separations technology in its own right, on all scales of industry.

1.2 The role of thermodynamic modelling within SFE

The design of a SFE process involves the following general steps:

- Obtain the required property information
- Develop a process model for the fractionation columns
- Design the fractionation process

This project focuses exclusively on the first step, namely obtaining a reliable source of property information for incorporation into the design of a SFE process. According to O' Connell et al. [28], there are three main sources of property and phase equilibrium information available to a process engineer, including:

Stellenbosch University https://scholar.sun.ac.za

- Self-conducted experiments
- Databases of published values from literature, and
- Estimation methods using correlation, prediction or computation.

1.2.1 Experimentation and databases

In most design circumstances conducting rigorous experiments is not feasible given time and resource requirements. Recent revolutions in computation and information science have allowed for many companies to access vast electronic databases of property information. These databases may be easily searched and updated, but the increasing demand of global industrial applications seems to always exceed the rate of data acquisition. According to O' Connell et al. [28], as of March 2009 the CAS (Chemistry Abstracts Service) registry contains 45 000 000 organic and inorganic substances, with a total of nearly 61 000 000 chemical sequences. Despite dealing with the problem of measuring data for the infinite combination of mixtures at the appropriate conditions, a substantial hurdle in managing this body of information is also determining the quality of the data. Errors of consistency, tabulation and omission could cause large problems in application for design purposes. It is therefore clear that obtaining the relevant property values solely through empirical means is not sustainable.

1.2.2 Correlation, prediction and simulation

The methods of correlation and prediction are in the form of mathematical property models within which substances are defined by a set of parameters specific to the model. The different forms which such a model may take can be related to the level of empiricism involved in describing the system.

If the property model is generated through curve-fitting all parameters to sparse experimental data using polynomials, log-log plots, time series analysis or ANOVA methods, the model may be regarded as a purely *empirical model*. Empirical models are generally only capable of approximate interpolation between points in the design space, with no reliable prediction capabilities outside the system conditions from which the data were obtained.

A purely *theoretical model* is based entirely on pre-established knowledge of the system components, conditions and the fundamental physical principles involved, with no parameters arbitrarily regressed to data. Such a model should ideally have a single parameter set for each chemical compound, rather than working with different parameter sets for estimating different properties; or as may also be necessary, different parameter sets for different operating

Stellenbosch University https://scholar.sun.ac.za

conditions for the same property [29]. Theoretical models should also have a functional form with minimal loss of accuracy upon differentiation with respect to any process variable. Theoretical models are generally derived from the disciplines of quantum mechanics and statistical mechanics, but can currently only provide precise predictions for highly simplified systems in which all initial conditions are known and intermolecular interactions are essentially negligible. Such systems are hardly ever encountered in engineering practice.

In between the empirical and theoretical approaches there is an approach which O' Connell et al. [28] refers to as "enlightened empiricism." This approach uses rigorous equations from chemical theory along with correlations and parameters adjusted to fit data. These models are referred to as *semi-empirical*and have been the dominant method for obtaining required property information inseparation process design.

Advances in processing power may soon see computational simulation becoming the primary method for obtaining property information in design applications, but the immense scale and complexity of chemical systems has so far prevented this transition.

1.3 Project objectives

The primary aim of this project is to establish an effective semi-empirical thermodynamic modelling methodology to obtain the required property information for designing a supercritical fluid extraction (SFE) process. This requires not only an understanding of thermodynamic models, but also of unique features of the critical point and the phase behaviour of the systems in terms of intermolecular interactions. The objectives of this project are therefore divided into theoretical and modelling objectives:

Theoretical objectives

1) Get acquainted with relevant theory regarding the critical point, binary phase diagrams and the challenges in obtaining the required property information for SFE applications
2) Gain a thorough understanding of how structural features of the solute such as functional end-group, carbon backbone and isomerism (side-branching), as well as temperatureinfluence the phase behaviour, solvent selection and feasibility for a SFE process.
3) Review existing thermodynamic models for obtaining the required property information and make an appropriate selection for SFE applications.

Stellenbosch University https://scholar.sun.ac.za

Modelling objectives

4) Determine the capabilities of the selected modelling approach in representing the pure component vapour pressure and saturated liquid volume for the components of interest to SFE applications.
5) Determine the capabilities of commercial process simulators to model the high-pressure binary VLE data for asymmetric systems of hydrocarbon-chain solutes in a supercritical solvent, approaching the mixture critical point.
6) Investigate model parameters for trends with solute structure for possible developmentof generalized correlations.
7) Determine the effect and relative importance of factors such as the pure component limit, the mixing rules and the system conditions on the thermodynamic modelling of high pressure VLE of the asymmetric binary systems of interest to SFE applications.
8) Determine the effect of different computational techniques on the final results.

The outcomes of the first three theoretical objectives involve making appropriate selections regarding the computational procedure to be used, systems (solutes and solvents) considered and thermodynamic models to be investigated for this study.Objectives 4 through 8 involve conducting the thermodynamic modelling of the selected systems using the selected modelling approach and numerical procedure. When a typical phase diagram is considered, the different regions are:

- Two-phase equilibrium regions
- Compressed liquid region
- Superheated vapour region
- Solid region
- The near critical region
- The above critical region

The regions to be modelled for this study are the high pressure vapour-liquid equilibrium (VLE) properties, namely T, P, {X}, {Y}, just above the critical temperature of the solvent at reduced temperature ($T_r = T/T_c$) of 02 – 1.3, and approaching the mixture critical point, which is where solubility is deemed to be most feasible. Pure component vapour pressure and saturated liquid densities will also be investigated.

Even though the focus of the project is primarily on obtaining the relevant property information through thermodynamic modelling, it is noted that the study strives for a holistic view by placing property modelling in the wider context of designing a SFE process.

Stellenbosch University https://scholar.sun.ac.za

1.4 Thesis layout

A thesis layout is subsequently given for addressing the project objectives. Chapter 2 addresses project objective 1 by discussing the unique characteristics of the supercritical phase and the general theory behind binary phase diagrams according to the classification of Van Konynenburg and Scott [30]. Unique challenges for obtaining property values in the high pressure region approaching the critical point are also discussed and a computational procedure is proposed for addressing the numerical challenges.

Chapter 3 addresses project objective 2 by investigating the phase behaviour of the systems considered for this thesis, with emphasis on process feasibility.Solvents and solutes are then selected for conducting the modelling for this study.

Chapter 4 addresses project objective 3through an overview of semi-empirical equations of sate (EOS) for high-pressure applications, with emphasis on the near-critical region. Model families considered include the virial EOS, the cubic equations of state (CEOS), the molecular models for polymer chains (Perturbed Hard Chain Theory and related models), the Statistical Association Fluid Theory (SAFT) models for association molecules, the group contribution methods and the crossover approach. An appropriate approach is thenselected for this study.

Chapter 5 outlines the precise modelling methodology followed for addressing project objectives 4 through 8 in the ensuing chapters using the selected approach from Chapter 4.

Chapter 6 addresses project objective 4 by investigating the representation of the pure component vapour pressure and saturated liquid volume by the selected modelling approach. Appropriate pure component model parameters are also obtained prior to conducting mixture modelling.

Chapter 7 addresses project objective 5 by investigating the ability of current simulation packages to model the high pressure VLE of the selected binary systems using the general modelling approach chosen from Chapter 4. Aspen Plus ® is used for this investigation due to its wide application in industry and academia, as well as the many property models it has available. Project objective 6 is also addressed in this chapter by investigating binary interaction parameters (BIPs) in the model mixing rules for trends with solute carbon number.

Chapter 8 addresses project objective 7 by investigating important factors in the chosen modelling approach using a design of experiments (DOE) statistical sensitivity analysis. 6 important modelling factors are identified, each at two levels, implying $2^6 = 64$ separate

Stellenbosch University https://scholar.sun.ac.za

treatments (modelling combinations). The first 4 factors are model dependent and include the temperature dependence of the model, the volume dependence, the source of the pure component constants and the mixing rules used. The remaining two factors are system dependent and include the operating temperature and the terminal functional group of the solute.The sensitivity of BIPs to modelling factors involving the pure component limit is also investigated.

Chapter 9 addresses project objective 8 by comparing results from self-developed MATLAB software with those obtained from Aspen Plus® using the same model. Project objective 6 is also addressed in this chapter through investigating the influence of *combining rules*on trends of BIPs with solute carbon number. Chapter 10 and 11 summarize the conclusions, recommendations and suggested future work from the study. The thesis layout is summarized in Figure 1-1.

Stellenbosch University https://scholar.sun.ac.za

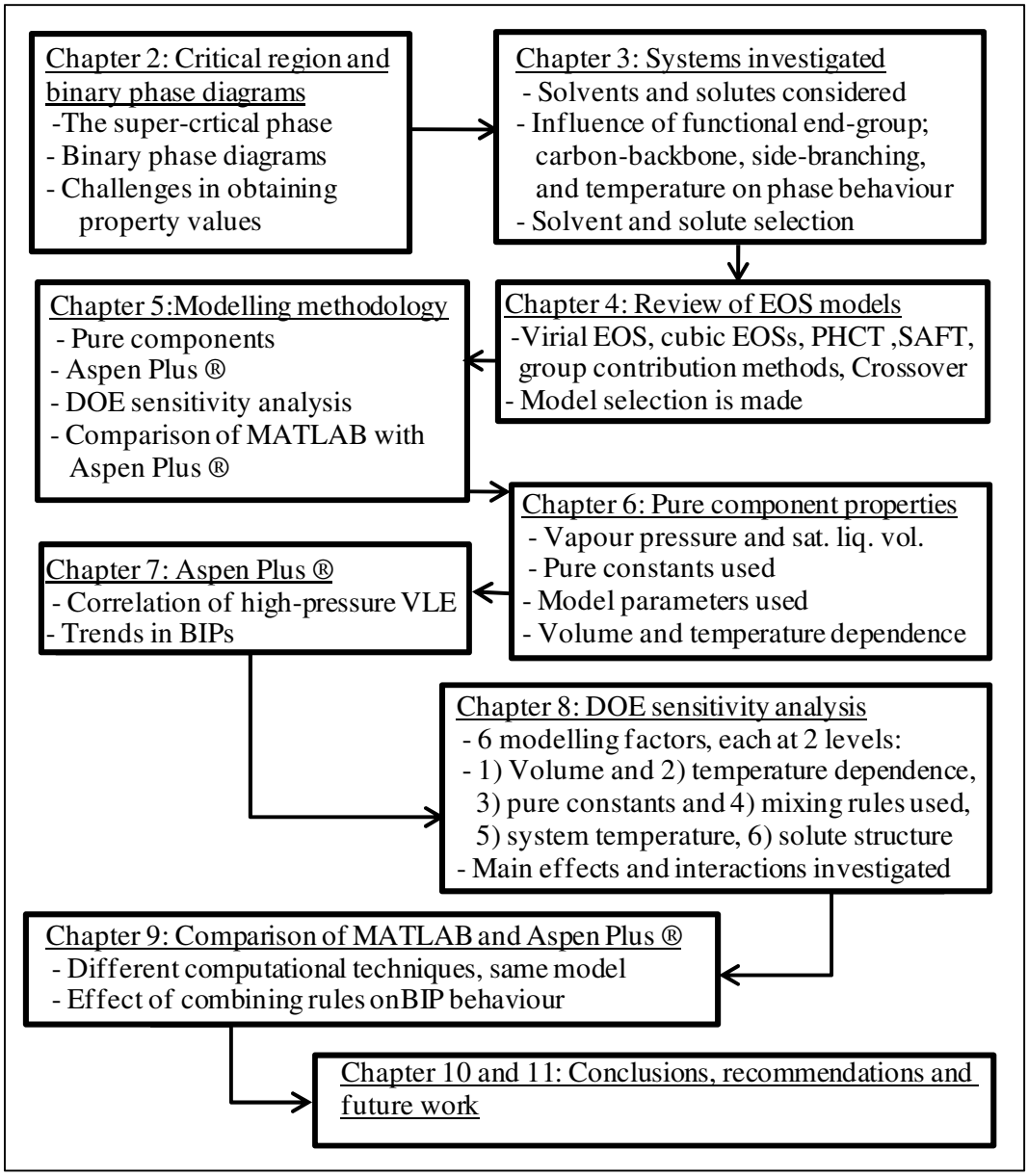

Figure 1-1 Diagram of thesis layout

Appendix A includes all of the working equations used and Appendix B gives the computational procedures used in the MATLAB software developed for conducting this study. Appendix C gives all of the pure constants used in the different sections of the project. Appendix D gives a chronological overview of important theoretical aspects in thermodynamic model development applicable to high pressure phase equilibrium and Appendix E contains additional figures and tables not included in the body of the thesis.

Stellenbosch University https://scholar.sun.ac.za

2. BINARY PHASE DIAGRAMS AND THE CRITICAL REGION

The aim of this chapter is to address project objective 1 from Section 1.3 by investigating the unique characteristics of a supercritical fluid (SCF) and to gain an understanding of binary phase diagrams and expected phase behaviour for systems of relevance to SFE applications. The 5 major types of binary phase diagrams as classified by Von Konynburg and Scott [30] are discussed. Particular difficulties in obtaining property values approaching the critical region are then discussed and a computational method is proposed for addressing these challenges.

2.1 The supercritical phase

Some general theory regarding the critical point is firstly presented, followed by a look at the physical fluid properties approaching the critical region.

2.1.1 General critical point theory

Stability and critical point conditions

Criteria for locating a critical point are found by investigating the limit of stability of single homogenous phases [31]. In Sections 6.1 and 8.1 it is shown how the Gibbs energy function (G) is minimized at equilibrium, and how a criterion for equilibrium can be derived from this fact in terms of *equality of fugacities*, which can be obtained directly from an EOS.

Even though equality of fugacities is a necessary condition for phase equilibrium, it is not sufficient to guarantee a global minimum in the Gibbs energy surface. This requires that the matrix of second derivatives of G with respect to independent composition variables be positive definite, meaning that the thermodynamic surface lies above its tangent plane and has positive curvature [32]. The classic criterion for this limit of stability was given by Gibbs:

$$\left(\frac{\partial^2 G}{\partial x_2^2}\right)_{P,T} = 0 \qquad 2\text{-}1$$

$$\left(\frac{\partial^3 G}{\partial x_2^3}\right)_{P,T} = 0 \qquad 2\text{-}2$$

$$\left(\frac{\partial^4 G}{\partial x_2^4}\right)_{P,T} > 0 \qquad 2\text{-}3$$

x_2 is the composition given in terms of component two of a mixture. In order to solve for the critical conditions using a pressure explicit EOS, it is more convenient to work in terms of the

Stellenbosch University https://scholar.sun.ac.za

Helmholtz energy (A), which is achieved by changing the constraints to temperature (T), volume (V) and mole number (n) as performed by Hicks and Young [33]. It can then be shown that the critical properties can be determined by finding the T, V and n which satisfy the following numerical conditions for a m component fluid [34]:

$$W = \begin{vmatrix} -\left(\frac{\partial^2 A}{\partial V^2}\right)_T & -\left(\frac{\partial^2 A}{\partial x_1\,\partial V}\right)_T \cdots & -\left(\frac{\partial^2 A}{\partial x_{m-1}\,\partial V}\right)_T \\ \left(\frac{\partial^2 A}{\partial x_1\,\partial V}\right)_T & \left(\frac{\partial^2 A}{\partial x_1^2}\right)_{T,V} \cdots & \left(\frac{\partial^2 A}{\partial x_1\,\partial x_{m-1}}\right)_{T,V} \\ \vdots & \vdots & \vdots \\ \left(\frac{\partial^2 A}{\partial x_{m-1}\,\partial V}\right)_T & \left(\frac{\partial^2 A}{\partial x_1\,\partial x_{m-1}}\right)_{T,V} & \left(\frac{\partial^2 A}{\partial x^2{}_{m-1}}\right)_{T,V} \end{vmatrix} = 0 \qquad 2\text{-}4$$

$$X = \begin{vmatrix} -\left(\frac{\partial W}{\partial V}\right)_T & -\left(\frac{\partial W}{\partial x_1}\right)_{T,V} \cdots & -\left(\frac{\partial W}{\partial x_{m-1}}\right)_{T,V} \\ \left(\frac{\partial^2 A}{\partial x_1\,\partial V}\right)_T & \left(\frac{\partial^2 A}{\partial x_1^2}\right)_{T,V} \cdots & \left(\frac{\partial^2 A}{\partial x_1\,\partial x_{m-1}}\right)_{T,V} \\ \vdots & \vdots & \vdots \\ \left(\frac{\partial^2 A}{\partial x_{m-1}\,\partial V}\right)_T & \left(\frac{\partial^2 A}{\partial x_1\,\partial x_{m-1}}\right)_{T,V} \cdots & \left(\frac{\partial^2 A}{\partial x^2{}_{m-1}}\right)_{T,V} \end{vmatrix} = 0 \qquad 2\text{-}5$$

All of the partial derivatives for constructing the matrices can be obtained directly from an EOS. The stability of the solution can then be verified by the following condition:

$$Y = \begin{vmatrix} -\left(\frac{\partial X}{\partial V}\right)_T & -\left(\frac{\partial X}{\partial x_1}\right)_{T,V} \cdots & -\left(\frac{\partial X}{\partial x_{m-1}}\right)_{T,V} \\ \left(\frac{\partial^2 A}{\partial x_1\,\partial V}\right)_T & \left(\frac{\partial^2 A}{\partial x_1^2}\right)_{T,V} \cdots & \left(\frac{\partial^2 A}{\partial x_1\,\partial x_{m-1}}\right)_{T,V} \\ \vdots & \vdots & \vdots \\ \left(\frac{\partial^2 A}{\partial x_{m-1}\,\partial V}\right)_T & \left(\frac{\partial^2 A}{\partial x_1\,\partial x_{m-1}}\right)_{T,V} \cdots & \left(\frac{\partial^2 A}{\partial x^2{}_{m-1}}\right)_{T,V} \end{vmatrix} > 0 \qquad 2\text{-}6$$

Pressure can be obtained from the partial derivative of the Helmholtz energy with volume:

$$P = -\left(\frac{\partial A}{\partial V}\right)_{T,n} \qquad 2\text{-}7$$

Stellenbosch University https://scholar.sun.ac.za

For a pure component, Equations 2-4 and 2-5 reduce to the following well known critical criterion for a pure component:

$$\left(\frac{\partial P}{\partial v}\right)_{T_c} = \left(\frac{\partial^2 P}{\partial v^2}\right)_{T_c} = 0 \qquad 2\text{-}8$$

Divergence of the compressibility

By the late 19th century, the characteristic empirical features of a pure fluid in its critical state were the visible scattering of light (critical opalescence), disappearance of the difference between vapour and liquid and the divergence of the isothermal compressibility [35]:

$$K_T \equiv -\frac{1}{v}\left(\frac{\partial v}{\partial P}\right)_T \qquad 2\text{-}9$$

This divergence is strong and compressibility values of a fluid near its critical density may become enhanced 100 K from the critical point, and differing by orders of magnitude within 10 K [35]. The Van der Waals EOS was the first model to explain vapour-liquid equilibrium from a single framework (see Appendix D.4). By further using Equation 2-8 for obtaining model parameters from critical point information, the termination of the phases and the divergence of the compressibility at the critical point was explained.

Typical PV behaviour for CO_2 is shown in Figure 2-1. The dashed lines give isotherms of how pressure varies with molar volume. The shaded area represents the region where the temperature and pressure are both higher than those at its critical point. The term "supercritical fluid" (SCF) is generally used for fluids in the following reduced temperature and pressure ranges [36]:

$T_r = 0.95 – 1.10$
$P_r = 1.01 – 1.5$

With an increase in temperature, the liquid density diminishes and the vapour density increases as the fluid vapour pressure increases [37]. At the critical point (CP), the densities converge and the dome shaped vapour-liquid equilibrium curve terminates. Not only the volumes and compositions converge at this point, but all other thermodynamic properties leaving no distinction between the phases.

Stellenbosch University https://scholar.sun.ac.za

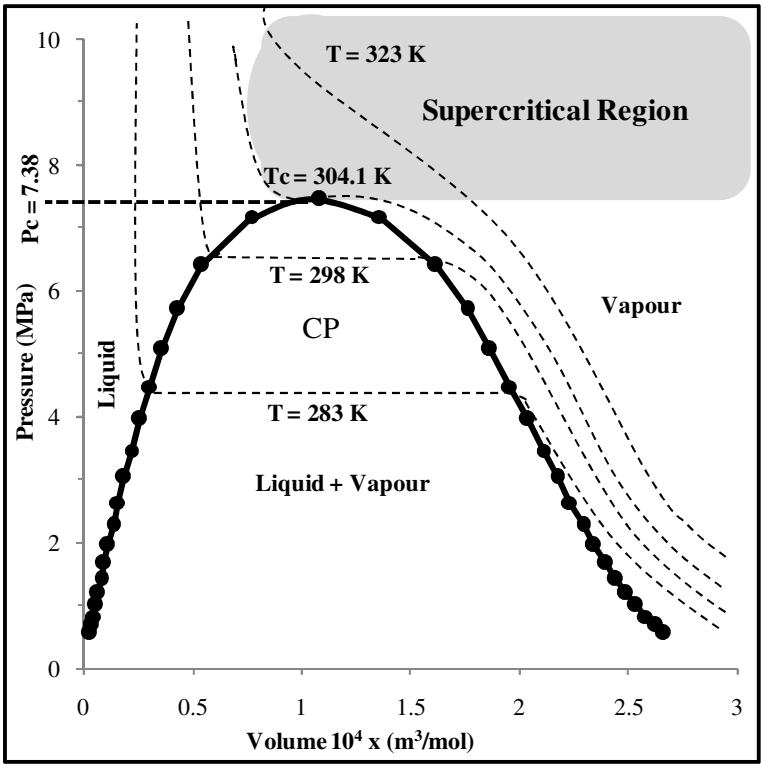

Figure 2-1: Pressure-volume diagram of CO_2 (redrawn from [36] using data from NIST)

In the vicinity of the critical point, small changes in pressure and temperature cause large changes in the volume, making super-critical solvents highly flexible for selective absorption of solutes [36]. As noted by Levelt Sengers [35], this sensitivity of density to system conditions has consequences for experimentation: errors in density will typically begin to exceed 1% in a region 10 K and 1 MPa from the critical point in fluids such as ethane and CO_2. At close approach to the critical point, a density gradient is unavoidable and even gravity may influence the measurement [38]. Experimentation is easier for mixtures, because the compressibility does not diverge, but the high pressures lead to process sensitivity and unique subtle complexities in phase behaviour are observed (see Section 2.2).

Density fluctuations

A fundamental assumption which is made in the development of most EOSs is the *mean-field* assumption, which models the fluid as having a homogenous potential field through which the molecules interact in a pair-wise fashion, according to the potential function used (see Appendix D.3). This view provides a realistic picture of fluid structure in the "classic", low pressure region, but is fundamentally incorrect approaching the critical point. The reason is related to the divergence of the compressibility and also offers an explanation for critical opalescence. Ornstein and Zernike [39] showed that the strong divergence of the

Stellenbosch University https://scholar.sun.ac.za

compressibility at the critical point culminated in the enhancement of long-range density fluctuations in a pure fluid, comparable with the wavelength of light, which exceeds the molecular dimensions considered in intermolecular potential functions. These fluctuations are responsible for critical anomalies which are not accounted for by classic mean-field models.

If a Taylor expansion is conducted for a classic EOS in volume and temperature at the critical point, the limiting behaviour of many thermodynamic properties can be given in the form of a power law for a given path. Some of these power laws are given in Table 2-1.

Table 2-1 Power law for the path to the critical point for selected properties and paths [35, 40]

Property	Power Law	Path
K_T (isothermal compressibility)	$K_T \propto \lvert\Delta T^*\rvert^{-\gamma}$	critical isochore ($\rho = \rho_c$)
C_V isochoric heat capacity	$C_V \propto \lvert\Delta T^*\rvert^{-\alpha}$	critical isochore ($\rho = \rho_c$)
Coexisting densities	$(\rho^L - \rho^v) \propto \lvert\Delta T^*\rvert^{\beta}$	two-phase region
P, pressure	$\Delta P^* \propto \lvert\Delta\rho^*\rvert^{\delta}$	critical isotherm
ξ, Correlation length	$\xi \propto \lvert\Delta T^*\rvert^{-\nu}$	critical isochore ($\rho = \rho_c$)

ξ is the *correlation length,* which gives the *spatial extent* of the density fluctuations [35]. The distance of a property from its critical value is defined as follows:

$$\Delta Val^* = \frac{Val - Val_c}{Val_c} \qquad 2\text{-}10$$

The values of the *critical exponents* for a classical mean-field equation and those for real fluids as determined by the "best" current means are given in Table 2-2 [35, 40].

Table 2-2 Critical exponent valuesfor the power laws in Table 2-1

Exponent	Classical Fluid	Real Fluid
γ	1	1.239
α	0	0.11
β	0.5	0.326
δ	3	4.8
ν	0.5	0.630

A relevant critical anomaly for determining VLE properties close to the critical point is the shape of the coexisting densities. For a classic fluid, the exponent β is 0.5, implying a parabolic shape to the coexistence curve. For real fluids, the shape of this dome has a flatter, shape with a β value of 0.326 [35].

Stellenbosch University https://scholar.sun.ac.za

Critical point universality

The reason the exponent values for real fluids can be presented as a single constant inTable 2-2 is that they are believed to be universal for a diverse range of fluids. This *principle of critical-point universality* follows from the density fluctuations: As can be seen from the behaviour of the a *correlation length,* ξ in Table 2-1, the closer to the critical point, the longer the extent of the fluctuations, which become greater than the scale of any intermolecular interactions in a fairly large near-critical region [41]. ξ diverges at the critical point, the microscopic structure of the fluid becomes unimportant and the thermodynamic properties of fluids become singular. For a mixture, ξ does not depict fluctuations in density but in *composition*, which results in similar universality [41]. Even though this universality has been demonstrated for a large range of fluids, studies have shown that complex solutions such as ionic liquids, electrolytes and polymers have a smaller "non-classical" region, with a sharp and even non-universal crossover into the critical region [38]

The mathematical nature of this asymptotic critical behaviour has been widely studied through *renormalization-group theory* and can be characterized by the scaling laws (as in Table 2-1) with universal critical exponents [41].

2.1.2 Physical properties of supercritcal fluids (SCFs)

Table 2-3 gives the typical range of four common properties for the gas, supercritical and liquid phases:

Table 2-3Comparison of physical properties of gases, liquids and SCF's (values obtained from [36] and [37])

Fluid Property	Gas	SCF	Liquid
Density (kg/m^3)	0.6 – 2	200 - 500	600 - 1600
Diffusivity (m^2/s)	1- 4x10^{-5}	2-7x10^{-8}	10^{-9}
Dynamic viscosity (Pa s)	1-3x10^{-5}	1-9x10^{-5}	10^{-3}
Surface tension (dyn/cm^2)	-	-	20 - 40

Density

The density values of fluids in the supercritical region are generally closer to those of the liquid phase and this is especially true at elevated pressures [36].According to Kikic and De Loos [40] the solubility of a given solute is practically exponentially related to the density of the solvent, making this liquid-like density key to the success of supercritical fluids as

Stellenbosch University https://scholar.sun.ac.za

solvents. The sensitivity of density to T and P due to the divergence of the compressibility allows for a great range of solvating power for minor adjustments of the process variables.

Diffusivity

The rate of mass diffusion of a chemical species A in a stagnant medium B in a specified direction is proportional to the local concentration gradient in that direction [42]:

$$\dot{m} = -D_{AB}A_s\left(\frac{dC}{dx}\right)\left[\frac{mol`}{s}\right] \qquad 2\text{-}11$$

The diffusivity coefficient D_{AB} is the unique proportionality constant by which species A moves through a certain surface area, A_s, against a certain concentration gradient, in a specific stagnant medium B. The diffusivity of gases generally increases with temperature and decrease with pressure, but show complex behaviour for liquids and solids [42]. It may be seen from Table 2-3 that the diffusivity coefficients of the SCF are closer to those of a liquid than a gas, however are still substantially higher than those of organic liquid solvents such as hexane, giving SCFs improved mass transfer properties for general process efficiency and improved contacting of solute and solvent. Figure 2-2 plots the diffusivity coefficient of ferrocene in $scCO_2$ as a function of the density of the fluid at 313 and 323 K.

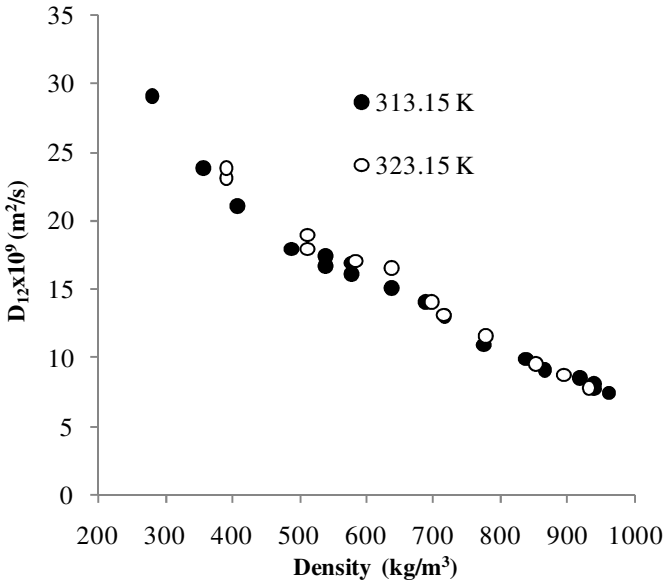

Figure 2-2 Diffusivity of ferrocene in $scCO_2$ as function of density $scCO_2$ (Redrawn from [35])

Stellenbosch University https://scholar.sun.ac.za

As the density increases the diffusivity decreases, but at constant density, a change in temperature does not bring a large change in diffusivity. This indicates that the density of the fluid is the controlling factor in determining the diffusivity [36].

Viscosity

The dynamic viscosity,μof a fluid may be defined by the following relation:

$$\tau = \mu \frac{du}{dy} \left[\frac{N}{m^2}\right] \qquad 2\text{-}12$$

τ is the shear stress of a layer of liquid and $\frac{du}{dy}$ is the velocity gradient (rate of deformation) of the contacting fluid layers moving parallel from a stationary point to the layer of the applied force, where the velocity is at a maximum [43]. The viscosity is a measure of the "resistance to deformation" of the fluid. Figure 2-3 shows the qualitative difference in the temperature dependence of viscosity between liquids and gases.

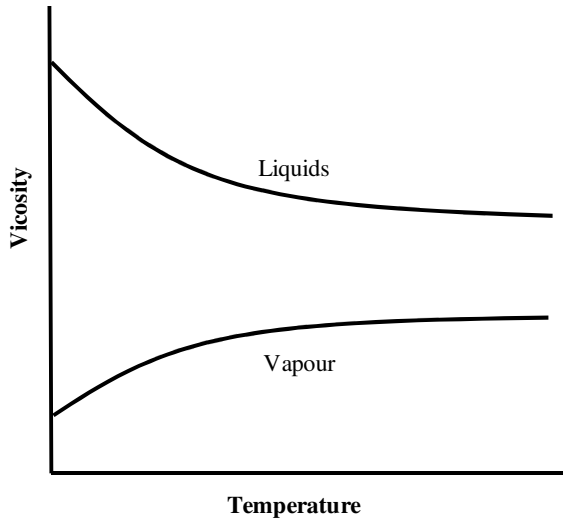

Figure 2-3Relationship of gas and liquid viscosities to temperature (Redrawn from Cengel et al. [42])

This behaviour can be explained by the molecular view of the phases: Viscosity in liquids is caused by the intermolecular forces (see Appendix D.3). As the temperature increases and the liquid molecules increase in kinetic energy, they oppose the intermolecular forces and the viscosity decreases. For gases, viscosity is proportional to molecular collisions, which

Stellenbosch University https://scholar.sun.ac.za

increase at higher temperatures [43]. From Table 2-3 it can be seen that the viscosity of the SCF is in a similar range to those of gases, resulting in improved hydrodynamic and mass transfer properties in process piping (lower pressure drop) and improved contacting between different phases [36]. Figure 2-4 plots the viscosity as a function of pressure and solvent density at different temperatures:

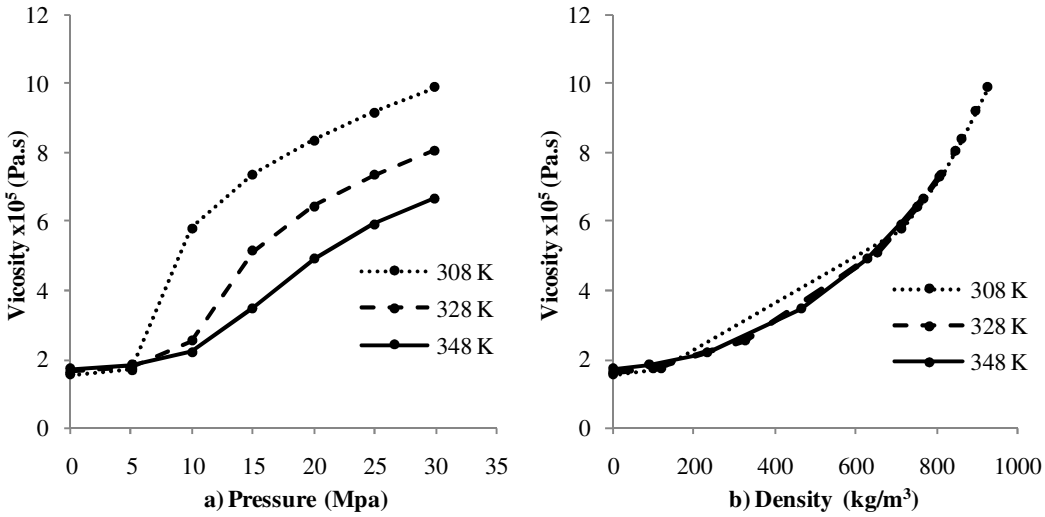

Figure 2-4 Variation of viscosity of $scCO_2$ as a function of (a) pressure and (b) density for various temperatures (Re-drawn from [35] using data from NIST)

From Figure 2-4 a) it is seen that viscosity of $scCO_2$ increases with pressure and decreases with temperature like liquids do, which is presumably because of the liquid-like density of the fluid. Figure 2-4 b) shows that at constant density, a change of temperature does not greatly influence the viscosity, however if the temperature is varied at constant pressure and the density is allowed to vary as in Figure 2-4 a), a marked change in the viscosity is observed [35]. This shows a similar linked relationship between viscosity and density as for diffusivity and density.

Surface Tension

Interfacial tension refers to an affinity that exists between the surfaces of two phases in equilibrium. This affinity changes drastically with changes in pressure, temperature and composition of the system, but approaches zero in the critical region where the border between phases disappears [37].

Stellenbosch University https://scholar.sun.ac.za

The range of liquid-like density with gas-like thermophysical properties which can be obtained with small variations in process conditions, makes SCF's an area of great potential and growing interest [36].

2.1.3 The mechanism of Supercritcal Fluid Extraction (SFE)

The mechanism of SFE is governed by the flexible density of the solvent approaching the critical point. The solubility of a solute in solvent is directly related to the density of the fluid, which is determined by the system pressure and temperature. The operating temperature for SFE is typically set close to the critical temperature of the solvent, which is where the density is most tuneable by system conditions. The pressure is optimised for the desired solubility of the component to be extracted compared to the other components present (see Chapter 3), which is often close to the total miscibility pressure of the desired solute in the solvent and thus closely related to the phase behaviour of the system [21].

2.2 Binary phase diagrams

The technical and economical feasibility of a SFE process is determined by the phase behaviour of the solvent/solute mixture [36, 37].The addition of a second component leads to highly complex phase behaviour not found in pure component mixtures [40]. Given the sensitivity of SFE to process conditions, a clear process path is necessary to assure that the preferred phase scenario is achieved [37]. In order to gain a proper understanding of the global phase behaviour that may be encountered for the systems of interest to this study, the 5 main types of binary phase behaviour according to the classification of van Konynenburg and Scott [30] are presented. The formation of solid phases at lower temperatures introduces additional complexities, however most supercritical separation processes select operating temperatures above the melting point of the heavier solute [22]. The formation of solid phases is therefore neglected in this discussion and De Loos [44] may be referenced for a more in depth discussion of these phenomena. The article by Privat and Jaubert [45] is also recommended for an up to date discussion on the global fluid-phase equilibrium behaviour in binary systems.

2.2.1 The general phase equilibrium problem

The state postulate stipulates that the state (all intensive properties) of a pure component, single-phase system can be fixed by 2 intensive variables. Considering the general case of a system with C components distributed throughout π phases, the state of the system can be

Stellenbosch University https://scholar.sun.ac.za

fixed by 2 + πC variables, namely the two independent variables for a pure, single phase species in addition to the composition of each multi-component phase.

Thermodynamics allows for the derivation of equations to solve for these variables and define the state of a multi-component, multi-phase system. The condition for phase equilibrium states that the chemical potential of each component in a mixture has the same value in each phase:

$$\mu_i^{\alpha} = \mu_i^{\beta} = \mu_i^{\gamma} = \ldots\ldots\ldots = \mu_i^{\pi} \text{ for } i = 1,2, \ldots\ldots, C \qquad 2\text{-}13$$

This is equivalent to the statement that the fugacity of each component is the same in each phase [46]:

$$f_i^{\alpha} = f_i^{\beta} = f_i^{\gamma} = \ldots\ldots\ldots = f_i^{\pi} \text{ for } i = 1,2, \ldots\ldots, C \qquad 2\text{-}14$$

These relations provide $(\pi - 1)C$ equations. π additional equations can be obtained by noting that the mole fractions of each phase sum to unity. Subtracting the equations from the variables gives the degrees of freedom (intensive variables) that need to be specified to fix the intensive state of each particular phase:

$$F = [2 + \pi C] - [(\pi - 1)C + \pi] \qquad 2\text{-}15$$

This reduces to the well known Gibbs phase rule:

$$F = C - \pi + 2 \qquad 2\text{-}16$$

If the full extensive state of the system is to be defined, then π phase fractions need to be additionally specified. By further adding the products of a phase fraction$(\alpha, \beta, \gamma \ldots \pi)$ and the component composition for each phase, C mass balance equations are obtained:

$$\alpha(y_i) + \beta(x_i) \ldots + \pi(s_i) = z_i \text{for } i = 1,2, \ldots\ldots, C \qquad 2\text{-}17$$

z_i is the composition of component i in the overall solution. Calculating the degrees of freedom for defining the extensive state shows that 2 variables are required, irrespective of the number of phases or components present:

$$F = [2 + \pi C + \pi] - [(\pi - 1)C + \pi + C] = 2 \qquad 2\text{-}18$$

Stellenbosch University https://scholar.sun.ac.za

This equation is known as Duhem's rule [46]. These variables can be extensive or intensive, but the Gibbs phase rule for intensive variables must still be obeyed.

2.2.2 Binary phase diagram definitions

At special regions in a phase diagram, such as azeotropes and critical points, additional equations become available:

$$F = N - \pi + 2 - \varphi \qquad 2\text{-}19$$

As the number of phases increase, less intensive variables are independent. The maximum number of intensive variables that need to be independently specified in order to constrain a system is therefore found in the one phase region and is given, for a binary system, by the following equation:

$$F_{max} = 4 - 1 = 3 \qquad 2\text{-}20$$

This result implies that all binary phase behaviour may be plotted on a three axis co-ordinate system, typically P,T and X. In order to get acquainted with binary phase diagrams, a couple of definitions will first be discussed at the hand of a type 5 phase diagram (see Figure 2-5).

The degrees of freedom decrease as the amounts of phases at equilibrium increase. This implies that a four phase region (F=0) region will be indicated by a single point in the PTXspace. Since each phase has a different composition (but the same T and P), this state is shown by four points in the phase space. A 3-phase region (F=1) will similarly be indicated by three curves; a 2-phase region (F=2) by two planes and a single phase (F=3) by a region in the phase space. These distinctions are labelled on Figure 2-5. An equilibrium with F = 0 is generally referred to as non-variant; F=1 is called mono-variant; F = 2 is referred to as bi-variant etc. [40].

Stellenbosch University https://scholar.sun.ac.za

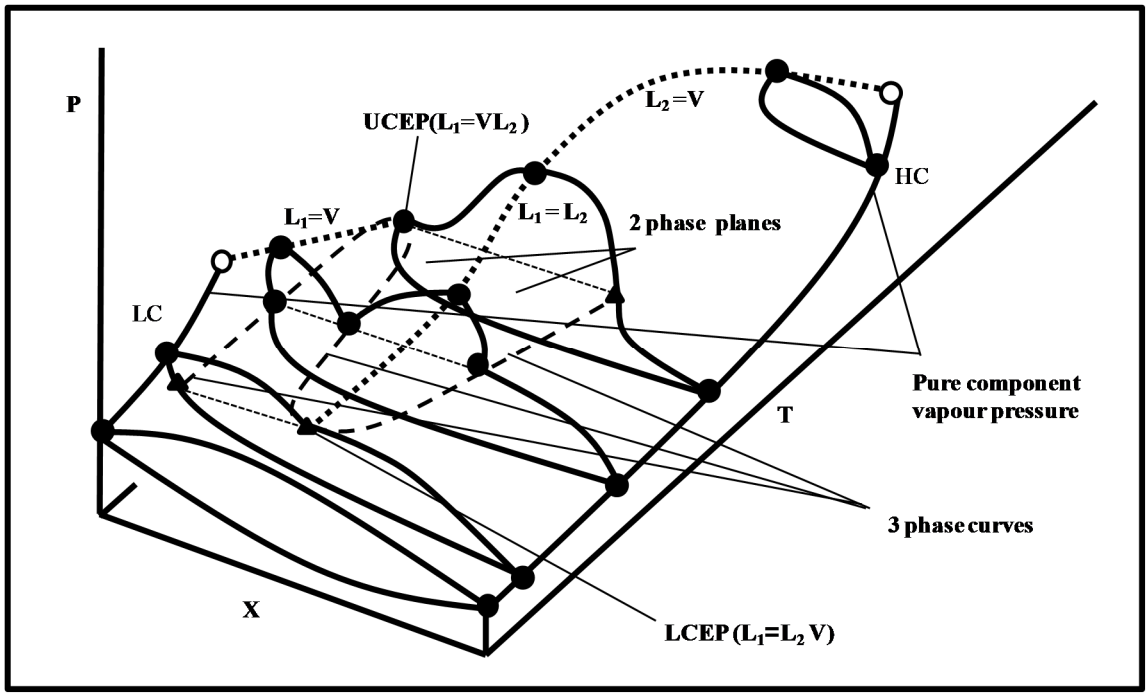

Figure 2-5 PTX diagram of a binary system showing type 5 fluid behaviour (Redrawn from De Loos [45])

From Figure 2-5 it is seen that the vapour pressure lines of the more volatile light component (LC) and the heavy component (HC) are found at solute fraction of X = 0 and X = 1 respectively and both terminate at their *critical points*, indicated by the non-filled circles. The two dotted lines are the *critical lines* of the mixture, extending from the pure component critical points to a point of intersection with a *three phase region*, the compositions of which are indicated by the three dashed curves, as labelled. The point (T,P,X) of intersection of a critical line and a three phase region is known as a *critical end point* (CEP). A critical line represents a two phase region, and its intersection with a 3-phase region implies that the *critical end point* is a point at which one phase transforms into a second, in the presence of a third phase. The highest temperature at which this occurs is termed the *upper critical end point* (UCEP) and the lowest temperature is termed the *lower critical end point* (LCEP). At the UCEP the lighter liquid phase L_1 turns into the vapour phase V, in the presence of the heavier liquid phase L_2 as indicated by the relation L_1=VL_2, leaving only V and L_2 at temperatures above the UCEP. Similarly the LCEP is defined by the relation L_1=L_2V [40]. These two points demarcate the limits of a three phase region. A critical line always emerges from a CEP [40]. The critical line terminating at the UCEP is characterized by the relation L_1 = V and the critical line terminating at the LCEP is characterized by the relation L_1=L_2. At temperatures above the UCEP where L_1 has turned into V, this critical line is defined as L_2=V.

Stellenbosch University https://scholar.sun.ac.za

Phase behaviour is seldom represented on a full global diagram, but rather as PT, PX or TX projections of the global diagrams. The discussion on the 5 types of phase behaviour to follow will be given with reference to a combined PT and TX projection of each type, as shown in Figure 2-6 for the type 5 phase behaviour just discussed.

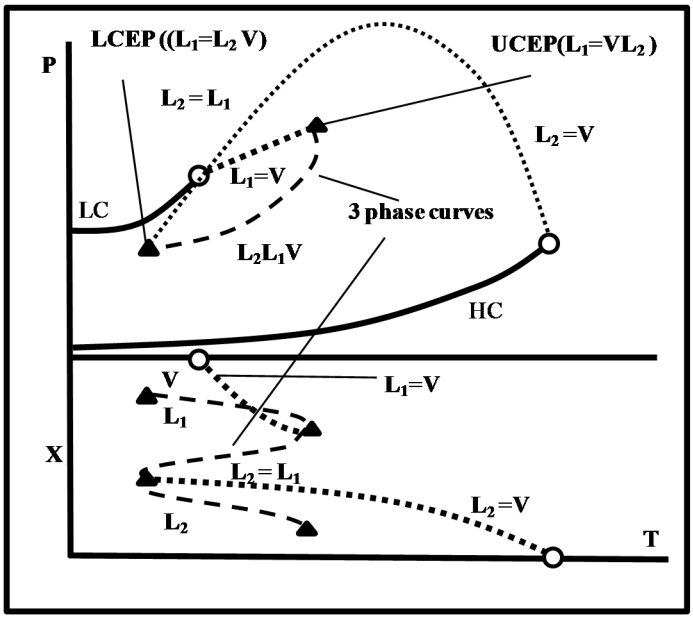

Figure 2-6 Combined PT and TX projections of type 5 phase behaviour (yet to be redrawn from De Loos [45])

The three phase region is indicated by one curve in the PT projection, since each phase is at the same temperature and pressure, but is given by three dashed-line curves in the TX projection.

2.2.3 Binary phase behaviour: Type 1 to 5

The 5 main types of global binary-phase behaviour as classified by van Konynenburg and Scott [30] can be related to the size and energy asymmetries between the solvent and the solute of a mixture. Figure 2-7 redrawn from Pereda et al. [37] and shows this general progression for a given solvent-solute series.

In general, three phase regions (liquid-liquid de-mixing) occurs at low temperatures for systems with appreciable non-ideality (energetic asymmetries), whereas de-mixing occurs at higher temperatures if the size asymmetry of the mixture is increased. In Appendix D.3 on intermolecular forces, it is seen that polar forces are inversely proportional to the temperature

Stellenbosch University https://scholar.sun.ac.za

(Equation D.12), which explains the liquid immiscibility at lower temperatures due to energetic asymmetries.

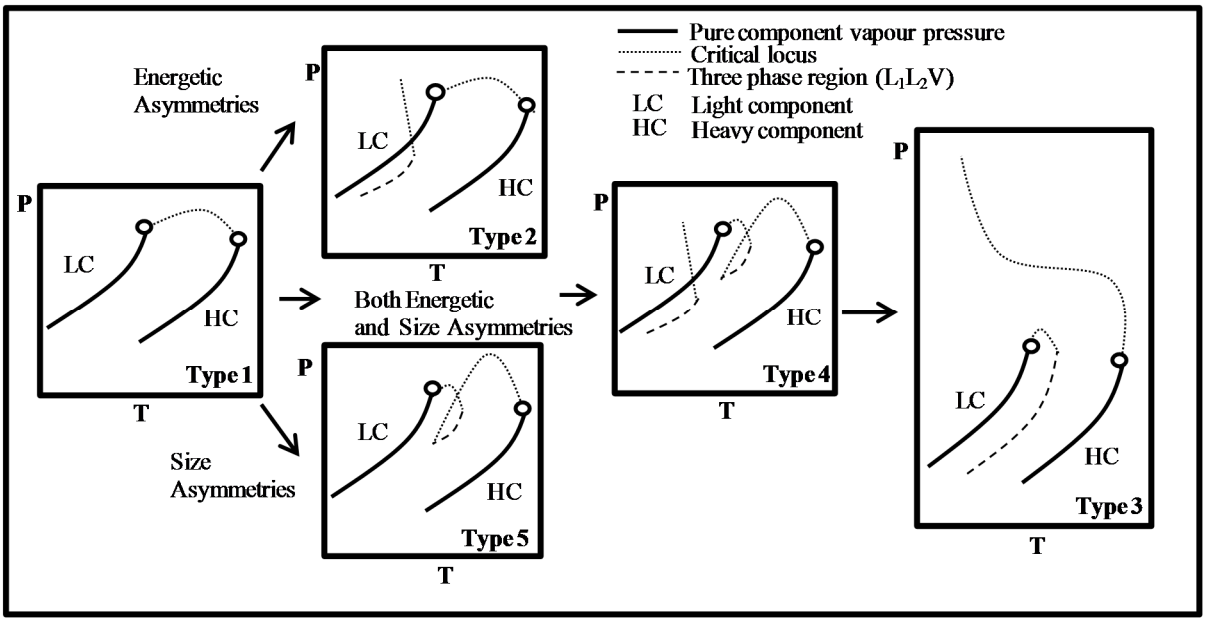

Figure 2-7 Progression of binary phase behaviour with size and energy asymmetries (Redrawn from Pereda et al [37])

The different types are now discussed in the context of Figure 2-7. Examples of how the different types of phase behaviour progress for particular solvent-solute series of interest are then given in Section 2.2.4.

Type 1

Type 1 phase behaviour is characterized by complete liquid miscibility at all temperatures, as shown by a single unbroken critical line from the pure solvent to the pure solute composition, representing a continuous vapour-liquid region (see Figure 2-8). This type of phase behaviour is typical of systems with components of similar size and chemical nature (similar critical temperatures) [37].

Stellenbosch University https://scholar.sun.ac.za

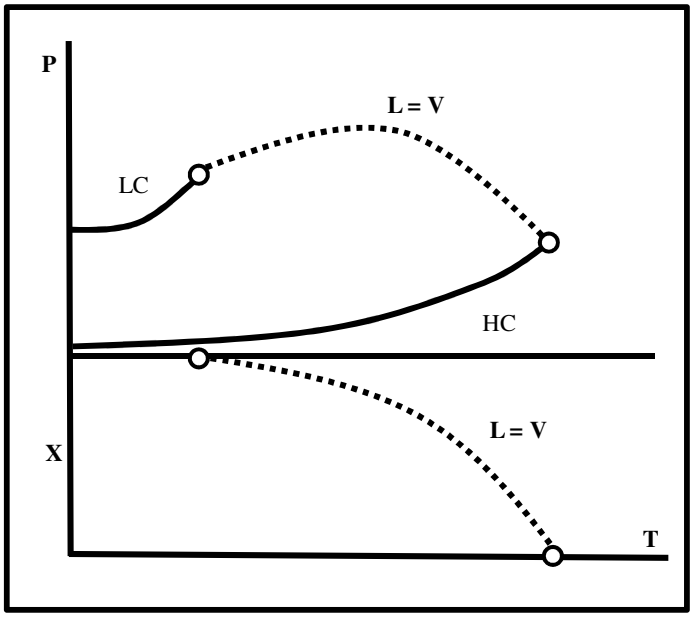

Figure 2-8 Combined PT and TX projections of type 1 phase behaviour (redrawn from De Loos [45])

Type 2

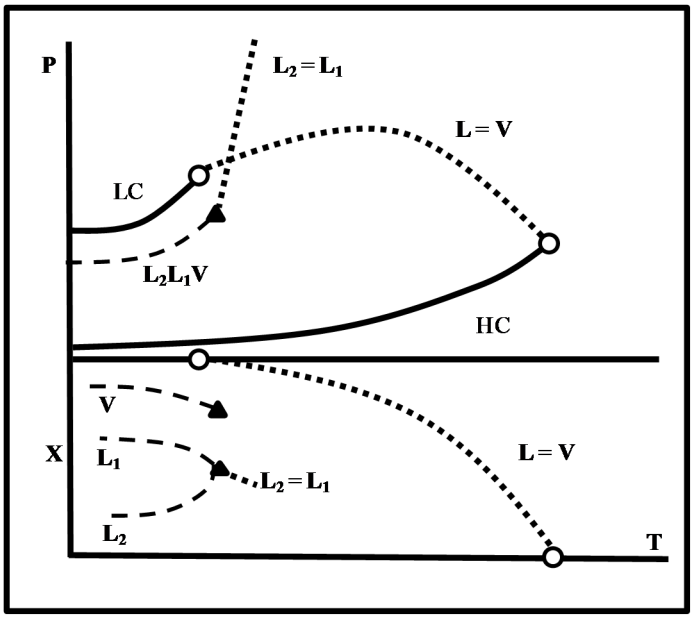

Figure 2-9 Combined PT and TX projections of type 2 phase behaviour (redrawn from De Loos [45])

Type 2 phase behaviour has a similar continuous critical curve as that observed in type 1, but at lower temperatures there is a phase split in the liquid resulting in a liquid-liquid critical line

Stellenbosch University https://scholar.sun.ac.za

$L_2 = L_1$ terminating at a three phase region L_2L_1V at the UCEP $L_2=L_1V$ (see **Error! Reference source not found.**). The $L_2=L_1$ critical curve may be interrupted by a solid phase at low temperature. If this does not occur the critical curve goes to infinite pressure [45]. This solid phase may in fact hide the three phase region, making it impossible to distinguish between type 1 and type 2 phase behaviour. Type 2 phase behaviour is typical of mixtures of similar sized components, but in which non-ideality (energetic asymmetries) lead to liquid split at subcritical temperatures [37].

Type 5

Type 5 behaviour is depicted in Figure 2-5 and is characterized by liquid-liquid immiscibility near the light component critical temperature (solvent critical temperature in SFE processes), resulting in the branching of the critical line into a three phase region at intermediate to elevated temperatures. One branch originates at the critical point of the more volatile component and ends at an UCEP. The other branch starts at the heavy component critical point, goes through a pressure maximum and terminates at a LCEP. As the size asymmetry (solute carbon number) increases, the LCEP moves to a lower temperature and the size of the three phase region stretches over a greater temperature range. Complete miscibility is retained at temperatures below the LCEP and above the UCEP. The entire three phase region is located close to the pure component vapour pressure of the volatile component [47]. This phase behaviour is typical of systems that are almost ideal (non-polar) but with significant difference in size [37].

Type 4

It can be seen from the combined PT and TX projections in Figure 2-10 that type 4 phase behaviour consists of two separate regions of liquid-liquid immiscibility:

Stellenbosch University https://scholar.sun.ac.za

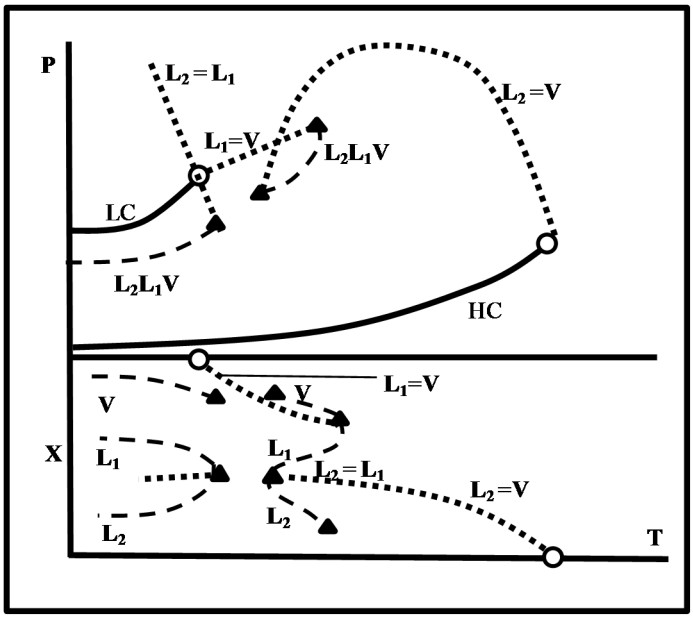

Figure 2-10 Combined PT and TX projections of type 4 phase behaviour (redrawn from De loos [45])

At higher temperatures, there exists a discontinuous critical curve as for type 5 phase behaviour. Complete liquid miscibility is observed at intermediate temperature, but at lower temperatures the liquid phase splits again, as observed for type 2 phase behaviour. This region may again be hidden by the formation of solid phase. Type 4 is encountered for molecules with appreciable size difference *and* polarity. The polarity or association causes de-mixing at lower temperatures and the size difference causes de-mixing at higher temperatures [37].

Type 3

It can be seen from Figure 2-11 that type 3 liquid-liquid de-mixing occurs continuously at low and high temperatures [37].The two 3-phase regions from the two branches of type 4 phase behaviour have merged, whereby the critical curve extending from the critical temperature of the more volatile component terminates at a UCEP, marking the upper limit of the 3-phase region [45]. The critical line extending from the critical point of the less volatile component may take on several forms. Since the critical curves (b) and (c) can exist at higher temperatures than the critical temperature of the less volatile component, these cases are often referred as gas-gas equilibria.

Stellenbosch University https://scholar.sun.ac.za

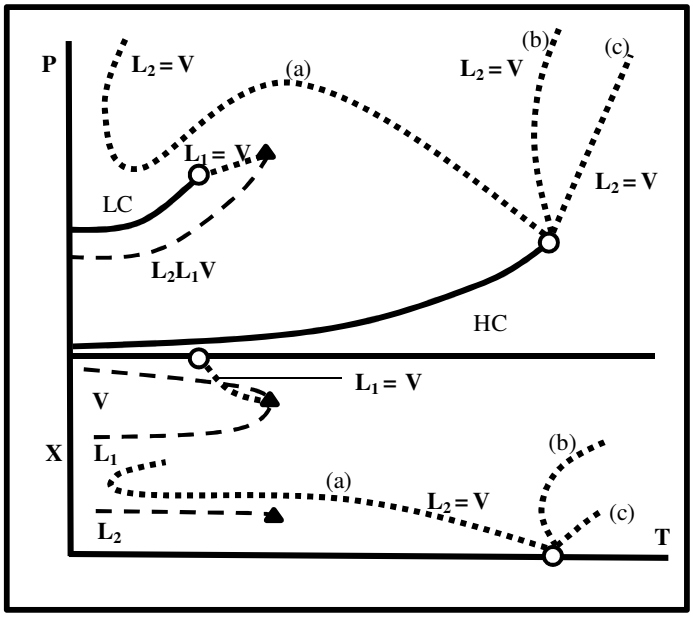

Figure 2-11Combined PT and TX projections of type 3 phase behaviour (redrawn from De loos [45]) (a) critical curve with pressure maximum and minimum and temperature minimum; (b) critical curve with a temperature minimum; (c) Critical curve without a pressure maximum or temperature minimum

Type 3 phase behaviour is observed for systems of significant size and energetic asymmetries, leading to liquid-liquid de-mixing at all temperatures and at high pressures.

2.2.4 Studies on homologous series

Considering the complex matrices encountered in industry, it is useful to know at what process conditions the different types of phase behaviour manifest themselves for a particular solvent with different homologous series. Of particular interest in applications with a volatile supercritical solvent and non-volatile solute, is the transition from type 1 to type 5 phase behaviour at a certain solute carbon number. At the onset of type 5 behaviour for a certain homologous series the LCEP and the UCEP coincide at the same temperature and the three phases emerging from the unbroken critical line (type 1) are essentially identical [47]. This phenomenon is known as *tri-criticality*. A further increase in solute carbon number causes the LCEP and UCEP to move to lower temperatures and the size of the three phase region, given as $\Delta T = T(UCEP) - T(LCEP)$, to increase [47].

The progression of types of phase behaviour as the solute carbon number is increased in supercritical solvents has been studied, amongst others, by Peters [47] and some results from

Stellenbosch University https://scholar.sun.ac.za

these investigations are summarized for typical light-weight solvents ethane, propane and CO_2.

Ethane

Mixtures of ethane with the n-alkane series show type 1 phase behaviour up to a carbon number of 17 (n-heptadecane), at which point tri-criticality occurs at a temperature of about 314 K [47]. A three phase region is observed for carbon numbers up to about 23, above which interference with a solid phase is observed [48].

For ethane with 1-alcohols, no tri-critical point has been observed and type 5 is believed to occur for the whole homologous series up to carbon number of 15 [47]. According to Peters [47], this de-mixing for low molecular weight 1-alcohols can be ascribed to aggregation into more than two molecules. The shift of the LCEP to lower temperature with carbon number is also much steeper for the 1-alcohols than the n-alkanes, leading to a larger overall size of the three phase region (270 – 316 K), compared to the n-alkanes (298 – 314 K) [47].

For ethylene as solvent, tri-criticality is observed for the carboxylic acid systems, which may imply its occurrence using ethane as solvent [47]. The occurrence of tri-criticality for the carboxylic acids, but not for the 1-alcohols, suggest a greater asymmetry for the 1-alcohol systems. According to Peters [47], this can be explained by the fact that the carboxylic acids form at most dimers due to hydrogen bonding, and not more complex aggregates such as is presumably the case with the 1-alcohols. The dimerization of acids is graphically illustrated in Figure 2-12.

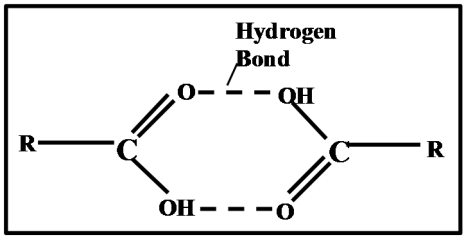

Figure 2-12 Dimerization of carboxylic acids

The double hydrogen bond between two carboxyl groups at the terminal end-point of a linear chain prevents aggregation of more than two molecules.

Stellenbosch University https://scholar.sun.ac.za

Propane

Mixtures of propane with the n-alkane series show type 1 phase behaviour up to a carbon number of 29 (nonacosane) at which point tri-criticality occurs at a temperature of about 377 K. A three phase region is observed for carbon numbers exceeding 50.

A tri-critical point is also observed for both the 1-alcohol and carboxylic acid in propane at carbon numbers of 18 and 14 respectively. The three phase region (type 5) is observed up to carbon number of approximately 26 and 22 for the 1-alcohols and carboxylic acids respectively. According to Peters [47], this shift of the three phase region to lower carbon numbers compared to the n-alkanes can be explained by aggregation in the 1-alcohols and dimerization of the acids, as was the case for ethane.In general, liquid-liquid immiscibility in propane binary mixtures requires much higher temperature and solute carbon numbers than in ethane due to the greater size of propane and increased symmetry of the mixture. For the 1-alcohols in propane, these conditions do not allow for the degree of aggregation which causes liquid-liquid immiscibility across the whole carbon number range for 1-alcohols in ethane [47]. Dimerization of the acids is less hindered and the liquid immiscibility occurs not only at lower carbon number than the 1-alcohols, but also at a slightly lower temperature [47].

Triglycerides were found to show an identical temperature range for the three phase region to the n-alkanes in propane at the same molecular mass, which suggests that the addition of non-polar functional groups does not greatly affect the phase behaviour of propane binaries. For non-linear solutes of a poly-aromatic nature, not only carbon number but also the molecular structure influences the phase behaviour. Type 2, 3 and 4 may occur, but a global classification is difficult due to the complexity of the interactions [47].

CO_2

Mixtures of CO_2 with the n-alkane series show type 1 phase behaviour for a carbon number in the range 1 – 6 and type 2 phase behaviour for carbon numbers 7 - 12. Type 4 phase behaviour occurs at carbon number of 13 and type 3 phase behaviour is generally found for solute carbon numbers 14 – 21 [45]. At carbon number greater than 22, the phase behaviour is influenced by the formation of a solid phase. These regions of liquid-liquid immiscibility are located at higher temperatures than for ethane. The progression of type 2 to type 3 via type 4 is typical of systems with CO_2 as the solvent [40]. Nieuwoudt and Du Rand [15] have further reported a three phase region for the CO_2/hexatriacontane system over the entire temperature range of interest for extraction.

Stellenbosch University https://scholar.sun.ac.za

For the 1-alcohols in CO_2, type 2 phase behaviour is observed at solute carbon numbers of 6 and 8, with type 3 observed at carbon number of 12. This shifting of the progression to lower carbon numbers than for the n-alkanes is due to the increased asymmetry caused by hydroxyl group [48].

Given the sensitivity of SFE to process conditions and the dependence of phase behaviour on the component interactions, an understanding of global binary phase behaviour provides valuable insight for designing these processes. Even though enhanced solubility has been observed close to a critical end point, 3-phase regions lead to additional complexities and aretypically avoided for SFE applications [45]. Operation temperatures above the UCEP and high enough to prevent the formation of solid phases are therefore typically chosen.

2.3 Summary of challenges

This section summarizes the challenges in obtaining VLE property values for the systems encountered in this study. These include unique complexities in the critical region, as well as those caused by the general mixture asymmetry (polarity and size differences). These complexities pose a problem not only for theoretical development, but also for numerical application of EOS models.

2.3.1 Critical point complexities

As shown by Equations 2-4 to 2-5, locating a critical point along the limit of stability is a numerically intensive procedure that involves higher order compositional derivates of the Helmholtz energy function. Solving for the critical conditions has undergone substantial mathematical development since the first formulation by Gibbs (equations 2-1 to 2-3), including the work of Hicks and Young [33], Heidemann and Khalil [31], Heidemann and Michelsen [49] as well as the application of the *tangent plane criterion* in the work of Michelsen [50 - 53]. Heidemann gives a good review of these developments [54]. Despite the progress made, the calculation is still numerically intensive and few commercial simulators allow for direct calculation of the critical point.

The power laws and critical exponents discussed in Section 2.1.1 give a true account of real fluid behaviour in the asymptotic critical region and a mean field EOS gives a reasonable account of classical low pressure region. As noted by Levelt-Sengers [35], the isothermal compressibility of a fluid near its critical density is already considerably enhanced at distances up to 100 K from a critical point, with a correlation length around twice the intermolecular distance. At distances farther from the critical point, a clear distinction cannot

Stellenbosch University https://scholar.sun.ac.za

be made between classical (short-range) effects and contributions from long range density fluctuations. The *crossover* theory has been developed to provide a consistent approach for obtaining thermodynamic properties across the whole region where critical enhancements are significant (the *global critical region*), which adheres to the scaling laws in the asymptotic critical region and reduces to the mean-field equation in the classic region. This includes the work of Tang and Sengers [56], Jin et al. [57], Kostrowicka Wyczalkowska et al [58] and Kiselev and co-workers [59 - 62]. More empirical methods, such as those of Solimando et al. [63], Firoozabadi et al. [64] and Kedge and Trebble [65] have also been developed, but are not as rigorous as the crossover models.

Even though experimental measurements in the near-critical region are easier for mixtures than for pure fluids since the compressibility does not diverge, application of these already complex theories are more difficult for mixtures because of the additional degrees of freedom from the composition variables [38].

2.3.2 System complexities

Apart from the unique complexities in the critical region, the following general modelling challenges are also presented by these systems:

- The non-spherical, chain-like structure of the solute
- The size asymmetry between solvents and solutes
- Polar effects of the different functional groups
- High pressures, far removed from ideal conditions

The performance of thermodynamic models in meeting theoretical challenges is investigated more thoroughly in Chapter 4. Some general comments on the numerical aspects of performing the required high-pressure phase equilibrium calculations are briefly made.

Trivial root problem

The calculation of phase equilibrium and thermodynamic properties from an EOS involves solving for the roots of the equation, either in volume or compressibility. As seen in Figure D.11 (Section D.4.2), a cubic equation of state has a three root region for a pure component at sub-critical temperatures and only one possible root above the critical temperature. In the two phase region ($P = P_{sat}$), fugacities are equal and the larger root corresponds to the vapour volume, the smaller root to that of the liquid and the middle root is thermodynamically unstable. In the one phase region, the stable root has the lower fugacity.

Stellenbosch University https://scholar.sun.ac.za

For mixtures, the allocation of roots to the correct phase is not as straight forward, even for simple cubic models. As described by Poling et al. [65], the pressure/volume derivative (Equation 2-8) at a certain composition does not represent the true critical point of a mixture as it does for a pure fluid, but rather a *pseudo-critical point.* (also referred to as the mechanical critical point). Below the pseudo-critical point, there is a range of temperatures for a given pressure and composition for which there are three real roots, making for simple phase identification. Outside this range, and at conditions above the pseudo-critical point, there is only one real root, which does not necessarily correspond to the phase for which the composition is specified. This may lead to incorrect fugacities and divergence of phase equilibrium calculations [38]. It may also lead to the *trivial solution* where the two phases converge to the same composition which automatically satisfies the equilibrium conditions, terminating the calculation pre-maturely. This is particularly prevalent in the near-critical region, which is always located substantially above the pseudo-critical point and where phase compositions are similar and change rapidly with pressure [66].

These problems are observed if the initial estimates for the phase equilibrium calculations are not of high quality [66]. As noted by Mathias et al. [67], good initial estimates are not always available, especially in commercial process simulators where different process models are required to provide values for various properties over a wide range of applications and process conditions. Data regression poses a particular challenge since the parameter values generated by the minimization algorithm are indifferent to these complexities.

Initial estimates (K values)

The most common method for generating initial estimates for phase equilibrium calculations is using the Wilson K-factor approximation [66]:

$$\ln K_i = \ln\left(\frac{P_{ci}}{P}\right) + 5.373(1 + \omega_i)\left(1 - \frac{T_{ci}}{T}\right) \qquad 2\text{-}21$$

As noted by Michelsen and Mollerup [66], this correlation is particularly useful for bubble point calculations at low pressure ($P < 1$ MPa), where the vapour phase for which the composition is to be solved is nearly ideal and non-idealities in the liquid phase don't matter since its composition is specified. This correlation loses accuracy at higher pressures and can not be used to start calculations in the relevant region for SFE. The most reliable way for calculating high-pressure VLE using a simple bubble point calculation is therefore construction of the phase envelope from low pressure, however this can be time consuming as convergence becomes very slow approaching the critical point, making it infeasible for

Stellenbosch University https://scholar.sun.ac.za

industrial applications. Various authors have therefore provided heuristic methods and algorithms to allow convergence of property calculations for infeasible specifications, including the work of Poling et al. [65], Mathias et al. [67], Gundersen [68], G.V. Pasad, G and Venkatarathnam [69] and Veeranna et al. [70].

2.3.3 Proposition for addressing the challenges

The data points for the systems modelled for this study were measured exclusively at high pressure approaching the critical region. Given the large size asymmetry between the solvent and solute, as well as the polar functional groups of the solutes, systems relevant to SFE are typically highly non-ideal. Providing good initial estimates for these high-pressure phase calculations is therefore particularly challenging, increasing the likelihood of the trivial solution. Since this study focuses primarily on investigating model performance, reliability is considered more important than speed of the calculation.

The approach proposed for calculating the high-pressure binary VLE in the software developed for this study therefore involves constructing the entire phase envelope using a standard bubble point pressure calculation. The calculation is started at the pure solute using a pure component vapour pressure calculation (see Appendix B.2) and stepped in liquid composition towards the pure solvent. Initial estimates for each step are obtained from the previous solution and the step-size is decreased in the near-critical region to ensure convergence and a close approach to the critical point. A detailed algorithm is presented in Appendix B.3. This study therefore does not investigate model performance in locating the critical point along the limit of stability, but rather just in correlating the high-pressure VLE approaching the critical point.

The theoretical challenges imposed by the density fluctuations in the critical region, the chain-structure of the solutes, the size asymmetry between the solvent and solutes, as well as the polarity introduced by solute functional group will be addressed in Chapter 4, which reviews EOS models for application in the high-pressure near critical region.

2.4 Conclusions

The aim of this chapter is to get acquainted with the theoretical aspects of the fluid critical point, binary phase diagrams and phase behaviour, as well as challenges in obtaining the relevant property information for designing a SFE process. The main outcomes from this chapter are given below:

Stellenbosch University https://scholar.sun.ac.za

- The criterion for a mixture critical point is located at the limit of stability where a single homogenous phase splits into two phases. Within thermodynamics, this criterion is represented by matrices of second order derivatives of the Gibbs energy with composition. Solving these criteria is quite analytically and numerically intensive.
- *Mean field*EOSs give a reasonable account of the classic low pressure region, but density and composition fluctuations approaching the critical point of a pure fluid and mixture, respectively, lead to anomalous behaviour not accounted for by the classic mean field models. Accounting for these fluctuations is addressed by *renormalization group theory* and reconciling classic low pressure behaviour with the asymptotic critical behaviour is addressed in the *crossover theory*. These theories are also complex.
- The tuneable density of SCFs, representing those of liquids, combined with transport properties representing those of gases, makes SCFspromising solvents for fractionating complex hydrocarbon mixtures.
- Solute solubility is exponentially related to the fluid density, which is largely tuneable by temperature and pressure in the vicinity of the solvent critical point. The solubility of a particular solute further determines the process feasibility and is closely related to the phase behaviour of the system.
- The 5 main types of binary phase behaviour as characterized by Van Konynenburg and Scott [30] are related to the energetic (polarity) and size asymmetries of a mixture. The nature of these intermolecular interactions leads to trends in the observed phase behaviour, particularly the carbon number and temperature range of three phase regions (liquid-liquid de-mixing), for different homologous series in a certain solvent.
- The location of three phase regions for the n-alkanes, triglycerides, 1-alcohols and carboxylic acids in CO_2, ethane and propane were discussed, providing useful insights for determining feasible operating conditions for processing the systems of interest to this study.
- The challenges in obtaining property values approaching the critical point of a mixture were summarized, which include unique complexities in the critical region, as well as general challenges leading to mixture non-ideality in the classic region, such as high-pressures, chained structure of the solutes and asymmetries between the solvent and solute.
- A simple method was proposed to overcome some numerical aspects of these challenges by approaching the critical point through stepping in liquid composition, X, from the pure solute (low pressure) towards the pure solvent using a standard bubble point calculation. Initial guesses are then carried over from each step to the next to avoid trivial solutions and failure of calculation convergence.

Stellenbosch University https://scholar.sun.ac.za

This chapter therefore addresses project objective 1 as given in section 1.3. The theoretical challenges in obtaining the required property information are addressed more thoroughly in Chapter 4, which reviews semi-empirical EOS models for high-pressure applications. Chapter 3 further investigates interesting phase behaviour for systems considered for this study.

Stellenbosch University https://scholar.sun.ac.za

3. SYSTEMS INVESTIGATED

System phase behaviour plays a determining role in the the feasibility of a SFE process. This chapter addresses project objective 2 by investigating the phase behaviour of systems considered for this study. The influence of the solute functional-end group, carbon backbone-length and isomerism, as well as temperature on the phase behaviour and solubility are discussed. Implications for process feasibility and setting operating conditions are discussed and solvents and solutes are then selected for the modelling to be conducted.

3.1 Solvents and solutes considered

Given the large degree of polydispersity of typical hydrocarbon mixtures encountered in industry, it is desirable to have a solvent that can distinguish between the following structural features of the solute:

- Functional end-group
- Carbon backbone length (molecular mass)
- Effects of isomerism(side-branching) on the carbon backbone

According to Pereda et al. [40], solvents used in a SFE process can be categorised as high and low T_c solvents. The high T_c solvents include water, ammonia, n-hexane or methanol. These solvents have a high solvating power, but show poorer selectivity among the molecules. The high operation temperatures required (500 to 700 K) furthermore lead to degradation of thermally labile solutes. The low T_c solvents typically include CO_2, (T_c = 304.1 K), ethane (T_c = 305.4 K) and propane (T_c = 369.8 K). These solvents require more moderate operating temperatures but have low solvating power due to higher degree of asymmetry between the solvent and the solute. The low solvating power implies higher pressures for complete miscibility, leading to a trade-off with equipment and maintenance costs; however by careful adjustment of the temperature and pressure, high selectivity for certain fractions of the mixture can be obtained due to this limited, but highly particular solvation. Low T_c solvents are also much easier to separate from the final extract since they are volatile gases at atmospheric conditions, leading to a purer product [19, 23].

The separations technology group at Stellenbosch University has been systematically collecting phase equilibrium data of various hydro-carbon derivatives in low T_c solvents for the purpose of investigating the feasibility of SFE as a viable fractionation technology of complex hydrocarbon-chain matrices. A summary of the measured data is presented in Table 3-1.

Stellenbosch University https://scholar.sun.ac.za

Table 3-1 Data collected for various hydrocarbon molecules (X : solute mass faction; CN : carbon number)

Solvent	Solute	CN	Temperature (K)	Composition (X)	Upper Pressure Limit (bar)	Reference
Ethane	Alkanes	10 -36	310-360	0.02-0.7	218.5	[1,2]
	Branched Alkanes	10	308-348	0.0120-0.662	83	[3]
	Alcohols	10-20	308-356	0.0173-0.648	250.1	[4]
	Branched Alcohols	10	308 -348	0.0120-0.662	152.2	[3]
	Methyl Esters	10-20	312-355	0.018-0.65	171.4	[5]
	Ethyl Esters	10-16	313-358	0.02-0.6	130	[6]
	Carboxylic Acids	10 - 22	308 - 353	0.016 – 0.68	272.8	[7]
Propane	Alkanes	14,32 -60	378- 408	0.015 - 0.566	142.6	[8,9,10]
	Alcohols	10-22	378-408	0.0175-0.600	83.7	[11]
	Carboxylic Acids	8-22	375-412	0.015-0.652	112	[12]
	Ethyl Esters	10-16	378-408	0.0151-0.655	73.6	[6]
CO_2	Alkanes	12-36	313-367	0.028-0.483	291	[13]
	Carboxylic Acids	8-18	308-358	0.595-0.621	272.2	[14]
	1,2,3,4 Octanols	8	308-348	0.017-0.712	180	[15]
	Branched Octanols	8	308-348	0.0162-0.660	160	[16]
	Branched Alkanes	10	308-348	0.0153-0.697	87	[17]
	Branched Alcohols	10	308-348	0.0153-0.697	152	[17]

The selectivity of a solvent for a specific solute can generally be deduced from the difference in phase-transition pressures observed for the different solutes in solution [9, 20]. Appreciable distinction between the saturation-pressure curves for molecules with different functional end-group, carbon-backbone length and side-branching over the entire composition range implies good selectivity amongst the features. This not only allows desired process conditions to be more easily identified, but also for a narrower cut to be obtained, making for a higher quality product and improved process feasibility [25].

3.2 Selectivity for functional group (energetic differences)

In order to isolate the energetic effects of the different homologous series functional groups, Figure 3-1 gives the phase transition pressure vs. solute mass fraction over the entire composition range for selected systems from Table 3-1 for constant solute carbon number of 16 and molecular mass of ± 300 g/mol.

Stellenbosch University https://scholar.sun.ac.za

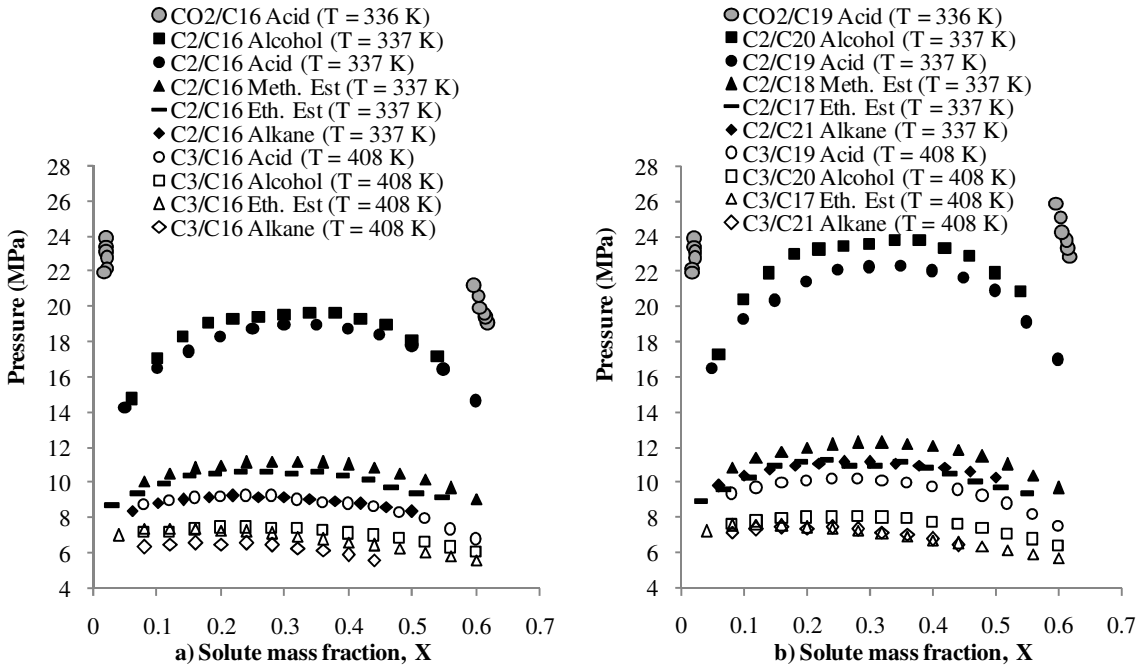

Figure 3-1 a) Pressure vs. solute mass fraction for selected homologous families in super-critical ethane (C2 : filled shapes) [1, 2 , 4-7], propane (C3 : open shapes) [6 , 8-12] and CO_2 (grey circles) [14] at a solvent-reduced temperature of $T_{r,\,solv}$ = 1.103 and for a) solute carbon number of 16 and b) solute molecular mass of $\pm$ 300 g/mol

The higher the pressure required for miscibility, the poorer the solubility and *solvating power* of the solvent. Solubility decreases as the degree of asymmetry between the solvent and the solute increase. Mixtures asymmetries are due to differences in molecular mass (carbon backbone length) of molecules and energetic asymmetries arise due to an uneven charge distribution around a molecule or part of a molecule, caused by electronegativity differences between atoms in a bond. These polar charge separations give rise to intermolecular forces (see Appendix D.3) which greatly influence mixture asymmetry and solubility.

Shielding

An important concept, which helps to explain the interplay between size and energetic asymmetry, is a type of steric-hindrance known as *shielding*. According to this concept, the effect of the polar functional group is most pronounced if it is located at the terminal position of the chained molecule where its interaction with surrounding molecules is more probable and severe. It has been observed, for example, by Fourie et al. [15] that in mixtures of 1, 2, 3 and 4-Octanols in CO_2, the solubility isgreatly increased as the location of the OH functional on the backbone moves inward towards the centre of the molecule, away from the terminal

Stellenbosch University https://scholar.sun.ac.za

position on the backbone. The improved solubility implies a reduction in polar effects upon shifting the functional group inward, since the mass and chain-length remain the same.

This idea can also be used to explain the higher phase transition pressures of the linear acid and 1-alcohol systems compared to the n-alkanes and esters, as seen in Figure 3-1:The carboxyl (COOH) and hydroxyl (OH) functional group of the acids and alcohols are located on the terminal position of the carbon backbone, which gives them a larger contribution to asymmetry and non-ideality of the mixture than the carbonyl group of the esters, which is shielded by methyl groups and not located on the terminal position of the backbone. Shielding also explains the slightly higher pressures of the methyl esters relative to the ethyl esters (as observed for the ethane systems in Figure 3-1) despite their lower molecular mass: The carbonyl group of the ethyl esters is farther from the terminal position than that of the methyl ester and thusmore shielded, leading to less energetic asymmetries and slightly improved solubility for the ethyl ester.

Figure 3-1 a) lumps the effect of both the mass and polarity of the functional groups for a specific backbone-length, whereas Figure 3-1 b) isolates only the energetic effects by plotting pressures for the same solute mass. Figure 3-1 b) (same molecular mass) shows a greater distinction (selectivity) between the polar (alcohol and acid) and the non-polar (alkane and ester) solutes than Figure 3-1 a) (same carbon number), which in turn shows a greater distinction *within* the non-polar solutes, since they have different molecular masses for the same carbon backbone length, but very little energetic differences at the same molecular mass. Despite these subtle differences, the following general trend can be observed for the pressure curves of the propane systems [10]:

Acid > Alcohol > Methyl Ester > Ethyl Ester > Alkane

The ethane/1-alcohol systems in Figure 3-1 show weaker solubility (higher saturation pressure) than the ethane/acid system, which contradicts the above trend. As mentioned in Section 2.2.4., Peters [47] observed that the ethane/1-alcohol series does not exhibit a tri-critical point, but that liquid de-mixing occurs for the whole series. This was attributed to a greater mixture asymmetry for the ethane/1-alcohols due to aggregation into more than two molecules whereas the acids form at most dimers.

For the CO_2/hexadecanoic acid system, a large miscibility gap is observed in the critical region due to the low solubility of the acids in CO_2. Pressures exceeding 30 MPa are typically required for complete miscibility of solutes larger than dodecanoic acid [16]. Nieuwoudt et al. [13] further report a similar miscibility gap for the CO_2/n-alkane family at solute carbon numbers above 20. Good selectivity is desirable, but as noted by these extreme pressures

Stellenbosch University https://scholar.sun.ac.za

required for complete miscibility, a trade-off exists between the selectivity and the solubility (solvating power) of a solvent and between the technical and financial feasibility of the process.

Phase curve profiles (composition dependence)

As noted by Fourie et al. [15] for the 1, 2, 3, 4-octanol systems in CO_2, the polar 1-octanol with its OH group on the terminal position of the backbone not only required higher pressures for miscibility, but showed a much more concave (less flat) envelope shape than when the OH group was located closer to the centre of the molecule and thus more shielded. This implies a greater dependence on the bulk composition of the mixture and a greater range of solubility for more polar systems.

From Figure 3-1 it is also seen that the shape of the phase envelope of the alcohols and acids are more concave, with flatter profiles observed for the esters and the n-alkane series. Following this trend, the propane systems all have lower phase transition pressure (greater solubility) and flatter phase envelopes than the ethane and CO_2 systems due to the smaller degree of asymmetry between the solute and the solvent for the propane systems. Accounting for the different composition dependencies of the different intermolecular interactions poses a considerable challenge to the development of mixing rules which seek to describe both size and polar effects accurately and consistently.

3.3 Selectivity for carbon backbone length (size and mass differences)

Figure 3-2 shows the phase transition pressure vs. carbon number for the homologous series from Figure 3-1 in solution with the three solvents at a reduced temperature of $T_r = 1.103$, corresponding to 337, 408 and 336 K for the ethane, propane and CO_2 systems respectively. A linear relationship is observed for the phase transition pressure with increasing carbon backbone for all of the systems depicted. The lines for the ethane and propane systems in Figure 3-2 are plotted at a solute mass fraction of X = 0.3, and thus approaches the pressure required for complete miscibility (see Figure 3-1), fixing the upper pressure limit for extracting the particular component. The pressure vs. carbon number line for the CO_2/acid system in Figure 3-1 is, however, plotted at a composition of X = 0.595 due to the mentioned miscibility gap in the critical region.

These linear relationships are not only useful for developing correlations for interpolating between systems, but also imply that at a certain temperature and composition, the larger molecules within a homologous series will be less soluble than the lower molecular mass solutes which can therefore be selectively fractionated [9]. The steeper the gradient of these

Stellenbosch University https://scholar.sun.ac.za

lines the greater the selectivity of the solvent for the carbon backbone length of the particular solute series.

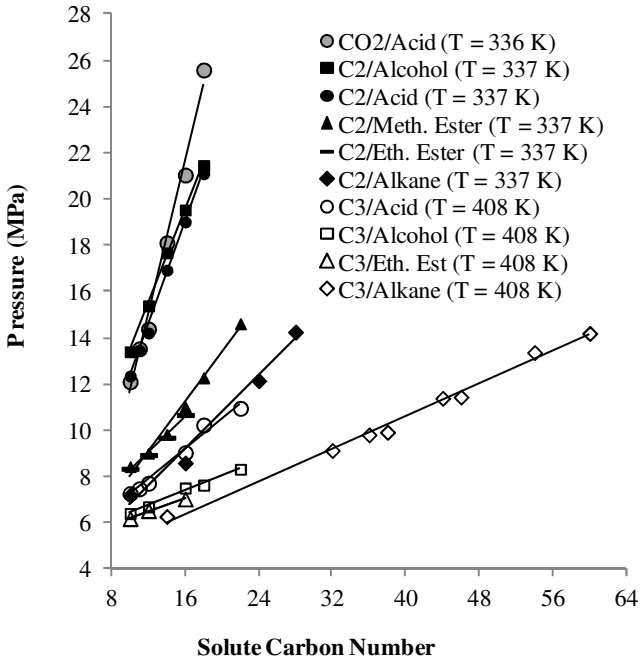

Figure 3-2: Pressure vs. carbon number plot for selected homologous series in supercritical ethane (C2 : filled shapes) [1, 2, 4-7], propane (C3 : open shapes) [6, 8-12] and CO_2 (grey circles) [14] at a solvent-reduced temperature of $T_{r,\,solv}$ = 1.103. Ethane and propane systems are at solute mass fraction of X = 0.3 (critical region), while CO_2/acid systems are at X = 0.595 (liquid region)

It is observed that the polar systems (alcohols and acids) not only exhibit higher pressures overall, but also much steeper gradients in these lines. Similarly CO_2 and ethane systems have steeper gradients than propane, due to the increased mixture asymmetry. This again implies improved selectivity for carbon-backbone length, but the pressure requirements quickly become substantial when using the lighter solvents.

Group additivity

These linear trends also imply that the addition of a -CH_2- group to the carbon backbone of these long-chain solutes leads to a fixed pressure increase at the same temperature and composition. This gives credence to a fundamental assumption in a popular modelling technique, namely the group contribution methods. This assumption of *group additivity* states that functional groups have a fixed effect on system conditions, irrespective of the existing chain-length to which it is added. This assumption loses accuracy for short, polar molecules

Stellenbosch University https://scholar.sun.ac.za

where the proximity of the added group to polar functional groups also influences the phase behaviour due to steric hindrance and shielding effects, leading to a non-linear relationship with pressure. Non-linear, increasing gradients of pressure vs. carbon number have, for example, been observed for the CO_2/acids at lower mass fractions and temperature [71].

3.4 Selectivity for the side-branching

Zamudio et al. [3, 17] compared the effects of structural isomers on nC10 n-alkanes and alcohols in supercritical ethane and CO_2, in order to see whether these solvents could distinguish between the various side-branching effects. It was found that the various isomers of n-decane do not show a significant change in phase transition pressure, unlike the case for alcohols where changing the shape of the carbon backbone causes a significant change: Improved solubility was generally observed with the presence of the methyl side branches [3, 17] which was attributed to the manner in which the added methyl groups shield the polar OH group of the alcohol.

Although this shielding phenomenon has not been modelled in detail, trends suggest that the phase transition pressure is reduced with the closeness of the methyl group to the OH group. It was reasoned that alkanes are not greatly affected by side branching due to their lack of polar functional groups and the relatively small impact of the size and mass increase of an additional methyl group, as also seen in Figure 3-1 for the methyl and ethyl esters. These results were observed for both CO_2 and ethane as solvent.

Fourie et al. [16] also studied the effect of side-branching and the position of the functional end-group of 1-octanol in CO_2, and observed that improved solubility was observed as the hydroxyl group is moved towards the middle of the carbon backbone and as the methyl side branches move closer to the functional group and the functional group becomes more shielded.

3.5 Influence of temperature

Solubility generally decreases with an increase in temperature, due to accompanied decrease in solvent density. As shown in Section 2.2 different types of phase behaviour may further be encountered in certain temperature ranges for different systems, due to the influence of size asymmetry and polarity on the interactions in a mixture. Figure 3-3 gives the phase curves for the n-alkane, methyl esters, 1-alcohols, and carboxylic acids of carbon number 16 in ethane, at various temperatures.

Stellenbosch University https://scholar.sun.ac.za

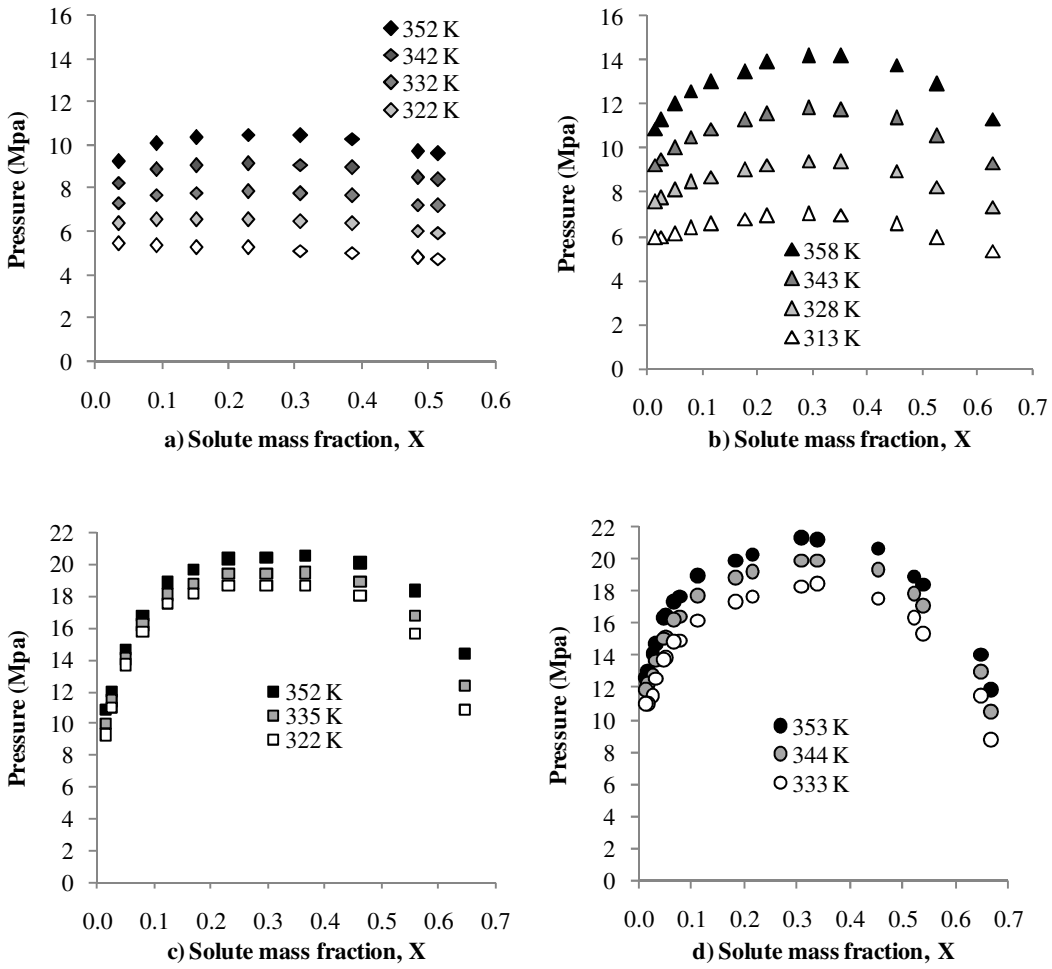

Figure 3-3 Pressure vs. X profiles at selected isotherms for ethane with solute carbon number 16 from the a) n-alkane [1, 2], b) methyl esters [5], c) alcohols [4] and d) carboxylic acid [7] homologous series

The phase transition pressure increases (solubility decrease) with increase temperature for all systems. It can also be seen that the shape of the phase curve becomes more concave (less flat) with increasing temperature, especially for the non-polar n-alkanes and methyl esters in Figure 3-3 a) and b). Figure 3-4 shows the same plots for the n-alkanes, 1-alcohols and carboxylic acids of carbon number 16 in propane:

Stellenbosch University https://scholar.sun.ac.za

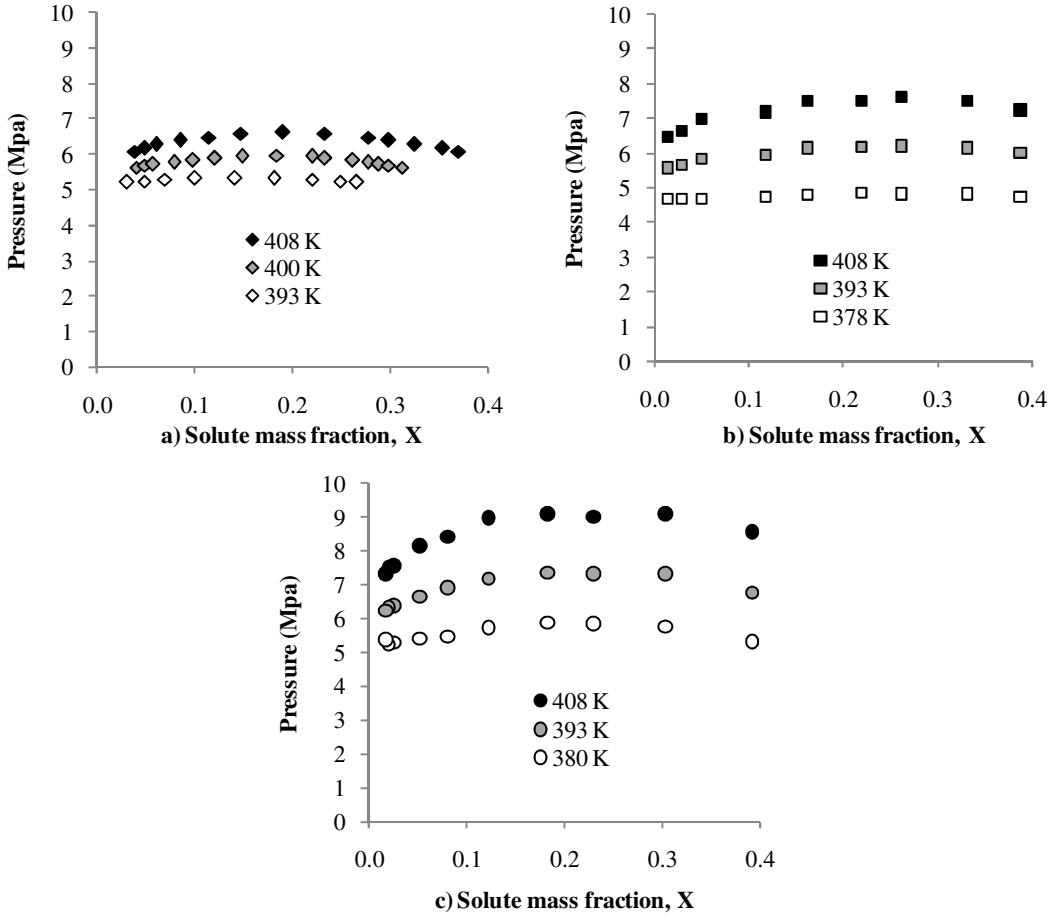

Figure 3-4 Pressure vs. X profiles at selected isotherms for propane with solute carbon number 16 from the a) n-alkane [8, 9, 10], b) alcohols [11] and c) carboxylic acid [12] homologous series

It is again noted that the pressures increase with temperature for all systems. The phase curves are also considerably flatter than for the ethane systems, but become slightly more concave with increasing temperature. Figure 3-5 gives the pressure vs. temperature diagram for various systems from Table 3-1 for solute carbon number of 16. Linear trends for equilibrium pressure vs. temperature are observed for these systems. It is also worth noting that the different gradients in these lines imply that different selectivity for certain solutes may be obtained at different temperatures. In comparing the n-alkane and 1-alcohols in ethane, for example, it is seen that the pressure vs. temperature gradient for the ethane/hexadecane system is steeper than that of the ethane/hexadecanol system, leading to a decrease in the solubility difference between the systems with increasing temperature. It is therefore expected that selectivity between these solutes in ethane decreases with increasing temperature, as was observed in a pilot plant study by Schwarz et al. [22]

Stellenbosch University https://scholar.sun.ac.za

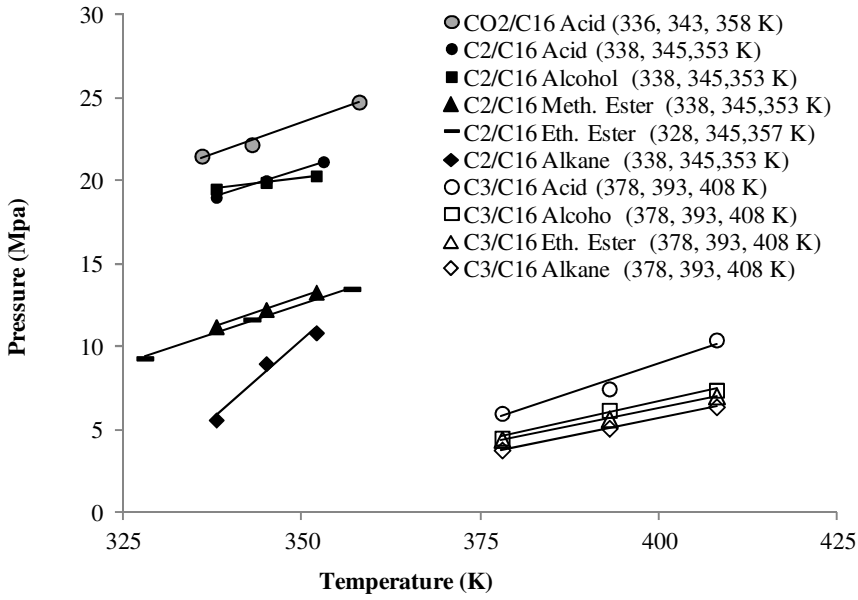

Figure 3-5 Pressure vs temperature lines for selected homologous series in supercritical ethane (C2) [1, 2, 4-7], propane (C3) [8, 10-12] and CO_2 [14] at solute carbon number of 16. Ethane and propane systems are at solute mass fraction of X = 0.3 (critical region), while CO_2/acid systems are at X = 0.595 (Liquid region)

These linear trends of pressure vs. temperature are common for systems with ethane and propane as solvent, but many CO_2 systems give a non-linear relationship. This can lead to aregion of temperature inversion, where solubility increases with temperature (lower pressures at higher temperature). This behaviour has been observed for the CO_2/1-alcohols with solute carbon number greater than 8 [15, 17, 21, 72, 73] as well as the CO_2/hexatriacontane system. However, it was not observed for CO_2/carboxylic acid systems of carbon numbers 8 – 18 in the 308 – 353 K range [14]. These inversions are presumably due to polar effects at low temperatures, which diminish with increasing temperature, counteracting the decreasing density of the solvent and causing better solubility than at lower temperatures.

As a final comparison of the influence of temperature on these systems, Figure 3-6 gives the pressure vs. carbon number for the n-alkanes, methyl esters and carboxylic acids in ethane and propane at three different temperatures. The general trend is that the gradients of the pressure vs. carbon number increase for increasing temperature, with the exception of the ethane/1-alcohol series: For increasing carbon number the difference between the pressures for different temperatures becomes smaller, with similar pressures observed at all three temperatures for the ethane/1-docosanol system. This suggests that at carbon numbers greater than 20, the pressure vs. carbon number lines may cross and those at low temperature could fall above those at high temperature, leading to a temperature inversion [4]. This behaviour

Stellenbosch University https://scholar.sun.ac.za

could also perhaps be linked to the aggregation of 1-alcohols into more than two molecules, which is less prevalent at higher temperatures and carbon numbers, leading to improved solubility (lower pressures) at these conditions, counter to what would be expected from the decreasing density of the solvent with temperature.

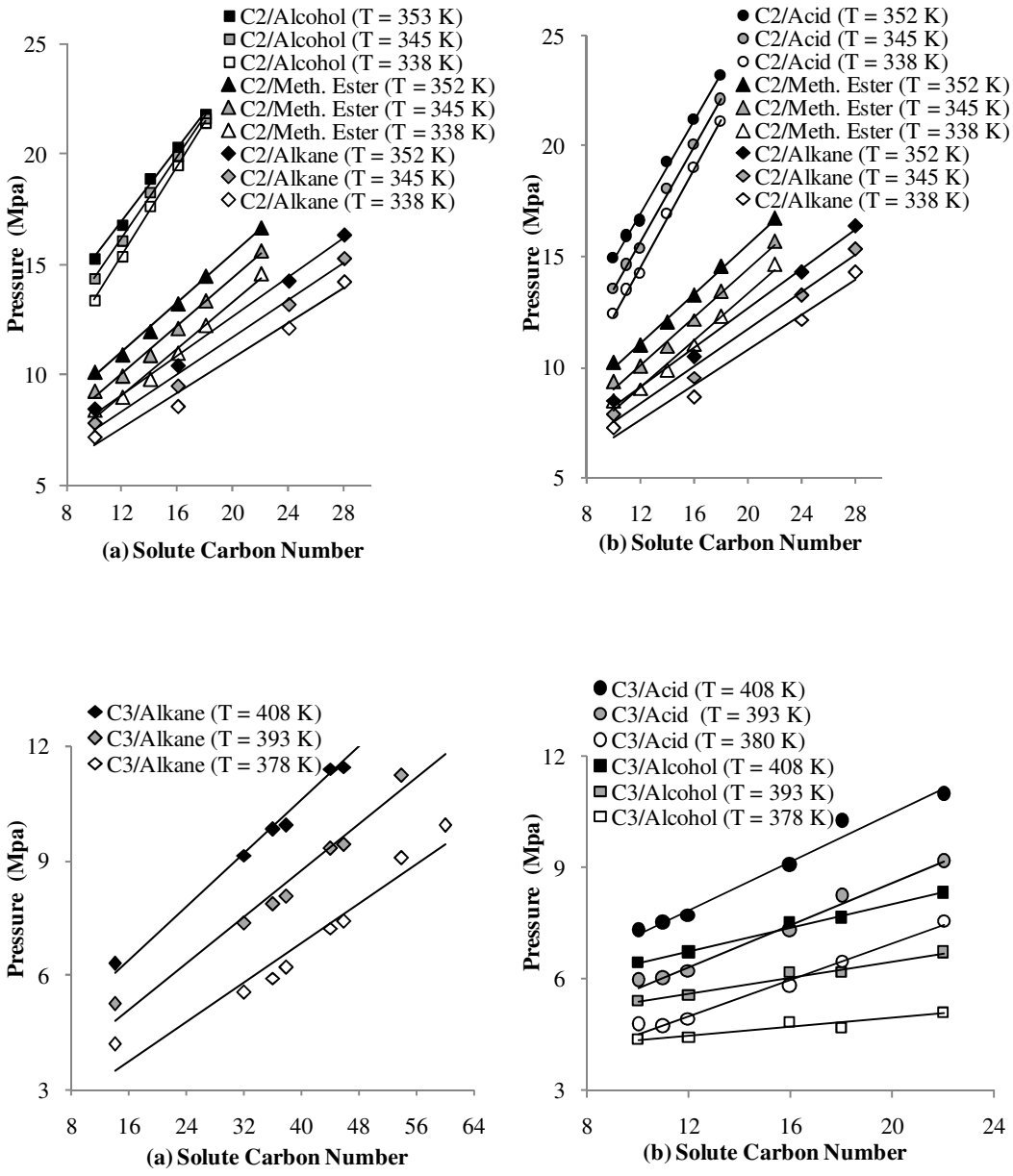

Figure 3-6 Pressure vs. solute carbon number for ethane (above) with n-alkanes [1,2] and methyl esters [5] plotted with a) alcohols [4] and b) carboxylic acids [7]; as well as propane (below) with a) n-alkanes [8, 9, 10] and b) 1-alcohols [11] and carboxylic acids [12]. Ethane and propane systems are at solute mass fraction of X = 0.3 (critical region)

As explained in Appendix D.3, dispersion forces are furthermore not directly related to temperature, however polar forces are inversely proportional to temperature. Explicitly

Stellenbosch University https://scholar.sun.ac.za

accounting for these effects is thus necessary for rigorous modelling of the various systems encountered in industry.

3.6 Solvent and solute selection for modelling

CO_2 is currently the most widely used supercritical solvent, which can be attributed to the following reasons:

- CO_2 is cheap, inert and widely available
- Has a relatively low critical temperature making for low processing temperatures
- Has a virtually negligible solvent residue after separation of the two final phases
- Has high selectivity for different features of hydro-carbon molecules
- Has a higher density than ethane, making for smaller column diameter
- Ethane and propane are more expensive and flammable

Despite these advantages a major drawback in the application of CO_2 as solvent is the extreme equilibrium pressures required for complete solubility of the organic product, as depicted in Figure 2-1and Figure 3-1. Crause et al. [19] further note the higher density of the CO_2 as solvent results in a smaller density difference between the solute and solvent phases in the extraction column, which may lead to premature flooding.

CO_2 is considered a non-polar molecule, however it is known to have a quadrupole moment (see Appendix D.3) which may contribute to non-ideality and asymmetry in solution with hydrocarbons, leading not only to higher phase transition pressures relative to hydrocarbon solvents, but also other complexities in phase behaviour such as the mentioned pressure-temperature inversions (pressure decreases with increasing temperature) and solvent-solute density inversions (CO_2 rich phase has higher density than the alkane phase at a certain pressure and composition) [13]. As discussed in Section 2.2.4, 3-phase regions within the operating range are also observed for many CO_2 systems, including the n-alkane and 1-alcohol series and are typically to be avoided during a SFE process [11].

In a pilot plant study of the feasibility of separating n-alkanes and alcohols using supercritical CO_2 and ethane, Bonthys et al. [21] found that pressure and temperature were the most important process parameters in determining a realistic operating range based on the overhead-to-feed ratio of the desired n-alkane product. It was further found that ethane offered much greater temperature control than CO_2 due to a wider available range (327.15 – 361.15 K for ethane vs. 310.15 – 317.15 K for CO_2) over the feasible overheads-to-feed ratio (0.1 – 0.9). Greater control in pressure was also demonstrated for ethane [22].

Stellenbosch University https://scholar.sun.ac.za

Despite the benefits of using CO_2, it is clear that ethane and propane demonstrate acceptable selectivity, improved solubility, greater controllability and simpler phase behaviour for the hydrocarbon solutes considered for this study. They also have great potential as co-solvents with CO_2. This study will therefore focus exclusively on binary mixtures with ethane and propane as solvent. Once these simpler systems have been modelled successfully, the methodology can be expanded to include CO_2 systems, which pose a greater challenge to thermodynamic models due to subtleties caused by its quadrapole moment.

The solutes to be modelled include the n-alkanes, 1-alcohols, methyl esters and carboxylic acids in ethane [1, 2, 4, 5, 7] and the n-alkanes, 1-alcohols and carboxylic acids in propane [8-10, 11, 12]. As seen in Table 3-1, these solutes in ethane and propane span the following operating conditions, over an extensive composition range (typically 0.015 – 0.7 solute mass fraction):

T : 313 – 408 K
P : 5 – 28 MPa

No three-phase regions have been reported for these systems within these operating conditions. The systems are chosen to cover a substantial range of both polar and non-polar solutes in two light-weight, non-polar, organic solvents. All data used for this study has been measured at Stellenbosch University and is included in Table 3-1.The carbon number range and temperatures modelled in this study for each solvent/series combination is given per chapter.

3.7 Conclusions

This chapter addresses project objective 2 (see Section 1.3) by determining how structural features of the solute such as functional end-group, carbon backbone and side-branching, as well as temperature influence the phase behaviour, solvent selection and feasibility for a SFE process. The following outcomes can be summarized from this chapter:

- Despite weaker *solvating power* (higher operating pressures required), low T_c solvents such as CO_2, ethane and propane are preferred for SFE applications due to better selectivity, lower operating temperatures and less solvent residue than high T_c solvents, including water, ammonia, n-hexane or methanol.
- The *solvating power* of a particular solvent is related to the phase transition pressure of a particular solute in the solvent: The higher the pressure required for complete phase miscibility, the poorer the solubility and the weaker the solvating power.

Stellenbosch University https://scholar.sun.ac.za

- Appreciable distinction between the phase transition pressures of various solutes in a solution shows a good selectivity between the molecules.
- The solute structure, specifically the functional end-group, carbon backbone length and isomerism (side-branching), as well as temperature, significantly influence the observed phase behaviour in different solvents.
- The following trend is observed for the phase transition pressures of different homologous series in propane at the same molecular mass:
  Acid > Alcohol > Ethyl Ester > Methyl Ester > Alkane
- Unlike the above trend with propane, the alcohols show poorer solubility than the acids in ethane due to the aggregation of the alcohols into more than two molecules which, according to Peters [47], does not occur for 1-alcohols in propane.
- The acids and alcohols show poorer solubility than the n-alkanes, methyl and ethyl ester of equal mass in ethane and propane due to the polar functional group and its position on the terminal end-point of the carbon backbone.
- The esters show similar solubility to the n-alkanes, because their polar carbonyl groups are *shielded* through steric hindrance by the methyl groups at the terminal end-point of the hydrocarbon backbone.
- Solvent selectivity for isomerism is therefore much more significant for molecules with a polar functional group at the terminal end-point than if polar groups are shielded by surrounding methyl groups.
- Propane shows greater solvating power of the mentioned organic hydrocarbonsthan bothethane and CO_2, however, haspoorer selectivity for the various solutes. This highlights a trade-off between selectivity and solubility, which is related to operating pressures and costs.
- Increasing linear trends of pressure vs. solute carbon number were observed for the n-alkanes, methyl and ethyl esters ,1-alcohols, and acids (solute mass fraction of 0.3) in ethane and propane, as well as the acids (solute mass fraction of 0.595) in CO_2, at a solvent reduced temperature if $T_r = 1.103$.
- Steeper gradients in these lines were observed for ethane and CO_2 as solvents than for propane, implying a greater selectivity for carbon backbone length using the lighter solvents.
- Increasing linear trends of pressure vs. temperature were also observed for all these systems, however the CO_2/alcohol and CO_2/n-alkane series are known to have systems exhibiting non-linear trends in these lines, leading to a region of temperature inversion (pressure decreases with temperature) at lower temperatures.
- The mentioned pressure vs. carbon number lines get steeper with increasing temperature, except for the ethane/1-alcohols, where a temperature inversion may occur at solute carbon number of 20.

Stellenbosch University https://scholar.sun.ac.za

- A more concave shape in the phase curve was observed for more polar solutes (acids and alcohols) and at higher temperatures.
- The solutes considered for this study are the n-alkanes, 1-acohols, carboxylic acids and methyl esters for carbon numbers greater than 10.
- The solvents considered are ethane and propane. CO_2 may be considered for future work if good results are obtained for the simpler phase behaviour of the ethane and propane binaries.
- No three-phase regions were observed for the binary systems selected for this study.
- All data to be modelled has been measured at Stellenbosch University and is included in Table 3-1.

This chapter therefore meets project objective 2 by presenting a thorough investigation into the phase behaviour of systems of importance in SFE applications and making appropriate solute and solvent selections for this study.

Stellenbosch University https://scholar.sun.ac.za

4. EQUATIONS OF STATE FOR APPROACHING THE CRITICAL REGION

This chapter addresses project objective 3 by giving a thorough overview of semi-empirical thermodynamic models for modelling high pressure VLE, especially of asymmetric binary systems approaching the mixture critical point. An appropriate approach is then chosen for modelling the systems selected in the previous chapter.

According to Deiters [29], the total count of published models, if variants are considered, exceeds 2000 (as of 1999). These models have varying theoretical backgrounds and mathematical complexity. This review looks at 6 potential modelling families, classified according to their theoretical background and the type of systems they seek to describe. These categories are:

- The Virial equation of state
- The Cubic/Van der Waals type equations of State
- The polymer-chain molecular models
- The SAFT molecular models
- The group contribution methods
- The crossover approach

Theoretical aspects and selected results from literature are firstly discussed for each model, followed by concluding remarks and model selection for this study. Appendix D.4 gives an overview of the Van der Waals equation of state, which provides useful insights into the cubic equations of state discussed in section 4.2 of this chapter. Section D.5 provides an overview of useful concepts for the discussion on the molecular polymer-chain and SAFT models in Sections 4.3 and 4.4.

4.1 The virial equation of state

This virial equation of state calculates the compressibility factor as an infinite power series in inverse molar volume, expanded as a Maclaurin series around the ideal-gas limit of zero density, where the compressibility factor is equal to 1 [74, 75]:

$$Z = \frac{Pv}{RT} = 1 + \frac{B}{v} + \frac{C}{v^2} + \frac{D}{v^3} + \qquad 4\text{-}1$$

The equation therefore represents the volumetric behaviour of a real fluid as a departure from the ideal gas condition [74]. The expansion may also be performed as a power series in pressure around the zero pressure limit:

Stellenbosch University https://scholar.sun.ac.za

$$Z = \frac{Pv}{RT} = 1 + B'P + C'P^2 + D'P^3 + \ldots \qquad 4\text{-}2$$

The parameters in Equations 4-1 and 4-2, known as virial coefficients, represent the order of interactions amongst molecules. B is called the "second virial coefficient" and represents deviations from ideality due to all two-body interactions. Similarly C is the "third virial coefficient" represents all three body interactions. The molar volume is influenced by intermolecular forces and investigation of the virial coefficients reveals the nature of these forces approaching the ideal gas limit where they become negligible.

The virial expansion has been found to converge very slowly at high densities, requiring evaluation of higher order coefficients [74]. Since very little is known theoretically about three-body interactions (three-body potential functions) and since these regions of poor convergence are at the experimental extremes, research has focused mainly on the evaluation of the second virial coefficients [75]. For spherically symmetric molecules, modern statistical mechanics provides the following exact relationship relating the second virial coefficient to the common pair-potential energy function, Γ(r) [46]:

$$B = 2\pi N_A \int_0^\infty \left(1 - e^{-\frac{\Gamma(r)}{kT}}\right) r^2 dr \qquad 4\text{-}3$$

Performing the integration for realistic potential functions (i.e. Lennard-Jones) is generally done numerically or by series techniques. This provides a valuable source of molecular parameters for substances where B has been measured experimentally (volumetric data of gases) and makes B a very important quantity for investigation of intermolecular forces [46].

The virial coefficients are functions of temperature only for pure species, but also composition for mixtures [75]. In a mixture, the second virial equation is proportional to the number of possible binary interactions, weighted by the amount of species present. Since three types of binary interactions may take place, namely Γ_{ii}, Γ_{jj} and Γ_{ij},each will have a unique coefficient $B_{ii,}$ B_{jj} and $B_{ij,}$. The overall mixture virial coefficient is simply the pure coefficient weighted by the fraction of each species present. This follows similarly for the higher order coefficients, allowing for theoretically sound mixing rules to be developed for the virial equation of state:

$$B_{mix} = \sum_i^n \sum_j^n y_i y_j B_{ij} \qquad 4\text{-}4$$

$$C_{mix} = \sum_i^n \sum_j^n \sum_k^n y_i y_j y_k C_{ij} \qquad 4\text{-}5$$

Stellenbosch University https://scholar.sun.ac.za

These mixing rules are considered theoretically correct mixing rules at the low density limit.

4.1.1 Theoretical low density limit for mixing rules

The sound theoretical basis of the virial equation at low densities has informed many developments of other thermodynamic models seeking to adhere to the theoretical constraints posed by the form of the virial equation [74-76]. An example of this may be seen upon the expansion of the Van der Waals equation [77] in terms of compressibility in powers of (b/v) at zero density:

$$z = \frac{Pv}{RT} = 1 + \sum_{n=0}^{\infty} \left(\frac{b}{v}\right)^n - \frac{a}{vRT} \qquad 4\text{-}6$$

This shows that the first 3 virial coefficients predicted from the Van der Waals [77] equations are given as follows:

$$B = b - \frac{a}{RT} \; ; C = b^2 \; ; D = b^3 \qquad 4\text{-}7$$

From Equation 4-4 it can be seen that the second virial coefficient B has a quadratic composition dependence at the low density limit, which through Equation 4-7, imposes this constraint on the mixing rules developed for a and b, if they are to adhere to true fluid behaviour at these limiting conditions. This result generally applies to all cubic equations [76]. Phase equilibrium calculations are done by calculating the fugacity coefficient for each species in each phase, which contains all the information of how true phase behaviour deviates from ideal behaviour. Calculation of fugacity coefficients of a species in solution for both vapour and liquid phase requires solving the partial derivative of pressure with respect to composition. This integration is taken from a reference state of zero density ($V = \infty$) to the system volume. Even though a correct composition dependence of B from an EOS does not necessary ensure a correct value prediction for B, adherence to the correct composition dependence does eliminate one source of error affecting the accuracy of predicted fugacity coefficients across all densities [76].

4.2 The cubic Van der Waals equations of state

Appendix D.4 discusses the development of the Van der Waals EOS, which provides a good overview for this section since all modern cubic equations of state (CEOS) are derived from its basic structure [77]:

Stellenbosch University https://scholar.sun.ac.za

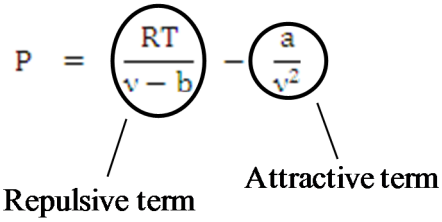

4-8

The constants a and b are substance specific parameters related to the intermolecular forces of attraction and to the molecular size modelled as a hard-sphere, henceforth referred to as the energy and size parameter respectively. The repulsive term is still used in most contemporary cubic models due to its simplicity. Modification of the volume and temperature dependence of the attractive term has lead to countless models that are still the most widely used in the petrochemical industry. The attractive term can be given by the following general expression:

$$P_{attraction} = -\frac{a}{g(V)} \qquad 4\text{-}9$$

The energy parameter, a, is typically deconstructed into a constant scaled to the critical point using Equation 2.8 (see Eection D.4.1) and a temperature dependent *alpha function*, correlated in terms of the acentric factor:

$$a = a_c(T_c, P_c)\alpha(T_r, \omega) \qquad 4\text{-}10$$

Modifications of the volume dependence are done by changing the form of $g(V)$ and the temperature dependence is improved through developing the dimensionless alpha function, $\alpha(T_r)$.

4.2.1 Volume dependence

Table 4-1 contains selected modifications to the volume dependence of the original Van der Waals EOS. The modification of the volume dependence by Redlich and Kwong (RK) [78] improved the critical compressibility, Z_c, of the Van der Waals [77] equation from 0.375 to 0.333. The form proposed by Peng and Robinson (PR) [79] improved this value further to 0.307, but still over-predicts values observed for real fluids, which is in the range of 0.29 – 0.24 for n-alkanes and can reach values as low as 0.22 for polar molecules. Given that the 2 model parameters are fitted to T_c and P_c , this error comes from a failure in representing the critical volume, which was explained in Section 2.1.2 by the critical exponent of the co-

Stellenbosch University https://scholar.sun.ac.za

existence densities, which gives a flatter profile than for classic fluids, more in-line with a 5th than 3rd order function [35].

Table 4-1 Volume dependence of attractive term for CEOS

Reference	g(V)	# of Parameters
Redlich and Kwong (1949) [78]	$\frac{a}{V(V+b)}$	2
Peng-Ronbinson (1976) [79]	$\frac{a}{V(V+b)+b(V-b)}$	2
Fuller (1976) [80]	$\frac{a}{V(V+cb)}$	3
Schmidt-Wenzel (1980) [81]	$\frac{a}{V^2+ubV+wb^2}$	3
Hermans and Knapp (1980)[82]	$\frac{a}{V^2+Vcb-(c-1)b^2}$	3
Patel-Teja (1982) [83]	$\frac{a}{V(V+b)+c(V-b)}$	3
Adachi et al. (1983) [84]	$\frac{a}{(V-b_2)(V+b_3)}$	4
Trebble and Bishnoi (1987) [85]	$\frac{a}{V^2+V(b+c)-(bc-d)}$	4

Any 2 parameter EOS gives a constant value for Z_c, and universal PVT behaviour for all fluids with the same T_c and P_c [86]. This is not in-line with real fluid behaviour, which is characterized by more than critical properties and where Z_c decreases with increasing molecular mass. If a third parameter is included in the volume dependence, the following equation can be utilised for the critical compressibility [46]:

$$Z_c = \frac{P_c v_c}{RT_c} \qquad 4\text{-}11$$

This allows for including the critical compressibility as an additional model parameter, leading to improved correlation of the critical volume. Wenzel et al. [81] has shown that fitting Z_c to experimental values leads to unacceptable errors in the volume for the low pressure region. Mollerup and Michelsen [66] has also shown that fitting Z_c is done at the expense of the correct critical fugacity, which would affect equilibrium properties, especially when an activity coefficient model is used for the liquid phase and K values are not determined from fugacity ratios. Trebble and Bishnoi [85] note that a 4th parameter allows for optimizing the "hardness" b_c, (slope in $\left(\frac{\partial P}{\partial V}\right)_T$) in addition to the critical compressibility. However, this is not widely used, presumably because of the added complexity in fitting parameters and extension to mixtures for only marginal improvement in model performance.

Stellenbosch University https://scholar.sun.ac.za

The attractive terms in Table 4-1 have varying degrees of success for saturation and PVT properties.

4.2.2 Volume translation

Peneloux et al. [87] improved the liquid volume correlations of a CEOS not by adjusting the critical volume through a third pure parameter, but by introducing a consistent volume correction, without altering the VLE conditions:

$$\nu_i^{\text{translated}} = \nu_i^{\text{original}} - c_i \qquad 4\text{-}12$$

c_i is the translation parameter. Although Peneloux developed his volume correction for the SRK equation, the cubic form allows this approach to be generalized. Volume corrections have also been developed for other cubic equations of state such as the Peng Robinson equation, however inaccuracies are still obtained, especially in the supercritical region [87, 88].

4.2.3 Temperature dependence (Alpha function)

Table 4-2 gives various proposed alpha functions for the temperature dependency of a cubic equation of state. In addition to the improved volume dependence, RK added temperature dependence to the attraction term, improving results for many gaseous systems [98]. Soave [89] noted that the acentric factor defines a specific saturation pressure at reduced temperature of 0.7 (see Equation D.43) for each substance. By including α(T)into the Redlich-Kwong EOS and adjusting its value to match this pressure at $T_r = 0.7$, the Soave expression in Table 4-2, designed to equal 1 at T_c, was used to correlate m for acentric factors up 0.5, which corresponds to an n-alkane of carbon number 10. This vastly improved the representation of vapour pressures for non-polar or weakly polar systems in the $0.6 < T_r < 0.9$ range. Poor results were obtained for polar systems due to the use a of single energy parameter for all intermolecular forces and the inadequacy of the acentric factor to distinguish between polar molecules. In order to improve vapour pressure representation for polar systems, additional parameters and terms are typically included in the alpha function, such as those proposed by Mathias [92], Mathias and Copeman [93] and Styjek-Vera [94] for modifying the Soave alpha function.

Stellenbosch University https://scholar.sun.ac.za

Table 4-2 Temperature dependency (alpha function) of attractive term for CEOS

Reference	$\alpha(T_r)$ (Alpha function)	# of Parameters
Redlich and Kwong (1949) [78]	$\alpha = \frac{1}{\sqrt{T}}$	0
Soave (1972)[89]	$\alpha(T_r) = \left(1 + m\left(1 - \sqrt{T_r}\right)\right)^2$	1 (m)
Heyen (1980) [90]	$\alpha(T_r) = \exp\left(k_1\left(1 - T_r^n\right)\right)$	2 (k_1 , n)
Boston-Mathias (1980) [91]	For $T > T_c$: $\alpha(T_r) = \left(\exp\left(c_i\left[1 - T_r^d\right]\right)\right)^2$ $c = 1 + \frac{m}{2} + 0.3p$ $d = \frac{c-1}{c}$	2 (m , p)
Mathias (1983)[92]	$\propto_i (T_r) = \left[1 + m\left(1 - \sqrt{T_{ri}}\right) - p(1 - T_{ri})(0.7 - T_{ri})\right]^2$	2 (m , p)
Mathias and Copeman (1983)[93]	$\alpha(T_r) = \left(1 + k_1\left(1 - \sqrt{T_r}\right) + k_2\left(1 - \sqrt{T_r}\right)^2 + k_3\left(1 - \sqrt{T_r}\right)^3\right)^2$	3 (k_1 , k_2 , k_3)
Stryjek-Vera (1986) [94]	$\alpha(T_r) = \left(1 + m\left(1 - \sqrt{T_r}\right)\right)^2$ $m = k_o + k_1(1 + \sqrt{T_r})(0.7 - T_r)$	2 (k_o , k_1)
Trebble and Bishnoi (1987) [85]	$\alpha(T_r) = \exp\left(q_1\left(1 - T_r\right)\right)$	1 (q_1)
Melhem et al. (1989)[95]	$\alpha(T_r) = \exp\left(M_1(1 - T_r)\right) + M_2\left(1 - \sqrt{T_r}\right)^2$	2 (M_1, M_2)
Twu et al.(1991)[96]	$\alpha(T_r) = T_r^{N(M-1)} \exp^{L\left(1 - T_r^{NM}\right)}$	3 (L,M,N)
Gasem et al.(2001)[97]	$\alpha(T_r) = \exp\left(G_1 + G_2 T_r\left[1 - T_r^{G_3}\right]\right)$	3 (G_1, G_2, G_3)

According to Twu et al. [96], a realistic alpha function must meet the following requirements:

1) It must be finite and positive for all temperatures.
2) It must be 1 at the critical point.
3) It must approach a finite value as the temperature approaches infinity

All of the alpha functions based on the Soave form go through a minimum of zero and then rise again with increasing temperature, which is not in-line with attractive forces, which diminish with temperature. This behaviour can often be avoided with use of an exponential alpha function, such as that of Melhem [95], Heyen [90] or Twu et al. [96]. The alpha function of Boston and Mathias [91] also provides a more realistic extrapolation to

Stellenbosch University https://scholar.sun.ac.za

temperatures above T_c. Many of the parameters in Table 4-2 can be reliably correlated in terms of the acentric factor while others (2nd and 3rd parameters) are purely empirical.

4.2.4 Mixing rules

The primary method for extending CEOSs to mixtures is through the use of *one-fluid* mixing rules [38]. This assumes that the fluid behaviour of a mixture of fixed composition can be described as an equivalent pure substance within the model framework with appropriate pure parameters. The parameters for a mixture are then obtained by varying the pure parameter values with composition, but still adhering to the pure-component limit. The classic quadratic mixing rules of Van der Waals are the most popular one-fluid mixing rules [77]:

$$a = \sum_i \sum_j x_i x_j \sqrt{a_i a_j}\left(1 - k_{aij}\right) \qquad 4\text{-}13$$

$$b = \sum_i \sum_j x_i x_j \frac{b_i + b_j}{2} \left(1 - k_{bij}\right) \qquad 4\text{-}14$$

The classic *combining rules* for the interaction terms, a_{ij} and b_{ij}, are the geometric and arithmetic mean in the energy and size parameter, respectively, and are independent of composition. Binary interaction parameters (BIPs), k_{aij} and $k_{bij,}$ are often incorporated into the combining rules to correlate the data by minimizing an objective function of the difference between model and experimental values. For highly non-ideal systems, additional terms and composition dependency have been incorporated into the combining rules for the energy parameter of the Van der Waals mixing rules. ‘
Table 4-3 gives three such modifications.The size parameter is typically obtained using the following linear mixing rule:

$$b = \sum_i \; x_i b_i \qquad 4\text{-}15$$

Each of the mixing rules in
Table 4-3 have shown improved accuracy in fitting systems of substantial size difference and polarity. Aside from not meeting the low density limit of quadratic composition dependence imposed by the second virial coefficient, higher order terms in composition and multiple BIPs may lead to other deficiencies.

When a component is divided into identical subcomponents, one would expect the mixture parameter to remain invariant to such a transformation, however this is not the case for the

Stellenbosch University https://scholar.sun.ac.za

Panagiotopoulos and Reid [99] or Schwartzenruber and Renon [100] mixing rules, which is a deficiency known as the "Michelsen-Kirtenmacher syndrome".

Table 4-3 Modified Van der Waals mixing rules

Reference	Mixing Rule
Panagiotopoulos and Reid (1985) [99]	$a = \sum_i \sum_j x_i x_j (a_i a_j)^{0.5} [1 - k_{aij} + (k_{aij} - k_{aji}) x_i]$
Schwartzenruber and Renon (1986) [100]	$a = \sum_i \sum_j x_i x_j (a_i a_j)^{0.5} [1 - k_{aij} - l_{a,ij}(x_i - x_j)]$
Mathias et al (1991)[101]	$a = a_0 + a_1$ $a_0 = \sum_i \sum_j x_i x_j (a_i a_j)^{0.5} (1 - k_{a,ij})$ $a_1 = \sum_{i=1}^{n} x_i \left(\sum_{j=1}^{n} x_j \left((a_i a_j)^{\frac{1}{2}} l_{a,ij} \right)^{\frac{1}{3}} \right)^3$

As with $l_{a,ij}$ in the Schwartzenruber and Renon mixing rule [100], the effect of a parameter which is the product of three mole fractions will become smaller for increasing number of components. This is known as the Dilution effect [102]. The mixing rule of Mathias et al. [101] was deliberately developed to avoid these problems. The papers of Schwartzenruber and Renon [103] and Zabaloy and Vera [104] are recommended for further information on these mixing rule deficiencies and how to avoid them.

4.2.5 Binary interaction parameters

Coutinho et al. [105] found that with use of appropriate combining rules, binary interaction parameters could be reliably correlated for the CO_2/hydrocarbons using both 1 and 2

Stellenbosch University https://scholar.sun.ac.za

BIPs.The authors warn against *inter-correlation* of parameters when 2 are simultaneously regressed. They further identified a definitive temperature dependence for k_{aij}, whereby its value decreases with temperature, reaching a minimum at $T_r = 0.55$ for each member of the methane/n-alkane series,. This minimum gradually moves to $T_r = 0.6$ for the nC30 solute [106]. This behaviour was linked to the theory of non-central forces between non-spherical molecules [105]. All correlations required only T_c , P_c and ω.

Stryjek developed a temperature dependent correlation for $k_{a,ij}$ of the SRK EOS, for the n-alkanes [107]. Gao [108] developed a correlation for $k_{a,ij}$ in the PR EOS for various light hydrocarbons in terms of T_c and Z_c, which is often not available. Kordas et al. [109] correlated $k_{a,ij}$ in terms of ω for the heavy component of the methane/n-alkanes series up to nC40 using a modified translated PR EOS. Different expressions were required below and above solute carbon number of 20. Kordas et al. [110] also correlated $k_{a,ij}$ in terms of T_r and $\omega$for CO_2/hydrocarbon binaries up to nC44 using their translated PR EOS with accuracies below %5 in the bubble point pressure. Nishiumi et al. [111] correlated $k_{a,ij}$ for the PR EOS for a large range of hydrocarbons,CO_2, N_2 and H_2S in terms of critical molar volume and acentric factor. $k_{a,ij}$ has also been determined in terms of groups using the promising predictive PR EOS by Jaubert et al. [112], which is discussed in Section 4.5.1.

Although these correlations vary in range, most are purely empirical and unsuitable for extrapolation. They also often require input information which is difficult to come by and many lack the correct temperature dependence. They are also almost exclusively for non-polar molecules. Many authors note that for more polar systems, a BIP in the size parameter is also required, which may lead to inter-correlation of parameters due to the various parameter sets that may satisfy the regression solution [106, 113] Jha et al.[114] were able to establish linear correlations for 2 BIPs in terms of the functional groups of various liquid solute molecules in CO_2, including alcohols from methanol to 1-decanol, using a more theoretically sound expression for the co-volume combining rule as developed by Kwak and Mansoori [115].

4.2.6 EOS/G_{ex} mixing rules

A promising approach for extending CEOSs to mixtures involves combining the CEOS with anexcess Gibbs energy (G_{ex}) model using the following relation:

$$G_{ex} = RT\,[\ln \varphi - \textstyle\sum_i x_i \ln \varphi_i] \qquad 4\text{-}16$$

Φ and φ_i are the fugacity coefficients of the mixture and pure compound, respectively. By equating an existing G_{ex} model to the right hand side of Equation 4-16 as determined from an

Stellenbosch University https://scholar.sun.ac.za

EOS at some reference pressure, the energy parameter, a, from an EOS can be related to a liquid activity coefficient model and a mixture expression derived. b is typically determined using the linear mixing rule (Equation 4-15)

Reference pressure

These mixing rules can be classified according to the reference pressure chosen for using Equation 4-16, which is crucial to subsequent assumptions in developing and applying the mixing rules. Kontogeorgis et al. [116] and Sacomani et al. [117] obtained an expression for the liquid activity coefficient (derivative of G_{ex} with component mole number) from any EOS/mixing rule combination using the right hand side of Equation 4-16. The resulting expression can be deconstructed into a "combinatorial" free-volume term, representing non-idealities due to size and shape differences, as well as a "residual" term, representing energetic asymmetries (polarity):

$$\ln \gamma_i = \ln \gamma_i^C + \ln \gamma_i^R \qquad 4\text{-}17$$

This deconstruction is also typical of many existing liquid activity models, including UNIQUAC and UNIFAC. At infinite pressure, the excess entropy ($-S_{ex}/R$) in the G_{ex} expression from the EOS is zero, which eliminates the combinatorial term, $\ln \gamma_i^C$ [118]. If an *infinite pressure reference*is used, only the residual term of the chosen external activity coefficient model should therefore be used in the left side of Equation 4-16. If a *zero pressure reference*is used, it is often the case that the combinatorial term originating from the EOS in using the linear mixing rule for b (Equation 4-15), only agrees with activity coefficient models for systems of small size and energetic asymmetries [118], causing errors for systems of large size asymmetry.

Infinite-pressure reference

The first successful matching of an EOS and G_{ex} model was done in 1978 and 1979 by Huron and Vidal [119, 120] who showed that accurate results could be obtained by relating the energy parameter, a, for the RK EOS to any model for G_{ex}. Huron and Vidal used an *infinite pressure reference* ($P = \infty$) for their derivation, where the molar volume of the EOS is assumed to be equal to the co-volume (b parameter) and the excess molar volume is equal to zero, $V_{ex} = 0$. The definition of the excess Gibbs energy ($G_{ex} = A_{ex} + PV_{ex}$) allows for a finite value of G_{ex} at infinite pressure. If Equation 4-16 is then solved for a binary mixture, the following relation can be derived for a:

Stellenbosch University https://scholar.sun.ac.za

$$\frac{a}{b} = \left[\sum_{i=1} x_i \frac{a_i}{b_i} - \frac{G_{ex}^{\infty}}{\ln 2}\right] \qquad 4\text{-}18$$

This can be generalized to other CEOSs than RK:

$$\frac{a}{b} = \left[\sum_{i=1} x_i \frac{a_i}{b_i} - C\, G_{ex}^{\infty}\right] \qquad 4\text{-}19$$

C is a numerical constant characteristic to equation of state and any activity model can be used to determine the excess Gibbs energy at infinite pressure, G_{ex}^{∞} .This methodology allowed for extending the liquid activity coefficient models, which are successful for polar systems at low pressure, to the high-pressure region where EOSs are better suited. Good correlations for VLE, LLE and VLLE for complex binary and multi-component mixtures containing water, alcohols, glycols and other hydrocarbons were obtained using these mixing rules [118].

Zero-pressure reference

A substantial drawback to the infinite reference pressure is that widely published low pressure parameters for G_{ex} models could not be used, since G_{ex} is pressure dependent. The derivation also strictly enforces the linear mixing rule for the co-volume b (Equation 4-15) which can be limiting to the accuracy of correlations. Mollerup [121] and Michelsen [122] abandoned the infinite pressure limit for a more realistic *exact zero reference pressure*, allowing for existing model parameters to be used for the G_{ex} model being applied.

Theoretical limitations in applying the exact-zero reference pressure lead to the development of the *approximate pressure models*, namely the modified Huron-Vidal first order (MHV1) by Michelsen [123], the modified Huron-Vidal second order (MHV2) by Dahl [124] and the PSRK model by Holderbaum and Gmehling [125]. These models provided good predictions for polar mixtures, like acetone and ethanol in water, over a wide temperature range and are often used in a purely predictive manner by incorporating the UNIFAC G_{ex} model. A severe limitation of these models is their poor performance for systems of great size asymmetry, which can be attributed to the increasing difference in the combinatorial terms from the EOS and G_{ex} model for these systems [118].

LCVM (Linear combination of Vidal and Michelsen)

The linear combination of Vidal and Michelsen (LCVM) model by Boukouvalas et al. [124] uses a linear combination of the original Vidal expression [119, 120] and that of Michelsen used in MHV1 [123] for the a parameter. This new mixing rule is used in conjunction with a

Stellenbosch University https://scholar.sun.ac.za

volume translated Peng-Robinson EOS, modified for polar effects by the Mathias-Copeman alpha function [93] and UNIFAC is used to obtain G_{ex}. If one lets $\alpha = \frac{a}{bRT}$, then the linear combination of the two mixing rule expressions for this parameter is given as follows:

$$\alpha = \lambda \cdot \alpha_V + (1 - \lambda) \cdot \alpha_M \qquad 4\text{-}20$$

Where α_V and α_M are the Vidal and Michelsen contributions respectively and λ is a parameter that determines their relative contributions and dependends on the EOS and G_{ex} models used. The authors suggest a value of 0.36 if the original UNIFAC model is used [124]. This combination was proposed primarily due to the observation that the Vidal mixing rules under-predicts and the Michelsen mixing rule over-predicts the bubble point pressure, especially as the size asymmetry of the species in the mixture increases [126]. The model has been criticized for the following reasons [118]:

- The combination of an infinite and zero reference pressure makes it unclear which are the correct UNIFAC parameters to use
- The value of λ is dependent on both EOS and G_{ex} and has no physical justification

Despite these issues, the LCVM has been reliably found to give excellent results for athermal asymmetric systems such as the methane, ethane, CO_2 and nitrogen with large hydrocarbons of different sizes [127, 128], with results for polar systems at high pressure comparable to that of the MHV2 model [118]. This good performance was explained in a phenomenological way by Kontogeorgis et al. [118], who showed that the value of 36 for λ, located the region where the difference between the combinatorial term of the activity coefficient from the EOS and the original UNIFAC model is lowest, leading to good correlation of athermal, size-asymmetric systems.

Wong-Sandler mixing rules

The Wong-Sandler mixing rules are deemed the most theoretically sound of the G_{ex}/EOS mixing rule models [129]. The model uses an *infinite pressure reference* to match the G_{ex} model and has been developed to give the quadratic composition dependence at the low density limit, which none of the other EOS/G_{ex} models do. This was achieved byincorporating the Helmholtz excess energy (A_{ex}) into the mixing rules, which unlike G_{ex}, is independent of pressure. The derivation starts with the Virial equation for gases:

$$z = \frac{Pv}{RT} = 1 + \frac{B}{v} + \frac{C}{v^2} + \frac{D}{v^3} + \ \ldots \qquad 4\text{-}21$$

Stellenbosch University https://scholar.sun.ac.za

Performing this expansion for a general Cubic EOS (as in Equation 4-6):

$$Z = \frac{Pv}{RT} = 1 + \sum_{n=0}^{\infty} \left(\frac{b}{v}\right)^n - \frac{a}{vRT} \qquad 4\text{-}22$$

Hence:

$$B(T) = b - \frac{a}{RT} \qquad 4\text{-}23$$

For a mixture, it can be derived from Statistical Mechanics that (see Equation 4-4):

$$B_m(T) = \sum_i \sum_j x_i x_j B_{ij}(T) \qquad 4\text{-}24$$

Hence for a Cubic EOS:

$$b_m - \frac{a_m}{RT} = B_m(T) = \sum_i \sum_j x_i x_j \left(b - \frac{a}{RT}\right)_{ij} \qquad 4\text{-}25$$

Now focussing on the liquid side, Wong and Sandler used the following expression:

$$G_{ex} = A_{ex} + PV_{ex} \qquad 4\text{-}26$$

They reasoned as follows:

$$G_{ex}(T, x, P = low) = A_{ex}(T, x, P = low) = A_{ex}(T, x, P = \infty) \qquad 4\text{-}27$$

This assumption is based on the empirical finding that A_{ex} is much less pressure dependent thanG_{ex}. This assumption has been questioned by Coutsikos et al. [130], especially for systems of large asymmetry.

This treatment results in two equations, 4-25 and 4-27, with two unknowns (a_m and b_m) which adhere to the theoretical quadratic composition dependence at low pressure, and the composition dependence of an existing G_{ex} model at infinite pressure. Solving simultaneously results in the Wong-Sandler mixing rule:

$$Q = \sum_i \sum_j x_i x_j \left(b - \frac{a}{RT}\right)_{ij} \qquad 4\text{-}28$$

$$D = \frac{1}{RT}\left(\sum_i x_i \frac{a_i}{b_i} + \frac{A_{ex}^{\infty}}{C}\right) = \frac{a_m}{b_m RT} \qquad 4\text{-}29$$

Stellenbosch University https://scholar.sun.ac.za

$$b_m = \frac{Q}{1-D} \qquad 4\text{-}30$$

$$\frac{a_m}{RT} = Q\left(\frac{D}{1-D}\right) \qquad 4\text{-}31$$

C is a constant unique to the model being used and the following combining rules can be used in Q:

Combining rule 1:

$$\left(b - \frac{a}{RT}\right)_{ij} = \frac{\left(b_i - \frac{a_i}{RT}\right) + \left(b_j - \frac{a_j}{RT}\right)}{2}\left(1 - k_{aij}\right) \qquad 4\text{-}32$$

Combining rule 2:

$$\left(b - \frac{a}{RT}\right)_{ij} = \frac{b_i + b_j}{2} + \frac{\sqrt{a_i a_j}}{RT}\left(1 - k_{aij}\right) \qquad 4\text{-}33$$

Combining rule 3:

$$\left(b - \frac{a}{RT}\right)_{ij} = \frac{b_i + b_j\left(1 - k_{bij}\right)}{2} + \frac{\sqrt{a_i a_j}}{RT}\left(1 - k_{aij}\right) \qquad 4\text{-}34$$

Combining rule 1 was published with the derivation of the original mixing rule by Wong and Sandler [129], and combining rule 2 has been recommended as an alternative by Sandler [76]. For combining rule 3, Valderrama [98] included a second BIP, $k_{b,ij,}$ for only the solute size parameter, b_j, in order to improve correlations in solubility calculations for asymmetric systems.

A_{ex}^{∞} is the excess Helmholtz energy at infinite pressure and any existing G_{ex} (liquid activity coefficient) model can be used for obtaining this value.k_{aij} and $k_{b,ij}$in the combining rules for the second virial coefficient expression can be adjusted to fit VLE data.

The WS mixing rule has shown reasonable correlation in the high-pressure region in conjunction with the NRTL local composition model for G_{ex} [131]. Caster and Sandler [132, 133] used the WS mixing rules with the PR EOS and NRTL G_{ex} model for critical point calculations of various mixtures. Quantitative agreement could only be obtained for some non-ideal systems ie. water, acetone and alcohols, while only qualitative agreement could be

Stellenbosch University https://scholar.sun.ac.za

obtained for highly asymmetric systems, such as water/n-dodecane. Lopez and Cardona [134] obtained good correlations for the CO_2/n-alkanes up to nC10 using the PR EOS with Stryjek-Vera (SV) alpha function and NRTL as G_{ex} model. Correlations were provided for the NRTL and second virial coefficient interaction parameters in terms of solute structure, but they give substantial error in the bubble pressure. Valderrama et al. [135] investigated CO_2/1-alcohols systems up to solute carbon number nC10 with the PR-SV model and the Van Laar G_{ex} model. Reliable correlations were obtained for the two Van Laar and second virial coefficient interaction parameters. Average errors in pressure, P, and solute concentration in the gas phase, Y_2, were 4.4 % and 25.1 % respectively. Yang et al. [136] extended the WS mixing rule to the 3 parameter Patel-Teja EOS, using the NRTL G_{ex} model. Good results were obtained for binary and multi-component mixtures of various classes of polar and non-polar molecules, with surprisingly good results reported approaching the critical point.

4.3 Polymer-chain molecular models

Traditionally, the chain-like fluid structure of polymers was described by equations of state from lattice theory [137]. These theories generally model the system as N molecules, consisting of r adjacent segments, arranged on a lattice specified by a co-ordination number Z_{cor}, resulting in a total of rN sites [137]. Particles are modelled as in a pseudo-solid phase by having more degrees of freedom than in an ordered crystal lattice [137]. Lattice theories may be divided into three categories:

- cell models,
- lattice-fluid models and
- hole models

The first two methods differ only in how they incorporate compressibility into the lattice. The hole models combine these two methods by either including lattice vacancies or by varying the cell volume. Lambert et al. [137] provides a good review on lattice theories.

Of late, the perturbation approach (see Section D.5.4) has been used in order to model polymers. This starts by taking molecules as tangent-spheres interacting through a specific potential function, and then imposing chain formation effects, thus abandoning lattice origins [137]. This development is portrayed in Figure 4-1.

Stellenbosch University https://scholar.sun.ac.za

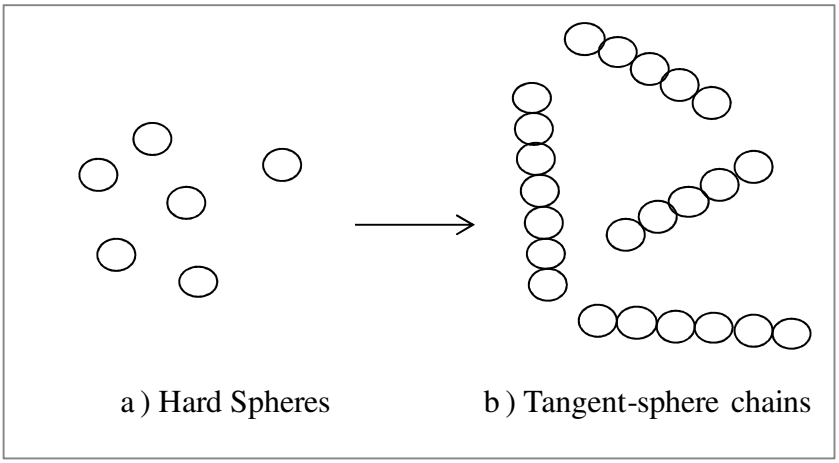

Figure 4-1Tangent-sphere chain formation

The models to be discussed in this section include:

- Perturbed Hard Chain Theory (PHCT) equations developed by Beret and Prausnitz [138] and Donohue and Prausnitz [139]
- Simplified Perturbed Hard Chain Theory (SPHCT) by Kim et al. [140]
- Perturbed Soft Chain Theory (PSCT) by Morris et al. [141]

Reference term expressions for mixtures are generally derived from statistical mechanics and empirical one-fluid mixing rules as those covered in Section 4.2 for the cubic models are only incorporated in the dispersion term, for which empirical interaction parameter may also be used. Since all the theoretical considerations are primarily aimed at the pure component model, mixture expressions for these models are not analyzed here, but are discussed in the review of Lambert et al. [137].

4.3.1 PHCT

The first model considered to successfully account for chain-like behaviour across all densities was the PHCT developed by Beret and Prausnitz [138], which was modified and extended to mixtures by Donohue and Prausnitz [139]. This model is based on the cell model approach of Prigogine [142] in 1957, which starts from the following partition function:

$$Q[N,V,T] = Q_{comb}\left(\frac{V_f}{\Lambda^3}\right)^{\mathbf{N}} q_{rot}^{N} q_{vib}^{N} \exp\left(-\frac{E_0}{kT}\right) \qquad 4\text{-}35$$

Stellenbosch University https://scholar.sun.ac.za

Q_{comb} is the combinatorial factor, which represents the number of ways of arranging Nr segments in a lattice of Nr sites, and $V_f$is the free volume. $\left(\frac{V_f}{\Lambda^3}\right)$ is the contribution due to translational motions and Λ is the *De Broglie wavelength* (see Section D.5.2). E_0 is the mean potential energy of the system with every r-mer in molecule N at the central position of its lattice site [137]. Q_{comb} is independent of the system volume, and falls away upon deriving a pressure explicit EOS (see Equation D.55)

In Section D.5.2, it was seen that the energies of translation, rotation and vibration etc. are separable from the contribution of intermolecular forces in deriving an expression for the partition function for *small, spherical molecules*. This treatment makes models derived from this partition function (Equation D.52) inadequate for representing chained molecules, because in chains the rotational and vibrational motions are influenced not only by internal temperature dependent modes, but by intermolecular forces, giving them external volumedependence [142, 137]. Prigogine [142] thus modified equation 4-35 by factoring the rotational and vibrational partition functions into an external volume dependent part and an internal temperature dependent part:

$$q_{rot}q_{vib} = q_{int}(T)q_{ext}(V) \qquad 4\text{-}36$$

To further approximate $q_{ext}(V)$, Prigogine [142] added a parameter c, to account for the additional external degrees of freedom required to account for the volume dependence of rotational and vibrational motions. As a lower limit, a single chained *molecule* free to move about in a system would have 3 translational degrees of freedom, the same as that of a spherical particle. An upper limit of 3 additional degrees of freedom*per segment*r could then be defined in order to account for the vibrational and rotational motions of a completely flexible r-mer molecule, with no constraints on its motion. Prigogine [142] then reasoned that the external degrees of freedom from these motions would fall somewhere in between these limits:

$$3 \leq 3c \leq 3r \qquad 4\text{-}37$$

3c are thusthe *effective external degrees* of freedom per r-mer molecule. By further assuming that the external rotational and vibrational degrees of freedom can be considered equivalent to translational degrees of freedom, the energy effects of all these motions can be grouped into temperature and volume dependent parts, while leaving c unspecified:

$$\left(\frac{V_f}{\Lambda^3}\right) q_{rot}q_{vib} = q_{int}(T)q_{ext}(V) = q_{int}(T)\left(\frac{V_f}{\Lambda^3}\right)^c \qquad 4\text{-}38$$

Stellenbosch University https://scholar.sun.ac.za

Prigogine's EOS derived from this partition function gave good results at high densities for liquid phase properties, but had the following short-falls [137]:

- It did not approach the ideal gas limit: $\lim_{V\to\infty}\left(\frac{V_f}{\Lambda^3}\right)q_{ext} = \frac{V}{\Lambda^3}$
- It did not meet the requirement of no external degrees of freedom as the system approached the closest-packing volume V_0: $\lim_{V\to V_0}\left(\frac{V_f}{\Lambda^3}\right)q_{ext} = 0$
- $q_{ext} = 1$ was not met for simple fluids at all densities
- q_{ext} did not satisfy equation 4-37 at liquid-like densities for large molecules.

Using the ideas of Prigogine [142], Beret and Prausnitz [138] proposed the Perturbed-Hard-Chain-Theory (PHCT). For their derivation, they used the hard-sphere partition function (Equation D.52), which is valid at all densities, however they kept Priogogine's separation of the rotational and vibrational energy contributions into an internal (temperature dependent) and external (volume dependent) energy contribution:

$$Q[N,V,T] = \frac{1}{N!}\left(\frac{1}{\Lambda^3}\right)^N q_{int}^N q_{ext}^N \left[V_f \exp\left(-\frac{\phi}{2kT}\right)\right]^N \qquad 4\text{-}39$$

The bracketed term represents the deconstruction of the *configurational integral* of Equation D.52 into the hard-sphere repulsion (reducing to V_f) and the attractive potential energy. ϕ, is the *mean potential energy,* defined so that $\left(\frac{1}{2}\right)N\phi = \bar{\Gamma}$, where $\bar{\Gamma}$ represents the intermolecular potential of the entire system, as given by Equation D. 56. In order to address the short-falls of Prigogine's work, Beret and Prausnitz proposed the following function:

$$q_{ext} = \left(\frac{V_f}{V}\right)^{c-1} \qquad 4\text{-}40$$

Donohue and Prausnitz [139] modified the equation of Beret and Prausnitz [138] by including attractive interactions in the expression:

$$q_{ext} = \left[\frac{V_f}{V}\exp\left(-\frac{\phi}{2kT}\right)\right]^{c-1} \qquad 4\text{-}41$$

This formulation leads to the following canonical partition function:

$$Q[N,V,T] = \frac{1}{N!}\left(\frac{V}{\Lambda^3}\right)^N q_{int}^N \left[V_f \exp\left(-\frac{\phi}{2kT}\right)\right]^{cN} \qquad 4\text{-}42$$

Stellenbosch University https://scholar.sun.ac.za

Upon deriving the final form for the PHCT model, the density dependence of the translational degrees of freedom, namelyV_f, was given by the Carnahan starling equation [143]:

$$Z = Z(\eta) = \frac{1+\eta-\eta^2-\eta^3}{(1-\eta)^3} \qquad 4\text{-}43$$

The Carnahan-Starling hard-sphere term was chosen because this term shows good correlation with simulation data and with considerable improvement over the Van der Waals hard-sphere term, especially at high densities [144].

It was further assumed that a chain molecule behaves like a chain of spherical beads or segments, each of which interacts with its neighbours with the attractive square-well potential [76]. The perturbation terms of a particular expansion around a reference system is often determined through empirical means by fitting models to molecular simulation data for a particular attractive potential. Alder et al. [145] developed an attractive perturbation expression for pressure in this manner for a square-well fluid with a well-width of $\gamma = 1.5$ over a specific density and temperature range:

$$P_{attr} = -\sum_n \sum_m A_{nm} \left(\frac{\epsilon}{kT}\right)^n \left(\frac{\eta}{\tau}\right)^m \qquad 4\text{-}44$$

η is the reduced volume ($\eta = \frac{b}{4v}$ with $b = \frac{2}{3} N_A \pi\sigma^3$ and σ is the hard-sphere diameter). ϵ is the well depth and A_{nm} are universal constants which were determined from statistical mechanical calculations for square-well simulation data.

Donohue and Prausnitz [138] refitted the Alder power series constants, $A_{nm,}$ to vapour pressure and liquid density data for methane, pre-disposing the model for improved performance for the n-alkane chain family. They also reduced the perturbation parameter matrix size to a 4 x 6 matrix facilitating faster computation times. Even though this makes the model essentially empirical, it corrects for the current lack in theoretical knowledge in both repulsive and attractive interactions during the fitting procedure of the universal parameters [75].

The final form for the PHCT EOS in terms of the compressibility is given as follows [76]:

$$Z = \frac{Pv}{RT} = \frac{1+(4c-3)r\eta+(3-2c)(r\eta)^2-(r\eta)^3}{(1-r\eta)^3} - c\sum_n \sum_m \frac{mA_{nm}}{v^m \tau^n} \qquad 4\text{-}45$$

Stellenbosch University https://scholar.sun.ac.za

The Alder power series is depicted above in the reduced variables:

$$\tau = \frac{ckT}{\varepsilon q} \quad 4\text{-}46$$

$$v = V\sqrt{\frac{2}{Nr\sigma^3}} \quad 4\text{-}47$$

Where ε is the intermolecular potential per unit surface area; q is the surface area per molecule;V is the system volume and r is the number of segments per molecule.The equation thus contains the following three substance dependent parameters:

- εq (related to the depth of the energy well)
- $r\sigma^3$(characteristic size parameter)
- c (one-third external degrees of freedom)

These parameters are generally determined from VLE data and have been demonstrated to scale reliably in terms of molecular weight for certain homologous series [75].

4.3.2 SPHCT

A useful attribute of the methodology followed by the PHCT for modelling chain effects is that different (simpler) reference and perturbation terms may be incorporated into the model without losing its chain-like capabilities for modelling more asymmetric systems [77]. Kim et al. [140] developed the Simplified Perturbed Hard Chain Theory by replacing the Alder perturbation term with a simpler expression based on a local composition model of Lee et al. [146]. The SPHCT is given as follows:

$$Z = 1 + c\left\{Z^{rep} - Z_M \frac{v^*Y}{v+v^*Y}\right\} \quad 4\text{-}48$$

With:

$$Z^{rep} = \frac{\frac{4\tau v^*}{v} - 2\left(\frac{\tau v^*}{v}\right)^2}{\left(1-\frac{\tau v^*}{v}\right)^3} \quad 4\text{-}49$$

$$Y = \exp\left(\frac{T^*}{2T}\right) - 1 \quad 4\text{-}50$$

Stellenbosch University https://scholar.sun.ac.za

$$\nu^* = N_A \frac{r\sigma^3}{\sqrt{2}} \quad 4\text{-}51$$

$$T^* = \frac{\varepsilon q}{ck} \quad 4\text{-}52$$

N_A is Avogadro's number, τ is a constant equal to 0.7405, Z_M is the maximum coordination number of a site on the chain (given a value of 36 by Kim et al. [140]), r is the number of segments in the molecule (defined arbitrarily as CH_2 for hydrocarbon chains), ε is the characteristic energy per unit surface area and q is the external area.

The SPHCThas three parameters:

- T^*(related to the depth of the energy well)
- ν^* (characteristic size parameter)
- c (one-third external degrees of freedom)

These parameters are generally fit to vapour pressure and liquid density data have also been reported to scale reliably with the molecular mass of certain homologous series .The SPHCT equation has been found to retain the advantages of the PHCT equation and can be used to predict properties across all densities for fluids with large size variations [140, 76].

4.3.3 PSCT

Another notable modification of the PHCT is the Perturbed Soft Chain Theory (PSCT) by Morris et al. [141] who replaced the fourth order perturbation term for the square well fluid by a second order perturbation term for the soft-core Lennard-Jones fluid. This modification introduces a temperature dependent hard-sphere diameter thereby incorporating electron cloud-like behaviour into the equation, making for a more realistic fluid description. The temperature dependent hard-sphere diameter was evaluated through the Barker Henderson approach (see section D.5.5) and then fitted to fourth order polynomial in T^* (same parameter as in SPHCT) [76, 141]. Improved performance at elevated temperatures was observed.This equation has the same characteristic parameters as the SPHCT, which also scale reliably with molecular weight up to carbon numbers of 8.Computational times were also reduced by 35% relative to the PHCT model, with no loss in accuracy [141].

Only a couple of polymer models are mentioned in this section, however many subsequent improvements have been made to these general equations, including the incorporation of multi-polar forces in the Perturbed Anisotropic Chain Theoryof (PACT). A review of

Stellenbosch University https://scholar.sun.ac.za

modelsemanating from PHCT is given by Donohue and Vimalchand and is recommended for a good background [147].

4.4 SAFT molecular models

In a series of articles from 1984 to 1986 Wertheim proposed his Thermodynamic Perturbation Theory (TPT) [148 - 151], defining a perturbation scheme which could incorporate hard-sphere repulsion, covalent chain formation and association effects into the reference system. All other intermolecular interactions, such as dispersion or polar effects may then be treated as a perturbation around the reference system through perturbation theory (see Section D.5.3).

Wertheim's TPT was extended to develop a real-fluid EOS, known as the Statistical Associating Fluid Theory (SAFT) [152]. The overall scheme of the original SAFT approach may be presented byFigure 4-2.

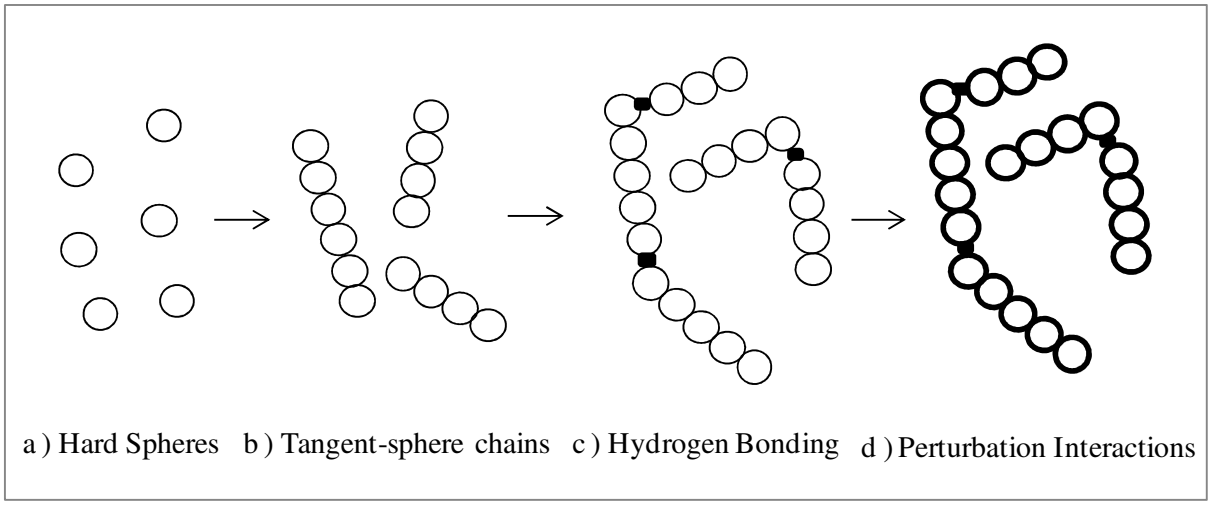

Figure 4-2 Physical representation of the original SAFT scheme: a) Hard-sphere reference b) Covalent bonds imposed between chains c) Hydrogen bonds imposed d) Dispersion effects through perturbation theory [5]

Many different versions of the SAFT equation have been developed based on the initial theory by Wertheim. These equations may be tailor made by expanding specific perturbation effects about any appropriate reference, leading to many variations depending on the potential function, choice of reference system and the treatment of the perturbation terms [152]. The following versions will be discussed:

- Original SAFT by Huang and Radosz [153, 154] and Chapman et al. [155, 156]
- Perturbed-Chain SAFT (PC-SAFT) by Gross and and Sadowski [157]

Stellenbosch University https://scholar.sun.ac.za

- Simplified Perturbed-Chain SAFT (sPC-SAFT) by Von Solms et al. [158]
- SAFT-Critical Point (SAFT-CP) by Chen and Mi [159, 160]
- SAFT+ Cubic by Polishuk [161, 162]

4.4.1 **Original SAFT (Huang and Radosz)**

All SAFT models view a molecule as consisting of segments and deconstructs the Helmholtz free energy into contributions from their various interactions, e.g. from an ideal gas, the intermolecular forces, the formation of chains and association [77]:

$$A = A^{IG} + A^{seg} + A^{chain} + A^{assoc} \qquad 4\text{-}53$$

Following the derivation of Huang and Radosz, the Helmholtz expansion may be represented as a mole *specific residual property* (difference between one mole of the true and the ideal gas property at the same temperature and density) [153]:

$$a^{res} = a^{seg} + a^{chain} + a^{assoc} \qquad 4\text{-}54$$

a_0^{seg} represents the segment-segment interactions as approximated by a repulsive hard-sphere term and an attractive dispersion termper mole of *segments* (as indicated by the 0 subscript):

$$a_0^{seg} = a_0^{hs} + a_0^{disp} \qquad 4\text{-}55$$

The segment Helmholtz energy per mole of *molecules* is then given as follows:

$$a^{seg} = m a_0^{seg} \qquad 4\text{-}56$$

Where m is defined as the segment number (segments per mole of molecules), and is a characteristic parameter of the equation.

Hard sphere contribution

The hard-sphere term that was used was the same as in the PHCT, namely the Carnahan and Starling term [143]:

$$\frac{a_0^{hs}}{RT} = \frac{4\eta - 3\eta^2}{(1-\eta)^2} \qquad 4\text{-}57$$

Stellenbosch University https://scholar.sun.ac.za

Withη defined as the segment packing factor:

$$\eta = \frac{\pi N_{AV}}{6} \rho m d^3 \qquad 4\text{-}58$$

ρ is the molar density and d is a temperature dependent effective segment diameter.

Dispersion term

For the perturbation term, the Alder series as refit by Chen and Kreglewski in 1977 to represent PVT and second virial coefficient data for argon was used [76, 152]:

$$\frac{a_0^{disp}}{RT} = \sum_i \sum_j D_{nm} \left(\frac{u(T)}{kT}\right)^n \left(\frac{\eta_{CK}}{\tau}\right)^m \qquad 4\text{-}59$$

$\frac{u(T)}{kT}$ is a temperature dependent energy parameter, related to the depth of the square energy well. η_{CK} is the reduced volume of a soft-sphere fluid as approximated by Chen and Kreglewski asa *hard-sphere model* with effective hard sphere diameter [156]. A simplified square-well-like potential function was used, namely the two step Chen and Kreglewski potential, which has a particle softness parameter to vary the repulsive diameter and could be solved analytically using the Barker and Henderson approach.This approach maps a soft-sphere potential onto a hard-sphere structure for which the radial distribution function (RDF) is known (see Sections D.5.3 – D.5.5) [156]. The hard-sphere and dispersion used in the SAFT equation are thus the same hard as those used for the PHCT equation [155, 156].

Chain contribution

The Helmholtz energy contribution due to chain formation per mole of molecules can be determined from the following expression initially proposed by Chapman et al. [155]:

$$\frac{a^{Chain}}{RT} = \sum_i X_i(1 - m_i) \ln(g_i(d_i)^{hs}) \qquad 4\text{-}60$$

Where $X_i$is mole fraction, m is the segment number and $g_i$is the correlation function of the reference system evaluated at the segment contact. As shown by the "hs" superscript, Chapman et al. [155] also considered a *hard-sphere*structure (RDF) for their segments and derived this expression by replacing the association bonds from Wertheim's theory with

Stellenbosch University https://scholar.sun.ac.za

covalent chain forming bonds approximated at the limit of total association [153]. The final expression for the Helmholtz contribution due to chain formation is given as follows:

$$\frac{a^{Chain}}{RT} = (1 - m) \ln \frac{1-\left(\frac{1}{2}\right)\eta}{(1-\eta)^3} \qquad 4\text{-}61$$

Association contribution

The association term is given as follows:

$$\frac{a^{Association}}{RT} = \sum_A \left[\ln X^A - \frac{X^A}{2}\right] + \frac{1}{2} M \qquad 4\text{-}62$$

Where M is the number of association sites on each molecule, X^A is the mole fraction of molecules NOT bonded at site A, and $\sum_A$ represents a sum over all associating sites on the molecule. The X^A term is generally implicit but may be approximated analytically under certain conditions using various association schemes. These schemes are selected from a list of analytically solvable expressions. Selecting the right expression requires spectroscopy data on the strength of the association sites, which is often difficult to obtain [153].

The auxiliary functions necessary for the full model derivation is given in the original article by Huang and Radosz and Chapman et al. [153, 155]. Three characteristic parameters emerge from this derivation, if association effects are neglected:

- m(segment number)
- ν^{00} (segment volume)
- $\frac{u^0}{kT}$(segment energy)

According to Huang and Radosz, the segment volume and segment energy are found to be nearly constant upon increasing the molecular mass, while the segment number is a linear function of the molecular mass. Correlations for all three parameters are provided in the original article [153]. This scaling of the parameters with homologous series is promising for extending this model to regions where data is not available. If association effects are included, two additional parameters are added to the model.

Stellenbosch University https://scholar.sun.ac.za

4.4.2 PC-SAFT

The reference system for the original SAFT equation was a hard-sphere reference. This reference system is used due to knowledge of the RDF for a hard-sphere which also allows for closed analytical evaluation of the perturbation integrals through the Barker and Henderson second order perturbation theory (see Section D.5.5). Since chain like structure was not incorporated into the reference fluid but merelyapproximated as a perturbation term connecting hard-sphere segments, the dispersion perturbation term did not take chain connectivity between segments into account. Gross and Sadowksi [157] therefore used the following grouping for their reference and perturbation terms in developing the Perturbed-Chain SAFT EOS:

$$A^{res}(T,V,N) = \left(A^{hs}(T,V,N) + A^{chain}(T,V,N)\right)^{Ref} + \left(A^{Assoc}(T,V,N) + A^{disp}(T,V,N)\right)^{Pert} \quad 4\text{-}63$$

The association and dispersion perturbations are now expanded around a *hard-sphere chain* reference in order to include chain connectivity into the dispersion term. This offers a considerable advantage since the larger volume of chain molecules reduces the space for dispersion interactions, which leads to their overestimation if a hard-sphere reference is used [163]. The new hard-sphere chain reference system is obtained by combining the Hemholtz energy contributions for the hard-sphere (Equation 4-57) and chain contributions (Equation 4-61) as proposed in the initial formulation by Chapman et al. [155, 156]:

$$\frac{a^{HSC\ ref}}{RT} = \left[m\frac{a^{hs}}{RT} - \sum_i X_i(1-m_i)\ln(g_i(d_i)^{hs})\right]_{ref} \quad 4\text{-}64$$

Solving for the perturbation terms for the above reference system involves the integration of the RDF for a hard-sphere chain structure [157]. To include chain structure in their reference system Gross and Sadowski used an analytical expression for the RDF for hard-sphere chains consisting of m hard-spheres at contact, as developed by Chiew in1991 [163]:

$$g_m(\sigma^+) = \frac{2+(3m-2)\eta}{2m(1-\eta)^2} \quad 4\text{-}65$$

Despite the Barker and Henderson second order perturbation theory being developed specifically for hard-sphere molecules, the theory may be applied to this hard-chain reference, since each chain segment is ultimately modelled as a sequence of hard-spheres [157]. Despite numerous simplifying assumptions by the authors, this treatment results in high overall

Stellenbosch University https://scholar.sun.ac.za

density dependence, greatly increasing the complexity of the perturbation terms and the computation times of the final model.

The new dispersion term used is similar to the Alder-series for square-well spheres, but requires a total of 36 universal parameters as fitted by Gross and Sadowski, which is 12 more than the Alder series used in the original SAFT and the PHCT [157]. The constants were obtained by regressing vapour pressure as well as liquid, vapour and supercritical volume data for the n-alkane series [157].

4.4.3 Simplified PC-SAFT

Von Solms et al. [158] developed a simplified PC-SAFT equation by assuming that all segments in the mixture have the same diameter, while keeping the volume fraction the same as that of the actual mixture. This assumption leads to a much simpler expression for the hard-sphere chain RDF thereby simplifying the hard-sphere, chain and association terms. Von Solms et al. [158] observed much faster computation times with no appreciable loss in the accuracy of the model over the original PC-SAFT.

Both PC-SAFT and simplified PC-SAFT have three characteristic parameters for non-associating fluids which are generally regressed from available vapour pressure and liquid density data. Generalized correlations have also been developed by the authors. One binary interaction parameter regressed from mixture VLE data is typically required for accurate results for mixtures and these models proved clearly superior to the original SAFT [158, 164].

4.4.4 SAFT-CP

Another method for incorporating non-sphericity of molecules is to model them as a hard-convex body with an included non-sphericity parameter into the hard-sphere EOS, as was done by Boublik [144]

$$Z = \frac{1+(3\alpha-2)\eta+(3\alpha-3\alpha+1)\eta^2-\alpha^2\eta^3}{(1-\eta\ )^3} \qquad 4\text{-}66$$

Where α, is the added non-sphericity parameter and may be determined from:

$$\alpha = \frac{R_0 S_0}{3V_0} \qquad 4\text{-}67$$

Stellenbosch University https://scholar.sun.ac.za

Where $R_{0,}S_0$ and V_0 are the mean curvature, mean surface area and volume of the convex body. It may be further noted that this equation reduces to the Carnahan-Starling expression for hard-spheres if α =1 [75]. This hard convex-body term was initially combined with an Alder series expansion as used in the original SAFT to give the Boublik-Alder-Chen-Kreglewski (BACK) EOS, which improved predictions for small non-spherical molecules like argon and nitrogen, especially in the critical region [75].

Pfohl and Brunner [165] incorporated the hard convex-body into the SAFT equation for improvement in the critical region for supercritical gas extraction processes with association. This new "SAFT BACK" model was tested for 40 sets of equilibrium data, covering temperatures from 230 to 540 K and pressures up to 200 bar, where the original SAFT fails due to over-prediction of the critical point [165]. The two convex-body parameters (η and α) were determined by Pfohl et al. [165] by regressing from VLE and critical point data. All remaining parameters may be obtained from the original SAFT correlations of Huang and Radosz [153].The new equation showed improved results for small, non-spherical molecules (solvents) across a wide range of conditions, but shortcomings were observed for longer chained molecules, which were therefore still modelled as spherical chains (α =1).

Chen and Mi [159] offered an empirical correction to the dispersion term of the modified SAFT BACK of Pfohl and Brunner [165] to correct for the over-estimation of dispersion effects for chain systems. They called their new equation SAFT Critical Point (SAFT CP), (also referred to as the modified SAFT BACK equation) [159, 160]. The new dispersion term is derived from statistical mechanics, but does not follow the rigorous second order Barker Henderson perturbation approach as with the development of the PC-SAFT dispersion term. Chen and Mi offered the following correction term to the Alder series dispersion term for spherical molecules to account for the effects of chain formation [159]:

$$A^{chain,disp} = \lambda\left(\frac{A^{chain,hcb}}{A^{hcb}}\right) A^{disp}$$

Correction term

Original SAFT Alder series

4-68

A^{hcb} and $A^{Chain,hcb}$ are the Helmholtz energy of the hard-convex body reference and chain perturbation, respectively, and are both functions of the RDF for a non-spherical hard convex body as derived by Boublik in 1975 [159]. λ is a conformal constant characteristic to a particular potential model [159].

Stellenbosch University https://scholar.sun.ac.za

Chen and Mi applied their equation in the modelling of pure equilibrium and PVT properties for a range of polar and non-polar fluids up to the critical point with good success [159, 160]. SAFT-CP has 4 characteristic parameters, namely the 3 non-associating SAFT parameters and the Boublik non-sphericity parameter. These parameters were regressed using the following objective function:

$$F = \left(\frac{T^{C,calc} - T^{C,exp}}{T^{C,exp}}\right)^2 + \left(\frac{P^{C,calc} - P^{C,exp}}{P^{C,exp}}\right)^2 + \left(\frac{\rho^{C,calc} - \rho^{C,exp}}{\rho^{C,exp}}\right)^2 + \sum_{j=1}^{NP}\left(\frac{P_j{}^{calc} - P_j{}^{exp}}{P_j{}^{C,exp}}\right)^2 + \left(\frac{\rho_j{}^{liq,calc} - \rho^{liq,exp}}{\rho^{liq,ex}}\right)^2 \quad 4\text{-}69$$

The component parameters were scaled to the critical properties, in contrast to the objective function generally used for the original SAFT model where parameters are simply fit to the saturation properties:

$$F = \sum_{i=1}^{NP}\left(\frac{P_i{}^{sat,calc} - P_i{}^{sat,exp}}{P_i{}^{sat,exp}}\right)^2 + \left(\frac{\rho_i{}^{sat,calc} - \rho_i{}^{sat,exp}}{\rho_i{}^{sat,exp}}\right)^2 \quad 4\text{-}70$$

4.4.5 Numerical pitfalls of the SAFT models

Despite the theoretical advantages of the SAFT models, it is well known that they suffer from the following numerical pitfalls:

- Up to 5 real roots in volume are obtained at low temperatures [166, 167]
- The isochoric heat capacity diverges at infinite pressures [167,168]
- Intersecting isotherms at high densities [169]

According to Privat et al. [166], the PC-SAFT equation may exhibit up to 5 different volume roots at low temperatures, where the cubic equations give at most 3 roots. Multiple equilibrium curves on a single isotherm have not been observed experimentally and may be considered non-physical. It also leads to the prediction of inconsistent phenomena, such as two critical points for a single pure component, as well as two different fluid-fluid coexistence lines. Privat et al [166] investigated close to 60 common pure components all showing this behaviour. Polishuk [167] notes that these unrealistic phase splits occur for feasible roots larger than the co-volume which are often also the stable roots, representing a global minimum in the Gibbs energy, whereas the roots that match the experimental VLE are meta-stable.

Stellenbosch University https://scholar.sun.ac.za

Polishuk [167] investigated the susceptibility of various common versions of SAFT to this behaviour and found that the original SAFT by Huang and Radosz, Soft-SAFT, SAFT CP and PC-SAFT all display this behaviour; however the SAFT version by Chapman et al. [155, 156] and the Simplified SAFT (SSAFT) by Fu and Sandler [170] did not. The reason for these unrealistic roots was attributed to the empirical polynomial series dispersion terms such as the Alder series or the newly fitted polynomial series for PC-SAFT, which may have a polynomial volume order up to 14 and 24, respectively [157]. Despite a polynomial order of 9 in volume for the SAFT model by Chapman et al. [155], this relative simplicity eliminates the problem. The same is true of SSAFT, which simply replaces the Alder series dispersion term with the same simplified expression as used in the development of the SPHCT by Kim et al. [140]

$C_v$diverges to negative infinity at the infinite pressure limit, which is also considered non-physical, since theory suggest that the mechanical stability limit will prohibit this value from occurring in reality [167, 168]. According to Kalikhman et al. [168] any temperature dependence enforced on the hard-sphere diameters and co-volumes of a model necessarily results in this divergence and intersecting isotherms at high densities [168]. This result is particularly problematic, since the temperature dependent hard-sphere diameter is crucial for extending soft-core behaviour such as that of the Lennard-Jones potential function to an analytical EOS via the Barker-Henderson perturbation theory [168].Polishuk [169] notes that for the SAFT model family, which aims at a theoretically sound representation of thermodynamic phase behaviour, these unrealistic limiting conditions are unacceptable and ways must be developed to repair these shortcomings.

4.4.6 SAFT + Cubic

In addition to the numerical pitfalls of SAFT models, Polishuk [161] also notes their poor estimation of T_c and P_c, which is achieved by the simpler cubic models. This leads to limited capability of predicting critical and subcritical PVT behaviour simultaneously. In addressing these issues, Polishuk [161] devised the SAFT + Cubic model, which simply attaches the cubic attractive term as a cohesive correction term to the existing SAFT model:

$$A^{res}(T,V,N) = A^{res,SAFT}(T,V,N) - \frac{a}{V+c} \qquad 4\text{-}71$$

The $A^{res,SAFT}$ term has the following conventional deconstruction of the residual Helmholtz energy:

Stellenbosch University https://scholar.sun.ac.za

$$A^{res,SAFT}(T,V,N) = A^{HS} + A^{disp} + A^{chain} + A^{assoc} \quad 4\text{-}72$$

A^{HS} and A^{disp} was further modified while the same chain and association terms were used as in the original SAFT. For the hard-sphere term, Polishuk [161] kept temperature dependence in the reduced volume, but removed the temperature dependence from the diameter term:

$$\eta = \frac{\pi N_{AV}}{6V}\sigma^3\theta(T) \quad 4\text{-}73$$

This modification completely avoided intersecting isotherms at the high densities, while the unrealistic isochoric heat capacity value was restricted to very high pressures and low temperatures outside industrial ranges. No loss of accuracy was observed relative to the original SAFT [169].

In selecting an appropriate dispersion term, Polishuk [161] chose the term from the initial SAFT of Chapman et al. [155], since it has not been found to predict the additional volume roots typical of most SAFT models at low temperatures. A similar correction to the dispersion term to that of Chen and Mi [159] in deriving SAFT-CP was also used:

$$A^{disp} = mR\left(a_{01}^{disp} + \frac{a_{01}^{disp}\left(\frac{\varepsilon}{k}\right)}{T}\right)\left(1 + \frac{2A^{chain}}{A^{HS}}\right) \quad 4\text{-}74$$

Original Chapman SAFT dispersion term

Correction term

Expressions for a_{o1}^{disp} and a_{o2}^{disp} are functions of reduced volume and are slightly altered from those used by Chapman et al. [155 162]. The newly proposed model has the following 5 substance dependent parameters, for non-associating compounds:

- m,
- σ,
- $\frac{\varepsilon}{k}$,
- a,
- c

Stellenbosch University https://scholar.sun.ac.za

Polishuk [171] generalized these parameters for heavy organic substances, considering 91 compunds of different chemical background with carbon numbers 18-39. The parameters m and c are obtained from generalized correlations in terms of molecular weight and T_c, while the remaining three paramters are obtained by scaling to the critical point:

$$\left(\frac{\partial P}{\partial v}\right)_{T_c} = \left(\frac{\partial^2 P}{\partial v^2}\right)_{T_c} = 0|_{v_{c,EOS}=1.1\, v_c^*} \qquad 4\text{-}75$$

The following condition is further to be satisfied at one arbitrary experimental or estimated liquid density data point:

$$\rho_{EOS} = \rho_{experimental} \qquad 4\text{-}76$$

In cases where the necessary T_c data were not available, this value was estimated and an additional data point was included in the regression to compensate for possible loss in accuracy [171].

4.5 Group contribution methods

The group contribution method is a modelling technique which derives all model parameters from the contributions of functional groups. This methodology is based on the assumption of *group additivity* whereby the system contributions from functional groups are assumed to be independent of that made by any other group. The success of the method relies on the validity of this assumption [75].

Since there is typically a smaller variety of functional groups in a mixture than chemical compounds, thousands of mixtures may be modelled by arranging a few dozen functional groups. This allows for predicting mixture properties of systems for which no data is available based entirely on pre-established information about the functional groups and their interactions, which may be more reliably correlated and logged in a database for repeated use. The accuracy of the method increases as more functional groups are identified for distinguishing compounds, but predictive capability is compromised as this number tends toward the number of individual compounds in the mixture. The following general criteria may be provided for identifying such functional groups [75]:

1. The geometry of the functional group should be the same independent of the molecule in which the group occurs.

Stellenbosch University https://scholar.sun.ac.za

2. Each atom in the functional group should have approximately the same charge in all molecules in which the group occurs and the group should be approximately electro-neutral.

3. Each group should be the smallest divisible entity for dividing a molecule into a collection of electro-neutral groups.

Given these criteria, these methods are not well suited for polar or associating systems in which proximity effects occur and the effect of adding a group to the solution depends on its relative location to a polar group. This inherently limits this method in describing more complex systems, although group contribution methods have been developed which show reasonable performance for polar systems [75].

The molecular polymer and SAFT models have parameters with clear physical meaning related to the molecular structure, making them especially susceptible to being reworked in terms of functional groups.

This section will discuss some existing equations of state reworked in terms of group contributions, as well as the the Group Contribution EOS derived by Skjold-JØrgensen [172, 173]. Existing equations that have been reworked in terms of groups discussed in this section include:

- The predictive 1978, Peng Robinson EOS (PPR78) by Jaubert et al. [112 ,174]
- The Group Contribution PSCT (GPSCT) by Jin et al. [175]
- The Group Contribution SPHCT (GSPHCT)by Georgeton and Teja [176]
- The Patel-Teja Group Contribution EOS (PT- GC) by Georgeton and Teja [177]
- The Group Contribution SAFT (GC-SAFT) by Tamouza et al. [178,179]
- The Group Contribution PC-SAFT (GC-PC-SAFT) by Peters et al. [180]

4.5.1 PPR78

This model, first proposed in 2004 by Jaubert et al. [112], involves the widely used PR EOS (1978 version) in conjunction the classic Van der Waals mixing rules, with the BIP for the energy parameter, $k_{aij,}$ given temperature dependence and calculated in terms of group contributions, making the model fully predictive.

k_{aij}, is determined as a function of the pure constants T_c, P_c and the acentric factor ω. Additional input information includes the number of existing groups defined by the method (currently 21) [106]; the fraction of a molecule occupied by a certain group and 2 previously

Stellenbosch University https://scholar.sun.ac.za

determined interaction parameter for each binary group interaction. For the 21 current groups, the 420 interaction parameters were regressed from an extensive database containing 100 000 data points made up of bubble, dew and critical points. This required sophisticated fitting procedures with a complex objective function minimizing errors in phase compositions and critical pressure. The following accuracies were obtained in this fitting procedure [106]:

- Overall deviation in liquid phase: 7.5% AAD
- Overall deviation in vapour phase: 8.0 % AAD
- Overall deviation in critical composition: 7.1 % AAD
- Overall deviation in critical pressure: 4.9 % AAD

The definition for %AAD is given by equation 6-24. Given the complex and broad ranging fitting procedures involved, these deviations suggest that the model can be used as an accurate predictive tool. The 21 current groups include the building blocks of alkanes, aromatics, naphthenes, mercaptans and alkenes, as well as CO_2, N_2, H_2S, H_2 and water across a wide temperature range. Jaubert and Privat [174] have also provided expressions for obtaining $k_{aij}$for the SRK EOS using any alpha function in terms of group parameters for the PR78 model, further extending the range of the method.

4.5.2 GPSCT

The original PSCT is discussed in Section 4.3 and has the same three characteristic pure compound parameters as the SPHCT:

- T^*(energy parameter)
- v^* (size parameter) and
- c(one third of the external degrees of freedom)

Jin et al. [175] reworked this equation by reformulating these pure parameters in terms of functional groups. 5 new parameters were defined in terms of functional groups and correlated in terms of carbon number. These correlations were normalized to take into account the position of the group. This may be necessary due to shielding effects, whereby contributions of groups depend on the length of the existing chain. Jin et al. [175] further provides mixing rules for these parameters, requiring no interaction parameter.

The average errors for 26 pure compounds of reasonably low molecular weight (nC2-30), was 3.5 %AAD for all liquid densities and 6.8 % for all vapour pressures. The ethane/n-decane system was correlated with similar accuracies to the original PSCT and PR EOSs [175].

Stellenbosch University https://scholar.sun.ac.za

4.5.3 GSPHCT

Georgeton and Teja [176] derived the original SPHCT parameters, T^*, v^* and c, in terms of CH_3, CH_2, CH_4, ACH, CO_2, groups, where the ACH indicates that the group is part of an aromatic compound.

Only n-hexane data were used to obtain the parameters for the CH_2/CH_2 interaction, however the authors comment that different molecules, ie. n-pentane, n-decane and n-hexadecane should be used, to average out the effect of adding the group to a different existing chain length. It was further remarked that the effect of each group reaches a state of constant change as the chain length increases, meaning that the validity of the group additivity assumption improves with increasing chain length [176]. If this limit is located for a particular group, then only data from that system would be required to accurately determine its contribution to larger chains.

A %AAD of less than 10 % for pressure and volume for propane, n-decane, n-octane and polyethylene was obtained. Improved performance was observed over the SPHCT for the n-butane/n-decane, propane/n-hexane and methane/n-heptane binary systems. For a highly non-ideal methane/benzene system a 4.68%AAD in bubble point pressure and a 0.038 average deviation in K values was observed [176]

4.5.4 PT-GC

Georgeton and Teja [177] derived the Patel Teja (PT) equation in terms of group contributions. The original PT equation required the following model parameters:

- T_c,
- P_c,
- ξ_c (an empirical compressibility factor)
- F (Soave alpha function parameter)

These parameters were correlated in terms of an effective carbon number (ECN), defined in terms of molecular structure and regressed interaction parameters. The authors fitted these parameters using a similar scheme as discussed for the GSPHCT [176]. Groups included for the GC-PT EOS are CH_3, CH_2, CH_4, ACH, AC,CO_2, and OH.

Stellenbosch University https://scholar.sun.ac.za

K values for the propane/decane and methane/n-pentane system were correlated very well by both the GC-PT and the original PT equation at wide ranges of temperature and pressure. Improved performance of the GC-PT over the PT was also observed for CO_2/n-alkane systems, as well as mixtures of polar compounds [177].

4.5.5 GC-SAFT

Tamouza et al. [178, 179] reworked the characteristic parameters ε, σ and m of the initial SAFT equation by Chapman et al.[155] in terms of group contributions for modelling both pure component and mixture properties.

This method was employed in predicting phase behaviour of n-alkanes, α −olefins, alkyl-benzenes, alkyl-cyclohexanes and 1-alkanols by defining the following 3 groups: CH_2, CH_3 and OH. Parameters were reworked by regressing from pure compound VLE data. A maximum deviation of 5% in vapour pressures and 1% in saturated liquid volumes were obtainedup to nC32 in this regression procedure, which makes for a promising VLE prediction tool [178]. Group interactions for the functional groups were based on the Lorentz-Berthelot combining rules for the energy, ε, and size $, \sigma$,parameters, while the segment number, m, was approximated as a simple linear summation of functional groups per molecule.

For non-polar n-alkane/n-alkane mixtures good predictive capabilities were observed with saturation pressures and liquid densities generally correlated to within 5%, however, deteriorated performance is observed at the critical point [179].

4.5.6 GC-PC-SAFT

Peters et al. [180] presented a group contribution model for the PC-SAFT equation by including liquid density and LLE data for long-chain polymers. Using the new parameters and employing a binary interaction parameter, vastly asymmetric systems could be satisfactorily modelled with a good degree of accuracy.

4.5.7 GC-EOS by Skjold-JØrgensen

The GC-EOS of state was developed by Skold-JØrgensen [172, 173] for the purpose of determining gas solubility in non-polar and polar solvents in a temperature range 100 -700 K

Stellenbosch University https://scholar.sun.ac.za

at pressures reaching 30 MPa. The equation is based on statistical mechanics, using a Van der Waals partition function, with the configurational term deconstructed into a hard-sphere and attractive term. A Carnahan-Starling repulsive termand a density dependent attractive term calculated from a NRTL-type local composition model is used.

The hard-sphere term is given as a function of hard-sphere diameter and total volume, and is not reworked in terms of groups. The hard-sphere diameter at the critical point, d_c, is obtained in terms of T_c and P_c, by solving for the pure component critical conditions. A variable hard-sphere diameter, d(T), is then derived.

The NRTL attractive term was reworked in terms of groups by altering the expression for the average potential energy at the level of the partition function. The final expression for the attractive term requires one adjustable interaction parameter for similar groups; with a non-randomness parameter and three additional temperature dependent parameters also regressed, if necessary. A complex objective function is used in reducing data, which minimizes errors in saturated liquid densities, vapour pressures, Henri's constant, dilute activity coefficients and any available volumetric data points. Contributions are weighted according to the accuracy of the data [172].

The authors remark that the quality of predictions should decrease as the size asymmetry in the system increase due to using the Carnahan-Starling free volume expression for hard-spheres, and neglecting additional degrees of freedom due to rotational or vibration motions. Improved predictions can be obtained for heavy hydrocarbons if d_c is adjusted to the vapour pressures of the components at a constant temperature. The data were further aimed at pressures ranging from 0 to 15 MPa, and the authors warn against inaccuracies outside this range, especially at 25 -30 MPa, which could cause problems for the systems investigated in this study. The attractive term is factorized into numerous auxiliary functions which leads to high model complexity, both for programming and in computational time required [181, 172].

Good accuracies were obtained for relatively asymmetric mixtures of CO_2 and hydrocarbons with K factors within 15% error in most cases [172]. Larger deviations are observed as the mixture critical point is approached [173].The model was first practically applied to supercritical extraction processes by Brignole et al. [181] who studied the extraction of alcohols from water. Temelli et al. [182] studied the extraction of Terpenes from cold-pressed orange peel.

Espinoza et al. [183] has extended the existing parameter tables to include ether, ester, chloro aromatic and triglyceride building blocks, as well as modifying the original aromatic/paraffinic, CO_2/paraffinic and CO_2/aromatic interaction parameters for improved

Stellenbosch University https://scholar.sun.ac.za

prediction for high molecular weight compounds. The best results were obtained for CO_2/paraffin mixtures for solute carbon numbers of nC10 -20, with average errors in liquid mole fractions not exceeding 10%. This showed vast improvement over the MHV2 and PSRK models, which predict errors approaching 30% for these systems.

Espinoza et al. [184] applied GC EOS to systems of CO_2 in mixture EPA and DHA esters with carbon number ranging up to 26 by correlatingthe hard-sphere diameter of the solutes, d_c, as a function of the Van der Waals volume. Satisfactory results were obtained in all cases.

4.6 The Crossover approach

As mentioned in Section 2.3.1, the crossover approach involves a rigorous theoretical attempt at describing the global critical region, thereby adhering to the known power laws from renormalization group theory in the asymptotic critical region, but reducing to mean-field theories in the classic low-pressure region.

4.6.1 Crossover and cubic models

Kostrowicka Wyczalkowska et al. [57] have incorporated critical fluctuations into the Van der Waals EOS. Their crossover Van der Waals equation uses the same asymptotic scaling laws (derived from the Landau-Ginzburg-Wilson theory) as initially employed by Tang and Sengers [55] and Jin et al. [56]. The derivation of this equation is complex, and may be obtained from the referenced articles. The equation required only one empirical parameter and could reach both the ideal gas and the hard-sphere limit. A more accurate reduced value of the critical point was observed relative to the original Van der Waals, while maintaining good prediction in the classical density range.

Kiselev et al. [58] was able to develop a method of extending any classical EOS into a crossover equation by defining a crossover function which approaches 1 as the system moves farther from the critical point, resulting in classical behaviour. The Patel-Teja EOS was used to demonstrate the procedure and was subsequently extended to mixtures through simple composition dependent mixing rules [60]. With the use of two previously determined interaction parameters, PVT data for methane and ethane was represented with % AAD of 2.3 %, compared to 50.2 % using the classical Patel-Teja EOS. Thermodynamic properties very near to the critical point were not well represented. Numerous parameters also had to be regressed from available VLE and PVT data [58].

Stellenbosch University https://scholar.sun.ac.za

4.6.2 Crossover and molecular models

Kiselev et al. [61] extended their general crossover method to the SAFT EOS. The model was applied to pure component chain molecules up to eicosane and all VLE and PVT correlations across a wide range of conditions were correlated below 4% AAD with no additional adjustable parameters required. This model was simplified to requiring only the three original SAFT parameters and also extended to mixtures. Good correlation of VLE, PVT and critical properties were found in all cases [185].

Based on theoretical work on Lennard-Jones fluids by Kolafa and Nezbeda [186], Kraska and Gubbins [187, 188] developed a modified LJ-SAFT equation, showing marked improvement over the original SAFT for both pure component and mixture properties. In a similar approach to Kraska and Gubbins, Blas and Vega [189] developed soft SAFT, which gave improved performance over the original SAFT for binary and ternary mixtures of the n-alkane series.

Lovell and Vega [190] extended this model using crossover treatment to develop the crossover soft-SAFT equation of state, which used the same pure component parameters as soft-SAFT. One BIP was used for the ethane/n-alkane systems, with a second constant parameter required for large solute carbon numbers.The authors were able to accurately predict phase behaviour of type 1 to 5 for methane and ethane with the n-alkane series. Good agreement between derivative properties such as speed of sound and heat capacities for mixtures were also obtained for selected systems [191]. Accurate results were obtained at sub- and supercritical regions using the same parameter set, however two additional crossover parameters were required for modelling the critical region [190].

4.7 Concluding remarks and modelling approach selection for this study

An appropriate approach can now be selected for conducting the modelling for this study by applying the following general criteria:

- Correlative capabilities of the model
- Predictive capabilities of the model
- Flexibility and range of the model
- Complexity in applying the model

In modelling hexane in supercritical CO_2, Schultz et al. [192] computed the virial coefficients up to the fourth order at a temperature of 353.15 K, but could not accurately represent the critical region of the mixture. Harvey et al. [193] used a truncated version of the virial

Stellenbosch University https://scholar.sun.ac.za

equation of state, with the second and third virial coefficients calculated from the Van der Waals, SRK and the Peng Robinson equations with no success. It is clear that despite the strong theoretical foundation of the virial EOS at low densities, it is not suited for a study in high-pressure VLE of non-ideal systems.

Group contribution methods are valuable in process design since they provide a consistent predictive approach, with results comparable to models fitted to specific systems and regions in phase space. The linear trends in equilibrium pressure vs. carbon number observed in chapter 3 (Figure 3-2) further suggests that the systems investigated for this study can be modelled with, or used in the development of, such a method. Developing such a method typically requires vast databanks and sophisticated fitting techniques in order to realistically account for the various group interactions under different circumstances. The data being modelled for this study (see Section 3.6) focuses exclusively on the high pressure region for highly asymmetric systems (nC10 – nC36 range), which is not necessarily representative of the effect of the functional groups in more moderate solution conditions. This study is also primarily aimed at accurate correlation of the high pressure VLE, with predictability being a secondary objective. This project will therefore neither develop nor use a group contribution method, but this approach could be considered for future work once an accurate correlation tool has been established for these systems.

The crossover methodology provides the most theoretically appropriate option for this study, since a single parameter set can be used for equilibrium and thermodynamic properties, with good results obtained at both sub- and super-critical conditions. These models are, however, quite complex, both conceptually and numerically. Up to 5 empirical parameters may be required, which would need sophisticated fitting techniques. This approach is thus not adopted for this study, but may be included in the developed software for future work.

This leaves the question as to whether a more theoretical molecular model or the simple CEOSs are to be adopted for this study. An extensive comparison by De Villiers [194] of different thermodynamic properties for various pure components using PC-SAFT and the CEOSs, found that the molecular model shows a particular advantage in the liquid density and pressure/volume derivative. The PSCT of Morris et al. [141] also performs much better than the PR EOS, especially at carbon numbers above 10 for the n-alkanes, where errors in liquid density for the PR EOS exceed 10%, but are kept below 2 % up to nC20 with the PSCT. Vapour pressure errors were also kept below 3 % for both PHCT and PSCT, with model parameters scaling linearly for the n-alkane series [141].

A notable advantage of the molecular models is furthermore that the perturbation expansion allows for including each molecular contribution (shape, chain-length, dipolar and polar

Stellenbosch University https://scholar.sun.ac.za

forces, association etc.) into the model as an explicit term, whereas the CEOSs only have a simple repulsive and attractive term, with known theoretical limitations [98]. The energy parameter, a, of the cubic models also lumps both dispersion and dipolar interactions together, which does not allow for adequate distinction between these effects, causing severe limitations for polar and associating systems [194]. The EOS/G_{ex} mixing rules discussed in Section 4.2.6, which incorporates a liquid activity coefficient model into the EOS, have addressed these shortcomings in an empirical manner by allowing for improved correlations of liquid properties for non-ideal systems at low-pressure, while maintaining the high-pressure performance and simplicity of classic cubic models.

For high-pressure mixtures approaching the critical point, the superiority of the molecular models is more contested than for pure component and low pressure properties. In modelling the CO_2/paraffins [13], propane/n-alkanes [8, 9] and the ethane/alcohols [4] the molecular models such as SAFT and simplified PC-SAFT required two BIPs to give a reasonable representation of the critical region and were often outperformed by the simpler PR and PT EOSs. Similar findings were made by Voutsas et al. [195], Alfradique and Castier [196], Diamantonis et al. [197] and Atilhan et al. [198]. The cubic models also avoid the numerical pitfalls of the SAFT models, as discussed in section 4.4.5.

CEOSs are still recommended for high-pressure applications by most process simulators, including Aspen Plus ® [199], due to the many alpha functions and mixing rules available. It was also shown in section 4.2.5, that despite the more empirical nature of CEOSs, many authors have succeeded in developing reliable correlations for up to two BIPs in the model mixing rules. These correlations have limited range, but as suggested by Coutinho et al. [105] and Jaubert et al. [112], BIPs have a definite temperature dependence and theoretical basis.

Due to their flexibility and reliability, the CEOSs have become established as the classical high-pressure models. Their simplicity is also a great advantage for SFE applications, since phase calculations struggle to converge approaching the critical point and can become very time consuming for complex models. The CEOSs are therefore deemed an appropriate methodology for application in the design of a SFE process and for conducting the modelling for this study.

Stellenbosch University https://scholar.sun.ac.za

5. MODELLING METHODOLOGY

The first 3 project objectives, as stated in Section 1.3 were achieved in Chapters 2 – 4, culminating in the following selections for conducting the modelling for this study:

- The solutes considered are the n-alkanes, 1-acohols, carboxylic acids and methyl esters for carbon numbers greater than 10.
- The solvents considered are ethane and propane.
- In order to an avoid infeasible specifications and assure convergence, the high-pressure VLE data of these binary systems are to be modelled by gradually stepping in liquid composition X, from the pure solute (low pressure) towards the pure solvent using a simple bubble point pressure calculation.
- The semi-empirical thermodynamic modelling approach to be used is the simple cubic equations of state (CEOSs).

Having made these selections, the methodology for reaching the modelling objectives 4 to 8 can now be presented in greater detail.

Objective4) : Pure component properties

Objective 4 is investigated in Chapter 6, which considers the following important factors in applying the CEOSs for modellingthe pure component vapour pressure and saturated liquid volume:

- Use of a 2 or 3 parameter model in the volume dependence
- Use of a 1 or 2 parameter alpha function in the temperature dependence
- The effect of using an estimation method for the required pure constants, namely T_c, P_c and acentric factor ω
- The applicability of published correlations in terms of the acentric factor, ω, for alpha function and other pure component parameters for components of interest

The choice of models, alpha functions and pure constants are further elucidated in Chapter 6. Appropriate pure component parameters are also to be obtained in this chapter.

Objective 5) : Results from a commercial process simulator

Objective number 5 is investigated in Chapter 7 by modelling the high pressure binary VLE of the n-alkane, 1-alcohol, methyl ester and carboxylic acid homologous series in ethane at

Stellenbosch University https://scholar.sun.ac.za

352 K, as well as the n-alkane, 1-alcohol and carboxylic acid series in propane at 408 K using property models from Aspen Plus ®. 5 CEOs which emanate from the PR and SRK EOS are investigated with different alpha functions and mixing rules. Various regression cases are formulated, incorporating up to 3 binary interaction parameters (BIPs) in the model mixing rules for correlating the binary VLE data.

Objective 6) : Investigate trends in BIPs with solute carbon number

In order to meet objective 6, the BIPs obtained from the various regression cases in Chapter 7 using Aspen Plus ® are plotted as a function of solute carbon number to see if trends exist for developing generalized correlations. Chapter 9 also investigates the influence of using a different combining rule in the Van der Waals quadratic mixing rules on the BIP vs. carbon number trends.

Objective 7) : Important factors in modelling the high pressure VLE

In order to meet objective 7, Chapter 8 investigates important factors for modelling the high-pressure VLE of asymmetric binaries using CEOSs through a factorial design of experiments (DOE) sensitivity analysis, conducted using STATISTICA 12 software and using ethane as solvent. The design is a 2 level factorial with 6 factors, amounting to 64 treatments (modelling combinations) to assess the effects and interactions amongst the considered factors. The first four factors are *model dependent*, including:

- Temperature dependence of the model (1 or 2 parameter alpha function)
- Volume dependence of the model (2 or 3 parameter model)
- Pure component constants used (Data or estimation method)
- Mixing rules used (classic Van der Waals or G_{ex}/EOS mixing rule)

The last two factors are *system dependent*:

- Temperature range (lower and higher temperature)
- Solute functional group (non-polar and polar)

The factors are assessed based on their effect on a *response variable*, defined as the average errors (%AAD) in bubble pressure and vapour composition of both components. The different factor *levels* chosen for this investigation are elucidated in Chapter 8.

Stellenbosch University https://scholar.sun.ac.za

Objective 8) : Effect of different computation techniques on the final results

Objective 8 is investigated in chapter 9 by comparing the correlation of the high-pressure VLE of the n-alkane, 1-alcohol, methyl ester and carboxylic acid homologous series in ethane at 352 K, as well as the n-alkane, 1-alcohol and carboxylic acid series in propane at 408 K, using two computational techniques, namely the Aspen Plus ® data regression routine and self-developed MATLAB software, but using the same model in both cases. The chosen model and details of the different computational techniques are given in Chapter 9.

The conclusions, recommendations and contributions from this study are presented in chapters 10 and 11.

Stellenbosch University https://scholar.sun.ac.za

6. PURE COMPONENTS

The primary aim of this project is thermodynamic modelling of the high-pressure VLE of asymmetric binary mixtures, however the pure component limit of a thermodynamic model is both of practical interest and fundamental to its theoretical framework. The aim of this chapter is to determine the capabilities of the cubic equations of state (CEOSs) in representing the vapour pressure and saturated liquid volume for the n-alkane, 1-alcohol, carboxylic acid and methyl ester series and to fit reliable model parameters to these properties.

The flexibility of the CEOSs provides different options with respect to the pure component model, which lead to a number of factors to be considered for any particular application. The following factors in applying the CEOSs for the components considered in this chapter are investigated:

- Use of a 2 or 3 parameter model in the volume dependence
- Use of a 1 or 2 parameter alpha function in the temperature dependence
- The effect of using an estimation method for the required pure constants, namely T_c, P_c and acentric factor ω
- The applicability of published correlations (alpha function and other pure component parameters in terms of the acentric factor, ω) for the components of interest

The models considered are the popular Peng-Robinson (PR), Soave-Redlich-Kwong (SRK) and Patel-Teja (PT) EOS. Three alpha functions are considered, namely the Soave, Stryjek-Vera and Mathias alpha functions. Two sources for the pure constants were incorporated, namely values from the DIPPR database and from the group contribution method of Constantinou and Gani (C&G).

6.1 Thermodynamic theory: Phase equilibrium for a pure component

For a closed system with an arbitrary number of components and phases in which the temperature and pressure are uniform, the following expression for the Gibbs free energy (G) can be derived from the 1st and 2nd law of thermodynamics:

$$dG^t + S^t dT - V^t dP \leq 0 \qquad 6\text{-}1$$

The equality holds for a reversible process, and the inequality for an irreversible process. The superscript t refers to the total bulk value of the property. At constant pressure and

Stellenbosch University https://scholar.sun.ac.za

temperature, which are necessary conditions for phase equilibrium, the condition is simplified as follows:

$$(dG^t)_{P.T} \leq 0 \qquad 6\text{-}2$$

This equation states that at constant temperature and pressure, any natural irreversible process proceeds in such a direction that the total Gibbs energy of a closed system decreases, reaching a minimum value at equilibrium. The Gibbs energy is thus the only fundamental energy function that does not change with a phase transition [200].From Equation 6-1 the following general expression is obtained for the pressure dependence of the Gibbs energy at constant temperature for a pure component i.

$$d(G_i) = V_i dP \qquad 6\text{-}3$$

The equality for a reversible process can be enforced because the Gibbs energy and its natural variables are state properties, and do not depend on the process path. Writing this equation for an ideal gas yields:

$$d\left(G_i{}^{ig}\right) = \frac{RT}{P} dP = RTd(\ln P) \qquad 6\text{-}4$$

This equation has some undesirable mathematical properties, namely that the Gibbs energy goes to negative infinity as the pressure goes to zero. In keeping with the form of equation 6-4, G.N. Lewis proposed the following expression for the change in Gibbs energy, which defines the fugacity, f [46]:

$$d(G_i) = RTd(\ln f_i) \qquad 6\text{-}5$$

By integrating Equations 6-4 and 6-5 and subtracting one from the other, the following expression can be obtained for a pure species i in any phase at any condition [48]:

$$\frac{\left(G_i - G_i{}^{ig}\right)}{RT} = \ln\left(\frac{f_i}{P}\right) = \ln(\varphi_i) \qquad 6\text{-}6$$

$G_i - G_i{}^{ig}$ is, by definition, the residual Gibbs energy $G^R{}_i$ and the dimensionless ratio $f_i/P$is defined as the *pure component fugacity coefficient,* for a pure speciesφ_i. The following low pressure limit is enforced to complete the definition of the fugacity:

$$\lim_{P\to 0}\left(\frac{f_i}{P}\right) \equiv 1 \qquad 6\text{-}7$$

Stellenbosch University https://scholar.sun.ac.za

It can be seen from Equation 6-6, that the denominator for the pure component fugacity coefficient, which is by definition the *fugacity for an ideal gas*, is simply equal to the system pressure, P. At the low-pressure, ideal gas limit $G^R{}_i = 0$ and $\varphi_i = 1$. If one finally considers a closed system in vapour/liquid equilibrium, in which mass transfer may occur between the phases, it can be seen from Equation 6-2 that the total Gibbs free energy is zero at constant temperature and pressure and internal changes in Gibbs energy of each phase due to mass transfer must therefore be equal:

$$d\left(G_i^L\right)_{T,P'} = d\left(G_i^V\right)_{T,P} \qquad 6\text{-}8$$

By substituting Equation 6-5 into 6-8, a condition for the vapour/liquid equilibrium of a pure species may be derived in terms of fugacity:

$$\ln f_i^L = \ln f_i^V \qquad 6\text{-}9$$

Since the pressure is constant at equilibrium, the following equivalent criterion is often used, since the *fugacity coefficient* can be obtained from an equation of state using Equation 6-6:

$$\ln\left(\varphi_i^L\right) = \ln\left(\varphi_i^V\right) \qquad 6\text{-}10$$

The only requirement for solving Equation 6-10 and obtaining the equilibrium properties of a pure component is an expression for the residual Gibbs energy from an EOS to be used in Equation 6-6 for each phase. This can be problematic because the natural independent variables for the Gibbs energy are T and P, but most EOSs are pressure explicit in terms of T and V. For this reason it is preferable to work in terms of the residual Helmholtz energy, which has natural variables of T and V, corresponding to those of an EOS. The residual Helmholtz energy can be obtained directly from an EOS by solving the following integral:

$$\frac{A_i^R}{RT} = \frac{\left(A_i - A_i{}^{ig}\right)}{RT} = \int_0^\rho \frac{Z-1}{\rho}\, d\rho = \int_0^{b\rho} \frac{Z-1}{b\rho}\, db\rho \qquad 6\text{-}11$$

The pure component fugacity coefficient can be calculated by the following expression [48]:

$$\ln\varphi_i = \frac{A_i^R}{RT} - \ln Z + Z - 1 \qquad 6\text{-}12$$

The phase of the fugacity coefficient is determined by the corresponding root for Z, as obtained from the EOS. Solving for the roots of a CEOS is discussed in Appendix B.1.

Stellenbosch University https://scholar.sun.ac.za

6.2 Models investigated

The pure component models chosen for this chapter are the widely used Peng-Robinson (PR) [79], the Patel-Teja (PT) [83] and the Soave-Redlich-Kwong (SRK) [89] EOS.

PR EOS: $$P = \frac{RT}{v-b} - \frac{a}{v(v+b)+b(v-b)} \quad 6\text{-}13$$

PT EOS: $$P = \frac{RT}{v-b} - \frac{a}{v(v+b)+c(v-b)} \quad 6\text{-}14$$

SRK EOS: $$P = \frac{RT}{v-b} - \frac{a}{v(v+b)} \quad 6\text{-}15$$

As discussed in Section 4.2, the energy parameter, a, is typically deconstructed into a constant scaled to the critical point and a temperature dependent alpha function, correlated in terms of the acentric factor, ω:

$$a = a_c(T_c, P_c)\alpha(T_r, \omega) \quad 6\text{-}16$$

Equations for obtaining a_c, b and c (see equations 6-13 to 6-15) in terms of the critical properties (including the empirical critical compressibility factor ξ_c for the Patel-Teja model) are provided in Appendix A.1. Three different alpha functions were applied to each model, namely the Soave [89], Stryjek-Vera (SV) [94] and Mathias (M) [92] alpha function:

Soave:

$$\alpha(T_r) = \left(1 + m\left(1 - \sqrt{T_r}\right)\right)^2 \quad 6\text{-}17$$

Stryjek-Vera:

$$\alpha(T_r) = \left(1 + m\left(1 - \sqrt{T_r}\right)\right)^2 \quad 6\text{-}18$$

$$m = k_o + k_1(1 + \sqrt{T_r})(0.7 - T_r) \quad 6\text{-}19$$

Mathias:

$$\alpha(T_r) = \left(1 + m\left(1 - \sqrt{T_r}\right) - p(1 - T_r)(0.7 - T_r)\right)^2 \quad 6\text{-}20$$

Stellenbosch University https://scholar.sun.ac.za

Appendix A.1 contains all the required mathematical expressions for calculating the pure component fugacity from Equations 6-11 and 6-12 analytically using these EOSs. The fugacity expressions are given in Appendix A.3

6.3 Reduction of data

An algorithm for calculating pure component vapour pressure and saturated liquid molar volume using an EOS is presented in Appendix B.2. The procedure involves finding the pressure at which the fugacity coefficient of a component in the vapour and liquid are equal (Equation 6-10), for a given temperature. The saturation densities are obtained from the roots of the equation where equality of fugacities is satisfied. The correlation between the property values from experiment and model can further be improved by regressing empirical model parameters to data. The following objective function was used in this study:

$$F = W_1 \sum_{i=1}^{np} \left[\frac{(P_{sat,i}^{exp} - P_{sat,i}^{calc})^2}{(P_{sat,i}^{exp})^2} \right]^{0.5} + W_2 \sum_{i=1}^{np} \left[\frac{(\rho_{sat\,liq.,i}^{exp} - \rho_{sat.liq,i}^{calc})^2}{(\rho_{sat.liq,i}^{exp})^2} \right]^{0.5} \qquad 6\text{-}21$$

The regression weights W_1 and W_2 for vapour pressure (P_{sat}) and saturated liquid density ($\rho_{sat\,liq.}$) respectively, were set to the following values for each EOS:

Table 6-1 Regression weights for each model

Model	W_1	W_2
PR	1	0
PT	0.8	0.2
SRK	1	0

For the PR and SRK models, alpha function parameters were fitted only to the vapour pressure, but saturated liquid density was included for the PT model because of the additional pure parameter, which allows for incorporating an empirical critical compressibility factor in the regression for better liquid volume correlations.

Both the saturation pressure and regressed parameters were obtained iteratively using the *fsolve* function in MATLAB, which uses the Levenberg-Marquardt non-linear least squares algorithm. This objective function with the weights as in Table 6-1, were applied with success by Forero and Velasquez [201]. Parameters were fitted to DIPPR correlations for 30 data points in the *reduced temperature* range of 0.5 to 0.9.

Stellenbosch University https://scholar.sun.ac.za

6.4 Pure component constants

The input information required for application of a CEOS are T_c, P_c and the acentric factor ω, as well as any additional empirical parameters fitted to data. Obtaining reliable values for the critical constants from experiment is often not possible for long hydrocarbon-chains, because the molecules thermally decompose before reaching the critical temperature [38]. Estimation methods are therefore often used to obtain *pseudo-critical* properties from correlations based on the molecular structure. Poling et al. [38] provide a good review of selected methods in chapter 2 of their book.

One such method is the group contribution method of Constantinou and Gani (C&G) [202]. Figure 6-1 shows the % deviation between pure constants obtained from the C&G method and those from the DIPPR databank, up to carbon number of 36 for the n-alkanes, 20 for the 1-alcohols and carboxylic acids and 10, 12, 16, 18 and 20 for the methyl esters.

The % deviation is calculated as follows:

$$\% \text{ Deviation} = \left|\frac{C_{DIPPR} - C_{C\&G}}{C_{DIPPR}}\right| \text{x } 100 \qquad 6\text{-}22$$

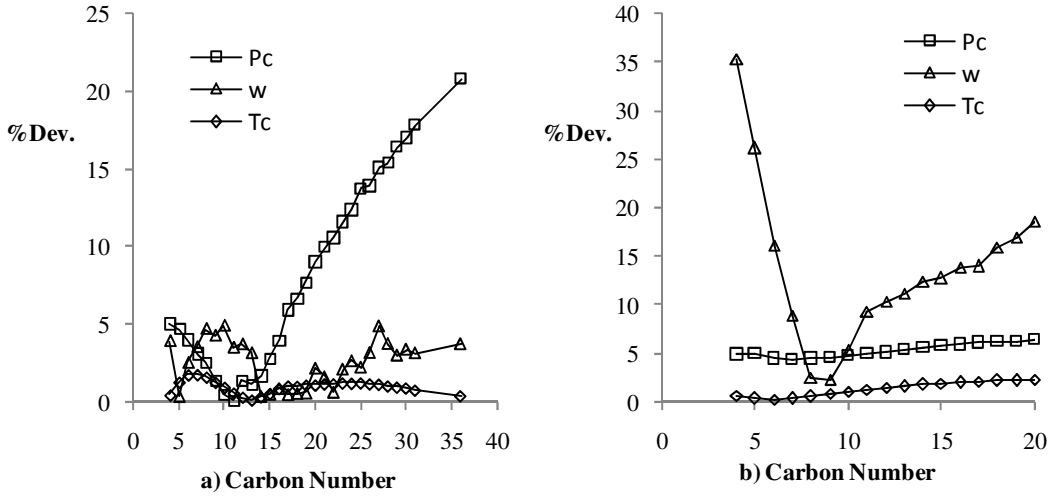

Stellenbosch University https://scholar.sun.ac.za

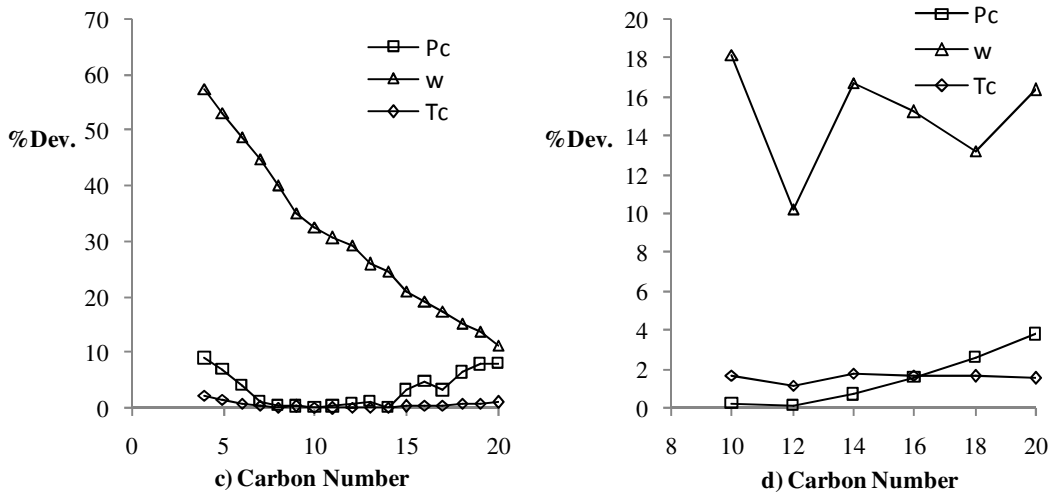

Figure 6-1 Percent deviation in T_c, P_c and ω between the Constantinou & Gani group contribution method and values from DIPPR for the a) n-alkane, b) 1-alcohol, c) carboxylic acids and d) methyl ester homologous series

The method of C&G provides a good estimation of T_c, P_c and ω for the n-alkanes (Figure 6-1 a)) with deviations below 5% up to a carbon number of about 15. For larger molecules, the errors in P_c increase sharply in a somewhat linear manner reaching 20% at carbon number of 36. Very good representation of T_c is seen over the whole carbon number range, with errors also remaining below 5 % for the acentric factor.

For the other systems (Figure 6-1 b) – d)), reasonable representation is given of P_c and T_c with errors typically below 5% for the whole carbon number range. The acentric factor is represented much worse, except for the 1-alcohols with carbon number 8, 9 and 10 where errors are below 5%. The error in acentric factor for the acids decreases more or less linearly from 60% to 10 % from carbon number 5 to 20, suggesting that the method struggles to account for the effect of the polar functional group on vapour pressure, which is more pronounced for lower carbon numbers.

The sensitivity of regressed model parameters to different pure constants is subsequently compared, as well as the effect on errors in vapour pressure and saturated liquid volumewhen a different source of pure constants (C&G) is used than those for which parameters were regressed (DIPPR). The numeric values of these constants for all components investigated, as well as the group parameters and correlations for the C&G method are given in Appendix C.

Stellenbosch University https://scholar.sun.ac.za

6.5 Obtaining model parameters

The Soave alpha function is a one parameter (m) alpha function, while the SV and M alpha functions have an additional empirical parameter (k_1 and p respectively), but both reduce to the Soave alpha function upon setting the additional parameter to zero. These additional parameters can thus be seen as a correction to the simpler Soave function and are totally empirical. They are meant to improve the correlation of vapour pressures for more polar systems.

6.5.1 Primary Soave parameter

The *primary* Soave parameter has similar functionality in all three alpha functions and is often correlated in terms of the acentric factor. This correlation is unique to the specific model/alpha function combination. Table 6-2 contains widely used correlations from literature:

Table 6-2 Literature correlations for the *primary (Soave)* alpha function parameter

Alpha function	EOS	Ref	Parameter Correlation
Soave	PR	[79]	$m = -0.37464 + 1.54226\omega - 0.26992\omega^2$
	PT	[83]	$m = 0.452413 + 1.30982\omega - 0.295937\omega^2$
	SRK	[89]	$m = -0.480 + 1.574\omega - 0.17\omega^2$
SV	PR	[94]	$k_o = 0.378893 + 1.4897153\omega - 0.17131848\omega^2 + 0.0196554\omega^3$
M	SRK	[92]	$m = -0.48508 + 1.55191\omega - 0.15613\omega^2$

As noted in Section 4.2, Soave fitted the m correlation in Table 6-2 at T_r =0.7, for acentric factors up 0.5, which corresponds to an n-alkane of carbon number 10. Peng and Robinson [79] incorporated a similar carbon number range, but for temperatures from the normal boiling point to the critical temperature. Patel and Teja [83] used data up to carbon number of 20 and Stryjek and Vera [94] up to 18 for correlating their alpha function. The correlation of Mathias was also fit to a larger data set than covered by the original method of Soave [89].

Given the range of data used in fitting these correlations and also the inadequacy of the acentric factor to distinguish between polar molecules (see Appendix D.4.1), the values obtained from these correlations were compared to those regressed to vapour pressure and saturated liquid volumes from DIPPR correlations for the n-alkane, 1-alcohol, carboxylic acid and methyl ester series using the procedure outlined in Section 6.3. The influence of pure constants was also incorporated into the comparison. Table 6-3 defines the cases compared in the figures to follow.

Stellenbosch University https://scholar.sun.ac.za

Table 6-3 Labels for investigating pure component parameter trends with carbon number

Case	Pure constants used	Source of empirical parameters
(1a)	DIPPR (Blue)	Regressed (solid line)
(1b)	DIPPR (Blue)	Literature Correlation (dashed line)
(2a)	C&G (Red)	Regressed (solid line)
(2b)	C&G (Red)	Literature Correlation (dashed line)

Blue represents pure constants from DIPPR and red represents values from the C&G method. A solid line means parameter values were then obtained through regression as outlined in Section 6.3 and a dashed line means the correlations from Table 6-2 were used.

Figure 6-2 compares the values of the Soave alpha function parameter m for the cases given in Table 6-3 for the PR EOS. For the n-alkanes (Figure 6-2 a)) it is seen that the blue (DIPPR) and red (C&G) lines of a given type follow one another quite closely, implying that using pure constants from the C&G method do not dramatically influence the alpha function parameter values, whether obtained from regression (solid line) or correlation (dashed line). At higher carbon numbers (above 20), the correlation (dashed lines) gives different values than obtained from regression (solid lines), which will undoubtedly affect the results adversely.

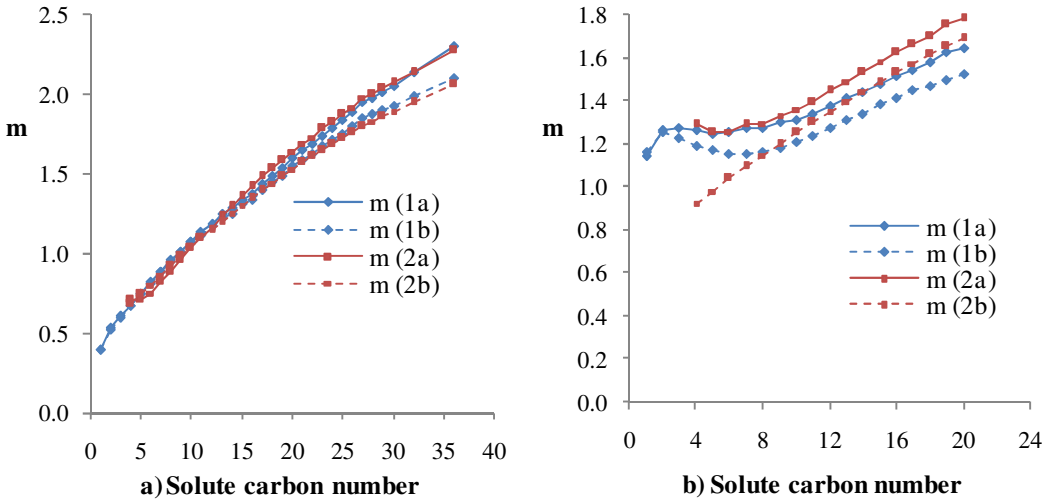

Stellenbosch University https://scholar.sun.ac.za

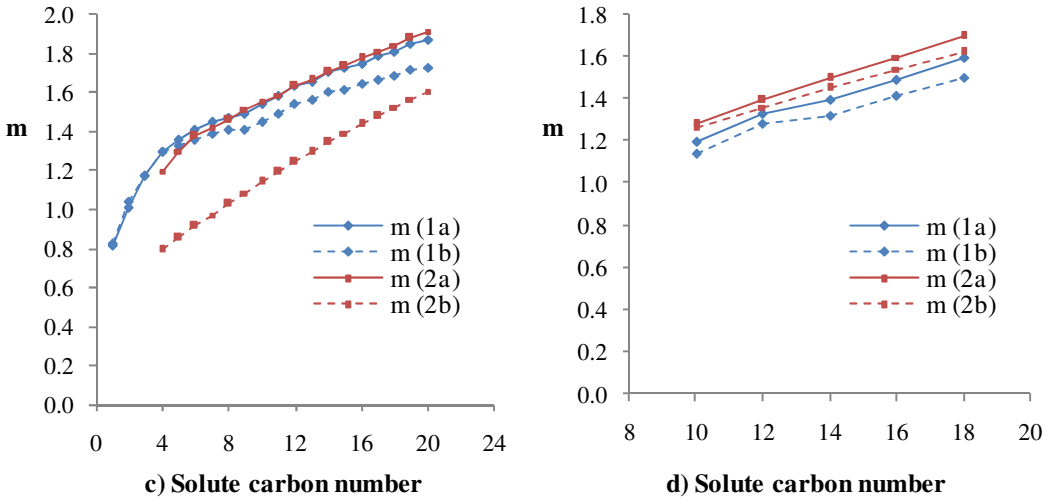

Figure 6-2 Soave alpha-function parameter m vs. carbon number for the a) n-alkanes, b) 1-alcohols, c) carboxylic acids and d) methyl esters in the PR model for cases given in Table 6-3

For the other series, the parameter is quite sensitive to both the pure constants used and whether the parameter is obtained from regression or the literature correlation.

Figure 6-3 shows the same plots but for the primary Soave parameter, k_o, in the SV alpha function, using the PR model.

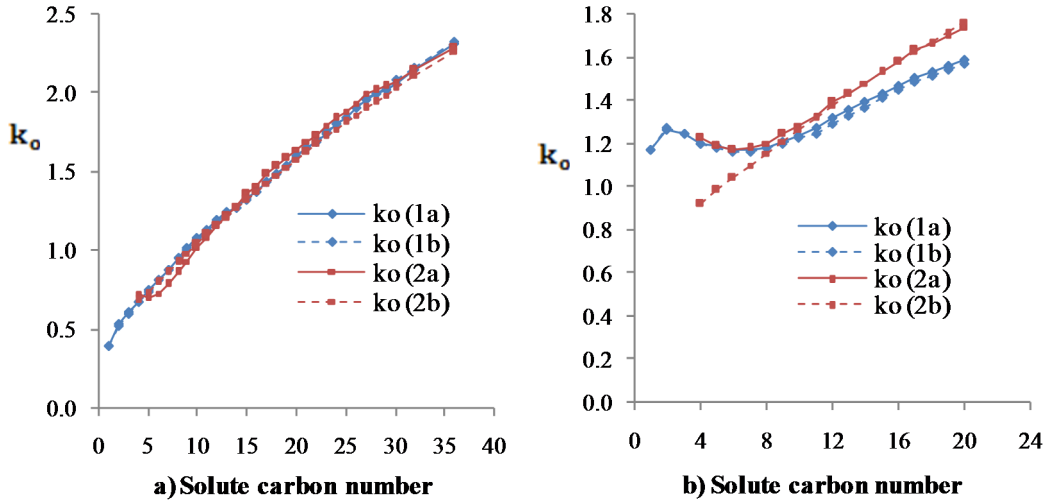

Stellenbosch University https://scholar.sun.ac.za

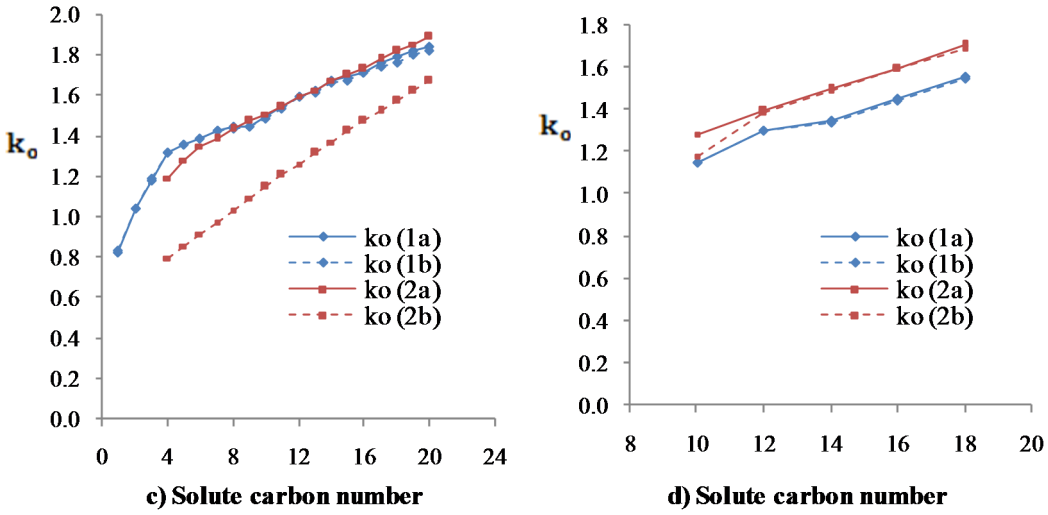

Figure 6-3 Stryjek-Vera alpha-function parameter k_o vs. carbon number for the a) n-alkanes, b) 1-alcohols, c) carboxylic acids and d) methyl esters in the PR model for cases given in Table 6-3

Even though there are expected differences between the blue and red lines (pure constants used), the solid and dashed lines of a given colour follow one another more closely than in Figure 6-2 for all series, meaning that the correlation is more reliable than for the Soave alpha function, since it more closely represents regressed parameter values.

This was found for all cases except where the k_o value was obtained from using the correlation *and* the C&G constants (red-dashed line) for the acids and the 1-alcohols, especially in the lower carbon number range. This can primarily be attributed to the poor representation of the acentric factor by the C&G method for these components, as shown in Figure 6-3 b) and c). In general it seems that incorporating an additional empirical parameter in the alpha function decreases the variability of the primary parameter for different compounds, "stabilizing" its value and making thegeneralized correlation more reliable. This was similarly observed in comparing the value of m from the Soave and Mathias alpha function using the SRK EOS (see Appendix E.3.5).

6.5.2 Empirical critical compressibility of the PT EOS

As discussed in Section 4.2, the PR and SRK EOS are 2 parameter models and predict a constant critical compressibility, Z_c, of 0.307 and 0.333, respectively, which is not in accordance with real fluid behaviour where the value is lower (0.25 – 0.29 for the n-alkanes and often as low as 0.22 – 0.24 for polar compounds) and decreases with increasing molecular mass. The PT EOS is a 3 parameter model, which allows for an adjustable critical

Stellenbosch University https://scholar.sun.ac.za

compressibility, giving it more theoretical credence than the 2 parameter models. As mentioned in Section 4.2, fitting this value to experimental values for Z_c is done at the expense of the correct critical fugacity coefficient [66]. Patel and Teja [83] therefore treated the critical compressibility as an empirical parameter (ξ_c in the original article) and provided the following correlation in terms of the acentric factor

$$\xi_c = 0.329032 - 0.076799\omega + 0.0211947\omega^2 \qquad 6\text{-}23$$

Figure 6-4 gives the values for this parameter for the cases in Table 6-3 :

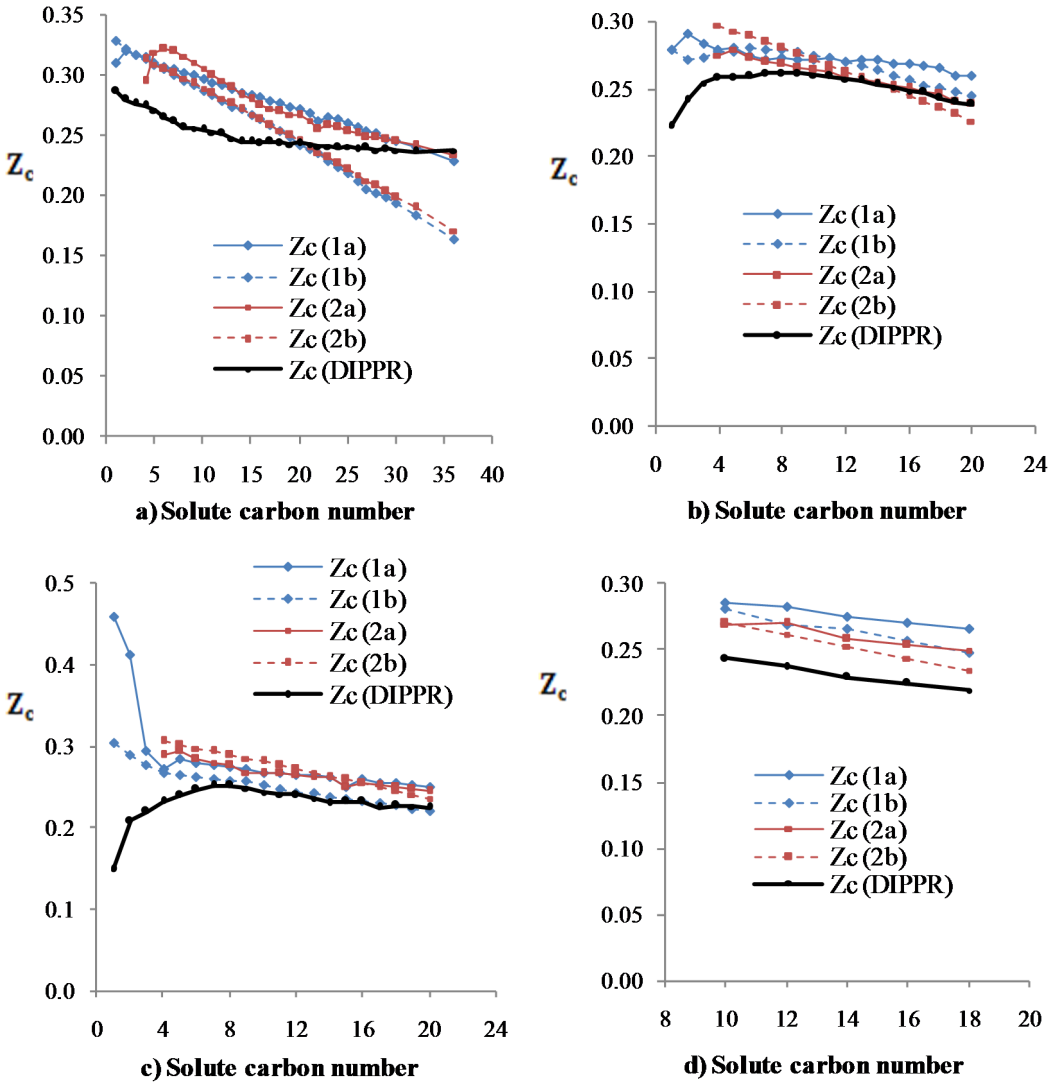

Figure 6-4 Critical compressibility (Z_c) vs. carbon number for the a) n-alkanes, b) 1-alcohols, c) carboxylic acids and d) methyl esters in the PT EOS for cases given in Table 6-3

Stellenbosch University https://scholar.sun.ac.za

The black line represents values for Z_c obtained from DIPPR. As expected, neither values fitted to data (solid lines) nor values from the correlation (dashed lines), corresponds precisely with experimental values (black lines), but trends are similar. For the n-alkanes (Figure 6-4 a)) the values fitted using the regression procedure outlined in Section 6.3 (solid lines) are both qualitatively and quantitatively closer to experimental values and differ quite substantially from those obtained from the Patel-Teja correlation (Equation 6-23). This is probably due to the use of different data, regression procedure and objective function. For the other series, the value for Z_c is again found to be sensitive to the pure constants used and whether values are obtained from the literature correlation or fitted to data.

6.5.3 Additional empirical alpha function parameters

The additional empirical parameters of the SV and M alpha functions are k_1 and p, respectively and were included in the regression procedure outlined in section 6.3 in using these alpha functions. These parameters are pure empirical with no clear trend with carbon number. The plots for all empirical parameters vs. carbon number not given in the preceding discussion are given in Appendix E.3.5.

Given the deviations of parameter values obtained from the literature correlations to those obtained from regression, especially for long-chain and polar molecules, it was decided to obtain all pure parameters used in this and subsequent chapters through regression in order to compare all models on an equal footing.

6.6 Vapour pressure and saturated liquid volume results

Table 6-4 gives cases for evaluating the effect of using different alpha functions and pure constants for the PR, PT and SRK EOSs on the correlation of vapour pressure and saturated liquid volume.

Table 6-4 Cases for evaluating the relationship between pure constants (Tc, Pc, w) and alpha function parameters used in determining vapour pressure and saturated liquid volume

		Pure constants used for:	
Case	Colour	Parameter regression	Property evaluation
1	Blue	DIPPR	DIPPR
2	Red	DIPPR	C&G
3	Green	C&G	C&G

Stellenbosch University https://scholar.sun.ac.za

The cases are defined in order to assess the effect of using a different set of constants than those with which parameters are regressed. For case 1 (blue), pure constants from DIPPR were used both in fitting parameters and calculating the correlation errors. Case 2 (red) involves using the alpha parameters determined from case 1 (regressed with DIPPR constants), but using pure constants from the C&G method for subsequently calculating the errors in property values. Case 3 (green) involves using the C&G constants for both fitting alpha parameters and determining the errors. These cases were applied for the n-alkanes, 1-alcohol, carboxylic acid and methyl ester series, for each model using all three alpha functions.

6.6.1 n-Alkanes

Figure 6-5 shows the %AAD in vapour pressure and saturated liquid volume for the n-alkane series up to carbon number of 36 for each case in Table 6-4, using the PR model with each alpha function. The %AAD is calculated as follows for a given property (defined as "Val"):

$$\%AAD = \frac{1}{N}\sum_{i=1}^{N}\left|\frac{Val_{exp} - Val_{calc}}{Val_{exp}}\right| \text{ x } 100 \qquad 6\text{-}24$$

It is clear from Figure 6-5 a), that using constants from the C&G method with parameters regressed using the DIPPR constants (red bars) introduces large errors in the vapour pressure, exceeding 10% for all components except for carbon numbers 11 to 15, where it is also seen from
Figure 6-1 a) that the errors between the C&G and DIPPR constants, especially the critical pressure, are lowest.

The errors in vapour pressure are largely reduced upon subsequently fitting the empirical alpha function parameters to data (green bars). For carbon numbers below 15, the 2 parameter alpha functions (SV and M) further give smaller errors (below 2%) than the Soave alpha function (around 5% AAD) for this case, suggesting that if an estimation method is used for the pure constants, then 2 or more parameters in the alpha function may be required in order to keep errors in vapour pressure below 5 %. For carbon numbers above 20 use of the C&G constants (green bars) seem to show slightly improved performance over the use of the DIPPR constants (blue bars), however errors approach 10% for carbon numbers above 30, irrespective of the pure constants used.

Stellenbosch University https://scholar.sun.ac.za

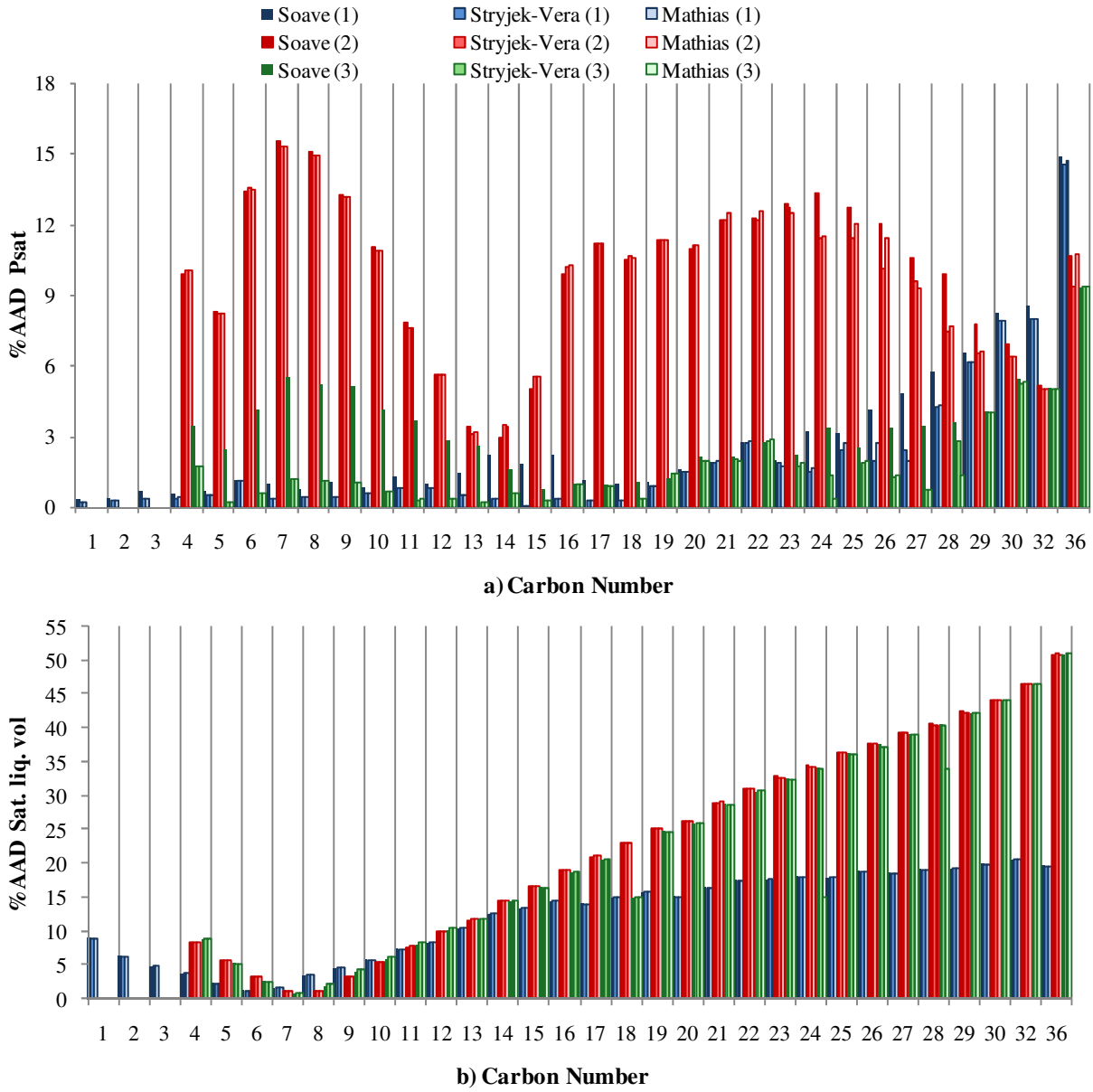

Figure 6-5 %AAD in a) vapour pressure and b) saturated liquid volume for the n-alkane series with the PR EOS using the Soave, Stryjek-Vera and Mathias alpha function for cases 1 (blue) ,2 (red) and 3 (green) as given in Table 6-4

Figure 6-5 b) shows the errors in saturated liquid volume for the same cases. It is seen that the type of alpha function has virtually no effect on the saturated liquid volume. The smallest %AAD is generally observed in using the DIPPR constants (blue bars), however errors still begin to exceed 5% for carbon number above 10 and increases gradually, approaching 15% at carbon number of 15. This shows the fundamental limitation of the PR model for modelling the liquid volume of chained molecules.

Stellenbosch University https://scholar.sun.ac.za

Similar plots to those in Figure 6-5 are constructed for the PT and SRK EOS, as well as for the other series, and are provided in Appendix E.3. For the remainder of this discussion only the average %AAD over the whole carbon number range for each series will be presented in order to allow for a more direct model comparison.

Figure 6-6 gives the average %AAD in vapour pressure and saturated liquid volume (from Figure 6-5) for the PR, SRK and PT models with each alpha function, over the whole carbon number range:

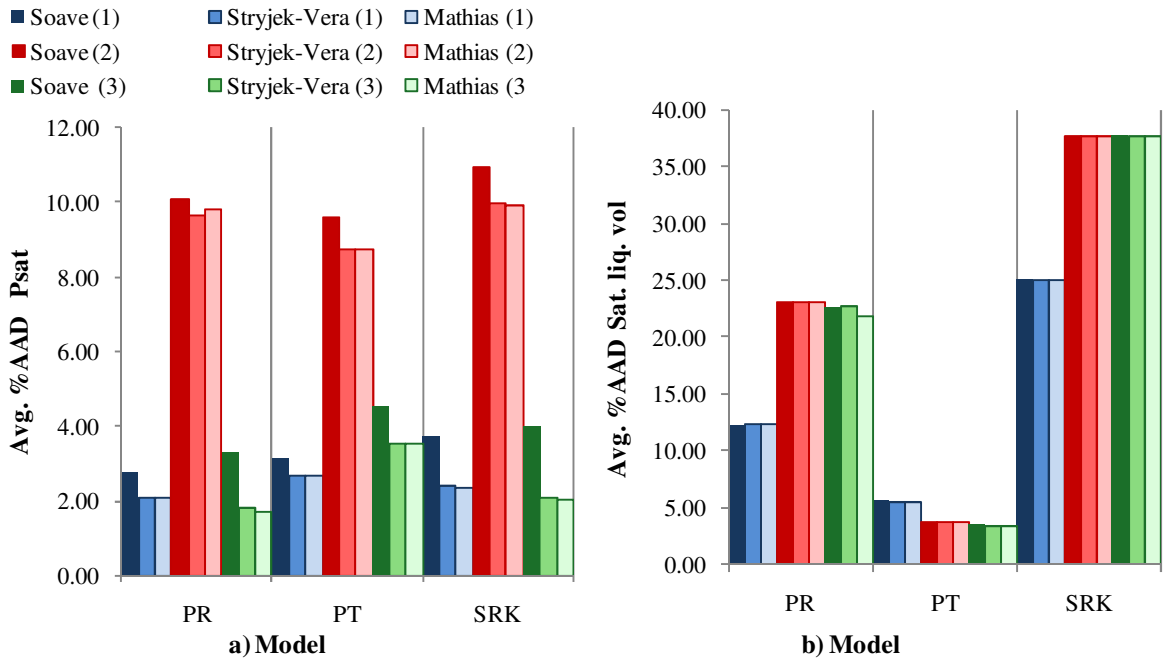

Figure 6-6 Avg. %AAD for a) vapour pressure and b) saturated liquid volume over carbon number range 1 – 36 for the n-alkane seriesfor cases 1 (blue) ,2 (red) and 3 (green) as given in Table 6-4 for the PR, PT and SRK EOS with the Soave, SV and M alpha function

It is seen that an additional alpha function parameter gives on average 1 to 2 % smaller errors in vapour pressure than the Soave function, with no clear advantage between the SV and M alpha functions. The PT EOS generally gives slightly higher errors in vapour pressure than the PR and SRK EOS, but considerably lower errors in saturated liquid volume (below 5 %), which can be attributed to the 3rd parameter in the volume dependence and the adjustable critical compressibility. The SRK EOS gives the largest errors in saturated liquid volume, implying that it struggles most with the chain structure and large size of the molecules.

Stellenbosch University https://scholar.sun.ac.za

Even though Figure 6-5 gives the %AAD over the whole carbon number range, it does not say whether the model over- or under-predicts the data. In order to get an impression of the qualitative representation of these saturation properties by the models, Figure 6-7 gives the fits obtained for carbon numbers 5, 10, 15 and 20 using the PR and PT EOS with the Soave and SV alpha functions.

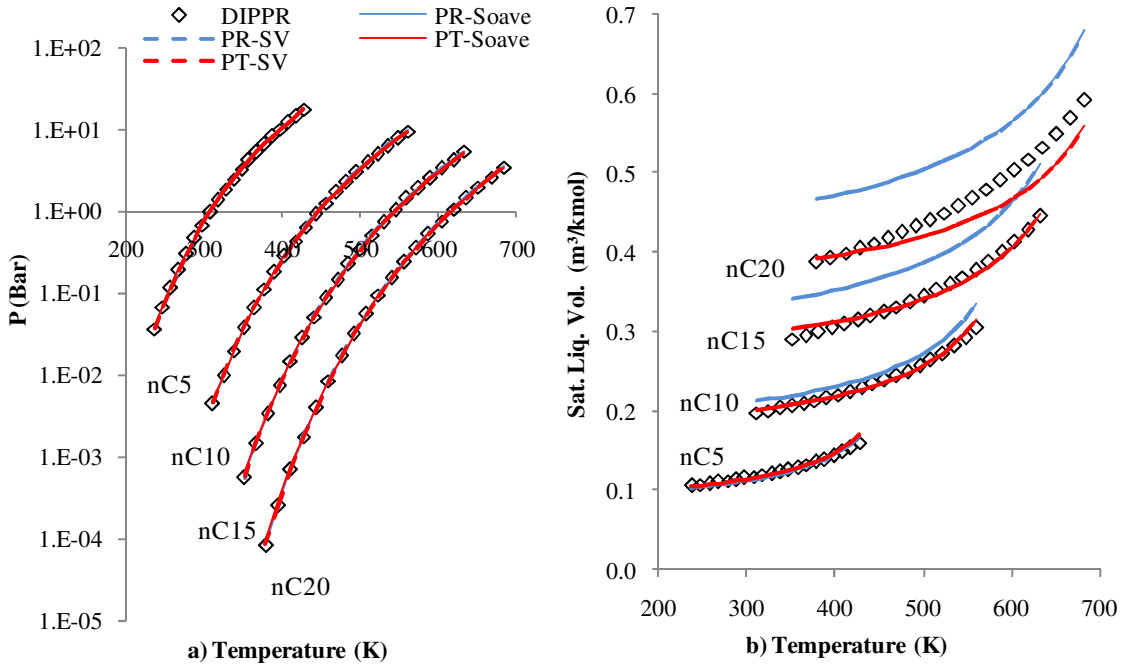

Figure 6-7 Model fits for a) vapour pressure and b) saturated liquid volume of the n-alkanes with carbon number 5, 10, 15 and 20 using the PR and PT EOS with the Soave and SV alpha functions

Table 6-5 gives the %AAD for each of the model fits in Figure 6-7.

Table 6-5 %AAD for the model fits for the n-alkanes fromFigure 6-7

%AAD								
Model:	PR-Soave		PR-SV		PT-Soave		PT-SV	
CN	P_{sat}	Sat. Liq. Vol.	P_{sat}	Sat. Liq. Vol.	P_{sat}	Sat. Liq. Vol.	P_{sat}	Sat. Liq. Vol.
5	0.66	2.42	0.53	2.43	0.6	1.83	0.58	1.85
10	0.82	5.89	0.56	5.94	1.58	1.13	1.24	1.14
15	1.92	13.46	0.17	13.58	4.21	1.6	3.48	1.56
20	1.66	15.24	1.58	15.23	3.28	4.33	2.27	4.3

Both the PR and PT EOS give good representation of the vapour pressure (errors generally below 3 %AAD), but the PR EOS begins to over-predict the saturated liquid data at carbon

Stellenbosch University https://scholar.sun.ac.za

numbers above 10. The PT EOS gives good representation of the saturated liquid volume, but as seen in Figure 6-7 b), under-predicts the data at carbon numbers above 15, especially at higher temperatures. The PT EOS clearly provides the best overall performance for the n-alkane series.

6.6.2 1-Alcohols

Figure 6-8gives the average %AAD in vapour pressure and saturated liquid volume for the PR, SRK and PT models with each alpha function for the 1-alchols of carbon number 1 – 20.

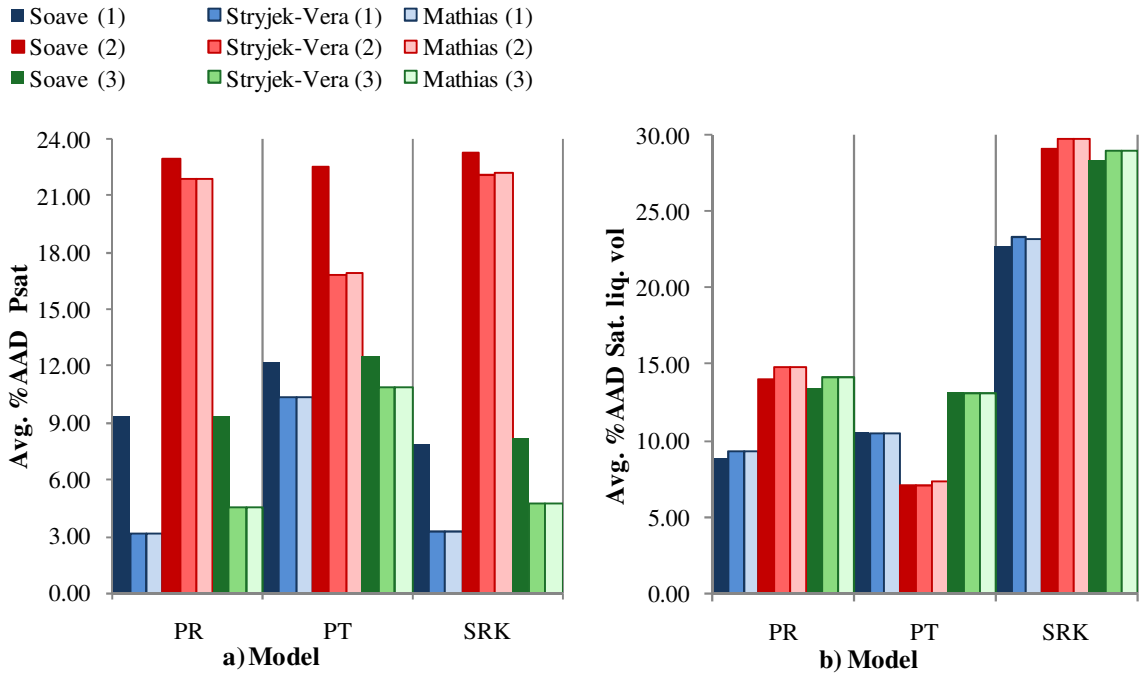

Figure 6-8 Avg. %AAD for a) vapour pressure and b) saturated liquid volume over carbon number range 1 – 20 for the 1-alcohol seriesfor cases 1 (blue) ,2 (red) and 3 (green) as given in Table 6-4 for the PR, PT and SRK EOS with the Soave, SV and M alpha function

The extra alpha function parameter of the SV and M alpha functions has negligible effect on saturated liquid volume, but gives up to 6 % smaller errors in vapour pressure (see PR and SRK EOS) than the Soave function, which is a greater improvement than observed for the non-polar n-alkanes in Figure 6-6 a). However errors are still slightly larger than for the n-alkanes. There is nothing to choose between the SV and M alpha functions.

Stellenbosch University https://scholar.sun.ac.za

In comparing the blue bars (DIPPR constants used) it can be seen that the PT EOS has substantially larger errors in vapour pressure (around 10%) than both PR and SRK (around 3 % using the SV and M alpha functions), but unlike the case for the n-alkanes, does not necessarily give improved performance for the saturated liquid volume. SRK still gives the largest average errors in saturated liquid volume (above 20%).

Figure 6-9 gives the model fits for carbon numbers 5, 10, 15 and 20 using the PR and PT EOS with the Soave and SV alpha functions.

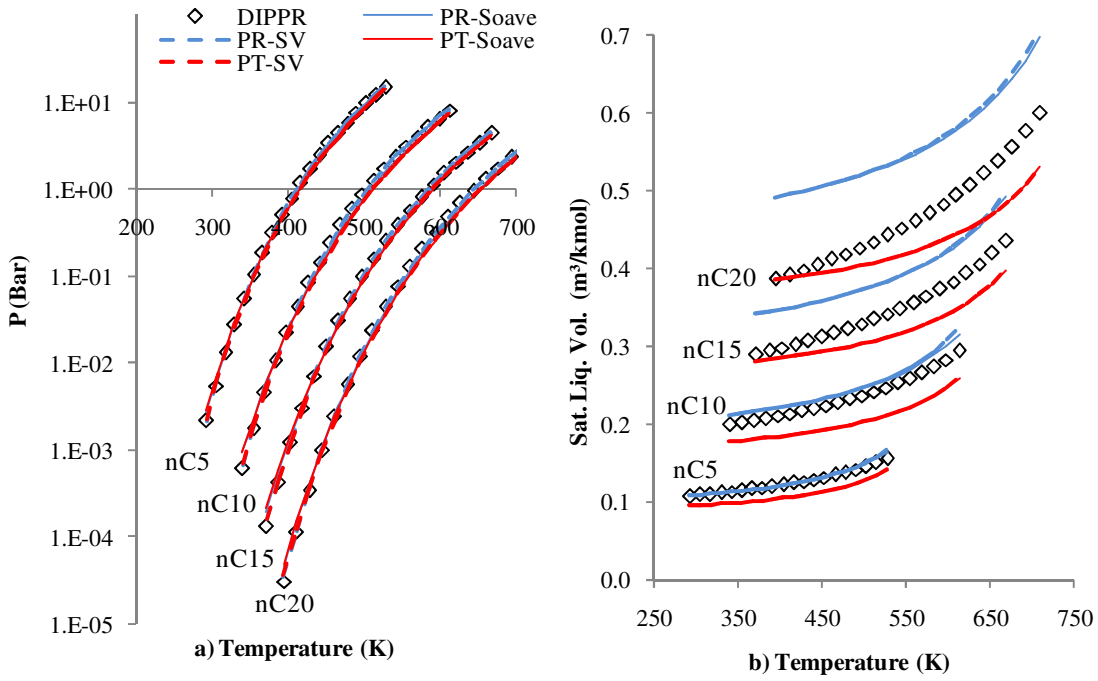

Figure 6-9 Model fits for a) vapour pressure and b) saturated liquid volume of the 1-alcohols with carbon number 5, 10, 15 and 20 using the PR (red) and PT EOS (blue) with the Soave (solid line) and SV (dashed line) alpha functions

Table 6-6 gives the %AAD for each of the model fits in Figure 6-9.

Table 6-6 %AAD for the model fits for the 1-alcohols from Figure 6-5

	%AAD							
Model:	PR-Soave		PR-SV		PT-Soave		PT-SV	
CN	P_{sat}	Sat. Liq. Vol.	P_{sat}	Sat. Liq. Vol.	P_{sat}	Sat. Liq. Vol.	P_{sat}	Sat. Liq. Vol.
5	8.75	1.16	0.75	1.47	11.11	12.75	8.81	12.7
10	13.28	4.79	2.83	5.62	16.47	13.26	13.52	13.21
15	10.24	13.25	5.43	13.71	14.03	7.68	10.71	7.64
20	12.29	19.93	3.11	20.46	17.51	7.32	13.87	7.29

Stellenbosch University https://scholar.sun.ac.za

As seen from Table 6-6 (and also Figure 6-8), rather large errors in the vapour pressure (often exceeding 10 % AAD) are encountered for all cases except the PR-SV model. These errors are not prevalent on Figure 6-9, due to using a log scale on the vertical axis, however it is seen that the models capture the general trend in vapour pressure. It is seen from Figure 6-9 b) that the PR EOS provides better saturated liquid volume correlations than the PT EOS for 1-alcohols of carbon number below 10, where the PT EOS under predicts the data. For larger carbon numbers, the PR EOS starts to severely over-predict the data and the fit for the PT EOS improves (especially at lower temperatures), but still under-predicts the data. The PR EOS with SV or M alpha function therefore seems to be the best model for the 1-alcohols with little improvement offered by the 3rd parameter in the PT EOS.

6.6.3 Carboxylic Acids

Figure 6-10gives the average %AAD in vapour pressure and saturated liquid volume for the PR, SRK and PT models with each alpha function for the linear carboxylic acids of carbon number 1 – 20.

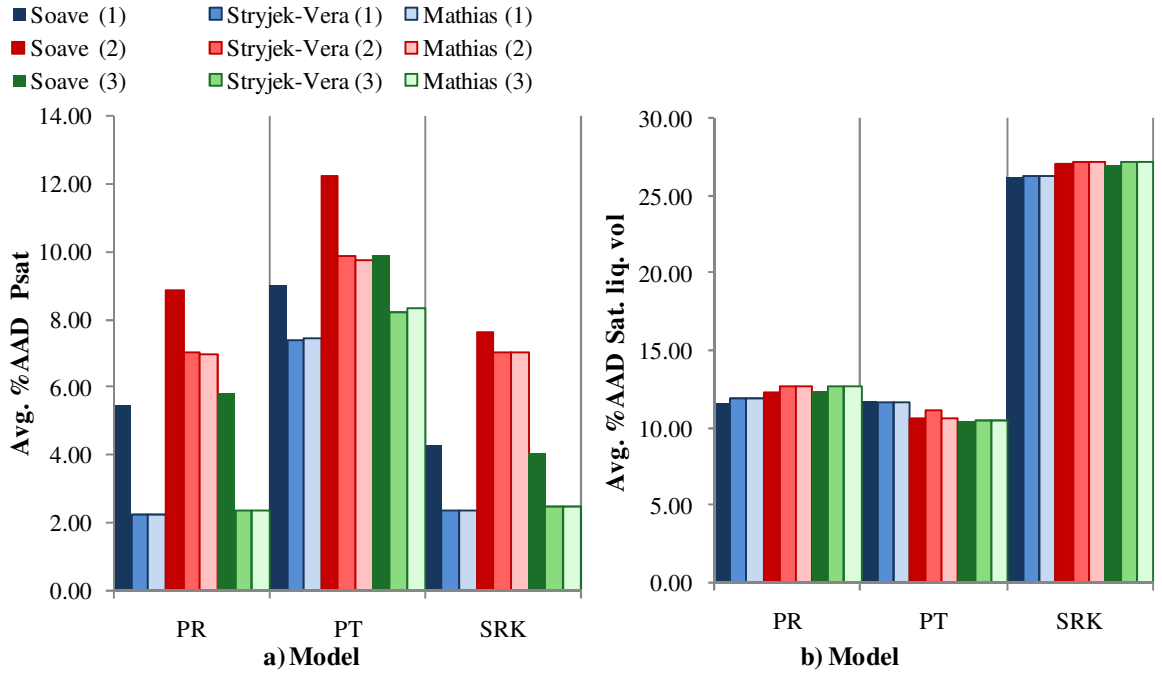

Figure 6-10 Avg. %AAD for a) vapour pressure and b) saturated liquid volume over carbon number range 1 – 20 for the carboxylic acid seriesfor cases 1 (blue) ,2 (red) and 3 (green) as given in Table 6-4 for the PR, PT and SRK EOS with the Soave, SV and M alpha function

Stellenbosch University https://scholar.sun.ac.za

The SV and M alpha functions again show considerable improvement in vapour pressure (up to 4 %) over the Soave function, but negligible effect on the saturated liquid volume. The PT EOS gives slightly better results for saturated liquid volume than the PR EOS, but the substantially larger errors in vapour pressure than both PR and SRK EOS (approaching 8 % AAD) again make the PR EOS the best overall choice in modelling these properties for the carboxylic acids.

Figure 6-11 gives the model fits for carbon numbers 5, 10, 15 and 20 using the PR and PT EOS with the Soave and SV alpha functions.

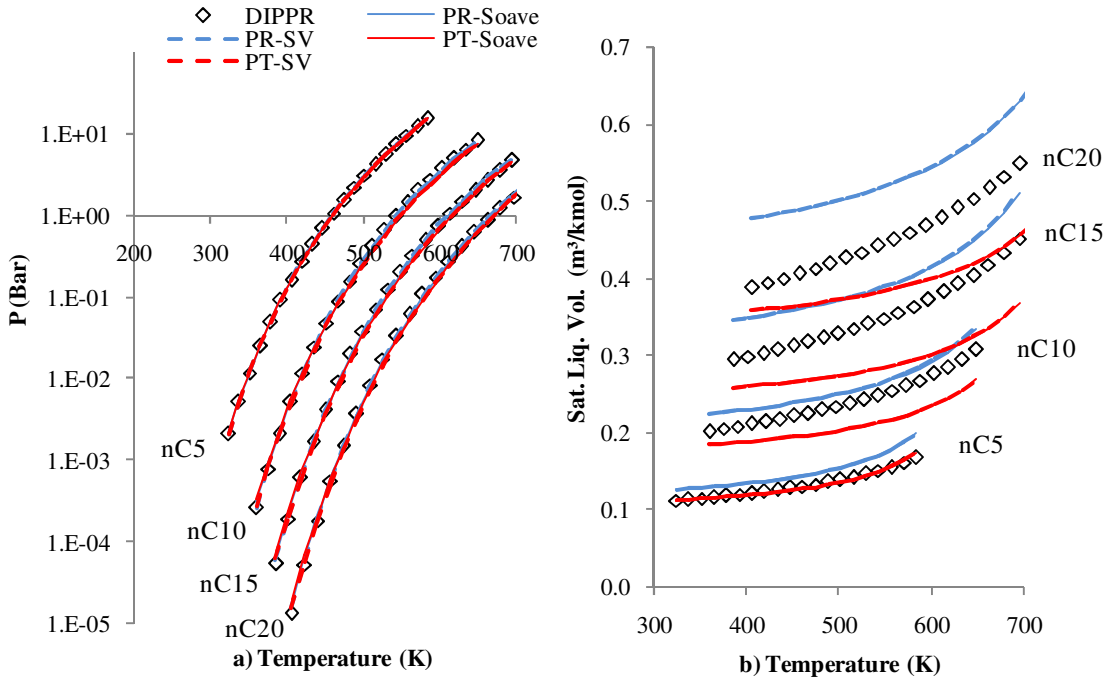

Figure 6-11 Model fits for a) vapour pressure and b) saturated liquid volume of the carboxylic acids with carbon number 5, 10, 15 and 20 using the PR (blue) and PT EOS (red) with the Soave (solid) and SV (dashed) alpha functions

Table 6-7 gives the %AAD for each of the model fits in Figure 6-11. As with the 1-alcohols, the PR EOS over-predicts and the PT EOS under-predicts the saturated liquid volume, especially for carbon numbers 10 and higher, where errors readily exceed 10 % AAD.

Stellenbosch University https://scholar.sun.ac.za

Table 6-7 %AAD for the model fits for the carboxylic acids from Figure 6-11

	%AAD							
Model:	PR-Soave		PR-SV		PT-Soave		PT-SV	
CN	P_{sat}	Sat. Liq. Vol.	P_{sat}	Sat. Liq. Vol.	P_{sat}	Sat. Liq. Vol.	P_{sat}	Sat. Liq. Vol.
5	0.42	11.89	0.34	11.91	2.59	1.81	2.3	1.82
10	8.17	7.33	1.33	7.82	12.13	12.83	10.14	12.79
15	7.03	12.92	4.13	13.25	13	17.22	10.61	17.18
20	8.38	17.05	6.34	17.24	13.63	13.73	10.65	13.69

6.6.4 Methyl Esters

Figure 6-12 gives the average %AAD in vapour pressure and saturated liquid volume for the PR, SRK and PT models with each alpha function for the linear methyl esters of carbon number 10, 12, 14, 16, 18 and 20.

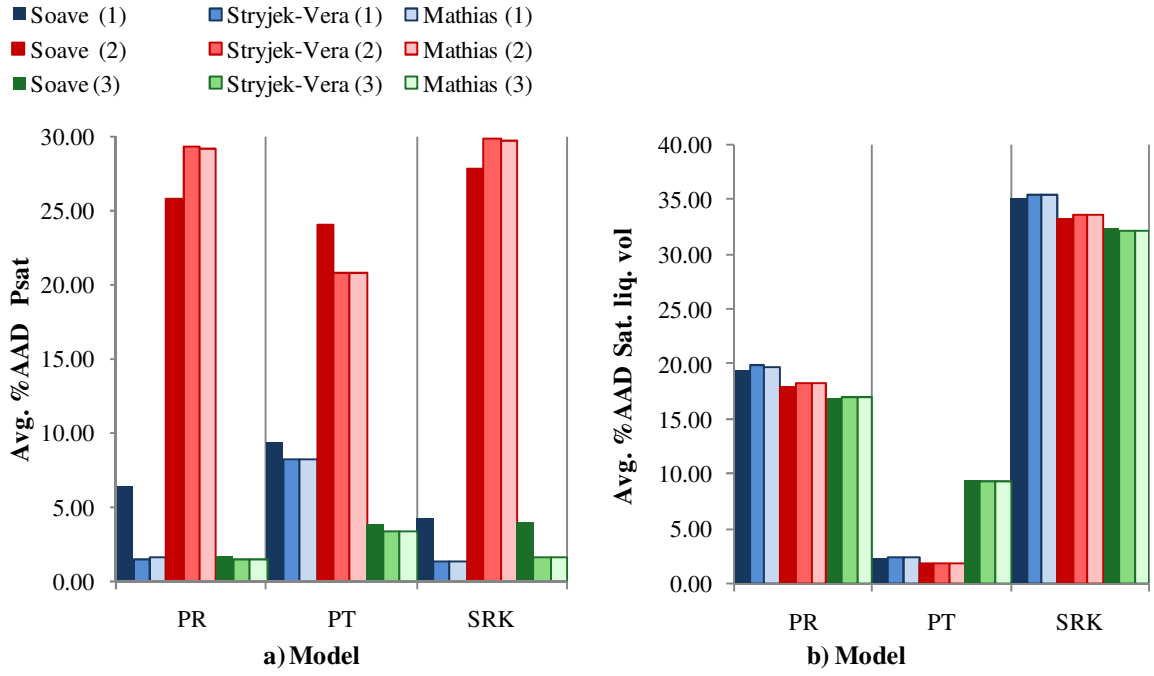

Figure 6-12 Avg. %AAD for a) pressure and b) saturated liquid volume over carbon number range 10– 18 for the methyl ester seriesfor cases 1 (blue) ,2 (red) and 3 (green) as given inTable 6-4 for the PR, PT and SRK EOS with the Soave, SV and M alpha function

Results for the methyl esters are similar to the n-alkanes, whereby improvement is observed in vapour pressure for the additional alpha function parameter, which is slightly less than for

Stellenbosch University https://scholar.sun.ac.za

the polar molecules. The PT EOS substantially out performs the PR and SRK models in saturated liquid volume, but larger errors (approaching 10 % AAD) than for the PR and SRK EOS (around 2 % for the SV and M alpha function) are observed in vapour pressure.

Figure 6-13 gives the model fits for carbon numbers 10, 12, 16 and 18 using the PR and PT EOS with the Soave and SV alpha functions.

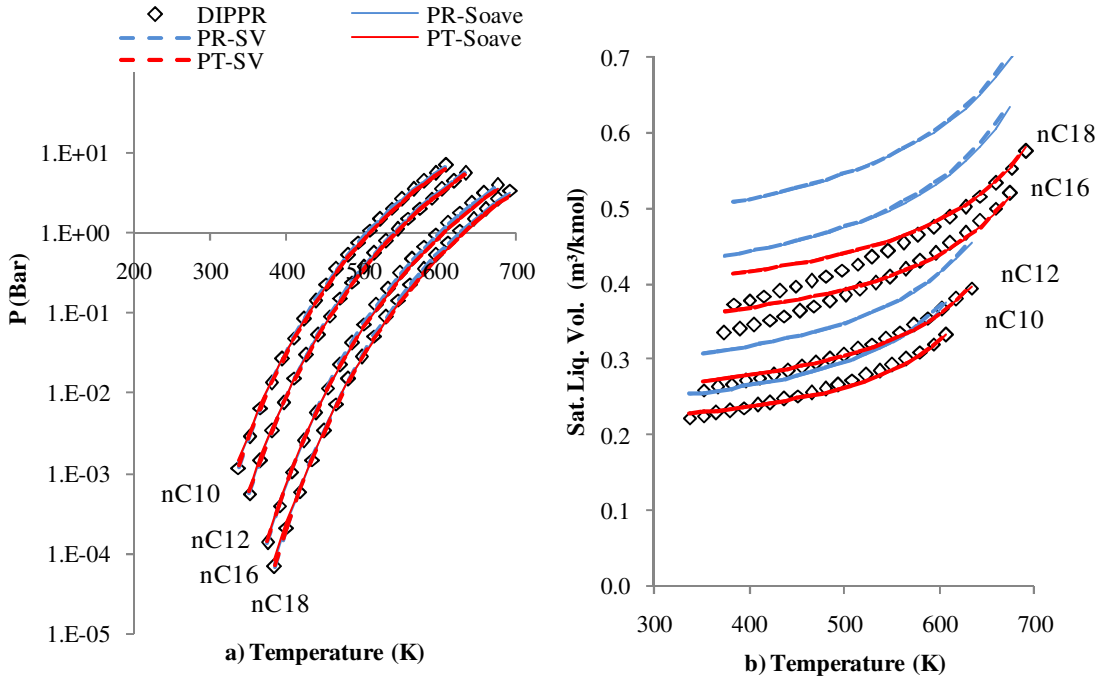

Figure 6-13 Model fits for a) vapour pressure and b) saturated liquid volume of the methyl esters with carbon number 5, 10, 15 and 20 using the PR (blue) and PT EOS (red) with the Soave (solid line) and SV (dashed line) alpha functions

Table 6-8 gives the %AAD for each of the model fits in Figure 6-13.

Table 6-8 %AAD for the model fits for the methyl esters from Figure 6-13

	%AAD							
Model:	PR-Soave		PR-SV		PT-Soave		PT-SV	
CN	P_{sat}	Sat. Liq. Vol.	P_{sat}	Sat. Liq. Vol.	P_{sat}	Sat. Liq. Vol.	P_{sat}	Sat. Liq. Vol.
10	6.6	11.19	0.62	11.7	8.57	1.57	6.94	1.51
12	3.85	14.74	0.45	14.98	6.26	1.64	5.04	1.58
16	7.9	23.62	2.23	24.07	11.64	2.95	9.68	2.85
18	7.34	29.45	2.78	29.85	11.7	4.23	9.93	4.25

Stellenbosch University https://scholar.sun.ac.za

The PT EOS gives good representation of the saturated liquid volume, however relatively large deviations are still observed for the higher carbon numbers (16 and 18), especially at lower temperatures. Errors in saturated liquid volume for the PR EOS exceed 10 % AAD over the whole carbon number range considered (10 – 18).

6.7 Influence of regression weights

It was found in the previous section that the 3 parameter PT EOS only offers an advantage for correlating vapour pressure and saturated liquid volume of non-polar molecules such as the n-alkanes and methyl esters. Large errors in vapour pressure with negligible improvement over 2 parameter models in saturated liquid volume were observed for the polar 1-alcohols and acids. This section investigates whether lower errors in vapour pressure can be obtained form the PT EOS by fitting parameters exclusively to this property, as was done for the PR and SRK EOSs. This offers a fairer comparison with the simpler 2 parameters models and takes a deeper look at the perceived limitations of the 3 parameter PT EOS for polar molecules observed in the previous section.

Table 6-9 gives the two sets of regression weights used in the current comparison.

Table 6-9 Labels for two sets of regression weights examined

Label	W_1	W_2
Set 1	0.8	0.2
Set 2	1	0

Table 6-10 gives the results in applying these regression weights in correlating the vapour pressure of n-alkanes and 1-alcohols with carbon number 5. 10, 15 and 20 using the PT and PR EOS with the Soave and SV alpha functions. It is seen that fitting parameters for the PT EOS exclusively to vapour pressure (right most column in Table 6-10 : set 2) does not provide an appreciable advantage for the non-polar n-alkanes. Marginal improvement is observed for the 1-alcohols, but results are still not better than obtained using the PR EOS, especially not when the SV alpha function is used. The PRSV model substantially outperforms the PT EOS for the 1-alcohol systems, irrespective of which set of regression weights or alpha function is used.

Stellenbosch University https://scholar.sun.ac.za

Table 6-10 Comparison of model fits in vapour pressure for the PR and PT EOS with Soave and SV alpha functions using different sets of regression weights as given in Table 6-9

	Weights:	Set 1		Set 2		Set 2	
Alkanes	CN	PT	PTSV	PR	PRSV	PT	PTSV
Pentane	5	0.61	0.58	0.67	0.53	1.69	1.68
Decane	10	1.63	1.28	0.82	0.55	3.32	2.16
Pentadecane	15	4.09	3.47	1.81	0.07	2.2	1.34
Eicosane	20	2.94	2.14	1.61	1.52	3.11	1.99
Average error:		2.32	1.87	1.23	0.67	2.58	1.79
Alcohols	CN	PT	PTSV	PR	PRSV	PT	PTSV
Pentanol	5	10.81	8.79	8.49	0.73	14.39	9.98
Decanol	10	15.42	13.23	12.17	2.75	13.85	13.7
Pentadecanol	15	12.05	10.05	8.78	5.11	9.42	9.4
Eicosanol	20	15.43	13.24	10.25	2.89	8.99	8.43
Average error:		13.43	11.33	9.92	2.87	11.66	10.38

Table 6-11 gives the results for applying the regression weights from Table 6-9 in correlating the saturated liquid volume of the same systems from Table 6-10.

Table 6-11 Comparison of model fits in sat. liq. vol. for the PR and PT EOS with Soave and SV alpha functions using different sets of regression weights as given in Table 6-9

	Weights:	Set 1		Set 2		Set 2	
Alkanes	CN	PT	PTSV	PR	PRSV	PT	PTSV
Pentane	5	1.65	1.66	2.31	2.31	1.01	1.01
Decane	10	1.05	1.05	5.76	5.81	11.87	6.98
Pentadecane	15	1.56	1.52	13.41	13.54	7.76	3.81
Eicosane	20	4.39	4.37	15.14	15.12	2.19	2.1
Average error:		2.16	2.15	9.16	9.20	5.71	3.48
Alcohols	CN	PT	PTSV	PR	PRSV	PT	PTSV
Pentanol	5	12.77	12.71	1.18	1.49	22.79	15.81
Decanol	10	13.28	13.22	4.8	5.69	9.42	9.28
Pentadecanol	15	7.85	7.79	13.14	13.65	4.43	4.42
Eicosanol	20	7.75	7.7	19.53	20.16	3.24	2.92
Average error:		10.41	10.36	9.66	10.25	9.97	8.11

Stellenbosch University https://scholar.sun.ac.za

It is observed that fitting parameters of the PT EOS solely to vapour pressure (set 2) slightly deteriorates the correlation of the saturated liquid volume for the n-alkanes, however actually seems to give slightly improved correlation of the saturated liquid volume for the 1-alcohols. Despite improved saturated liquid volume correlation for the non-polar n-alkanes, it is again noted that the PT EOS offers no significant advantage over the simpler 2 parameter PR EOS for the 1-alcohols, irrespective of which set of regression weights is used.

The results from this section therefore seem to support the idea that the 3rd parameter from the PT EOS only offers an advantage in correlation the saturated liquid volume of non-polar molecules like the n-alkanes and methyl esters, but not for more polar systems such as alcohols or acids. Pure parameters obtained using the regression weights initially given in Table 6-1 are used in the subsequent chapters of this thesis.

6.8 Conclusions

The aim of this chapter is to determine the capabilities of CEOSs to correlate the pure component vapour pressure and saturated liquid density for the n-alkane, 1-alcohol, carboxylic acid and methyl ester homologous series, thereby addressing project aim number 4 (see Section 1.3). The following factors in applying the CEOSs for pure component modelling are investigated:

- Use of a 2 or 3 parameter model in the volume dependence
- Use of a 1 or 2 parameter alpha function in the temperature dependence
- The effect of using an estimation method for the requisite pure constants (T_c, P_c and acentric factor ω)
- The applicability of literature correlations for alpha function and other pure component parameters in terms of the acentric factor, ω.

The outcomes from this chapter are summarized as follows:

- Large errors are observed in the vapour pressure and saturated liquid volume if different pure constants are used than those for which empirical parameters have been fitted to data. Model parameters should therefore be used in conjunction with a specific set of pure constants.
- Caution should be taken in using literature correlations in terms of the acentric factor for alpha function parameters of long-chain or polar molecules, especially for the 1 parameter Soave alpha function. Including additional empirical parameters in the alpha function seems to makegeneralized correlations for the *primary (*Soave like)

Stellenbosch University https://scholar.sun.ac.za

parameter more reliable, but the additional correction parameters are highly empirical and do not follow any trend with acentric factor or carbon number. Fitting pure parameters to data therefore seems required for optimal results.

- The choice of alpha function has negligible effect on the saturated liquid volume, but the 2 parameter alpha functions (SV and M) show a considerable improvement (typically 2 – 5 %AAD) in vapour pressure correlationover the Soave alpha function, especially for the more polar 1-alcohols and carboxylic acids and in cases where the C&G method was used to estimate the pure constants.
- Errors in vapour pressure were kept below 5% AAD for all series using the PR and SRK EOS, provided a 2 parameter alpha function was used. Average vapour pressure errors exceeded 7 % for the PT EOS for all series except the n-alkanes, irrespective of the alpha function used.
- For the non-polar n-alkane and methyl esters the 3 parameter PT EOS with its adjustable critical compressibility shows a substantial improvement in saturated liquid volume (% AAD below 5%) over the PR (%AAD > 10 %) and SRK EOS (%AAD > 20%).
- For the more polar 1-alcohols and carboxylic acids, the 3 parameter PT EOS does not offer any improvement over the simpler 2 parameter models. %AAD in saturated liquid volume approaches % 10 for both PR EOS and PT EOS, and approaches 25 % for the SRK EOS. Much better correlation of the vapour pressure is also achieved with both PR and SRK EOS for these systems.
- An investigation into the influence of regression weights on the performance of the PT EOS showed that only very marginal improvement in vapour pressure correlation can be achieved for the polar 1-alcohols, despite fitting pure parameters exclusively to this property.
- Qualitatively, the PR EOS generally over-predicts saturated liquid volume, whereas the PT EOS under-predicts this property. This is especially true at carbon numbers above 10 for each series.

In general, the flexible volume dependence and temperature dependent alpha functions available to CEOSs allow for good vapour pressure representation over a large carbon number range for all series investigated, provided a 2 parameter alpha function is used, parameters are fitted through regression and the same pure constants are used as those in the fitting procedure.

A 3rd parameter in the volume dependence generally offers improved correlationof saturated liquid volume for the non-polar n-alkanes and methyl esters, but could not provide good

Stellenbosch University https://scholar.sun.ac.za

correlation at both high and low temperatures for these series, especially at high carbon numbers (exceeding 15), nor for the polar systems in general.

It is further clear that substantial theoretical development is required to allow the simple CEOSs to simultaneously represent vapour pressure and saturated liquid volume for both polar and non-polar molecules at both low and high temperatures, across the whole carbon number range of interest to SFE.More theoretical models such as PHCT and SAFT will undoubtedly give better performance for pure component properties, especially volumetric properties, due to their ability to account for chain formation and polarity.

In the design of a SFE process, it may therefore be advisable that the simpler CEOSs models be used to design the high-pressure fractionation column, and that the low-pressure separation chamber be modelled using a more theoretical molecular model, where improved representation of volumetric properties are preferred to accurately quantify the product yield

Stellenbosch University https://scholar.sun.ac.za

7. MODELLING WITH A COMMERCIAL PROCESS SIMULATOR: ASPEN PLUS ®

The general steps for designing a SFE process (also given in Section 1.2) are as follows.

- Obtain the required property information
- Develop a process model for the fractionation columns
- Design the fractionation process

The focus of this study is primarily on obtaining the required high-pressure VLE property information through thermodynamic modelling, however this is only a pre-requisite for developing a process model and designing the physical process. In developing a process model, it may be useful to use commercially available software which already incorporates the required thermodynamic models and design equations for modelling the necessary process units. Such simulators may not always provide the best option for design, since their general applicability may overlook details required for a particular application. In particular, the critical region of a mixture poses subtle challenges, especially in thermodynamic modelling (see Section 2.3), which are seldom addressed in commercially available software.

Weber et al. [204] and Stoldt and Brunner [205] have applied cubic models from Aspen Plus ® with success for modelling high pressure VLE of various hydrocarbons in CO_2 and propane. Zamudio [206] recently established a process model for separating detergent range alkanes and alcohols with supercritical CO_2 using a CEOS in Aspen Plus ®.

The aim of this chapter is to determine the capability ofcubic models from Aspen Plus ® for modellinghigh pressure binary VLE of the n-alkane (nC10-C36), 1-alcohol (nC10-nC18) and methyl ester (nC10-nC18) homologous series in ethane (353 K), as well as the n-alkane (nC14-nC36), 1-alcohol (nC10-nC18) and carboxylic acid (nC10-nC18) series in propane (408 K), thereby addressing project objective 5 (see Section 1.3).Various regression cases are formulated, incorporating up to 3 binary interaction parameters (BIPs) in the mixing rules for correlating the binary VLE data. The sensitivity and qualitative effect of the BIPs are also investigated. BIP values are then plotted as a function of solute carbon number to see if any trends exist for developing generalized correlations for possiblty meeting project objective 6.

If the systems considered may be accurately modelled and generalized correlations developed for BIPs, the process modelling methodology of Zamudio [206] may be extended to model and design a SFE process for separating these components.

Stellenbosch University https://scholar.sun.ac.za

7.1 Systems modelled

The carbon number, composition and pressure ranges for the ethane systems investigated in this chapter are presented in Table 7-1:

Table 7-1 Ethane systems (X is the solute mass fraction)

Ethane (352 K)				
Alkanes [1,2]	CN	Tr (solute)	X	P (MPa)
N-Decane	10	0.57	0.053-0.440	7.9-8.5
N-Hexadecane	16	0.49	0.070-0.500	9.8-10.3
N-Tetracosane	24	0.44	0.078-0.550	12.9-14.1
N-Octacosane	28	0.42	0.068-0.580	14.2-16.2
N-Hexatriacontane	36	0.40	0.018-0.600	16.4-20.4
Alcohols [4]	CN	Tr (solute)	X	P (MPa)
1-Decanol	10	0.51	0.069-0.630	12.8-15.2
1-Dodecanol	12	0.49	0.090-0.570	14.5-16.5
1-Tetradecanol	14	0.47	0.057-0.630	14.2-18.6
1-Hexadecanol	16	0.46	0.052-0.640	14.6-20.0
1-Octadecanol	18	0.45	0.072-0.590	17.8-21.6
Carboxylic Acids [7]	CN	Tr (solute)	X	P (MPa)
Decanoic acid	10	0.49	0.094-0.557	13.0-14.5
Dodecanoic acid	12	0.47	0.110-0.540	15.0-16.5
Tetradecanoic acid	14	0.46	0.094-0.57	16.5-18.5
Hexadecanoic acid	16	0.45	0.067-0.592	17.0-20.0
Octadecanoic acid	18	0.44	0.140-0.530	21.0-22.5
Methyl Esters [5]	CN	Tr (solute)	X	P (MPa)
Methyl Decanoate	10	0.51	0.073-0.515	9.5-9.9
Methyl Dodecanoate	12	0.49	0.020-0.630	9.2-10.7
Methyl Tetradecanoate	14	0.47	0.023-0.650	9.8-11.7
Methyl Hexadecanoate	16	0.46	0.026-0.628	10.7-13.0
Methyl Octadecanoate	18	0.45	0.024-0.612	11.5-14.3

The carbon number, composition and pressure ranges for the propane systems are presented in Table 7-2.

Stellenbosch University https://scholar.sun.ac.za

Table 7-2 Propane systems (X is the solute mass fraction)

Propane (408 K)				
Alkanes [8,9,10]	CN	Tr (solute)	X	P (MPa)
N-Tetradecane	14	0.59	0.026-0.385	5.8-6.5
N-Hexadecane	16	0.56	0.047-0.382	6.2 - 6.5
N-Tetracosane	24	0.51	0.056-0.386	7.4-7.9
N-Octacosane	28	0.49	0.058-0.397	8-8.6
N-Hexatriacontane	36	0.47	0.031-0.459	8.6-9.6
Alcohols [11]	CN	Tr (solute)	X	P (MPa)
1-Decanol	10	0.59	0.03-0.410	6.3-6.8
1-Dodecanol	12	0.57	0.024-0.500	6.2-6.7
1-Tetradecanol	14	0.55	0.039-0.467	6.6-7.1
1-Hexadecanol	16	0.53	0.022-0.510	6.5-7.5
1-Octadecanol	18	0.52	0.017-0.537	6.7-7.6
Carboxylic Acids [12]	CN	Tr (solute)	X	P (MPa)
Decanoic acid	10	0.57	0.028-0.475	6.6-7.2
Undecanoic acid	11	0.56	0.023-0.470	6.9-7.5
Dodecanoic acid	12	0.53	0.027-0.467	7.0-7.6
Hexadecanoic acid	16	0.52	0.039-0.504	7.8-8.8
Octadecanoic acid	18	0.51	0.034-0.527	8.5-10

Data for systems which were not directly measured were obtained from the linear trends in Figure 3-6 through interpolation for the desired carbon number at the temperature of interest. These include the propane/n-alkane systems for carbon numbers 16, 24 and 28, as well as the propane/tetradecanol system at 408 K. The R^2 values for these linear interpolated data were above 0.96 in all cases. The required pure constants (T_c, P_c and the acentric factor, ω) for all components were obtained from the Pure20 database in Aspen Plus®, except for the methyl ester systems for carbon number 14 to 18, in which case values from the DIPPR database were used, since they were not available in the Pure 20 database. The values for these constants are given in Appendix C.3.

7.2 Models investigated

The models recommended by Aspen Plus ® documentation for SFE applications fall under the classification of “Flexible and predictive equation-of-state property methods” and include exclusively CEOSs [199]. 5 models are investigated in this chapter, which emanate from the basic SRK [89] (Equation 6-15) and PR [79] (Equation 6-17) models, but with various alpha functions and mixing rules. The form of each investigated model is subsequently discussed.

Stellenbosch University https://scholar.sun.ac.za

PR and SRK EOSs

The standard PR and SRK models with the Soave alpha function were investigated using the following mixing rules by Mathias et al. [101]:

$$a = a_0 + a_1 \quad 7\text{-}1$$

$$a_0 = \sum_i \sum_j x_i x_j (a_i a_j)^{0.5} (1 - k_{a,ij}) \quad 7\text{-}2$$

$$a_1 = \sum_{i=1}^{n} x_i \left(\sum_{j=1}^{n} x_j \left((a_i a_j)^{\frac{1}{2}} l_{a,ij} \right)^{\frac{1}{3}} \right)^3 \quad 7\text{-}3$$

$$b = \sum_i x_i b_i \quad 7\text{-}4$$

This approach includes 2 interaction parameter for the energy parameter, $k_{a,ij}$ and $l_{a,ij}$, however no interaction parameters for the co-volume parameter b were used. The mixing rule is meant to improve property estimation for asymmetric and polar mixtures, and furthermore does not suffer from common deficiencies of mixing rules with higher order composition dependence such as the dilution effect or the Michelsen-Kirstenmacher syndrome, as discussed in Section 4.2 [102].

PR/BM EOS

A variation of the PR model also investigated in this chapter is the PR model with an extrapolated alpha function for temperatures above the critical temperature of the component as developed by Boston and Mathias [91]:

$$\alpha(T_r) = \left(\exp\left(c\left[1 - T_r^d\right]\right)\right)^2 \quad 7\text{-}5$$

$$c = 1 + \frac{m}{2} + 0.3p \quad 7\text{-}6$$

$$d = \frac{c-1}{c} \quad 7\text{-}7$$

The standard Soave type alpha function gives unrealistic results at high reduced temperatures, where the alpha function should go asymptotically to zero. This boundary condition is met by the extrapolation of Boston and Mathias, making it more consistent for application in the

Stellenbosch University https://scholar.sun.ac.za

critical region. The mixing rules of Mathias et al. [101], given by Equations 7-1 to 7-4, were also used for this model.

RK-ASPEN EOS

The next model investigated in this chapter has been given the title RK-ASPEN in the Aspen Plus ® documentation [199] and consists of the SRK EOS with the Mathias [92] alpha function, also used in chapter 6 (Equation 6-20):

$$\alpha(T_r) = \left(1 + m\left(1 - \sqrt{T_r}\right) - p(1 - T_r)(0.7 - T_r)\right)^2 \quad 7\text{-}8$$

$$m = -0.48508 + 1.55191\omega - 0.15613\omega^2 \quad 7\text{-}9$$

The Boston-Mathias alpha function extrapolation [91] (Equations 7-5 to 7-7) was also used for $T_r > 1$ for a given component. The classic Van der Waals mixing rules were used with two binary interaction parameters; one for the energy parameter a (k_{aij}) and one for the size parameter b (k_{bij}):

$$a = \sum_i \sum_j x_i x_j a_{ij} \quad 7\text{-}10$$

$$b = \sum_i \sum_j x_i x_j b_{ij} \quad 7\text{-}11$$

$$a_{ij} = (a_i a_j)^{0.5}(1 - k_{aij}) \quad 7\text{-}12$$

$$b_{ij} = \frac{b_i + b_j}{2}(1 - k_{bij}) \quad 7\text{-}13$$

This model was applied with success in the Aspen Plus ® process model developed by Zamudio [206] for separating detergent range alkanes and alcohols in supercritical CO_2.This model was also identified as the best model in Aspen Plus ® for SFE applications in the work of Weber et al. [204] and Stoldt and Brunner [205].

SR-POLAR EOS

The final model being investigated has been given the title SR-POLAR in the Aspen Plus ® documentation and consists of the SRK EOS with the following mixing rule by Schwartzenruber and Renon [103] for the energy parameter, a:

Stellenbosch University https://scholar.sun.ac.za

$$a = \sum_i \sum_j x_i x_j (a_i a_j)^{0.5} [1 - k_{aij} - l_{a,ij}(x_i - x_j)] \quad 7\text{-}14$$

The mixing rule has 2 BIPs in the energy parameter, namely $k_{a,ij}$ and $l_{a,ij}$, and a 3rd BIP, $k_{b,ij}$, is used in the size parameter, b:

$$b = \sum_i \sum_j x_i x_j \frac{b_i + b_j}{2} (1 - k_{bij}) \quad 7\text{-}15$$

This model also has a modified Soave type alpha function with three additional polar parameters, but these were set to zero, reducing it to the standard Soave alpha function.

7.3 Reduction of data

This section briefly outlines the procedures followed in reducing the data for obtaining BIPs in the model mixing rules.

7.3.1 Data smoothing

The data in Table 7-1 and Table 7-2 were published as dew and bubble point data at a fixed temperature. In order to fit parameters and evaluate model performance, the data was smoothed into VLE sets of {X}, {Y} and P at a specific temperature. This was done by firstly interpolating between the measured isothermal data points linearly or through a cubic-spline interpolation using the *spline* function in MATLAB. An appropriate interpolation is selected, depending on which one best represents the general curvature of the data through visual inspection. The *ginput* function in MATLABwas then used in order to obtain the VLE sets. This function generates a crosshair over the plot of the interpolated data, with which data values can be selected at fixed pressure intervals for both the vapour and liquid phases. 4 to 7 sets of {X}, {Y} and P were selected per system, at pressure intervals of 0.2 – 0.6 MPa, in the high-pressure region. The near-critical region, approximately 0.5 MPa from the maximum pressure for complete miscibility, was excluded since the regression procedure struggles to generate representative parameters if this part of the phase curve is included.

7.3.2 Regression

BIPs were obtained through the “Data regression” run type in Aspen Plus ®, and using the Britt-Luecke solution algorithm [203].The objective function used in Aspen Plus ® is minimized using a maximum likelihood approach as given by the following expression:

Stellenbosch University https://scholar.sun.ac.za

$$Q = \sum_{n=1}^{NDG} w_n \sum_{i=1}^{NP} \left[\left(\frac{T_{exp} - T_{calc}}{\sigma_{Ti}} \right)^2 + \left(\frac{P_{exp} - P_{calc}}{\sigma_{pi}} \right)^2 + \sum_{j=1}^{NC-1} \left(\frac{X_{exp,ij} - X_{calc,ij}}{\sigma_{x,ij}} \right)^2 + \left(\frac{Y_{exp,ij} - Y_{calc,ij}}{\sigma_{y,ij}} \right)^2 \right] \quad 7\text{-}16$$

NDG is the number of data groups, NP the number of data points and NC the number of components. σ is the standard deviation of the measured property and w_n the weight assigned to a data group. This method is deemed more sophisticated than least squares methods due to incorporating all experimental data and associated errors for the best statistical estimates of parameters. Table 7-3 gives the regression cases formulated for each model.

Table 7-3 Regression cases investigated for each model

EOS	Regression cases
SRK/PR/PR-BM	$k_{a,ij}$/ $l_{a,ij}$/ Both $k_{a,ij}$ and $l_{a,ij}$
RK-ASPEN	$k_{a,ij}$/$k_{b,ij}$/ Both $k_{a,ij}$ and $k_{b,ij}$
SR-POLAR	$k_{a,ij}$/$l_{a,ij}$/ $k_{b,ij}$ / Both $k_{a,ij}$ and$l_{a,ij}$/ Both $k_{a,ij}$ and $k_{b,ij}$/$k_{a,ij}$, l_{aij} and $k_{b,ij}$

The RK-ASPEN EOS further employs the Mathias [92] alpha function, which has an additional pure parameter, p, for polar systems (see Equation 7-8). The values for this parameter were fitted to DIPPR correlations for vapour pressure for each component in Table 7-1 and Table 7-2 and are given in Appendix E.2.

7.4 Results

The %AAD (see Equation 6-24) in T, P and solute composition of each phase, X_2 and Y_2, were generated by Aspen Plus ®for each of the regression cases in Table 7-3. These errors are statistically estimated and not based on any specific specification variable. Results are firstly presented for the ethane systems and then for the propane systems.

7.4.1 Overall results: Ethane

Table 7-4 contains results for the ethane systems for each regression case for each model as given in Table 7-3. The results are presented as an average %AAD over the 5 systems chosen for each homologous series as given in Table 7-1..

Stellenbosch University https://scholar.sun.ac.za

Table 7-4 Overall results for ethane systems

Ethane

RK-ASPEN

Alkanes

Case	Avg. %AAD T	P	X_2	Y_2
$k_{a,ij}$	1.07	1.17	0.16	35.24
$k_{b,ij}$	3.99	0.81	1.42	49.08
$k_{a,ij}/k_{b,ij}$	0.40	0.35	0.08	6.54

Alcohols

Case	Avg. %AAD T	P	X_2	Y_2
$k_{a,ij}$	1.41	1.75	0.33	60.80
$k_{b,ij}$	11.24	7.82	3.32	40.87
$k_{a,ij}/k_{b,ij}$	0.80	0.76	0.25	6.92

Acids

Case	Avg. %AAD T	P	X_2	Y_2
$k_{a,ij}$	0.76	0.95	0.18	22.50
$k_{b,ij}$	2.07	1.35	0.80	32.20
$k_{a,ij}/k_{b,ij}$	0.45	0.43	0.11	4.82

Methyl Esters

Case	Avg. %AAD T	P	X_2	Y_2
$k_{a,ij}$	1.05	1.19	0.17	24.36
$k_{b,ij}$	5.47	2.15	1.21	35.31
$k_{a,ij}/k_{b,ij}$	0.54	0.51	0.15	12.95

PR

Alkanes

Case	Avg. %AAD T	P	X_2	Y_2
$k_{a,ij}$	1.16	1.38	0.31	78.28
$l_{a,ij}$	0.87	1.20	0.29	71.13
$k_{a,ij}/l_{a,ij}$	0.91	0.87	0.19	6.81

Alcohols

Case	Avg. %AAD T	P	X_2	Y_2
$k_{a,ij}$	1.36	1.91	0.55	108.51
$l_{a,ij}$	0.77	1.12	0.49	69.82
$k_{a,ij}/l_{a,ij}$	1.53	1.67	0.58	13.61

Acids

Case	Avg. %AAD T	$k_{a,ij}/l_{a,ij}$	X_2	Y_2
$k_{a,ij}$	0.73	1.00	0.23	36.28
$l_{a,ij}$	0.60	0.70	0.19	29.43
$k_{a,ij}/l_{a,ij}$	0.77	0.86	0.20	5.98

Methyl Esters

Case	Avg. %AAD T	P	X_2	Y_2
$k_{a,ij}$	1.80	2.20	0.21	49.39
$l_{a,ij}$	1.23	1.68	0.22	42.68
$k_{a,ij}/l_{a,ij}$	1.08	1.00	0.15	12.96

PR-BM

Alkanes

Case	Avg. %AAD T	P	X_2	Y_2
$k_{a,ij}$	1.16	1.34	0.30	75.15
$l_{a,ij}$	0.90	1.20	0.28	68.71
$k_{a,ij}/l_{a,ij}$	0.87	0.81	0.17	6.73

Alcohols

Case	Avg. %AAD T	P	X_2	Y_2
$k_{a,ij}$	1.56	2.04	0.53	104.51
$l_{a,ij}$	0.81	1.11	0.47	68.37
$k_{a,ij}/l_{a,ij}$	1.53	1.55	0.54	12.80

Acids

Case	Avg. %AAD T	P	X_2	Y_2
$k_{a,ij}$	0.61	0.84	0.25	37.20
$l_{a,ij}$	0.60	0.68	0.20	28.96
$k_{a,ij}/l_{a,ij}$	0.76	0.80	0.18	5.67

Methyl Esters

Case	Avg. %AAD T	P	X_2	Y_2
$k_{a,ij}$	1.76	2.12	0.20	46.97
$l_{a,ij}$	1.20	1.63	0.21	40.97
$k_{a,ij}/l_{a,ij}$	1.02	0.94	0.14	13.02

SRK

Alkanes

Case	Avg. %AAD T	P	X_2	Y_2
$k_{a,ij}$	6.92	1.39	0.11	37.39
$l_{a,ij}$	5.42	1.38	0.35	35.06
$k_{a,ij}/l_{a,ij}$	2.75	2.41	1.33	29.81

Alcohols

Case	Avg. %AAD T	P	X_2	Y_2
$k_{a,ij}$	8.78	2.44	0.12	56.67
$l_{a,ij}$	4.76	1.31	0.49	45.89
$k_{a,ij}/l_{a,ij}$	3.10	2.17	1.27	36.11

Acids

Case	Avg. %AAD T	P	X_2	Y_2
$k_{a,ij}$	13.97	2.03	0.06	72.56
$l_{a,ij}$	8.29	0.33	0.23	72.29
$k_{a,ij}/l_{a,ij}$	4.73	3.71	3.44	45.24

Methyl Esters

Case	Avg. %AAD T	P	X_2	Y_2
$k_{a,ij}$	2.18	1.15	0.10	28.90
$l_{a,ij}$	1.80	2.28	0.52	41.14
$k_{a,ij}/l_{a,ij}$	2.41	1.03	0.14	23.90

SR POLAR

Alkanes

Case	Avg. %AAD T	P	X_2	Y_2
$k_{a,ij}$	0.95	1.05	0.16	34.24
$l_{a,ij}$	0.95	1.05	0.16	32.93
$k_{a,ij}/l_{a,ij}$	0.51	0.44	0.10	6.29
$k_{b,ij}$	5.02	1.75	1.54	48.22
$k_{a,ij}/k_{b,ij}$	0.53	0.51	0.09	7.45
$k_{a,ij}/k_{b,ij}/l_{a,ij}$	0.28	0.28	0.07	6.79

Alcohols

Case	Avg. %AAD T	P	X_2	Y_2
$k_{a,ij}$	1.06	1.59	0.36	57.24
$l_{a,ij}$	0.74	1.04	0.33	39.28
$k_{a,ij}/l_{a,ij}$	0.82	0.94	0.31	8.01
$k_{b,ij}$	4.84	2.74	2.58	53.82
$k_{a,ij}/k_{b,ij}$	0.74	0.81	0.27	6.98
$k_{a,ij}/k_{b,ij}/l_{a,ij}$	0.30	0.30	0.10	4.81

Acids

Case	Avg. %AAD T	P	X_2	Y_2
$k_{a,ij}$	0.72	0.98	0.18	19.46
$l_{a,ij}$	0.61	0.87	0.20	17.35
$k_{a,ij}/l_{a,ij}$	0.41	0.46	0.12	5.20
$k_{b,ij}$	1.52	1.18	0.65	26.56
$k_{a,ij}/k_{b,ij}$	0.38	0.42	0.12	3.83
$k_{a,ij}/k_{b,ij}/l_{a,ij}$	0.27	0.29	0.08	3.98

Methyl Esters

Case	Avg. %AAD T	P	X_2	Y_2
$k_{a,ij}$	1.30	1.50	0.18	31.74
$l_{a,ij}$	0.96	1.17	0.17	27.03
$k_{a,ij}/l_{a,ij}$	0.65	0.64	0.13	12.39
$k_{b,ij}$	6.82	3.14	1.38	36.06
$k_{a,ij}/k_{b,ij}$	0.59	0.58	0.13	12.65
$k_{a,ij}/k_{b,ij}/l_{a,ij}$	0.57	0.59	0.10	11.26

Key	Description
	Best fit within a homologous series
	2nd best fit within a homologous series
	3rd best fit within a homologous series
	Best fit for a single BIP within a homologous series

Stellenbosch University https://scholar.sun.ac.za

As noted by the key, the results highlighted in green, yellow and red give the first, second and third best fit obtained across all models and regression cases within a particular homologous series, as determined by the error in Y_2, which is the variable for which the %AAD is most sensitive to deviation from experimental values, because of its small absolute value

The results high-lighted in blue give the best fit within a series using a single BIP. As noted in Section 4.2.5, correlations for BIPs are typically only developed for a single BIP in the energy parameter, $k_{a,ij}$. Once two or more BIPs are used, the parameters become inter-correlated, trends become non-monotonic and reliable correlations become difficult to develop. Multiple BIPs should therefore only be incorporated if necessary for a reasonable fit.

Comparing the best cases firstly just in terms of BIPs used, it is seen from Table 7-4 that errors in T,P and X_2 are reasonable for use of a single BIP, hardly exceeding 1%AAD for the best cases (high-lighted in blue). However errors in Y_2 are 20 – 25 % for the acids and methyl esters and exceed 30% for the n-alkanes and 1-alcohols. Valderrama [98] reports that %AAD in Y_2 can be as high as 200% for asymmetric systems such as these, but are usually not reported or discussed in literature. Even though the small absolute value of Y_2 exaggerates the %AAD, the improvement observed with the inclusion of 1 or more additional BIPs is substantial for all systems and seems necessary for design of a SFE process, especially since Y_2 gives the solubility of the heavy solute in the solvent and determines the expected product yield.

The relative improvement upon including a 3rd BIP in the SR-POLAR model is slightly greater for the polar 1-alcohols and acids than for the n-alkanes and methyl esters, where 2 BIPs give essentially equivalent performance and even slightly better results than the 3 BIP case for the n-alkanes, albeit only in Y_2.

Comparing performance in terms of models, it is seen that the best cases are distributed throughout the SR-POLAR and RK-ASPEN models. However, the superiority of these models are very marginal once two BIPs are included in the model mixing rules, irrespective of the model or whether the BIPs are only incorporated into the energy parameter or both the energy and size parameter.

7.4.2 BIP values: Ethane systems

Table 7-5 gives the values of the BIPs for the best cases using the SR-POLAR and RK-ASPEN models for each homologous series. For all cases where 2 BIPs are used, the values are smaller than for 3 BIPs in the SR-POLAR EOS, which suggest that the 2 BIPs offer a

Stellenbosch University https://scholar.sun.ac.za

correction to the pure prediction of the mixing rule (no BIPs), whereas use of 3 BIPs force the model through the data.

Table 7-5 BIPs for best regression cases for ethane systems using the SR-POLAR and RK-ASPEN models (CN : carbon number)

Ethane (T = 352 K)					
Model:	SR-POLAR			RK-ASPEN	
Solute	BIP's			BIP's	
n-Alkanes (CN)	$k_{a,ij}$	$k_{b,ij}$	$l_{a,ij}$	$k_{a,ij}$	$k_{b,ij}$
10	-0.00601		0.00481	-0.01621	-0.00683
16	0.11875		0.07246	0.02681	-0.04326
24	0.04761		0.01368	0.03373	0.00444
28	-0.02567		-0.05005	0.03360	0.02126
36	-0.47505		-0.44909	0.02350	0.08489
1-Alcohols (CN)	$k_{a,ij}$	$k_{b,ij}$	$l_{a,ij}$	$k_{a,ij}$	$k_{b,ij}$
10	1.61813	0.90762	1.18924	0.03678	0.03887
12	1.38041	0.70348	1.05082	0.02977	0.06692
14	0.36029	0.19818	0.26358	0.03548	0.05959
16	0.07680	0.06916	0.03464	0.03852	0.06090
18	0.36174	0.18518	0.27271	0.03707	0.07830
Acids (CN)	$k_{a,ij}$	$k_{b,ij}$	$l_{a,ij}$	$k_{a,ij}$	$k_{b,ij}$
10	-0.32050	-0.21352	-0.25045	-0.00636	-0.05844
12	-0.26139	-0.15949	-0.21082	0.00279	-0.03410
14	0.02232		0.01145	0.01260	0.00563
16	-0.15170	-0.04285	-0.13738	0.01653	0.02644
18	1.08342	0.36943	0.89047	0.02438	0.02609
Meth. Est. (CN)	$k_{a,ij}$	$k_{b,ij}$	$l_{a,ij}$	$k_{a,ij}$	$k_{b,ij}$
10	-0.61235	-0.34601	-0.48789	0.01451	-0.03721
12	-0.27357	-0.10952	-0.22975	0.01249	0.01480
14	0.42048	0.18533	0.32571	0.01835	0.02858
16	-0.31504	-0.10041	-0.29403	0.03532	0.01109
18	0.20587	0.12825	0.13312	0.03929	0.05140

7.4.3 Ethane plots

In order to provide a more qualitative comparison of the results, figures are subsequently presented which compare the fit for the best cases from Table 7-4 for the SR-POLAR and RK-ASPEN models, as well as the best case for a single BIP for each series, as also highlighted in blue in Table 7-4. These fits are given in Figure 7-1 for all systems with ethane as solvent.

Stellenbosch University https://scholar.sun.ac.za

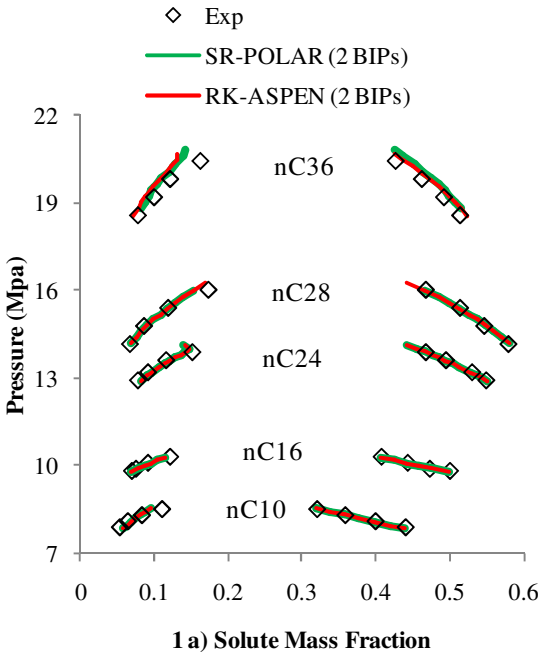

1 a) Solute Mass Fraction

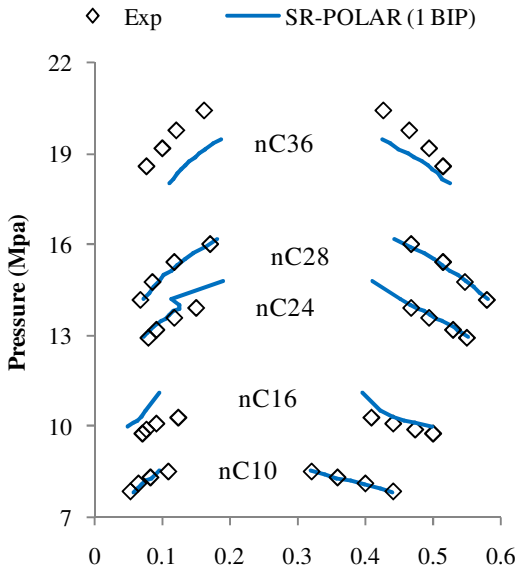

1 b) Solute Mass Fraction

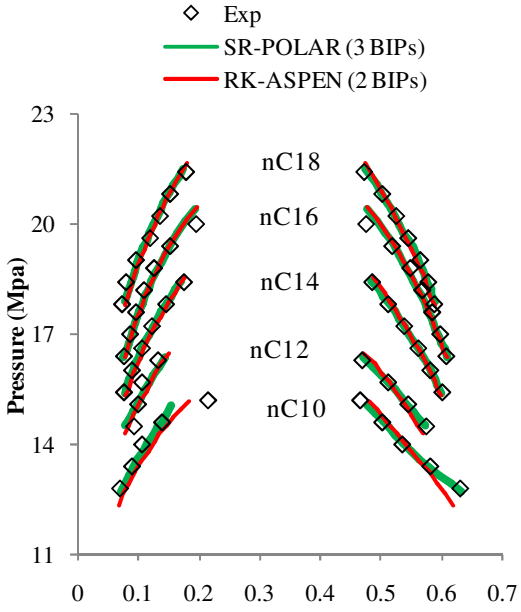

2 a) Solute Mass Fraction

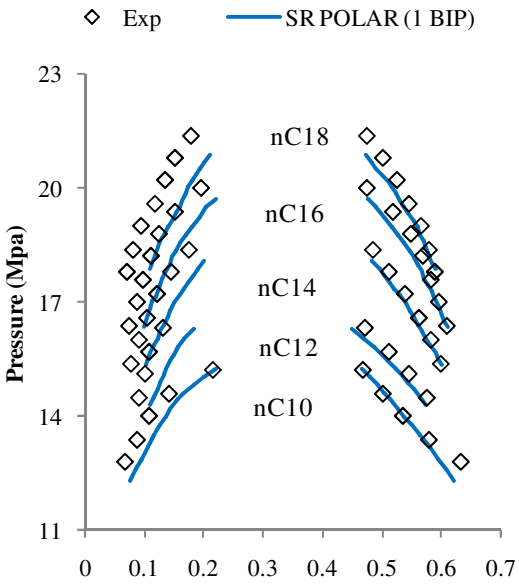

2 b) Solute Mass Fraction

Stellenbosch University https://scholar.sun.ac.za

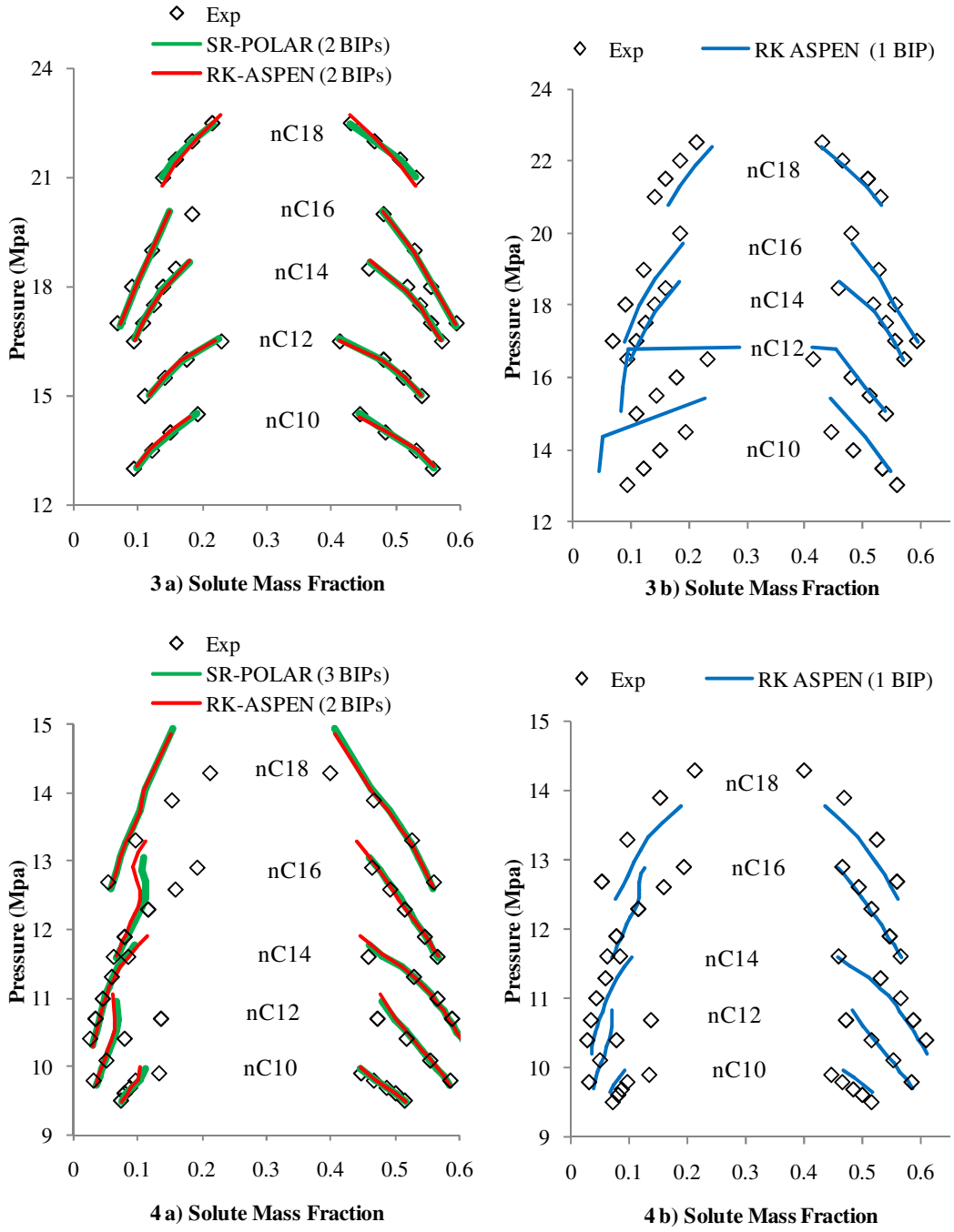

Figure 7-1 Model fits for SR-POLAR and RK-ASPEN EOS using a) 2 or 3 BIPs and using b) 1 BIP for ethane with the (1) n-alkanes [1, 2], (2) 1-alcohols [4], (3) carboxylic acids [7] and (4) methyl esters [5] systemsat 352 K

From Figure 7-1 1b) it is seen that the SR-POLAR model with a single BIP ($l_{a,ij}$) gives a reasonable representation of the data for the n-alkanes, however as shown in Table 7-4 (highlighted in blue), the %AAD in Y_2 are above 32 %AAD and deviations increase with larger carbon numbers, as seen for the ethane/hexatriacontane (nC36) system in Figure 7-1 1b).

Stellenbosch University https://scholar.sun.ac.za

Figure 7-1 1 a) shows that a very good fit is obtained with use of an additional BIP for both the SR-POLAR and RK-ASPEN models over the whole n-alkane series.

For the alcohols (Figure 7-1 2 a) and b)), use of a single BIP gives reasonable correlation of the nC10 system, but under-predicts the data, especially the dew curve (vapour phase), with increasing carbon number. For the ethane/octadecanol (nC18) system, the dew curve predicted by the model falls on the ethane/hexadecanol (nC16) data points, confirming that more than 1 BIP is required to accurately distinguish between members of the 1-alcohol series.

For the carboxylic acids (Figure 7-1 3 a) and b)), a single BIP gives a good fit for the ethane/tetradecanoic acid (nC14) system. Convergence errors are observed for the lower carbon numbers, but deteriorated model performance for larger solutes again enforces the use of more than 1 BIP for good correlation of all systems in the series. It may be noted that these parameters have been used to construct the phase envelope in MALTAB software (see also Chapter 9) and the observed convergence errors are therefore not deemed to have an effect on the regression routine and parameters obtained, but rather seems to culminate from the property evaluation method in Aspen Plus ® after parameters have been regressed.

The errors observed in Figure 7-1 4 a) upon approaching the critical region for the methyl esters are most likely due to convergence errors rather than model inadequacy. Figure 7-1 4 b) shows that a single BIP provides a good representation of the lower carbon number systems but loses accuracy with increasing asymmetry. Multiple BIPs therefore again seem to be a necessity.

From Table 7-4, it is generally seen that slightly better results are obtained for the polar 1-alcohols and acids than for the n-alkanes and methyl esters. It can also be seen from Figure 7-1 that the phase curves of the more polar 1-alcohols and acids have a more concave (less flat) profile than the n-alkanes and methyl esters, as was also pointed out in Section 3.2. The results from Table 7-4 therefore suggest that with use of BIPs in the mixing rules, the more concave phase curve for the polar solutes in the high-pressure region is correlated with slightly better accuracy than the flatter phase curves of the non-polar substances.

7.4.4 Overall results: Propane

Table 7-6 contains the results for the propane systems for each regression case. The results are presented as an average %AAD over the 5 systems chosen for each homologous series as given in Table 7-2.

Stellenbosch University https://scholar.sun.ac.za

Table 7-6 Overall results for propane systems

Propane

RK ASPEN — Alkanes

Case	Avg. %AAD T	P	X_2	Y_2
$k_{a,ij}$	0.80	0.94	0.24	21.10
$k_{b,ij}$	1.41	2.04	1.58	38.48
$k_{a,ij}/k_{b,ij}$	0.44	0.20	0.12	11.28

RK ASPEN — Alcohols

Case	Avg. %AAD T	P	X_2	Y_2
$k_{a,ij}$	1.34	1.73	0.49	11.41
$k_{b,ij}$	2.58	1.96	1.14	22.42
$k_{a,ij}/k_{b,ij}$	0.80	1.14	0.51	11.22

RK ASPEN — Acids

Case	Avg. %AAD T	P	X_2	Y_2
$k_{a,ij}$	0.59	0.88	0.15	11.96
$k_{b,ij}$	0.67	0.58	0.48	23.58
$k_{a,ij}/k_{b,ij}$	0.27	0.37	0.14	11.08

PR — Alkanes

Case	Avg. %AAD T	P	X_2	Y_2
$k_{a,ij}$	1.44	2.32	0.15	29.59
$l_{a,ij}$	1.26	2.04	0.16	28.87
$k_{a,ij}/l_{a,ij}$	0.32	0.15	0.10	9.96

PR — Alcohols

Case	Avg. %AAD T	P	X_2	Y_2
$k_{a,ij}$	0.86	1.43	0.39	14.43
$l_{a,ij}$	0.91	1.30	0.43	12.15
$k_{a,ij}/l_{a,ij}$	0.89	1.17	0.45	10.35

PR — Acids

Case	Avg. %AAD T	P	X_2	Y_2
$k_{a,ij}$	0.89	1.40	0.14	22.94
$l_{a,ij}$	0.65	1.06	0.14	19.80
$k_{a,ij}/l_{a,ij}$	0.53	0.66	0.16	11.61

PR-BM — Alkanes

Case	Avg. %AAD T	P	X_2	Y_2
$k_{a,ij}$	1.39	2.22	0.14	28.47
$l_{a,ij}$	1.23	1.95	0.16	27.86
$k_{a,ij}/l_{a,ij}$	0.33	0.16	0.10	10.09

PR-BM — Alcohols

Case	Avg. %AAD T	P	X_2	Y_2
$k_{a,ij}$	0.87	1.41	0.45	13.53
$l_{a,ij}$	0.98	1.35	0.44	13.30
$k_{a,ij}/l_{a,ij}$	0.83	1.23	0.45	11.01

PR-BM — Acids

Case	Avg. %AAD T	P	X_2	Y_2
$k_{a,ij}$	0.86	1.32	0.14	21.96
$l_{a,ij}$	0.63	1.01	0.14	19.04
$k_{a,ij}/l_{a,ij}$	0.51	0.63	0.15	11.64

SRK — Alkanes

Case	Avg. %AAD T	P	X_2	Y_2
$k_{a,ij}$	2.37	1.09	0.16	36.10
$l_{a,ij}$	1.70	0.81	0.25	32.93
$k_{a,ij}/l_{a,ij}$	2.87	2.13	1.97	37.03

SRK — Alcohols

Case	Avg. %AAD T	P	X_2	Y_2
$k_{a,ij}$	2.39	4.17	0.53	21.42
$l_{a,ij}$	3.24	4.29	1.11	21.34
$k_{a,ij}/l_{a,ij}$	4.22	3.37	1.16	21.46

SRK — Acids

Case	Avg. %AAD T	P	X_2	Y_2
$k_{a,ij}$	2.22	1.03	0.14	36.40
$l_{a,ij}$	2.18	1.00	0.26	35.55
$k_{a,ij}/l_{a,ij}$	2.18	0.81	0.21	37.84

SR POLAR — Alkanes

Case	Avg. %AAD T	P	X_2	Y_2
$k_{a,ij}$	0.78	0.92	0.29	20.94
$l_{a,ij}$	0.77	1.03	0.21	21.02
$k_{a,ij}/l_{a,ij}$	0.44	0.21	0.12	11.17
$k_{b,ij}$	1.26	0.93	0.68	38.79
$k_{a,ij}/k_{b,ij}$	0.45	0.20	0.13	11.31
$k_{a,ij}/k_{b,ij}/l_{a,ij}$	0.08	0.07	0.08	3.57

SR POLAR — Alcohols

Case	Avg. %AAD T	P	X_2	Y_2
$k_{a,ij}$	1.32	1.70	0.51	11.50
$l_{a,ij}$	1.47	1.99	0.49	12.63
$k_{a,ij}/l_{a,ij}$	1.06	1.09	0.57	12.26
$k_{b,ij}$	2.68	1.91	1.20	22.84
$k_{a,ij}/k_{b,ij}$	0.81	1.13	0.53	11.07
$k_{a,ij}/k_{b,ij}/l_{a,ij}$	0.47	0.59	0.30	5.50

SR POLAR — Acids

Case	Avg. %AAD T	P	X_2	Y_2
$k_{a,ij}$	0.57	0.85	0.15	12.19
$l_{a,ij}$	0.49	0.75	0.15	12.30
$k_{a,ij}/l_{a,ij}$	0.28	0.38	0.14	11.22
$k_{b,ij}$	0.67	0.61	0.48	23.52
$k_{a,ij}/k_{b,ij}$	0.27	0.37	0.14	11.09
$k_{a,ij}/k_{b,ij}/l_{a,ij}$	0.26	0.38	0.12	8.88

Key	Description
	Best fit within a homologous series
	2nd best fit within a homologous series
	3rd best fit within a homologous series
	Best fit for a single BIP within a homologous series

Stellenbosch University https://scholar.sun.ac.za

As expected, the SR-POLAR model with 3 BIPs gives a good representation of the data, providing the best results for all three homologous series. There is little to choose between the PR, PR/BM and RK-ASPEN models when using 2 BIPs, however as with the ethane systems, the SRK EOS struggles, despite using 2 BIPs. When 3 BIPs are used (SR-POLAR), the best results are obtained for the n-alkanes, followed by the 1-alcohols and then the acids.

7.4.5 BIP values: Propane systems

Table 7-7 gives the values of the BIPs for the best cases using the SR-POLAR and RK-ASPEN models for each homologous series in propane.

Table 7-7BIPs for best regression cases for propane systems using the SR-POLAR and RK-ASPEN models (CN : carbon number)

Propane (T = 408 K)					
Model:	SR-POLAR			RK-ASPEN	
Solute	BIP's			BIP's	
Alkanes (CN)	$k_{a,ij}$	$k_{b,ij}$	$l_{a,ij}$	$k_{a,ij}$	$k_{b,ij}$
14	-6.60909	-2.96890	-5.32856	0.03407	0.01283
16	-5.12155	-2.19084	-4.15632	0.04687	-0.03919
24	-1.54344	-0.50449	-1.29802	0.03308	0.00204
28	-1.36516	-0.37121	-1.17107	0.02736	0.01823
36	-2.81974	-0.53069	-2.48578	0.01514	0.04840
Alcohols (CN)	$k_{a,ij}$	$k_{b,ij}$	$l_{a,ij}$	$k_{a,ij}$	$k_{b,ij}$
10	-2.22036	-1.29888	-1.65724	0.02295	0.01159
12			-0.01502	0.02360	-0.02083
14	-0.55231	-0.35680	-0.43561	0.02660	-0.05278
16	-1.36255	-0.72991	-1.08810	0.03283	-0.02336
18	-0.82279	-0.39606	-0.66333	0.01511	-0.02870
Acids (CN)	$k_{a,ij}$	$k_{b,ij}$	$l_{a,ij}$	$k_{a,ij}$	$k_{b,ij}$
10	-0.86512	-0.56421	-0.64899	0.00777	-0.04400
11	-0.04097	-0.03507	-0.03147	0.00040	-0.01751
12	-0.43720	-0.24721	-0.32853	-0.00287	-0.01659
16	0.49879	0.21507	0.37655	0.01392	-0.00459
18	-0.07881	-0.02779	-0.08067	0.02302	0.01757

As with the ethane systems, BIP values are much larger when 3 BIPs are used, suggesting the model is forced through the data in these cases.

Stellenbosch University https://scholar.sun.ac.za

7.4.6 Propane plots

Figure 7-2compares the fit for the best cases from the SR-POLAR and RK-ASPEN models from Table 7-6and the best case for a single BIP for each series, as also high-lighted in blue in Table 7-6.

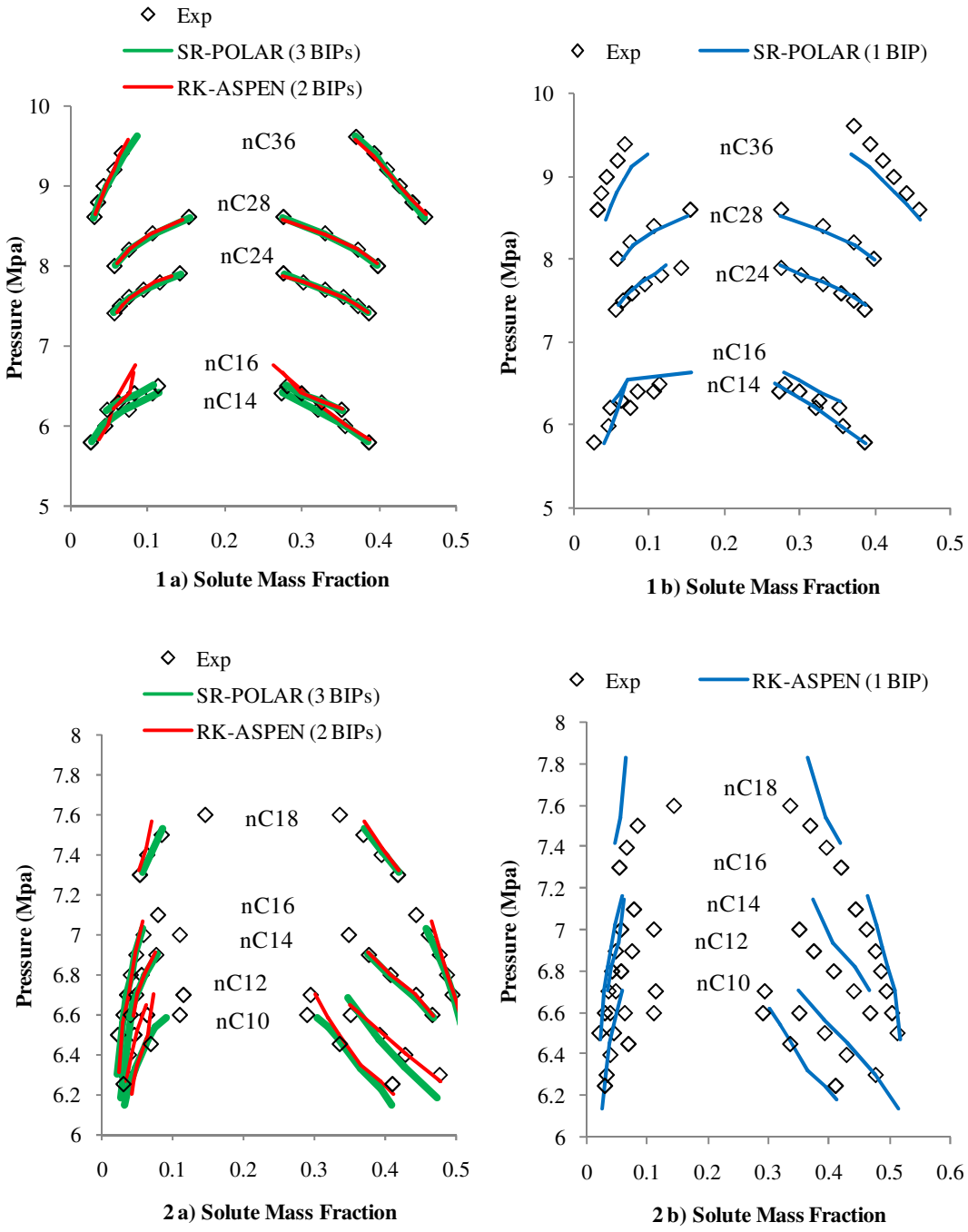

Stellenbosch University https://scholar.sun.ac.za

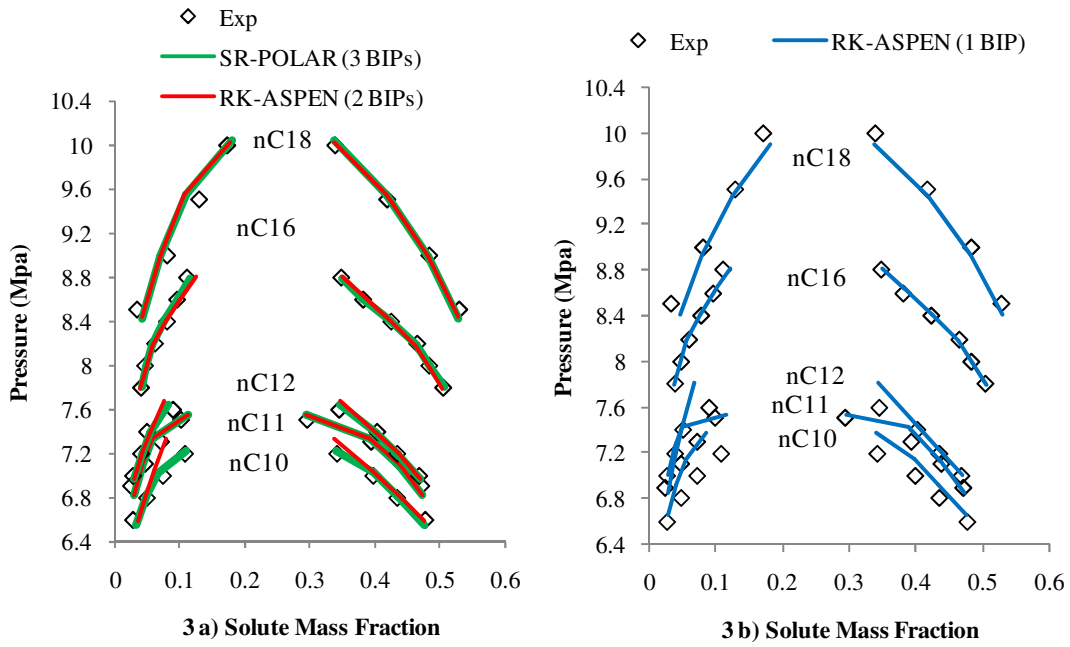

Figure 7-2 Model fits for the SR-POLAR and RK-ASPEN EOS using a) 2 or 3 BIPs and using b) 1 BIP for propanewith the (1) n-alkanes [8 , 9, 10] , (2) 1-alcohols [11] and (3) carboxylic acids [12]at 408 K

As with the ethane systems, Figure 7-21b) shows that reasonable results are obtained for the n-alkane solutes with a single BIP in the SR-POLAR model, however errors increase with asymmetry of the mixture and multiple BIPs are required for carbon number above 30. The deviations observed in Figure 7-2 1a) for the RK-ASPEN model in the critical region of the propane/tetradecane (nC14) and propane/hexadecane (nC16) systems are probably due to convergence problems rather than model inadequacy. Good representation of the data is achieved with use of multiple BIPs in the SR-POLAR and RK-ASPEN models.

Figure 7-22 a) for the 1-alcohols shows that use of multiple BIPs in the SR-POLAR and RK-ASPEN model give a very good representation of the data, but large errors, especially for the propane/octadecanol (nC18) system and for the vapour phase in general, are observed for use of 1 BIP in the RK-ASPEN model.

Figure 7-22 b) shows that surprisingly good correlation for the carboxylic acids is obtained for 1 BIP, however deviations are observed for the lower carbon number systems propane/nC10, nC11 and nC12, especially in the dew curve. This is presumably due to the more pronounced effect of the polar functional group for these systems. Use of additional BIPs again provides a very good fit for the whole acid series in propane.

Stellenbosch University https://scholar.sun.ac.za

For the 1-alcohols and the acids, use of 1 BIP in the energy parameter of RK-ASPEN gives results comparable to use of 2 BIPs, but not for the n-alkanes. This again suggests that fitting BIPs allows for a slightly improved correlation of the more concave phase curves of the polar solutes.

7.5 Including data in the critical region

It was noted in Section 7.3.1 that the near critical region was excluded from the fitting of BIPs since this region is generally over-predicted by mean-field equations such as the CEOSs. Including this regionalso typically leads to convergence errors and would result in parameters which compromise the representation of the classic, non-critical region for which the models are better suited. Figure 7-3 shows the nC16 solute for selected homologous series in ethane and propane, using the RK-ASPEN EOS with 2 BIPs, but with data points included in the near-critical region.

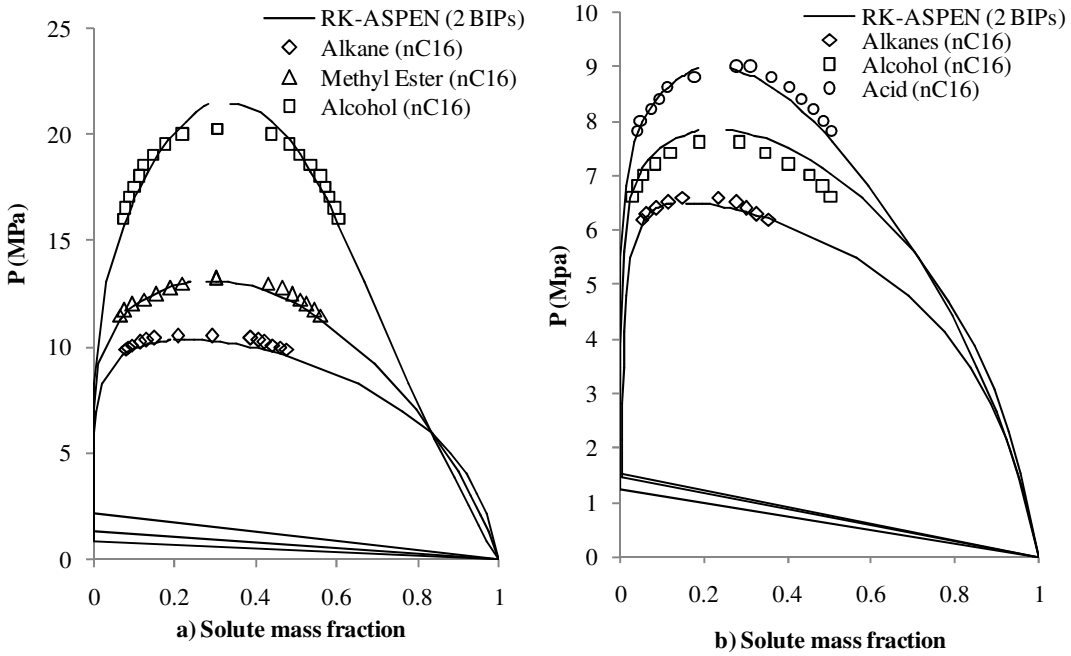

Figure 7-3 Model fits for RK-ASPEN EOS (2 BIPs) for a) ethane with n-alkanes [1,2], 1-alcohols [4] and methyl esters [5]at 352 K, as well as b) propane with the n-alkanes [8, 9, 10], 1-alcohols [11] and carboxylic acids [12]at 408 K with data points in the near critical region included

These plots were generated using a bubble point calculation in MATLAB software, as outlined in Appendix in B.3. The BIPs from Table 7-5 and Table 7-7 for the RK-ASPEN

Stellenbosch University https://scholar.sun.ac.za

model were used, as well as the same pure constants and alpha function parameters as used in obtaining the parameters using the Aspen Plus ® "data regression" routine (see Section 7.3.2). Table 7-8 gives the %AAD in P, Y_1 and Y_2 for each system in Figure 7-3 for both the case when data in the critical region is included and excluded (as in Figure 7-1 and Figure 7-2).

Table 7-8 Model fit comparison for ethane (352 K) and propane (408 K) with the nC_{16} n-alkane1-alcohol, methyl ester and carboxylic acid when data points in the critical region are excluded and included

	Ethane (352 K)					
	Critical region excluded			Critical region included		
	%AAD P	%AAD Y_1	%AAD Y_2	%AAD P	%AAD Y_1	%AAD Y_2
n-Hexadecane	2.18	0.08	0.88	3.23	2.18	14.56
1-Hexadecanol	3.31	0.41	3.08	4.31	0.8	4.03
Methyl Hexanoate	2.12	0.3	3.76	2.41	3.99	16.82
	Propane (408 K)					
	Critical region excluded			Critical region included		
	%AAD P	%AAD Y_1	%AAD Y_2	%AAD P	%AAD Y_1	%AAD Y_2
n-Hexadecane	0.94	1.64	18.03	1.23	2.53	20.25
1-Hexadecanol	5.59	1.3	39.64	4.46	1.48	23.21
Hexadecanoic acid	2.19	0.45	8.66	2.45	5.1	27.83

It is seen that errors increase when data for the critical region is included for all systems, except the propane/1-hexadecanol system. As seen in Figure 7-3 b), this exception is observed because the parameters obtained from the Aspen Plus ® regression routine for this system over-predicts the classical high pressure region when T and X are used as the specification variables. Upon including data for the critical region, the fit is thus improved, since this region is naturally over-predicted relative to the classic high-pressure region. If the classic region isbetter correlated, the qualitative shift in the phase curve should lead to greater over-prediction of the critical point, as observed for the ethane/1-hexadecanol system in Figure 7-3 a). It is also noted that the %AAD for the systems in Table 7-8, especially the ethane/1-hexadecanol system, do not fully reflect the observed over-prediction of the critical point observed from Figure 7-3 a), because the calculation terminates before taking into account the maximum pressure datum for which the model fit is worst.

Figure 7-3 a) also puts into perspective the slight improvement observed for the correlation of the polar 1-alcohols and acids relative to the n-alkanes and methyl esters in ethane (see Table 7-4). The more concave high-pressure region of the polar systems is easier to correlate than the curvature of the non-polar systems, but this is done at the expense of greater over-prediction of the critical region. This also holds for the propane systems, where it is seen in

Stellenbosch University https://scholar.sun.ac.za

Figure 7-3 b) that the flatter profiles lead to smaller over-prediction of the critical pointas, for example, compared tothe ethane/hexadecanol system in Figure 7-3 a).

7.6 Qualitative effect of BIPs

In order to assess the qualitative effect of BIPs in both the size and energy parameter, a sensitivity analysis was conducted using the classic Van der Waals mixing rules (Equation 7-10 to 7-13) with the PR EOS and the Stryjek-Vera (SV) alpha function (Equation 6-18 and 6-19). Parameters were regressed using MATLAB software and using the computational procedure outlined in Appendix B.3 (also see Section 8.2). Figure 7-4 compares the pure prediction (no BIPs) and use of 2 BIPs in the mixing rules for the ethane/hexadecane system.

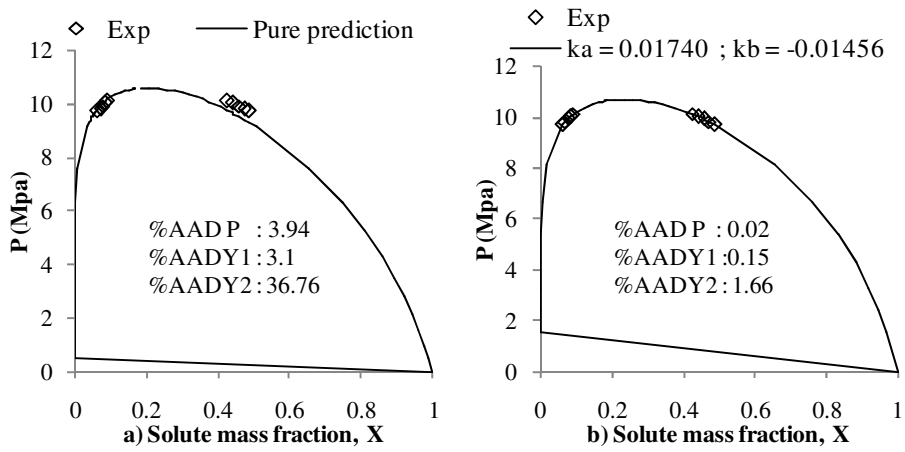

Figure 7-4Ethane/hexadecane [1] system with the PR-SV model and Van der Waals mixing rules for a) pure prediction and b) using 2 BIPs

A reasonable qualitative representation of the ethane/hexadecane system is obtained with no BIPs, even though the error in the vapour phase for the heavier component (Y_2) approaches 40%. The BIPs improve the quantitative fit dramatically, but not much can be deduced about the qualitative impact of the BIPs from Figure 7-4 b). Figure 7-5 shows the same comparison for the ethane/1-hexadecanol system.

Stellenbosch University https://scholar.sun.ac.za

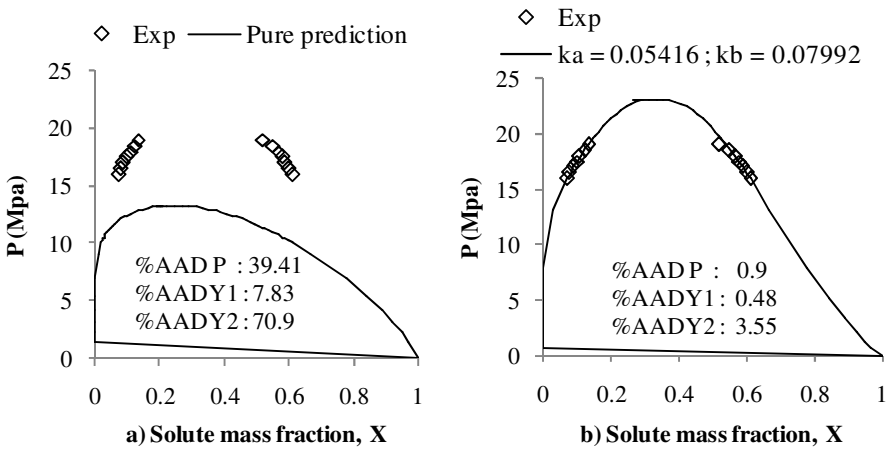

Figure 7-5 Ethane/1-hexadecanol system with the PR-SV model and Van der Waals mixing rules for a) pure prediction and b) using 2 BIPs

It is seen that the pure prediction significantly under-predicts the data, but good correlation is obtained with 2 BIPs. Given the large difference between the pure prediction and the case with 2 BIPs, the ethane/hexadecanol system is used to investigate the qualitative impact of each BIP in both the energy ($k_{a,ij}$) and size parameter ($k_{b,ij}$) using the classic Van der Waals mixing rules. Table 7-9 gives the cases investigated for this analysis:

Table 7-9 Cases for investigating the qualitative effect of BIPs inthe Van der Waals mixing rulesfor both the size and energy parameters using the PR-SV model

Case	BIP changed	Relative value
a)	$k_{a,ij}$	0
b)	$k_{a,ij}$	1/3
c)	$k_{a,ij}$	2/3
d)	$k_{b,ij}$	0
e)	$k_{b,ij}$	1/3
f)	$k_{b,ij}$	2/3

The “relative value” column gives the fraction of the final regressed value (as in Figure 7-5 b)) for the particular BIP, while the other BIP is held constant at its final regressed value. Figure 7-6 gives the results of this qualitative investigation.

Stellenbosch University https://scholar.sun.ac.za

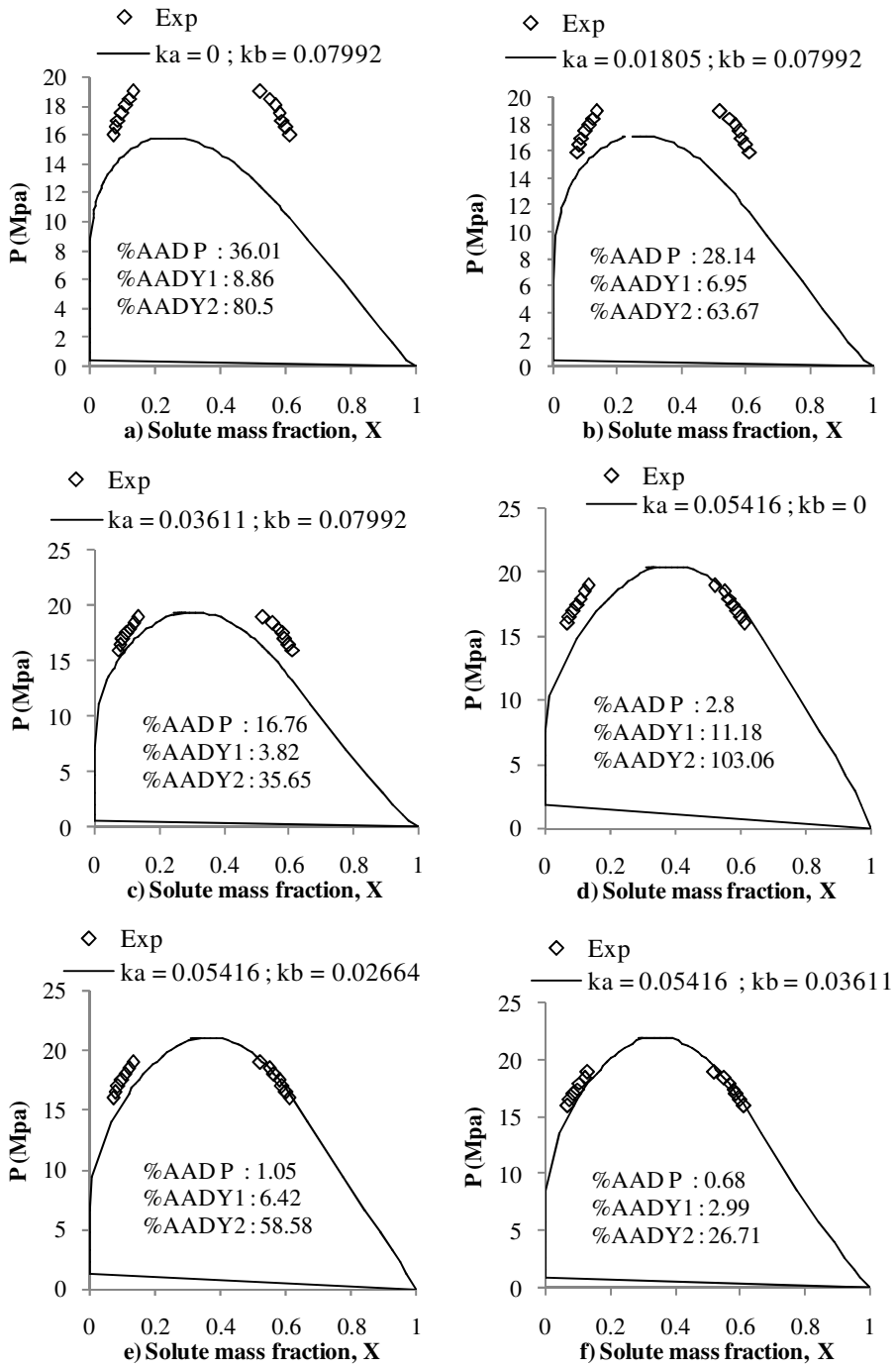

Figure 7-6BIP sensitivity for ethane/1-hexadecanol system with the PRSV model and Van der Waals mixing rules for cases a) – f) as given in Table 7-9

Figure 7-6 a) – c) gives the effect of increasing $k_{a,ij}$, while keeping $k_{b,ij}$ constants at its final regressed value, and Figure 7-6 d) – f) gives the effect of increasing $k_{b,ij}$ while keeping $k_{a,ij}$ at its final value. In general, $k_{a,ij}$ clearly has a larger qualitative and quantitative impact on the phase curve than $k_{b,ij}$. Even though the BIPs are not mutually orthogonal, meaning the

Stellenbosch University https://scholar.sun.ac.za

influence of a particular BIP is dependent on the value of the other, it is seen that $k_{a,ij}$ is largely responsible for a vertical translation along the pressure axis, whereas $k_{b,ij}$ influences more the lateral dimension along the compositional axis.

These results support the idea that BIPs in both the energy and size parameters are necessary for full qualitative flexibility of the mixing rules. The results from Tables 7-4 and 7-6 show, however, that there is little to choose between the models once 2 BIPs are used irrespective, of whether the parameters are only used in the energy parameter or split between the parameters. A qualitative investigation into the flexibility that can be achieved by incorporating multiple BIPs within each pure parameter is required for further clarification on this point.

7.7 BIPs vs. Solute carbon number

In an attempt to see whether any trends may be observed in the BIPs for possible development of generalized correlations, the BIPs for all cases were plotted as a function of carbon number. Figure 7-7 shows the BIPs vs. carbon number for the ethane/1-alcohol systems for the PR model, as obtained from the Aspen Plus ® data regression routine.

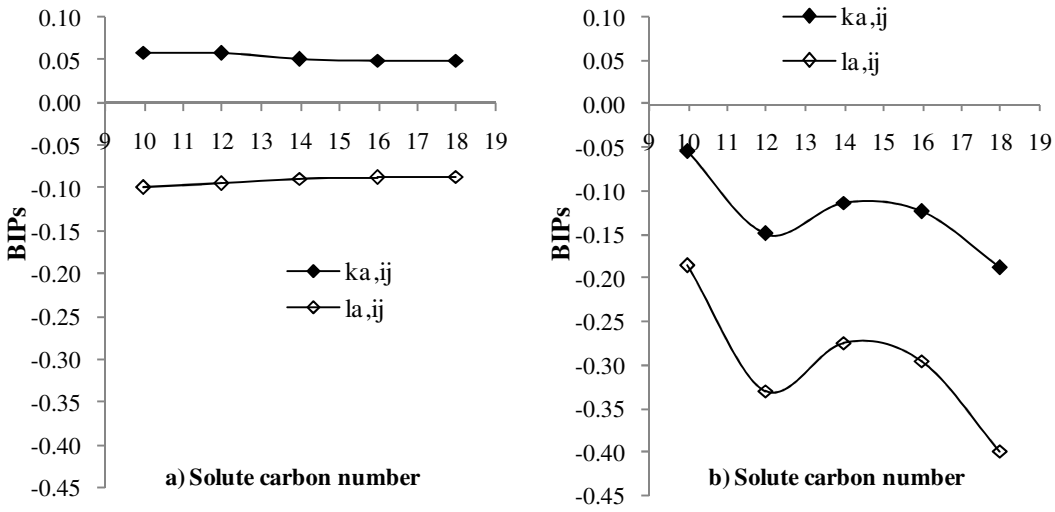

Figure 7-7 BIP vs. Solute carbon number for the PR model regressing a) 1 BIP at a time and b) both simultaneously for the ethane/1-alcohols

Figure 7-7 a) shows the BIPs vs. solute carbon number if 1 BIP is used. Both interaction parameters available in the Mathias et al. [101] mixing rule are *well behaved*, showing a monotonic trend over the carbon number range with a small range in the values. Figure 7-7 b) shows the BIP behaviour if both of these parameters are regressed simultaneously. As shown

Stellenbosch University https://scholar.sun.ac.za

in Table 7-4, this greatly improves the correlation, but the monotonic nature of the parameters is lost and values take on larger absolute values. Figure 7-8 shows the BIPs vs. carbon number for the ethane/1-alcohol systems for the RK-ASPEN model, which unlike the PR model in Figure 7-7, incorporates BIPs into both the energy and size parameter.

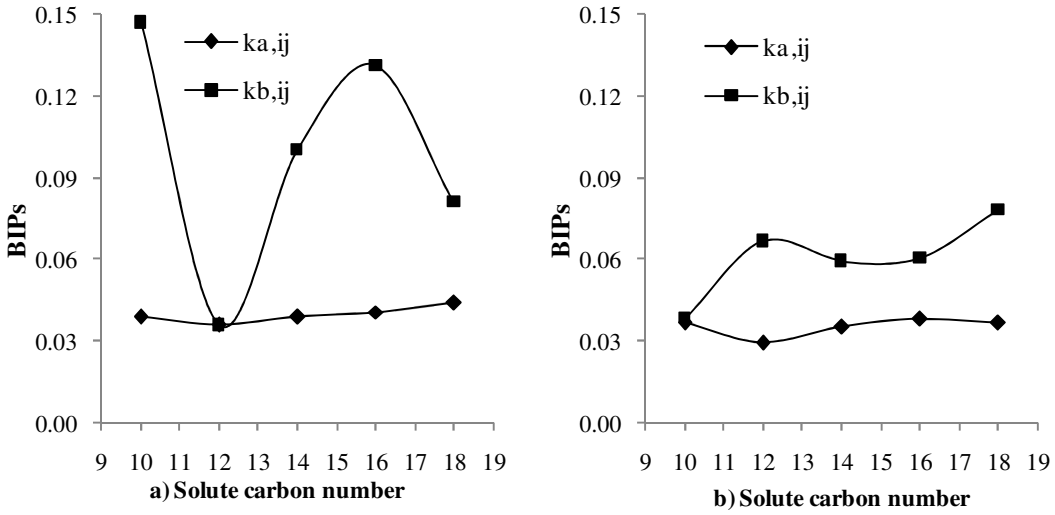

Figure 7-8 BIP vs. Solute carbon number for the RK-ASPEN model regressing a) a single BIP and b) both simultaneously for the ethane/1-alcohols

Even though non-monotonic behaviour is observed for $k_{b,ij}$,, even when it is regressed exclisively (Figure 7-8 a)), two things are worth noting when comparing the BIP behaviour in Figures 7-7 and 7-8. Firstly, the 2 BIPs seem to take on smaller values when they are split between the parameters as done in the quadrtic Van der Waals mixing rules used in the RK-ASPEN model (Figure 7-8) vs. when they are incorporated into the same parameter (Figure 7-7). The BIPs also become less inter-correlated when split between the parameters. This encourages the BIPs to be split between the energy and size parameter when 2 BIPs are used in the mixing rules.

These observations were made through-out all cases in Tables 7-4 and 7-6, however a degree of inter-correlation was typical of all systems. The plots for BIPs vs. solute carbon number for all cases investigated in this chapter are given in Appendix E.1.

It is furthermore likely that these parameters are temperature dependent and that different values may be obtained for fitting the low pressure region, which further implies the requirement of density dependence in the mixing rules for fitting the whole phase envelope. None of the cases investigated were therefore deemed appropriate for developing reliable generalized correlations.

Stellenbosch University https://scholar.sun.ac.za

7.8 Conclusions

This chapter addresses project objective 5 (see Section 1.3) by determining the capabilities of the Aspen Plus ® process simulation package for correlating the high-pressure VLE of asymmetric binaries of the n-alkane, 1-alcohol, carboxylic acid and methyl ester series with ethane (353 K) and propane (408 K) as solvents, for the design of a SFE process. 5 CEOS modelsfrom the Aspen Plus ®process simulator are investigated, incorporating various mixing rules and alpha functions. Objective 6 is also addressed by investigating the sensitivity and qualitative effect of BIPs in the model mixing rules and plotting their behaviour vs. solute carbon number for possible development of generalized correlations. The main outcomes from this chapter are summarized below:

- Use of at least 2 BIPs in the model mixing rules are required to achieve a reasonable correlation of the data, with errors in P, T and X_2 typically below 1 %AAD and errors in Y_2 ranging from 4 to 12 %AAD, across the entire solute carbon number range for all the systems investigated, using both ethane and propane solvents.
- Large BIP value sare obtained when using 3 BIPs in the SR-POLAR model, suggesting the model is forced through the data in correlating the errors.
- A qualitative investigation into BIP behaviour suggests that BIPs in both the energy and size parameter are required for full flexibility of the mixing rules.
- Monotonic and often linear trends for BIPs vs. solute carbon number are observed for the use of 1 BIP, however at least 2 BIPs are required for reasonable representation of the data in all models, which leads to inter-correlation of the BIPs, greatly impeding the development of reliable correlations.
- When 2 BIPs are used, it may be recommended to split the BIPs between the pure parameters, since this leads to smaller BIP values and smoother trends with solute carbon number.
- Due to general model inadequacy and convergence problems in the near-critical region, a large part of the phase curve approaching the critical point is typically excluded in fitting parameters.
- Including data in the critical region for model evaluation shows a general increase in errors due to over-estimation of the critical point.
- The shape of the phase curve seems to influence the correlation of data, whereby the more concave shape of the polar 1-alchols and acids (especially in ethane) shows improved correlations over the flatter profiles of the non-polar solutes in the classic high-pressure region, however the more concave shape leads to a greater over-estimation of the critical point.

Stellenbosch University https://scholar.sun.ac.za

It has therefore been shown that simple cubic models available in Aspen Plus ® can be used to satisfactorily correlate the high pressure VLE of various long-chain hydrocarbon solutes in ethane (353 K) and propane (408 K) at solvent reduced temperatures of 1.153 and 1.106, respectively. Aspen Plus ® is therefore deemed a suitable tool for developing a process model for SFE applications at the investigated process conditions.

Zamudio [206] and Stoldt and Brunner [205] note that model performance deteriorates drastically at lower temperatures closer to the solvent critical temperature, where the isothermal compressibility diverges. Improvement of EOS models for accurate VLE correlation at these temperatures is of great value to SFE applications and a good area for future study.

Zamudio et al. [207] have also found that modelling a multi-component mixture of CO_2 with (n-dodecane + 1 decanol + 3,7 dimethyl-1-octanol), using only BIPs obtained for the binary solvent/solute interactions, proved inadequate for accurate correlation of the VLE for the multi-component system, especially at high solute mass fractions. Obtaining BIPs for the solute/solute interactions and possible modification of mixing rules for multi-component mixtures is therefore also a worthy subject for future study.

Stellenbosch University https://scholar.sun.ac.za

8. STATISTICAL SENSITIVITY ANALYSIS FOR BINARY VLE MODELLING

The flexibility of the CEOSs allow for many modelling options, which lead to many factors to be taken into account for any particular application. This chapter addresses project objective 7, by investigating factors of importance in modelling high pressure VLE data of asymmetric binaries with the CEOSs using ethane as solvent. The effects of these factors are investigated through a factorial design of experiments (DOE) statistical sensitivity analysis, conducted using STATISTICA 12 software. The design is a 2 level factorial with 6 factors. This amounts 64 treatments (modelling combinations) to assess the effects and interactions amongst the considered factors.The first four factors are *model dependent*, including:

- Temperature dependence of the model (1 or 2 parameter alpha function)
- Volume dependence of the model (2 or 3 parameter model)
- Pure component constants used (Data or estimation method)
- Mixing rules used (classic Van der Waals or G_{ex}/EOS mixing rule)

The last two factors are *system dependent*:

- Temperature range (lower and higher temperature)
- Solute functional group (non-polar and polar)

The *response variable* used to investigate the effect of these factors on the modelling problem is an average in the %AAD of the output variables:

$$\text{Response} = \frac{\%\text{AAD P} + \%\text{AAD Y}_1 + \%\text{AAD Y}_2}{3} \qquad 8\text{-}1$$

P, Y_1 and Y_2 are the output variables since the MATLAB software developed for conducting this investigation performs a bubble point pressure calculation, which uses T and X as specification variables to determine P and Y iteratively. The procedure is outlined in Section 8.2, with a full algorithm presented in Appendix B.3.

8.1 Thermodynamic theory: Phase equilibrium of a mixture

In Section 6.1 it was shown how the fundamental property relation for the total Gibbs free energy can be used as a basis for deriving the phase equilibrium conditions for a pure component. For the more general case of a single-phase open system in which material may pass into and out of the system, the fundamental property relation may be given as follows:

Stellenbosch University https://scholar.sun.ac.za

$$d(nG^t) = (nV^t)dP - (nS^t)dT + \sum_i \mu_i dn_i \quad 8\text{-}2$$

μ_i is the *chemical potential* (also called the molar Gibbs energy) and is defined as the partial derivative of the Gibbs free energy with molar amount of a species i:

$$\mu_i \equiv \left[\frac{\partial(nG^t)}{\partial n_i}\right]_{P,T,n_j} \quad 8\text{-}3$$

By applying Equation 6-1 to a *closed* system consisting of vapour and liquid phases, which can exchange mass and therefore be modelled as *open* systems via Equation 8-2, the common criterion for equilibrium in terms of chemical potential can be derived [46]:

$$\mu_i^\alpha = \mu_i^\beta = \mu_i^\gamma = \ldots\ldots\ldots = \mu_i^\pi \text{ for } i = 1,2,\ldots\ldots, C \quad 8\text{-}4$$

Following an analogous procedure to Section 6.1 for a pure component, it can be shown that by taking the partial molar derivative of Equation 6-5 on both sides and integrating the result, a new criterion for equilibrium can be derived in terms of the *fugacity of component i in solution:*

$$\hat{f}_i^\alpha = \hat{f}_i^\beta = \hat{f}_i^\gamma = \ldots\ldots\ldots = \hat{f}_i^\pi \text{ for } i = 1,2,\ldots\ldots, C \quad 8\text{-}5$$

In order to calculate these component fugacities in solution from an EOS, it is necessary to relate them to the residual Gibbs energy of the mixture by taking the partial molar derivative of Equation 6-6 on both sides [48]:

$$\frac{\mu_i(T,P) - \mu_i^{ig}(T,P)}{RT} = \left(\frac{\partial\left(\frac{nG - nG^{ig}}{RT}\right)}{\partial n_i}\right)_{T,P,nj\neq i} = \left(\frac{\partial(\ln\varphi_i)}{\partial n_i}\right)_{T,P,n_j} = \ln(\hat{\varphi}_i) \quad 8\text{-}6$$

$\hat{\varphi}_i$ is the *fugacity coefficient for component i in solution* and is defined as follows:

$$\hat{\varphi}_i \equiv \frac{\hat{f}_i}{y_i P} \quad 8\text{-}7$$

It can be noted that the denominator of $\hat{\varphi}_i$ (defined as the fugacity of species i in an *ideal* mixture) is no longer the total system pressure, as was the case for a pure component (Equation 6-6), but rather the partial pressure $y_i P$.

Stellenbosch University https://scholar.sun.ac.za

All that is now required in order to calculate the component fugacities in solution is an expression for the residual Gibbs energy from an EOS. As mentioned in Section 6.1, this can be problematic, because the natural independent variables for the Gibbs energy are T and P, however a pressure explicit EOS is in terms of T and V. The fugacity of component i in solution is therefore more conveniently obtained using the following expression in terms of the residual Helmholtz energy [48]:

$$\ln\hat{\varphi}_i = \ln\left(\frac{\hat{f}_i}{y_i P}\right) = \frac{\partial\left(\frac{nA^R{}_i}{RT}\right)_{T,V}}{\partial n_i} - \ln Z \qquad 8\text{-}8$$

The $\hat{\varphi}_i$ expressions for the models and mixing rules used in this study are presented in Appendix A. Validation of their consistency is given in Appendix B.4 and Appendix B.3 contains information on the computational procedures used in performing the required phase equilibrium calculations and fitting binary interaction parameters to VLE data.

8.2 Reduction of data

An algorithm for performing the VLE calculations by matching the component fugacities in solution for each species in each phase is presented in Appendix B.3. A standard bubble point calculation is used which takes temperature, T and liquid composition X as input variables and returns the equilibrium pressure P and vapour composition Y.

Different methods can be used to fit BIPs in the model mixing rules to binary VLE data through regression. One method is by constructing the phase envelope and minimizing the errors in P and Y by iterating the BIP values to minimize the following *explicit* objective function [208]:

$$F = \sum_{i=1}^{np}\left[\frac{(P_i{}^{exp} - P_i{}^{calc})^2}{(P_i{}^{exp})^2}\right]^{0.5} + \sum_{i=1}^{np}\sum_{j=1}^{nc}\left[\frac{y_j{}^{exp} - y_j{}^{calc})^2}{(y_j{}^{exp})^2}\right]^{0.5} \qquad 8\text{-}9$$

This objective function is computationally intensive since the entire phase envelope must be constructed for each iteration in the BIP values and convergence is typically slow in the high pressure region approaching the critical point. The small absolute values of the heavy component in the vapour phase for these asymmetric systems also lead to exaggerated relative errors, which causes the objective function to converge on BIP values that give unacceptable errors in the bubble point pressure, especially when data is only limited to the high pressure region. The following *implicit* objective function therefore provides a better option for fitting BIPs for the systems and data range investigated in this study:

Stellenbosch University https://scholar.sun.ac.za

$$F = \sum_{i=1}^{np} \sum_{i=1}^{nc} \left[\frac{(K_{i,j}^{exp} - K_{i,j}^{calc})^2}{(K_{i,j}^{exp})^2} \right]^{0.5} \quad 8\text{-}10$$

This objective function is referred to as implicit, because the K factors for a specific component can be calculated directly from an EOS as follows:

$$K_i = \frac{\hat{\varphi}^l{}_i}{\hat{\varphi}^v{}_i}$$

The fugacities are calculated from the experimental VLE values, eliminating the need for iterative calculations, which leads to much faster computational times. This objective function is also more robust than the explicit method, because it does not depend on minimization of error in any specific output variable. Lopez et al. [208] investigated the use of both explicit and implicit objective functions for asymmetric mixtures at high pressures and found an implicit method to not only be considerably faster, but also provides more reliable values for the BIPs. Equation 8-10 was therefore used as the objective function in this study and BIPs were obtained using the *fminsearch* function in MATLAB, which uses the Nelder-Mead simplex method as minimization algorithm.

8.3 Factor levels

This section summarizes the factors being investigated, their corresponding labels for the ensuing discussion and the 2 levels chosen for each factor. Table 8-1shows this information.

Table 8-1 Summary of factors, their corresponding labels and the levels selected for testing the effect on the response variable

Number	Factor	label	level 1	level 2
1	Volume dependence	Vol	PR EOS	PT EOS
2	Temperature dependence	Alpha	Soave	SV
3	Solute functional group	System	Alkane	Alcohol
4	Temperature range	T	338	352
5	Pure constants	Pure	DIPPR	C&G
6	Mixing rules	Mixing rule	VdW	WS

Stellenbosch University https://scholar.sun.ac.za

1. Volume dependence (2 or 3 parameter model)

In Chapter 6 it was found that the 3 parameter PT EOS provides substantial improvement in correlating the saturated liquid volume for the non-polar n-alkanes and methyl esters, while maintaining reasonable representation of the vapour pressure. This advantage of the PT EOS was lostfor the more polar 1-alcohols and carboxylic acids since larger errors were observed in the vapour pressure than for the PR and SRK EOS without significant improvement in the saturated liquid volume over that of the simpler PR EOS.

In order to assess the effect of the volume dependence of the model on the correlation of high-pressure binary VLE through the response variable, the 2 parameters PR EOS (level 1) and the 3 parameter PT EOS (level 2), were chosen as the 2 levels for this factor.

2. Temperature dependence (alpha function)

It was found in Chapter 6 that the 2 parameter Stryjek-Vera (SV) and Mathias alpha function improved the correlation of the pure component vapour pressure over the simpler Soave alpha function. In order to assess the effect of the temperature dependenceof the model on the response variable, the 1 parameter Soave (level 1) and 2 parameter SV (level 2) alpha functions were chosen as the 2 levels of this factor.

3. Solute functional group

Given the importance of phase behaviour on both SFE and thermodynamic modelling, the effect of the solute functional group on the response variable was determined by selecting the non-polar n-alkane (level 1) and the more polar 1-alcohols (level 2) series as the two levels for this factor. 5 systems were modelled for each series, namely those with carbon numbers 10, 12, 14, 16 and 18 and the values in response variable were averaged.

4. Temperature range

The two levels selected to include the effect of temperature on the response variable was determine by the availability of data and are 338 K (level 1) and 352 K (level 2).

5. Pure constants

In Chapter 6 it was determined that using pure component constants in a CEOS other than those for which model parameters were regressed leads to large errors in the vapour pressure

Stellenbosch University https://scholar.sun.ac.za

and saturated liquid volume of the pure component. Such a practice may often be necessary when data are not available, both for pure constants and properties for re-fitting parameters.

In order to assess the effect that such a practice may have on the correlation of high-pressure binary VLE, pure component parametersin the PR and PT EOS with each alpha function were regressed using the DIPPR constants (level 1). Pure constants from the Constantinou and Gani (C&G) method for both solvent and solute were then used without regressing new pure parameters (level 2), in order to assess the effect that such a deviation in the pure component limit may have on the correlation of binary VLE in the high pressure region.

6. Mixing rules

The previous chapter investigated various mixing rules in conjunction with different CEOSs, including the classic quadratic Van der Waals mixing rules with 2 BIPs (used in the RK-ASPEN model), as well as mixing rules with higher order composition dependence, namely the Mathias et al. [101] mixing rule with 2 BIPs (used in the PR, SRK and PR/BM models) and the 3 BIP mixing rule of Schwartzenruber and Renon (used in the SR-POLAR model) [100]. Various mixing rules for the CEOSs were also reviewed in Section 4.2.4, including those that incorporate activity models for excess Gibbs energy (G_{ex}) into the mixing rule for improved correlation of more complex systems exhibiting polarity and size asymmetry.

In Chapter 7 it was found that among the mixing rules investigated, that of Schwartzenruber and Renon [100] as used in the SR-POLAR model gave the best overall correlation due to use of 3 BIPs and higher order composition dependence. This mixing rule suffers from well-known inconsistencies, such as the Michelsen-Kirstenmacher syndrome and the dilution effect (discussed in Section 4.2.4) and furthermore does not meet the theoretically correct quadratic composition dependence as imposed by the second virial coefficient (see Section 4.1).

The RK-ASPEN model gave comparable results to the SR-POLAR model, despite use of one less BIP in the classic Van der Waals mixing rules, which also meet the constraint of quadratic composition dependence and does not suffer from any inconsistencies. The Van der Waals mixing rules with 2 BIPs are therefore selected as level 1 for investigating mixing rules as a modelling factor in this chapter.

It was further found in Section 4.2.4, that Wong and Sandler found a way of incorporating an activity model into the mixing rules which meets the quadratic composition of the second virial coefficient at low pressures and converges to the liquid properties of the selected G_{ex} model at high pressures [129]. Despite questions raised regarding the fundamental

Stellenbosch University https://scholar.sun.ac.za

assumptions made in its derivation, especially for systems of large size asymmetry (see the work of Coutsikos et al. [130]), the Wong-Sandler (WS) mixing rule is nevertheless selected as level 2 for investigating the effect of mixing rules on the response variable.

Having selected the Van der Waals (VdW) (level 1) and Wong-Sandler (WS) (level 2) mixing rules as the two levels, there are still some decisions which need to be made in order to apply the mixing rules and compare them on an equal footing. These considerations include which G_{ex} model and combining rule for the second virial coefficient expression to use for the WS mixing rule, as well as which parameters to include in the regression for both mixing rules.

Van der Waals mixing rules

For the Van der Waals mixing rules, it was established in Chapter 7 (see Section 7.6) that 2 BIPs, one in both the energy and size parameter, seems necessary to achieve the full qualitative flexibility of these mixing rules. This approach, as given by Equations 7-10 to 7-13, is therefore followed in this chapter for the Van der Waals mixing rule. The following linear mixing rule is used for the third parameter, c, in the PT EOS:

$$c_m = \sum_j x_i c_i \qquad 8\text{-}11$$

Wong-Sandler mixing rules

In order to decide on the G_{ex} model and combining rule to use in the WS mixing rule, a preliminary investigation is conducted for the ethane/hexadecane and ethane/hexadecanol systems. The PR model with SV alpha function is used as the pure component model for this investigation.

Two combining rules are compared, which were introduced in Section 4.2.4 and are given as follows:

Combining rule 1:

$$\left(b - \frac{a}{RT}\right)_{ij} = \frac{\left(b_i - \frac{a_i}{RT}\right) + \left(b_j - \frac{a_j}{RT}\right)}{2}\left(1 - k_{aij}\right) \qquad 8\text{-}12$$

Combining rule 2:

$$\left(b - \frac{a}{RT}\right)_{ij} = \frac{b_i + b_j\left(1 - k_{bij}\right)}{2} + \frac{\sqrt{a_i a_j}}{RT}\left(1 - k_{aij}\right) \qquad 8\text{-}13$$

Stellenbosch University https://scholar.sun.ac.za

Combining rule 1 was published with the derivation of the original mixing rule by Wong and Sandler [129], and the general form of combining rule 2 (without the BIP $k_{b,ij}$) has been recommended as an alternative by Sandler [76]. Valderrama included the second BIP $k_{b,ij}$ for only the solute size parameter, b_j, in order to improve correlations in solubility calculations for asymmetric systems [98].

The two G_{ex} models investigated are the UNIFAC group contribution method and the NRTL model. UNIFAC parameters were obtained from Poling et al. [38]. The form of the G_{ex} models, as well as group parameters for the UNIFAC model, is given in Appendix A.1.4 and A.1.5. Figure 8-1 compares the pure prediction (no BIPs) and use of BIPs in both combining rule 1 and 2 for use of the UNIFAC G_{ex} model in the WS mixing rules:

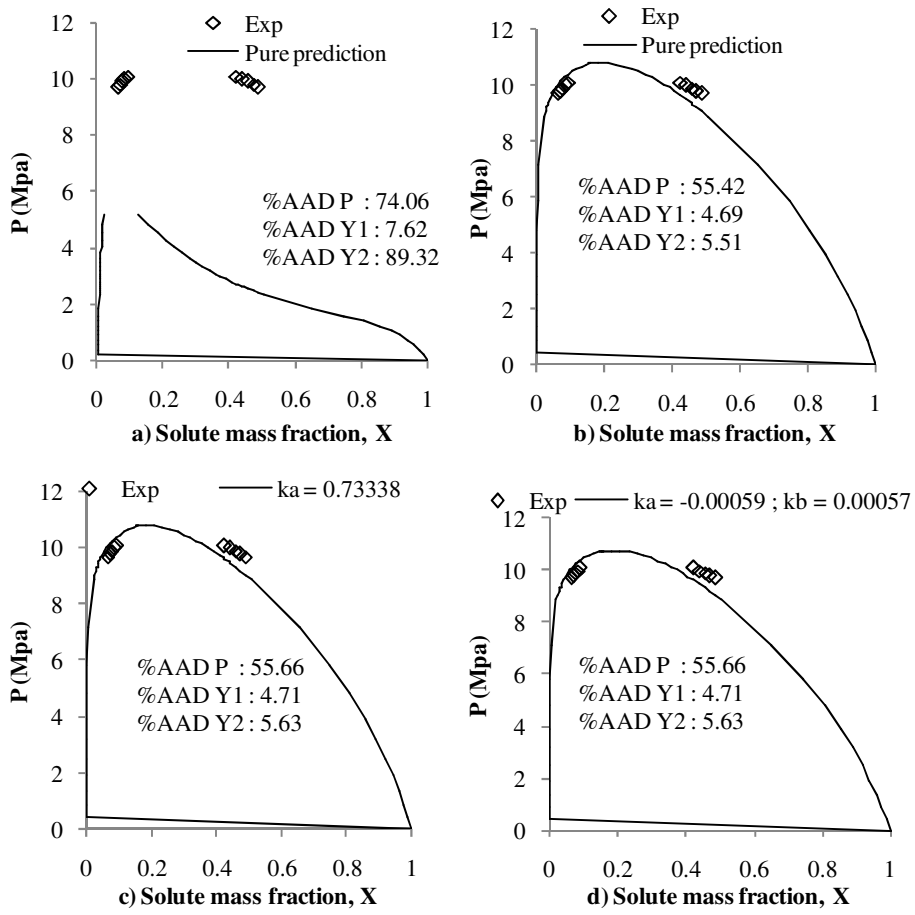

Figure 8-1 Ethane/hexadecane [1] system with the PR-SV model and WS mixing rules with the UNIFAC G_{ex} model: Pure prediction for a) combining rule 1 and b) combining rule 2 and fitting BIPs for c) combining rule 1 and d) combining rule 2

Stellenbosch University https://scholar.sun.ac.za

As discussed in Section 4.2.6, only the residual term of the UNIFAC model was used in the mixing rule. Figure 8-1 a) and b) show that combining rule 2, which uses the arithmetic mean in the size parameter b and the geometric mean in the energy parameter a, gives much better performance than combining rule 1 if no BIPs are used.

Figure 8-1 c) and d) also show that inclusion of the BIPs for the second virial coefficient expression has a large impact for combining rule 1, but does not significantly influence the results for combining rule 2. This comparison using the UNIFAC G_{ex} model could furthermore not be done for the ethane/hexadecanol system since the calculation terminated only a couple of steps into constructing the phase envelope. This could be due to the inadequacy of the use of the original UNIFAC parameters or due to the theoretical limitations in the WS mixing rules for asymmetric systems as discussed by Coutsikos et al [130]. It thus seems that combining rule 2 is better than combining rule 1, but use of the UNIFAC G_{ex} model with parameters from Poling et al. [38] is not suited for the investigation conducted in this chapter.

It can be seen from Appendix A.1.5 that the NRTL G_{ex} model contains three parameterswhich can all be incorporated into the fitting procedure:

- Interaction parameters τ_{ij} and τ_{ji}
- "Non-randomness" parameter, α_{ij},

$\alpha_{ij}$is the only parameter with any concrete physical meaning. In deriving the NRTL model, Renon and Prausnitz [131] related α_{ij} to a value of $2/Z_{cor}$ in the quasichemical theory of Guggenheim, where Z_{cor} is the co-ordination number of a lattice, which varies between 8 and 12 for liquids. A value of 0.3 is typically recommended in the absence of data, but if data is available, α_{ij} is often included inthe fitting procedure. As discussed by Kontogeorgis et al. [209], negative values and values above 0.5 are not in agreement with the physical meaning of α_{ij}. They provide the following recommended values for $\alpha_{ij}$for selected types of systems:

Table 8-2Recommended values for NRTL non-randomness parameter, α_{ij} [209]

α_{ij}	Recommended Systems
0.2	Hydrocarbons-polar non-associated compounds
0.3	Non polar compounds, polar mixtures with slight deviations for Raoult's law
0.4	Hydrocarbons-perfluorocarbons
0.47	Alcohols-non-polars

Stellenbosch University https://scholar.sun.ac.za

Table 8-3 gives results for the ethane/hexadecane and ethane/1-hexadecanol system using the NRTL G_{ex} model in the WS mixing rules with values of α_{ij} set to a constant value increasing in increments from 0 to 0.45 while regressing the other interaction parameters using combining rule 1.

Table 8-3 NRTL and binary interaction parameters with results obtained for the ethane/hexadecane [1] and ethane/1-hecadecanol [4] systems using combining rule 1

Ethane/Hexadecane [1]						
α_{ij}	τ_{ij}	τ_{ji}	$k_{a,ij}$	%AAD P	%AAD Y1	%AAD Y2
0	-0.51648	-0.28037	0.72094	6.47	5.33	62.93
0.2	-0.28016	-0.51599	0.72027	6.56	5.38	63.56
0.3	-0.28005	-0.51575	0.71993	6.61	5.41	63.91
0.45	-0.27964	-0.51536	0.71942	6.7	5.46	64.47
-29.57306	-0.47363	0.11072	0.72416	2.88	2.6	30.89
Ethane/1-Hexadecanol [4]						
α_{ij}	τ_{ij}	τ_{ji}	$k_{a,ij}$	%AAD P	%AAD Y1	%AAD Y2
0	-0.56631	-0.30503	0.78970	12.27	6.52	59.35
0.2	-0.56597	-0.30483	0.78924	12.19	6.49	59.08
0.3	-0.56581	-0.30477	0.78903	12.15	6.47	58.97
0.45	-0.56559	-0.30465	0.78873	12.11	6.46	58.83
-32.63634	0.12379	-0.52502	0.80029	10.83	5.92	53.73

The last row for each system gives the case where α_{ij} is included in the regression. These results suggest that the α_{ij} value does not largely influence the model fit and the WS mixing rule generally struggles with these asymmetric systems in the high-pressure region. Results are improved upon including α_{ij} in the regression, but the unrealistic values of α_{ij} obtained suggest that this does not improve the correlation, but rather forces the model through the data.

Table 8-4 gives the same cases as Table 8-3 but with combining rule 2, which includes an additional BIP for the solute size parameter in the second virial coefficient expression. Combining rule 2 does not significantly improve the correlation, but smaller values are obtained for the interaction parameters and more reasonable values are obtained for α_{ij} upon including it in the regression.

Stellenbosch University https://scholar.sun.ac.za

Table 8-4 NRTL and binary interaction parameters with results obtained for the ethane/hexadecane and ethane/1-hecadecanol systems using combining rule 2

Ethane/Hexadecane							
α_{ij}	τ_{ij}	τ_{ji}	$k_{a,ij}$	$k_{b,ij}$	%AAD P	%AAD Y1	%AAD Y2
0	0.00023	0.00015	-0.00061	0.00038	5.63	4.71	55.66
0.2	0.00023	0.00015	-0.00061	0.00038	5.63	4.71	55.66
0.3	0.00023	0.00015	-0.00061	0.00038	5.63	4.71	55.66
0.45	0.00023	0.00015	-0.00061	0.00038	5.63	4.71	55.66
0.30290	0.00019	0.00022	-0.00061	0.00032	5.63	4.71	55.66
Ethane/1-Hexadecanol							
α_{ij}	τ_{ij}	τ_{ji}	$k_{a,ij}$	$k_{b,ij}$	%AAD P	%AAD Y1	%AAD Y2
0	-0.09288	0.01956	0.13762	0.08962	10.69	5.87	53.31
0.2	-0.09296	0.01956	0.13759	0.08951	10.68	5.87	53.29
0.3	-0.09282	0.01955	0.13757	-0.08959	10.68	5.87	53.28
0.45	-0.09276	0.01955	0.13754	-0.08962	10.68	5.86	53.27
-1.47754	-0.02464	-0.00092	0.13832	-0.09645	10.6	5.83	52.95

Figure 8-2 gives the qualitative representation of the case given in the last row of Table 8-4 for each system.

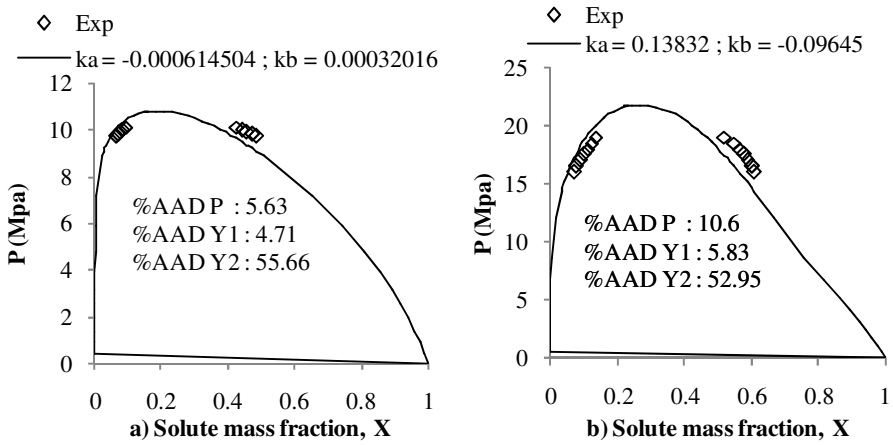

Figure 8-2 Qualitative representation of model fit for a) ethane/hexadecane and b) ethane/1-hexadecanol using the PRSV model with WS mixing rule with NRTL gex model and using combining rule 2

Based on this preliminary investigation, it seems that the WS mixing rules with the NRTL G_{ex}model struggles to correlate the data for these asymmetric systems, despite including 5 empirical parameters. This application of the WS mixing rule, namely all three NRTL

Stellenbosch University https://scholar.sun.ac.za

parameters and 2 BIPs in combining rule 2, was nevertheless chosen to allow for full flexibility in the WS mixing rule in determining the value of the response variable.

Having established the full statistical design, the sensitivity analysis can now be performed and the results discussed. It is also worth noting that for a fair analysis into the effect of the factors, BIPs were re-fitted for each treatment (combination of factor levels) before calculating the response variable.

8.4 Results of statistical analysis

A normal probability of residuals is firstly given in order to validate the statistical model applied. Some useful statistical concepts for interpreting the results of the analysis are then discussed and a Pareto chart of effects is presented to get an initial impression of the relative importance of the factors and their interactions. Diagrams are then presented for analysing the main and interaction effects, followed by an optimization analysis for obtaining the best combination of the modelling factors as determined by the lowest value in the response variable. The book by Montgomery [210] is recommended for a thorough overview for conducting and interpreting a design and analysis of experiments.

8.4.1 Normal probability plot of residuals

A factorial analysis of variance model of 3rd order interactions was applied using STATISTICA 12. This analysis of variance can only be reliably used for hypothesis testing of treatment means and quantifying the effects of the factors if certain basic assumptions are met. A fundamental assumption for application of the analysis of variance is that the errors in observations are normally and independently distributed, with mean zero and constant but unknown variance [210]. Testing this assumption can be done through examination of the residuals, defined as the difference between an observation and its treatment average. If the model is adequate, the residuals should be structureless with no obvious pattern. Figure 8-3 gives the normal probability plot of residuals for this model:

Stellenbosch University https://scholar.sun.ac.za

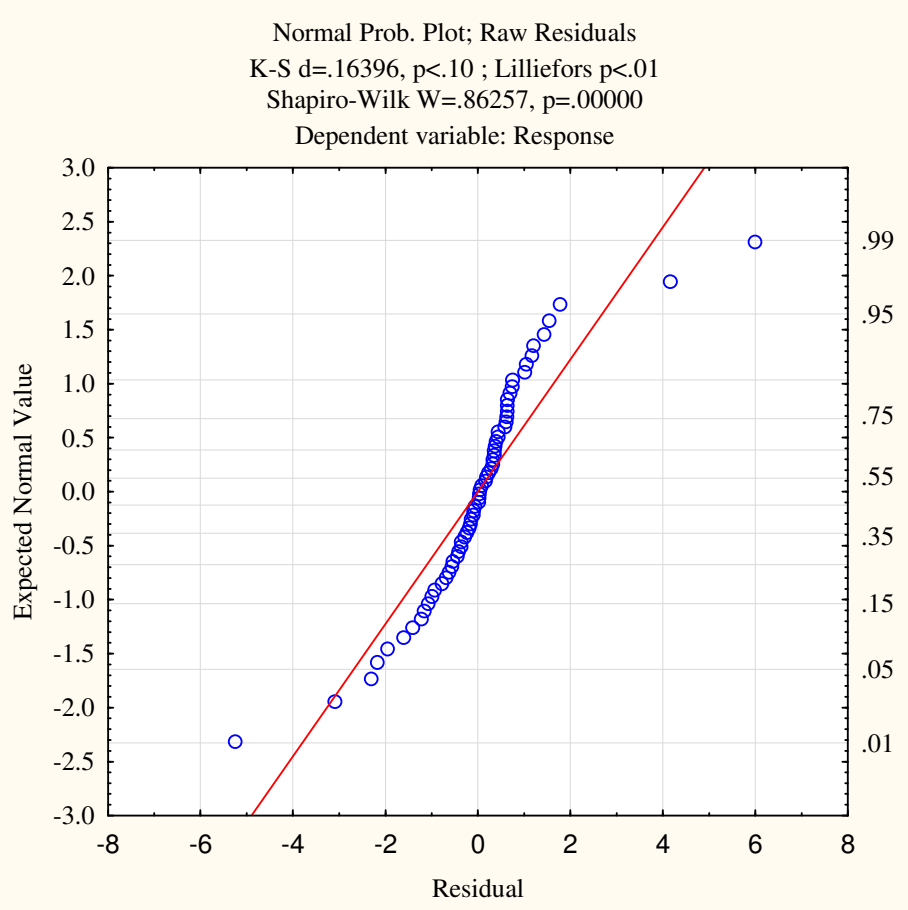

Figure 8-3 Normal probability plot of residuals for factorial analysis of variance

If the underlying error distribution is normal, this plot will resemble a straight line, with greater emphasis on the points near the middle of the plot than the extreme points. The plot shows that the residuals for this analysis are not grossly non-normal and the model may be trusted to give a reliable account of the factors and their effect on the response variable.

8.4.2 Statistical concepts

This section outlines some useful statistical concepts for interpreting the results of the statistical sensitivity analysis.

Main- and interaction effects

The *effect* of a factor is defined as the change in the response produced by a change in the level of a factor. The *main effect* of a 2 level design is the difference between the average response at the low level (level 1) and at the high level (level 2) of a particular factor. When the effect of a factor depends on the level of another factor, there is said to be an *interaction*

Stellenbosch University https://scholar.sun.ac.za

between the two effects. This occurs when the difference between the average responses at the 2 levels of a particular factor is not the same at all levels of the other factors. The results of a factorial experiment can also be represented as a regression model of the following form:

$$y = \beta_0 + \beta_1 x_1 + \beta_2 x_2 + \beta_{12} x_1 x_2 + \ldots \qquad 8\text{-}14$$

y is the response, the β coefficients are the regression parameters and the x values are variables representing the factors.The regression parameters can be related to the effect estimates: The$\beta_1$coefficient represents the main effect of factor 1 (x_1); the β_{12} coefficient represents the effect of the interaction between factors 1 (x_1) and 2 (x_2) etc.

Pareto chart

A chart comparing the values of the regression parameters, and thus the relative importance of the factors and their interactions, is known as a Pareto chart. Figure 8-4 shows the Pareto chart for the statistical analysis up to 3rd order interactions.

Statistical significance and the p value

It is seen from Figure 8-4 that none of the 3rd order interactions can be considered *statistically significant*, as determined by a p value of 0.05, which is the pre-defined cut-off for statistical significance of an effect and is given by the red-line in Figure 8-4.

The p value and the idea of statistical significance can be explained in the context of hypothesis testing. In the context of this chapter, consider the *nul hypothesis*, H_o, to be that the average response for a change in the level of a particular factor is the same, implying the factor is not significant and has no effect on the response:

$$H_o : \mu_1 = \mu_2$$

With $\mu_1$and $\mu_2$being the average of the response at level 1 and 2 of the factor, respectively. This hypothesis may be either rejected or accepted by a statistical test, which leads to two possible errors, each with their own probability. Either the null hypothesis is rejected when it is in fact true (type 1 error), or it is accepted when it is false (type 2 error).

The probability of a type 1 error is often called the *significance level* of the hypothesis test. The p value gives the smallest level of significance (probability of a type 1 error) that would lead to the rejection of the null hypothesis. A p value smaller than the defined significance level of 0.05 implies that a type 1 error is less probable than 5 % and that the null hypothesis

Stellenbosch University https://scholar.sun.ac.za

can be rejected with reasonable confidence, which implies that changing the level of the factor has a statistically significant effect on the response.

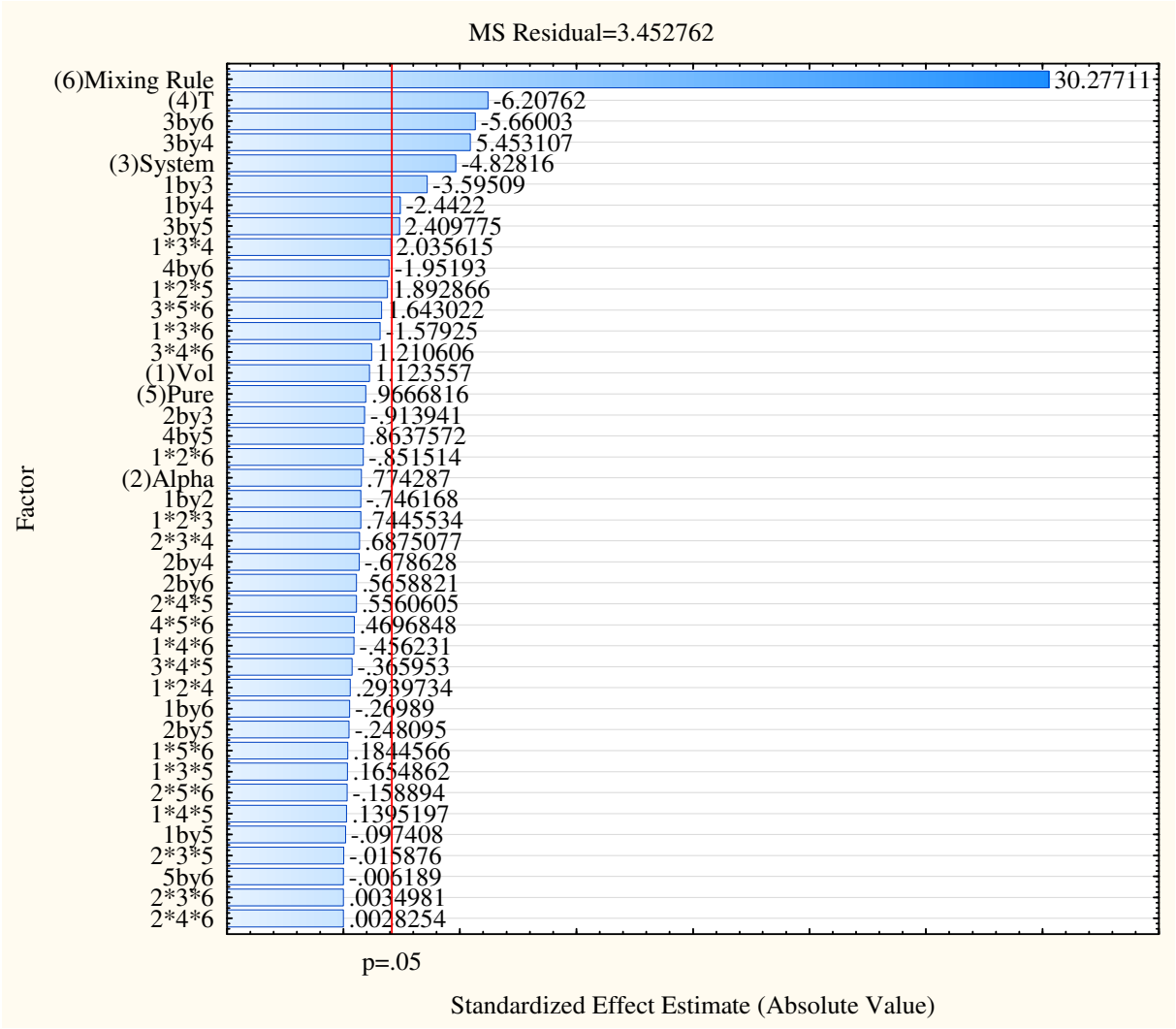

Figure 8-4 Pareto chart for main, binary (2nd order) interaction and ternary (3rd order) interaction effects for factors

Given that none of the 3rd order interactions in Figure 8-4 were found to be statistically significant (p value below 0.05), Figure 8-5 gives the Pareto chart for only main effects and 2nd order interactions:

Stellenbosch University https://scholar.sun.ac.za

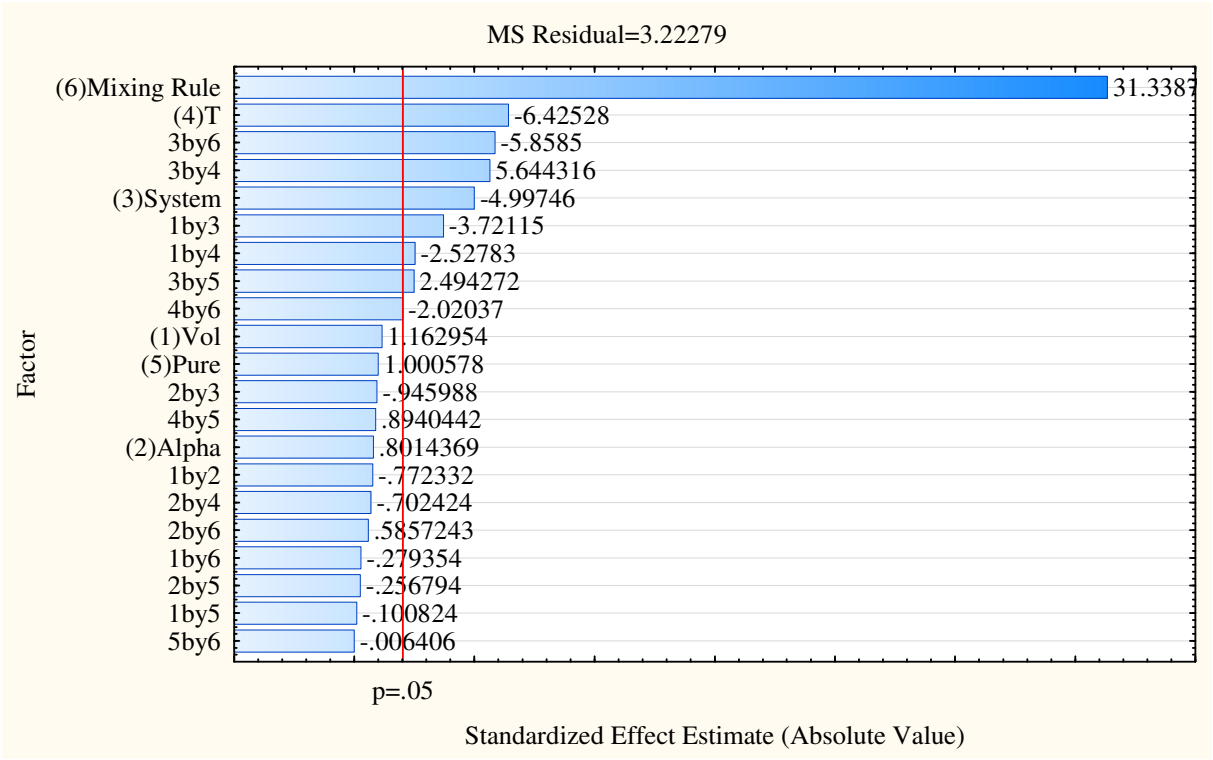

Figure 8-5 Pareto chart for main and binary (2nd order) interaction effects for factors

This chart gives a good first impression of the relative significance of the investigated factors. The mixing rules had the biggest effect on the response, followed by the temperature. The interaction effects between the system (solute functional group) and both the mixing rules (3 by 6) and temperature (3 by 4) have the next biggest effect, followed by the main effect of the system. It is also interesting to note that even though the main effect of the volume dependence (PR or PT EOS) does not seem to have a statistically significant effect on the response once BIPs are fitted, its interaction with the system (1 by 3) and temperature (1 by 4) seems to be significant.

The main and interaction effects can be more thoroughly investigated graphically. Diagrams for the main and interaction effects are subsequently presented, with focus on those that are shown to be statistically significant from the Pareto chart in Figure 8-5.

8.4.3 Main effects

For ease of reference, the factors will be referred to by their labels given in Table 8-1. Figure 8-6 gives diagrams for the main effects of each factor investigated for this investigation:

Stellenbosch University https://scholar.sun.ac.za

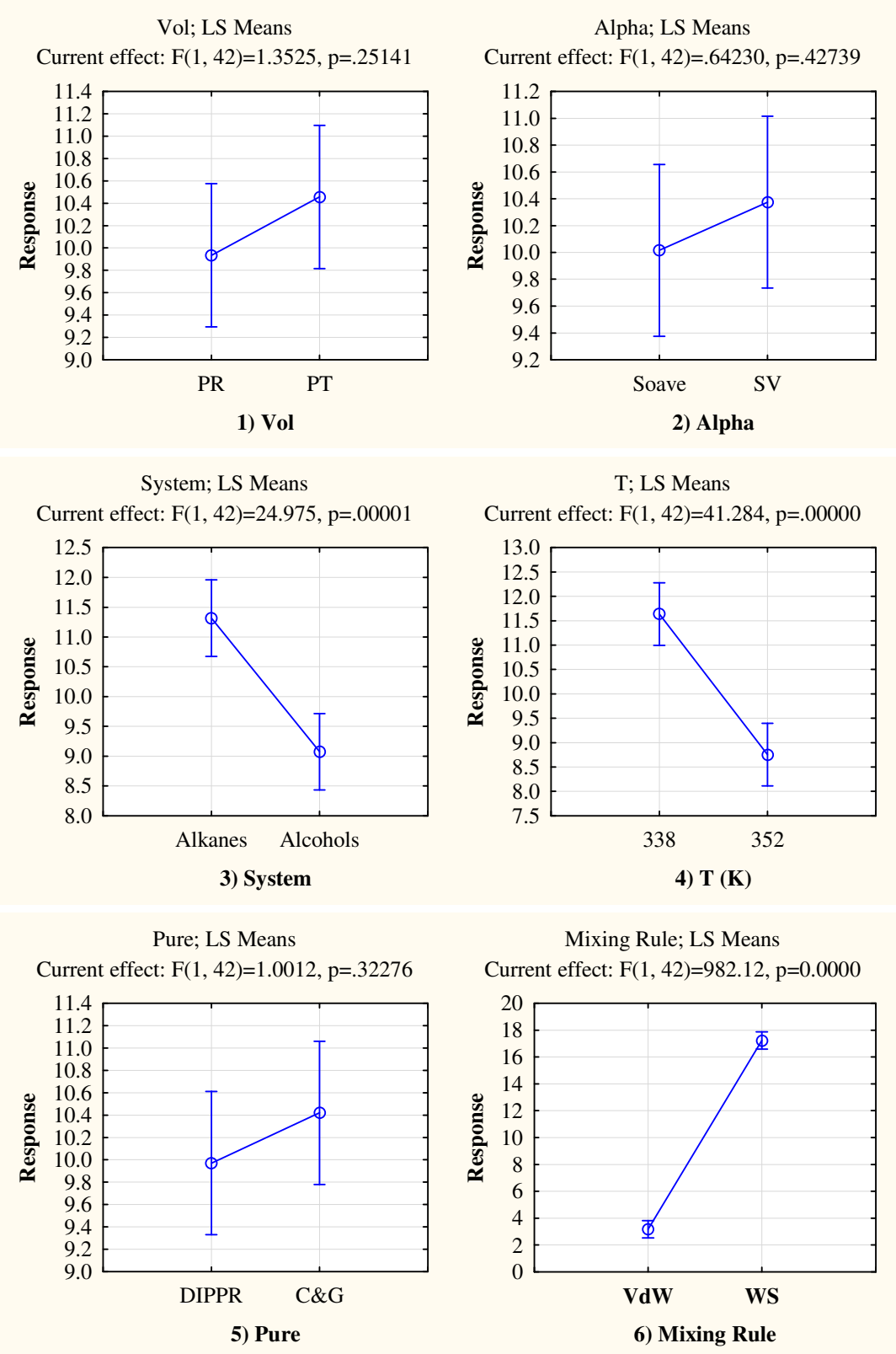

Figure 8-6 Main effects for factorial design

Stellenbosch University https://scholar.sun.ac.za

The horizontal axis gives the level of the specific factor and the vertical axis gives the average response at that level. The cross bars give the 95 % confidence interval around the average. A p value of exactly 0.05 means that the differences between the average response at the two levels of a factor differs by the extent of the cross bars, which is the cut-off for statistical significance.

Pure component factors (Vol, Alpha and Pure)

As seen for factor 1, Vol, the p value is 0.25141. This means that even though the PR EOS gave a lower average response than the PT EOS, these average responses at the two levels do not differ by significantly more than the range of responses at each level, and there is a 25 % chance of falsely attributing significance to this factor (type 1 error). The same can be said for the other two factors to do with the pure component limit, namely the alpha function and the pure constants used. Slightly lower values in the average response is obtained for the Soave alpha function and the DIPPR constants, however the difference in response for the levels of these factors fall within the cross-bars and are not deemed statistically significant in terms of their effect on correlating the high-pressure VLE of the binary systems, once BIPs are fitted to data.

Mixing rules and system dependent factors

In contrast to the factors related to the pure component limit, the system (solute functional group), temperature and mixing rules had a significant effect on the response variable. Better correlations (lower response) were definitively observed for the 1-alcohols, the higher temperature of 352 K and for the Van der Waals mixing rules.

As discussed in Chapter 3 (Sections 3.1 and 3.5), both higher temperatures and polarity of the solute leads to a more concave shape in the phase envelope, which seems easier to correlate than the flatter envelopes of the non-polar n-alkanes in the high-pressure region approaching the critical point, as discussed in Chapter 7 (Sections 7.4.3, 7.4.6 and 7.5). The higher temperature is also farther from the solvent critical temperature where the isothermal compressibility diverges and results deteriorate drastically.

8.4.4 Interaction effects

As seen in the Pareto chart (Figure 8-5), the main effects do not tell the full story and it is necessary to investigate the interactions. The interaction effects discussed are those with p value greater than 0.05 and include:

Stellenbosch University https://scholar.sun.ac.za

- The Mixing rule/System interaction
- The Temperature (T)/System interaction
- The System/Vol interaction
- The T/Vol interaction

Figure 8-7 gives the interaction diagram between the “mixing rule” and “system” factors.

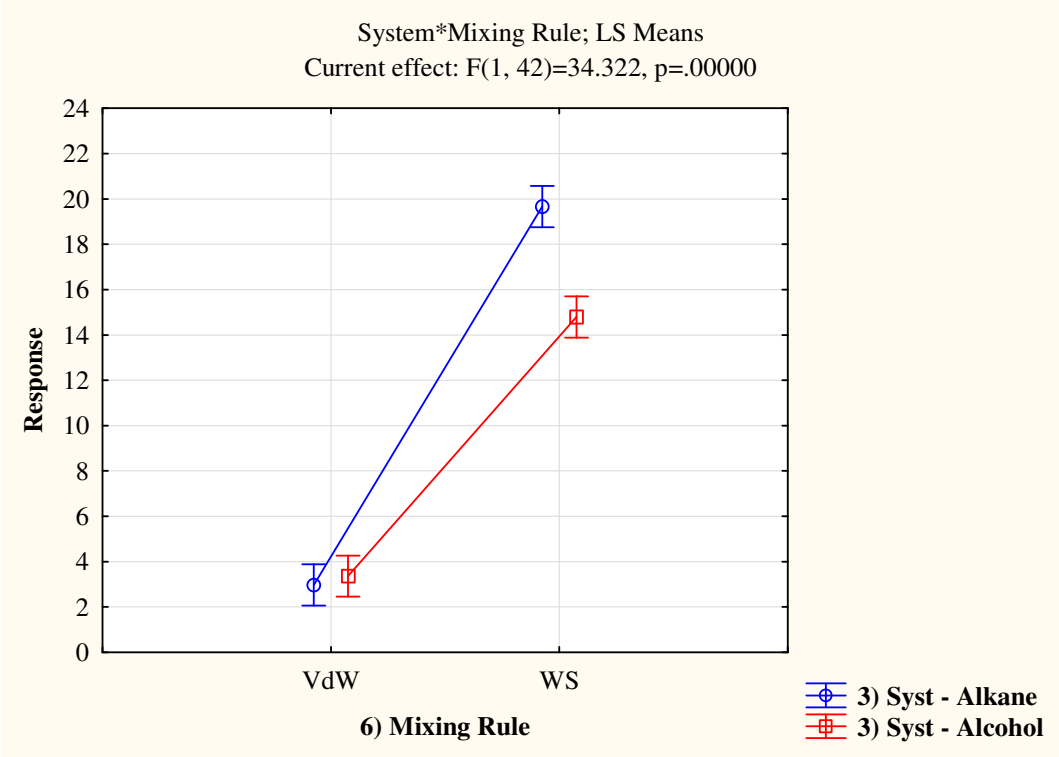

Figure 8-7 Interaction effect for “Mixing rule” and “System” factors

A significantly lower response (smaller error) is obtained for the alcohols than the alkanes using the WS mixing rules, but there is very little to choose between the correlations of the two series using the Van der Waals mixing rules, which substantially out-perform the WS in general.

Figure 8-8 gives the interaction diagram between the “T” and the “System” factors.A significant interaction is observed, whereby a change from low (338 K) to high (352 K) temperature has a significantly larger effect on the n-alkane series than on the alcohols.

Stellenbosch University https://scholar.sun.ac.za

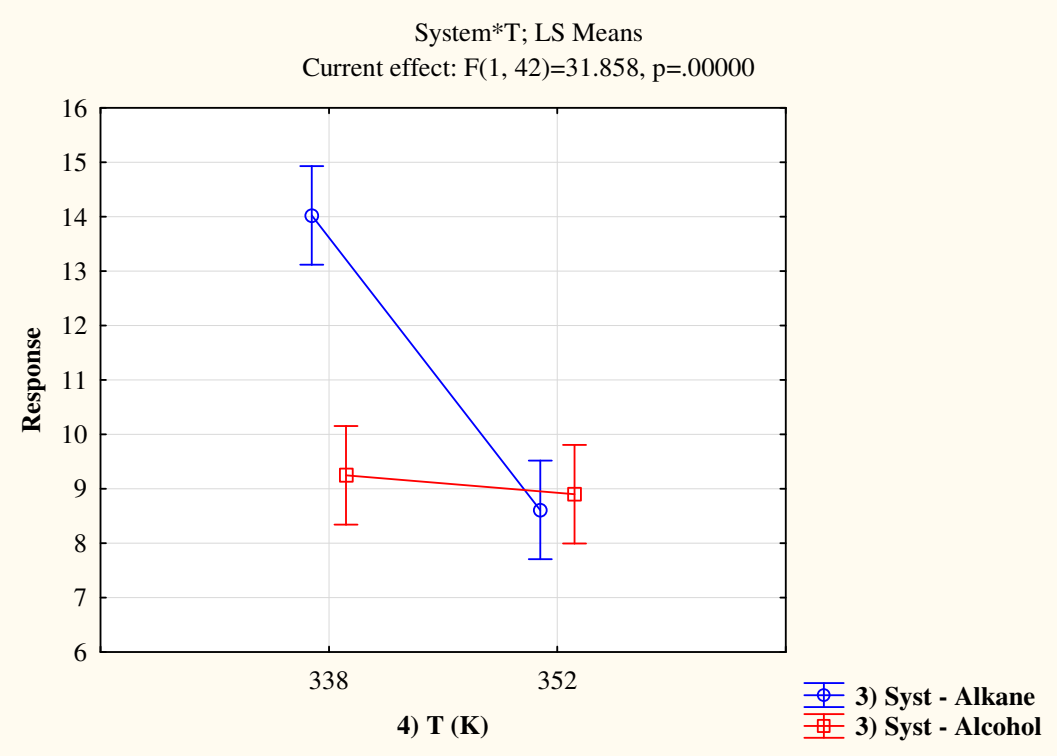

Figure 8-8 Interaction effect for "T" and "System" factors

In Chapter 3 it was found that the phase curve is more concave at higher temperatures and for more polar solutes. Results from Chapter 7 (Sections 7.4.3, 7.4.6 and 7.5) also suggest that models more easily correlate the concave shape in the high-pressure region, at the expense of over-predicting the critical point. An increase in temperature may therefore have a larger influence on the correlation of the n-alkanes, because they have a flatter profile than the 1-alcohols series for which the temperature increase has a smaller qualitative impact on the shape of the phase curve, as can also be seen in Figure 3-3 c).

Figure 8-9 gives the interaction between the "System" and "Vol" factors. From the Pareto chart in Figure 8-5 and the main effect diagrams in Figure 8-6, it is seen that the main effects of factors involving the pure component limit do not have a statistically significant effect on the binary VLE in the high-pressure region, however Figure 8-9 shows a significant interaction between the pure component EOS used and the system modelled.

Stellenbosch University https://scholar.sun.ac.za

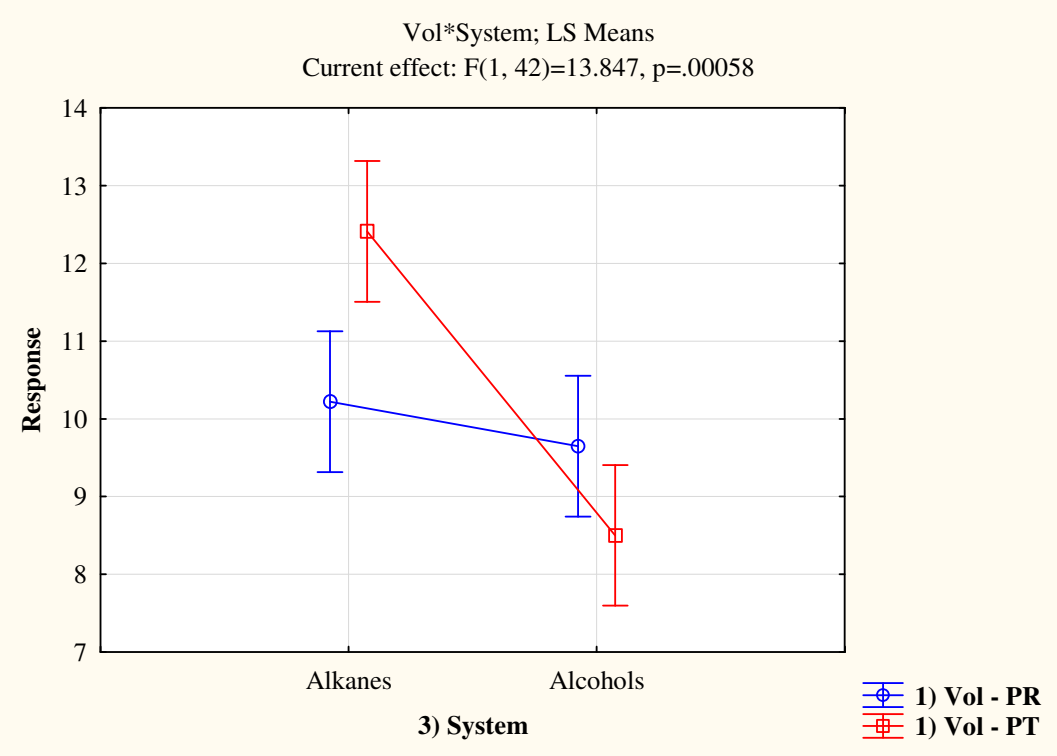

Figure 8-9 Interaction effect for "System" and "Vol" factors

The PT EOS gives a significantly better correlation of the alcohols than for the n-alkanes, whereas there is very little separating the results for the two homologous series using the PR EOS.

Figure 8-9 is especially curious because it shows an inversion of the results for the pure component properties from Chapter 6: For the n-alkanes, the PT EOS showed the best overall performance in pure component vapour pressure and saturated liquid volume (Figure 6-6) due to its 3rd parameter and adjustable compressibility, however the PR EOS gave better results than the PT EOS in both pure component properties for the alcohols (Figure 6-8). For the ethane mixtures, it seems from Figure 8-9 that the PR EOS gives better results for the n-alkane solutes, whereas the PT EOS gives better results for the 1-alcohol solutes. Figure 8-10 gives the interaction between "Vol" and "Temperature" factors, which is related to this finding.

Stellenbosch University https://scholar.sun.ac.za

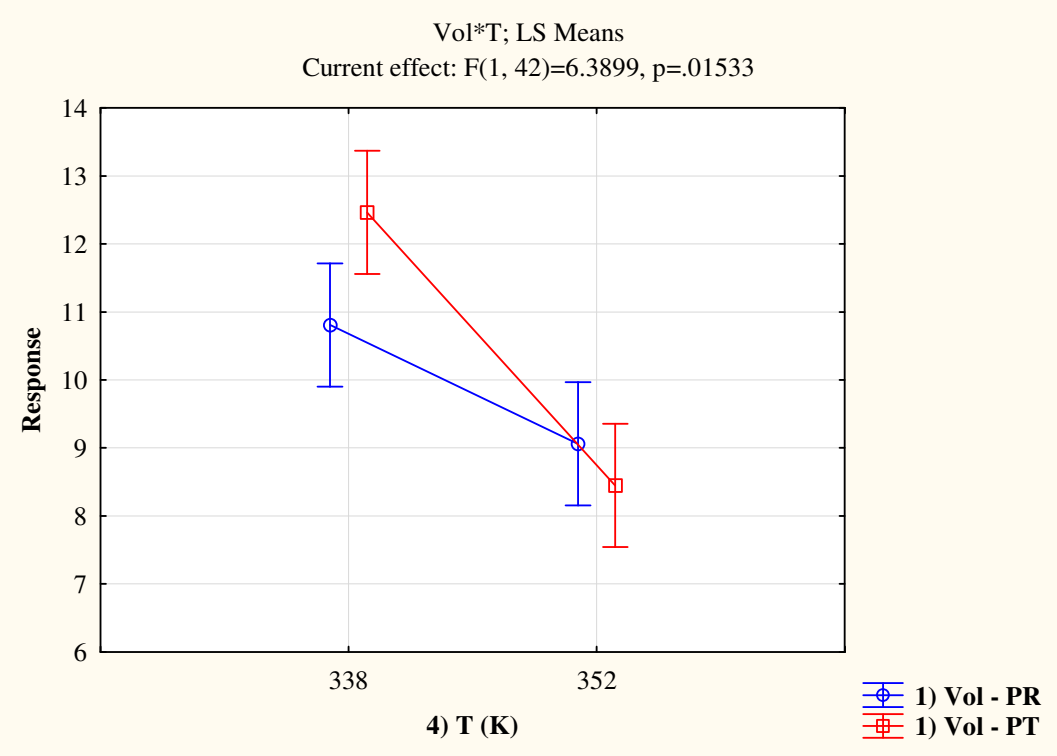

Figure 8-10 Interaction effect for "T" and "Vol" factors

As mentioned, the two *system dependent* factors ("System" and "T"), can be related to the shape of the phase curve: more polar solutes and higher temperature leads to a more concave phase curve. Within this context it is seen that there are similarities between the interaction effects of Figure 8-9 and Figure 8-10: Both the PR and PT EOS show improved performance for the more concave phase curves (higher temperature and more polar alcohols) over the flatter profiles, however the PT EOS shows a greater dependence on this qualitative aspect.

A tentative conclusion can therefore be made based on Figure 8-9 and Figure 8-10 that the PR EOS is better for the non-polar mixtures and lower temperatures and the PT EOS is better suited at higher temperatures and more polar systems, however the advantage of the PT EOS at these conditions is not substantial and the precise temperature range where one model should be preferred over the other is not clear from these results. As mentioned, this result is also somewhat at odds with the pure component performance of the models, whereby the PT EOS only offers an advantage for the non-polar n-alkanes. The PR EOS therefore seems to be the most reliable overall choice of the two pure component models in addressing the mixture modelling problem.

The observed interactions between the pure model (PR EOS or PT EOS) and the system components (Figure 8-9) and conditions (Figure 8-10), shows that the pure component and

Stellenbosch University https://scholar.sun.ac.za

mixture modelling problems cannot be considered independently, as was suggested when only the main effects were investigated. An appropriate modelling selection for correlating the high-pressure VLE of different asymmetric binaries at different conditions using the CEOSs therefore does not only rely on appropriate mixing rule selection, but also the form of the pure model. The exact manner in which the pure model influences the correlation for mixtures warrants further investigation. A third level could possibly be included in the statistical design for future work.

8.4.5 Optimization

An optimization analysis was also conducted using STATISTICA in order to find the optimum factor levels for minimization of the response variable. Figure 8-11 gives the best combination of factors for the overall lowest value in the response variable.

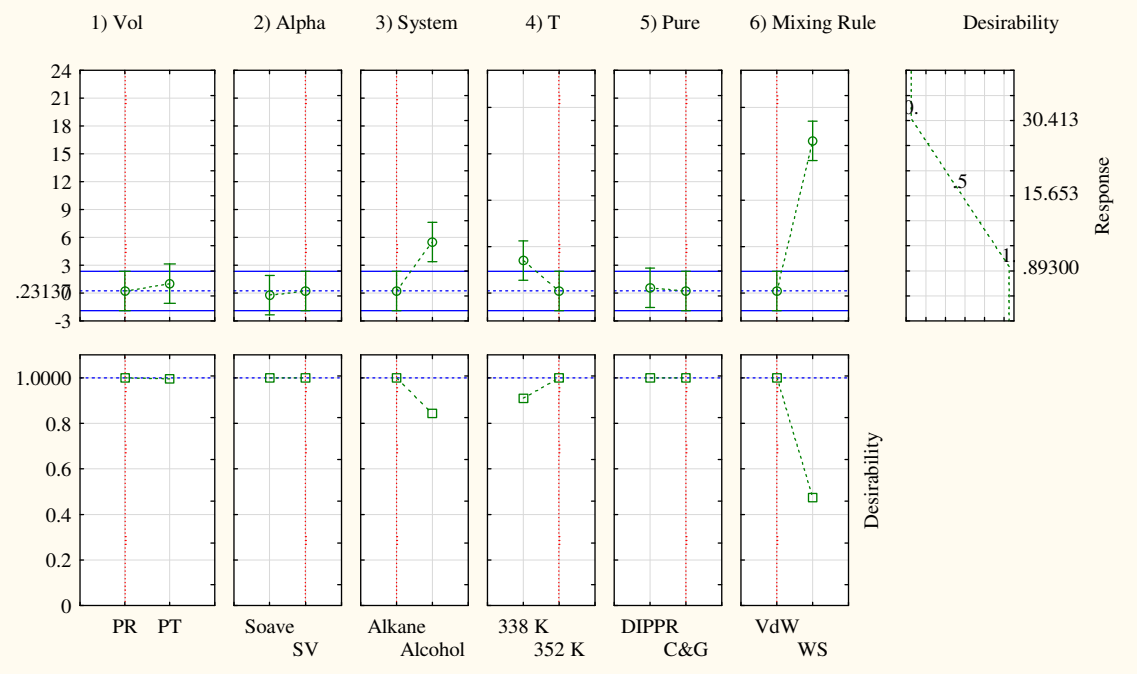

Figure 8-11 Optimization procedure: Best overall factor combination

The optimization is performed by attaching a "desirability" of 0 to the largest value in the response (30.413) and a value of 1 to the lowest value in the response (0.893). The vertical red line running down for each factor listed across the top of the figure gives the recommended level of the particular factor. The statistical significance is also included in these figures: If the green cross-bars at each level of a factor fall fully outside the blue bars running across the top section of the figure, then the effect of the factor is considered

Stellenbosch University https://scholar.sun.ac.za

statistically significant. The best overall levels give a value of 0.893 in the response variable is summarized in Table 8-5.

Table 8-5 Optimum overall factor levels

Factor	Optimum level
1) Vol	PR
2) Alpha	SV
3) System	Alkane
4) T	352
5) Pure	C&G
6) Mixing rule	VdW

The PR-SV model with the Van der Waals mixing rules for the n-alkanes at 352 K gave the lowest value in the response variable of all the treatments investigated. The optimization also found that use of the pure constants from the C&G method are preferred, however given that this pure component factor was not found to be of much significance in correlating the high-pressure binary VLE, it is simply recommended that pure component parameters of the model be fitted to the pure constants used, as was found in Chapter 6.

Given that different process conditions may be required for different industrial applications, it is desirable to optimize for the model dependent factors at specific levels of the system dependent factors. Figure 8-12 gives the results of the optimization at the low temperature of 338 K for both n-alkanes and alcohols.

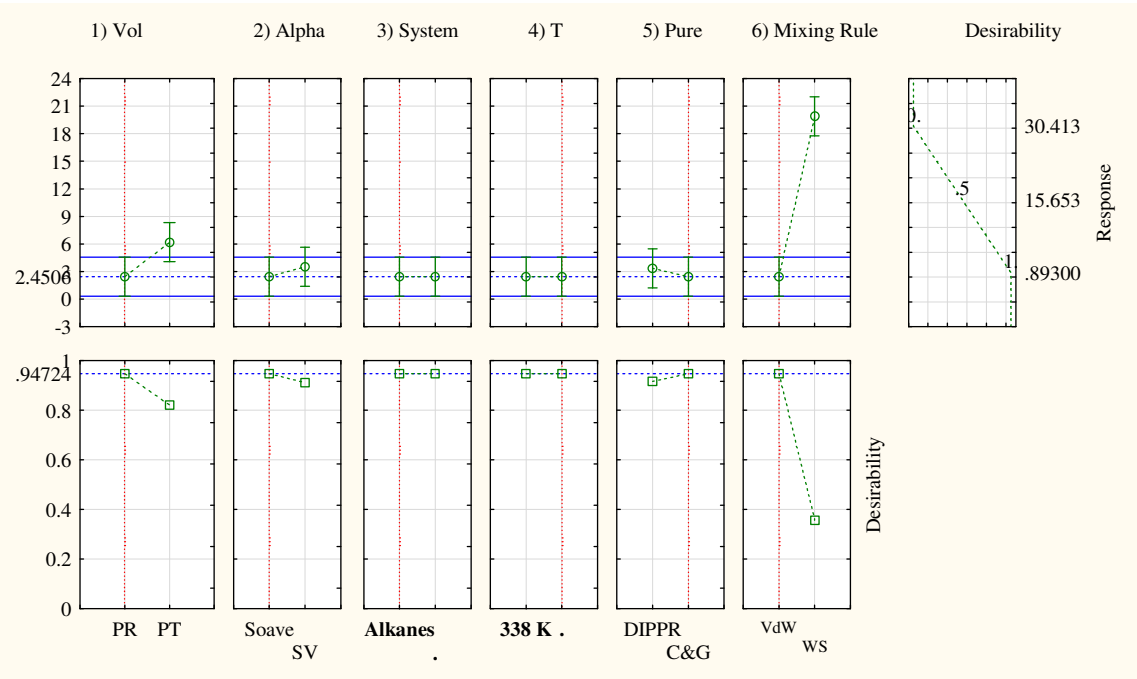

(a)

Stellenbosch University https://scholar.sun.ac.za

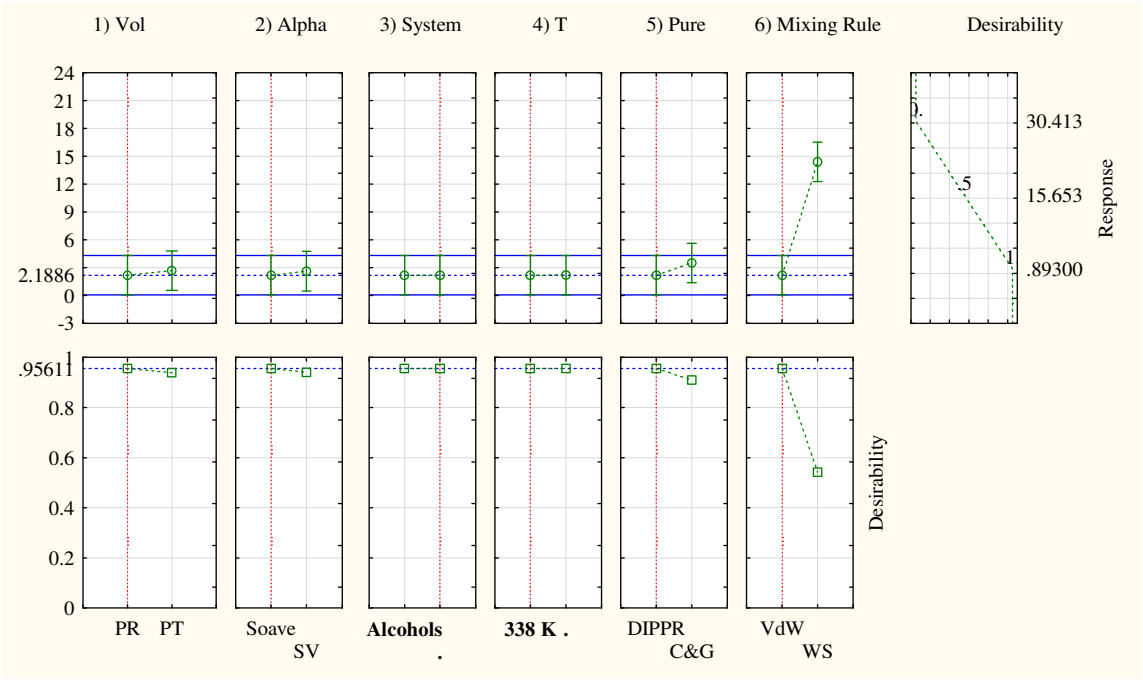

(b)

Figure 8-12 Optimization procedure: Best combination at lower temperature (338 K) for (a) n-alkanes and (b) 1-alcohols in ethane

Table 8-6 summarizes the optimum levels at 338 K as in Figure 8-12:

Table 8-6 Optimum model-dependent factor levels at low temperature 338 K from Figure 8-12

Factor	Alkanes	Alcohols
1) Vol	PR	PR
2) Alpha	Soave	Soave
5) Pure	DIPPR	DIPPR
6) Mixing rule	VdW	VdW

At the lower temperature 338 K, the PR model with Soave alpha function and Van der Waals mixing rule was the best model choice for both the alkane and alcohol series. Even though the Soave alpha function gives better results, the alpha function was generally found to not be statistically significant for the mixture correlation as represented by the response variable and the SV alpha function should therefore still be preferred due to improved correlation for pure component vapour pressure as shown in Chapter 6.

It should be noted that the recommended factor levels from this optimization procedure are based on the value of the lowest response variable and therefore do not incorporate the statistical significance in making a recommendation. Table 8-6 should therefore not be seen as

Stellenbosch University https://scholar.sun.ac.za

necessarily establishing the best modelling approach, but does high-light the usefulness of using such a statistical method to make modelling selections. Figure 8-13 gives the optimization results at the higher temperature of 352 K for both series.

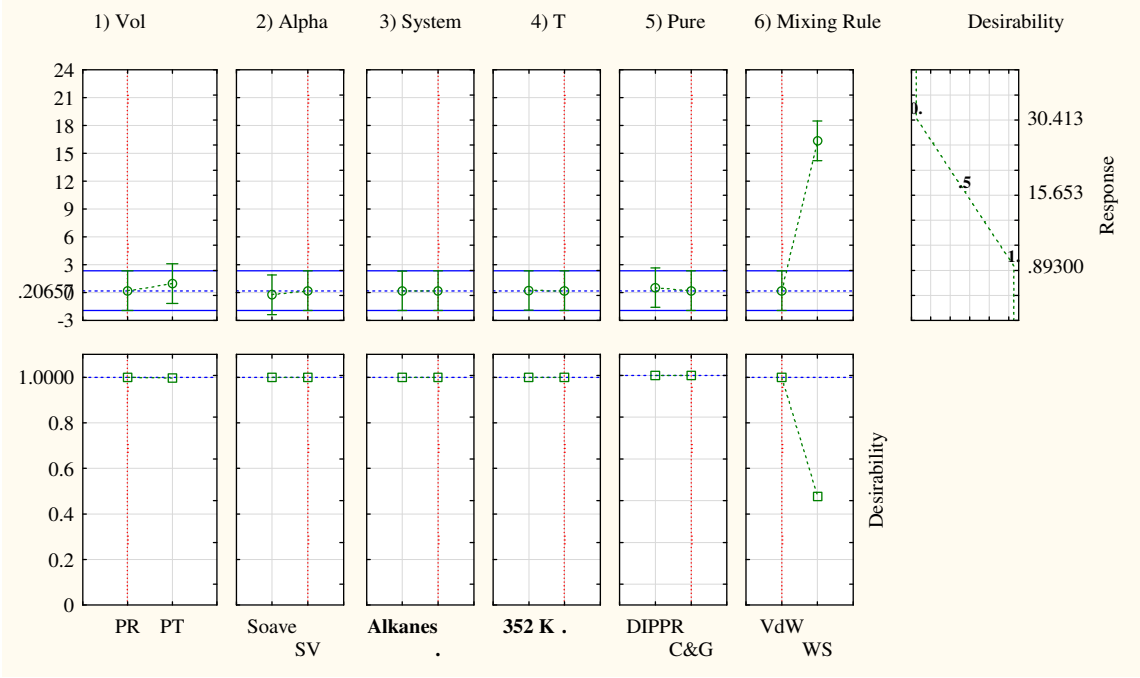

(a)

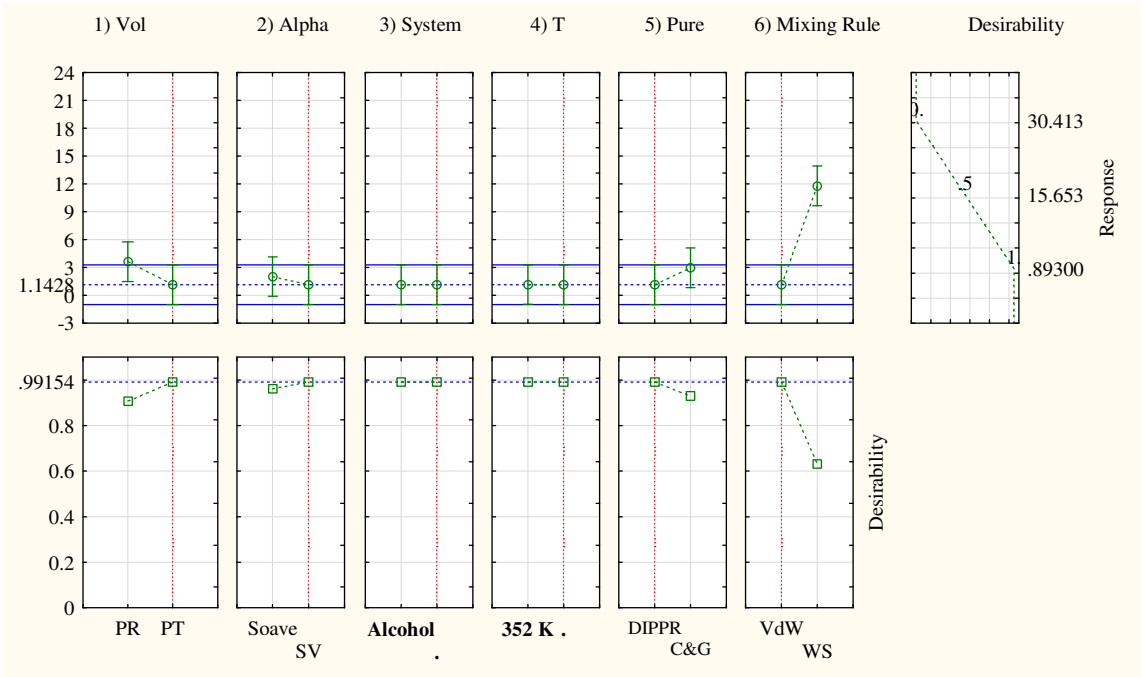

(b)

Figure 8-13 Optimization procedure: Best combination at higher temperature (352 K) for (a) n-alkanes and (b) 1-alcohols

Stellenbosch University https://scholar.sun.ac.za

Table 8-7 summarizes the optimum levels at 352 K as in Figure 8-13.

Table 8-7 Optimum model-dependent factor levels at high temperature 352 K from Figure 8-13

Factor	Alkanes	Alcohols
1) Vol	PR	PT
2) Alpha	SV	SV
5) Pure	C&G	DIPPR
6) Mixing rule	VdW	VdW

The PR-SV model gave the best results for the alkanes, while the PT- SV gave the best results for the alcohols, both using the Van der Waals mixing rules. As previously discussed and also seen from Figure 8-13, improvement with the PT EOS for the alcohols is marginal and the PR EOS can still be considered to give a better performance for these systems due to also providing better correlation of the pure component vapour pressure and saturated liquid volume for the alcohols (see Figure 6-8).

8.4.6 The effect of the pure component limit on BIPs

The statistical analysis revealed that the alpha function and pure constants used in the pure component model does not have a significant effect on the accuracy of high pressure binary VLE results. The mixing rules are thus sufficiently flexible to compensate for deviations in these aspects of the pure component limit through changing the BIP values in the fitting procedure.

If data is not available, one may be forced to use generalized empirical correlations for the BIPs and alpha-function parameters. If an estimation method for the pure constants is also used, errors could accumulate and greatly affect the results in the high-pressure region. In order to determine the effect that these practices could have, the BIPs obtained using different pure component factors (alpha function and pure constants) are used within the same pure component EOS.

Table 8-8 defines the different cases for which BIPs were firstly obtained. The BIPs obtained for each case are then used in the PR-SV model, with pure constants from DIPPR, defined as the *base model*. The influence of temperature was also investigated by repeating the analysis for BIPs obtained at 338 K for each of the cases. Model performance was compared for the ethane/hexadecane and ethane/1-hexadecanol systems at 352 K using these different BIP sets (from cases 1 to 4) in the base model.

Stellenbosch University https://scholar.sun.ac.za

Table 8-8 Cases for testing accuracy in high-pressure VLE region to sensitivity in BIPs regressed using different alpha function and pure constants in the PR model

Case	Alpha	Pure
1	SV	DIPPR
2	Soave	DIPPR
3	SV	C&G
4	Soave	C&G

Ethane/Hexadecane [1]

The BIPs from each of the cases in Table 8-8 are given in Table 8-9 for the ethane/hexadecane system.

Table 8-9 BIP values used for sensitivity analysis on the ethane/hexadecane [1] system corresponding to the cases in Table 8-8

Model:	PRSV			
	(a) Parameters regressed at 352 K		(b) Parameters regressed at 338 K	
Parameters:	$k_{a,ij}$	$k_{b,ij}$	$k_{a,ij}$	$k_{b,ij}$
Case 1	0.01740	-0.01456	0.02728	-0.05539
Case 2	0.01760	-0.01187	0.02656	-0.05009
Case 3	0.02362	0.00401	0.03050	-0.03357
Case 4	0.02387	0.00642	0.03102	-0.03018

The model fits obtained when these sets are used in the base case model (PRSV with DIPPR constants) is given in Figure 8-14:

Stellenbosch University https://scholar.sun.ac.za

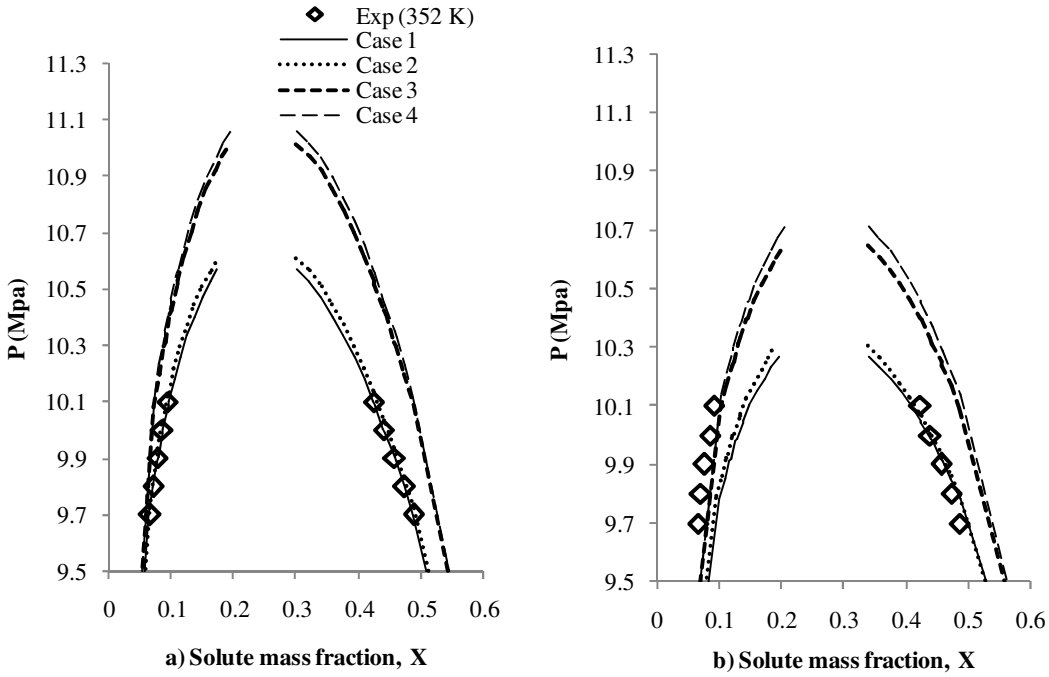

Figure 8-14 BIP sensitivity analysis for the ethane/hexadecane [1] system (352 K) using the PRSV model with the Van der Waals mixing rules and BIPs from each case given in Table 8-8 , obtained at a) 352 K and b) 338 K

The numerical errors for these cases are given in Table 8-10.

Table 8-10 Numerical errors for the fits shown in Figure 8-14

Model:	PRSV					
	(a) Parameters regressed at 352 K			(b) Parameters regressed at 338 K		
	%AADP	%AAD Y1	%AAD Y2	%AADP	%AAD Y1	%AAD Y2
Case 1	**0.02**	**0.15**	**1.66**	0.44	4.48	52.78
Case 2	0.32	0.16	1.76	0.45	3.94	46.37
Case 3	4.15	1.27	14.58	3.51	4.97	58.35
Case 4	4.5	1.28	14.71	4.07	5.06	59.32

Errors when BIPs are regressed to the base model (case 1) are printed in bold as a reference for the errors in using the other BIP sets which were not regressed for the base model. The BIPs obtained from using the Soave alpha function at the same temperature of 352 K does not introduce large errors, but when different pure constants are used (C&G method), the error in pressure and Y_2 increases by about 4% and 13%, respectively. Using BIPs at a temperature of 338 K does not greatly affect the pressure correlation, but the errors in vapour composition, especially Y_2, increases dramatically, exceeding 50%, even for case 1.

Stellenbosch University https://scholar.sun.ac.za

Ethane/1-Hexadecanol [4]

The BIPs from each of the cases in Table 8-8 are given in Table 8-11 for the ethane/hexadecanol system:

Table 8-11 BIP values used for sensitivity analysis on the ethane/hexadecanol [4] system corresponding to the cases in Table 8-8

Model:	PRSV			
	(a) Parameters regressed at 352 K		(b) Parameters regressed at 338 K	
Parameters:	$k_{a,ij}$	$k_{b,ij}$	$k_{a,ij}$	$k_{b,ij}$
Case 1	0.05416	0.07992	0.05801	0.09215
Case 2	0.05690	0.09392	0.06285	0.10323
Case 3	0.06655	0.11208	0.07230	0.11615
Case 4	0.06989	0.12126	0.07614	0.12931

Figure 8-15 gives the fits obtained when using the BIPs from Table 8-11 in the base case model:

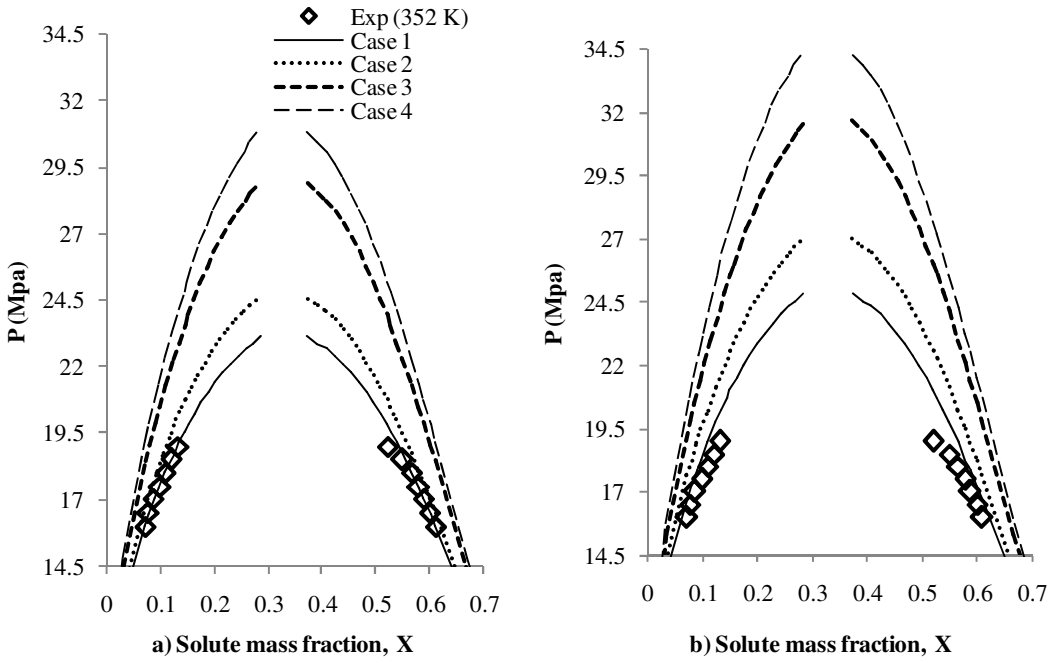

Figure 8-15 BIP sensitivity analysis for the ethane/1-hexadecanol [4] system (352 K) using the PRSV model with the Van der Waals mixing rules and BIPs from each case given in Table 8-8 , obtained at a) 352 K and b) 338 K

The numerical errors of these fits are presented in Table 8-12:

Stellenbosch University https://scholar.sun.ac.za

Table 8-12 Numerical errors for the fits shown in Figure 8-15

Model:	PRSV					
	(a) Parameters regressed at 352 K			(b) Parameters regressed at 338 K		
Parameters:	%AADP	%AAD Y1	%AAD Y2	%AADP	%AAD Y1	%AAD Y2
Case 1	**0.9**	**0.48**	**3.55**	5.86	0.44	3.33
Case 2	4.5	0.54	4.56	12.74	0.48	3.66
Case 3	18.44	0.48	3.71	27.94	1.13	9.78
Case 4	23.92	0.42	3.16	34.89	0.65	5.42

For the ethane/hexadecanol system, using BIPs from the Soave alpha function and pure constants from the C&G method in the base model at the same temperature (352 K) does not have much effect on the errors in composition, but errors in pressure increase quite dramatically, especially for use of the C&G pure constants. Using BIPs obtained for each case at 338 K further deteriorates the correlation.

Even though the alpha function or pure constants used does not affect the correlation of the high-pressure VLE data once BIPs are regressed, these BIPs cannot be used for different alpha functions or pure constants. Such a practice was found to introduce large errors in composition for the non-polar ethane/hexadecane system and large errors in pressure for the ethane/hexadecanol system. BIPs obtained at a different temperature also lead to substantial deterioration in the correlation of the high-pressure VLE. It is therefore clear that any attempt to develop generalized correlations for BIPs is highly dependent on the pure component model, pure constants used, as well as on the temperature.

8.5 Conclusions

The aim of this chapter is to determine the effect and relative importance of factors considered in the modelling of high-pressure VLE properties of asymmetric binary mixtures with ethane as solvent using the CEOSs, thereby addressing project objective 7. The factors investigated were the following:

- Temperature dependence of the model (1 or 2 parameter alpha function)
- Volume dependence of the model (2 or 3 parameter model)
- Pure component constants used (Data or estimation method)
- Mixing rules used (classic Van der Waals or G_{ex}/EOS mixing ruled)
- Temperature range (lower and higher temperature)
- Solute functional group (non-polar and polar)

Stellenbosch University https://scholar.sun.ac.za

The effect of these factors was assessed with a design of experiments sensitivity analysis using STASTITICA 12 software. The outcomes of this analysis can be summarized as follows:

- Considering only the main effects of the factors suggests that the pure component limit (volume dependence, alpha function and pure constants used) does not significantly influence the correlation obtained for the binary mixtures in the high-pressure region once BIPs are fitted to data.
- The mixing rules had the largest effect on the response variable, with the quadratic Van der Waals mixing rules with 2 BIPs substantially out-performing the Wong-Sandler mixing rules, despite the use of 5 empirical parameters in the latter.
- A lower value in the response variable (improved correlation) is observed at higher temperatures and for the more polar 1-alchols over the n-alkanes in ethane. This is presumably because of the more concave shape of the phase curve, which seems easier to correlate than the flatter profile of the n-alkanes at lower temperatures. The higher temperature is also farther from the solvent critical temperature where results deteriorate quite drastically due to the divergence of the compressibility.
- A significant interaction is observed between the system (solute functional group) and the temperature, whereby a larger decrease in the response variable occurs in changing from lower (338 K) to higher (352 K) temperature for the n-alkanes, with temperature having a much smaller effect on the alcohols. This was attributed to the flatter profiles of the n-alkanes, which undergo a larger qualitative change with increases in temperature, becoming relatively more concave than the 1-alcohols and therefore easier to correlate in the fitting procedure.
- Despite the main effect of the volume dependence of the pure model, as determined by a 2 parameter (PR EOS) or 3 parameter (PT EOS) model, not having a statistically significant effect on the response variable, it does have a statistically significant interaction with both the solute functional group and system temperature.
- The PR EOS shows improved performance over the PT EOS for the non-polar n-alkanes at lower temperature and although both models show improvement in modelling the 1-alcohols and at higher temperature, the PT EOS shows a larger relative improvement, also outperforming the PR EOS at these conditions.
- The pure component limit and mixture modelling problems can therefore not be independently considered, as might be suggested when only the main effects of the factors are taken into account. The precise nature of this relationship between the pure model and mixing rules warrants further study.

Stellenbosch University https://scholar.sun.ac.za

- In conducting an optimization procedure for the different levels of the various factors, it is found that except for the alcohols at high temperature (352 K), the PR EOS with SV alpha function, using the Van der Waals mixing rules, is the most promising property method from the combinations considered in this chapter.
- Even though the pure component limit is not significant in fitting the high-pressure VLE region once BIPs have been regressed to data, it was shown that the different BIP values obtained for the different pure component factors (ie. different alpha functions and pure constants), cannot be used in other pure component models. BIPs were found to be highly sensitive to the pure component limit as well as temperature and these aspects have to be taken into account when developing generalized correlations for these parameters.

The flexibility of the CEOSs leads to many modelling factors to be considered for any given application. Due to the significant interactions between these factors, an optimization analysis as conducted in this chapter could prove valuable in helping chemical engineers make the appropriate modelling selection for a specific application. Such an analysis could provide a promising alternative to the typical heuristic selection-trees provided in the documentation of most current commercial process simulators.

It should also be noted that since the mixing rules were deemed the most important factor and given that multiple BIPs were fitted to the mixing rules, the analysis does not necessarily reflect which models are fundamentally better or worse, but rather just identifies which is the most effective correlation tool for a specific application. In order to extend the power of such an analysis to theoretical model development and not just to model selection, the analysis should be done without fitting any BIPs. This, however, falls outside the scope of the current study.

Stellenbosch University https://scholar.sun.ac.za

9. COMPARISON OF SELF-DEVELOPED SOFTWARE WITH RESULTS FROM ASPEN PLUS ®

An important aspect in the application of semi-empirical thermodynamic models is the computational technique used for obtaining model parameters. Different algorithms and fitting procedures may be required to obtain different property values, depending on the process conditions and the model used. The primary aim of this chapter is to compare the influence that different computation techniques may have on correlating the high pressure binary VLE of the n-alkane (nC10-C36), 1-alcohol (nC10-nC18) and methyl ester (nC10-nC18) homologous series in ethane (353 K), as well as the n-alkane (nC14-nC36), 1-alcohol (nC10-nC18) and carboxylic acid (nC10-nC18) series in propane (408 K) (same systems as investigated in chapter 7 and given in Table 7-1 andTable 7-2)

Model fits using parameters obtained from the Britt-Luecke minimization [203] algorithm and a maximum-likelihood objective function, as used in the Aspen Plus ®regression routine (see Section 7.3.2), are compared to results obtained using self-developed software in MATLAB, which employs the Nelder-Mead simplex minimization algorithm and an implicit objective function in terms of equilibrium ratios (K values) (see Section 8.2 and Appendix B.3). The RK-ASPEN model is used for this comparison, since parameters from the Aspen Plus ® regression routine have already been obtained in Chapter 7 and good correlation of the systems investigated were obtained using this model.

Ashour and Aly [211] conducted a similar comparison of two computational techniques using the SRK and PR EOS with the quadratic Van der Waals mixing rulesfor various systems, including asymmetric binaries. The first method usedthe non-linear least squaresalgorithm of Levenberg-Marquardt (LM) for minimizing deviations in the natural logarithm of equilibrium K factors, very similar to the objective function used in MATLAB for this chapter (see Section 8.2). This method was compared to the same maximum likelihood approachinvestigated in this chapter, which uses the Britt-Luecke minimization algorithm [203] as implemented in Aspen Plus ® (Section 7.3.2). The authors found the second method to be superior and note that different BIP values are obtained using the same model and experimental property values, high-lighting the importance of the computation technique on the final results.

A final attempt is also made in this chapter to see whether generalized correlations can be developed for BIPs as a function of carbon number by using a different combining rule in the mixing rules. The best overall model from the statistical analysis in chapter 8 is used for this investigation, namely the PR EOS with the Stryjek-Vera (SV) alpha function. This chapter therefore addresses project objectives 8 and 6 as given in Section 1.3.

Stellenbosch University https://scholar.sun.ac.za

9.1 Models

The models investigated in this chapter are briefly out-lined.

RK-ASPEN

The form of this model has already been presented in Section 7.2. For the purposes of this chapter, the name RK-ASPEN refers specifically to the following details in applying the model:

The pure constants (T_c, P_c and ω)from the pure 20 data bank in Aspen Plus ®were used and are given in Appendix C.3. The primary parameter for the Mathias alpha function (Equation 7.8) was obtained from the accompanied literature correlation (Equation 7-9) [92]. The additional polar parameter in this alpha function was fit to DIPPR correlations in vapour pressure using the Aspen Plus ® data regression routine. The parameter values are presented in Appendix E.2. The 2 BIPs used in the Van der Waals mixing rules (Equations 7-10 to 7-13) were also obtained from the Aspen Plus ® regression routine and given in Table 7-5 and Table 7-7 for the ethane and propane systems respectively.

SRKM

This model has the same form as the RK-ASPEN model as was given in Section 7.2, but the name SRKM refers to the following details in applying the model:

Pure constants from DIPPR were used and are given in Appendix C.1. Both alpha function parameters in the Mathias alpha function (Equation 6-20) [92] were obtained using the *fsolve* function in MATLAB, which uses the Levenberg-Marquardt non-linear least squares algorithm. This is the same method as was used for investigating pure properties in Chapter 6 and is discussed in detail in Appendix B.2. The 2 BIPs in the Van der Waals mixing rules (Equations 7-10 to 7-13) were obtained using an implicit objective function in terms of K factors, which was minimized using the *fminsearch* function in MATLAB, which uses the Nelder-Mead simplex method. This routine is out-lined in Section 8.2 and a detailed algorithm is presented in Appendix B.3.

It is noted that given the description of the RK-ASPEN and SRKM models above, the models are not completely identical in the sense that different sources were used for both the pure constants and pure parameters. Comparison of the DIPPR constants in Appendix C.1 (used in MATLAB software) with the pure constants from the Pure 20 database (used in Aspen Plus ®) as given in Appendix C.2 reveals that the values used are very similar. Figure E.52 in

Stellenbosch University https://scholar.sun.ac.za

Appendix E.3.5 also shows the close relationship between the regressed values for the primary Soave-like parameter in the Mathias alpha function (used in MATLAB software) and that obtain from the literature correlation (used in Aspen Plus ®). The fitting of the additional empirical parameter in the Mathias alpha function using two different computational techniques therefore is not deemed to have too large of an impact on the pure component representation of the two respective models. These discrepancies in the pure component limit are therefore not deemed to greatly undermine the comparison of computational techniques conducted in this chapter.

PRSV-KM

In applying the quadratic Van der Waals mixing rules throughout this study, the following standard combining rules were used for the cross-interaction term, which apply the geometric and arithmetic mean for the energy parameter, a, and size parameter, b, respectively:

$$a_{ij} = \sqrt{a_i a_j}\left(1 - k_{aij}\right) \qquad 9\text{-}1$$

$$b_{ij} = \frac{b_i + b_j}{2}\left(1 - k_{bij}\right) \qquad 9\text{-}2$$

As noted in Section 4.2.5, Jha and Madras [114] was able to correlate the high-pressure VLE of various binary mixtures with CO_2, including alcohols from methanol to 1-decanol, using the PR EOS with quadratic Van der Waals mixing rules and 2 BIPs using the following combining rules:

$$a_{ij} = \sqrt{a_i a_j}\left(1 - k_{aij}\right) \qquad 9\text{-}3$$

$$b_{ij} = \left(\frac{\left(b_i^{\frac{1}{3}} + b_j^{\frac{1}{3}}\right)}{2}\right)^3 \left(1 - k_{bij}\right) \qquad 9\text{-}4$$

The geometric mean was kept for the energy parameter, but an expression derived by Kwak and Mansoori [115] was used for the size parameter, b, which is deemed to be more in-line with statistical mechanical theory.

In addition to providing a good correlation to the data, Jha and Madras [114] found that the two BIPs vary linearly with the solute carbon number for the systems investigated. In order to see whether such linear trends may be attained for the systems investigated in this chapter,

Stellenbosch University https://scholar.sun.ac.za

these combining rules were used with the PR-SV model and the data was correlated. This model is henceforth called the PRSV-KM model.

PRSV

In order to provide a reference for the model fits obtained using the combining rules given by Equations 9-3 and 9-4 in the PRSV-KM model, the PR-SV model using the classic combining rules (Equations 9-1 and 9-2) is also used in this chapter, and given the name PRSV. This model was found to give the best overall performance of the various modelling combinations (treatments) used in the statistical analysis conducted in Chapter 8 for modelling the ethane/alkanes and ethane/alcohols at 338 and 352 K.

The BIPs for both the PRSV-KM and PRSV models were determined using the self-developed MATLAB software, with the techniques out-lined in Section 8.2 and described in detail in Appendix B.3.

9.2 Model fit results

Table 9-1 presents the model fits for the high pressure binary VLE of the n-alkane, 1-alcohol, methyl ester and carboxylic acid homologous series in ethane at 352 K, as well as the n-alkane, 1-alcohol and carboxylic acid series in propane at 408 K using all 4 models investigated for this chapter. The data used are the same as that from Chapter 7 and presented in Table 7-1 and Table 7-2 for the ethane and propane systems respectively.The data was modelled using a bubble point pressure calculation (see Appendix B.3) and results are therefore presented as %AAD in P, Y_1 and Y_2.

9.2.1 Comparison of different computational techniques

The RK-ASPEN model represents the maximum-likelihood approach with the Britt-Luecke minimization [203] algorithm (see Section 7.3.2) and SRKM represents the minimization of an implicit objective function in K values, using the Nelder-Mead simplex method (see Section 8.2 and Appendix B.3). Even though differences are expected between these methods, they should not be drastic since correlations should be more dependent on the model used than on the computational procedure. In order to elucidate these differences in Table 9-1, the lowest error obtained for a particular *variable* within a given solvent/homologous series combination, is high-lighted in green. The 2nd and 3rd best fit is high-lighted in yellow and red, respectively.

Stellenbosch University https://scholar.sun.ac.za

Table 9-1 Comparison of results from self-developed software with those from ASPEN

Solvent:	Ethane												Propane											
Model:	RK-ASPEN			SRKM			PRSV			PRSV-KM			RK-ASPEN			SRKM			PRSV			PRSV-KM		
	%AAD			%AAD			%AAD			%AAD			%AAD			%AAD			%AAD			%AAD		
Alkanes (CN):	P	Y_1	Y_2	P	Y_1	Y_2	P	Y_1	Y_2	P	Y_1	Y_2	Alkanes (CN):	P	Y_1	Y_2	P	Y_1	Y_2	P	Y_1	Y_2	P	Y_1	Y_2
10	3.21	0.16	4.23	0.89	0.52	4.63	1.67	0.43	4.39	1.67	0.43	4.39	14	1.31	2.06	32.2	1.76	3.42	41	2.6	3.74	46.69	2.6	3.74	46.68
16	2.18	0.08	0.86	1.31	1.15	11.4	1.3	1.14	11.24	1.3	1.15	11.32	16	0.94	1.64	18.03	0.75	1.58	18.07	0.62	1.6	17.07	0.62	1.6	17.08
24	3.72	0.56	3.84	0.53	0.36	2.35	0.55	0.38	2.45	0.55	0.38	2.46	24	1.28	0.91	7.34	1.29	2.25	26.11	0.83	0.95	12.29	0.82	0.94	12.06
28	3.74	0.9	5.72	0.41	0.82	5.37	0.36	0.79	5.14	0.35	0.78	5.14	28	1.39	0.87	6.39	0.83	0.89	11.28	0.66	0.67	8.11	0.66	0.67	8.06
36	1.73	1.1	7.26	0.91	1.33	9.15	0.55	0.93	5.98	0.55	0.93	6	36	1.53	0.71	9.22	0.97	1.01	13.72	0.98	1.09	15.22	0.98	1.1	15.29
Avg.	2.92	0.56	4.38	0.81	0.84	6.58	0.89	0.73	5.84	0.88	0.73	5.86	Avg.	1.29	1.24	14.64	1.12	1.83	22.04	1.14	1.61	19.88	1.14	1.61	19.83
Alcohols (CN):	P	Y_1	Y_2	P	Y_1	Y_2	P	Y_1	Y_2	P	Y_1	Y_2	Alcohols (CN):	P	Y_1	Y_2	P	Y_1	Y_2	P	Y_1	Y_2	P	Y_1	Y_2
10	2.1	2.17	17.69	4.88	2.08	16.53	4.87	2.07	16.45	4.87	2.07	16.45	10	0.53	1.85	27.11	1.01	2.55	26.04	1.23	2.59	26.13	1.23	2.59	26.14
12	3.72	1.12	9.38	3.11	1.89	16.09	3.11	1.9	16.17	3.11	1.9	16.17	12	0.89	0.88	9.28	1.22	0.79	8.81	1.45	0.79	9.11	1.45	0.79	9.11
14	3.83	0.17	1.43	2.13	0.69	6	2.11	0.68	5.95	2.11	0.68	5.95	14	0.99	0.93	9.62	0.49	1.42	16.71	0.57	1.53	18.29	0.57	1.53	18.33
16	3.31	0.41	3.08	2.28	0.18	1.45	2.21	0.21	1.65	2.21	0.21	1.65	16	5.3	1.22	35.64	1.63	1.26	22.71	1.5	1.17	21.06	1.5	1.17	21.06
18	3.61	0.47	3.41	1.94	0.53	3.97	1.86	0.5	3.78	1.86	0.5	3.8	18	0.69	1.92	15.52	0.56	2.07	18.49	0.74	2.14	19.37	0.74	2.14	19.33
Avg.	3.31	0.87	7.00	2.87	1.07	8.81	2.83	1.07	8.80	2.83	1.07	8.80	Avg.	1.68	1.36	19.43	0.98	1.62	18.55	1.10	1.64	18.79	1.10	1.64	18.79
Acids (CN):	P	Y_1	Y_2	P	Y_1	Y_2	P	Y_1	Y_2	P	Y_1	Y_2	Acids (CN):	P	Y_1	Y_2	P	Y_1	Y_2	P	Y_1	Y_2	P	Y_1	Y_2
10	3.2	1.48	7.91	0.86	0.85	6.26	0.83	0.82	6.03	0.84	0.83	6.08	10	0.79	1.34	18.56	0.45	1.39	18.68	0.49	1.53	19.73	0.49	1.53	19.74
12	3.24	1.46	6.86	2.16	5.03	25.23	2.16	5.04	25.29	2.17	5.05	25.35	12	1.99	1.01	18.43	5.88	1.67	31.18	4.45	1.66	30.6	4.45	1.66	30.55
14	3.35	1.14	7.27	0.94	0.89	5.03	0.92	0.9	5.12	0.92	0.9	5.12	14	1.45	0.5	6.43	1.05	1.43	25.29	0.86	0.67	10.6	0.86	0.67	10.58
16	3.17	1.23	7.07	2.39	2.08	13.36	1.55	1.43	8.08	1.55	1.43	8.07	16	1.9	0.66	8.48	0.89	0.83	7.87	0.89	0.82	7.7	0.89	0.81	7.67
18	3.2	0.88	4.1	2.31	2.46	11	7.08	8.7	41.43	2.18	2.39	10.65	18	1.91	1.21	14.18	3.25	2.03	17.68	3.31	2.07	18.09	3.32	2.07	18.04
Avg.	3.23	1.24	6.64	1.73	2.26	12.18	2.51	3.38	17.19	1.53	2.12	11.05	Avg.	1.61	0.94	13.22	2.30	1.47	20.14	2.00	1.35	17.34	2.00	1.35	17.32
Meth. Est. (CN):	P	Y_1	Y_2	P	Y_1	Y_2	P	Y_1	Y_2	P	Y_1	Y_2													
10	3.47	1.3	10.76	1.17	1.96	17.86	1.48	1.98	18.03	1.48	1.99	18.07													
12	2.82	2.35	20.65	1.67	2.29	20.43	1.8	2.33	20.93	1.79	2.29	20.43													
14	4.2	0.52	7.9	2.99	0.86	10.77	3.11	0.81	10.19	3.11	0.81	10.19													
16	3.64	3.15	16.84	1.45	2.79	14.57	1.48	2.85	14.96	1.5	2.88	15.15													
18	3.24	2.67	15.21	2.69	3.88	24.37	2.68	3.93	24.7	2.68	3.93	24.69													
Avg.	3.47	2.00	14.27	1.99	2.36	17.60	2.11	2.38	17.76	2.11	2.38	17.71													

Key	Description
	Best fit within a homologous series for particular variable and solvent
	2nd best fit within a homologous series for particular variable and solvent
	3rd best fit within a homologous series for particular variable and solvent

Stellenbosch University https://scholar.sun.ac.za

For ethane as solvent it can be seen that the RK-ASPEN model gives the lowest error in the composition variables for all systems, but the SRKM gives lower error in the pressure. These differences are typically only 1 or 2 %, which suggests that the overall performance of the computational techniques is similar, but give slightly different deviations in the different variables. Similar results were observed for the propane systems, with no clear preference for one computational technique over the other, except for the propane/carboxylic acids, where the parameters obtained from Aspen Plus ® show a clear advantage. In general, the results from Table 9-1 suggest that both computational techniques give good correlations to the data, and one technique is not definitively superior to the other.

9.2.2 Overall model comparison

In comparing the SRKM, PRSV and PRSV-KM models, it can be seen that very similar results were obtained across all systems, with none of the models showing definitive superiority over the others. This suggests that the use of the Van der Waals mixing rules with BIPs in both the energy and size parameter is the determining factor, irrespective of whether the SRK or PR EOS is used. This corresponds to the results from the statistical analysis in the previous chapter, which found the mixing rules to be the most important factor in modelling the high-pressure VLE of asymmetric binaries. These results also suggest that the superiority of the RK-ASPEN and SR-POLAR models in Chapter 7 is probably due to the inclusion of BIPs in the energy and size parameter for the mixing rules used, rather than the SRK EOS form. As suggested by the established interaction between the volume dependence and the phase behaviour (solute structure and temperature) from the statistical analysis in Chapter 8 (Figure 8-9 and Figure 8-10), the pure model could very well influence the mixture results, but this interaction requires more detailed investigation.

9.3 BIPs vs. CN for PRSV-KM

Table 9-1 shows that changing the combining rules in the PRSV model does not adversely affect the correlation of high-pressure VLE once BIPs are fitted to data. If BIPs obtained from the combining rules used in the PRSV-KM model (Euations 9-3 and 9-4) can be shown to have linear trends with carbon number, this would encourage their use for developing generalized correlations. Figure 9-1 shows the plots of the 2 BIPs from the PRSV-KM model with carbon number for the n-alkanes, 1-alcohols, carboxylic acids and methyl esters in ethane.

Stellenbosch University https://scholar.sun.ac.za

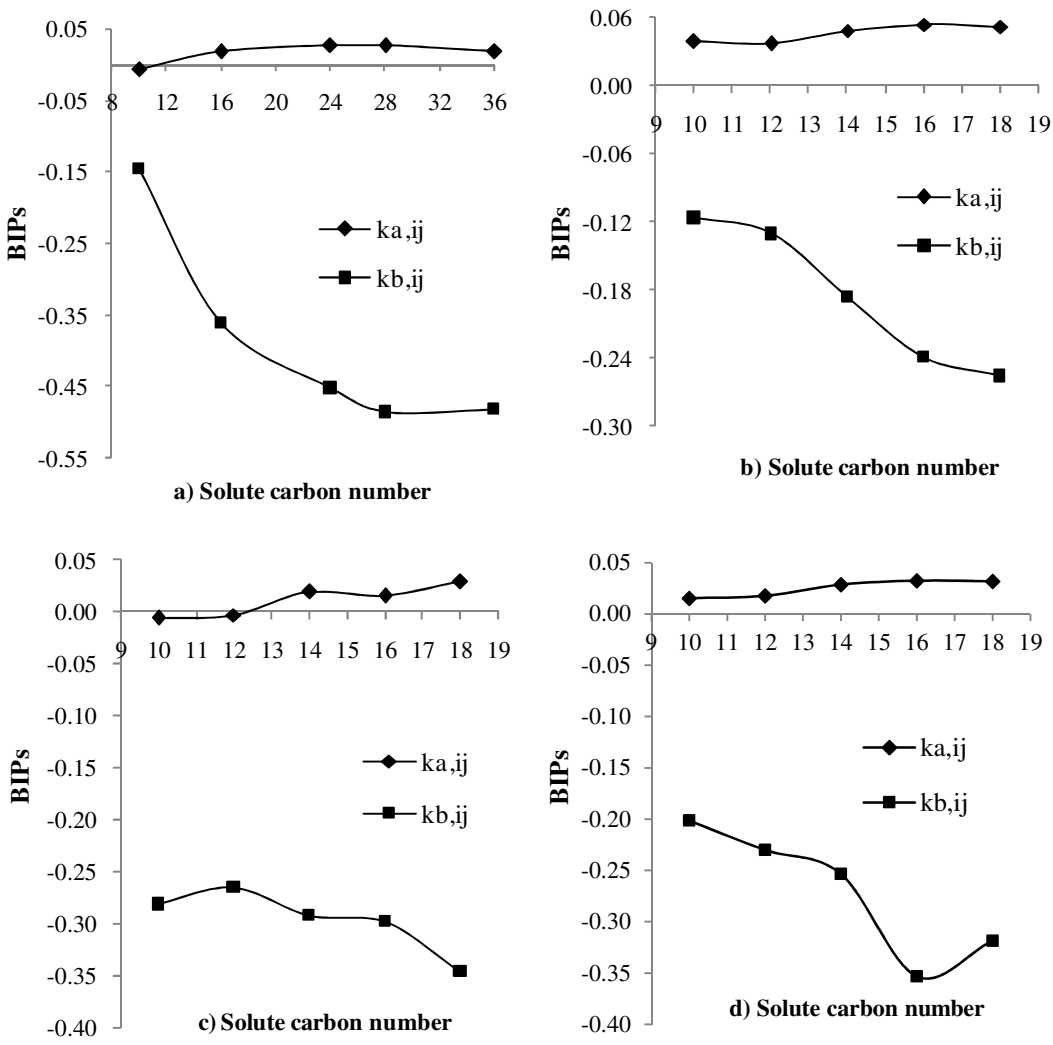

Figure 9-1 BIPs vs. solute carbon number for the a) n-alkane, b) 1-alcohol, c) carboxylic acid and d) methyl ester series in solution with ethane, using the PRSV-KM EOS

Although the trends are not strictly linear, the behaviour in both BIPs is more or less monotonic, showing much better trends with carbon number than any of the cases investigated in Chapter 7 using different mixing rules and the standard combining rules given by Equations 9-1 and 9-2. Figure 9-2 shows the same plots for the propane cases:

Stellenbosch University https://scholar.sun.ac.za

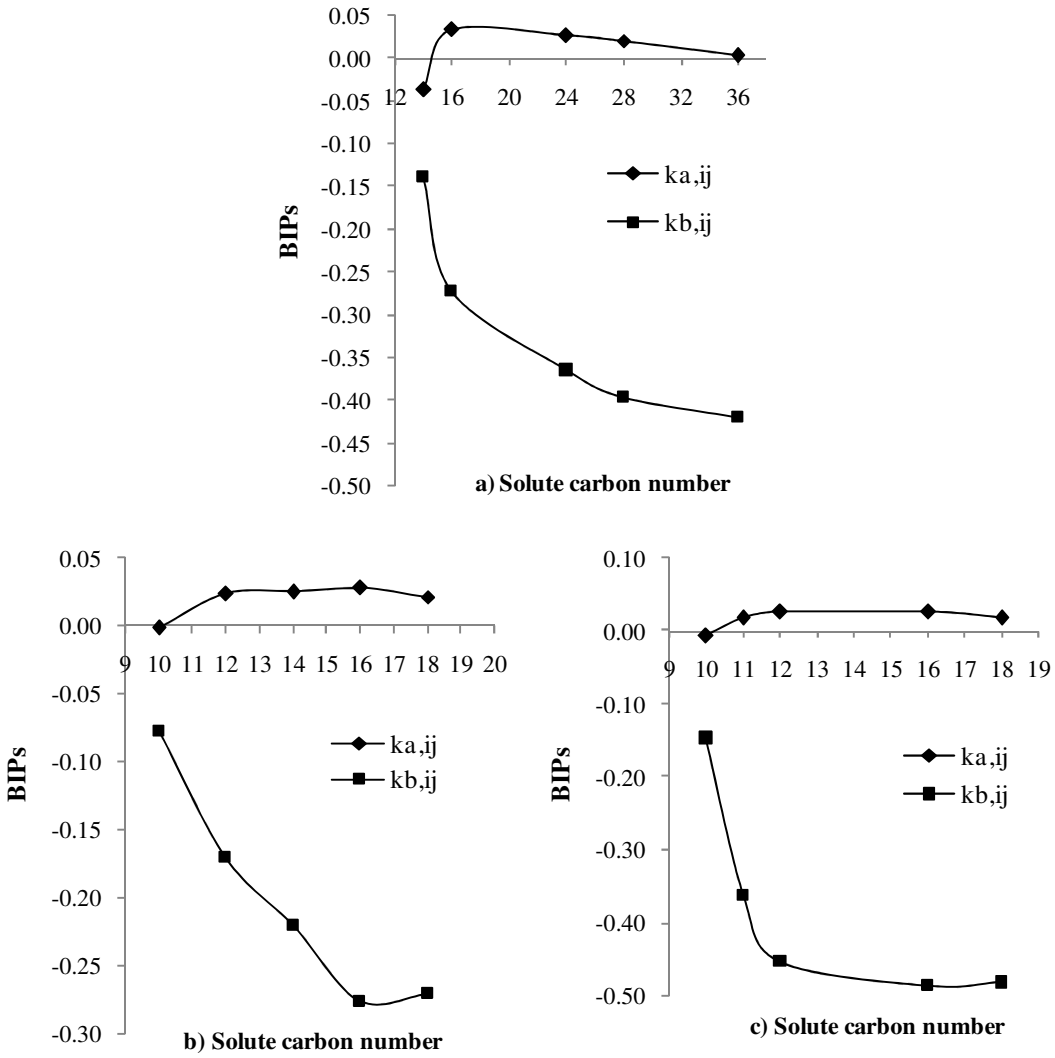

Figure 9-2BIPs vs. solute carbon number for the a) n-alkane, b) 1-alcohol, and c) carboxylic acid in solution with propane, using the PRSV-KM EOS

It is clear that these combing rules show greater promise for developing correlations, however it should also be noted that the values are quite large, especially the BIP for the size parameter $k_{b,ij}$, ranging from -0.1 to -0.5 over the carbon number range considered. These large BIP values suggest that the pure prediction of these combining rules do not provide a good correlation of the data. Figure 9-3 compares the pure prediction of these combining rules (Equations 9-3 and 9-4) with the standard combining rules (Equations 9-1 and 9-2) for the ethane/hexadecane and ethane/hexadecanol systems within the PRSV model:

Stellenbosch University https://scholar.sun.ac.za

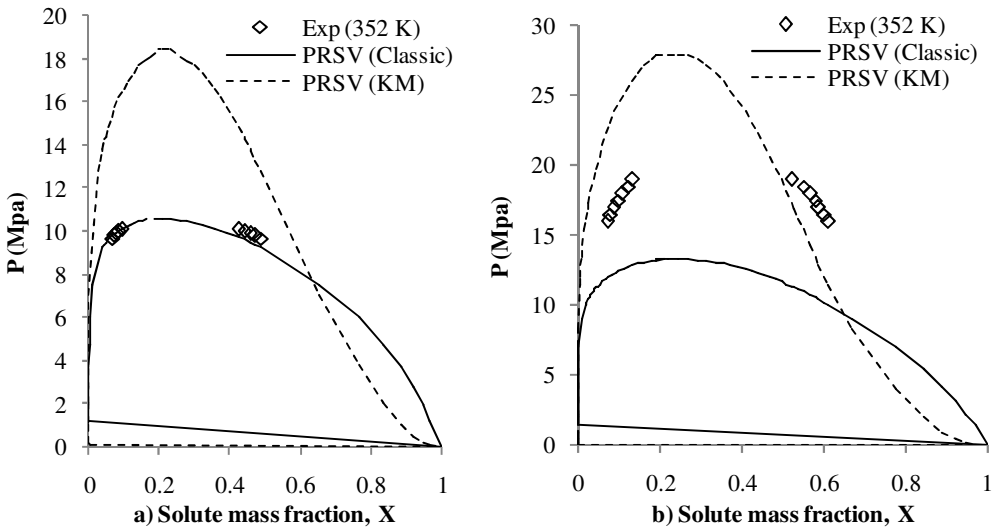

Figure 9-3 Pure prediction of the PRSV model with Van der Waals mixing rules using classic and Kwak-Mansoori combining rules for the a) ethane/hexadecane [1] and ethane/1-hexadecanol [4] systems

Even though the combining rules given by Equations 9-3 and 9-4 show better trends with solute carbon number, they give a worse pure prediction than the standard combining rules, especially for the non-polar ethane/hexadecane system, where the standard combining rules give a reasonable qualitative description of the phase curve, as also shown in Section 8.3.

It is clear that despite obtaining improved trends for BIPs for different combining rules from which simpler correlations may be developed, such correlations remain largely empirical. As also shown in Section 8.4.6, these BIPs are largely sensitive to the pure constants used, as well as temperature. It is also suspected that different BIP values may be obtained in fitting the data in the low pressure region, which further implies the requirement of density dependence in the mixing rules.

A systematic study taking all of these factors into account is therefore necessary for developing reliable mixing rules with predictive capabilities across a range of systems and process conditions and falls outside the range of this project.

9.4 Conclusions

The aim of this chapter is to determine the significance of different computational techniques for correlating the high-pressure VLE of asymmetric binaries of the n-alkane, 1-alcohol, carboxylic acid and methyl esters with ethane and propane as solvent, using the same model.The computational techniques compared are the maximum-likelihood approach with

Stellenbosch University https://scholar.sun.ac.za

the Britt-Luecke minimization algorithm as applied in Aspen Plus ® and the minimization of an implicit objective function in K values, using the Nelder-Mead simplex method, as applied in self-developed MATLAB software. The RK-ASPEN model is used for this investigation. The influence of different combining rules, as developed by Kwak and Mansoori [115], on the model fit and BIP behaviour vs. solute carbon number is also investigated using the PR-SV model. This method is referred to as the PRSV-KM model. The outcomes from this chapter are summarized below:

- The maximum likelihood approach used in Aspen Plus ® generally gives lower errors in the composition variables and the Nelder-Mead simplex method used in MATLAB gives lower errors in pressure, especially for the ethane systems. In general, the two computational methods give slightly different errors in the output variables, but there is very little to choose between them in terms of overall performance.
- There is very little to choose between the correlations obtained for the SRKM, PRSV and PRSV-KM models, presumably because they all use 2 BIPs in the Van der Waals mixing rules, namely one BIP in the energy and size parameter.
- Trends of BIPs vs. carbon number for the PRSV-KM model are found to be more or less monotonic and better suited for developing correlations than when the classic combining rules (Equations 9-1 and 9-2) are used.
- Despite improved trends in BIPs, the pure prediction (no BIPs) obtained in using the alternative combining rules in the PRSV-KM model is worse than observed when using the classic combining rules (Equations 9-1 and 9-2) for the ethane/hexadecane and ethane/hexadecanol systems.
- A systematic study taking into account the influence of temperature, density, as well as the influence of the pure component limit on BIP behaviour is required for developing reliable generalized correlations for these empirical parameters and thus falls outside the scope of the current project.

As mentioned in the introduction to Chapter 7, commercial process simulators often do not provide the best option for process design since their general applicability may overlook more subtle details required for a particular niche application. This may be especially true for a SFE process, since most process simulators do not allow for analytical calculation of the mixture critical point and do not include crossover models that can account for the fluctuations in density and compositionwhich greatly influences fluid behaviour in the extended critical region (see Sections 2.3.1 and 4.6).

Even though these rigorous methods are not applied in this study, the results from this chapter suggest that the parameters obtained from the Aspen Plus ® regression routine give

Stellenbosch University https://scholar.sun.ac.za

equivalent or better correlations of high-pressure VLE than those obtained using standard non-linear regression methods, as applied in independently developed software. These results, as well as the recent process model developed by Zamudio [206], validate Aspen Plus ® as a highly capable thermodynamic tool for correlating the high-pressure VLE of asymmetric binaries.

Stellenbosch University https://scholar.sun.ac.za

10. CONCLUSIONS

The high-pressure binary VLE properties of long-chain hydrocarbon solutes (carbon number greater than 10) from different homologous series are of importance to many lucrative industries. Supercritical Fluid Extraction (SFE) has emerged as a viable technique for treating such systems. The following steps are typically required in the design of such a process:

- Obtain the required property information
- Develop a process model for the fractionation columns
- Design the fractionation process

The focus of this project was primarily on the first step, namely obtaining a reliable source of property information for incorporation into the design of a SFE process. The specific project objectives were given in Section 1.3 and this chapter summarizes the main outcomes from each chapter in addressing these objectives.

10.1 Objective 1 : Review theory on critical points, binary phase diagrams and obtaining the required property information for SFE applications

Chapter 2 provided a review of relevant critical theory and phase behaviour, as well as a discussion on both the theoretical and numerical challenges in obtaining high-pressure VLE properties for asymmetric binaries approaching the mixture critical point. This chapter revealed the fundamental inadequacy of classic mean field models, which do not account for the density and composition fluctuations approaching the critical point and therefore invariably over-predicts the critical point. The relationship between different types of phase behaviour as classified by Konynenburg and Scott [30] and size and energetic asymmetries in a mixture was elucidated. The carbon number and temperature range of three phase regions, as well as the occurrence of tri-criticalty was discussed for selected homologous series in CO_2, ethane and propane as solvents.

A simple computational procedure was proposed for conducting the modelling for this study and addressing the numerical challenges caused by the system non-ideality. The phase curve is constructed by stepping in liquid compostion X from the pure solute (low pressure) towards the pure solvent using a bubble point pressure calculation and carrying all intial guesses from one step to the next. This procedure avoids problems such and the trivial solution and convergence errors and achieves a fairly close and reliable approach to the mixture critical point.

Stellenbosch University https://scholar.sun.ac.za

10.2 Objective 2 : Review interesting phase behaviour of systems considered

Chapter 3 provided a thorough investigation into interesting aspects of the phase behaviour for the systems considered in this project. This investigation revealed that the solute structure and temperature largely influence the solute solubility and therefore the process feasibility. Despite weaker solvating power (higher operating pressures required), low T_c solvents such as CO_2, ethane and propane are preferred for SFE applications due to better selectivity, lower operating temperatures and less solvent residue than high T_c solvents, including water, ammonia, n-hexane or methanol.

Despite CO_2 currently being the most widely used supercritical solvent, ethane and propane were selected for conducting the modelling for this study since they show improved solubility and greater controllability than CO_2, as well as exhibiting linear trends in pressure vs. carbon number and temperature for the considerd hydrocarbon solutes. More complex phase behaviour is observed for the CO_2 systesms due to its quadrupole moment, especially the CO_2/alkanes and CO_2/alcohols.

The solutes considered were selected as then-alkane (nC10-C36), 1-alcohol (nC10-nC18) and methyl ester (nC10-nC18) homologous series.

10.3 Objective 3 : Give overview of semi-empirical EOS models

Chapter 4 reviewed semi-empirical equations of state (EOS) of varying levels of theoretical rigour. The modelling families considered were the following:

- The Virial equation of state
- The Cubic/Van der Waals type equations of State
- The polymer-chain molecular models
- The SAFT molecular models
- The group contribution methods
- The crossover approach

Due to their simplicity, flexibility and reliability, especially in the high-pressure region, the simple CEOSs were deemed an appropriate modelling approach for application in the design of a SFE process and for conducting the modelling for this study.

Stellenbosch University https://scholar.sun.ac.za

10.4 Objective 4 : The pure component limit

It was established that pure component model parameters should always be used in conjunction with a specific set of pure constants for which they are regressed. Literature correlations in terms of the acentric factor for empirical pure component parameters proved less reliable for long-chain or polar molecules. Parameters should rather be regressed in these cases if reliable data is available.The alpha function in the energy parameter of the pure CEOS model has little effect on the saturated liquid volume, but use of a 2 parameter alpha function shows a considerable improvement in the vapour pressure correlation over the simpler 1 parameter Soave alpha function (typically from 2 – 5% smaller errors over the carbon number range), especially for the more polar 1-alcohols and carboxylic acids and when an estimation method was used for the pure constants. The 3 parameter PT EOS with adjustable critical compressibility only show an advantage over the simpler 2 parameter models (SRK and PR EOS) for the non-polar n-alkanes and methyl esters. In general, the CEOSs struggle to simultaneously represent the vapour pressure and saturated liquid volume of a substance and further theoretical improvement of these models are required.

10.5 Objective 5 : Determine capabilities of commercial process simulator

The n-alkanes, 1-alcohols, carboxylic acids and methyl esters in ethane (352 K) and propane (408 K) were investigated in Chapter 7 using property models from Aspen Plus ®. Various regression cases were formulated using 5 CEOSs with different alpha functions and mixing rules.

Good correlations of the data were achieved, with errors in P, T and X_2 typically below 1 % for the best cases. Errors in Y_2 were larger, often exceeding 10 %, however this is due to the small absolute value of the solute concentration in the vapour phase, and these results are typical or better than reported in the literature [98].

Use of at least 2 BIPs were required to achieve a reasonable correlation of the data across the entire solute carbon number range for all the systems investigated, irrespectrive of the model used. The SR-POLAR can be said to have given the best overall performance due to the use of 3 BIPs and higher order composition mixing rules, but large BIP values were observed which suggest that the model does not correlate the data, but rather just fits the errors

The more concave phase curve for the 1-alcohols and carboxylic acid systems were better correlated in the classic high-pressure region than the non-polar alkanes and methyl esters in ethane, however a larger over-estimation of the critical point is observed for these systems.

Stellenbosch University https://scholar.sun.ac.za

This chapter thus showed that thermodynamic models from Aspen Plus ® can provide good correlation of the systems of interest to SFE application at temperatures substantially above the sovent critical temperature and can be used for developing a reliable process model at these conditions.

10.6 Objective 6 : Investigate trends in BIPs for developing generalized correlations

The sensitivity and qualitative effect of BIPs on the phase curve were investigated in Chapter 7. These interaction parameters were also plotted as a function of solute carbon number for the various regression cases evaluated in this chapter. Chapter 9 further investigated the effect of using an alternative combining rule as developed by Kwak and Mansoori [115] in the Van der Waals mixing rules.

Inter-correlation of BIPs occurs when more than 1 BIP is used in the mixing rules, which prevents developing generalized correlations in terms of the solute structure. Smaller vaues and smoother trends were further observed when 2 BIPs were split between the energy and size parameter, rather than applied solely to the energy parameter. Improved trends of BIPs vs. carbon number for the PRSV model with an alternative combining rule of Kwak and Mansoori (Equations 9-3 and 9-4) were observed over use of the classic combining rules, however the pure prediction (no BIPs used) obtained in using these alternative combining rules are worse than those for the classic combining rules in the Van der Waals mixing rules for both the ethane/hexadecane and ethane/hexadecanol systems

Given the sensitivity of BIPs to the pure component limit, temperature, combining rules and probably density, developing reliable correlations were deemed to fall outside the scope of the current investigation

10.7 Objective 7 : Investigate the effect and relative importance of modelling factors for binary VLE at high pressure

A statistical design of experiments sensitivity analysis was conducted in Chapter 8 for investigating important factors in the high-pressure VLE modelling of asymmetric binaries using the CEOSs and ethane as solvent. The factors investigated included:

- Temperature dependence of the model (Soave vs. SV alpha function)
- Volume dependence of the model (2 (PR EOS) vs. 3 (PT EOS) parameter model)
- Pure component constants used (Data (DIPPR) vs. estimation method (C&R))
- Mixing rules used (Vdw vs. WS)

Stellenbosch University https://scholar.sun.ac.za

- Temperature range (338 K vs. 352K)
- Solute functional group (n-alkanes vs. 1-alcohols)

The factors were assesed based on their effect on a *response variable*, defined as the average errors in bubble pressure and vapour composition of both components.

The mixing rules had the largest effect on the response variable, with the quadratic Van der Waals mixing rules with 2 BIPs substantially out-performing the Wong-Sandler mixing rules. A lower value in the response variable was also observed at 352 K and for the 1-alcohols over the n-alkanes, which was attributed to the concave shape of the phase curve for these cases, which seems easier to correlate.

The main effects of the pure component factors (volume dependence, alpha function and pure constants used) did not have a significant effect on the response variable. Despite the main effect of the volume dependence not having a significant effect, significant interactions were observed between the volume dependence and both the temperature and solute structure. This suggests that the pure component model influences the correlation of the high-pressure VLE region and that mixing rules are not the only important factor for the correlating asymmetric mixtures.

An optimization analysis revealed that the PR EOS with SV alpha function, using the Van der Waals mixing rules gave the best overall performance from the combinations considered. BIPs were further found to be highly sensitive to the pure component limit as well as temperature.

It was thus shown that a systematic statistical analysis of important modelling factors reveals interactions and effects which are not immediately obvious from considering the factor effects separately. This could warrant extension of the size of the statistical analysis and incorporation of such an analysis in process simulators to allow for a better model selection strategy than proposed by the heauristic selection trees used in most commercial process simulators.

10.8 Objective 8 : Investigate the effect of different computational procedures on the results

Chapter 9 compared two computational techniques for the RK-ASPEN model, namely a maximum likelihood approach using the Britt-Luecke minimization [203] algorithm in Aspen Plus ® and an implicit objective function in terms of equilibrium K ratios minimized using the Nelder-Mead simplex method in MATLAB. Very similar results for the two

Stellenbosch University https://scholar.sun.ac.za

computational techniques were obtained with slightly different errors in the output variables (P, Y_1 and Y_2).

These results partially validate the use of Aspen Plus ® as a reliable thermodynamic and process modelling tool for SFE applications since similar model fits were obtained using two entirely separate computational techniques using the same model.

Stellenbosch University https://scholar.sun.ac.za

11. RECOMMENDATIONS AND FUTURE WORK

A number of recommendations can be made based on the results from this study. These include reworking selected thesis chapters into literature publications, possibly upgrading the existing study into a doctorate dissertation, as well as work recommended for future studies.

11.1 Possible contributions and motivation for upgrade of current study

The following possible publications may be adapted from the work done for this project, which may offer a good motivation for upgrading the study into a doctorate dissertation:

- Chapter 3 may be adapted into a review article on interesting aspects of the phase behaviour for systems of interest to SFE applications.
- Chapter 6 offers a thorough investigation of important factors to consider in applying the CEOSs to the pure component vapour pressure and saturated liquid volume for long-chain hydrocarbons of interest to SFE applications and may be adapted into a publication.
- Chapter 7 offers a thorough investigation into the capabilities of CEOS models inthe Aspen Plus ® process simulator for correlating the high pressure VLE of long-chain hydrocarbons in supercritical ethane and propane. BIP behaviouris also investigated in this chapter for various regression cases and this chapter may thus be adapted into a publication.
- Chapter 8 provides a thorough statistical analysis into important modelling factors to be considered in applying the CEOS models to the high-pressure VLE of asymmetric binary systems of interest to SFE applications and may also be adapted into a publication.
- Chapter 9 compares different computational techniques for modelling asymmetric binaries of interest to SFE applications and helps establish Aspen Plus ® as a viable tool for developing a realistic process model. This chapter can also contribute to a literature publication.

The statistical analysis conducted in chapter 8 also made the interesting finding that significant interactions exist amongst modelling factors which are not readily observed upon considering each factor independently. Extending the range of this investigation may therefore yield interesting results. A recommendation for extending the statistical analysis is to increase the size of the design to 7 factors, each at two levels, amounting to 128 treatments (modelling combinations), rather than the current size of 2^6 = 64 treatments. Given the importance of phase behaviour on the results obtained, the 7^{th} factor is recommended to be the

Stellenbosch University https://scholar.sun.ac.za

solvent used, with ethane and propane as the two levels. Data for the n-alkanes and 1-alcohols in the appropriate carbon number and temperature range using propane as solvent has already been measured at Stellenbosch University and MATLAB and STATISTICA software is already in place for conducting such an investigation with minimal additional time (one to two months) and including these results in the current thesis.

11.2 Future work

Model inadequacy of classic mean-field equations in accounting for the long range density fluctuations and divergence of the isothermal compressibility approaching the critical point pose a considerable theoretical challenge in obtaining reliable property values for SFE applications. Even though the cubic equations of state provide a very useful methodology for calculating high-pressure VLE due to their simplicity, flexibility and reliability, the methods employed in this study will not suffice for a rigorous solution to the problems which the critical region pose for thermodynamic modelling. The following recommendations are therefore made to address these issues more thoroughly in future studies:

- A procedure for analytical calculation of the critical point should be included in the software such as that of of Hicks and Young [33], Heidemann and Khalil [31], Heidemann and Michelsen [49] or the application of the *tangent plane criterion* in the work of Michelsen [50 - 53]
- More sophisticated models should be incorporated into the software which can account explicitly for chain-formation, polarity and association such as those from the SAFT or PHCT family.
- The theoretical aspects approaching the critical region should be addressed either via heuristic or empirical means, such as through the work of Solimando et al. [63], Firoozabadi et al. [64] and Kedge and Trebble [65]; or the more rigorous crossover theory such as applied by Tang and Sengers [56], Jin et al. [57], Kostrowicka Wyczalkowska et al [58] and Kiselev and co-workers [59 - 62] and Lovell and Vega [190]
- Zamudio [206] found that thermodynamic models struggle significantly at lower temperatures, close to the critical temperature of the solvent, due to divergence of the isothermal compressibility in this region. The temperature range considered for this study was above this range and lower temperatures should be considered in future work.
- Modelling of multi-component mixtures with more than two components is also of vital importance to the design of a SFE process and is recommended for future studies.

Stellenbosch University https://scholar.sun.ac.za

Having shown the importance of mixing rules in Chapter 8, an alternative to the rigorous theoretical approach would be to develop reliable mixing rules that could give a good generalized description of the systems in this study across a large temperature, density and carbon number range for different solvents. As elucidated by the sensitivity of BIPs, this is an inevitably empirical affair, however the MATLAB software developed for this study has the following features which could greatly aid such a study:

- The software allows for easy data importation from an existing and growing data-base established at the Separation Technology group at Stellenbosch University
- Utilization of the *ginput* function from MATLAB allows for checking the consistency and smoothing of data into VLE sets before regression, to make sure the same region of the phase curve is modelled for different systems.
- A script has been developed which allows specification of different binary systems of a specific homologous series for a given solvent and temperature. The systems are then imported from the data-base, the mutually available composition range is identified and correlations of pressure vs. carbon number (as shown in Figure 3-2) can be exported to excel for a given number of data points or at given increments over the composition range. The R^2 value of these correlations can be observed and the correlations can be used to generate data for intermediate carbon numbers to the measured systems.
- The software allows for the calculation of the fugacity of component in solution from the numerical derivative of the pure component fugacity. As explained in Appendix B.4, this is useful for developing mixing rules, since testing new expressions does not require the analytical calculation of the derivative with mole number, which can be quite complicated and tedious if intermediate changes are made in mixing rule development.
- The software allows for testing the analytical expressions for the fugacity of a component in solution for consistency using the method recommended by Michelsen and Mollerup [66], as also explained in Appendix B.4. This test identifies problems such as the dilution effect or the Micheslen-Kirstenmacher syndrome.

It is therefore clear that even though novel mixing rules and generalized correlations for BIPs were not developed in this study, the software developed provides a useful tool for such investigations for various solvent/homologous series combinations and over a large range of both temperature and carbon numbers of relevance to SFE applications.

Stellenbosch University https://scholar.sun.ac.za

12. REFERENCES

[1] M. Du Rand, I. Nieuwoudt, Measurement of phase equilibria of supercritical ethane and paraffins., J. Supercritical Fluids 21 (2001) 181-193

[2] C.E. Schwarz, I. Nieuwoudt, J.H. Knoetze, Phase equilibira of long chain n-alkanes in supercritical ethane: Review, measurements and prediction, J. Supercritical Fluids 46 (2008) 226-232

[3] M. Zamudio, C.E. Schwarz, J.H. Knoetze, Phase equilibria of branched isomers of C_{10}-alcohols and C_{10}-alkanes in supercritical ethane, J. Supercritical Fluids 58 (2011) 330-342

[4] C.E. Schwarz, A.J. De Villiers, C.B. McClune, G.J.K Bonthuys, A.J Burger, J.H. Knoetze, High pressure phase equilibirum measurements of long chain alcohols in supercritical ethane, J. Supercritical Fluids 55 (2010) 554-565

[5] C.E. Schwarz, M.L. Hahn, A.J. De Villiers, J.H. Knoetze, Phase behaviour of high molecular mass methyl esters in supercritical ethane, Fluid Phase Equilibria 311 (2011) 36-44

[6] C.E. Schwarz, C. Schlechter, J.H. Knoetze, Phase equilibria of ethyl esters in supercritical ethane and propane, J. Supercritical Fluids 79 (2013) 19-26

[7] C.E. Schwarz, K.G. Chobanov, Phase equilibria of linear saturated high molecular mass acids in supercritical ethane, J. Supercritical Fluids 87 (2014) 40-49

[8] C.E. Schwarz, I. Nieuwoudt, Phase equilibrium of propane and alkanes part I: Experimental procedures, dotriacontane equilibrium and EOS modelling, J. Supercritical Fluids 27 (2003) 133-144

[9] C.E. Schwarz, I. Nieuwoudt, Phase equilibrium of propane and alkanes part II: hexatriacontane through hexacontane, J. Supercritical Fluids 27 (2003) 145-156

[10] C.E. Schwarz, G.J.K Bonthys, J.H. Knoetze, A.J. Burger, The influence of functional end groups on the high pressure phase equilibria of long chain molecules in supercritical propane, J. Supercritical Fluids 46 (2008) 233-237

[11] C.E. Schwarz, J.H. Knoetze, Phase equilibria of high molecular mass 1-alcohols in supercritical propane, Fluid Phase Equilbria 258 (2007) 51-57

[12] C.E. Schwarz, M. Zamudio, J.H. Knoetze, Phase equilibria of long-chain carboxylic acids in supercritical propane, J. Chemical &Engineering Data 56 (2011) 1116-1124

[13] I. Nieuwoudt, M. Du Rand, Measurement of phase equilibria of supercritcal carbon dioxide and paraffins, J. Supercritical Fluids 22 (2002) 185-199

[14] C.E. Schwarz, J.H. Knoetze, Phase equilibria of long-chain acids in supercritical carbon dioxide, J. Supercritical Fluids 56 (2011) 1116-1124

Stellenbosch University https://scholar.sun.ac.za

[15] F.C.v.N. Fourie, C.E. Schwarz, J.H. Knoetze, Phase equilbira of alcohols in supercritical fluids Part 1: The effect of the position of the hydroxyl group for linear C_8 alcohols in supercritical carbon dioxide, J. Supercritical Fluids 47 (2008) 161-167

[16] F.C.v.N. Fourie, C.E. Schwarz, J.H. Knoetze, Phase equilibria of alcohols in supercritical fluids Part II: The effect of side branching on C_8 alcohols in supercritical carbon dioxide, J. Supercritical Fluids 51 (2009) 128-135

[17] M. Zamudio, C.E. Schwarz, J.H. Knoetze, Phase equilibria of branched isomers of C_{10}-alcohols and C_{10}-alkanes in supercritical carbon dioxide, J. of Supercritical Fluids 59 (2011) 14-26

[18] G. Brunner, Counter-current separations, J. Supercritical Fluids 47 (2009) 574-582

[19] J.C. Crause, I. Nieuwoudt, Paraffin wax fractionation: state of the art vs. supercritical fluid fractionation, J. Supercritical Fluids 27 (2003) 39-54

[20] C.E. Schwarz,The phase equilibrium of alkanes and supercritical fluids, Master's Thesis, University of Stellenbosch, 2001

[21] G.J.K. Bonthys, C.E. Schwarz, A.J. Burger, J.H. Knoetze, Separation of alkanes and alcohols with supercritical fluids. Part 1: Phase equilibria and viability study, J. Supercritical Fluids 57 (2011) 101-111

[22] C.E. Schwarz, G.J.K. Bonthys, R.F. van Schalkwyk, D.L. Laubscher, A.J. Burger, J.H. Knoetze, Separation of alkanes and alcohols with supercritical fluids. Part 2 Influence of process parameters and size of operating range, J. of Supercritical Fluids 58 (2011) 352-359

[23] F. Temelli, Perspectives on supercritical fluid processing of fats and oils, J. of Supercritical fluids 47 (2009) 583-590

[24] A.S. Teja, C.A. Eckert, Commentary on supercritical fluids: Research and applications, Industrial &Engineering Chemistry Research 39 (2000) 4442-4444

[25] I. Nieuwoudt, C. Crause, M. Du Rand, Oligomer fractionation with supercritical fluids, J. of Supercritical Fluids 24 (2002) 47-55

[26] M. Perrut, Supercritical fluid applications: Industrial developments and economic issues, Industrial &Engineering and Chemistry Research 39 (2000) 4531-4535

[27] M. Perrut, J. Clavier, Supercritical fluid formulation: Process choice and scale up, Industrial& Engineering and Chemistry Research 42 (2003) 6375-6383

[28] J.P. O'Connell, R. Gani, P.M. Mathias, G. Maurer, J.D. Olson, P.A. Crafts, Thermodynamic property modeling for chemical process and product engineering: Some perspectives, Industrial & Engineering Chemistry Research 48 (2009) 4619-4637

[29] U.K. Deiters, Remarks on publications dealing with equations of state, Fluid Phase Equilibria 161 (1999) 205-219

Stellenbosch University https://scholar.sun.ac.za

[30] P.H. Van konynenburg, R.L. Scott, Critical lines and phase equilibrium in binary Van der Waals mixtures, Philosophical transactions of the Royal Society of London, Series A: Mathematical, Physical and Engineering Sciences 298 (1980d) 495–540

[31] R.A. Heidemann, A.M. Khalil, The Calculation of critical points, AIChE Journal 26 (1980) 769–778

[32] M.L. Michelsen, Phase equilibrium calculations. What is easy and what is difficult?, Computers & Chemical Engineering 17 (1993) 431–439

[33] C.P. Hicks, C.L. Young, Theoretical prediction of phase behaviour at high temperatures and pressures for non-polar mixtures Part 1 – Computer solution techniques and stability tests, J. Chem. Soc., Trans. Faraday Soc. 11, 73 (1976) 597–612

[34] Y. S. Wei, R.J. Sadus, Phase behaviour of ternary mixtures: a theoretical investigation of the critical properties of mixtures with equatl size components, Phys. Chem. Chem. Phys. 1 (1999) 4329–4336

[35] J.M.H. Levelt-Sengers, Critical behaviour of fluids: Concepts and applications, in: E. Kiran, J.M. Levelt Sengers, NATO Advanced Study Institute on Supercritical Fluids-Fundamentals for application , Kluwer Academic Publishers Turkey,1994, pp. 65-89.

[36] C. Erkey, Supercritical fluids and organometallic compounds: From recovery of trace metals to synthesis of nanostructured material, Elsevier,. Amsterdam, Netherlands, 2011, pp. 11-19

[37] S. Pereda, S.B. Bottini, E.A. Brignole, Fundamentals of supercritical fluid technology, in:J.L. Martinez, Supercritical fluid extraction of nutraceuticals and bioactive compounds, CRC Press, Boca Raton, FL, USA,2007, pp. 2-33

[38] B.E. Poling, J.M. Prausnitz, J.P. O'Connel, The properties of gases and liquids, 5th edition, McGraw Hill, 2001, Chapter 2 (pp. 2.2 – 2.38), Chapter 4 (pp 4.9, 4.30), Chapter 5 (pp. 5.2 , 5.21), Chapter 6 (pp. 6.30,), Chapter 8 (pp. 8.122)

[39] L.S. Ornstein, F. Zernike, Accidental deviations of density and opalescence at the critical point of a single substance, Proc. Sec. Sci. Kon. Akad. Wetensch. Amsterdam, 73 (1914) 793-805

[40] I. Kikic, T. de Loos, Thermodynamic Properties Phase Equilibriua, Presented at Socrates Intensive Course in Basics, Developments, Research and Industrial Applications in High Pressure Chemical Engineering Processes, Prague, 2005, pp.1-45

[41] M.A. Ansimov, J.V. Sengers, Critical Region. In: J. Sengers, R. Kayser, C. Peters, H. White, Equations of State for Fluids and Fluid Mixtures,Amsterdam, The Netherlands, IUPAC, 2000,pp. 381-426.

[42] Y. Cengel,Heat and Mass Transfer: A Preactical Approach,3rd ed,McGraw Hill, New York, 2006: pp. 776

Stellenbosch University https://scholar.sun.ac.za

[43] Y. Cengel,. Fluid Mechanics: Fundametntals and Applications,1st ed,McGraw Hill, New York, 2006 pp. 46-47

[44] Th. W. De Loos, Understanding Phase Diagrams, in: E. Kiran, J.M. Levelt Sengers, NATO Advanced Study Institute on Supercritical Fluids-Fundamentals for application ,Kluwer Academic Publishers Turkey, 1994, pp. 65-89

[45] R. Privat, J.N. Jaubert, Classification of global fluid-phase equilibrium behaviours in binary systems, Chemical Engineering Research and Design 91 (2013) 1807–1839

[46] J.M. Smith, H.C. Van Ness, M.M. Abbot. Introduction to Chemical Engineering Thermodynamics. New York: McGraw Hill, 7th edition, 2005

[47] C.J. Peters, Multiphase equilibria in near-critical solvents, in: E. Kiran, J.M. Levelt Sengers, NATO Advanced Study Institute on Supercritical Fluids-Fundamentals for application , Kluwer Academic Publishers Turkey, 1994, pp. 117-145

[48] J.R. Elliot, C.T. Lira, Introductory Chemical Engineering Thermodynamics, Prentice Hall PTR, New Jersey, 1999, Chapter 7, pp. 229–256

[49] M.L. Michelsen, R.A. Heidemann, Calculation of critical points from cubic two-constant equations of state, AIChE Journal 27 (1981) 521–523

[50] M.L. Michelsen, Calculation of phase envelopes and critical points for multicomponent mixtures, Fluid Phase Equilibria 4 (1980) 1 -10

[51] M.L. Michelsen, Calculation of critical points and phase boundaries in the critical region, Fluid Phase Equilibria 16 (1984) 57–76

[52] M.L. Michelsen, The isothermal flash problem. Part 1: Stability, Fluid Phase Equilibria 9 (1982) 1-19

[53] M.L. Michelsen, The isothermal flash problem. Part 2 : Phase split calculation, Fluid Phase Equilibria 9 (1982) 21-40

[54] R.A. Heidemann, The classical theory of critical pointsn, in: E. Kiran, J.M. Levelt Sengers, NATO Advanced Study Institute on Supercritical Fluids-Fundamentals for application , Kluwer Academic Publishers Turkey,1994, pp. 39-64

[55] S. Tang, J.V. Sengers, Thermodynamic behaviour of fluids in the supercritical region, J. Supercritical Fluids 4 (1991) 209–214

[56] G.X. Jin, S. Tang, J.V. Sengers, Thermodynamic behaviour of fluid mixtures in the critical region, Fluid Phase Equilibria 75 (1992) 1-10

[57] A. Kotrowicka Wycsalkowska, M.A. Anisimov, J. Sengers, Global crossover equation of state of a Van der Waals fluid,Fluid Phase Equilbiria 158-160 (1999) 523-535.

[58] S.B. Kiselev, Cubic crossover equation of state,Fluid Phase Equilibria, 147 (1998) 7-23

Stellenbosch University https://scholar.sun.ac.za

[59] S.B. Kiselev, J.C. Rainwater, M.L. Huber, Binary mixtures in and beyond the critical region: thermodynamic properties, Fluid Phase Equilibria 150–151 (1998) 469-478

[60] S. B. Kiselev, D.G Friend, Cubic crossover equation of state for mixtures. Fluid Phase Equilibria 162 (1999) 51-82

[61] S. B. Kiselev, J.F. Ely, Crossover SAFT equation of state: Application for normal alkanes,Industrial &Engineering Chemistry Research 38 (1999) 4993-5004

[62] R. Solimando, M. Rogalski, E. Neau, A. Peneloux, Modelling of the phase behaviour of mixtures in the critical region using the augemented Peng-Robinson equation of state, Fluid Phase Equilibria 82 (1993) 369–377

[63] A. Froozabadi, S. Arbabi, B. Dindoruk, Near-critical phase behaviour of mixtures using equations of state, The Canadian Journal of Chemical Engineering 72 (1994) 134-141

[64] C.J. Kedge, M.A. Trebble, An empirical near-critical correction for cubic and non-cubic equations of state, Fluid Phase Equilibria 194–197 (2002) 401 – 409

[65] B.E. Poling, E.A. Grens, J.M. Prausnitz, Thermodynamic properties from a cubic equation of state: Avoiding trivial roots and spurious derivatives, Industrial & Engineering Process Design & Development 20 (1981) 127-130

[66] M.L. Michelsen, J.M. Mollerup, Thermodynamic models: Fundamentals & computational aspects, 2nd edition, Tie-line publications, Denmark, 2007, pp. 223,77

[67] P.M. Mathias, J.F. Boston, S. Wantanasiri, Effective utilization of equations of state for thermodynamic properties in process simulation, AIChE Journal 30 (1984) 182–186

[68] T. Gundersen, Numerical aspects of the implementation of cubic equations of state in flash calculation routines, Computers &Chemical Engineering 6 (1982) 245–255

[69] G.V. Pasad, G. Venkatarathnam, A method for avoiding trivial roots in isothermal flash calculations using cubic equations of state, Industrial & Engineering Chemistry Research 38 (1999) 3530–3534

[70] D. Veeranna, A. Husain, S. Subrahmanyam, M.K. Sarkar, An algorirthm for flash calculations using an equation of state, Computers & Chemical Engineering 11 (1987) 489–496

[71] C.E. Schwarz, J.H. Knoetze, Comparison of the phase behaviour of alkanes and acids in supercritical fluids, Keynote presentation at the 13th European meeting on Supercritical Fluids, Den Haag, Netherlands, 9 – 12 October 2011

[72] A. Kramer, G. Thodos, Solubility of 1-hexadecanol and palmitic acid in supercritical carbon dioxide, J. Chemical Engineering Data 33 (1998) 230–234

Stellenbosch University https://scholar.sun.ac.za

[73] J.S. Yau, F.N. Tsai, Solubilities of 1-eicosanol and eiconsanoic acid in supercritical carbon dioxide from 308.2 to 328.2 K at pressures 21.26 MPa, J. Chemical Engineering Data 39 (1994) 827 - 829

[74] A. Anderko, Cubic and Generalized Van der Waals Equations. In: J.V. Sengers, R.F. Kayser, C.J. Peters, H.J. White, eds. Equations of state for fluids and fluid mixtures, Part 1. Amsterdam, The Netherlans: IUPAC,2000, pp. 75-126

[75] A. Anderko,S. Malanowski, Modelling Phase Equilibria,New York, John Wiley & Sons, Inc., 1992

[76] S. Sandler, Equations of State for Phase Equilibrium Computations. In: E. Kiran, J. L. Sengers, NATO Advanced Study Institute on Supercritical Fluids-Fundamentals for application. Turkey: Kluwer Academic Publishers, 1994, pp. 147-175.

[77] J. D. Van der Waals, On the continuity of gaseous and liquid states, Ph.D. Dissertation, Universiteit Leiden, Leiden, The Netherlands, 1873

[78] O. Redlich, J.N.S. Kwong, On thermodynamic solutions, Chem. Rev. 44 (1949) 233-244

[79] D. Peng, D.B. Robinson, A new two-constant equation of state, Industrial &Engineering Chemical Fundamentals 15 (1976) 59 – 63

[80] G.G. Fuller, A modified Redlich-Kwong-Soave equation of state capable of representing the liquid state, Industrial & Engineering Chemistry Research 15 (1976) 254–257

[81] G. Scmidt, H. Wenzel, A modified van der Waals type equation of state, Chemical Engineering Science 35 (1980) 1503–1512

[82] A. Harmens, H. Knapp, Three-parameter cubic equation of state for normal substances, Industrial & Engineering Chemistry Research 19 (1980) 291–294

[83] N.C. Patel, A.S. Teja, A new cubic equation of state for fluids and fluid mixtures, Chemical Engineering Science 37 (1982) 463-473

[84] Y. Adachi, B.C.Y. Lu, H. Sugie, A four-parameter equation of state, Fluid Phase Equilibria 11 (1983) 29–48

[85] M.A. Trebble, P.R. Bishnoi, Development of a new four-parameter cubic equation of state, Fluid Phase Equilibria 35 (1987) 1–18

[86] M. Cismondi, J. Mollerup, Development and application of a three-parameter RK-PR equation of state, Fluid Phase Equilibrium 22 (2005)74-89

[87] A. Peneloux, E.F.R. Rauzy, R. Fréze Consistent correction for Redlich-Kwong-Soave,Fluid Phase Equilibria 32 (1982) 139

[88] P.M. Mathias, T. Naheiri, E.M Oh, A density correction for the Peng-Robinson equation of state, Fluid Phase Equilibria 47 (1989) 77–87

[89] G. Soave, Equilibrium constants for a modified Redlich-Kwong equation of state, Chemical Engineering Science 27 (1972) 1197–1203

Stellenbosch University https://scholar.sun.ac.za

[90] G. Heyen, Proceeding of the 2nd international conference on phase equilibira fluids and properties in the chemical industry, 1, Dechema, Frankfurt 1980

[91] J.F. Boston, P.M. Mathias, Phase equilibrium in a third generation process simulator, in: Proceedings of the 2nd international conference on phase equilibrium and fluid properties in the chemical process industries, West Berlin (17 – 21 March 1980), pp. 823 – 849

[92] P. M. Mathias, A versatile equation of state, Industrial &Engineering Chemistry Process Design &Development 22 (1983) 385-391

[93] P. Mathias, T. Copeman, Extension of the Peng-Robinson Equation of State to complex mixtures: Evaluation of the various forms of the local composition concept Fluid Phase Equilibira13 (1983) 91-108

[94] R. Stryjek, J.H. Vera, PRSV: An improved Peng-Robinson equation of state for pure compounds and mixtures, Canadian J. Chemical Engineering, 64 (1986) 323–333

[95] G.A. Melhelm, R. Saini, B. M. Goodwin, A modified Peng-Robinson equation of state, Fluid Phase Equilibria, 47 (1989) 189

[96] C.H. Twu, D. Bluck, J.R. Cunningham, J.E. Coon, A cubic equation of state with a new alpha function and a new mixing rule, Fluid Phase Equilibria 69 (1991) 33–50

[97] K.A.M. Gasem, W. Gao, Z. Pan, R.L. Robinson Jr., A modified temperature dependence for the Peng-Robinson equation of state, 181 (2001) 113–125

[98] J.O. Valderrama, The state of the cubic equations of state. Industrial & Engineering Research 42(2003) 1603-1618.

[99] A.Z. Panagiotopoulos, R.C. Reid, A new mixing rule for cubic equations of state for highly polar, asymmetric system, Presented at the 189th American Chemical Society Meeting, Miami Beach, FL, April 29 – May 3, 1985

[100] J. Schwartzenruber, H. Renon, Extension of UNIFAC to high pressures and temperatures by the use of cubic equation of state, Industrial & Engineering Chemisty Research28 (1989) 1049-1055

[101] P.M. Mathias, H.C. Klotz, J.M. Prausnitz, Equation-of-state mixing rules for multicomponent mixtures: The problem of invariance, Fluid Phase Equilibria 67 (1991) 31-44

[102] M.L. Michelsen, H. Kirtstenmacher, On composition-dependent interaction coefficients, Fluid Phase Equilibria, 58 (1990) 229–230

[103] J. Schwartzentruber, H. Renon, Equations of state: how to reconcile flexible mixing rules, the virial coefficient constraint and the “Michelsen-Kirtenmacher syndrome” for multicomponent systems, Fluid Phase Equilibria 67 (1991) 99-110

Stellenbosch University https://scholar.sun.ac.za

[104] M.S. Zabaloy, J.H. Vera, Identification of variant and invariant properties in the thermodynamics of mixtures: tests for models and computer codes, Fluid Phase Equilibria 119 (1996) 27– 49

[105] J.A.P. Coutinho, G.M. Kontogeorgis, E.H. Stenby, Binary interaction parameters for non-polar systems with cubic equations of state: a theoretical approach 1. CO_2/hydrocarbons using SRK equation of state, Fluid Phase Equilibria, 102 (1994) 31–60

[106] R. Privat, J. Jaubert, Thermodynamic models for the prediction of pertroleum-fluid phase behaviour. Crude-oil emulsions- composition stability and characterization, Prof. Manar El-Sayad Abdul-Raouf (Ed.), ISBN: 978-958-51-0220-5, In Tech, Available from: http://www.intechopen.com/books/crude-oil-emulsions-composition-stability-and-chracterization/thermodynamic-models-for -the-prediction-of-petroleum-fluid-phase-behaviour

[107] R. Stryjek, Correlation and prediction of VLE data for n-alkane mixtures,Fluid Phase Equilibria 56 (1990) 141-152

[108] G Gao, A simple correlation to evaluate binary interaction parameters of the Peng-Robinson equation of state:binary light hydrocarbon systems,Fluid Phase Equilibria, 74 (1992) 85-93

[109] A. Kordas, K. Magoulas, S. Stamataki, D.Tassios, Methane-hydrocarbon interaction parameters correlation for the Peng-Robinson and the t-mPR equation of state,Fluid Phase Equilibria,112 (1995) 33-44

[110] A. Kordas, K. Tsoutsouras, S. Stamataki, D.Tassios, A generalized correlation for the interaction coefficients of CO_2-hydrocarnon binary mixtures,Fluid Phase Equilibria,93 (1994) 141-166

[111] H. Nishiumo,A. Tsutomu, Generalization of the binary interaction parameter of the Peng-Robinson equation of state by component family,Fluid Phase Equilibria, 42 (1988) 43-62

[112] S. Vitu, R. Privat, J. Jaubert,F. Mutelet, 2008. Predicting the phase equilibria of CO2 + hydrocarobn systems with the PPR78 model (PR EOS and kij calculated through group contribution method),J. Supercritical Fluids45 (2008) 1-26

[113] W. Gao, R. Robinson, K. Gasem, Alternate equation of state combining rules and interaction paramter generalizations for asymmetric mixtures, Fluid Phase Equlibiria 213 (2003) 19-37

[114] S.K. Jha, G. Madras, Correlations for binary phase equilibria in high-pressure carbon dioxide, Fluid Phase Equilibria, 238 (2005) 174-179

[115] T.Y. Kwak, G.A. Mansoori, Van der Waals mixing rules for cubic equatios of state. Applications for supercritical fluid extraction modelling,Chemical Engineering Science 41 (1986) 1303-1309

Stellenbosch University https://scholar.sun.ac.za

[116] G.M. Kontogeorgis, P. Coutsikos, V.I. Harismiadis, A. Fredeslund, D.P. Tassios, A novel method for investigating the repulsive and attractive parts of cubic equations of state and the combining rules used with the vdW-1f theory,Chemical Engineering Science53 (1997) 541-552

[117] P.A. Sacomani, E.A. Brignole, Predictions of activity coefficients of nearly athermal binary mixtures using cubic equations of state, Industrial & Engineering Chemistry Research 42 (2003) 4143–4145

[118] G.M. Kontogeorgis, P. Coutsikos, Thirty years with the EOS/G_{ex} models-What have we learned?, Industrial & Engineering Chemistry Research 51 (2012) 4119-4142

[119] J. Vidal,Mixing rules and excess properties in cubic equations of state. Chemical Engineering Science 33 (1978) 787-791

[120] M. Huron, J. Vidal, New mixing rule in simple EOS for representing VLE of strongly non-ideal mixtures, Fluid Phase Equilibria 3 (1979) 255-271

[121] J. Mollerup, A note on derivation of mixing rules from excess gobbs energy models,Fluid Phase Equilbiria 25 (1986) 323-327.

[122] M. Michelsen, A method for incorporating excess Gibbs energy models into equations of state, Fluid Phase Equilibria 60 (1990) 47-58

[123] M. Michelsen, A modified Huron-Vidal mixing rule for cubic equations of stateq. Fluid Phase Equibliria 60 (1990) 213-219

[124] S. Dahl, A. Fredenslund, P. Rasmussen,The MHV2 Model: A UNIFAC-Based equation of state model for prediction of gas solubility and vapour-liquid equilibria at low and high pressures,Industrial & Engineering Chemistry Research 30 (1991) 1936-1945

[125] T. Holdebaum, J. Gmehling, PSRK: A group contribution equation of state based on UNIFAC,Fluid Phase Equlibria 70 (1991) 251-265

[126] C. Boukouvalas, Prediction of vapor-liquid equilbirium with the LCVM model: a linear combination of the Vidal and Michelsen mixing rules coupled with the original UNIFAC and the t-mPR equation of state,Fluid Phase Equilbiria 92 (1994) 75-106

[127] E. Voutsas, C. Boukouvalas, N. Kalospiros, P. Tassios, The performance of EOS/Gex models in the prediction of Vapour-Liquid Equilbria in Asymmetric systems, Fluid Phase Equilbiria 116 (1996) 480-4487

[128] I. Yakoumis, Application of the LCVM model to systems containing organic compounds and supercritical carbon dioxide, J. Supercritical Fluid 9 (1996) 88-98

[129] D.S.H. Wong, S.I. Sandler, A theoretically correct mixing rule for cubic equations of state, AIChE Journal 38 (1992) 671-680

[130] P. Coutsikos, N. Kalospiros, D. Tassios, Capabilities and limitations of the Wong-Sandler mixing rules,Fluid Phase Equilbria 108 (1995) 59-78

Stellenbosch University https://scholar.sun.ac.za

[131] H.I. Renon, J.M. Prausnitz, Local compositions in thermodynamic excess functions of liquid mixtures, AIChE Journal 14 (1968) 135-144

[132] M. Castier, S. Sandler, Critical points with the Wong-Sandler mixing rule - I. Calculations with the Van der Waals equation of state,Chemical Engineering Science 19 (1997) 3393-3399

[133] M. Castier, S. Sandler, Critical points with the Wong-Sandler mixing rule - II. Calculations with a modified Peng-Robinson equation of state,Chemical Engineering Science 52 (1997) 3579-3588

[134] J.A. Lopez, C.A. Cardona, Phase equilibrium calculations for carbon dioxide + n-alkanes binary mixtures with the Wong-Sandler mixing rules, Fluid Phase Equilibria 239 (2006) 206–212

[135] J.O. Valderrama, J. Zavaleta, Generalized binary interaction parameters in the Wond-Sandler mixing rules for mixtures containing n-alkanols and carbon dioxide, Fluid Phase Equilibria 234 (2005) 136-143

[136] T. Yang, G.J. Chen, W. Yan, T.M. Guo, Extension of the Wong-Sandler mixing rule to the three-parameter Patel-Teja equation of state: Application up to the near-critical region, Chemical Engineering Journal 67 (1997) 27–36

[137] S. Lambert,Y. Song, J. Prausnitz, Equations of state for polymer systems. In: J. Sengers, R. Kayser, C. Peters, H. White, eds. Equations of state for fluids and fluid mixtures . Amsterdam, The Netherlands: IUPAC, 2000, pp. 523-582

[138] S. Beret, J.M. Prausnitz, Perturbed Hard-Chain Theory: An Equation of State for Fluids Containing Small or Large Molecules, AIChE Journal 21 (1975) 1123-1132

[139] M.D. Donohue, J.M. Prausnitz, Perturbed Hard Chain Theory for Fluid Mixtures: Thermodynamic Properties for Mixtures in Natural Gas and Petroleum Technology, AIChE Journal 25 (1978) 849-860

[140] C.H. Kim, P. Vimalchand, M.D. Donohue, S.I. Sandler, Local Composition Model for Chain-Like Molecules: A new simplified version of the Perturbed Hard Chain Theory, AIChE Journal 32(1986) 1726–1734

[141] M. Morris, P. Vimalchand, M. Donohue, The Perturbed Soft Chain Theory: An Equation of state based on the Lennard-Jones potential,Fluid Phase Equilibria 32 (1987) 103-115

[142] I. Prigogine, A. Bellemans, V. Mathot, The molecular theory of solutions, North-Holland, Amsterdam (1957)

[143] Carnahan, N. & Starling, K.,. Equation of state for nonattracting rigid spheres. The Journal of Chemical Physics, 51 (1969) 635-636.

[144] R. Sadus, Y. Wei, Equations of state for the calculation of fluid phase equilibria. American Institute of Chemical Engineers 46 (2000) 169-196

[145] B.J. Alder, D.A. Young, M.A. Mark, J. Chem. Phys 56 (1972) 3013

Stellenbosch University https://scholar.sun.ac.za

[146] K.H. Lee, M. Lombardo, S.I. Sandler, The Generalized van der Waals Partition Function: II. Application to the square-well fluid, Fluid Phase Equilibria 21 (1985) 177

[147] M. Donohue, The Perturbed-Hard-Chain Theory: Extension and Applications Fluid Phase Equilibria 40 (1988) 185-211

[148] M. Wertheim, Fluid with highly hirectional attractive forces I. Statistical Thermodynamics, J. Statistical Physics 35 (1984) 19-34

[149] M. Wertheim, Fluid with highly directional attractive forces II.Thermodynamic Perturbation Theory and Integral Equations. J. Statistical Physics 35 (1984) 35-47

[150] M. Wertheim, Fluid with highly directional attractive forces III. Multiple Attraction Sites,J. Statistical Physics 42 (1986) 459-476.

[151] M. Wertheim, Fluid with highly directional attractive forces IV. Equilibrium Polymerization,J. Statistical Physics 42 477-492

[152] E. Muller, K. Gubbins,Associating fluids and fluid mixtures. In: J.V. Sengers, R.F. Kayser, C.J. Peters, H.J. White, eds. Equations of state for fluids and fluid mixtures, Part 2. Amsterdam, The Netherlans: IUPAC,2000, pp. 435-465.

[153] S. Huang, M. Radosz, Equation of State for Small, Large, Polydisperse, and Associating Molecules. Industrial &Engineering Chemistry Research 29 (1990) 2284-2294

[154] S. Huang, M. Radosz, Equation of State for Small, Large, Polydisperse, and Associating Molecules: Extensions to Fluid Mixures. Industrial Journal of Chemistry Research 30 (1991) 1994-2005

[155] W. Chapman, K. Gubbins, G. Jackson, M. Radosz, SAFT: Equation-of-State Solution Model for Associating Fluids,Fluid Phase Equilbiria 52 (1989) 31-38.

[156] W. Chapman, K. Gubbins, G. Jackson, M. Radosz, New Reference Equation of State for Associating Liquids, Industrial & Engineering Chemistry Research 29(1990) 1709-1721

[157] J. Gross, G. Sadowki, Perturbed-Chain SAFT: An equation of state based on a Perturbation Theory for chain molecules, Industrial &Engineering Chemistry Research 40 (2001) 1244-1260

[158] N. Van Solms, M. Michelsen, G. Kontogeorgis, Computational and physical performance of a Modified PC-SAFT equation of state for highly asymmetric and associating mixtures,Industrial &Engineering Chemistry Research 42 (2003) 1098-1105

[159] J. Chen, J. Mi, Equation of state extended from SAFT with improved results for non-polar fluids across the critical point, Fuid Phase Equilbiria 186 (2001) 165-184

Stellenbosch University https://scholar.sun.ac.za

[160] J. Mi, J. Chen, G. Gao, W. Fei, Equation of state extended from SAFT with improved results for polar fluids across the critical point,Fluid Phase Equilibiria 201 (2002) 295-307

[161] I. Polishuk, Till which pressures the fluid phase EOS models might stay reliable. J. Supercritical Fluids 58 (2011) 204-215

[162] I. Polishuk, Hybridizing SAFT and Cubic EOS: What can be achieved. Industrial &Engineering Chemistry Research 50 (2011) 4183-4198.

[163] S. Tan,H. Adidharma,M. Radosz, Recent advances and applications of Statistical Associating Fluid Theory,Industrial &Engineering Chemistry Research 47 (2008) 8063-8082

[164] N .Van Solms, I. Kouskoumvekaki, M. L. Michelsen. G.M. Kontogeorgis,Capabilities, limitations and challenges of a simplified PC-SAFT equation of state, Fluid Phase Equilbiria 241 (2006) 344-353.

[165] O. Pfohl, G. Brunner, 2. Use of BACK to modify SAFT in order to enable density and phase equilibrium calculations to gas-extraction processes, Industrial & Engineering Chemistry Research 37 (1998) 2966-2976

[166] R. Privat, R. Gani, J. Jaubert, Are safe results obtained when the PC-SAFT equation of state is applied to ordinary pure chemicals?Fluid Phase Equilibria 295 (2010) 76-92.

[167] I. Polishuk, About the numerical pitfalls characteristic for SAFT EOS models, Fluid Phase Equilibria 298 (2010) 67-74.

[168] V. Kalikhman, D. Kost, I. Polishuk, About the physical validity of attaching the repulsive terms of analtical EOS models by temperature dependencies,Fluid Phase Equilibria 293 (2010) 164-167

[169] I. Polishuk, Addressing the issue of numerical pitfalls characteristic of SAFT EOS models, Fluid Phase Equilibria 301 (2011) 123-129

[170] Y. Fu, S. Sandler, A simplified SAFT Equation of state for associating compounds and mixtures, Inustrial &Engineering Chemistry Research 34 (1995) 1897-1909

[171] I. Polishuk, Generalization of SAFT+Cubic equation of state for predicting and correlating thermodynamic properties of heavy organic substances, J. Supercritical Fluids 67 (2012) 94-107

[172] S. Skjold-Jorgensen, Gas Solubility Calculations II. Applications of a new Group-Contribution Equation of State, Fluid Phase Equilbiria 16 (1984) 317-351.

[173] S. Skjold-Jorgensen, Group Contribution Equation of State (GC-EOS): A predictive method for phase equilbirium computations over wide ranges of temperatures and pressures up to 30 MPA,Industrial &Engineering Chemistry Research 27 (1988) 110-118.

Stellenbosch University https://scholar.sun.ac.za

[174] J. Jauber, R. Privat, Relationship between the binary interaction parameters (k_{ij}) of the Peng-Robinson and those of the Soave-Redlich-Kwong equations of state: Application to the definition of the PR2DRK model,Fluid Phase Equilibiria295 (2010) 26-37

[175] G. Jin, J. Walsh, M. Donohue,A group-contribution correlation for preduicting thermodynamic properties with the perturbed-soft-chain theory,Fluid Phase Equilibria 31 (1986) 123-146

[176] G. Georgeton, A. Teja, A group contribution equation of state based on the simplified perturbed hard chain theory. Industrial&Engineering Chemistry Research 27 (1988) 657-664.

[177] G. Geoergeton, A. Teja, A simple group contribution equation of state for fluid mixtures,Chemical Engineering Science 44 (1989) 2703-2710

[178] S. Tamouza, J. Passarello, P. Tobaly, J. Hemptinne, Group contribution method with SAFT EOS applied to vapor liquid equilbiria of various hydrocarbon series, Fluid Phase Equlibiria 222-223 (2004) 67-76

[179] S. Tamouza, J. Passarello, P. Tobaly, J. Hemptinne, Application to binary mixrures of a group contribution SAFT EOS (GC-SAFT),Fluid Phase Equlibria 228-229 (2005) 409-419

[180] F. Peters, F. Laube, G. Sadowski, Development of a group contribution method for polymers within the PC-SAFT model, Fluid Phase Equilbirium 324 (2012) 70-79

[181] E. Brignole, P.Andersen, A. Fredenslund, Supercritical fluid extraction of alcohols from water, Industrial &Engineering Chemistry Research 26 (1987) 254-261

[182] F. Temelli, J. O'Connell, C. Chen, R. Braddock, Thermodynamic analysis of supercritical carbon dioxide extraction of terpenes from cold-pressed orange oil, Industrial &Engineering Chemistry Research 29 (1990) 618-624

[183] S. Espinosa, G. Foco, A. Bermudez, T. Fornari, Revision and extension of the group contribution equation of state to new solvent groups and higher molecualr wights alkanes, Fluid Phase Equilibria 172 (2000) 129-143

[184] S. Espinosa, S. Diaz, E. Brignole, 2002. Themodynamic modeling and process optimization of supercritical fluid fractionation of fish oil fatty acid ethyl esters. Industrial &Engineering Chemistry Research, Volume 41 (2002) 1516-1527

[185] S. Kiselev, J. Ely, Simplified crossover SAFT equation of state for pure fluids and fluid mixtures, Fluid Phase Equilibria 174 (2000) 93-113

[186] J. Kolafa, I. Nezbeda, The Lennard-Jones fluid: An accurate analytic and theoretically-based equation of state, Fluid Phase Equilibria 100 (1994) 1-34

[187] T. Kraska, K.E. Gubbins, Phase equilibria calculations with a modified SAFT equation of state 1. Pure alkanes, alkanols, and water. Industrial &Engineering Chemistry Research 35 (1996) 4727-4737

Stellenbosch University https://scholar.sun.ac.za

[188] T. Kraska, K. Gubbins, Phase Equilibria Calculations with a modified SAFT Equation of State. 2. Binary mixtures of n-Alkanes, 1-Alkanols, and water. Industrial &Engineering Chemistry Research 35 (1996) 4738-4746

[189] F. Blas, L.Vega, Prediction of binary and ternary diagrams using the Statistical Associating Fluid Theory (SAFT) Equation of State, Industrial &Engineering Chemistry Research 37 (1998) 660-674

[190] F. Llovell, L. Vega, Phase equilibiria, critical behaviour and derivative properties of selected n-alkane/n-alkane and n-alkane/1-alkanol mixtures by the crossover soft-SAFT equation of state. J. Supercritical Fluids 41 (2007) 204-216.

[191] F. Llovell, C. Peters, L. Vega, Second-order thermodynamics derivative properties of selected mixrtures by the soft-SAFT equation of state. Fluid Phase Equilbiria 248 (2006) 115-122

[192] A. Schultz, K.R.Y. Shaul, D.Kofke, Modeling solubility in supercritical fluids via the virial equation. J. Supercritical Fluids, 55 (2010) 479-484.

[193] A. Harvey, On the suitability of the virial equation for modeling the solubility of solids in supercritical fluids. Fluid Phase Equilibria 130 (1997) 87-100.

[194] R. De Villiers, PhD Thesis. Evaluation and improvement of the sPC-SAFT EOS for complex mixtures, Stellenbosch: Department of Chemical Engineering at the Universtiy of Stellenbosch, 2011

[195] E.C. Voutsas, G.D. Pappa, K. Magoulas, D.P. Tassios, Vapour liquid equilibrium modelling of alkane systems with Equations of State: "simplicity versus complexity", Fluid Phase Equilibria 240 (2006) 127-139

[196] M.F. Alfradique, M. Castier, Critical points of hydrocarbon mixtures with the Peng-Robinson, SAFT and PC-SAFT equations of state., Fluid Phase Equilibria 257 (2007) 78-101

[197] N.I. Diamantonis, G.C. Boulougouris, E. Mansoor, D.M. Tsangaris, I.G. Economou, Evaluation of cubic, SAFT and PC-SAFT equations of state for the vapour-liquid equilibrium modelling of CO_2 mixtures with other gases, Industrial & Engineering Chemistry Research, 52 (2013) 3933–3942

[198] M. Atilhan, S. Aparicio,K.R. Hall, Optimized binary interaction parameters for VLE calculations of natural gas mixtures via cubic and molecular bases equations of state, Industrial & Engineering Chemistry Research, 51 (2012) 9687 - 9699

[199] ASPEN Technology Inc., ASPEN Physical Property System - Physical Property Methods and Models 11.1, 2.1, Property Method Descriptions, ASPEN Technology Inc., Cambridge, MA, U.S.A, 2001.

[200] A. M. Martinez, C.J. Peters, Fundamental Considerations, in: A.R.H. Goodwin, J.V. Sengers, C.J. Peters, Applied Thermodynamics of Fluids, RSC Publishing , Cambridge, 2010, pp. 5 – 30

Stellenbosch University https://scholar.sun.ac.za

[201] L.A. Forero, J.A. Velasquez, The Patel-Teja and the Peng Robinson EOSs performance when the Soave alpha function is replaced by an exponential function, Fluid Phase Equilibria, 332 (2012) 55 – 76

[202] L. Constantinou, R. Gani, New group contribution method for estimating properties of pure compounds, AIChE Journal 40 (1994)1697-1710

[203] H.I. Britt, R.H. Luecke, The estimation of parameters in non-linear implicit models, Technometrics 15 (1973) 233 – 247

[204] W. Weber, S. Petkov, G. Brunner, Vapour-liquid-equilibria and calculations using the Redlich-Kwong-Aspen-equation of state for tristearin, tripalmitin, and triolein in CO_2 and propane, Fluid Phase Equilibria 158 – 160 (1999) 695 - 706

[205] J. Stoldt, G. Brunner, Phase equilibria in complex systems of palm oil deodorizer condensates and supercritical carbon dioxide: experiments and correlation, J. of Supercritical Fluids 14 (1999) 181 - 195

[206] M. Zamudio, PhD Thesis, The separation of detergent range alkans and alcohols with supercrtical CO_2, Stellenbosch Department of Chemical Engineering at University of Stellenbosch, March 2014

[207] M. Zamudio, C.E. Schwarz, J.H. Knoetze, Experimental measurement and modelling with Aspen Plus ® of the phase behaviour of supercritical CO_2 + (n-dodecane + 1-decanol + 3,7-dimethyl-1-octanol), J. Supercritical Fluids 84 (2013) 132 - 145

[208] J.A. Lopez, V.M. Trejos, C.A. Cardona, Objective functions analysis in the minimization of binary VLE data for asymmetric mixtures at high pressures, Fluid Phase Equilibria, 248 (2006) 147 – 157

[209] G. Kontogeorgis, G. Folas,Thermodynamic Models for Industrial Applications - From Classical and Advanced Mixing Rules to Association Theories,United Kingdom: John Wiley & Sons Ltd,1st ed. West Sussex, PO19 8SQ, 2010, pp. 5.3

[210] D.C. Montgomery, Design of Experiments, 7th edition, John Wiley and Sons, Hoboken, N.J., 2009, pp. 162 – 165

[211] I. Ashour, G. Aly, Effect of computation techniques for equation of state binary interaction parameters on the prediction of binary VLE data, Computers and Chemical Engineering 20 (1996) 79-91

Stellenbosch University https://scholar.sun.ac.za

13. NOMENCLATURE

13.1 List of symbols

Symbol	Description	Units
A	Helmholtz energy	J
A	Species A	-
A	Dimensionless variable in CEOSs	-
A	Expression used in analytical root determination of cubic equation	-
a	Molar Helmholtz energy	J/mol
a	Coefficient for cubic polynomial	-
a	Energy parameter in CEOSs	(Depends on model form)
A_s	Surface area	m^2
A_{nm}	Universal constants in Alder perturbation matrix	-
B	Species B	-
B	Expression used in analytical root determination of cubic equation	-
B	Dimensionless variable in CEOSs	-
B	Second virial coefficient	Depends on expansion (in P or v)
b	Size parameter in CEOSs	m^3/mol
b	Coefficient for cubic polynomial	-
b_2	3rd parameter in Adachi et al. CEOS	m^3/mol
b_3	4th parameter in Adachi et al. CEOS	m^3/mol
C	Concentration	mol
C	Number of components	-
C	Dimensionless variable in CEOSs	-
C	Third virial coefficient	Depends on expansion (in P or v)
C	Unique constant for EOS in G_{ex}/EOS combination	-
C	Energy constant in potential energy functions	J
C2	Ethane	-
C3	propane	-
C2	Coefficient for cubic polynomial	-
C1	Coefficient for cubic polynomial	-
C0	Coefficient for cubic polynomial	-
C_v	Isochoric heat capacity	J/K
c	Coefficient for cubic polynomial	-
c	Property in calculating the % deviation	-

Stellenbosch University https://scholar.sun.ac.za

c	3rd volume parameter in CEOS	m^3/mol
c	One third external degrees of freedom (PHCT parameter)	-
c	Volume translation parameter in CEOS	m^3/mol
c	Expression used in Boston-Mathias alpha function	-
c	SAFT + Cubic correction term parameter	-
D	Wong-Sandler mixing rule expression	-
D	Fourth virial coefficient	Depends on expansion (in P or v)
D_{AB}	Diffusivity	m^2/s
D_{nm}	Universal constants in Alder perturbation matrix (SAFT models)	-
d	4th parameter in treble-bishnoi CEOS	m^6/mol^2
d	Hard-core diameter in potential energy functions	m
d	Kihara potential function parameters	-
d	Expression used in Boston-Mathias alpha function	-
d	Effective segment diameter (SAFT models)	-
d	Expression for deriving PT EOS fugacity in solution using Wong-Sandler mixing rules	-
e	Expression for deriving PT EOS fugacity in solution using Wong-Sandler mixing rules	-
e	energy	J
E_0	Mean potential energy of the system	J
F	Degrees of freedom for Gibbs phase rule	-
F	Soave alpha function parameter in original PT EOS publication	-
F	Objective function	-
f	Fugacity	MPa
$\hat{f}$	Fugacity of component in solution	MPa
G	Gibbs energy	J
G_{ji}	NRTL interaction expression	-
$G_{1,}$	Gasem et al. alpha function parameter	-
$G_{2,}$	Gasem et al. alpha function parameter	-
G_3	Gasem et al. alpha function parameter	-
g(r)/ g(1,2)/g(i)	Radial distribution function	-
K_T	Isothermal compressibility	$m\ s^2/kg$
K	Equilibrium factor (y/x)	-
k	Binary interaction parameter	-
k_o	Stryjek-Vera alpha function parameter	-
k_1	Stryjek-Vera, Heyen and Mathias-Copeman alpha function parameters	-

Stellenbosch University https://scholar.sun.ac.za

k_2	Mathias-Copeman alpha function parameter	-
k_3	Mathias-Copeman alpha function parameter	-
I	Perturbation integral	-
I	Ionization potential	-
L	Liquid	-
L	Twu et al. alpha function parameter	-
l_i	UNIFAC model expression	-
l	Distance from a defined origin	m
l	Binary interaction parameter	-
M	Twu et al. alpha function parameter	-
M	Expressions used in pure component fugacity expression for the PT EOS	-
M	Number of association sites	-
$M_{1,}$	Melhem et al. alpha function parameter	-
M_2	Melhem et al. alpha function parameter	-
M_r	Molecular weight	g/mol
$\dot{m}$	mass flow-rate	kg/s
m	Segment number (SAFT parameter)	-
m	Mie potential function parameters	-
m	Soave, Boston-Mathias and Mathias alpha function parameter	-
N	Mole number	mol
N	Number of molecules	-
N	Expressions used in pure component fugacity expression for the PT EOS	-
N	Twu et al. alpha function parameter	-
n	Heyen alpha function parameter	-
n	Mie potential function parameters	-
P	Pressure	MPa
p	Mathias alpha function parameter	-
p	degeneracy	-
pc1k	Constantinou & Gani group specification for P_c	$Bar^{0.5}$
Q	Expression used in analytical root determination of cubic equation	-
Q	Quadrapole moment	Cm^2
Q	Canonical partition function	-
Q	UNIFAC group (surface area)	-
Q	Wong-Sandler mixing rule expression	-
q_1	Trebble-Bishnoi alpha function parameter	-
q	Molecular partition function	-
q	charge	C

Stellenbosch University https://scholar.sun.ac.za

q	UNIFAC component parameter (combinatorial term)	-
R	UNIFAC group (volume)	-
R	Expression used in analytical root determination of cubic equation	-
$R_{0,}$	Mean curvature of hard-convex body	-
r_0	Equilibrium separation in potential energy functions	m
r	UNIFAC component parameter (combinatorial term)	-
r	Segments in molecule	-
r	Radial distance	m
S	Entropy	J/s
S_0	Mean surface area of hard-convex body	-
T	Temperature	K
T^*	SPHCT parameter	-
t	time	s
tc1k	Constantinou & Gani group specification for T_c	K
u	Fluid velocity	m/s
u	Schmidt-Wentzel CEOS parameter	-
$\frac{u^0}{kT}$	Segment energy (SAFT parameter)	-
V	Vapour	-
V	volume	m^3
$\vec{V}$	Molecule Velocity	m/s
V_0	Mean volume of hard-convex body	-
v	Molar volume	m^3/mol
v	Reduced variable in Alder perturbation series	-
W_1	Regression weight 1	-
W_2	Regression weight 2	-
w	Schmidt-Wentzel CEOS parameter	-
w1k	Constantinou & Gani group specification for ω	-
X, x	Overall or liquid composition	-
X^A	Mole fraction of molecules NOT bonded at site A	-
Y, y	Vapour composition	-
Y	SPHCT expression	-
y	Distance	m
Z	Compressibility factor	-
Z_{cor}	Co-ordination number	-
Z_{config}	Configurational integral	-
Z_M	Maximum co-ordination number	-
z	Overall mixture composition	-

Stellenbosch University https://scholar.sun.ac.za

13.2 Greek symbols

Symbol	Description	Units
α	Phase label	-
α	Alpha function	-
α	Parameter in LCVM model derivation	-
α	Polarizability	-
α	Non-sphericity parameter in hard-convex body term of Boublik	-
α	NRTL non-randomness parameter	-
α	Critical exponent ()	-
β	Critical exponent ()	-
β	Phase label	-
$\hat{\varphi}_i$	Fugacity coefficient for component in solution	-
φ	Fugacity coefficient of mixture	-
φ_i	Fugacity coefficient of pure compound	-
φ	Additional equations in Gibbs phase rule	
θ_i	UNIFAC combinatorial term expression	-
$\theta(T)$	Temperature dependence of reduced volume in SAFT + Cubic model	-
θ	Expression used in analytical root determination of cubic equation	-
ϕ_i	UNIFAC combinatorial term expression	-
ϕ	Mean potential energy	J
γ	Critical exponent ()	-
γ	Phase label	-
γ	Activity coefficient	-
γ	Square-well potential function parameter	-
λ	Conformal constant in SAFT-CP perturbation correction term	-
λ	Constant in LCVM model	-
ω	Acentric factor	
ε	Termination tolerance	-
ε	Depth of energy well in potential functions	J
ε	Energy level	J/molecule
εq	PHCT energy parameter	-
ε_r	Dielectric constant of the medium	-
μ	Dynamic viscosity	Pa s
μ	Chemical potential	J/mol
μ	Dipole moment	Debye (3.336×10^{-30} Cm)
ψ	UNIFAC interaction expression (residual term)	-
ψ	Expression for deriving PT EOS fugacity in solution using Wong-	-

Stellenbosch University https://scholar.sun.ac.za

	Sandler mixing rules	
σ	collision diameter in potential functions	m
σ	Standard deviation	-
$r\sigma^3$	PHCT size parameter	-
ρ	Density	Kg/m^3
δ	Critical exponent ()	-
π	Number of phases	-
τ	Shear stress	N/m^2
τ	Reduced variable in Alder perturbation series	-
τ	NRTL interaction parameter	-
ν	Critical exponent ()	-
ν^*	SPHCT parameter	-
ν	Group frequency in UNIFAC model	-
ν^{00}	Segment volume (SAFT parameter)	-
Γ	Potential energy	J
$\bar{\Gamma}$	Average intermolecular potential energy of the system	J
Γ	UNIFAC residual term expression	-
Ω_a	Parameter used in derivation of PT EOS	-
Ω_b	Parameter used in derivation of PT EOS	-
Ω_c	Parameter used in derivation of PT EOS	-
η	Reduced volume	-
Λ	De Broglie Wavelength	m
ξ	Expression for deriving PT EOS fugacity in solution using Wong-Sandler mixing rules	-
ξ	Correlation length	
ξ_c	Empirical critical compressibility in PT EOS	-

13.3 Superscripts

Symbol	Description
assoc	Helmholtz energy contribution of association
C	"Combinatorial"
calc	Model calculation
chain	Helmholtz energy contribution of chain formation
exp	Experimental value
disp	Helmholtz energy contribution of dispersion interactions
hcb	Hard convex body
hs	Helmholtz energy contribution of hard-sphere
HSC ref	Hard-sphere-chain reference
ig	Helmholtz energy contribution of ideal gas

Stellenbosch University https://scholar.sun.ac.za

Pert	Perturbation terms
R	“Residual”
res	Residual property
seg	Helmholtz energy contribution of segment
t	Total bulk value
0	Reference part
1	Perturbation part
γ	Phase label
α	Phase label
β	Phase label
∞	Infinite pressure

13.4 Subscripts

Symbol	Description
A	Species A
a	Energy parameter in CEOSs
AB	Species A in medium B
B	Species B
b	Size parameter in CEOSs
BH	“Barker and Henderson”
c	Value at critical point
ck	Chen and Kreglewski
comb	“combinatorial”
cor	Co-ordination number
ex	Excess property
ext	“external”
elec	Electrical energy contributions
f	Free-volume
i	Energy state
i	Species i
ij	Interaction between species i and j
int	“internal”
j	Energy level
j	Species j
K	Kinetic energy
k	Group indicator
M	“Michelsen”
m	mixture property
m	UNIFAC interaction indicator
m	Component label

Stellenbosch University https://scholar.sun.ac.za

n	UNIFAC interaction indicator
nucl	Nuclear energy contributions
r	Reduced value
ref	Reference term
rot	"Rotational motions"
trans	"translational motions"
V	"Vidal"
vib	"Vibration motions"
WCA	"Weeks, Chandler and Anderson"
o	Per mole of segments
1	Component 1
2	Component 2

13.5 Value of constants

Symbol	Description	Value
R	Universal gas constant	8.314 J/mol K
N_A	Avagadro's constant	6.02×10^{23}
k	Boltzman's constant	1.38×10^{-23} J / (molecule K)
π	pie	3.14159
ε_0	dielectric permittivity of vacuum	8.854×10^{-12} C^2J/m
τ	SPHCT model constant	0.76

13.6 Abbreviations

Abbreviation	Description
C&G	Constantinou and Gani
CEOS	Cubic equation of state
CEP	Critical end-point
CN	Carbon number
DOE	Design of Experiments
EOS	Equation of state
HC	Heavy component
LC	Light component
LCEP	Lower critical end-point
M	Mathias
NP	Number of data points
NC	Number of components
NDG	Number of data groups
UCEP	Upper critical end-point

Stellenbosch University https://scholar.sun.ac.za

Sat	Saturation property
Sat. liq. vol.	Saturated liquid (molar) volume
SCE	Supercritical Fluid Extraction
SCF	Supercritical Fluid
SPD	Short Path Distillation
SV	Stryjek-Vera
VLE	Vapour-Liquid Equilibrium

Stellenbosch University https://scholar.sun.ac.za

APPENDIX A: Working Equations

A.1 Pure models

The following useful groupings are used in order to give the equations in terms of dimensionless variables:

$$Z = \frac{Pv}{RT} = \frac{P}{\rho RT} \quad \text{A. 1}$$

$$A = \frac{Pa}{(RT)^2} \quad \text{A. 2}$$

$$C = \frac{Pc}{RT} \quad \text{A. 3}$$

$$B = \frac{Pb}{RT} \quad \text{A. 4}$$

$$\frac{B}{Z} = b\rho \quad \text{A. 5}$$

$$\frac{A}{B} = \frac{a}{bRT} \quad \text{A. 6}$$

$$\rho = \frac{1}{v} \quad \text{A. 7}$$

A.1.1 Peng-Robinson [1]

$$P = \frac{RT}{v-b} - \frac{a}{v(v+b)+b(v-b)} \quad \text{A. 8}$$

$$P = \frac{RT\rho}{1-b\rho} - \frac{a\rho^2}{1+2b\rho-(b\rho)^2} \quad \text{A. 9}$$

$$Z = \frac{1}{1-b\rho} - \frac{a}{bRT}\left[\frac{b\rho}{1+2b\rho-b\rho^2}\right] \quad \text{A. 10}$$

$$Z = \frac{1}{1-\left(\frac{B}{Z}\right)} - \frac{A}{B}\left[\frac{\frac{B}{Z}}{1+2\left(\frac{B}{Z}\right)-\left(\frac{B}{Z}\right)^2}\right] \quad \text{A. 11}$$

$$Z^3 + (B-1)Z^2 + \left(A - 3B^2 - 2B\right)Z + (B^2 + B^3 - AB) = 0 \quad \text{A. 12}$$

Stellenbosch University https://scholar.sun.ac.za

$$Z - 1 = \frac{b\rho}{1-b\rho} - \frac{a}{bRT}\left[\frac{b\rho}{1+2b\rho-b\rho^2}\right] \quad \text{A. 13}$$

Additional equations:

$$a(T) = 0.45724\left(\frac{R^2T_c^2}{P_c}\right)\alpha(T_r) \quad \text{A. 14}$$

$$b = 0.07780\left(\frac{RT_c}{P_c}\right) \quad \text{A. 15}$$

$$Z_c = 0.307 \quad \text{A. 16}$$

A.1.2 Patel Teja [2]

$$P = \frac{RT}{v-b} - \frac{a}{v(v+b)+c(v-b)} \quad \text{A. 17}$$

$$P = \frac{RT\rho}{1-b\rho} - \frac{a\rho^2}{1+\rho(b+c)-cb\rho^2} \quad \text{A. 18}$$

$$Z = \frac{1}{1-b\rho} - \frac{a}{bRT}\left[\frac{b\rho}{1+\rho(b+c)-cb\rho^2}\right] \quad \text{A. 19}$$

$$Z = \frac{1}{1-\left(\frac{B}{Z}\right)} - \frac{A}{B}\left[\frac{\frac{B}{Z}}{1+\left(\frac{B+C}{Z}\right)-\left(\frac{BC}{Z^2}\right)}\right] \quad \text{A. 20}$$

$$Z^3 + (C-1)Z^2 + \left(A - 2BC - B - C - B^2\right)Z + (B^2C + BC - AB) = 0 \quad \text{A. 21}$$

$$Z - 1 = \frac{b\rho}{1-b\rho} - \frac{a}{bRT}\left[\frac{b\rho}{1+\rho(b+c)-cb\rho^2}\right] \quad \text{A. 22}$$

Additional equations:

$$a(T) = \Omega_a\left(\frac{R^2T_c^2}{P_c}\right)\alpha(T_r) \quad \text{A. 23}$$

$$b = \Omega_b\left(\frac{RT_c}{P_c}\right) \quad \text{A. 24}$$

Stellenbosch University https://scholar.sun.ac.za

$$c = \Omega_c \left(\frac{RT_c}{P_c}\right) \quad \text{A. 25}$$

$$\Omega_c = 1 - 3\xi_c \quad \text{A. 26}$$

$$\Omega_a = 3\xi_c^2 + 3(1 - 2\xi_c)\Omega_b + \Omega_b^2 + 1 - 3\xi_c \quad \text{A. 27}$$

$$\Omega_b^3 = (2 - 3\xi_c)\Omega_b^2 + 3\xi_c^2\Omega_b - \xi_c^3 \quad \text{A. 28}$$

A.1.3 SRK [3]

$$P = \frac{RT}{v-b} - \frac{a}{v(v+b)} \quad \text{A. 29}$$

$$P = \frac{RT\rho}{1-b\rho} - \frac{a\rho^2}{1+b\rho} \quad \text{A. 30}$$

$$Z = \frac{1}{1-b\rho} - \left(\frac{a}{bRT}\right)\frac{b\rho}{1+b\rho} \quad \text{A. 31}$$

$$Z = \frac{1}{1-\left(\frac{B}{Z}\right)} - \frac{A}{B}\left[\frac{\frac{B}{Z}}{1+\left(\frac{B}{Z}\right)}\right] \quad \text{A. 32}$$

$$Z^3 - Z^2 + (A - B - B^2)Z - AB = 0 \quad \text{A. 33}$$

$$Z - 1 = \frac{b\rho}{1-b\rho} - \left(\frac{a}{bRT}\right)\frac{b\rho}{1+b\rho} \quad \text{A. 34}$$

Additional equations:

$$a(T) = 0.42747\left(\frac{R^2T_c^2}{P_c}\right)\alpha(T_r) \quad \text{A. 35}$$

$$b = 0.08664\left(\frac{RT_c}{P_c}\right) \quad \text{A. 36}$$

$$Z_c = 0.333 \quad \text{A. 37}$$

Stellenbosch University https://scholar.sun.ac.za

A.1.6 Alpha functions

The reduced temperature is defined as follows:

$$T_r = \frac{T}{T_c} \qquad \text{A. 38}$$

Soave [3]:

$$\alpha(T_r) = \left(1 + m\left(1 - \sqrt{T_r}\right)\right)^2 \qquad \text{A. 39}$$

Stryjek-Vera [4]:

$$\alpha(T_r) = \left(1 + m\left(1 - \sqrt{T_r}\right)\right)^2 \qquad \text{A. 40}$$

$$m = k_o + k_1(1 + \sqrt{T_r})(0.7 - T_r) \qquad \text{A. 41}$$

Mathias [5]:

$$\alpha(T_r) = \left(1 + m\left(1 - \sqrt{T_r}\right) - p(1 - T_r)(0.7 - T_r)\right)^2 \qquad \text{A. 42}$$

Boston-Mathias [6]:

For $T > T_c$

$$\alpha(T_r) = \left(\exp\left(c\left[1 - T_r^d\right]\right)\right)^2 \qquad \text{A. 43}$$

$$c = 1 + \frac{m}{2} + 0.3p \qquad \text{A. 44}$$

$$d = \frac{c-1}{c} \qquad \text{A. 45}$$

The following correlations are typically used for these alpha functions in combination with selected CEOS:

Stellenbosch University https://scholar.sun.ac.za

Tabel A.1. 1 Literature correlations for alpha function parameters

Alpha function	EOS	Ref	Parameter Correlation
Soave	PR	[1]	$m = -0.37464 + 1.54226\omega - 0.26992\omega^2$
	PT	[2]	$m = 0.452413 + 1.30982\omega - 0.295937\omega^2$
	SRK	[3]	$m = -0.480 + 1.574\omega - 0.17\omega^2$
SV	PR	[4]	$k_o = 0.378893 + 1.4897153\omega - 0.17131848\omega^2 + 0.0196554\omega^3$
M	SRK	[5]	$m = -0.48508 + 1.55191\omega - 0.15613\omega^2$

A.1.4 UNIFAC [7]

$$\ln \gamma_i = \ln\gamma_i^C + \ln\gamma_i^R \quad \text{A. 46}$$

Combinatorial:

$$\ln\gamma_i^C = \ln\left(\frac{\phi_i}{x_i}\right) + \frac{Z_{cor}}{2} q_i \ln\left(\frac{\theta_i}{\phi_i}\right) + l_i - \frac{\phi_i}{x_i}\sum_j x_j l_j \quad \text{A. 47}$$

$$l_i = \frac{Z_{cor}}{2}(r_i - q_i) - (r_i - 1)\,; Z_{cor} = 10 \quad \text{A. 48}$$

$$\theta_i = \frac{q_i x_i}{\sum_j q_j x_j} \quad \text{A. 49}$$

$$\phi_i = \frac{r_i x_i}{\sum_j r_j x_j} \quad \text{A. 50}$$

$$r_i = \sum_k \nu_k^i R_k \quad \text{A. 51}$$

$$q_i = \sum_k \nu_k^i Q_k \quad \text{A. 52}$$

Table A. 1 UNIFAC group parameters

Group nr.	Formula	Volume (R)	Surface Area (Q)
1	CH3	0.9011	0.848
2	CH2	0.6744	0.54
3	OH	1	1.2
4	CH2COO	1.6764	1.42
5	COOH	1.3013	1.224

Stellenbosch University https://scholar.sun.ac.za

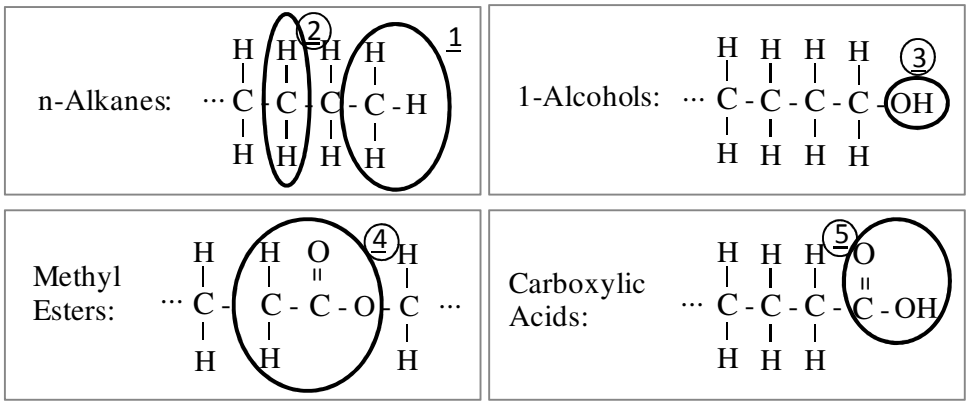

Figure A. 1Molecular deconstruction in terms of functional groups for use in the UNIFAC group contribution method

Residual:

$$\ln\gamma_i^R = \sum_k \nu_k^i \left(\ln\Gamma_k - \ln\Gamma_k^i\right) \qquad \text{A. 53}$$

$$\ln\Gamma_k = Q_k\left[1 - \ln\left(\sum_m \theta_m \psi_{mk}\right) - \sum_m \frac{\theta_m \psi_{km}}{\sum_n \theta_n \psi_{nm}}\right] \qquad \text{A. 54}$$

$$\theta_m = \frac{Q_m X_m}{\sum_n Q_n X_n} \qquad \text{A. 55}$$

$$\psi_{mn} = \exp\left(-\frac{a_{mn}}{T}\right) \qquad \text{A. 56}$$

Table A. 2 UNIFAC group interaction parameters

	n = 1	2	3	4	5
m = 1	0	0	986.5	232.1	663.5
2	0	0	986.5	232.1	663.5
3	156.4	156.4	0	101.1	199
4	114.8	114.8	245.4	0	660.2
5	315.3	315.3	-151	-256.3	0

Poling et al. [7] give example problems in applying the UNIFAC model in Chapter 8 of their book which elucidates all symbols and definitions given above.

Stellenbosch University https://scholar.sun.ac.za

A.1.5 NRTL [8]

$$\ln\gamma_i = x_j^2\left[\tau_{ji}\left(\frac{G_{ji}}{x_i+G_{ji}x_j}\right)^2 + \frac{\tau_{ij}G_{ij}}{(G_{ij}x_i + x_j)^2}\right] \quad \text{A. 57}$$

$$\tau_{ji} = \frac{g_{ji} - g_{ii}}{RT} = \frac{\Delta g_{ji}}{RT} \quad \text{A. 58}$$

$$G_{ji} = \exp(-\alpha_{ji}\tau_{ji}) \quad \text{A. 59}$$

Parameters:

- α
- τ_{ij}
- τ_{ji}

For both the UNIFAC and NRTL models, G_{ex} can be calculated from activity coefficieicnts using the summability relationship:

$$\frac{G_{Ex}}{RT} = \sum x_i\gamma_i \quad \text{A. 60}$$

A.2 Mixing rules

A.2.1 Van der Waals mixing rules

$$a_m = \sum_i\sum_j x_i x_j a_{ij} \quad \text{A. 61}$$

$$b_m = \sum_i\sum_j x_i x_j b_{ij} \quad \text{A. 62}$$

$$c_m = \sum_j x_i c_i \quad \text{A. 63}$$

Combining rule 1 (Classic) [9]:

$$a_{ij} = \sqrt{a_i a_j}(1 - k_{aij}) \quad \text{A. 64}$$

$$b_{ij} = \frac{b_i+b_j}{2}(1 - k_{bij}) \quad \text{A. 65}$$

Stellenbosch University https://scholar.sun.ac.za

Combining rule 2 (KM) [10]:

$$a_{ij} = \sqrt{a_i a_j}(1 - k_{aij}) \quad \text{A. 66}$$

$$b_{ij} = \left(\frac{(b_i^{\frac{1}{3}} + b_j^{\frac{1}{3}})}{2}\right)^3 (1 - k_{bij}) \quad \text{A. 67}$$

A.2.2 Wong-Sandler mixing rules

General expressions for the PR and SRK EOS [11]:

$$Q = \sum_i \sum_j x_i x_j \left(b - \frac{a}{RT}\right)_{ij} \quad \text{A. 68}$$

$$D = \frac{1}{RT}\left(\sum_i x_i \frac{a_i}{b_i} + \frac{A_{ex}^{\infty}}{C}\right) \quad \text{A. 69}$$

$$b_m = \frac{Q}{1-D} \quad \text{A. 70}$$

$$\frac{a_m}{RT} = Q\left(\frac{D}{1-D}\right) \quad \text{A. 71}$$

Table A. 2 C value in Wong-Sandler mixing rule

EOS	Value for C
SRK	$-\ln 2$
PR	$-\frac{1}{\sqrt{2}}\ln(\sqrt{2}-1)$

General expressions for the PT EOS [12]:

$$d = \frac{-(b+c)+\sqrt{b^2+6bc+c^2}}{2} \quad \text{A. 72}$$

$$e = \frac{-(b+c)-\sqrt{b^2+6bc+c^2}}{2} \quad \text{A. 73}$$

$$\psi_i = \frac{c_i}{b_i} \quad \text{A. 74}$$

Stellenbosch University https://scholar.sun.ac.za

$$\xi_i = \frac{1}{\sqrt{1+6\psi_m+\psi_m^2}} \ln\left(\frac{3+\psi_i+\sqrt{1+6\psi_i+\psi_i^2}}{3+\psi_i-\sqrt{1+6\psi_i+\psi_i^2}}\right) \quad \text{A. 75}$$

$$\xi_m = \frac{1}{\sqrt{1+6\psi_m+\psi_m^2}} \ln\left(\frac{3+\psi_m+\sqrt{1+6\psi_m+\psi_m^2}}{3+\psi_m-\sqrt{1+6\psi_m+\psi_m^2}}\right) \quad \text{A. 76}$$

$$Q = \sum_i \sum_j x_i x_j \left(b - \frac{a}{RT}\right)_{ij} \quad \text{A. 77}$$

$$D = \frac{1}{\xi_m RT}\left(\sum_i x_i \xi_i \frac{a_i}{b_i} - A_{ex}^{\infty}\right) \quad \text{A. 78}$$

$$b_m = \frac{Q}{1-D} \quad \text{A. 79}$$

$$\frac{a_m}{RT} = Q\left(\frac{D}{1-D}\right) \quad \text{A. 80}$$

$$c_m = \psi_m b_m \quad \text{A. 81}$$

Combining rule 1:

$$\left(b - \frac{a}{RT}\right)_{ij} = \frac{\left(b_i - \frac{a_i}{RT}\right)+\left(b_j - \frac{a_j}{RT}\right)}{2}\left(1 - k_{aij}\right) \quad \text{A. 82}$$

Combining rule 2:

$$\left(b - \frac{a}{RT}\right)_{ij} = \frac{b_i + b_j(1-k_{bij})}{2} + \frac{\sqrt{a_i a_j}}{RT}\left(1 - k_{aij}\right) \quad \text{A. 83}$$

A.3 Expressions for pure component fugacity

A.3.1 Peng Robinson [1]

$$\ln\varphi = Z - 1 - \ln(Z - B) - \frac{A}{B\sqrt{8}} \ln\left[\frac{Z+(1+\sqrt{2})B}{Z+1(1-\sqrt{2})B}\right] \quad \text{A. 84}$$

Stellenbosch University https://scholar.sun.ac.za

A.3.2 Patel Teja [2]

$$\ln\varphi = Z - 1 - \ln(Z - B) - \frac{a}{2RTN}\ln\left[\frac{Z+M}{Z+Q}\right] \quad \text{A. 85}$$

$$M = \left(\frac{b+c}{2} - N\right)\left(\frac{P}{RT}\right) \quad \text{A. 86}$$

$$Q = \left(\frac{b+c}{2} + N\right)\left(\frac{P}{RT}\right) \quad \text{A. 87}$$

$$N = \left[bc + \frac{(b+c)^2}{4}\right]^{\frac{1}{2}} \quad \text{A. 88}$$

A.3.3 SRK [3]

$$\ln\varphi = Z - 1 - \ln(Z - B) - \frac{A}{B}\ln\left[\frac{Z+B}{Z}\right] \quad \text{A. 89}$$

A.4 Expressions for fugacity of component in solution

A.4.1 Peng-Robinson

$$\ln\hat{\varphi}_i = \frac{1}{b_m}\left(\frac{\partial n b_m}{\partial n_i}\right)(Z - 1) - \ln(Z - B) - \frac{A}{B\sqrt{8}}\ln\left[\frac{Z+(1+\sqrt{2})B}{Z+(1-\sqrt{2})B}\right]\left[\frac{1}{a_m}\left(\frac{1}{n}\frac{\partial n^2 a_m}{\partial n_i}\right) - \frac{1}{b_m}\left(\frac{\partial n b_m}{\partial n_i}\right)\right] \quad \text{A. 90}$$

Van der Waals mixing rules [1]:

$$\left(\frac{\partial n b_m}{\partial n_i}\right) = 2\left(\sum_i^n x_i b_{ij}\right) - b_m \quad \text{A. 91}$$

$$\left(\frac{1}{n}\frac{\partial n^2 a_m}{\partial n_i}\right) = 2\left(\sum_i^n x_i a_{ij}\right) \quad \text{A. 92}$$

Wong Sandler mixing rules [11]:

$$\left(\frac{\partial n b_m}{\partial n_i}\right) = \frac{1}{1-D}\left(\frac{1}{n}\frac{\partial n^2 Q}{\partial n_i}\right) - \frac{Q}{(1-D)^2}\left(1 - \frac{\partial n D}{\partial n_i}\right) \quad \text{A. 93}$$

$$\frac{1}{RT}\left(\frac{1}{n}\frac{\partial n^2 a_m}{\partial n_i}\right) = D\left(\frac{\partial n b_m}{\partial n_i}\right) + b_m\left(\frac{\partial n D}{\partial n_i}\right) \quad \text{A. 94}$$

Stellenbosch University https://scholar.sun.ac.za

$$\frac{1}{n}\frac{\partial n^2 Q}{\partial n_i} = 2\left(\sum_i x_i \left(b - \frac{a}{RT}\right)_{ij}\right) \quad \text{A. 95}$$

$$\frac{\partial nD}{\partial n_i} = \frac{a_i}{b_i RT} + \frac{\ln\gamma_i^{\infty}}{-\frac{1}{\sqrt{2}}\ln(\sqrt{2}-1)} \quad \text{A. 96}$$

A.4.2 Patel Teja

Van der Waals mixing rules [2]:

$$\ln\hat{\varphi}_i = -RT\ln(Z-B) + RT\left(\frac{\left(\frac{\partial nb_m}{\partial n_i}\right)}{v-b_m}\right) - \frac{\left(\frac{1}{n}\frac{\partial n^2 a_m}{\partial n_i}\right)}{2d}\ln\left(\frac{Q+d}{Q-d}\right) + \frac{a_m}{2}\left[\frac{\left(\frac{\partial nb_m}{\partial n_i}\right)-\left(\frac{\partial nc_m}{\partial n_i}\right)}{Q^2-d^2}\right] + \frac{a_m}{8d^3}\left[\left(\frac{\partial nc_m}{\partial n_i}\right)(3b_m + c_m) + \left(\frac{\partial nb_m}{\partial n_i}\right)(3c_m + b_m)\right]\left[\ln\left(\frac{Q+d}{Q-d}\right) - \frac{2Qd}{Q^2-d^2}\right] \quad \text{A. 97}$$

Expressions:

$$Q = v + \frac{b_m + c_m}{2} \quad \text{A. 98}$$

$$d = \sqrt{b_m c_m + \frac{(b_m+c_m)^2}{4}} \quad \text{A. 99}$$

$$\left(\frac{1}{n}\frac{\partial n^2 a_m}{\partial n_i}\right) = 2\left(\sum_i^n x_i a_{ij}\right) \quad \text{A. 100}$$

$$\left(\frac{\partial nb_m}{\partial n_i}\right) = 2\left(\sum_i^n x_i b_{ij}\right) - b_m \quad \text{A. 101}$$

$$\left(\frac{\partial nc_m}{\partial n_i}\right) = c_m \quad \text{A. 102}$$

Wong Sandler mixing rules [12]:

$$\ln\hat{\varphi}_i = \ln\left(\frac{v}{v-b_m}\right) + \left[\left(\frac{\partial nb_m}{\partial n_i}\right)\right]\left(\frac{1}{v-b_m}\right) + \left(\frac{1}{RT}\right)\left[\frac{\left(\frac{1}{n}\frac{\partial n^2 a_m}{\partial n_i}\right)}{d_m - e_m} - \frac{a_m\left(\left(\frac{\partial nd_m}{\partial n_i}\right)-\left(\frac{\partial ne_m}{\partial n_i}\right)\right)}{(d_m-e_m)^2}\right]\ln\left(\frac{v-d_m}{v-e_m}\right) - \frac{\frac{a_m}{RT}\left[\left(\frac{\partial nd_m}{\partial n_i}\right)\right]}{(v-d_m)(d_m-e_m)} + \frac{\frac{a_m}{RT}\left[\left(\frac{\partial ne_m}{\partial n_i}\right)\right]}{(v-e_m)(d_m-e_m)} - \ln Z \quad \text{A. 103}$$

Stellenbosch University https://scholar.sun.ac.za

Expressions:

$$Q = \sum_i \sum_j x_i x_j \left(b - \frac{a}{RT}\right)_{ij} \quad \text{A. 104}$$

$$D = \frac{1}{\xi_m RT}\left(\sum_i x_i \xi_i \frac{a_i}{b_i} - A_{ex}^{\infty}\right) = \frac{a_m}{b_m RT} \quad \text{A. 105}$$

$$\left(\frac{\partial n b_m}{\partial n_i}\right) = \frac{1}{1-D}\left(\frac{1}{n}\frac{\partial n^2 Q}{\partial n_i}\right) - \frac{Q}{(1-D)^2}\left(1 - \frac{\partial nD}{\partial n_i}\right) \quad \text{A. 106}$$

$$\frac{1}{RT}\left(\frac{1}{n}\frac{\partial n^2 a_m}{\partial n_i}\right) = D\left(\frac{\partial n b_m}{\partial n_i}\right) + b_m\left(\frac{\partial nD}{\partial n_i}\right) \quad \text{A. 107}$$

$$\frac{1}{n}\frac{\partial n^2 Q}{\partial n_i} = 2\left(\sum_i x_i \left(b - \frac{a}{RT}\right)_{ij}\right) \quad \text{A. 108}$$

$$\left(\frac{\partial nD}{\partial n_i}\right) = \frac{\xi_i \frac{a_i}{b_i} - RT\ln\gamma_i^{\infty}}{\xi_m RT} - \frac{\frac{n}{RT}\left(\frac{\partial \xi_m}{\partial n_i}\right)\left(\sum_i x_i \xi_i \frac{a_i}{b_i}\right)}{(\xi_m RT)^2} \quad \text{A. 109}$$

$$n\left(\frac{\partial \xi_m}{\partial n_i}\right) = -\frac{3\frac{c_i}{b_i} - 3\psi_m + \frac{c_i}{b_i}\psi_m - \psi_m^2}{\sqrt{(1+6\psi_m+\psi_m^2)^3}} \ln\left(\frac{3+\psi_m+\sqrt{1+6\psi_m+\psi_m^2}}{3+\psi_m-\sqrt{1+6\psi_m+\psi_m^2}}\right) +$$
$$\frac{1}{\sqrt{1+6\psi_m+\psi_m^2}}\left[\frac{(\psi_i-\psi_m)+\frac{3\frac{c_i}{b_i}-3\psi_m+\frac{c_i}{b_i}\psi_m-\psi_m^2}{\sqrt{1+6\psi_m+\psi_m^2}}}{3+\psi_m+\sqrt{1+6\psi_m+\psi_m^2}} - \frac{(\psi_i-\psi_m)-\frac{3\frac{c_i}{b_i}-3\psi_m+\frac{c_i}{b_i}\psi_m-\psi_m^2}{\sqrt{1+6\psi_m+\psi_m^2}}}{3+\psi_m-\sqrt{1+6\psi_m+\psi_m^2}}\right] \quad \text{A. 110}$$

$$\left(\frac{\partial nc_m}{\partial n_i}\right) = \left(\frac{\partial n b_m}{\partial n_i}\right)\sum_i x_i\left(\frac{c_i}{d_i}\right) + b_m\left(\frac{c_i}{b_i}\right) - b_m\sum_i x_i\left(\frac{c_i}{d_i}\right) \quad \text{A. 111}$$

$$\left(\frac{\partial nd_m}{\partial n_i}\right) = \frac{1}{2}\left[-\left(\left(\frac{\partial n b_m}{\partial n_i}\right) + \left(\frac{\partial nc_m}{\partial n_i}\right)\right) + \frac{b_m\left(\frac{\partial n b_m}{\partial n_i}\right) + 3b_m\left(\frac{\partial nc_m}{\partial n_i}\right) + 3c_m\left(\frac{\partial n b_m}{\partial n_i}\right) + c_m\left(\frac{\partial nc_m}{\partial n_i}\right)}{\sqrt{b_m + 6b_m c_m + c_m^2}}\right] \quad \text{A. 112}$$

$$\left(\frac{\partial ne_m}{\partial n_i}\right) = \frac{1}{2}\left[-\left(\left(\frac{\partial n b_m}{\partial n_i}\right) + \left(\frac{\partial nc_m}{\partial n_i}\right)\right) - \frac{b_m\left(\frac{\partial n b_m}{\partial n_i}\right) + 3b_m\left(\frac{\partial nc_m}{\partial n_i}\right) + 3c_m\left(\frac{\partial n b_m}{\partial n_i}\right) + c_m\left(\frac{\partial nc_m}{\partial n_i}\right)}{\sqrt{b_m + 6b_m c_m + c_m^2}}\right] \quad \text{A. 113}$$

Stellenbosch University https://scholar.sun.ac.za

A.4.4 SRK

$$\ln\widehat{\varphi}_i = \frac{1}{b_m}\left(\frac{\partial n b_m}{\partial n_i}\right)(Z-1) - \ln(Z-B) - \frac{A}{B}\ln\left(1+\frac{B}{Z}\right)\left[\frac{1}{a_m}\left(\frac{1}{n}\frac{\partial n^2 a_m}{\partial n_i}\right) - \frac{1}{b_m}\left(\frac{\partial n b_m}{\partial n_i}\right)\right] \quad \text{A. 114}$$

Van der Waals mixing rules [3]:

$$\left(\frac{\partial n b_m}{\partial n_i}\right) = 2\left(\sum_i^n x_i b_{ij}\right) - b_m \quad \text{A. 115}$$

$$\left(\frac{1}{n}\frac{\partial n^2 a_m}{\partial n_i}\right) = 2\left(\sum_i^n x_i a_{ij}\right) \quad \text{A. 116}$$

Wong Sandler mixing rules [11]:

$$\left(\frac{\partial n b_m}{\partial n_i}\right) = \frac{1}{1-D}\left(\frac{1}{n}\frac{\partial n^2 Q}{\partial n_i}\right) - \frac{Q}{(1-D)^2}\left(1-\frac{\partial nD}{\partial n_i}\right) \quad \text{A. 117}$$

$$\frac{1}{RT}\left(\frac{1}{n}\frac{\partial n^2 a_m}{\partial n_i}\right) = D\left(\frac{\partial n b_m}{\partial n_i}\right) + b_m\left(\frac{\partial nD}{\partial n_i}\right) \quad \text{A. 118}$$

$$\frac{1}{n}\frac{\partial n^2 Q}{\partial n_i} = 2\left(\sum_i x_i\left(b-\frac{a}{RT}\right)_{ij}\right) \quad \text{A. 119}$$

$$\frac{\partial nD}{\partial n_i} = \frac{a_i}{b_i RT} + \frac{\ln\gamma_i^{\infty}}{-\ln 2} \quad \text{A. 120}$$

References

[1] D. Peng, D.B. Robinson, A new two-constant equation of state, Industrial &Engineering Chemical Fundamentals 15 (1976) 59 – 63

[2] N.C. Patel, A.S. Teja, A new cubic equation of state for fluids and fluid mixtures, Chemical Engineering Science, 37(1982) 463-473

[3] G. Soave, Equilibrium constants for a modified Redlich-Kwong equation of state 27 (1972) 1197–1203

[4] R. Stryjek, J.H. Vera, PRSV: An improved Peng-Robinson equation of state for pure compounds and mixtures, Canadian J. Chemical Engineering 64 (1986) 323–333

[5] P. M. Mathias, A versatile equation of state,Industrial &Engineering Chemistry Process Design & Development 22 (1983) 385-391

[6] J.F. Boston, P.M. Mathias, Phase equilibrium in a third generation process simulator, in: Proceedings of the 2nd international conference on phase equilibrium and fluid

Stellenbosch University https://scholar.sun.ac.za

properties in the chemical process industries, West Berlin (17 – 21 March 1980), pp. 823 – 849

[7] B.E. Poling, J.M. Prausnitz, J.P. O'Connel, The properties of gases and liquids, 5th edition, McGraw Hill, 2001, Chapter 2 (pp. 2.2 – 2.38), Chapter 4 (pp 4.9, 4.30), Chapter 5 (pp. 5.2 , 5.21), Chapter 6 (pp. 6.30,), Chapter 8 (pp. 8.122)

[8] H.I. Renon, J.M. Prausnitz, Local compositions in thermodynamic excess functions of liquid mixtures, AIChE Journal 14 (1968) 135-144

[9] J. D. Van der Waals, On the continuity of gaseous and liquid states, Ph.D. Dissertation, Universiteit Leiden, Leiden, The Netherlands, 1873

[10] T.Y. Kwak, G.A. Mansoori, Van der Waals mixing rules for cubic equatios of state. Applications for supercritical fluid extraction modelling,Chemical Engineering Science 41 (1986) 1303-1309.

[11] D.S.H. Wong, S.I. Sandler, A theoretically correct mixing rule for cubic equations of state, AIChE Journal 38 (1992) 671 - 680

[12] T. Yang, G.J. Chen, W. Yan, T.M. Guo, Extension of the Wong-Sandler mixing rule to the three-parameter Patel-Teja equation of state: Application up to the near-critical region, Chemical Engineering Journal 67 (1997) 27–36

Stellenbosch University https://scholar.sun.ac.za

APPENDIX B: Algorithms and numerical methods

B.1 Root solving

Property calculations using an EOS all rely on solving for the roots in volume or compressibility. A pressure explicit cubic equation of state can generally be expanded in a cubic polynomial in compressibility of the following general form:

$$Z^3 + (C2)Z^2 + (C1)Z + (C0) = 0 \qquad \text{B. 1}$$

A notable advantage of the cubic equations of state is that their roots can be obtained analytically, which can lead to simpler and faster calculations than if iterative numerical methods were used. The method for solving the roots analytically, known as Cardano's method [1], is subsequently described. Consider a polynomial of the following general form:

$$x^3 + ax^2 + bx + c = 0 \qquad \text{B. 2}$$

The following variables can be defined in terms of the coefficients:

$$Q = \frac{a^2 - 3b}{9} \qquad \text{B. 3}$$

$$R = \frac{2a^2 - 9ab + 27c}{54} \qquad \text{B. 4}$$

If Q and R are real, and $R^2 \leq Q^3$ then the equation has 3 real roots. By defining θ:

$$\theta = \arccos\left(\frac{R}{\sqrt{Q^3}}\right) \qquad \text{B. 5}$$

The three roots are obtained as follows:

$$x_1 = -2\sqrt{Q}\cos\left(\frac{\theta}{3}\right) - \frac{a}{3} \qquad \text{B. 6}$$

$$x_2 = -2\sqrt{Q}\cos\left(\frac{\theta + 2\pi}{3}\right) - \frac{a}{3} \qquad \text{B. 7}$$

$$x_3 = -2\sqrt{Q}\cos\left(\frac{\theta - 2\pi}{3}\right) - \frac{a}{3} \qquad \text{B. 8}$$

Stellenbosch University https://scholar.sun.ac.za

The largest value is attributed to the vapour phase, the smallest to the liquid phase and the middle value has no significance. If $R^2 \geq Q^3$, the equation has one real root, which can be obtained by defining A and B:

$$A = -\frac{R}{|R|}\left[|R| + \sqrt{R^2 - Q^3}\right]^{\frac{1}{3}} \qquad \text{B. 9}$$

$$B = \begin{cases} \frac{Q}{A} & A \neq 0 \\ 0 & A = 0 \end{cases} \qquad \text{B. 10}$$

and solving for the root as follows:

$$x_1 = (A + B) - \frac{a}{3} \qquad \text{B. 11}$$

As noted by Monroy-Loperena [1], as well as Zhi and Lee [2], this method suffers from some drawbacks, particularly at low temperatures and for heavy non-volatile components, such as the solutes investigated in this study. The problems arise from rounding errors because of the finite precision with which numerical values are stored in computer memory when numerical methods are used for the analytical calculation. For the vapour phase, where compressibility values are typically close to 1, rounding errors are not significant. However for the liquid phase, the compressibility for heavy components is easily in the $1x10^{-10}$ range and rounding errors can be significant, even if double-precision numbers are used. This may lead to infeasible results (liquid volumes smaller than the co-volume b), which leads to termination of the calculation. In order to avoid these shortfalls, but still keep the advantage of an analytical solution, the expansion in compressibility can be transformed into an expansion in density using the following expression:

$$Z = \frac{PM_r}{\rho R_o T} \qquad \text{B. 12}$$

Equation B.1 can be re-written in terms of density as follows:

$$\left(\frac{1}{\rho^3}\right)\left(\frac{PM_r}{R_o T}\right)^3 + \left(\frac{1}{\rho^2}\right)C2\left(\frac{PM_r}{R_o T}\right)^2 + \left(\frac{1}{\rho}\right)C2\left(\frac{PM_r}{R_o T}\right) + C0 \quad = 0 \qquad \text{B. 13}$$

This leads to the following expression in the appropriate form (Equation B.2) for the analytical calculation of the roots:

Stellenbosch University https://scholar.sun.ac.za

$$\rho^3 + \left(\frac{C1}{C0}\right)\left(\frac{PM_r}{RT}\right)\rho^2 + \left(\frac{C2}{C0}\right)\left(\frac{PM_r}{RT}\right)^2\rho + \left(\frac{1}{C0}\right)\left(\frac{PM_r}{RT}\right)^3 \qquad \text{B. 14}$$

Since the liquid density is numerically much larger than the liquid molar volume or compressibility, the drawbacks of round-off error are generally avoided and analytical determination of the roots are much more reliable for heavy components at low temperature.

B.2 Pure Components

The computation procedure for calculating the pure component phase equilibrium and regressing model parameters to data is presented in Figure B.1.

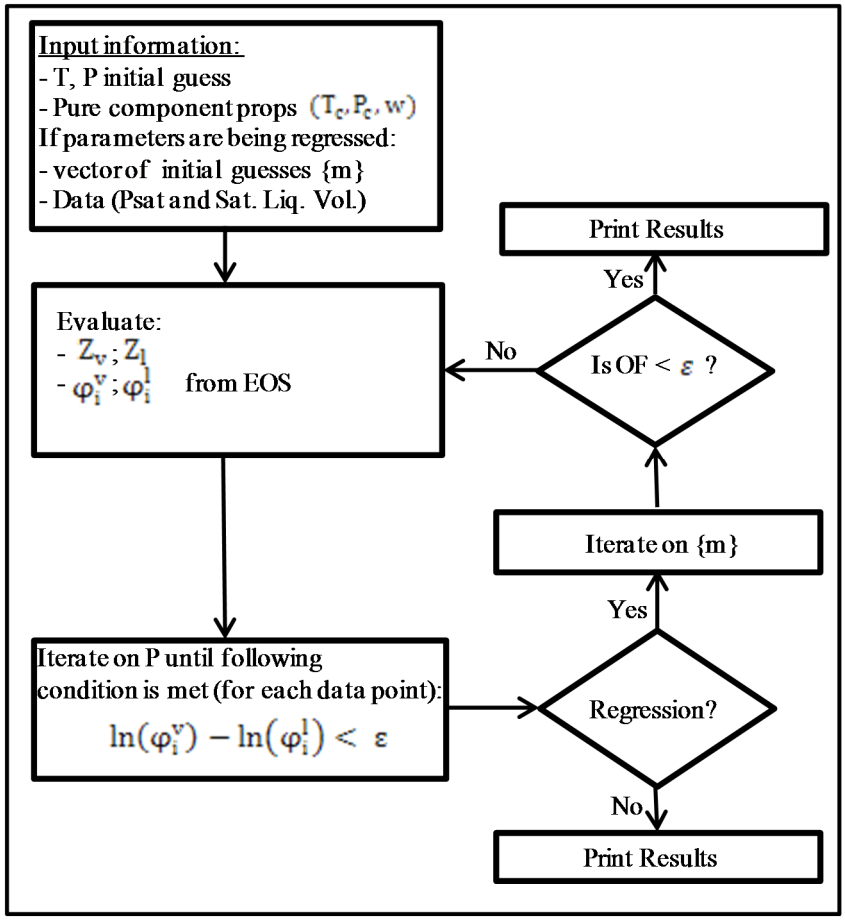

Figure B. 1 Computation procedure for vapour pressure and saturation liquid volume calculation and parameter regression for pure components

As explained in Section 6.1, the condition for vapour/liquid phase equilibrium of a pure component i can be given as the equality of the fugacity coefficient in each phase:

Stellenbosch University https://scholar.sun.ac.za

$$\ln\left(\varphi_i^L\right) = \ln\left(\varphi_i^V\right) \qquad \text{B. 15}$$

The input information required is the pure component constants T_c, P_c and the acentric factor ω and an initial guess for the final pressure. Three different sources were used for the constants in this project, namely the DIPPR database, the Constantinou and Gani (C&G) group contribution method and the ASPEN Plus® (Pure 20) database. The values for these constants are given in Appendix C. The pressure value from the DIPPR correlations at the specified temperature was used as an initial guess.

The next step is to solve for the vapour and liquid compressibility. CEOSs can readily be formulated as a cubic function in compressibility that must be solved for vapour, liquid and fluid roots, as discussed in Section B.1 of this appendix. Once these roots are obtained, the pure component fugacity is calculated using the expressions given in Appendix A.3. Using the initial guess for pressure from the DIPPR correlations, the pressure was iterated using the *fsolve* function in MATLAB, which uses the Levenberg-Marquardt non-linear least squares algorithm. Pressure was iterated until the following condition was met:

$$\ln\left(\varphi_i^L\right) - \ln\left(\varphi_i^V\right) < \varepsilon \qquad \text{B. 16}$$

A value of 1e-6 was chosen for ε.

If parameters are being regressed, then the procedure requires a vector, $\{m\}$, of initial guesses for all pure component parameters selected for regression, as well as the data to which parameters are being regressed. The DIPPR correlations for vapour pressure and saturated liquid density were used as data in this studyand parameters were fit to 30 data points in the *reduced temperature* range of 0.5 to 0.9. The following objective function was used to minimize the errors between the model and experimental values:

$$F = W_1 \sum_{i=1}^{np} \left[\frac{(P_i^{exp} - P_i^{calc})^2}{(P_i^{exp})^2}\right]^{0.5} + W_2 \sum_{i=1}^{np} \left[\frac{(\rho_{sat\,liq.,i}^{exp} - \rho_{sat.liq,i}^{calc})^2}{(\rho_{sat.liq,i}^{exp})^2}\right]^{0.5} \qquad \text{B. 17}$$

The weights used in this study are given in Table 6-1. Parameters being regressed for the pure model were also iterated using the *fsolve* function until the objective function reached a tolerance of 1e-6 or the value for the objective function for each subsequent regression iteration was below tolerance.

Stellenbosch University https://scholar.sun.ac.za

B.3 Binary Mixtures

Figure B.2 gives the algorithm for the binary VLE phase calculations performed for this study.

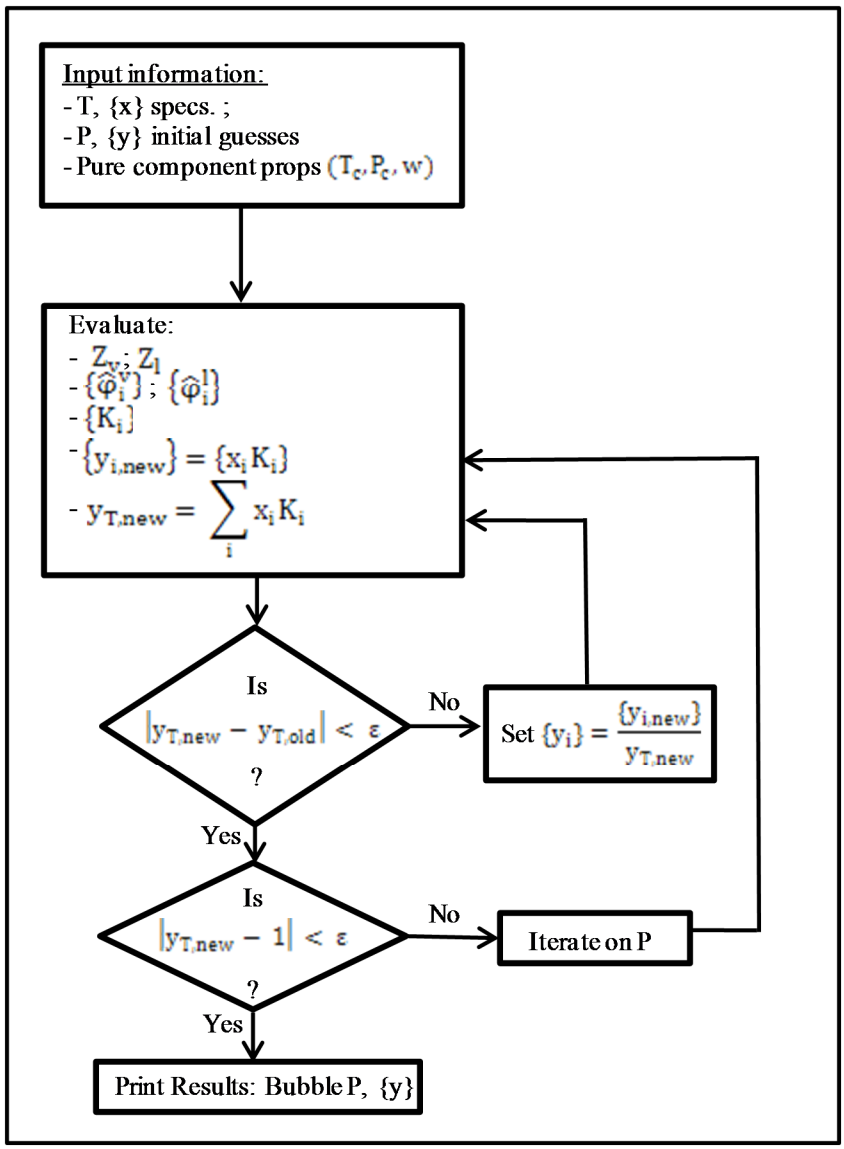

Figure B. 2 Computation procedure for bubble point calculation of a binary mixture

The procedure uses a standard isothermal bubble point pressure calculation which uses temperature T and liquid composition {x} as the specification variables, and returns pressure P and vapour composition {y} at equilibrium. The pure constants T_c, P_c and ω is required as input information for each species, as well as initial guesses for P and {y}. The calculation is started at the pure solute (X_2 = 1) using a pure component vapour pressure calculation at the

Stellenbosch University https://scholar.sun.ac.za

specified temperature as in Section B.2. The phase envelope is then constructed by gradually stepping in X from the pure solute towards the pure solvent.

The first step in X after the initial vapour pressure calculation is taken as 0.2. The subsequent step sizes are determined by the distance of the current liquid composition from the composition at the maximum pressure of the VLE data for which the fit is being determined. At a distance of 0.08 from this composition, the step-size of 0.05 is taken; at a distance of 0.04 a step-size of 0.01 is taken and at distance of 0.02 from this composition a step-size of 0.005 is taken until the phase compositions converge, the K values become 1 and the calculation terminates. If the current step crosses the liquid composition of a data point for which the fit is being determined, this value is taken as the specification in order to determine the %AAD in pressure and vapour composition for evaluating model performance. The initial guesses in P and {y} for each step is obtained from the previous calculation. At each new specification, the vapour and liquid compressibility is firstly calculated using the EOS, from which the fugacity of component in solution is obtained for each component. The K factor for each species is then calculated from the following relation:

$$K_i = \frac{y_i}{x_i} = \frac{\hat{\varphi}^l{}_i}{\hat{\varphi}^v{}_i} \qquad \text{B. 18}$$

The new vapour pressure composition is calculated for each species:

$$y_{i,new} = \{x_i K_i\} \qquad \text{B. 19}$$

The total vapour composition is then calculated and compared to that from the previous *inner loop* iteration until the following condition is met:

$$\left|y_{T,new} - y_{T,old}\right| < \varepsilon \qquad \text{B. 20}$$

The tolerance for ε was taken as $1e^{-5}$. The pressure used as an initial guess at the specified temperature is not necessarily the equilibrium pressure, and the vapour compositions which converge for the inner loop do not necessarily sum to unity. The inner loop is thus repeated for an improved guess for pressure in an outer loop.

The secant method was used for updating the pressure:

$$P_{k+2} = P_{k+1} - \frac{g(P_{k+1})(P_{k+1} - P_k)}{g(P_{k+1}) - g(P_k)} \qquad \text{B. 21}$$

Stellenbosch University https://scholar.sun.ac.za

With g(P) defined as follows:

$$g(P) = \ln \sum K_i x_i \qquad \text{B. 22}$$

It is seen that the new pressure from the secant method requires values from the two previous iterations P_k and P_{k+1}. For the 1st iteration following that of the initial guess, P_k, the following value is used for the outer loop iteration:

$$\begin{aligned} &if\, y_{T,new} > 1 \;\; ; \;\; P_{k2} = P_{k1} + 0.0001x\, P_{k1} \\ &if\, y_{T,new} < 1 \;\; ; \;\; P_{k2} = P_{k1} - 0.0001x\, P_{k1} \end{aligned} \qquad \text{B. 23}$$

Equation B.21 is then used for subsequent iterations until the inner loop converges on a vapour composition which satisfies the mass balance:

$$\left| y_{T,new} - 1 \right| < \varepsilon \qquad \text{B. 24}$$

The tolerance is again selected as $1e^{-}5$ and the equilibrium pressure and vapour composition is obtained when this condition is met.

The data regression routine for fitting binary interaction parameters (BIPs) involves solving for the following implicit objective function:

$$F = \sum_{i=1}^{np} \sum_{i=1}^{nc} \left[\frac{(K_{i,j}{}^{exp} - K_{i,j}{}^{calc})^2}{(K_{i,j}{}^{exp})^2} \right]^{0.5} \qquad \text{B. 25}$$

K values are calculated directly from the EOS using Equation B.18 at the conditions of the experimental data. The iterative procedure from Figure B.2 is therefore not required, leading to a considerably faster procedure than if an explicit objective function is used. The objective function was minimized by iterating BIPs using the *fminsearch* function, which uses the Nelder-Mead simplex minimization algorithm, until F reaches a value of $1e^{-}5$ or the decrease in F for each subsequent iteration stabilizes.

B.4 Validation of the code

This section discusses the validation of the MATLAB software developed for this thesis, in particular, the analytical expressions for the fugacity of a component in solution. As shown by Equation 8-8, obtaining these expressions analytically involves the derivative of the Helmholtz energy with mole number of the component. Given the complex composition dependence which various mixing rules may have, this derivative can be quite involved,

Stellenbosch University https://scholar.sun.ac.za

leading to complicated expressions for the component fugacity. Michelsen and Mollerup [3] provide the following equation for numerically testing the consistency of these analytical expressions, in order to prevent coding errors from sneaking in:

$$\ln\hat{\varphi}_i = \ln\left(\frac{\hat{f}_i}{x_i P}\right) = \frac{\partial(\sum n_i \ln\hat{\varphi}_i)_{T,P,n_j}}{\partial n_i} \qquad \text{B. 26}$$

The derivative on the right can be solved using central differences as follows:

$$\ln\hat{\varphi}_i = \frac{\left[(n_i+\varepsilon\ )\ln\hat{\varphi}_{i_{T,P,n+\varepsilon_i}} + n_j\ln\hat{\varphi}_{j_{T,P,n+\varepsilon_i}}\right] - \left[(n_i-\varepsilon\ )\ln\hat{\varphi}_{i_{T,P,n+\varepsilon_i}} + n_j\ln\hat{\varphi}_{j_{T,P,n-\varepsilon_i}}\right]}{2\varepsilon} \qquad \text{B. 27}$$

The subscript $n + \varepsilon_i$ means that the specific component fugacity is calculated at the renormalized composition where mole number of component i is increased by amount ε_i while keeping that of the other component constant. For testing the analytical expressions used in this thesis as presented in Appendix A.4, a total mole number of 7 was chosen and ε_i was taken as $1e^{-5}$ times the total mole number. As noted by Michelsen and Mollerup [3], consistency in the fugacity expressions should give agreement between the left and right hand side of Equation B.27 up to 8 – 10 digits.

The test was performed using a phase composition of $X_1 = 0.9$ and $X_2 = 0.1$ for the light component (1) of the ethane/hexadecane system at P = 12 MPa and T = 352 K. Results are given in Table B.1.

Table B. 1 Consistency test for analytical fugacity of component in solution

Model	LHS	RHS	%Dev
PR-VDW	-0.5626147794	-0.5626147794	1.54E-09
PT-VDW	-0.5190792244	-0.5190792244	5.42E-09
SRK-VDW	-0.5063488704	-0.5063488704	1.72E-09
PR-WS (UNIFAC)	-0.5666464114	-0.5666464114	8.10E-10
PT-WS (UNIFAC)	-0.5441407768	-0.5441407767	2.40E-08
SRK-WS (UNIFAC)	-0.5089671950	-0.5089671950	8.64E-09
PR-WS (NRTL)	-0.5664403262	-0.5664403263	1.23E-08
PT-WS (NRTL)	-0.5369875686	-0.536987562	1.30E-08
SRK-WS (NRTL)	-0.5078666720	-0.5078666720	1.60E-09

It is seen that all expressions give good agreement between the left and right hand side of Equation B.27 and the code can be considered validated. An additional test that can be

Stellenbosch University https://scholar.sun.ac.za

applied is to determine the fugacity of component in solution numerically from the derivative of the pure component fugacity for a particular mixing rule:

$$\ln\hat{\varphi}_i = \ln\left(\frac{\hat{f}_i}{x_i P}\right) = \left.\frac{\partial[n\ln\varphi]}{\partial n_i}\right|_{T,P,n_j} \qquad \text{B. 28}$$

This can again be done through the use of central differences, as follows:

$$\ln\hat{\varphi}_i = \ln\left(\frac{\hat{f}_i}{x_i P}\right) = \frac{(n+\varepsilon_i)\ln\varphi_{T,P,n+\varepsilon_i} - (n-\varepsilon_i)\ln\varphi_{T,P,n-\varepsilon_i}}{2\varepsilon_i} \qquad \text{B. 29}$$

Table B.2 gives the agreement between the values obtained from the analytical expressions in Appendix A.4 and those from numerical derivation of the pure component fugacity as given in Appendix A.3, calculated with the corresponding mixing rule:

Table B. 2 Analytical vs. numerical value of fugacity of component in solution

Model	Analytical	Numerical	%Dev
PR-VDW	-0.5626147794	-0.562614779	2.9546E-11
PT-VDW	-0.5190792244	-0.519079224	5.0821E-12
SRK-VDW	-0.5063488704	-0.50634887	4.251E-11
PR-WS (UNIFAC)	-0.5666464114	-0.566414214	0.00040977
PT-WS (UNIFAC)	-0.5441407768	-0.544140777	3.9889E-11
SRK-WS (UNIFAC)	-0.5089671950	-0.508967195	1.3649E-10
PR-WS (NRTL)	-0.5664403262	-0.56620812	0.00040994
PT-WS (NRTL)	-0.5369875686	-0.536987569	2.6012E-10
SRK-WS (NRTL)	-0.5078666720	-0.507866672	1.4112E-10

Good agreement is again obtained. Using this methodology for obtaining the expressions for the fugacity of a component in solution may be very useful, since the expression for the pure component fugacity is much simpler than the analytical expression of its derivative with mole number for a particular mixing rule. Many different mixing rules may therefore be applied for a particular model without having to solve the component fugacity in solution analytically. Given the empirical nature of mixing rules, this may be particularly useful in developing new expressions, since analytical derivation for each new case being tested can become quite tedious.

Given the deficiencies of many empirical mixing rules, such as the dilution effect and Michelsen-Kirstenmacher syndrome, it may further be useful to apply the consistency test of Michelsen and Mollerup (Equation B.26) for fugacities of components in solution obtained

Stellenbosch University https://scholar.sun.ac.za

from the numerical derivative in Equation B.29. This will undoubtedly lead to accumulation of round-off errors and accuracies up to 8 – 10 digits cannot be expected as for the analytical expressions. Table B.3 gives the results of the consistency test (Equation B.27) using this method.

Table B. 3 Consistency test for numerical fugacity of component in solution

Model	LHS	RHS	%Err
PR-VDW	-0.562614779	-0.562616048	2.26E-04
PT-VDW	-0.519079224	-0.519079478	4.89E-05
SRK-VDW	-0.50634887	-0.506351598	5.39E-04
PR-WS (UNIFAC)	-0.566414214	-0.566415483	2.24E-04
PT-WS (UNIFAC)	-0.544140777	-0.544141792	1.87E-04
SRK-WS (UNIFAC)	-0.508967195	-0.508972524	0.00104705
PR-WS (NRTL)	-0.56620812	-0.5662059	3.92E-04
PT-WS (NRTL)	-0.536987569	-0.536993342	0.0010751
SRK-WS (NRTL)	-0.507866672	-0.507867243	1.12E-04

It is seen that even though agreement between the left and right side of Equation B.27 is not as good as for the analytical expressions, accuracies up to 4 or 5 digits are still achieved, which should suffice for confirming consistent expressions in mixing rule development.

References

[1] R. Monroy, A note on the analytical solution of cubic equations of state in process simulation, Industrial Engineering Chemistry Research, 51 (2012) 6972–6976

[2] Y. Zhi, H. Lee, Fallibility of analytic roots of cubic equations of state in low temperature region, Fluid Phase Equilibria 201 (2002) 287-294

[3] M.L. Michelsen, J.M. Mollerup, Thermodynamic models: Fundamentals & computational aspects, 2nd edition, Tie-line publications, Denmark, 2007, pp. 223,77

Stellenbosch University https://scholar.sun.ac.za

APPENDIX C: Pure component constants used

This appendix contains all of the pure component properties that were used in performing the modelling for this project. This includes the n-alkane series with carbon numbers 1 – 30, 32 and 36; the 1-alcohols with carbon number 1 -20, the methyl esters with carbon number10, 12, 14, 16 and 18, as well as the carboxylic acids with carbon number 1 – 20. Three different sources were used for this project, namely the DIPPR data base, the Constantinou and Gani group contribution method and the Pure20 database from ASPEN Plus ®.

C.1 DIPPR

Table C. 1Pure component constants from DIPPR for the n-alkanes

Component	CN	MW (g/mol)	Tc (K)	Pc (Bar)	w
Methane	1	16.04	190.564	45.99	0.0115
Ethane	2	30.07	305.32	48.72	0.0995
Propane	3	44.09	369.83	42.48	0.1523
n-Butane	4	58.12	425.12	37.96	0.2002
n-Pentane	5	72.15	469.70	33.70	0.2515
n-Hexane	6	86.18	507.60	30.25	0.3013
n-Heptane	7	100.21	540.20	27.40	0.3495
n-Octane	8	114.23	568.70	24.90	0.3996
n-Nonane	9	128.26	594.60	22.90	0.4435
n-Decane	10	142.29	617.70	21.10	0.4923
n-Undecane	11	156.31	639.00	19.50	0.5303
n-Dodecane	12	170.34	658.00	18.20	0.5764
n-Tridecane	13	184.37	675.00	16.80	0.6174
n-Tetradecane	14	198.39	693.00	15.70	0.6430
n-Pentadecane	15	212.42	708.00	14.80	0.6863
n-Hexadecane	16	226.45	723.00	14.00	0.7174
n-Heptadecane	17	240.75	736.00	13.40	0.7697
n-Octadecane	18	254.50	747.00	12.70	0.8114
n-Nonadecane	19	268.53	758.00	12.10	0.8522
n-Eicosane	20	282.56	768.00	11.60	0.9069
n-Heneicosane	21	296.58	778.00	11.10	0.9420
n-Docosane	22	310.61	787.00	10.60	0.9722
n-Tricosane	23	324.63	796.00	10.20	1.0262
n-Tetracosane	24	338.66	804.00	9.80	1.0710
n-Pentacosane	25	352.68	812.00	9.50	1.1053
n-Hexacosane	26	366.71	819.00	9.10	1.1544
n-Heptacosane	27	380.73	826.00	8.83	1.2136
n-Octacosane	28	394.76	832.00	8.50	1.2375

Stellenbosch University https://scholar.sun.ac.za

n-Nonacosane	29	408.79	838.00	8.26	1.2653
n-Triacontane	30	422.81	844.00	8.00	1.3072
n-Dotriacontane	32	450.87	855.00	7.50	1.3766
n-Hexatriacontane	36	506.97	874.00	6.80	1.5260

Table C. 2Pure component constants from DIPPR for the 1-alcohols

Component	CN	MW (g/mol)	Tc (K)	Pc (Bar)	w
Methanol	1	32.04	512.6	80.90	0.556
Ethanol	2	46.07	513.9	61.40	0.644
1-Propanol	3	60.10	536.8	51.70	0.623
1-Butanol	4	74.12	563.1	44.20	0.588
1-Pentanol	5	88.15	588.1	38.97	0.575
1-Haxanol	6	102.18	611.3	34.46	0.559
1-Heptanol	7	116.20	632.3	30.85	0.562
1-Octanol	8	130.23	652.3	27.83	0.570
1-Nonanol	9	144.26	670.9	25.27	0.584
1-Decanol	10	158.29	688.0	23.08	0.607
1-Undecanol	11	172.31	703.9	21.19	0.624
1-Dodecanol	12	186.34	718.7	19.54	0.656
1-Tridecanol	13	200.37	732.4	18.10	0.688
1-Tetradecanol	14	214.39	745.3	16.82	0.717
1-Pentadecanol	15	228.42	757.3	15.69	0.751
1-Hexadecanol	16	242.45	768.6	14.68	0.779
1-Heptadecanol	17	256.47	779.2	13.77	0.812
1-Octadecanol	18	270.50	789.3	12.95	0.832
1-Nonadecanol	19	284.00	798.5	12.20	0.858
1-Eicosanol	20	298.56	807.7	11.54	0.879

Table C. 3 Pure component constants from DIPPR for the methyl esters

Component	CN	MW (g/mol)	Tc (K)	Pc (Bar)	w
Methyl decanoate	10	186.291	686.9	19.42	0.549138
Methyl dodecanoate	12	214.344	712	16.5	0.664389
Methyl tetradecanoate	14	242.398	741.2	14.21	0.697887
Methyl hexadecanoate	16	270.451	762.2	12.35	0.776457
Methyl octadecanoate	18	298.504	781.1	10.84	0.859477

Table C. 4 Pure component constants from DIPPR for the carboxylic acids

Component	CN	MW (g/mol)	Tc (K)	Pc (Bar)	w
Methanoic acid	1	46.026	588	58.10	0.312521
Ethanoic acid	2	66.053	591.95	57.86	0.466521

Stellenbosch University https://scholar.sun.ac.za

Propanoic acid	3	74.08	600.81	46.68	0.579579
Butanoic acid	4	88.106	615.7	40.60	0.675003
Pentanoic acid	5	102.133	639.16	36.30	0.706632
Hexanoic acid	6	116.16	660.2	33.08	0.733019
Heptanoic acid	7	130.187	677.3	30.43	0.759934
Octanoic acid	8	144.211	694.26	27.79	0.773427
Nonanoic acid	9	158.241	710.7	25.14	0.778706
Decanoic acid	10	172.268	722.1	22.80	0.813724
Undecanoic acid	11	186.291	732	20.90	0.85309
Dodecanoic acid	12	200.318	743	19.30	0.89828
Tridecanoic acid	13	214.344	754	17.90	0.913368
Tetradecanoic acid	14	228.371	763	16.40	0.953534
Pentadecanoic acid	15	242.398	774	15.70	0.963881
Hexadecanoic acid	16	256.424	785	14.90	0.991904
Heptadecanoic acid	17	270.451	792	13.70	1.01866
Octadecanoic acid	18	284.477	803	13.30	1.03936
Nonadecanoic acid	19	298.504	811	12.70	1.06769
Eicosanoic acid	20	312.53	820	12.00	1.08228

C.2 Constantinou & Gani group contribution method

This method uses only the component structure as input information. The equations for estimating T_c, P_c and ω are provided below [1]:

$$T_c = 181.128\ \ln[\sum_k N_k(tc1k)] \tag{C.2.1}$$

$$P_c = [\sum_k N_k(pc1k) + 1.0022]^{-2} + 1.3705 \tag{C.2.2}$$

$$\omega = 0.4085\{\ln[\sum_k N_k(w1k) + 1.1507]\}^{\frac{1}{0.5050}} \tag{C.2.3}$$

N_k is the number of time the functional group appears in the molecule. The following table provides the necessary parameters for the functional groups relevant to this study:

Table C. 5Constantinou & Gani group specifications

Group nr.	Formula	tc1k (K)	pc1k ($Bar^{0.5}$)	w1k
1	CH_3	1.6781	0.0199	0.296
2	CH_2	3.492	0.0106	0.147
3	OH	9.7292	0.0051	0.737
4	CH_2COO	13.8116	0.0218	0.765
5	COOH	23.7593	0.0115	0.57

Stellenbosch University https://scholar.sun.ac.za

The location of these functional groups on the 4 homologous series investigated is depicted below:

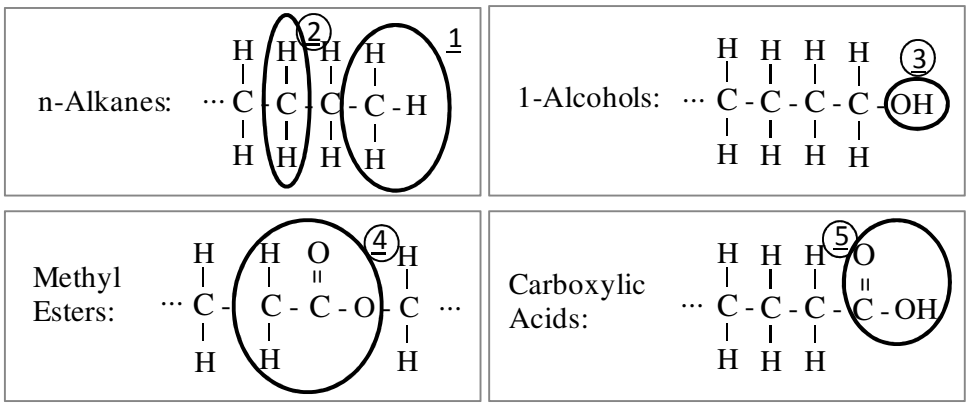

Figure C. 1Molecular deconstruction in terms of functional groups for use in the Constantinou and Gani group contribution method

The values obtained for T_c, P_c and ω using this method are tabulated below:

Table C. 6 Pure component constants from the Constantinou & Gani group contribution method for the n-alkanes

Component	CN	MW (g/mol)	Tc (K)	Pc (Bar)	w
n-Butane	4	58.124	423.1221	39.88034	0.208096
n-Pentane	5	72.151	475.8231	35.28999	0.250405
n-Hexane	6	86.178	516.596	31.47402	0.293456
n-Heptane	7	100.205	549.856	28.26756	0.336945
n-Octane	8	114.232	577.9457	25.5474	0.380648
n-Nonane	9	128.259	602.2584	23.21994	0.424392
n-Decane	10	142.286	623.6905	21.21309	0.46805
n-Undecane	11	156.313	642.8528	19.47054	0.511523
n-Dodecane	12	170.34	660.1805	17.94785	0.554738
n-Tridecane	13	184.367	675.9942	16.60952	0.597638
n-Tetradecane	14	198.394	690.5375	15.42696	0.640182
n-Pentadecane	15	212.421	703.9993	14.37689	0.682339
n-Hexadecane	16	226.448	716.5295	13.44023	0.724084
n-Heptadecane	17	240.75	728.2486	12.60124	0.765403
n-Octadecane	18	254.504	739.2554	11.84677	0.806285
n-Nonadecane	19	268.529	749.6315	11.16586	0.846722
n-Eicosane	20	282.556	759.4452	10.54923	0.886711
n-Heneicosane	21	296.58	768.7544	9.98905	0.926251
n-Docosane	22	310.607	777.6085	9.478629	0.965342
n-Tricosane	23	324.634	786.0498	9.012245	1.003989

Stellenbosch University https://scholar.sun.ac.za

n-Tetracosane	24	338.661	794.1153	8.584973	1.042194
n-Pentacosane	25	352.68038	801.8368	8.192559	1.079962
n-Hexacosane	26	366.70696	809.2425	7.831312	1.117299
n-Heptacosane	27	380.73354	816.3574	7.498018	1.154212
n-Octacosane	28	394.76012	823.2032	7.189864	1.190707
n-Nonacosane	29	408.7867	829.7998	6.904384	1.22679
n-Triacontane	30	422.81328	836.1645	6.639408	1.262469
n-Dotriacontane	32	450.86644	848.2598	6.163514	1.332645
n-Hexatriacontane	36	506.97276	870.2677	5.386548	1.468475

Table C. 7 Pure component constants from the Constantinou & Gani group contribution method for the 1-alcohols

Component	CN	MW (g/mol)	Tc (K)	Pc (Bar)	w
1-Butanol	4	74.123	558.911	41.96802	0.380648
1-Pentanol	5	88.15	585.7274	37.01148	0.424392
1-Haxanol	6	102.177	609.0808	32.9102	0.46805
1-Heptanol	7	116.204	632.238	30.945	0.574466
1-Octanol	8	130.231	648.3259	26.57727	0.554738
1-Nonanol	9	144.258	665.161	24.10336	0.597638
1-Decanol	10	158.285	680.5636	21.97655	0.640182
1-Undecanol	11	172.311	694.7584	20.13482	0.682339
1-Dodecanol	12	186.339	707.9211	18.5294	0.724084
1-Tridecanol	13	200.365	720.1918	17.12154	0.765403
1-Tetradecanol	14	214.392	731.6837	15.8801	0.806285
1-Pentadecanol	15	228.419	742.4897	14.77984	0.846722
1-Hexadecanol	16	242.446	752.6872	13.80015	0.886711
1-Heptadecanol	17	256.474	762.3411	12.92403	0.926251
1-Octadecanol	18	270.499	771.5063	12.13738	0.965342
1-Nonadecanol	19	284	780.23	11.42842	1.003989
1-Eicosanol	20	298.555	788.5528	10.78724	1.042194

Table C. 8 Pure component constants from the Constantinou & Gani group contribution method for the methyl esters

Component	CN	MW (g/mol)	Tc (K)	Pc (Bar)	w
Methyl decanoate	10	186.291	675.3147	19.36565	0.648818
Methyl dodecanoate	12	214.344	703.4173	16.52846	0.732552
Methyl tetradecanoate	14	242.398	727.7397	14.31295	0.814573
Methyl hexadecanoate	16	270.451	749.1792	12.54992	0.894816
Methyl octadecanoate	18	298.504	768.3476	11.12405	0.973265

Stellenbosch University https://scholar.sun.ac.za

Table C. 9 Pure component constants from the Constantinou & Gani group contribution method for the carboxylic acids

Component	CN	MW (g/mol)	Tc (K)	Pc (Bar)	w
Butanoic acid	4	88.106	630.1115	44.23467	0.287567
Pentanoic acid	5	102.133	648.6394	38.8711	0.331012
Hexanoic acid	6	116.16	665.4467	34.4547	0.374696
Heptanoic acid	7	130.187	680.826	30.77489	0.418443
Octanoic acid	8	144.211	695.001	27.67654	0.462119
Nonanoic acid	9	158.241	708.1468	25.0433	0.505622
Decanoic acid	10	172.268	720.4027	22.78652	0.548876
Undecanoic acid	11	186.291	731.8816	20.83772	0.591822
Dodecanoic acid	12	200.318	742.6762	19.14331	0.634416
Tridecanoic acid	13	214.344	752.8635	17.66086	0.676627
Tetradecanoic acid	14	228.371	762.5082	16.35644	0.718429
Pentadecanoic acid	15	242.398	771.6652	15.20264	0.759807
Hexadecanoic acid	16	256.424	780.3814	14.17714	0.800749
Heptadecanoic acid	17	270.451	788.6974	13.2616	0.841246
Octadecanoic acid	18	284.477	796.6483	12.44083	0.881296
Nonadecanoic acid	19	298.504	804.2648	11.70221	0.920897
Eicosanoic acid	20	312.53	811.574	11.03511	0.96005

C.3 Aspen Plus ® (Pure 20 database)

Table C. 10 Pure component constants from the ASPEN Plus ® Pure20 database for the n-alkanes

Component	CN	MW (g/mol)	Tc (K)	Pc (Bar)	w
Methane	1	16.04	190.564	45.99	0.0115478
Ethane	2	30.07	305.32	48.72	0.099493
Propane	3	44.094	369.83	42.48	0.152291
n-Butane	4	58.124	425.12	37.96	0.200164
n-Pentane	5	72.151	469.7	33.7	0.251506
n-Hexane	6	86.178	507.6	30.25	0.301261
n-Heptane	7	100.205	540.2	27.4	0.349469
n-Octane	8	114.232	568.7	24.9	0.399552
n-Nonane	9	128.259	594.6	22.9	0.44346
n-Decane	10	142.286	617.7	21.1	0.492328
n-Undecane	11	156.313	639	19.5	0.530316
n-Dodecane	12	170.34	658	18.2	0.576385
n-Tridecane	13	184.367	675	16.8	0.617397
n-Tetradecane	14	198.394	693	15.7	0.643017
n-Pentadecane	15	212.421	708	14.8	0.68632

Stellenbosch University https://scholar.sun.ac.za

n-Hexadecane	16	226.448	723	14	0.717404
n-Heptadecane	17	240.75	736	13.4	0.769688
n-Octadecane	18	254.504	747	12.7	0.811359
n-Nonadecane	19	268.529	758	12.1	0.852231
n-Eicosane	20	282.556	768	11.6	0.906878
n-Heneicosane	21	296.58	778	11.1	0.942004
n-Docosane	22	310.607	787	10.6	0.97219
n-Tricosane	23	324.634	796	10.2	1.02617
n-Tetracosane	24	338.661	804	9.8	1.07102
n-Pentacosane	25	352.68038	812	9.5	1.10526
n-Hexacosane	26	366.70696	819	9.1	1.15444
n-Heptacosane	27	380.73354	826	8.83	1.21357
n-Octacosane	28	394.76012	832	8.5	1.23752
n-Nonacosane	29	408.7867	838	8.26	1.26531
n-Triacontane	30	422.81328	844	8	1.30718
n-Hexatriacontane	36	506.97276	874	6.8	1.52596

Table C. 11 Pure component constants from the ASPEN Plus ® Pure20 database for the 1-alcohols

Component	CN	MW (g/mol)	Tc (K)	Pc (Bar)	w
Methanol	1	32.042	512.5	80.84	0.565831
Ethanol	2	46.069	514	61.37	0.643558
1-Propanol	3	60.096	536.8	51.69	0.620432
1-Butanol	4	74.123	563	44.14	0.589462
1-Pentanol	5	88.15	588.1	38.97	0.57314
1-Hexanol	6	102.177	610.3	34.17	0.576355
1-Heptanol	7	116.204	632.6	30.58	0.567024
1-Octanol	8	130.231	652.5	27.77	0.58291
1-Nonanol	9	144.258	670.7	25.28	0.599685
1-Decanol	10	158.285	687.3	23.15	0.621924
1-Undecanol	11	172.311	703.6	21.47	0.624739
1-Dodecanol	12	186.339	719.4	19.94	0.666353
1-Tridecanol	13	200.365	734	19.35	0.712411
1-Tetradecanol	14	214.392	747	18.1	0.743185
1-Pentadecanol	15	228.419	759	17	0.779668
1-Hexadecanol	16	242.446	770	16.1	0.816283
1-Heptadecanol	17	256.474	780	15	0.849235
1-Octadecanol	18	270.499	790	14.4	0.888625
1-Nonadecanol	19	284	799	13.8	0.908171
1-Eicosanol	20	298.555	809	13	0.918342

Stellenbosch University https://scholar.sun.ac.za

Table C. 12 Pure component constants from the ASPEN Plus ® Pure20 database for the methyl esters

Component	CN	MW (g/mol)	Tc (K)	Pc (Bar)	w
Methyl decanoate	10	186.291	671	19.9	0.699294
Methyl dodecanoate	12	214.344	712	17.4	0.692419
Methyl tetradecanoate	14	242.398	738	15.1339	0.771061
Methyl hexadecanoate	16	270.451	768	12.7945	0.781369
Methyl octadecanoate	18	298.504	797	11.0717	0.772988

Table C. 13 Pure component constants from the ASPEN Plus ® Pure20 database for the carboxylix acids

Component	CN	MW (g/mol)	Tc (K)	Pc (Bar)	w
Methanoic acid	1	46.026	588	58.1	0.317268
Ethanoic acid	2	66.053	591.95	57.86	0.466521
Propanoic acid	3	74.08	600.81	46.17	0.574521
Butanoic acid	4	88.106	615.7	40.64	0.680909
Pentanoic acid	5	102.133	639.16	35.72	0.698449
Hexanoic acid	6	116.16	660.2	33.08	0.729866
Heptanoic acid	7	130.187	677.3	30.43	0.756364
Octanoic acid	8	144.211	694.26	27.79	0.770625
Nonanoic acid	9	158.241	710.7	25.14	0.772351
Decanoic acid	10	172.268	722.1	22.5	0.805989
Undecanoic acid	11	186.291	732	20.8	0.83455
Dodecanoic acid	12	200.318	743	19.4	0.879987
Tridecanoic acid	13	214.344	754	18.1	0.903891
Tetradecanoic acid	14	228.371	765	17	0.935637
Pentadecanoic acid	15	242.398	775	16	0.95857
Hexadecanoic acid	16	256.424	785	15.1	0.982707
Heptadecanoic acid	17	270.451	793	14.3	1.02787
Octadecanoic acid	18	284.477	804	13.6	1.03597
Nonadecanoic acid	19	298.504	812	13	1.06278
Eicosanoic acid	20	312.53	821	12.4	1.08673

References

[1] L. Constantinou, R. Gani, New group contribution method for estimating properties of pure compounds, AIChE Journal, 40, (1994), pp 1697 - 1710

Stellenbosch University https://scholar.sun.ac.za

Appendix D: Important theoretical developments applicable to high pressure phase equilibrium

This section gives a theoretical background of relevant developments in defining the thermodynamic state of a system. The discussion starts with the culmination of the ideal gas law from experiments perfumed in the mid seventeenth century, and chronicles the subsequent developments from the kinetic theory of gases, the Van der Waals law (1873) up to the unification of these ideas with present day molecular theory, in particular statistical mechanical perturbation theory.

D.1 The ideal gas law

The attempts at describing the thermodynamic state of a system dates back to the mid seventeenth century, whereby experimental investigations were made into the relationship between temperature, pressure and the volume of a system containing gases at moderate temperatures and pressures. In 1662, British chemist and physicist, Robert Boyle (1627 – 1691) observed that at constant temperature, the volume occupied by a fixed amount of gas is inversely proportional to the applied pressure:

$$V = \left(\frac{\text{Constant}}{P}\right)_{T,n} \qquad \text{D. 1}$$

In 1801, the French chemist and physicist, Louis Joseph Gay-Lusaac (1778 – 1850) published the following relationship between volume and temperature:

$$V = (\text{Constant x } T)_{P,n} \qquad \text{D. 2}$$

Gay-Lusaac accredited this discovery to unpublished work by fellow French scientist and mathematician, Jacques Charles (1746 – 1823), and subsequently named it Charles's law. In 1811, an Italian scientist by the name Amedeo Avogadro (1776 – 1856) discovered that at constant temperature and pressure, the volume occupied by a gas is directly proportional to the amount (mol) of gas:

$$V = (\text{Constant x } n)_{P,T} \qquad \text{D. 3}$$

By combining the three laws above, the following relation was first published in 1834 by French engineer and physicist Emile Clapeyron (1799 - 1864) and is known as the ideal gas law:

Stellenbosch University https://scholar.sun.ac.za

$$P = \frac{nRT}{V} = \frac{RT}{\nu} \qquad D.4$$

Having experimentally obtained this relationship, the next challenge was to develop a theory which could explain this gas behaviour.

D.2 The kinetic theory of gases

Around the same time that the empirical laws relating to the ideal gas law were being discovered, a theory which could explain this behaviour was postulated, namely the kinetic theory of gases. The publication which most strongly spurred the development of this theory wasa work entitled Hydrodynamica (1738) by Swiss mathematician; Daniel Bernoulli (1700 – 1782) [1]. In this work, Bernoulli argues that the macroscopic phenomena that we experience daily such as pressure and temperature can be explained solely by the random molecular motions of material points called atoms. It was argued that the impact of these atoms on a particular surface results in the pressure that we feel and measure, while the heat we experience at different temperatures is a result of the kinetic energy of the atoms in motion. This theory was initially met with scepticism, as the conservation of energy had not yet been established and the view did not comply with contemporary intuitions. The popular view at the time was that there was an universal "ether" through which energy is transmitted by light and radiation heat. It was believed that this ether fills the space between bodies, which suspends them at certain equilibrium points, thus influencing their motion. It was the properties of this ether that was presumed to be responsible for the phenomena of pressure and temperature.

Kinetic theory experienced a revival in the mid-19th century with a series of groundbreaking publications by Herman Helmholtz (1821 – 1894), Rudolf Clausius (1822 – 1888) and others, in which it was shown that energy is conserved and that heat, or thermal energy, is a type of mechanical energy, resulting from the cumulative motions of the molecules in a system. In particular, Clausius showed in his treatise on the nature of heat (1857) that Boyle's law can be derived on the assumption that a gas consists of material points which move at high velocity similar to that of sound and is proportional to the square root of the temperature [2]. In 1860 the renowned Scottish physicist and mathematician, James Clerk Maxwell (1831 -1879) published a paper in which he introduced the idea of a precise velocity distribution of ideal gas molecules corresponding to a particular temperature. This may be depicted by the well-known Maxwell-Boltzmann distribution curve, shown in Figure D.1.

Stellenbosch University https://scholar.sun.ac.za

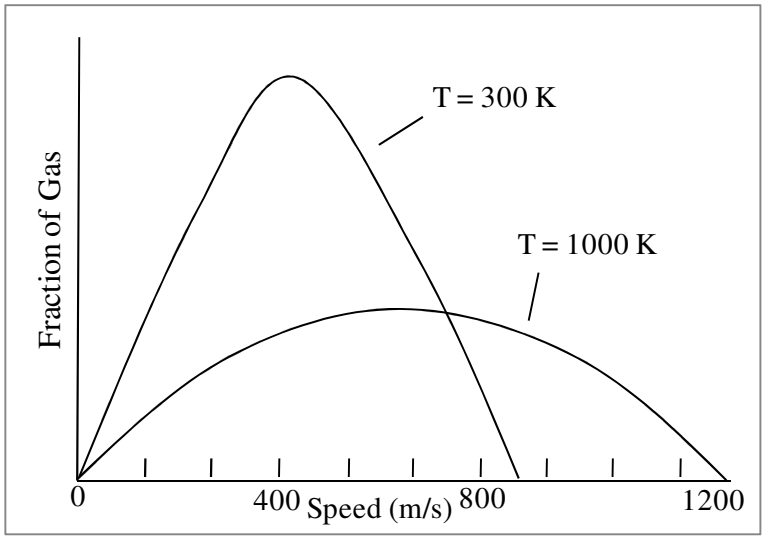

Figure D. 1Maxwell-Boltzmann distribution of O2 molecules at 300 and 1000 K [3]

These curves show that at a given temperature, the distribution of velocitiesof all the gas molecules in a system becomes constant and well defined in terms of the law governing the distribution [3]. The curves further show that the velocities of the molecules of a particular species become dispersed over a larger range as the temperature is increased. These developments therefore showed that temperature of an ideal gas is related to the mean square molecular velocity due to translational motions:

$$T \approx \frac{1}{2} m\overline{\overrightarrow{V^2}} = \overline{e_K^{molecular}} \qquad D.5$$

In the above relation, m is the mass of an individual molecule and $\overline{\overrightarrow{V^2}}$ is the mean square velocity of all the molecules.$\overline{e_K^{molecular}}$ represents the average kinetic energy of the centre-of-mass motion of the molecules due to translation (larger, chain-like molecules will have rotational and vibrational motions that would also contribute to the kinetic energy). By relating temperature to the average molecular kinetic energy of the system, it may be seen that the temperature of system is independent of the chemical nature of the particular substance in the system for an ideal gas. On average, heavier molecules will move more slowly while lighter atoms will have greater velocity, but as long as the average kinetic energy remains constant, the measured temperature is the same and does not depend on any other distinction between the molecules.

A further implication of this finding is that an absolute temperature scale may be established whereby a temperature of absolute zero corresponds to a state with zero kinetic energy. The Kelvin temperature scale may be defined by the following relation:

Stellenbosch University https://scholar.sun.ac.za

$$\overline{e_K^{molecular}} \equiv \left(\frac{3}{2}\right) kT \qquad D.6$$

The proportionality constant is defined as 3/2 times the value of Boltzmann's constant, (k = 1.38 x 10^{-23} [Joule / (molecule Kelvin)]), thereby defining the Kelvin temperature scale. It may also be noted that temperature is defined per molecule, so it does not depend on the size of the system, making it an inherently intensive property [3].

In the view of kinetic theory, pressure is the normal force per unit area exerted by a substance on the physical boundary which defines the system [3]. If a traditional piston-cylinder set-up is visualized, the pressure which the molecules exert on the surface area, A_s, of the piston may be given by the following equation:

$$P = \frac{1}{A_s}\sum_{i=1}^{N}\left[\frac{d(m\vec{V}_z)}{dt}\right] \qquad D.7$$

Since the force exerted by a particle mass is equal to the time rate of change of its momentum, $m\vec{V}$, the total pressure which the gas exerts on the face of the piston is the sum of the change in the momentum of all the individual atoms. By incorporating the definitions of temperature and pressure as defined by the kinetic theory (Equations D.6 and D.7), the ideal gas law may be derived quite readily [3]. The three main postulates of the kinetic theory of gases are as follows:

Postulate 1: Particle volume: Because the volume of an individual gas particle is so small compared to the volume of its container the gas particles are considered to have mass, but no volume. Particles are modelled as small, hard round spheres.

Postulate 2: Particle motion: Gas particles are in constant, random, straight-line motion except when they collide with each other or with the container walls.

Postulate 3: Particle collisions: Collisions are elastic therefore the total kinetic energy of the particles is constant. These collisions are furthermore the only interaction amongst the particles which do not have any intermolecular forces between them [4].

Althoughthe ideal gas law, with the kinetic theory behind it, could accurately describe many systems at intermediate temperatures and pressures, it was observed that real system behaviour deviated from this relationship at lower temperatures and elevated pressures.

Stellenbosch University https://scholar.sun.ac.za

D.3 Intermolecular forces and potential-energy functions

The observed deviations from ideal behaviour can be attributed to the finite volume occupied by molecules due to the repulsive interactions of their electron clouds, as well as intermolecular forces caused by net charges of ions, or by a permanent polarized charge distribution within a net-neutral molecule. The interactions between these polarized charges are of an electrostatic nature, since they are a permanent characteristic of the molecules involved.

Much like gravitation, the forces between electric charges can be considered to be conservative forces, since they allow us to keep track of the energy of a charge in the electromagnetic force field. This means that when work is done in order to move a a particle against such a force, along a path which starts and ends in the same place, the total work done is zero, irrespective of the path taken. If one imagines dragging a cube across a frictional surface, the work done is highly dependent on the path, because energy is dissipated all along the length of the path, making friction a non-conservative force. Since the work done in moving a particle against a conservative force is independent of the path, the force which a particle experiences is solely dependent on its position relative to the source of the force. A numerical value may therefore be assigned which gives the energy which a particle has solely due to its position in a particular force field. This value is termed the potential energy and may beconceived of as the predicted motion of a particle under the influence of a specific force field. As a particle moves from one position to another the potential energy is merely transferred to kinetic energy, but may be retrieved upon returning to its initial position. Having defined the potential energy for an isolated pair of molecules separated by distance r, $\Gamma(r)$, the force between them can be calculated by the following general expression:

$$F = -\frac{d\Gamma(r)}{dr} \qquad \text{D. 8}$$

By convention, a negative (minus) sign in the potential energy $\Gamma(r)$ indicates attractive forces and a positive (plus) sign indicates repulsive forces [5].

The first empirical insights into the electrostatic forces between charges were made by Priestly (1767), Cavendish (1771) and Coulomb (1784), who observed that all charged bodies interact through an inverse-square force law [6]. These investigations finally culminated into the well-known Coulomb's law, which gives the electrostatic potential energy between two point charges 1 and 2:

$$\Gamma_{12} = \frac{q_1 q_2}{(4\pi\varepsilon_0\varepsilon_r)r} \qquad \text{D. 9}$$

Stellenbosch University https://scholar.sun.ac.za

Where q_1 and q_2 are the charges (units of coulomb C), r is the distance between the charges (m), ε_0 is the dielectric permittivity of vacuum, a constant equal to 8.854 x 10^{-12} (C^2J/m), and ε_r is the dimensionless dielectric constant of the medium. If the length between the bodies carrying these charges is much greater than their respective radii, then the charges are defined as point charges [3]. Figure D.2 shows the "lines of force" between two point charges.

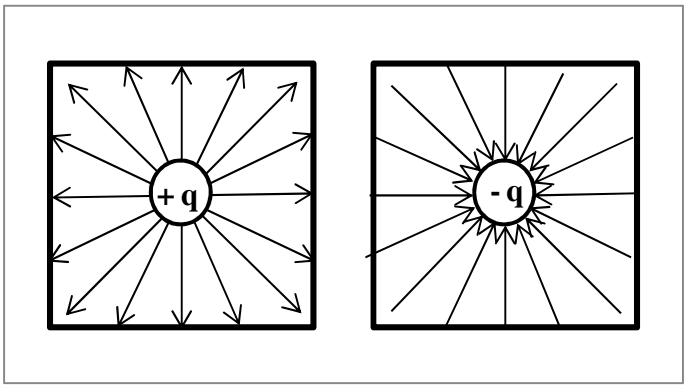

Figure D. 2Electric field lines from positive and negative point charges [3]

The lines point in the direction in which a positive charge (also called a test charge) would move under the influence of the force exerted by a surrounding charge. If the distances between molecules are sufficiently small that the lines affect the bulk system behaviour, then the relationship between pressure, temperature and volume can no longer be predicted by the ideal gas law, whereby molecules are thought to have only kinetic energy, with no other forces between them. These forces naturally become more appreciable at high pressures and low temperatures, where the molecules are closer together and their kinetic energy is lower.

Point charges exert strong forces (typically 100 – 600 kJ/mol) and generally fall off slowly, making the existence of isolated charges in nature quite uncommon, as opposite charges generally combine to form more stable molecules [3, 5]. Some molecular examples include:

- Ionic solids (NaCl crystals)
- Electrolyte solutions and molten salts in media with high dielectric constants (such as water)
- Ionized gases (plasmas)

In addition to being less prevalent, the strong interaction between point charges makes general theories difficult to formulate and these interactions are therefore not discussed further in this text.

Stellenbosch University https://scholar.sun.ac.za

By viewing molecules as *a distribution of charges*, Coulomb's law (Equation D.9) can be generalized to account for the intermolecular forces between net-neutral species with an internal polarized separation of charge, which is much more prevalent in nature than isolated point charges [6]:

$$\Gamma(r) = \frac{1}{(4\pi\varepsilon_0)} \sum_i^A \sum_j^B \frac{q_i q_j}{r_{ij}} \qquad D.10$$

Where q_i is a charge in distribution (molecule) A, q_j is a charge in distribution B, and r_{ij} the distance between the charges. Using this equation as starting point, several contributing mechanisms to intermolecular interactions can be elucidated, each with its own general potential-energy function.

D.3.1 Attractive potential-energy functions

Typical intermolecular forces present in a mixture include:

- Polar forces
- Induction forces
- Dispersion (London) forces

It is noted that only pair-wise interactions amongst different charged molecules are generally considered in defining these intermolecular forces and their potential-energy functions. This assumption of explaining a system in terms of pair-wise interactions, whereby higher order (three and four body) interactions are neglected, is a fundamental assumption from the statistical mechanical derivations of analytical thermodynamic equations. If higher order interactions are to be included, more complex potential functions must be employed.

Polar forces

If a net-neutral molecule can be represented by a region of net-positive charge next to a region of net-negative charge, this molecule can be treated as a dipole [3]. This is depicted in Figure D.3.

Stellenbosch University https://scholar.sun.ac.za

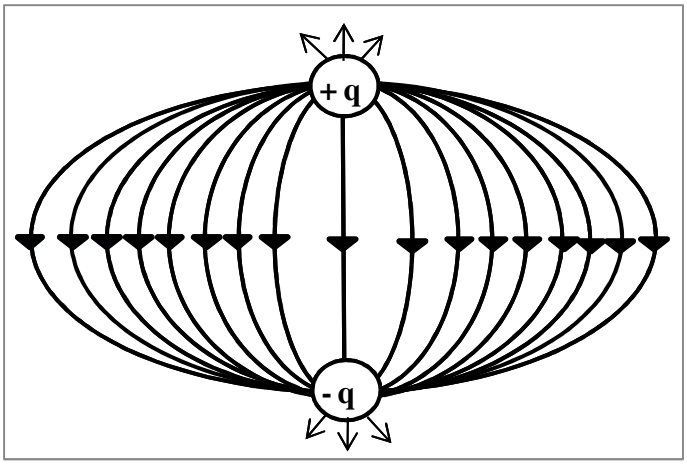

Figure D. 3Lines of force in a dipole interaction between two atoms of a molecule [3]

The dissimilarity of atoms in a dipole molecule results in a non-symmetric distribution of the electron cloud around the molecule, which is determined by the difference in electronegativity of the atoms in the molecule.

From the force lines in Figure D.3it is clear that dipoles may exert forces on surrounding molecules in their vicinity. The size of this force increases with the degree of asymmetry between the atoms in the molecule. This asymmetry may be characterized by a vector quantity, the dipole moment(μ), that points from the negative charge to the positive charge (see Figure D.4).

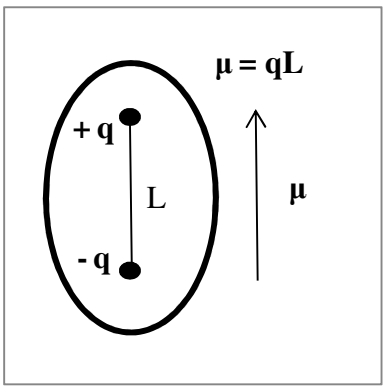

Figure D. 4Portrayal of dipole moment in a dipole interaction

As seen in Figure D.4 the dipole moment is defined as the electric charges q (C) multiplied by the distance between them L (m), although values are commonly reported in units Debye (1 Debye = 3.336 x 10^{-30} Cm)[5]. Molecules with dipole moments greater than 0 are considered *polar molecules*and dipole moments greater than 1 are considered highly polar [5].

Stellenbosch University https://scholar.sun.ac.za

Similarly, if a molecule can be represented by the concentration of charges at four separate points in the molecule, the molecule is regarded as a quadrapole [5]. For a simple linear molecule, the quadrapole moment (Q) is defined as follows:

$$Q = \sum_i \; q_i l_i^2 \qquad \text{D. 11}$$

Again q_i are the charges and l the distance from a defined origin. Molecules like Benzene, nitrogen, CO and CO_2 have appreciable quadrapole moments [5].

The interaction between two dipole molecules is called a dipole-dipole interaction; quadrapoles are engaged in qudrapole-qudrapole interactions and a dipole and quadrapole is engaged in a dipole-quadrapole interaction. In order to calculate the contribution of these interactions to the potential energy of the system from Equation D.10, the charge separation r_{ij} is replaced by the centre-of-mass separation r of the two distributions, and the interaction is statistically averaged over each possible orientation of the molecules, since opposite charges attract and likes repel. In general, molecules prefer the lower energy state offered by attraction whereby opposite charges align; however thermal energy favours randomization of orientation. This trade-off can be quantified by the Boltzmann factor, $(e^{-\frac{\Gamma}{kT}})$, where k is Boltzmann's constant (1.38 x 10^{-23} J/molecule K) [3]. By weighting each orientation by its Boltzmann factor, the following expression for each mentioned interaction may be derived from Equation D.10:

Dipole-dipole interaction:

$$\overline{\Gamma_{12}} = -\frac{1}{3}\frac{\mu_1^2\mu_2^2}{kT(4\pi\varepsilon_0)^2 r^6} \qquad \text{D. 12}$$

Dipole-quadrapole interaction:

$$\overline{\Gamma_{12}} = -\frac{\mu_1^2 Q_2^2}{kT(4\pi\varepsilon_0)^2 r^8} \qquad \text{D. 13}$$

Quadrapole-quadrapole interaction:

$$\overline{\Gamma_{12}} = -\frac{7}{40}\frac{Q_1^2 Q_2^2}{kT(4\pi\varepsilon_0)^2 r^{10}} \qquad \text{D. 14}$$

Stellenbosch University https://scholar.sun.ac.za

It is interesting to note that upon averaging, all of these interactions have negative potentials, resulting in a net-effect of attraction. In a medium other than air or a vacuum, in which the refractive index is in between that of the two molecules, these interactions can be repulsive [5]. These polar interactions are all furthermore directly proportional to the fourth power of the dipole or quadrapole moments and inversely related to the temperature. This implies that the potential energy may be highly sensitivity to small changes in polarity; however these effects diminish as temperature is increased. It can also be seen that the effect of quadrapoles are much less than those of dipoles, due to the relative decrease in the range of these forces: dipoles are proportional to the 6th power of the inverse distance between molecules, whereas quadrapoles are related to the 10th power of the inverse distance, making multi-poles higher than dipoles extremely short range. These higher multi-poles are therefore often assumed negligible, however can be appreciable in special cases.

Induction forces

If a non-polar molecule is in close enough proximity to the electric field of a dipole, then its electrons can become displaced and a dipole can be induced in the non-polar molecule. Following a similar averaging procedure, the potential-energy of such an interaction can be expressed as follows:

$$\overline{\Gamma_{12}} = -\frac{\alpha_1 \mu_2^2}{(4\pi\varepsilon_0)^2 r^6} \qquad \text{D. 15}$$

The parameter α_1 is the polarizability of the non-polar molecule 1 being induced into a dipole by the electric field of the dipole of molecule 2, which is proportional to the square of its dipole moment(μ_2). The polarizability is related to how easily the valence electrons of a molecule can be displaced by an electric field, whereby the more easily an electron may be displaced, the larger the value of α_1 . Electrons are generally more easily from larger molecules, since the electrons in the valence shell are farther away from the attractive nucleus and also shielded by inner electrons. If both molecules involved in an interaction are polar, then the complete expression for the contribution of induction to the potential energy is given as follows:

$$\overline{\Gamma_{ij}} = -\frac{\alpha_1 \mu_2^2 + \alpha_2 \mu_1^2}{(4\pi\varepsilon_0)^2 r^6} \qquad \text{D. 16}$$

Similarly, induction caused by interaction of quadrapoles is given as follows:

Stellenbosch University https://scholar.sun.ac.za

$$\overline{\Gamma_{ij}} = -\frac{3}{2}\frac{\alpha_1 Q_2^2 + \alpha_2 Q_1^2}{(4\pi\varepsilon_0)^2 r^8} \qquad \text{D. 17}$$

It can be noted that these interactions are also attractive and proportional to the 6th power of the inverse distance between molecules for induction by dipoles.

Dispersion (London) Forces

There is another type of intermolecular interaction, namely dispersion forces, which are not related to permanent or induced charge distributions within asymmetric molecules, but rather more instantaneous fluctuations in the electron clouds of any mixture. If it were not for these fluctuations, non-polar molecules would not condense or freeze, as no asymmetries would exist, and thus no intermolecular forces of attraction [3, 5]. The formula for potential energy of dispersion interactions between two symmetric (non-polar) molecules 1 and 2 was developed from quantum mechanics, and given below as finally formulated by London (1930)[6]:

$$\Gamma_{ij} \approx -\frac{3}{2}\frac{\alpha_1^2\alpha_2^2}{(4\pi\varepsilon_0)^2 r^6}\left(\frac{I_1 I_2}{I_1 + I_2}\right) \qquad \text{D. 18}$$

I, is the first ionization potential, which is the energy required to displace the first electron from the valence electron cloud of the species. It can further be expected that dispersion forces are greater for larger molecules with greater polarizability, just as was the case for induction forces. Even though Equation D.18 was derived for symmetric molecules, these forces are universal to all molecules.

General comments

The specific polar and induction forces, as well as the universal dispersion forces have become known as the *Van der Waals forces*. They are all attractive and of the following general form:

$$\Gamma_{ij} = -\frac{C_a}{r^m} \qquad \text{D. 19}$$

Where C_a is a constant proportional to the size of the attractive forces (generally in the 1kJ/mol range) and m = 6since the potential varies inversely to the 6th power of the distance for dipoles. As mentioned dispersion forces are always present and furthermore dominate the Van der Waals forces except for small, highly polar molecules (like water and methanol). Induction forces are typically below 7%, even for highly polar molecules, while dipolar and

Stellenbosch University https://scholar.sun.ac.za

higher multi-pole forces are only significant for molecules with dipole moments greater than 1 [5,6].

Although Equation D.19 is a good general expression, it fails to distinguish between the different dependencies of dispersion and the various polar forces on inter-particle distance, as well as their relative magnitude and temperature dependence.

D.3.2 Repulsive potential functions

According to the kinetic theory of gases, particles were considered to be small, round hard spheres, however were assumed to occupy no volume. Despite this assumption Newton and others recognized that repulsive forces must exist at short distances due to the incompressibility of dense fluids and materials [6]. Considering the potential-energy of hard-sphere repulsion, molecules can be modelled as billiard balls with diameter σ which only repel once the diameters touch ($r \leq \sigma$), at which point the potential energy jumps to infinity [3]:

$$\Gamma = \begin{cases} 0 & \text{for } r > \sigma \\ \infty & \text{for } r \leq \sigma \end{cases} \qquad \text{D. 20}$$

The potential is plotted in Figure D.5.

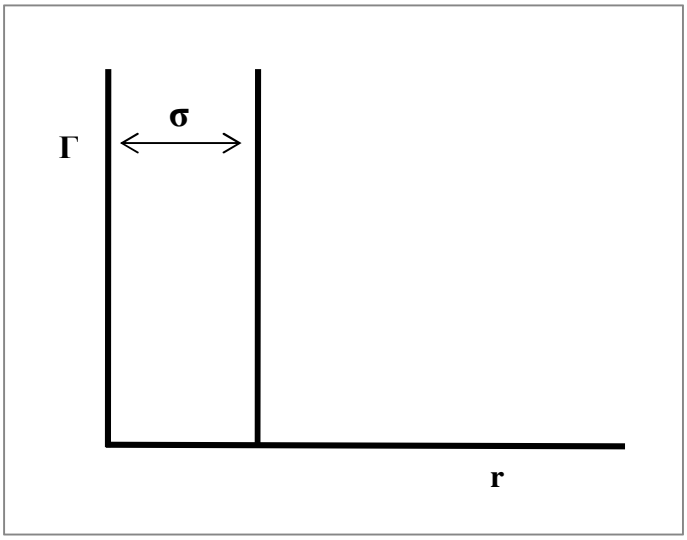

Figure D. 5 Hard-sphere potential-energy function

In reality, atoms and molecules are not hard spheres with rigid borders and fixed diameters, but are bound by diffuse electron clouds in rapid motion. This view was already incorporated

Stellenbosch University https://scholar.sun.ac.za

by Maxwell as soon as 1867, who found that treating molecules as spherical hard cores fails to describe the diffusion of gases [6]. Maxwell therefore postulated a pair-wise repulsive force inversely proportional to a power n of separation between their centres of mass:

$$\Gamma_{ij} = \frac{(C_r)}{r^n} \qquad \text{D. 21}$$

The constant C_r is proportional to the size of the repulsion. Through the study of the viscosity of air at different temperatures, Maxwell obtained a value of 4 for n. In 1903 Mie also used a generic inverse power law of the form of Equation D.20, but found that in order to provide a consistent description for the compressibility of metals, a steeper (n>4) repulsive exponent was required [6].

The precise dependence of repulsive forces on inter-particle distance is still not nearly as well understood as those of the attractive interactions; however the advent of quantum mechanics and the Pauli Exclusion Principle seems to suggest that these interactions depend exponentially on position. An inverse power function of the form of Equation D.21 still remains the most convenient for practical applications [3].

D.3.4 Combined potential functions

According to Lafitte et al. [6], Grüneisen, in his study of metallic systems, was the first to explicitly publish a fully generic expression for the potential-energy function, combining Equations D.19 and D.21 for both repulsive and attractive interactions:

$$\Gamma_{ij} = \frac{(C_r)}{r^n} + \frac{(C_a)}{r^m} \qquad \text{D. 22}$$

Some full potential-energy functions derived from this expression are listed below. The number in brackets refers to the number of molecular parameters used:

- Lennard Jones potential (2)
- Mie potential (4)
- Kihara potential (3)
- Square-well potential (3)
- Sutherland potential (2)

It should be noted that all of these functions consider the pair potential-energy functions as function of solely the distance of separation between the molecules and not their orientation,

Stellenbosch University https://scholar.sun.ac.za

which can be a significant limitation for complex systems. This weakness becomes apparent in the fact that molecular parameters of a species, which should be invariant for different properties, differ with respect to the properties they are fitted to (virial coefficients and transport properties) and also over the relevant temperature range for the second virial coefficient, even for simple molecules like Argon [5].

Lennard Jones potential

The most widely applied form of this general potential function is the Lennard-Jones potential, which selects the power of the distance dependence of the repulsive interaction to be n = 12 and that of the attractive interaction to be m = 6 (as corresponds to London's theory (equation (18)) and the Van der Waals forces):

$$\Gamma = 4\varepsilon\left[\left(\frac{\sigma}{r}\right)^{12} - \left(\frac{\sigma}{r}\right)^{6}\right] \qquad \text{D. 23}$$

Where the following values have been substituted into Equation D.22:

$C_r = 4\varepsilon\sigma^{12}$ and $C_a = 4\varepsilon\sigma^{6}$

These values were selected due to their empirical success, rather than rigorous theoretical derivation. The molecular parameters ε and σ are called the *well depth* and *collision diameter* respectively and are related to the potential energy magnitude at equilibrium due to the attractive interaction and the distance between molecules at which $\Gamma = 0$, respectively [7]. The parameters may be physically understood by a plot of this potential function, as shown in Figure D.6.

Stellenbosch University https://scholar.sun.ac.za

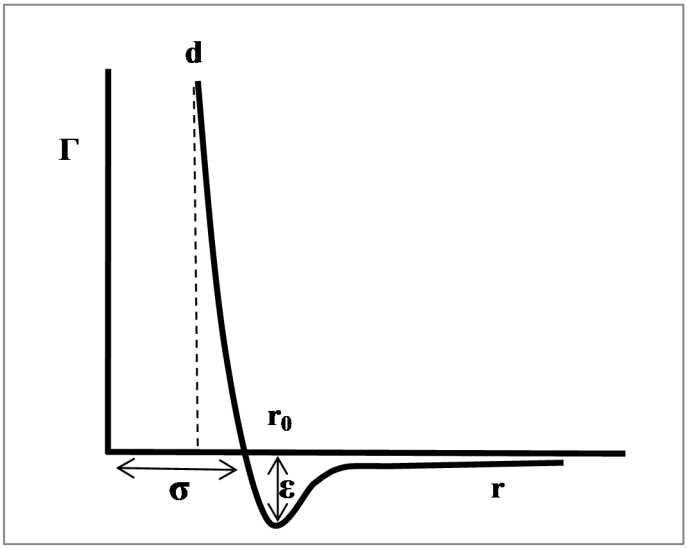

Figure D. 6 Lennard-Jones potential energy function

The *hard core diameter* d is a measure of the centre-to-centre separation for which the potential energy becomes infinite and can also be used as a third modelling parameter in some potential-energy functions; however the Lennard-Jones potential neglects this parameter, allowing for full penetration of the electron clouds [5]. r_0 is referred to as the *equilibrium separation* [7].

Mie potential

Despite the popularity of the Lennard-Jones potential, especially for simpler non-polar molecules, many researchers find value in using a more generic expression given the empirical nature of potential-energy functions and the general lack of theoretical understanding in repulsive and polar forces. The Mie potential energy function provides such a generic expression, allowing for explicit expression of repulsive interactions of varying softness/hardness and any appropriate power law for attraction by varying parameters and m and n, respectively:

$$\Gamma = \frac{m}{m-n}\left(\frac{m}{n}\right)^{\frac{n}{m-n}} \varepsilon \left[\left(\frac{\sigma}{r}\right)^{m} - \left(\frac{\sigma}{r}\right)^{n}\right] \qquad \text{D. 24}$$

Kihara potential-energy function:

The Kihara potential is a 3 parameter potential function which represents molecules as having a hard core, surrounded by a soft penetrable cloud and offers improved results over the 2 parameter functions.

Stellenbosch University https://scholar.sun.ac.za

$$\Gamma = \begin{cases} 4\varepsilon\left[\left(\frac{\sigma-2d}{r-2d}\right)^{12} - \left(\frac{\sigma-2d}{r-2d}\right)^{6}\right] & \text{for } r \geq 2d \\ \infty & \text{for } r < 2d \end{cases} \qquad \text{D. 25}$$

The d parameter represents the impenetrable spherical core of the molecules as represented in Figure D.6.

Square-well potential-energy function:

Another popular potential function is the square-well potential function, which combines a hard-sphere repulsive potential with a square-well attractive contribution and is shown in Figure D.7.

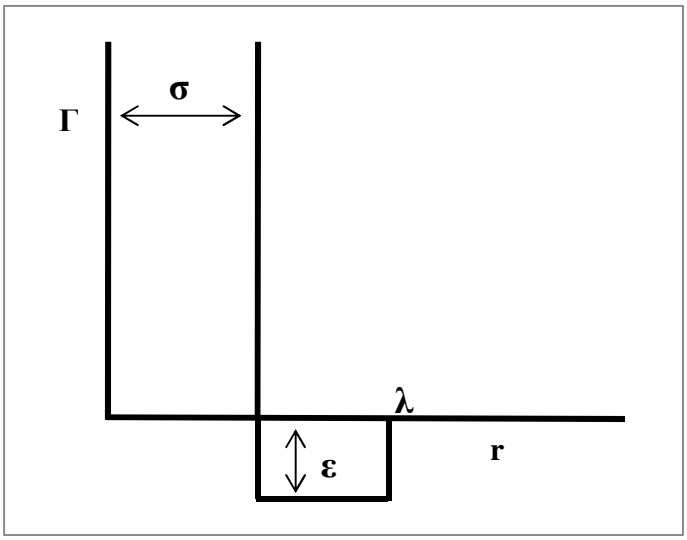

Figure D. 7 Square-well potential energy function

The energy parameter εrepresents the well depth,σ is the hard-sphere diameter and λ controls the width of the well and generally varies between 1.5 and 2. The function is given as follows:

$$\Gamma = \begin{cases} \infty & \text{for } r \leq \sigma \\ -\varepsilon & \text{for } \sigma < r < \lambda\sigma \\ 0 & \text{for } r > \lambda\sigma \end{cases} \qquad \text{D. 26}$$

The Lennard-Jones, Mie and Kihara potential functions provide a much more realistic molecular representation than the square well potential, however practical applications generally involve integration of these expressions, which must be done numerically or by series techniques [7]. The rectilinear form of the square-well potential allows closed-form

Stellenbosch University https://scholar.sun.ac.za

analytical expression to be obtained, while still providing a reasonably sound molecular representation.

Sutherland potential

The Sutherland potential energy function combines a hard-sphere repulsive potential with a Van der Waals attraction and is shown in Figure D.8.

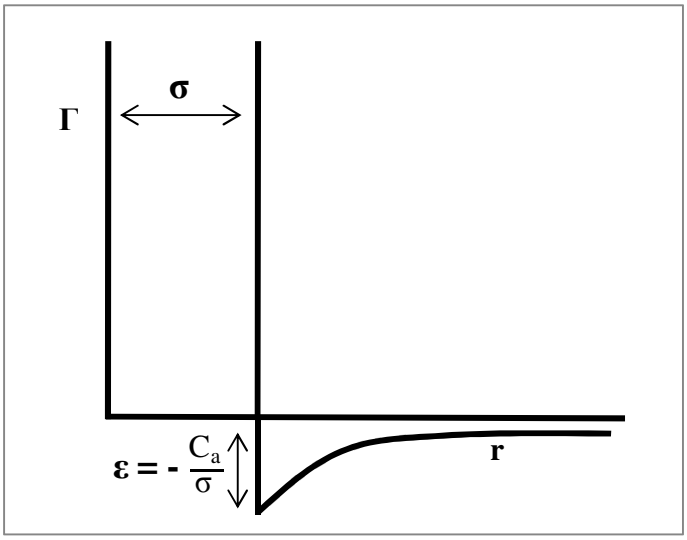

Figure D. 8 The Sutherland potential energy function

$$\Gamma = \begin{cases} -\frac{C_a}{r^6} & \text{for } r > \sigma \\ \infty & \text{for } r \leq \sigma \end{cases} \qquad \text{D. 27}$$

D.3.5 Quasi-chemical forces

In addition to the Van der Waals intermolecular forces, it is further the case that certain systems may exhibit unique quasi-chemical forces with a different magnitude and dependence on distance than the Van der Waals forces. These include hydrogen bonds and acid-base complexes [5].

These interactions are known as quasi-chemical forces because unlike the intermolecular forces discussed so far, in which molecules maintain their physical identity, these forces lead to the formation of weak complexes with a unique chemical identity [7]. Such complexes include:

Stellenbosch University https://scholar.sun.ac.za

- Dimers (from organic acids)
- Linear or cyclic oligemers (from alcohols and phenols)
- Hexamers (from hydrogen floride)
- Three dimensional networks (water) [5]

Due to its greater prevalence in thermodynamic systems, this text focuses exclusively on hydrogen bonds. These bonds form between an electronegative atom (F, O or N atoms) of a molecule and the hydrogen atom of another molecule, also bonded to an electronegative atom [3]. This is illustrated in Figure D.9, depicting two water molecules where the O atom is highly electronegative (3.5 on the Pauling scale):

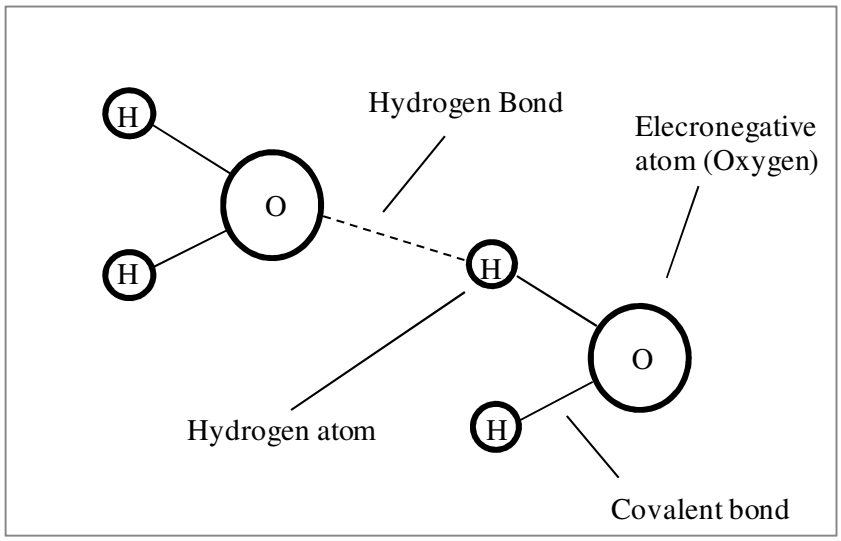

Figure D. 9Hydrogen bond between two water molecules in solution

Hydrogen bonds are approximately two orders of magnitude larger than the Van der Waals forces (typically around 3 - 40 kJ/mol), but one order of magnitude smaller than covalent bonds. These bonds lead to three main types of behaviour which may influence the thermodynamic properties, namely:

1) Intermolecular self-association (bonding between different molecules of same type):
$A + A \leftrightarrow A^2$

2) Intramolecular self-association (bonding between different atoms in the same molecule)

3) Cross-association or solvation (bonding between different types of molecules):

Stellenbosch University https://scholar.sun.ac.za

$$A + B \leftrightarrow AB$$

The influence of these cases on system behaviour can be elucidated by visualizing a binary mixture of species A and B in vapour-liquid equilibrium:

Case 1) Self-association of a species A causes the formation of dimers (A^2) in the liquid phase, which can be seen as a distinct chemical species and is generally less volatile due to its increased mass. This causes an increase in the asymmetry of the mixture, which allows more of the volatile component B to escape into the vapour phase, leading to an increase in the system pressure, relative to the case of no association (positive deviation from Raoult's law) [3].

Case 2) Intramolecular-association of molecules causes a change in their structure which may influence their intermolecular interactions via Van der Waals forces.

Case 3) Cross-association causes formation of dimers (AB), which depletes the relative amounts of A and B in the liquid. This causes condensation of A and B from the vapour phase, which leads to lower system pressures (negative deviation from Raoult's law)

These effects are typically observed in systems containing water, alcohols, organic acids, amines, glycols as well as bio-molecules and polymers [5].

The Hydrophobic effect

In addition to the mentioned effects, there is an additional effect known as the *hydrophobic effect*. This occurs when non-polar molecules are added to water, which consists of a strong extensive network of hydrogen bonds. This forces the hydrogen bond network to become even more structured, leading to a higher degree of local order than for pure water. This in turn forces the polar molecules to aggregate, forcing a stronger attraction between them than predicted by the Van der Waals forces. This is known as the hydrophobic interaction [5].

D.4 The Van der Waals equation of state

This section takes a brief look at how the Van der Waals equation of state was developed by modifying the basic structure of the ideal gas law in order to account for the proper volume of the particles (repulsive forces) and intermolecular forces (attractive forces).

In a Nobel Lecture by Van der Waals in 1910, it is mentioned what a profound influence the revival of kinetic theory by the work of Clausius, Maxwell and Boltzman had on the

Stellenbosch University https://scholar.sun.ac.za

development of his equation in 1873. Van der Waals's insight was to realize that if ideal gases may be considered material points in constant motion, then this must certainly still be true at reduced volumes. Van der Waals thus realized that despite the large macroscopic differences between liquid and gas phases, a liquid may simply be seen as a compressed gas at low temperatures and that the factors which influence the deviations from ideal gas behaviour are always present, but merely has quantitative differences as the density and temperature changes. Van der Waals named this concept "continuity" and it is this reasoning which led him to postulate that if the system may be corrected for the pressure and volume differences, then it should still obey the general form of the ideal gas law.

In developing his equation, Van der Waals used as a starting point the virial theorem, an expression published by Clausius in 1870 in a paper entitled "On a Mechanical Theorem Applicable to Heat". The theorem relates the the internal and external forces acting on a system of particles (a term Clausius defined as "the virial") to the average kinetic energy of a system [8]. Being acutely aware of the simplifying assumptions of kinetic theory and the ideal gas model, Van der Waals replaced the virial term by an effective pressure term, incorporating two parameters a and b to account for intermolecular forces and the proper volume occupied by molecules, respectively. By further assuming the average kinetic energy to be equal to Equation D.6, shown to only be valid for one mole of an ideal gas, he arrived at his seminal equation:

$$P = \frac{RT}{v-b} - \frac{a}{v^2} \qquad D.28$$

The form of the attractive term was determined largely through intuitive reasoning, by which intermolecular forces cause fewer collisions with the system boundary (lowering the pressure), and further diminish as the molecular volume increases. Similarly, the b parameter decreases the mean free path between molecules, leading to more collisions (increasing the pressure).

The next step in defining the Van der Waals equation was to relate the parameters a and b to the particular system. In his 1910 Nobel lecture, Van der Waals remarks that he expected to find that the appropriate value for the size parameters b would simply be the total volume of all the molecules [2]. The volume occupied by one mole of molecules would then be given by the following expression:

$$b = \frac{\pi\sigma^3}{6} \times N_A \qquad D.29$$

Stellenbosch University https://scholar.sun.ac.za

N_A is Avogadro's number. Van der Waals observed; however, that this did not give accurate results. The manner in which the value for b was eventually determined was by calculating the excluded volume of two particles and summing this value over all pairs of molecules [3]. The excluded volume is defined as the volume of sphere of which the radius is equal to the diameter of one molecule, as shown in Figure D.10.

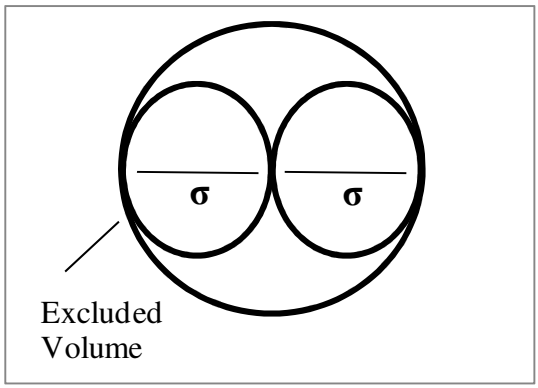

Figure D. 10 Excluded volume of two molecules

The value of the excluded volume of two molecules could therefore be calculated as follows:

$$b = \frac{\pi(2\sigma)^3}{6} = \frac{4\pi\sigma^3}{3} \qquad \text{D. 30}$$

Since one such excluded volume is comprised of two molecules, the final value for total volume to be excluded from the ideal gas volume term for one mole of a species can be calculated. This value is commonly referred to as the "co-volume" and is given as follows:

$$b = \frac{4\pi\sigma^3}{3} x \frac{N_A}{2} = \frac{2\pi\sigma^3}{3} x\, N_A \qquad \text{D. 31}$$

It may be noted that this value is 4 times larger than the total molecular volume initially anticipated by Van der Waals and given by Equation D.29. The molecules therefore not only occupy appreciable volume, but occupy more than is to be anticipated from just accounting for their individual sizes.

The value for the energy parameter a may be determined in terms of molecular considerations by integrating a particular potential function. It is clear from Figure D.10 that Van der Waals assumed particles to be small hard spheres with rigid boundaries The overall potential function which can therefore be integrated to represent a Van der Waals fluid is that of Sutherland (Equation D.27), since the attractive forces are considered proportional to the 6^{th}

Stellenbosch University https://scholar.sun.ac.za

power of the inverse distance between molecules ($C_a \approx \frac{1}{r^6}$), which is proportional to the square of the molar volume($v^2 \approx r^6$) which is used as the denominator for a in the Van der Waals equation. The value for a obtained when integrating the Sutherland potential is therefore given as follows [3]:

$$a = \frac{2\pi N_A^2 C_6}{3\sigma^3} \qquad \text{D. 32}$$

The parameters a and b are not generally used in their molecular form but rather fitted to data as purely empirical parameters or estimated from critical properties of a substance using a technique called the *principle of corresponding states.*

D.4.1 The principle of corresponding states

Van der Waals adopted a clever way of determining model parameters in a semi-theoretical fashion when data is not available. This technique follows from the recognition that the critical point of a substance represents a unique state for each molecule, characteristic of its intermolecular forces. In a paper from 1880, Van der Waals reasoned that even though the EOS relation of P to v at constant T is different for each substance, they are related to the critical properties in a universal way. By dividing these values by their corresponding critical value (introducing "reduced" variables), they should obey a general universal function for the following form:

$$F\left(\frac{T}{T_c}, \frac{P}{P_c}, \frac{v}{v_c}\right) = 0 \qquad \text{D. 33}$$

Substances with the same reduced properties are said to be in *of corresponding states*, since they are deemed to have the same deviations from ideality (ie. the same compressibility factor).The *principle of corresponding states.*is even more general than the Van der Waals equation of state and regarded by many as perhaps a greater, if not equal contributionto physical science than the Van der Waals Equation [9].

Van der Waals obtained an expression of the form of Equation D.29 by applying the following known condition for the critical point, namely an inflection point in the critical isotherm:

$$\left(\frac{\partial P}{\partial v}\right)_{T_c} = \left(\frac{\partial^2 P}{\partial v^2}\right)_{T_c} = 0 \qquad \text{D. 34}$$

Stellenbosch University https://scholar.sun.ac.za

By taking the Van der Waals equation at the critical point:

$$P_c = \frac{RT_c}{v_c - b} - \frac{a}{{v_c}^2} \qquad \text{D. 35}$$

and getting an expression for the first and second derivative according to Equation D.30, the two parameters a and b may be solved simultaneously in terms of critical temperature and volume:

$$a = \frac{9}{8} v_c RT_c \qquad \text{D. 36}$$

$$b = \frac{v_c}{3} \qquad \text{D. 37}$$

If these expressions are substituted back into the original Van der Waals equation, the parameters may be expressed as constants, in terms of critical temperature and pressure:

$$a = \frac{27}{64} \frac{(RT_c)^2}{P_c} \qquad \text{D. 38}$$

$$b = \frac{RT_c}{8P_c} \qquad \text{D. 39}$$

Substituting these expressions back into the original form of the Van der Waals equation as *a reference fluid* EOS, the equation may be rearranged in terms of reduced variables:

$$\frac{P}{P_c} = P_r = \frac{8\left(\frac{T}{T_c}\right)}{3\left(\frac{v}{v_c}\right) - 1} - \frac{3}{\left(\frac{v}{v_c}\right)^2} = \frac{8T_r}{3v_r - 1} - \frac{3}{{v_r}^2} \qquad \text{D. 40}$$

Although the property values obtained from fixing a and b to data values will ultimately be more accurate, the expression given above is of the form of Equation D.29 and therefore provides a universal function for reduced pressure in terms of reduced volume and temperature which are properties which are known and readily obtained for most species.

The expression in Equation D.36 can be regarded as a 2 parameter corresponding states model, since reduced pressure is a function of only reduced temperature and reduced volume:

$$P_r = F(T_r, v_r) \qquad \text{D. 41}$$

Stellenbosch University https://scholar.sun.ac.za

Unfortunately this formulation does not provide a universal function as Van der Waals hoped, but can only distinguish between non-polar molecules for which molecular interactions scale reliably with size. In order to distinguish between additional molecular characteristics, such as moment of inertia, radius of gyration, polar effects and chemical reactivity, other dimensionless *scale factors* need to be considered to group the molecules into classes within which they can be scaled more reliably[10]:

$$F\left(\frac{T}{T_c}, \frac{P}{P_c}, \frac{v}{v_c}, w_1, w_2 \ldots\right) = 0 \qquad \text{D. 42}$$

The most widely used additional parameter is the Pitzer acentric factor ω, and is defined as follows [10]:

$$\omega = -1 - \log\left[\frac{P_{sat}(T_r=0.7)}{P_c}\right] \qquad \text{D. 43}$$

This parameter uses the reduced vapour pressure at $T_r = 0.7$, to distinguish between substances and characterizes how non-spherical a molecule is [3]. Although greatly improving results, this parameter still does not distinguish between largely polar substances. As mentioned, the *principle of corresponding states* has found much wider application than its humble beginnings in the work of Van der Waals. A good review of the range of these applications is given by Ely [11].

D.4.2 VLE from the Van der Waals equation

Figure D.11 depicts isotherms plotted on a PV diagram of the pressure as predicted by the Van der Waals law for a pure component.

Stellenbosch University https://scholar.sun.ac.za

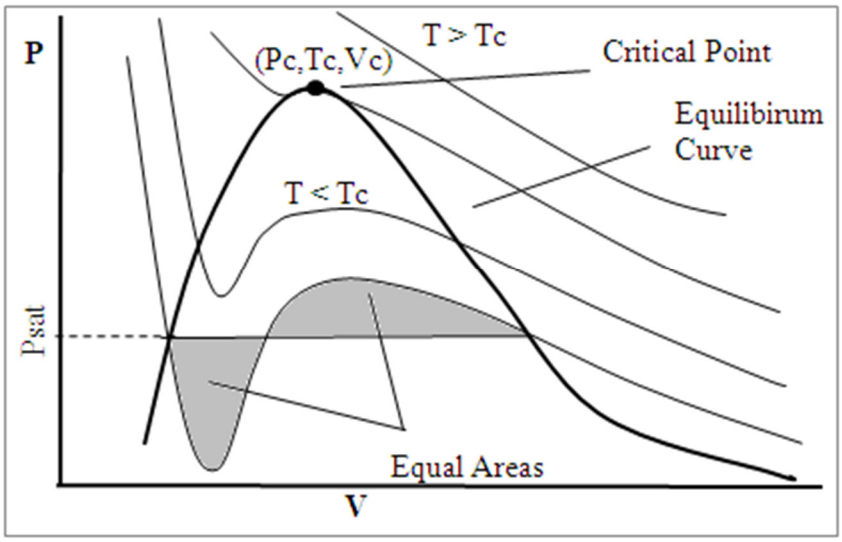

Figure D. 11PV behaviour of the Van der Waals equation for a pure component

If the Van der Waals equation is expanded, it may be seen that there are three roots for the volume:

$$Pv^3 - (RT + Pb)v^2 + av - ab = 0 \qquad \text{D. 44}$$

Figure D.11 is useful for understanding how the three roots generated from this equation of state may qualitatively describe the thermodynamic state of the system at a given equilibrium pressure along different isotherms. This is done by relating the obtained roots to the pure component vapour-liquid equilibrium curve for a real system, which is also depicted by the bolder bell-shaped curve. The critical isotherm is characterized by an inflection point (P_c,T_c, v_c) at the maximum equilibrium pressure on the bell curve (see Equation D.30). It can be seen that for temperatures below the critical temperature ($T < T_c$) the model predicts three real roots. The middle root obeys the following condition: $\frac{dP}{dV} > 0$. This root is thermodynamically unstable and at constant temperature the volume will always decrease as the pressure increases, making it un-physical [3]. The two remaining roots may be taken to represent the specific volume of the saturated liquid (smaller root) and the saturated vapour (larger root). Above the critical point there is only one positive real root, with the two other having either negative or imaginary values. This root represents the specific volume of the supercritical phase, and varies continuously between vapour- and liquid-like densities.

In reality the isotherm is horizontal in the two phase region (constant pressure), however this discontinuity has not yet been accounted for by any models to date [3]. According to Maxwell's equal area rule, however the saturation pressure P_{sat} for a given temperature may

Stellenbosch University https://scholar.sun.ac.za

be determined from an equation of state by locating the P value at which the isobar equally divides the area between the equation of state curve above and below the isobar, also depicted in Figure D.11 [10]. This calculation allowed the Van der Waals equation to predict VLE properties of a substance, making it the first equation to account for the properties of both phases of matter from a unified framework.

D.4.3 The critical compressibility factor (Z_c)

Equations of state are often represented in the form of a dimensionless parameter called the compressibility factor which is given as follows:

$$Z = \frac{Pv}{RT} \qquad D.45$$

It can be seen that the value for the compressibility factor is 1 for an ideal gas. Since the pressure is lower in real systems due to the net attractive forces involved, compressibility factors generally have values less than 1 for real system, although this value may exceed 1 at temperatures and pressures substantially larger than the critical values. The compressibility at the critical point Z_c, is of particular interest because it defines the deviation of a particular substance from ideal behaviour in terms of its unique critical properties.

By combining Equations D.34 and D.35 to solve for the critical compressibility factor of the Van der Waals equation, it can be seen that this model predicts a constant Z_c for all species.

$$Z_c = \frac{P_c v_c}{RT_c} = \frac{3}{8} = 0.375 \qquad D.46$$

Experimental values for the compressibility factor at the critical point generally range between 0.24 and 0.29 for most substances.The accuracy of a particular EOS is often qualitatively estimated by how well it predicts this value, however a close correlation to the experimental value does not necessarily imply better model performance. Given the many gaps in theoretical understanding, fitting data to reproduce experimental values for the critical compressibility may reduce the accuracy in predicting the rest of the general phase space, many regions of which are often of more practical importance than the critical point. The large value obtained from the Van der Waals equation nevertheless emphasizes the empirical nature of the Van der Waals model and its limitations in accurately predicting the PVT behaviour of fluids [3]. The insights of Van der Waals presented in this section, despite their limitations, had a determining influence on the subsequent development of thermodynamic

Stellenbosch University https://scholar.sun.ac.za

models. The modern cubic EOSs are perhaps still the most widely applied, and are all derived from the basic ideas and structure of the Van der Waals equation.

D.5 Molecular models and perturbation theory

For more complex systems, such as those that associate or contain chained and polar molecules, a more theoretically rigorous approach needs to be developed. This section provides a general introduction to the class of thermodynamic models which can be referred to as "molecular models." These models are generally developed from statistical mechanics, which derives macroscopic system properties such as temperature, pressure etc. from the motions and interactions of molecules, by incorporating a probabilistic framework of distribution functions. Statistical mechanics is a vast field and only a brief introduction is given to how this framework is generally used as a starting point for developing equations of sate.

D.5.1 The Boltzmann Distribution

James Maxwell was able to demonstrate how a specific temperature was related to a fixed distribution for the translational kinetic energy of the molecules in a system (Figure D.1).The advent of quantum mechanics showed however that energy is not distributed continuously among molecular motions and interactions, but that the relationship between energy and motion on the molecular scale is a discrete function where molecules have quantifiable jumps between molecular *energy levels.* A more general distribution function could therefore be derived which gives not only the fraction of molecules at a specific kinetic energy due to translational velocity for a given overall temperature (Figure D.1) but gives the most probable fraction of molecules per *energy level*, due to translational, rotational and vibrational motions, as well as electronic, nuclear and interaction energy effects, given a specific total energy of the system [12].

This distribution function is known as the Boltzmann distribution and may be given as follows [12]:

$$\frac{N_j}{N} = \frac{p_j \exp\left(-\frac{\varepsilon_j}{kT}\right)}{\sum_j p_j \exp\left(-\frac{\varepsilon_j}{kT}\right)} \qquad \text{D. 47}$$

Where j is the specific *energy level*, N_j is number of molecules at a specific discrete *energy level*, ε_j, and k is the Boltzmann constant (see Equation D.6). p_j is known as the degeneracy of the *energy level* and represents the number of possible*energy states*(arrangement of

Stellenbosch University https://scholar.sun.ac.za

molecules) within that *energy level*, having a value ofε_j. N is the total number of molecules in the system, over all the various *energy levels*[12].

D.5.2 The Partition function

The denominator of Equation D.47 which serves as the normalizing function in the overall energy distribution is known as the *molecular partition function*, q (also called the *single particle partition function)*:

$$q = \sum_j p_j \exp\left(-\frac{\varepsilon_j}{kT}\right) \qquad \text{D. 48}$$

The *total partition function* of a particular system is merely the product of all the individual *molecular partition functions*,q^N and contains all of the thermodynamic information of a particular system [12, 13]. Since the description of a system depends on the independent variables that are chosen, different types of partition function exist. For a closed isothermal system, with N,V and T taken as the independent variables, the total partition function is known as the *canonical partition function* and may be given as follows [13]:

$$Q(N,V,T) = \frac{1}{N!}q^N = \frac{1}{N!}\sum_i \exp\left(-\frac{\varepsilon_{i\,(N,V)}}{kT}\right)^N \qquad \text{D. 49}$$

The $\frac{1}{N!}$ term is included to show that the molecules in the system must be statistically indistinguishable [12]. It may be noted that in Equation D.49 the degeneracy term has been removed from equation D.48 and the summation is done over all quantum *energy states*i within each *energy level.*ε_i is thus the energy of the ith *quantum state*, and the summation is over all *states* of the molecules consistent with a given macroscopic N and V [13]. It may also be noted that the overall energy of a molecule can be separated into different types of energy which each contribute to the overall partition function individually:

$$Q(N,V,T) = \frac{1}{N!}\sum_i \exp\left(-\frac{(\varepsilon_{trans} + \varepsilon_{rot} + \varepsilon_{vib} + \varepsilon_{elec} + \varepsilon_{nucl})}{kT}\right)^N$$
$$= \frac{1}{N!}q_{trans}^N q_{rot}^N q_{vib}^N q_{elec}^N q_{nucl}^N \qquad \text{D. 50}$$

The translational molecular partition function for ideal gas molecules has been shown to have the following value [12]:

Stellenbosch University https://scholar.sun.ac.za

$$q_{trans} = \left(\frac{V}{\Lambda^3}\right) \qquad D.51$$

WhereΛ is the *De Broglie wavelength* and is a function of temperature and the mass of the particle and contains both the Boltzmann and Planc's constant [12]:

For real fluid systems an additional contribution must be added to the partition function to account for the intermolecular forces and for the true volume of the system particles.

For *small, spherical molecules*, the energies of translation, rotation and vibration etc. are separable from the contribution of intermolecular forces and the partition function can be written in the following form [13]:

$$Q(N,V,T) = \frac{1}{N!}\frac{1}{\Lambda^{3N}} q_{rot}^N q_{vib}^N q_{elec}^N q_{nucl}^N \mathbf{Z_{config}}(\mathbf{N},\mathbf{V},\mathbf{T})$$

$$= \frac{q(T)^N}{N!}\mathbf{Z_{config}}(\mathbf{N},\mathbf{V},\mathbf{T}) \qquad D.52$$

$q(T)$ is the *molecular partition function*due to all effects except the intermolecular forces and is only a function of temperature [13]. Z_{config} is called the *configurational integral* and accounts for all intermolecular forces and contains all of the volume dependent properties of the system. It is determined by integrating the Boltzmann factor $\left(e^{-\frac{\Gamma(r)}{kT}}\right)$over all locations of the particles:

$$Z_{config}(N,V,T) = \int \ldots \int e^{-\left(\frac{\Gamma(r_1,r_2,\ldots r_n)}{kT}\right)} dr_1 dr_2 dr_3 \qquad D.53$$

Once the partition function for a particular system has been defined, the macroscopic properties of a system may readily be derived. In particular the Helmholtz free energy (A) and the system pressure (P) are generally of interest [13]:

$$A(N,V,T) = -kT\,\ln Q(N,V,T) \qquad D.54$$

$$P(N,V,T) = kT\left(\frac{\partial \ln Q}{\partial V}\right)_{T,N} = -\left(\frac{\partial A}{\partial V}\right)_{T,N} \qquad D.55$$

As shown by Equation D.55, the pressure explicit EOS is obtained from the partial derivative of the canonical partition function in terms of volume, and is thus only a function of Z_{config}, since it contains all the volume dependent information for the system [12,13].

Stellenbosch University https://scholar.sun.ac.za

D.5.3 The Radial Distribution Function (Pair correlation function)

As has been mentioned, the *configurational integral*represents the average potential energy of the system, making it not only a function of temperature, but also the term containing the volume dependence of the system. In order to solve the Equation D.53 and D.55 it is generally necessary to make simplifying assumptions about the *configurational integral*. A fundamental simplifying assumption is that of *pair-wise additivity*, which approximates the total potential energy of the system as additive between pairs of molecules such as given by traditional potential-energy functions discussed in Section D.3.4. If this approximation is made (which loses accuracy at high densities), it can be shown that the average intermolecular potential energy of the entire system can be given as follows [14]:

$$\bar{\Gamma} = \frac{N^2}{2V}\int \Gamma(r)g(r)4\pi r^2\, dr \qquad D.56$$

An important function which emerges from this averaging procedure is the *radial distribution function* (RDF), g(r), which contains all the density dependent information of the system, involving the arrangement or distribution of the molecules in a fluid [12]. The RDF is defined in relation to the probability of finding the centre of a molecule at a given distance r from the centre of another molecule. The RDF is generally normalized so that $g(r) \to 0$ as $r \to 0$ and$g(r) \to 1$ as $r \to \infty$, therefore representing the factor by which the local density at some radial distance r from a central molecule deviates from the average bulk density of 1, to which the RDF converges as the extent of the system increases [12]. g(r) = 1 is also the limiting condition taken in the one-fluid approximation, where the fluid is viewed as having a homogonous structure with no local density variations from the mean bulk density. In a real fluid the local density may therefore fluctuate above or below a RDF value of 1 as r increases. For a Lennard-Jones fluid, a strong first peak is observed in the RDF, which corresponds to the interaction potential minimum. At low densities the function falls-off of smoothly towards 1, however the higher density, liquid-like states at lower temperature often show oscillations in the RDF, since molecules are arranged in relatively symmetric shells about a central molecule [15].

The potential function thus contains information regarding the interactive forces, and the radial distribution function uses this information to derive the structural properties of the fluid throughout which these forces act. If the intermolecular potential function Γ(r) and the RDF, g(r) for a particular fluid system is known in a closed analytical form, all of the thermodynamic behaviour of a fluid system may be completely described [12, 16].

Stellenbosch University https://scholar.sun.ac.za

Although work is continually being done on developing improved potential functions [17, 18], simple models like the Lennard-Jones potential still offer a reasonable account of real fluid behaviour, and are simple enough to be employed in the development of an analytically solvable EOS through perturbation theory. Obtaining a reasonable expression for the RDF for a real system has however proven to be substantially more challenging [12]: Although not explicitly stated in the foregone discussion, the RDF is not only a function of the intermolecular distance, r, but also system density and temperature, $g(r, \rho, T)$, making analytical evaluation of this term a difficult task. Most of modern statistical mechanics is aimed at calculating the RDF for fluid systems for a given potential function [19] There are generally four available methods of determining this function, namely:

- Experimental techniques
- Computer simulation
- Intergro-differential methods
- Integral equation methods

In the first method, radiation scattering experiments may be performed, whereby the pattern by which X-rays are diffracted by the particular system may be used to establish g(r) [12, 19]. This function may also be determined through the use of *monte-carlo simulations* (determining average value of properties over likely states) or *molecular dynamics simulations* (solving the dynamical equations and following the time evolution of the system) [13]. Both of the mentioned methods (experimental and simulation) are exact methods, whereby experiments give exact values for a particular real system and simulations give exact values for a model as determined by the potential-function used [19]. These methods therefore solve for precise numerical values for g(r) given a certain state of the system. These values may be used to derive both thermodynamic and transport properties, however they are in the form of raw data points and need to be correlated either statistically or with an existing EOS for analytical use in process design [13].

The integro-differential and integral methods seek to derive equations for g(r) fundamentally in terms of a specific fluid potential function by making various simplifying assumptions. These functions are generally derived from graph theory, function analysis or by truncating a hierarchy of equations and are thus approximate methods. For real systems, these equations generally need to be solved numerically, also generating numeric values for the RDF at fixed points of temperature and density, which must then be correlated afterwards [19].

Stellenbosch University https://scholar.sun.ac.za

Given the mentioned complications in obtaining the RDF it is clear that an alternative method is required to obtain an analytically solvable EOS with which to generate system properties from statistical mechanical theory. The perturbation theory, to be discussed next, offers such a method and has been the source of the EOS family commonly referred to in the literature as "molecular" models.

D.5.4 Perturbation theory

The first integral equation derived for the RDF which could be solved analytically for system properties was the Percus-Yevick approximation derived in 1958 [14]. This was applied in 1963 by Wertheim and Thiele for a hard-sphere fluid and marks a pivotal achievement in the subsequent development of the statistical mechanical description of fluid systems [19]. It was further found that due to the in-exact nature of the integral equation methods, two separate hard-sphere equations are found depending on whether the EOS is derived from the partition function in terms of compressibility or pressure [12, 19].

The reason why obtaining an analytical solution for the RDF of a hard-sphere fluid had such a large impact on EOS development, was that theoretical investigations into the RDF of non-polar fluids were beginning to show that the structure of real fluids, as well as those calculated using more realistic potential functions (LJ) closely resemble those of hard-spheres [20, 21]. This led to the speculation that the structural behaviour of a single phase fluid was governed by short-range repulsive forces, of which the hard-sphere is a reasonable approximation.

Zwansig also made this observation in 1954, when he saw that at high temperatures, the equation of state for gas behaviour is predominantly dominated by repulsive forces, and that the long range Van der Waals forces have a small effect on the system behaviour [22]. Based on this observation, Zwansig reasoned that these long range forces may be treated as a perturbation about a hard-sphere reference term, for which the RDF is known [22]. Zwansig therefore conceived the internal potential energy of the system, $\Gamma_N$as consisting out of an unperturbed reference part (0) and a perturbation part (1):

$$\Gamma_N = \Gamma_N^{(o)} + \Gamma_N{}^{(1)} \qquad \text{D. 57}$$

Substituting this decomposition into Equation D.53, the *configurational integral* can be shown to be given by the following expression:

Stellenbosch University https://scholar.sun.ac.za

$$Z_{config} = Z^{(0)}_{config}\langle \exp(-\beta\Gamma_N^{(1)})\rangle_0 \qquad \text{D. 58}$$

$\beta = \frac{1}{kT}$ and the square bracket term $\langle \quad \rangle_0$ indicates that the perturbation potential interaction $\Gamma_N^{(1)}$ is averaged over the structural properties of the reference system for which the RDF is known. Zwansig then expanded the exponential term as a MacLaurin series expansion (Taylor series expansion about a value of zero) around the properties of the reference fluid, resulting in a power series in β with the perturbation terms as coefficients, representing the contributions to the internal energy by long range forces, such as polar or dipolar forces defined by $\Gamma_N{}^{(1)}$. Nezbeda gives a three step procedure for conducting a general perturbation expansion for arriving at an EOS: [16]:

1) The internal potential energy function is decomposed into a reference and a perturbed part(s) as in Equation D.57

2) The Helmholtz free energy, A, is then obtained using Equation D.54 from the (volume dependent) *configurational integral,* expanded in powers of $\beta\Gamma_N{}^{(1)}$ from Equation D.58:

$$A = A_{ref} + \beta\Delta A_1\left(\Gamma_N{}^{(1)}\right) + \beta^2\Delta A_2\left(\Gamma_N{}^{(1)}\right) \qquad \text{D. 59}$$

A_{ref} is determined from a well defined reference term, for which g(r) is known, with the perturbation terms ΔA_ibeing functions of the structure of this reference fluid.

3) After the perturbation terms, ΔA_1, ΔA_2 ... are evaluated, the final EOS may then be derived in terms of pressure or compressibility:

$$Z = Z_{ref} + \Delta Z_1 + \Delta Z_2 \qquad \text{D. 60}$$

A very useful attribute of these more theoretical models may be seen from Equation D.57 through D.60 whereby each of the unique perturbation effects results in an explicit term for the particular effect in the final EOS. Although each term generally contains additional parameters, this allows for isolated analytical study of each effect [16, 23].

D.5.5 Evaluation of reference and perturbation terms

According to Nezbeda, undergoing a physically plausible analysis of the perturbation terms $\Delta A_{1\ldots}$ remains the greatest challenge for developing purely theoretical equations of state from

Stellenbosch University https://scholar.sun.ac.za

statistical mechanical perturbation theory. In general, this may be achieved by solving equations of the following form [16]:

$$\Delta A = \frac{1}{2}\rho N[I(\rho,T) - \text{constant}] \qquad \text{D. 61}$$

Where $I(\rho,T)$is the perturbation integral:

$$I(\rho,T) = \rho \int [g_{ref}(1,2) - 1]\Delta\Gamma(1,2)d(1)d(2) \qquad \text{D. 62}$$

$\Delta\Gamma(1,2)$ is furthermore usually made up of several terms for each perturbation effect (dispersion, polar etc), which may require solving several perturbation integral terms [16]. As mentioned, the perturbation should theoretically be expanded around the structure of the reference fluid, as portrayed by$g_{ref}(1,2)$. The perturbation converges faster as the properties of the reference fluidand selection of the reference and perturbation potentials resemble those of the true fluid. This not only leads to more accurate predictions but the evaluation of the higher-order perturbation terms further pose problems for developing a closed analytically solvable EOS [12,16].

For these reasons, it is generally desirable to choose a more realistic reference system than the hard-sphere fluid. Currently only two main methods are available by which a more realistic, soft-repulsive reference fluid such as the LJ fluid may be used in the expansion of an analytically solvable equation. These are the general methods of Barker and Henderson (BH; 1967) and Weeks, Chandler and Anderson (WCA; 1971) [20]. Although these methods will not be reviewed here, it may be stated that both methods result in mapping the properties of the soft-repulsive reference system onto those of an existing hard-sphere model with a variable diameter [12, 16]. With the BH approach, the new diameter is a function of temperature ($d_{BH}(T)$) and the potential function only, whereas the WCA approach gives a temperature and density dependent hard-sphere diameter ($d_{WCA}(\rho,T)$) [12, 20]. Any hard-sphere modelmay then be used in conjunction with a variable diameter term (either $d_{BH}(T)$ or $d_{WCA}(\rho,T)$) in calculating the reduced volume $\eta = \frac{b}{4v}$,with b a function of molecular diameter. This approach is capable of representing a more realistic electron cloud, rather than a rigid diameter in the reference term.

Analytical expressions for a simple square-well fluid have been determined by Chang and Sandler (1994), however these expressions involve the definite integration of the RDF, which results in complex property functions containing exponential and trigonometric functions [12].

Stellenbosch University https://scholar.sun.ac.za

In general, the perturbation terms of analytically solvable equations of state are not evaluated in the theoretically rigorous manner as proposed by Equations D.61 and D.62 but are determined as approximations by fitting simulation results or by making simplifying assumptions [12, 20]. Since most molecular models being used today employ an empirical representation of the perturbation terms, these models are still considered only semi-theoretical, despite being substantially more theoretically grounded than the cubic equations of state which are based purely on intuition from kinetic theory.

References

[1] Levermore, D., 2011. Homepage of Dave Levermore. [Online] Available at: http://www.terpconnect.umd.edu/~lvrmr/index.shtml [Accessed 23 April 2012].

[2] J. van der Waals, Reprint of: The equation of state for gases and liquids, J. Supercritical Fluids 55 (2010) 403-414

[3] M. Koretsky, Engineering and Chemical Thermodynamics, Hoboken, N.J.: John Wiley & Sons., 2004

[4] K.G. Clarke, T. Pistorius, IC Engineering Chemistry Course Lectures, Stellenbosch: Department of Process Engineering, University of Stellenbosch, 2012

[5] G. Kontogeorgis, G. Folas, Thermodynamic Models for Industrial Applications - From Classical and Advanced Mixing Rules to Association Theories,United Kingdom: John Wiley & Sons Ltd,1st ed. West Sussex, PO19 8SQ, 2010, pp. 5.3

[6] T.Lafitte, A. Apostolako,C.Avendao,A.Galino,C.S. Adjiman, E.A.Muller,G.Jackson, Accurate statistical associating fluid theory for chain molecules formed from Mie segments,J. of Chemical Physics 39 (2013)154504

[7] J.M. Smith, H.C. Van Ness, M.M. Abbot. Introduction to Chemical Engineering Thermodynamics. New York: McGraw Hill, 7th edition, 2005.

[8] M.J. Klein, The historical origins of the Van der Waals equation, Physica (1974) 73, 28-47

[9] J. De Boer, Van der Waals in his time and the present revival: opening address, Physica (1974) 1- 27

[10] S.M. Walas, Phase equilibria in chemical engineering,Butterworth Publishers, Stoneham, MA, 1985, Vol. 1

[11] J.F. Ely, The corresponding states principle, in: A.R.H. Goodwin, J.V. Sengers, C.J. Peters, Applied Thermodynamic s of Fluids, RSC Publishing, Cambridge, UK, 2010, pg 135 – 171

[12] Du Rand, M., 2004, PhD Thesis,. Practical Equation of State for Non-Spherical and Asymmetric Systems, Stellenbosch: Department of Chemical Engineering at the Universtiy of Stellenbosch.

Stellenbosch University https://scholar.sun.ac.za

[13] S. Sandler, Equations of state for phase equilibrium computations. In: E. Kiran & J. L. Sengers, eds. NATO Advanced Study Institute on Supercritical Fluids-Fundamentals for application. Turkey: Kluwer Academic Publishers, 1994, pp. 147-175.

[14] G.A. Mansoori, Radial Distribution Functions and their Role in Modelling of Mixtures Behaviour, Fluid Phase Equilibria, 1993, 87, 1-22

[15] J.M.H Levelt Sengers, Critical Behaviour of fluids: Concepts and applications, in: E. Kiran, J.M. Levelt Sengers, NATO Advanced Study Institute on Supercritical Fluids-Fundamentals for application , Kluwer Academic Publishers Turkey, 1994, pp. 65 - 89.

[16] I. Nezbeda, On molecular-based equations of state: rigor versus speculation, Fluid Phase Equilibria182 (2001) 3-15.

[17] I. Nezbeda, On the way from theoretical calculations to practical equations of state for real fluids,Fluid Phase Equilibria52 (1989) 39-46

[18] I. Nezbeda, Role of the range of intermolecular interactions in fluid. Current Opinion in Colloid and Interface Science 9 (2004) 107-111

[19] P. Cummings, Y.V. Kalyushnyi, Equations of state from analytically solvable intergral-equation approximations. In: J. Sengers, R. Kayser, C. Peters, H.White, eds. Equations of state for fluids and fluid mixtures. Amsterdam, The Netherlands: IUPAC, pp. 169-241.

[20] T.Boublik, I.Nezbeda, K. Hlavaty, Statistical thermodynamics of simple fluids and their mixtures, Elsevier, Amsterdam, 1980

[21] C.G. Gray, K.E. Gubbins, Theory of Molecular Fluids, 1, Clarendon Press, Oxford, 1984

[22] R.W. Zwanzig, Temperature Equation of State by a Perturbation Method. I. Nonpolar Gases, J. Chem. Phys. 22 (1954) 1420-1426

[23] T. Boublik, Perturbation Theory. In: J. Sengers, R. Kayser, C. Peters & J. H.J. White, eds. Equations of State for Fluids and Fluid Mixtures. Amsterdam, The Netherlands: IUPAC, 2000, pp. 127-166

Stellenbosch University https://scholar.sun.ac.za

APPENDIX E: Additional figures and tables

E.1 ASPEN regression: BIP vs. CN plots for each case

E.1.1 Ethane/n-Alkanes

RK-ASPEN:

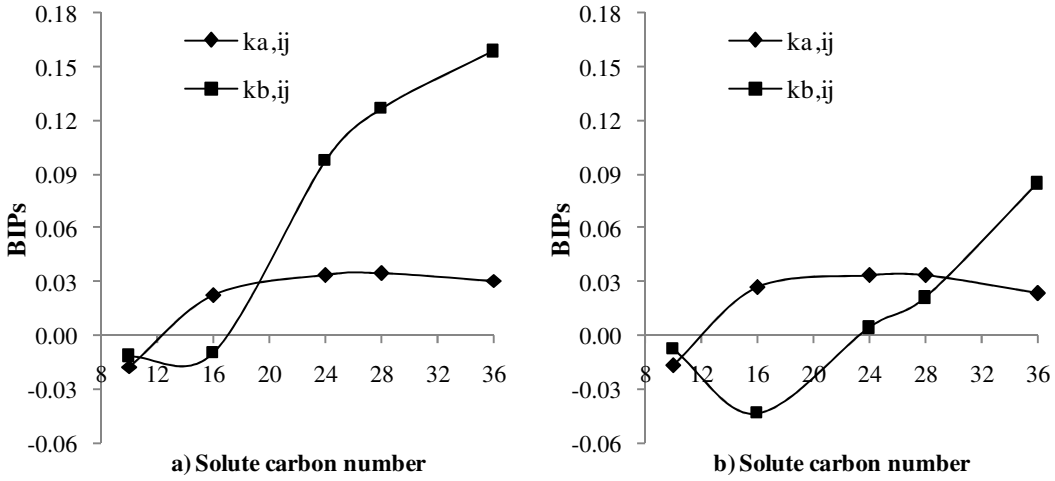

Figure E. 1 BIP vs. Solute carbon number for the RK-ASPEN model regressing a) a single BIP and b) both simultaneously for the ethane/n-alkanes

PR-BM:

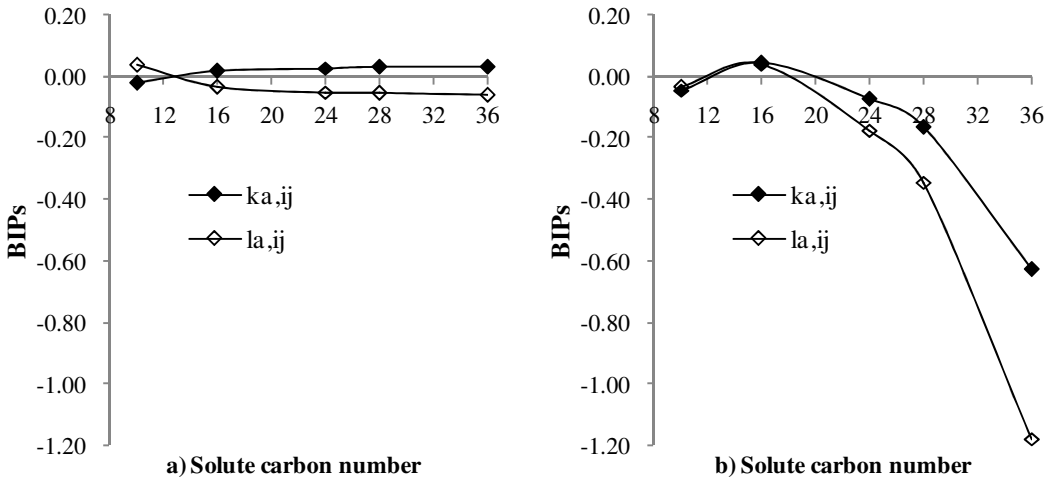

Figure E. 2 BIP vs. Solute carbon number for the PR-BM model regressing a) a single BIP and b) both simultaneously for the ethane/n-alkanes

Stellenbosch University https://scholar.sun.ac.za

PR:

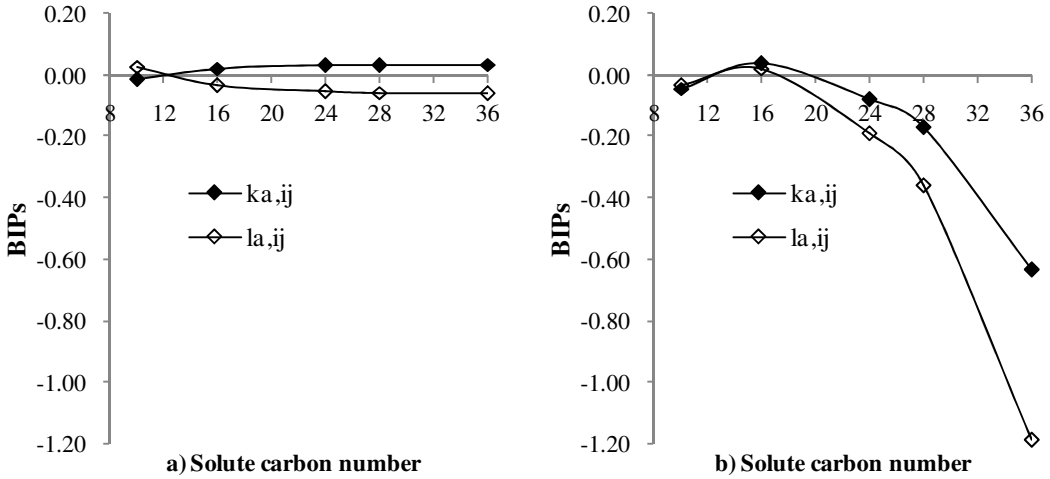

Figure E. 3 BIP vs. Solute carbon number for the PR model regressing a) a single BIP and b) both simultaneously for the ethane/n-alkanes

SRK:

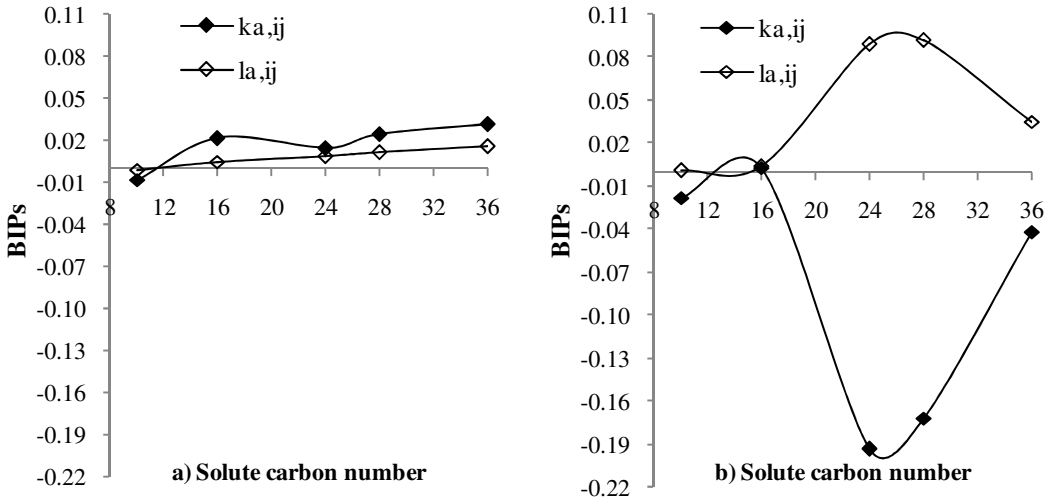

Figure E. 4 BIP vs. Solute carbon number for the SRK model regressing a) a single BIP and b) both simultaneously for the ethane/n-alkanes

Stellenbosch University https://scholar.sun.ac.za

SRPOLAR:

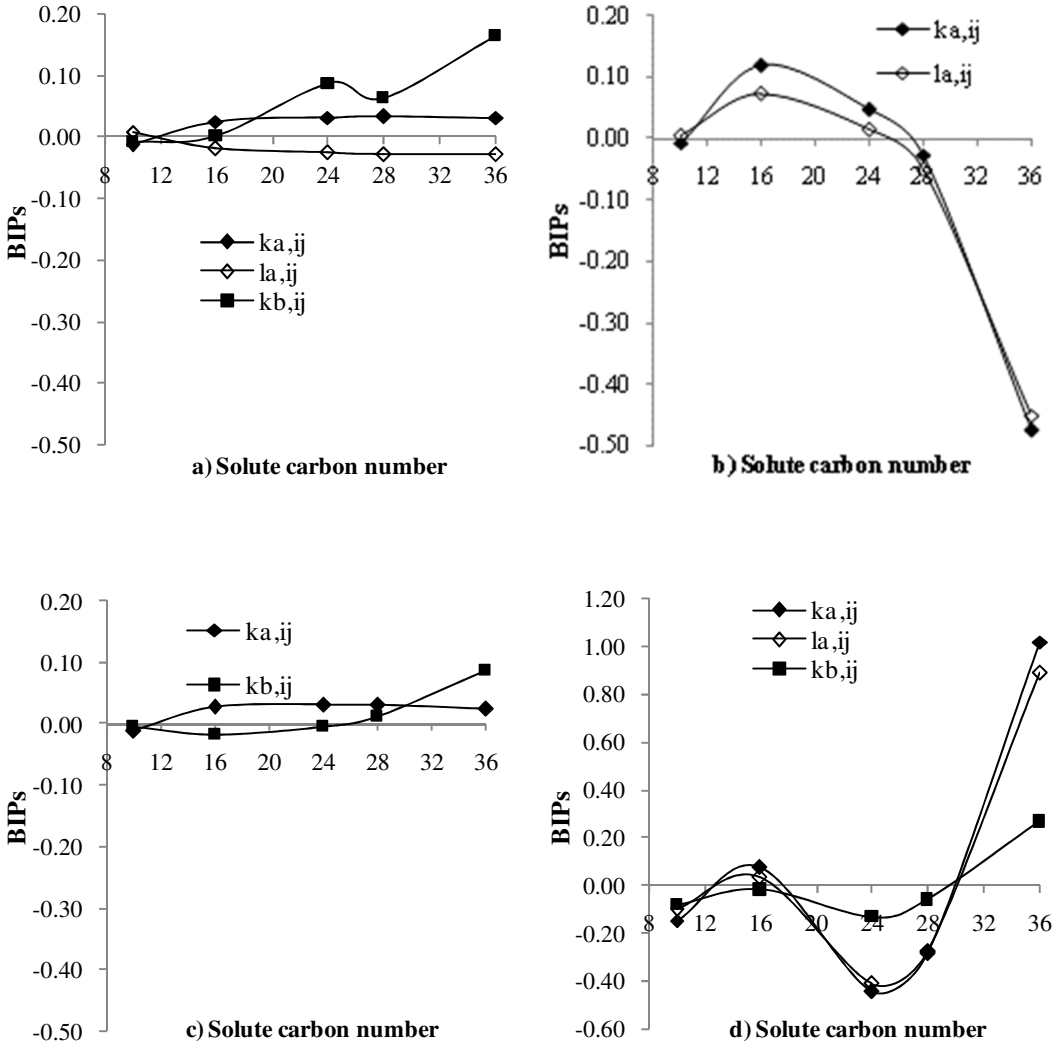

Figure E. 5 BIP vs. Solute carbon number for the SR-POLAR model regressing a) a single BIP, b) both $k_{a,ij}$ and $l_{a,ij}$, c) both $k_{a,ij}$ and $k_{b,ij}$ and d) all three simultaneously for the ethane/n-alkanes

Stellenbosch University https://scholar.sun.ac.za

E.1.2 Ethane/1-Alcohols

RK-ASPEN:

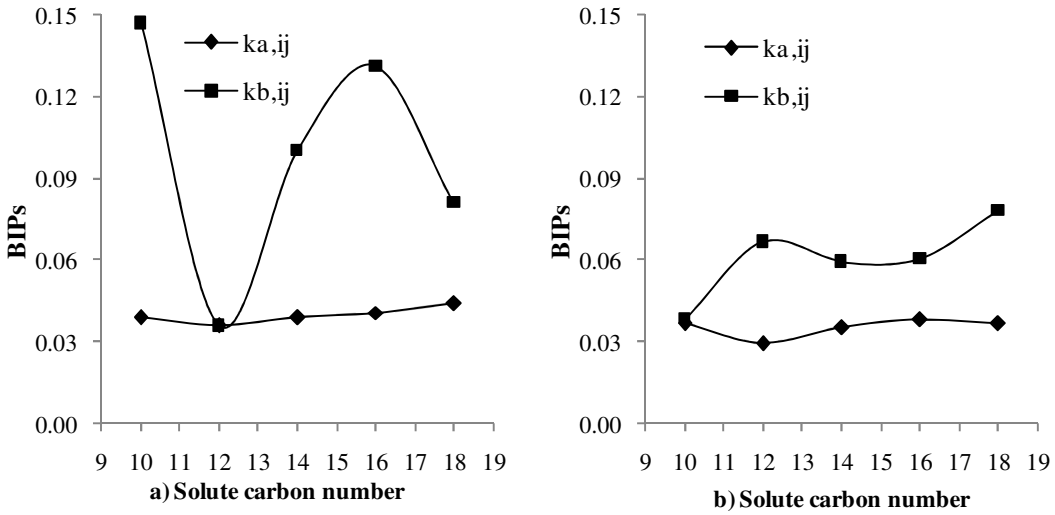

Figure E. 6 BIP vs. Solute carbon number for the RK-ASPEN model regressing a) a single BIP and b) both simultaneously for the ethane/1-alcohols

PR-BM:

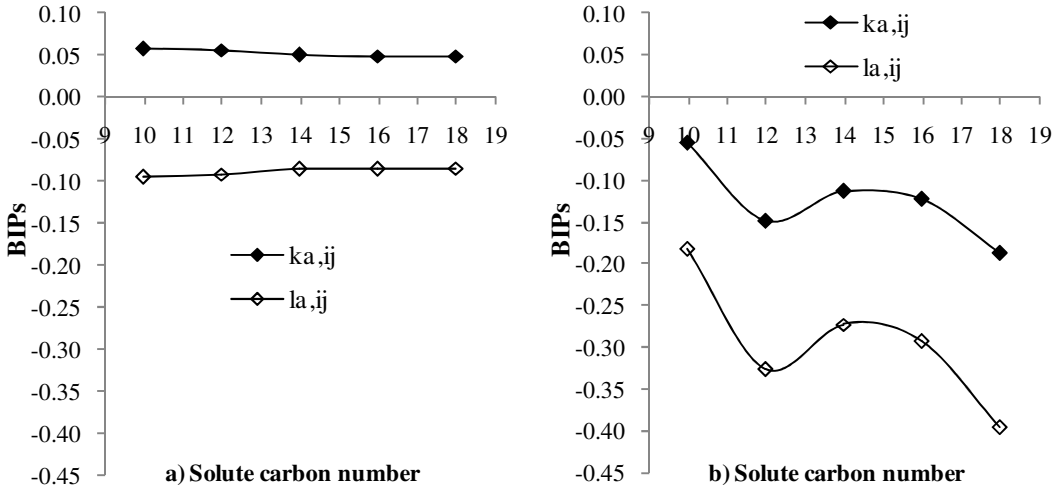

Figure E. 7 BIP vs. Solute carbon number for the PR-BM model regressing a) a single BIP and b) both simultaneously for the ethane/1-alcohols

Stellenbosch University https://scholar.sun.ac.za

PR:

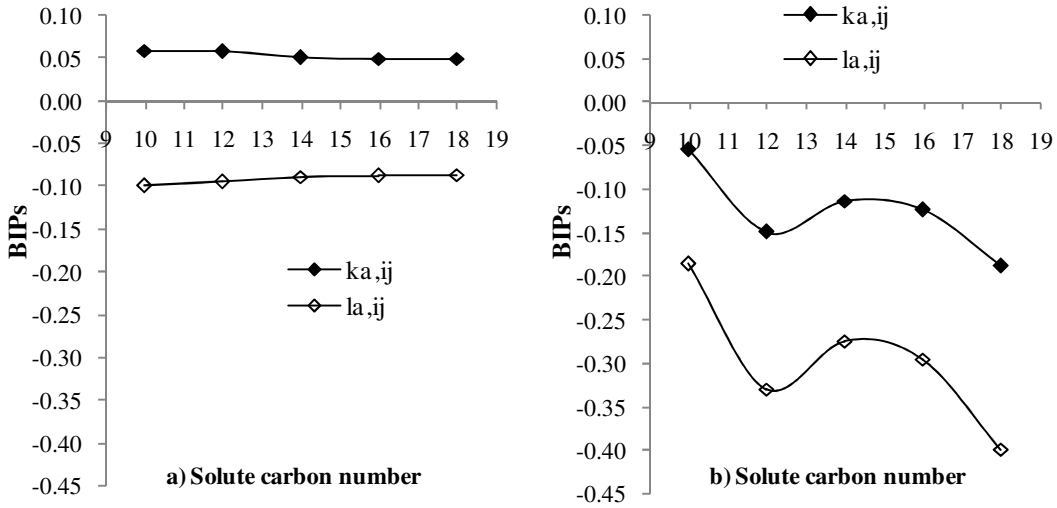

Figure E. 8 BIP vs. Solute carbon number for the PR model regressing a) a single BIP and b) both simultaneously for the ethane/1-alcohols

SRK:

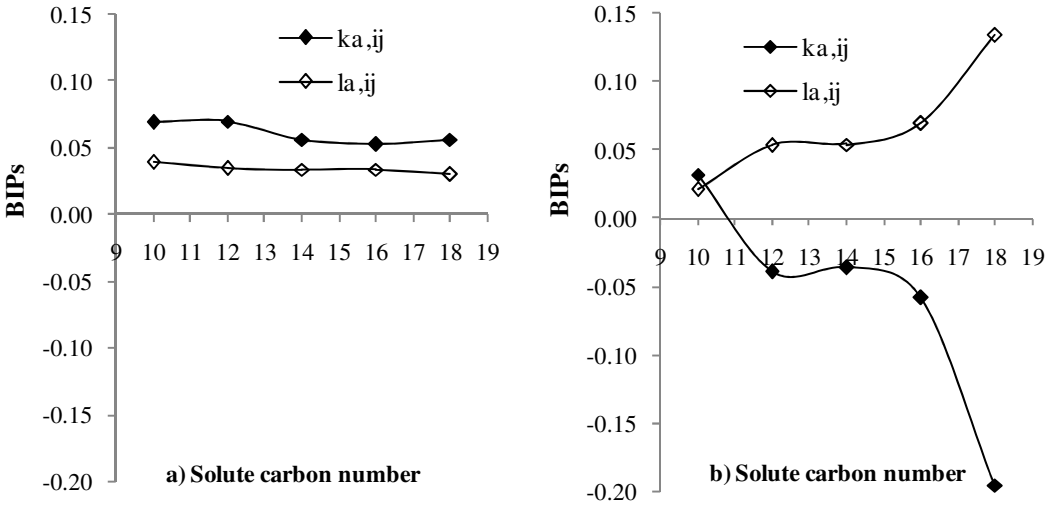

Figure E. 9 BIP vs. Solute carbon number for the SRK model using a) a single BIP and b) both simultaneously for the ethane/1-alcohols

Stellenbosch University https://scholar.sun.ac.za

SR-POLAR:

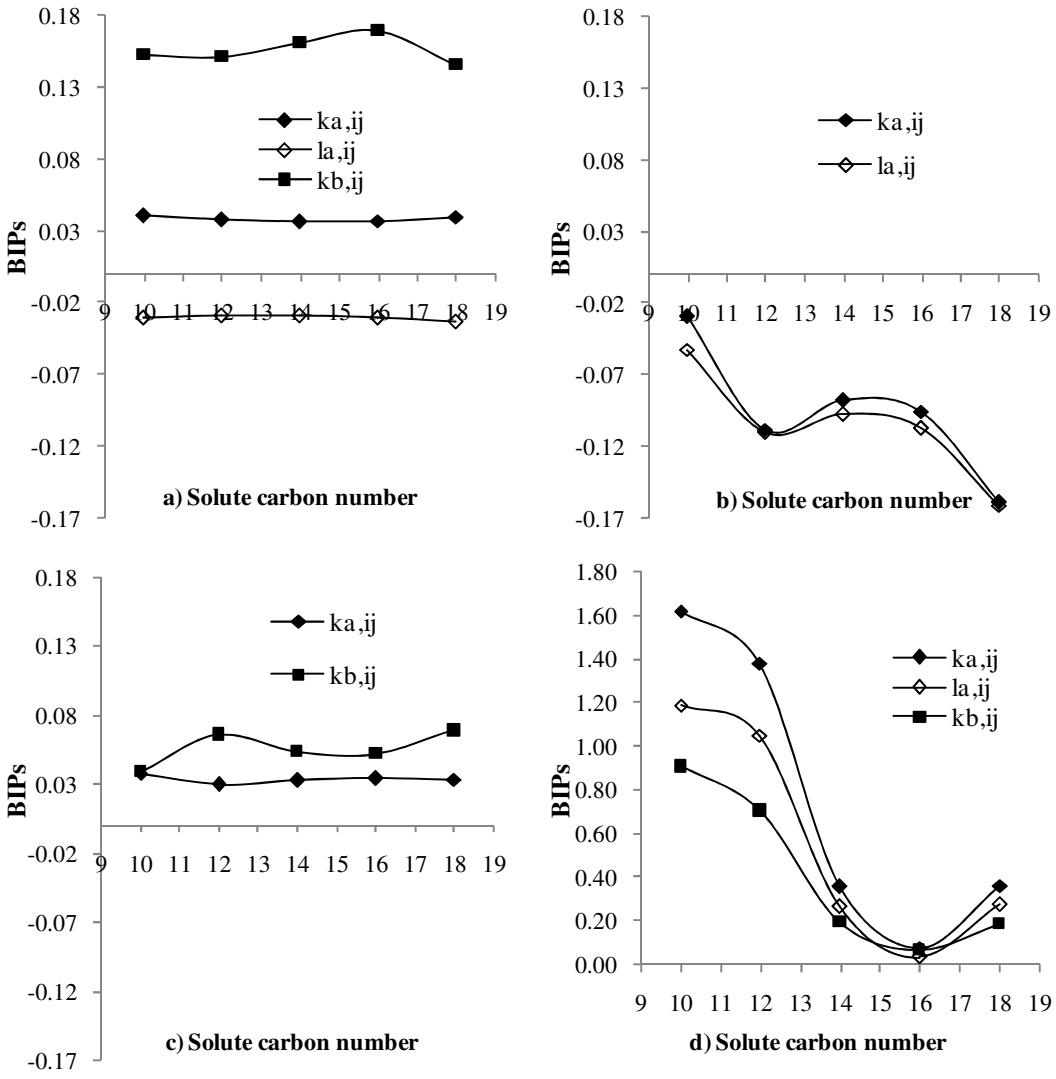

Figure E. 10 BIP vs. Solute carbon number for the SR-POLAR model regressing a) a single BIP, b) both $k_{a,ij}$ and $l_{a,ij}$, c) both $k_{a,ij}$ and $k_{b,ij}$ and d) all three simultaneously for the ethane/1-alcohols

Stellenbosch University https://scholar.sun.ac.za

E.1.3 Ethane/Carboxylic Acids

RK-ASPEN:

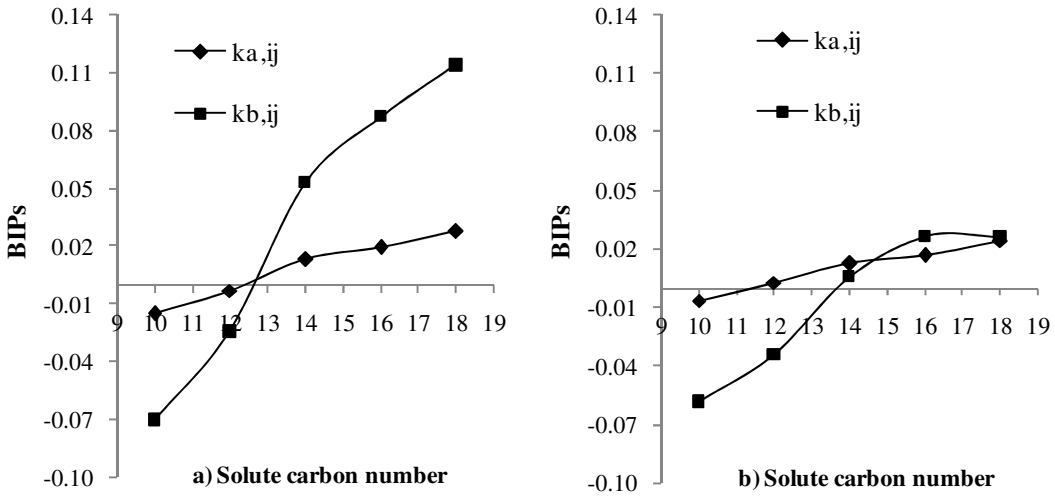

Figure E. 11 BIP vs. Solute carbon number for the RK-ASPEN model using a) a single BIP and b) regressing both simultaneously for the ethane/carboxylic acids

PR-BM:

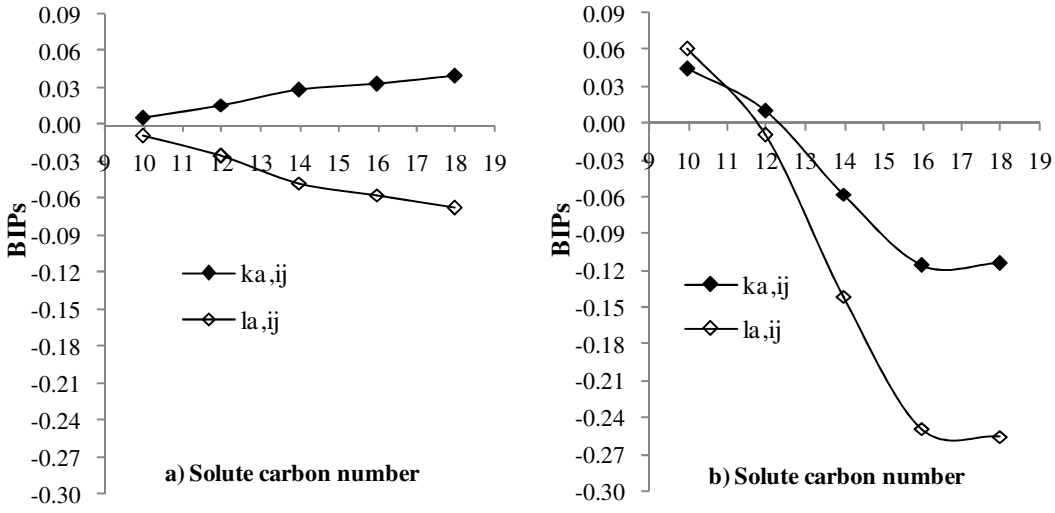

Figure E. 12 BIP vs. Solute carbon number for the PR-BM model using a) a single BIP and b) regressing both simultaneously for the ethane/carboxylic acids

Stellenbosch University https://scholar.sun.ac.za

PR:

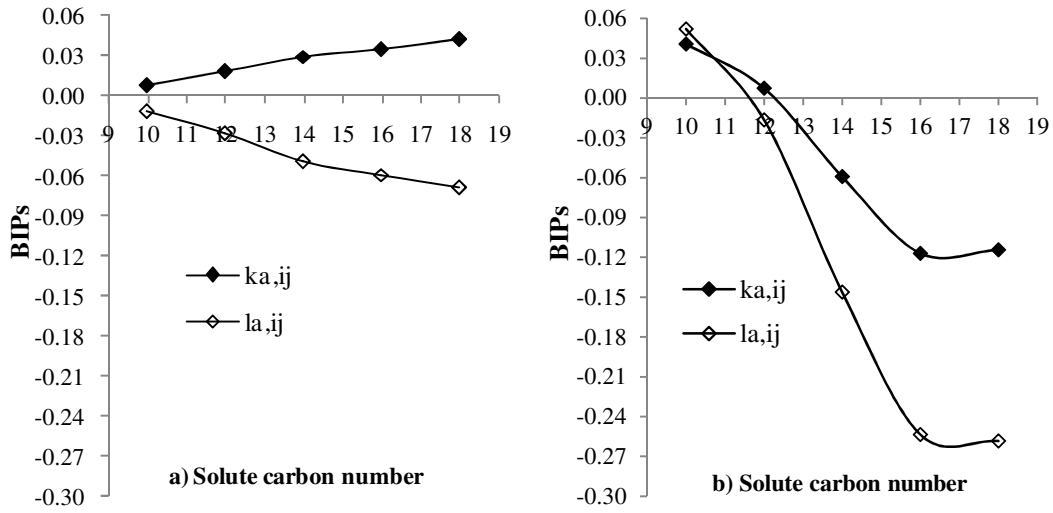

Figure E. 13 BIP vs. Solute carbon number for the PR model using a) a single BIP and b) regressing both simultaneously for the ethane/carboxylic acids

SRK:

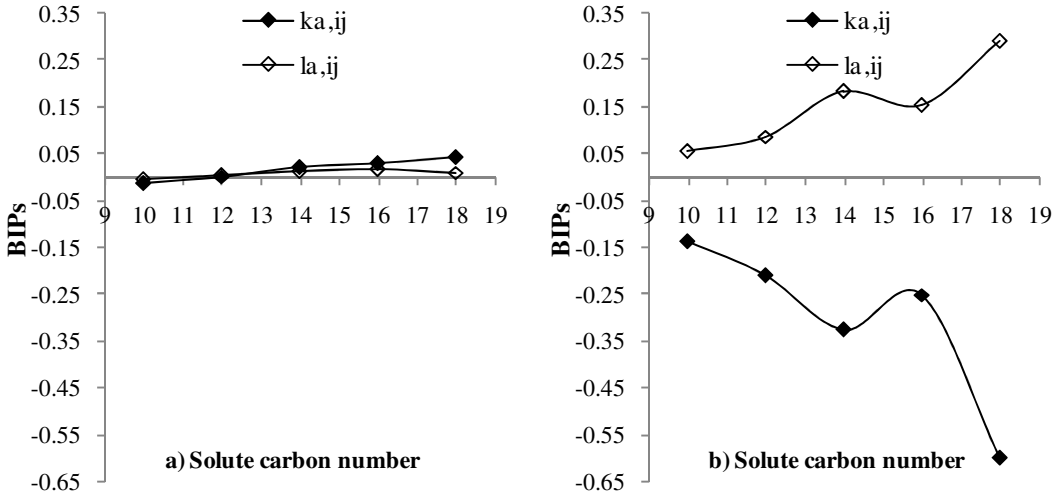

Figure E. 14 BIP vs. Solute carbon number for the SRK model using a) a single BIP and b) regressing both simultaneously for the ethane/carboxylic acids

Stellenbosch University https://scholar.sun.ac.za

SR-POLAR:

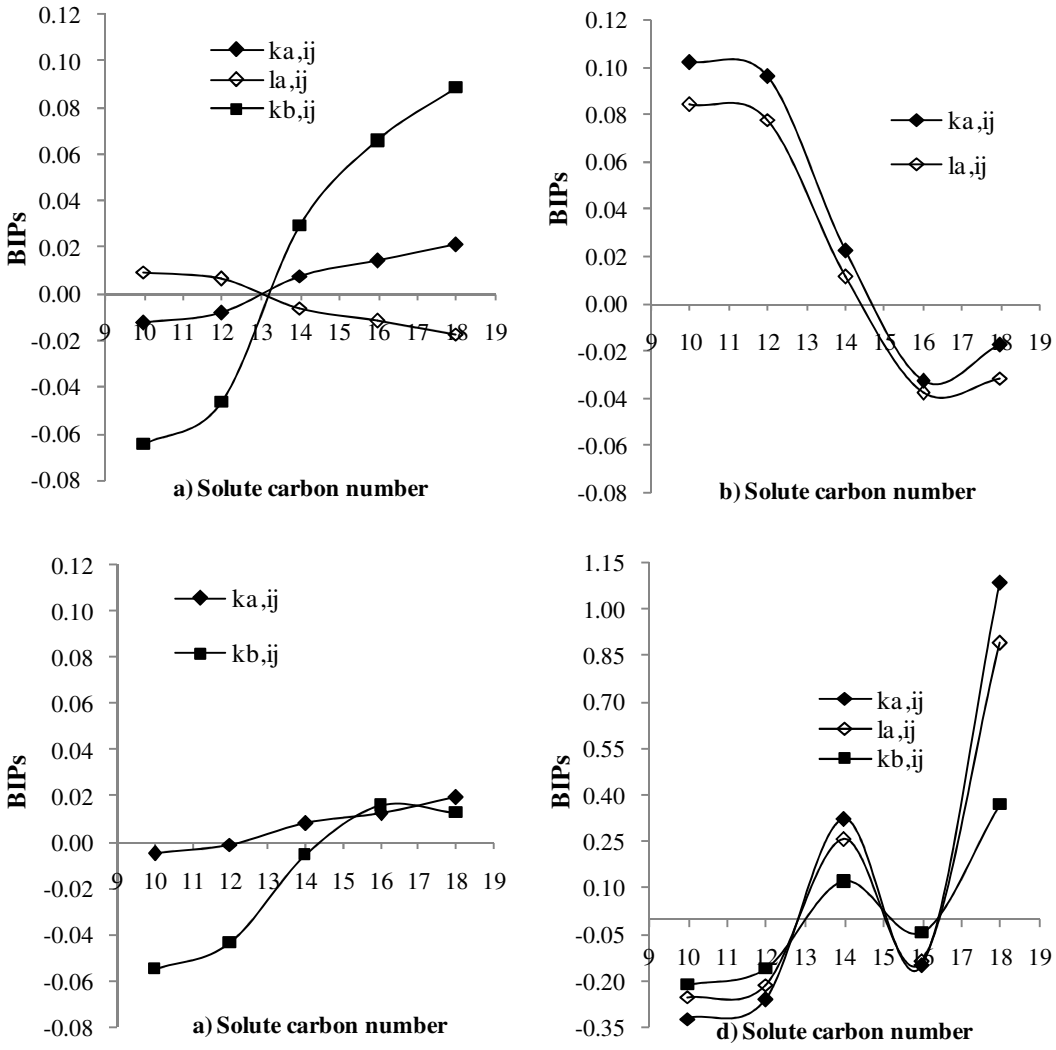

Figure E. 15 BIP vs. Solute carbon number for the SR-POLAR model regressing a) a single BIP, b) both $k_{a,ij}$ and $l_{a,ij}$, c) both $k_{a,ij}$ and $k_{b,ij}$ and d) all three simultaneously for the ethane/carboxyix acids

Stellenbosch University https://scholar.sun.ac.za

E.1.4 Ethane/Methyl Esters

RK-ASPEN:

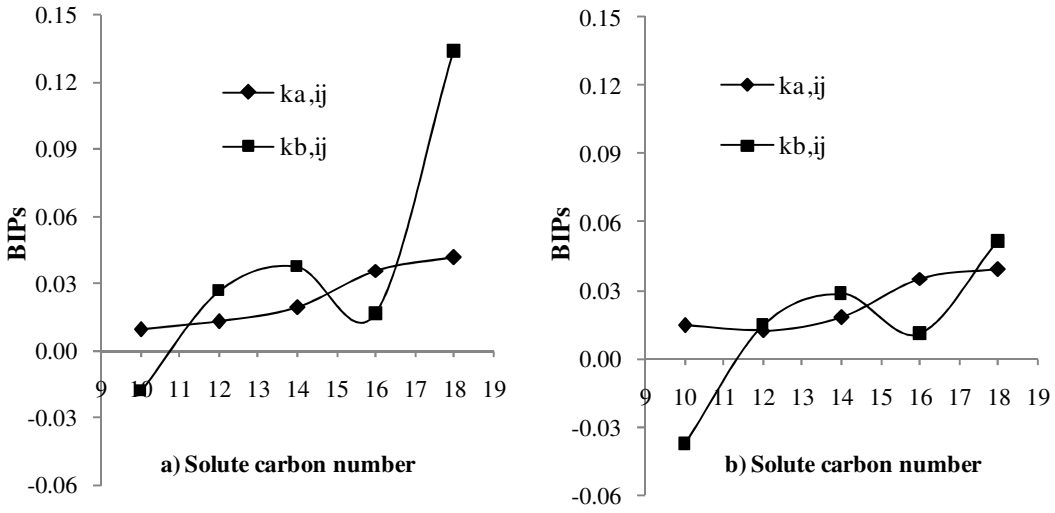

Figure E. 16 BIP vs. Solute carbon number for the RK-ASPEN model using a) a single BIP and b) regressing both simultaneously for the ethane/methyl esters

PR-BM:

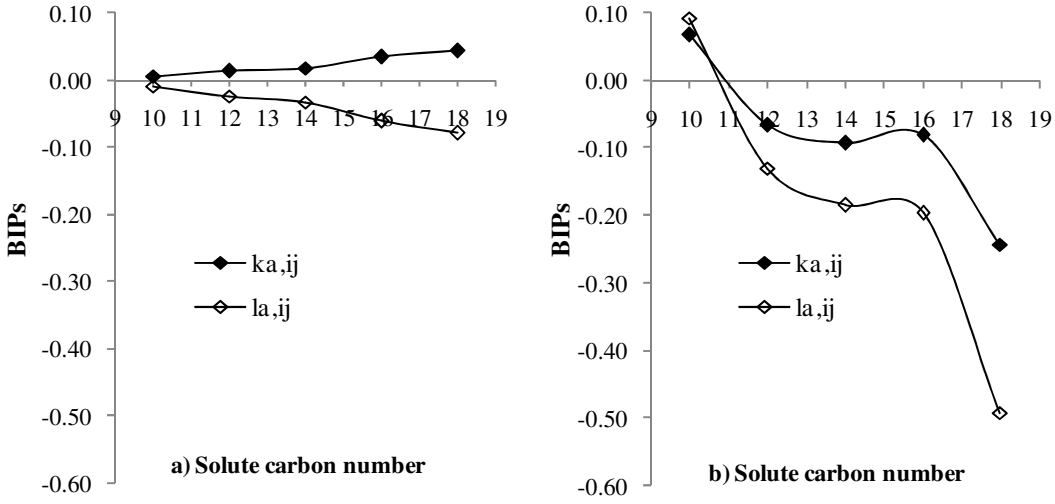

Figure E. 17 BIP vs. Solute carbon number for the PR-BM model using a) a single BIP and b) regressing both simultaneously for the ethane/methyl esters

Stellenbosch University https://scholar.sun.ac.za

PR:

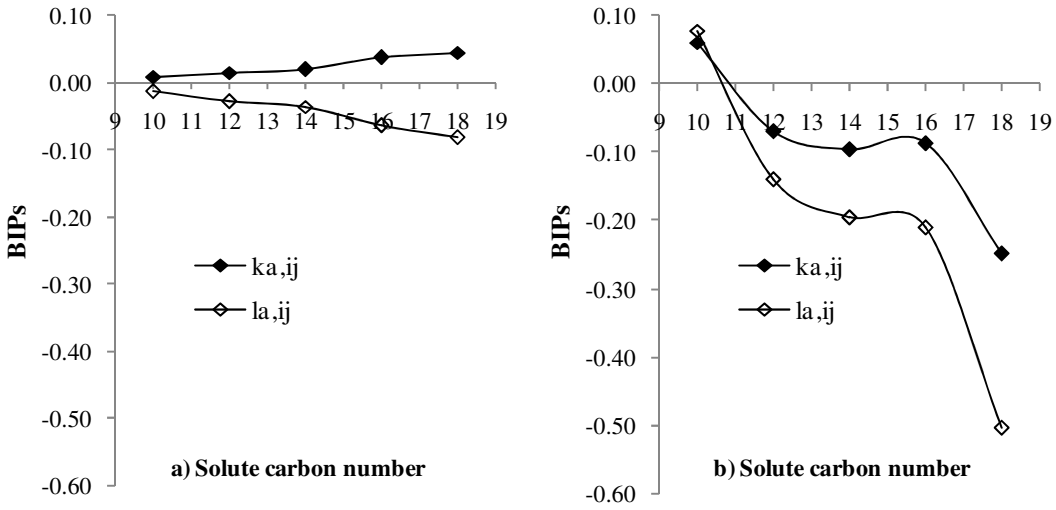

Figure E. 18 BIP vs. Solute carbon number for the PR model using a) a single BIP and b) regressing both simultaneously for the ethane/methyl esters

SRK:

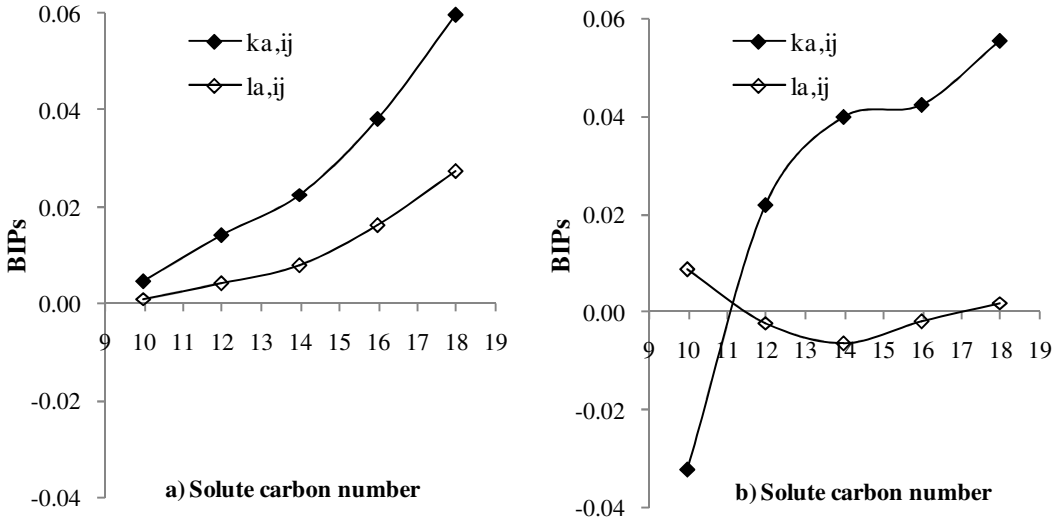

Figure E. 19 BIP vs. Solute carbon number for the SRK model using a) a single BIP and b) regressing both simultaneously for the ethane/methyl esters

Stellenbosch University https://scholar.sun.ac.za

SR-POLAR:

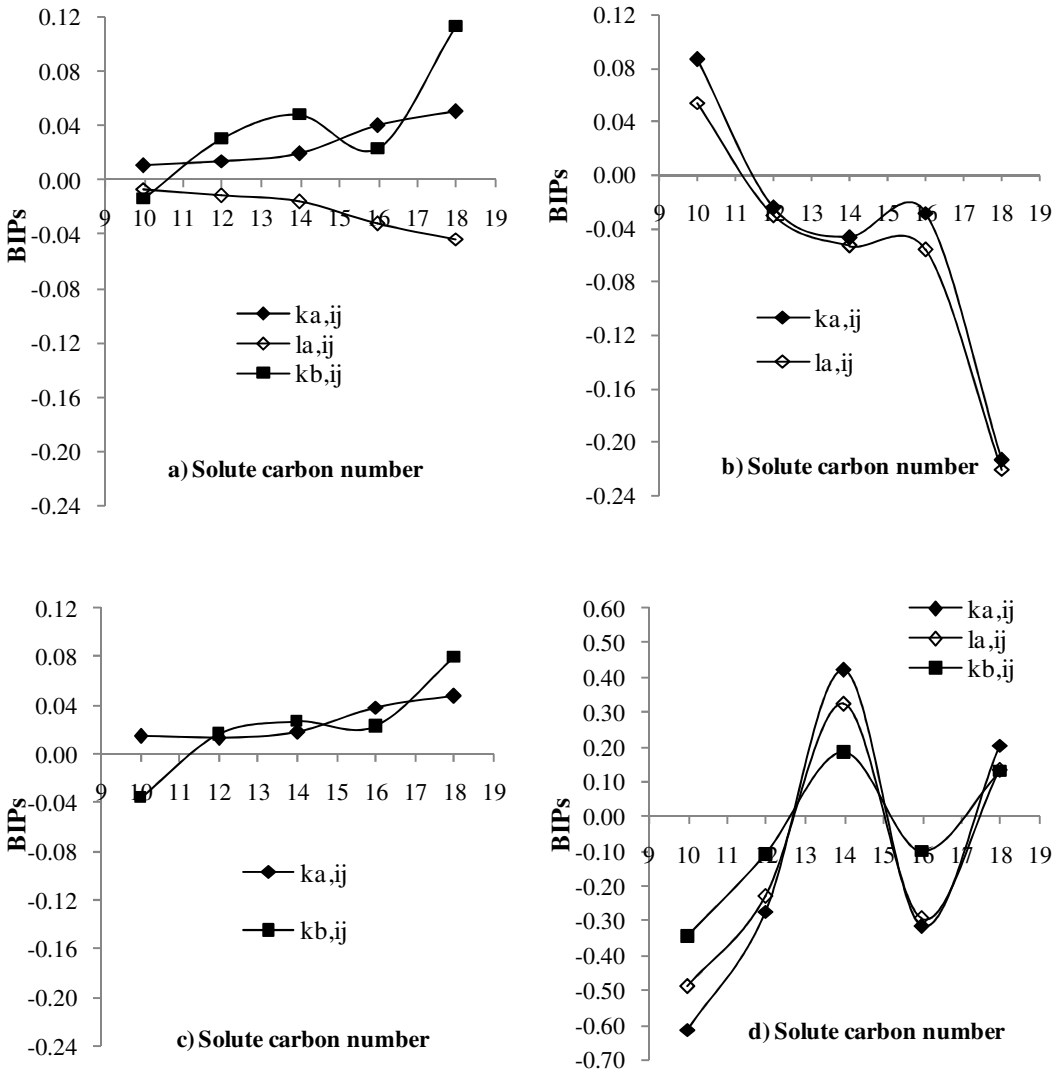

Figure E. 20 BIP vs. Solute carbon number for the SR-POLAR model regressing a) a single BIP, b) both $k_{a,ij}$ and $l_{a,ij}$, c) both $k_{a,ij}$ and $k_{b,ij}$ and d) all three simultaneously for the ethane/methyl esters

Stellenbosch University https://scholar.sun.ac.za

E.1.5 Propane/n-Alkanes

RK-ASPEN:

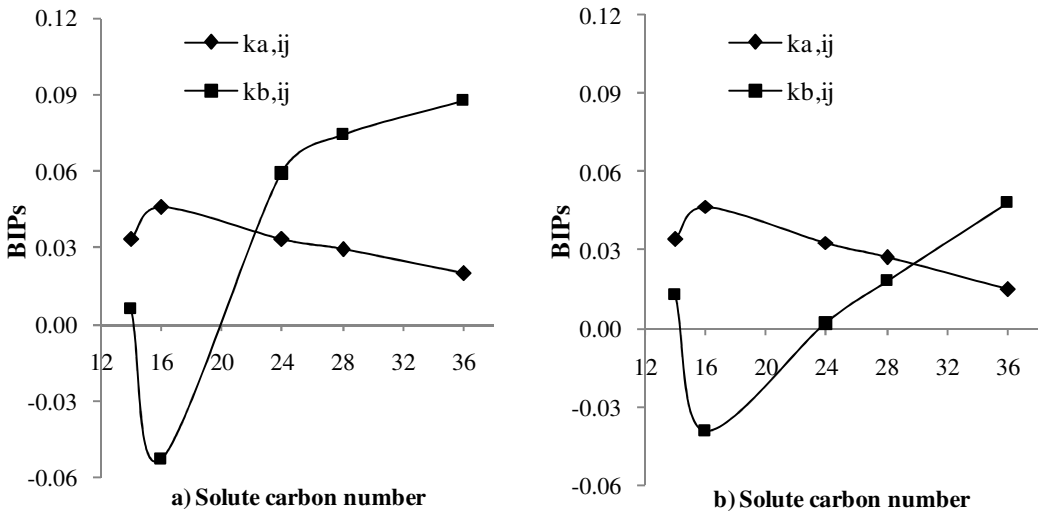

Figure E. 21 BIP vs. Solute carbon number for the RK-ASPEN model regressing a) a single BIP and b) both simultaneously for the propane/n-alkanes

PR-BM:

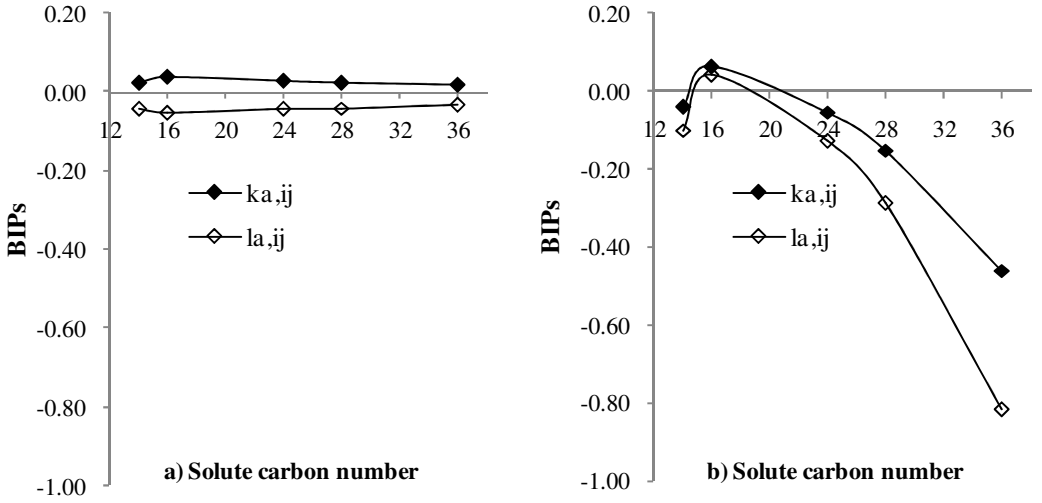

Figure E. 22 BIP vs. Solute carbon number for the PR-BM model regressing a) a single BIP and b) both simultaneously for the propane/n-alkanes

Stellenbosch University https://scholar.sun.ac.za

PR:

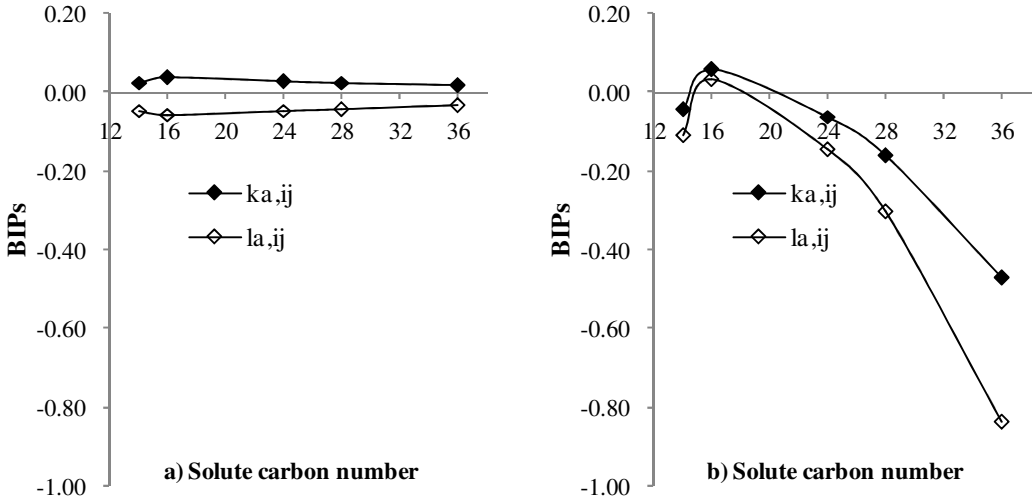

Figure E. 23 BIP vs. Solute carbon number for the PR model regressing a) a single BIP and b) both simultaneously for the propane/n-alkanes

SRK:

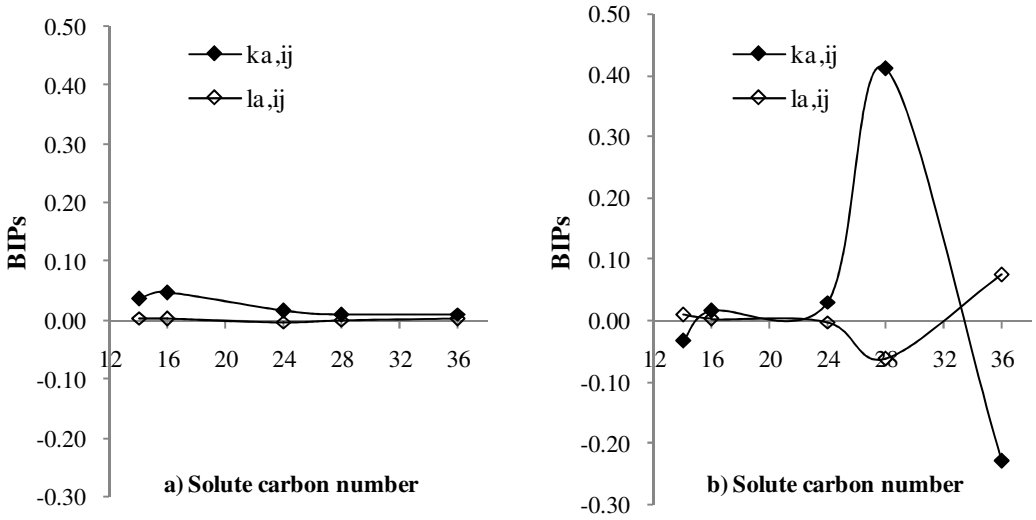

Figure E. 24 BIP vs. Solute carbon number for the SRK model regressing a) a single BIP and b) both simultaneously for the propane/n-alkanes

Stellenbosch University https://scholar.sun.ac.za

SR-POLAR:

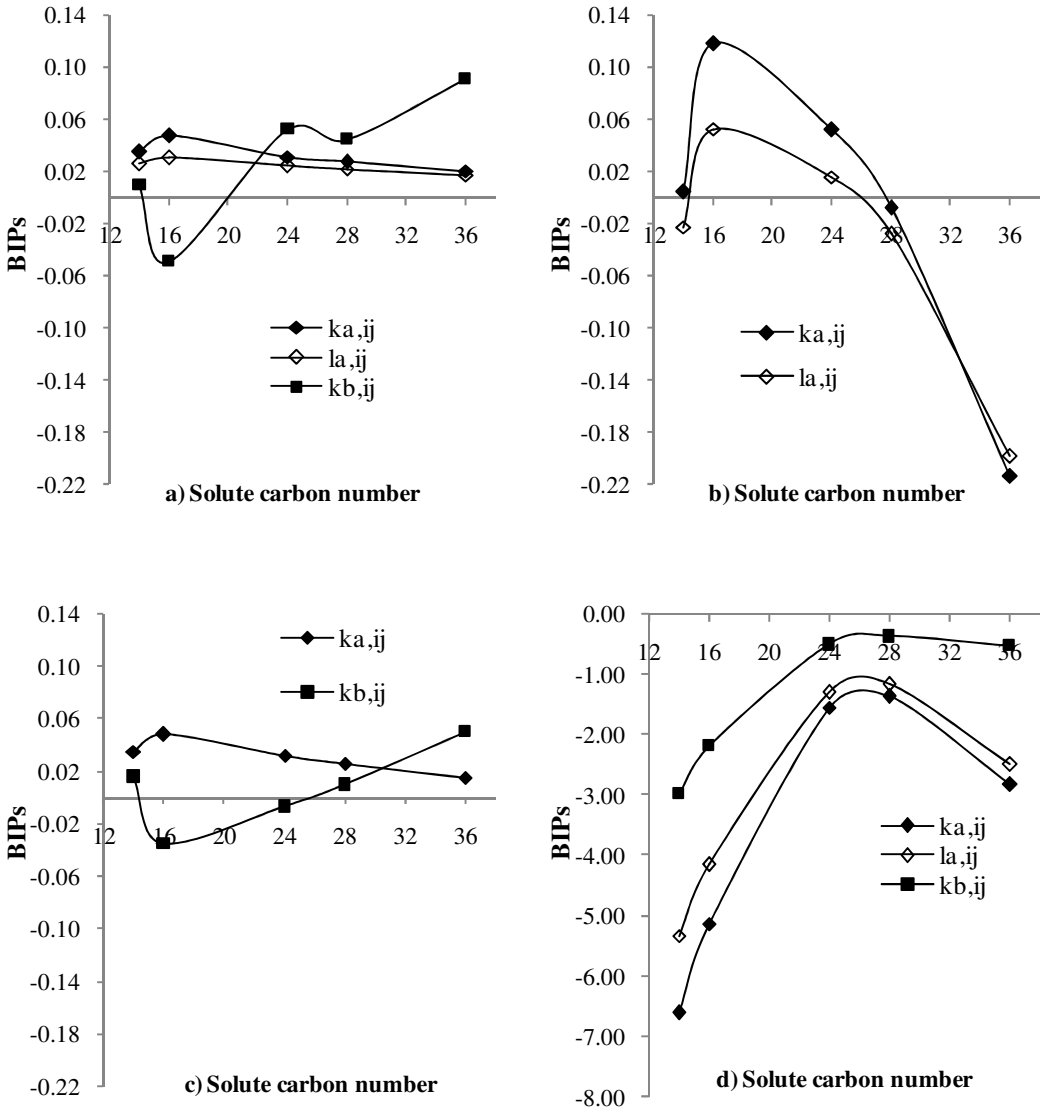

Figure E. 25 BIP vs. Solute carbon number for the SR-POLAR model regressing a) a single BIP, b) both $k_{a,ij}$ and $l_{a,ij}$, c) both $k_{a,ij}$ and $k_{b,ij}$ and d) all three simultaneously for the propane/n-alkanes

Stellenbosch University https://scholar.sun.ac.za

E.1.6 Propane/1-Alcohols

RK-ASPEN:

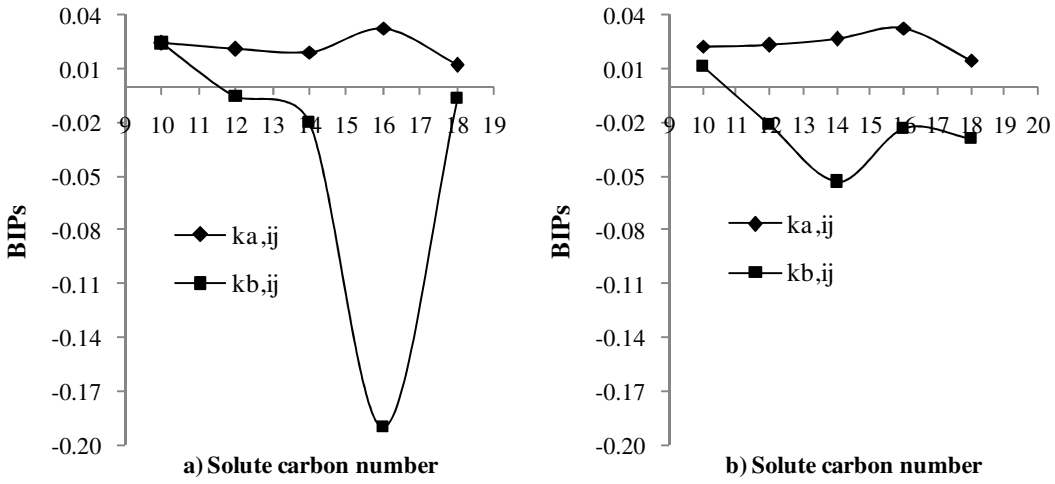

Figure E. 26 BIP vs. Solute carbon number for the RK-ASPEN model regressing a) a single BIP and b) both simultaneously for the propane/1-alcohols

PR-BM:

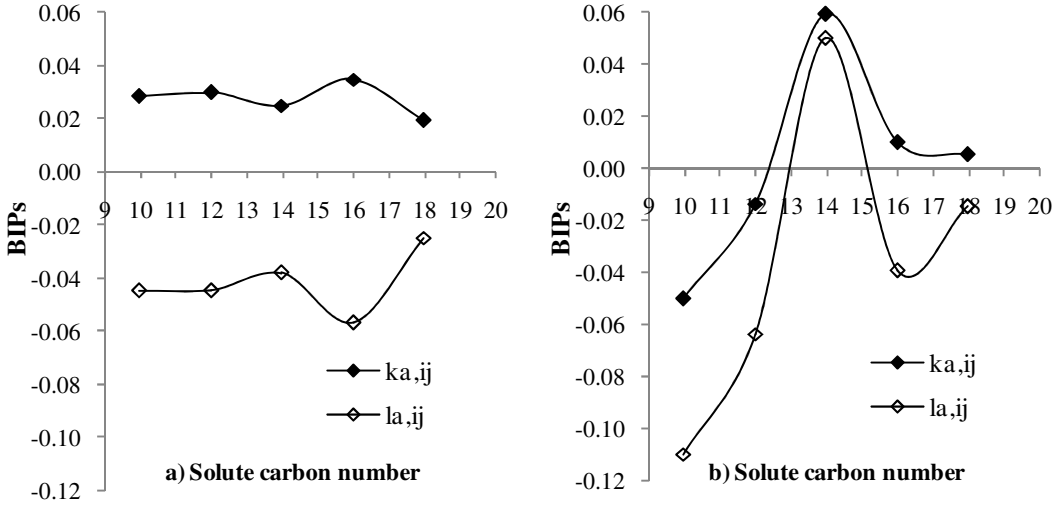

Figure E. 27 BIP vs. Solute carbon number for the PR-BM model regressing a) a single BIP and b) both simultaneously for the propane/1-alcohols

Stellenbosch University https://scholar.sun.ac.za

PR:

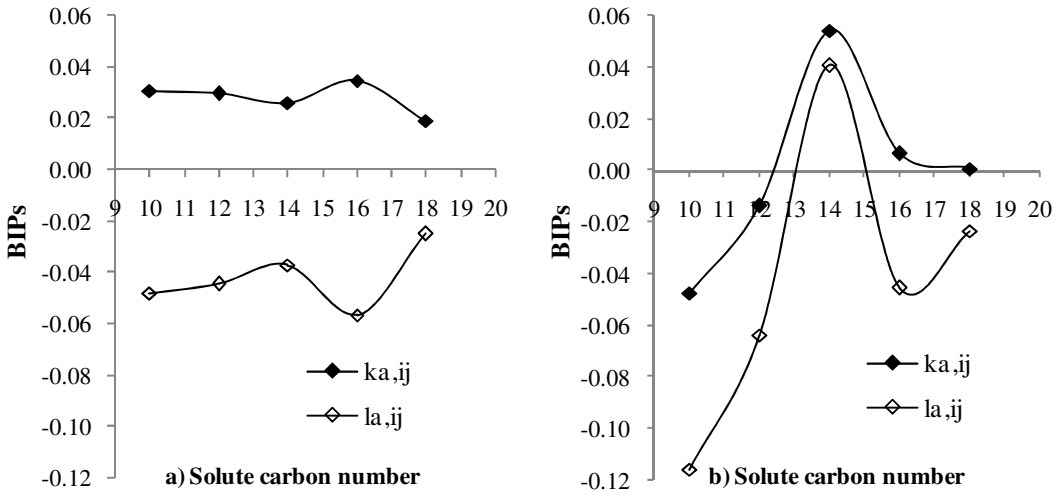

Figure E. 28 BIP vs. Solute carbon number for the PR model regressing a) a single BIP and b) both simultaneously for the propane/1-alcohols

SRK:

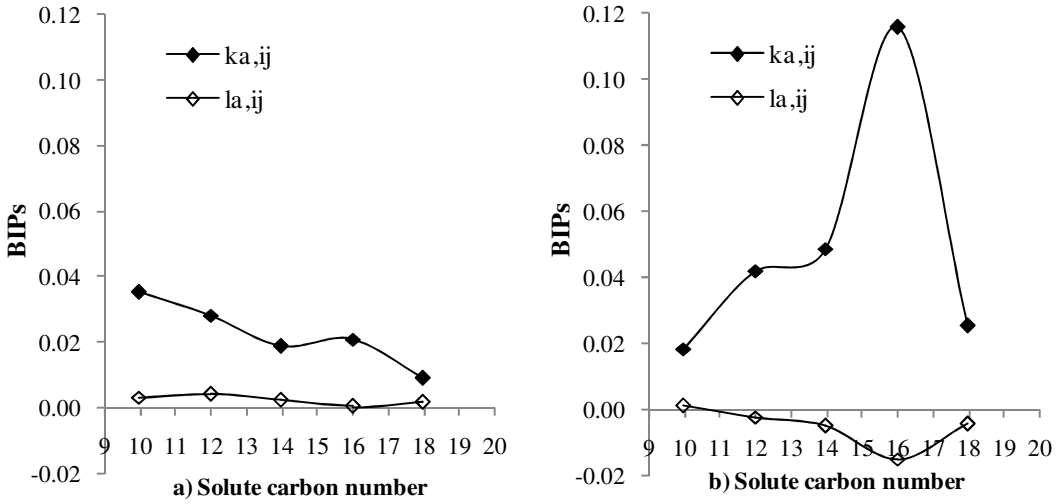

Figure E. 29 BIP vs. Solute carbon number for the SRK model regressing a) a single BIP and b) both simultaneously for the propane/1-alcohols

Stellenbosch University https://scholar.sun.ac.za

SR-POLAR:

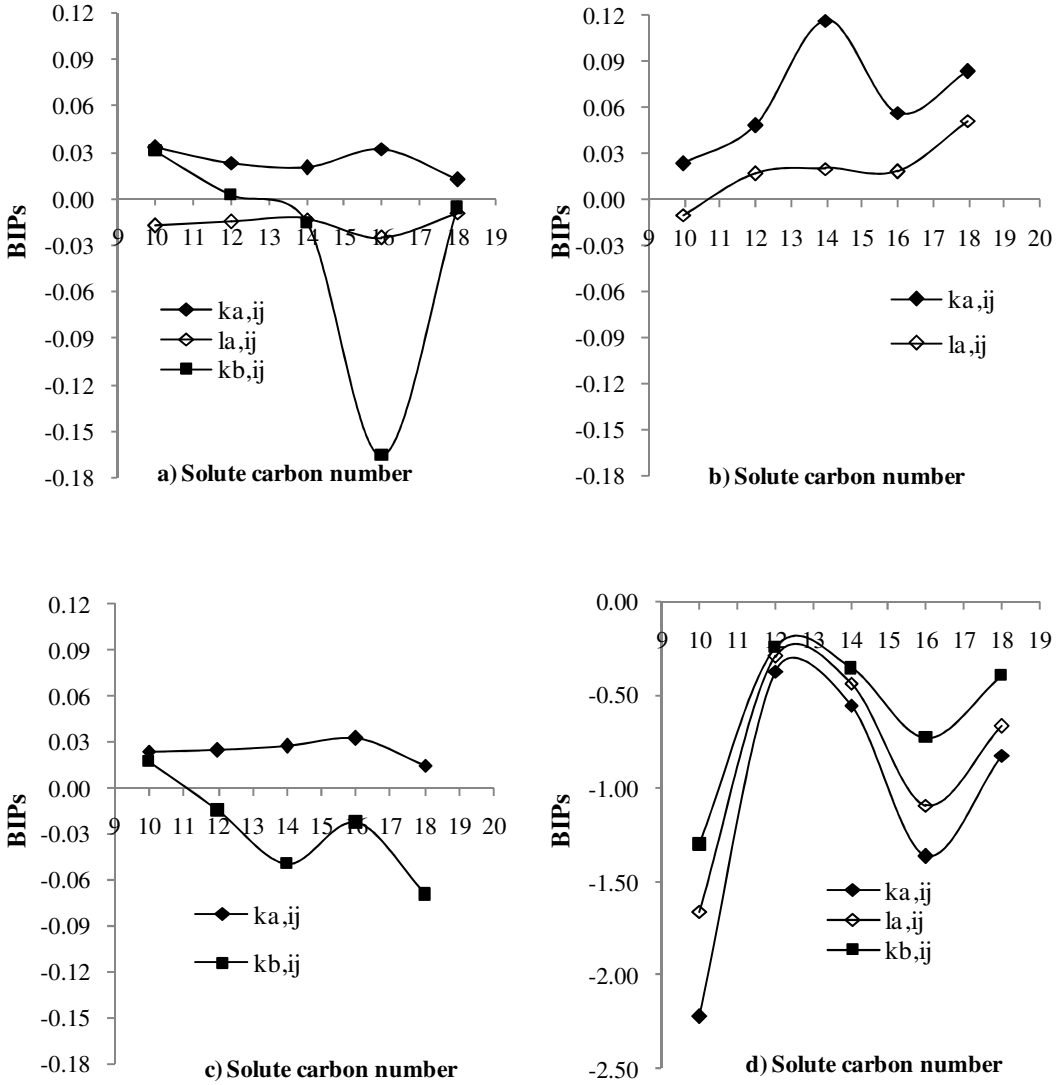

Figure E. 30 BIP vs. Solute carbon number for the SR-POLAR model regressing a) a single BIP, b) both $k_{a,ij}$ and $l_{a,ij}$, c) both $k_{a,ij}$ and $k_{b,ij}$ and d) all three simultaneously for the propane/1-alcohols

Stellenbosch University https://scholar.sun.ac.za

E.1.7 Propane/Carboxylic Acids

RK-ASPEN:

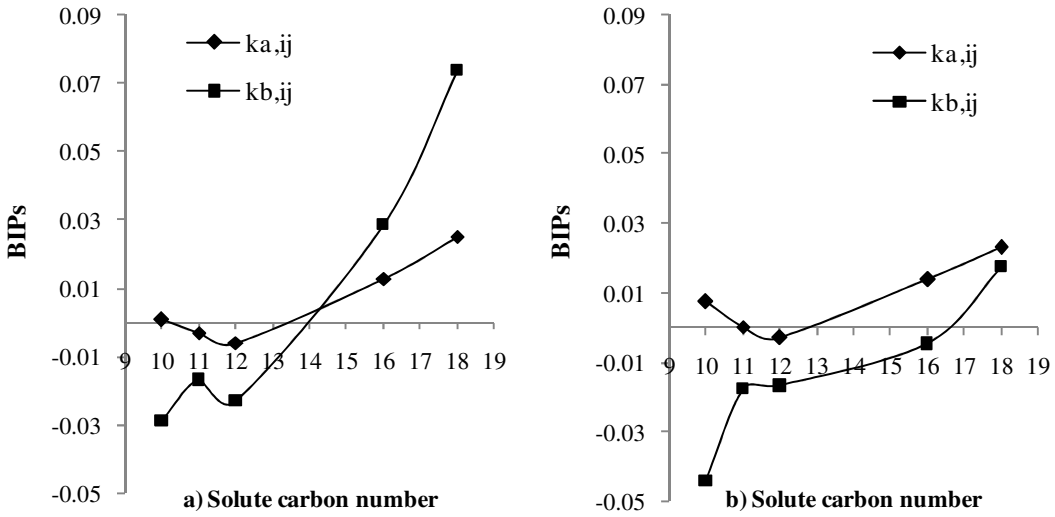

Figure E. 31 BIP vs. Solute carbon number for the RK-ASPEN model regressing a) a single BIP and b) both simultaneously for the propane/carboxylic acids

PR-BM:

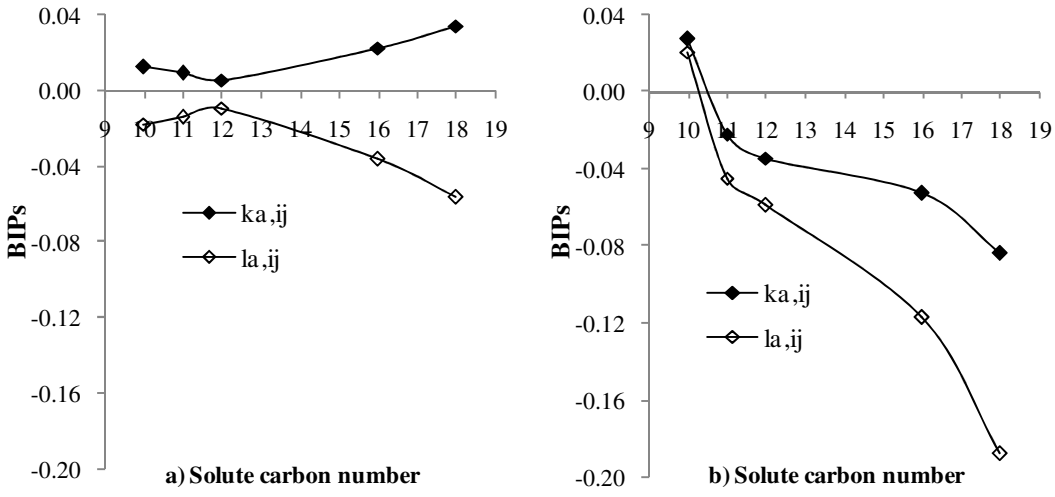

Figure E. 32 BIP vs. Solute carbon number for the PR-BM model regressing a) a single BIP and b) both simultaneously for the propane/carboxylic acids

Stellenbosch University https://scholar.sun.ac.za

PR:

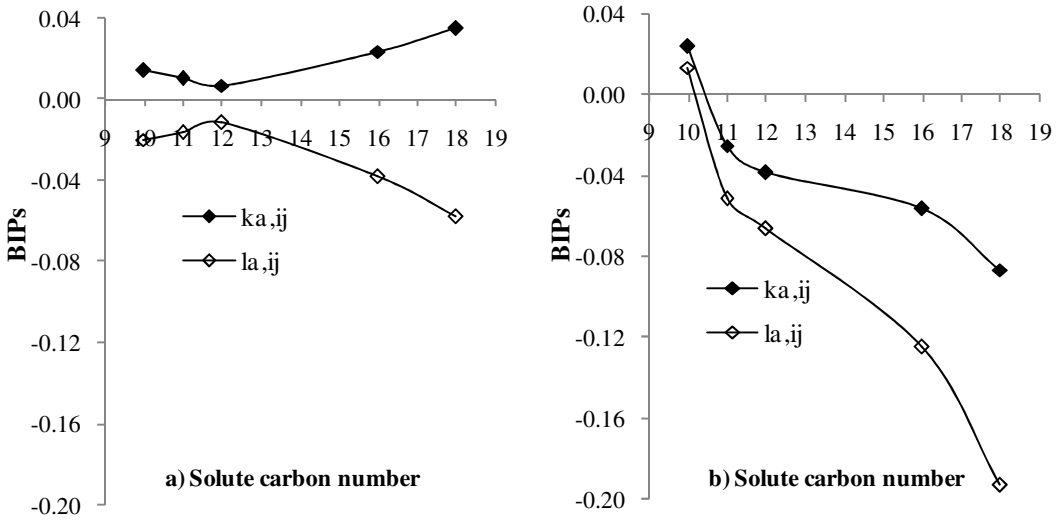

Figure E. 33 BIP vs. Solute carbon number for the PR model regressing a) a single BIP and b) both simultaneously for the propane/carboxylic acids

SRK:

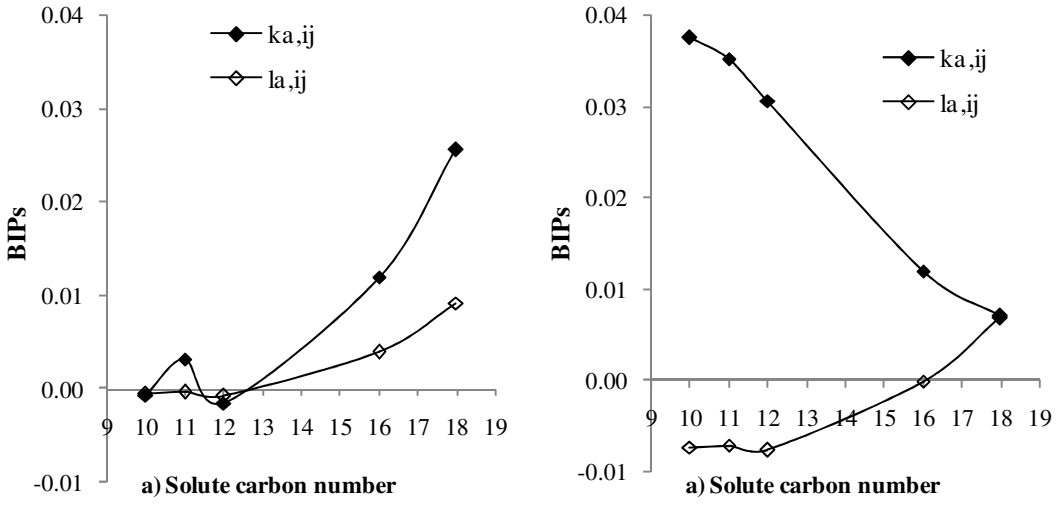

Figure E. 34 BIP vs. Solute carbon number for the SRK model regressing a) a single BIP and b) both simultaneously for the propane/carboxylic acids

Stellenbosch University https://scholar.sun.ac.za

SR-POLAR:

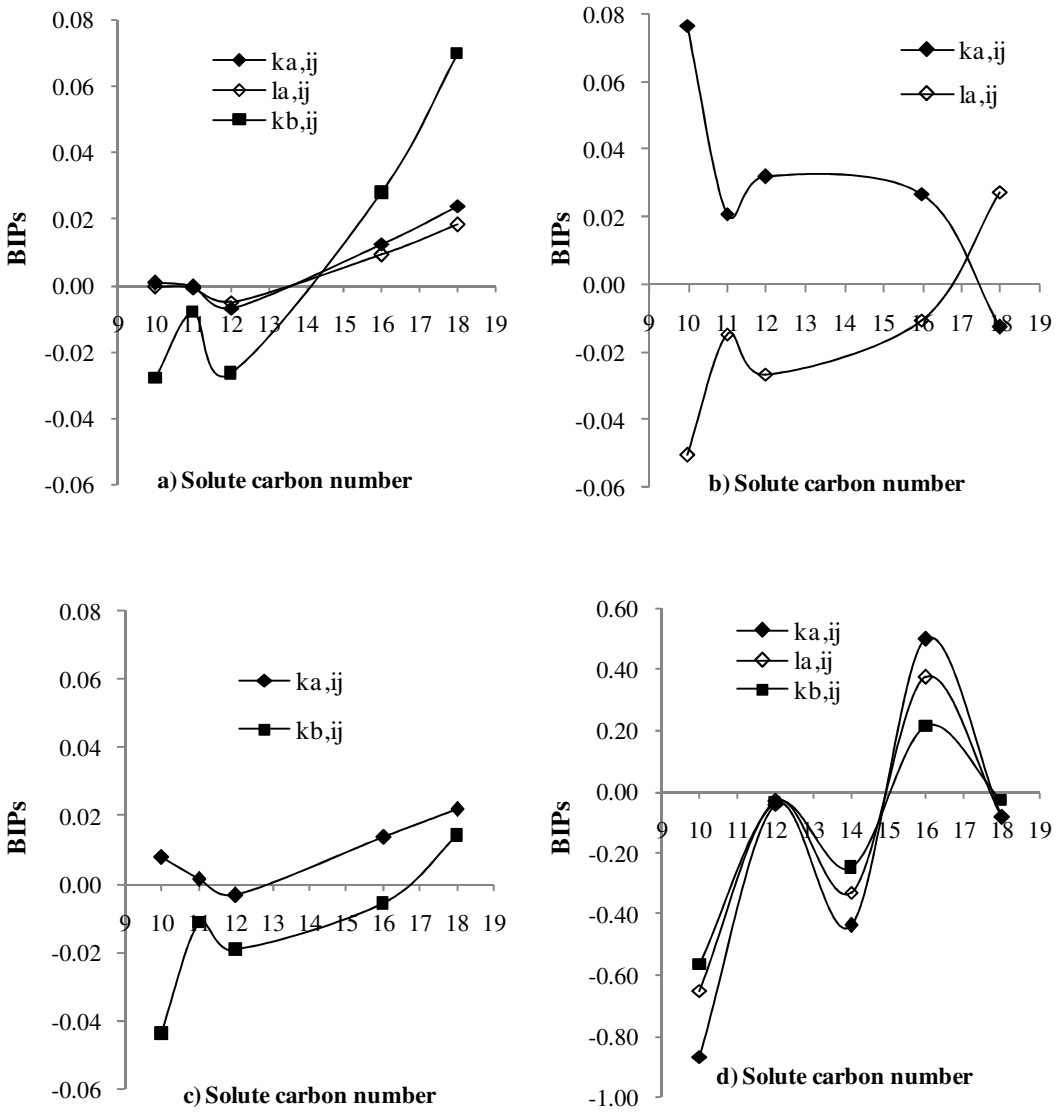

Figure E. 35 BIP vs. Solute carbon number for the SR-POLAR model regressing a) a single BIP, b) both $k_{a,ij}$ and $l_{a,ij}$, c) both $k_{a,ij}$ and $k_{b,ij}$ and d) all three simultaneously for the propane/carboxylic acid

Stellenbosch University https://scholar.sun.ac.za

E.2 ASPEN regression: Parameter values

Table E. 1 Regressed values for additional pure polar parameter, p, in RK-ASPEN model

n-Alkanes	CN	p_i
Ethane	2	0.0309122
Propane	3	0.0114435
N-Decane	10	0.0188267
N-Tetradecane	14	-0.0247356
N-Hexadecane	16	-0.0251255
N-Tetracosane	24	0.1131957
N-Octacosane	28	0.1071697
N-Hexatriacontane	36	-0.0117877
1-Alcohols		
1-Decanol	10	-0.3456655
1-Dodecanol	12	-0.3244521
1-Tetradecanol	14	-0.1679846
1-Hexadecanol	16	-0.1143628
1-Octadecanol	18	-0.0528363
Carboxylic Acids		
Decanoic acid	10	-0.2044598
Undecanoic acid	11	-0.2163252
Dodecanoic acid	12	-0.1862341
Tetradecanoic acid	14	-0.1518723
Hexadecanoic acid	16	-0.1659127
Octadecanoic acid	18	-0.1489059
Methyl Esters		
Methyl Decanoate	10	0.1712581
Methyl Dodecanoate	12	0.0274692
Methyl Tetradecanoate	14	0.0423834
Methyl Hexadecanoate	16	-0.0770793
Methyl Octadecanoate	18	-0.2288297

Stellenbosch University https://scholar.sun.ac.za

Table E. 2BIPs for best regression case for each model – Ethane systems

Solvent:	Ethane										
Model:	PR		PR-BM		SRK		SR-POLAR			RK-ASPEN	
Solute	BIP's:		BIP's:		BIP's:		BIP's:			BIP's:	
Alkanes (CN):	$k_{a,ij}$	$l_{a,ij}$	$k_{a,ij}$	$l_{a,ij}$	$k_{a,ij}$	$l_{a,ij}$	$k_{a,ij}$	$k_{b,ij}$	$l_{a,ij}$	$k_{a,ij}$	$k_{b,ij}$
10	-0.04266	-0.03439	-0.04266	-0.03439	-0.01786	0.00125	-0.14705	-0.07837	-0.10092	-0.01706	
16	0.02246		0.04536	0.04038		0.00506	0.07382	-0.01760	0.03640	0.02681	-0.04326
24	-0.08130	-0.19160	-0.07193	-0.17333	-0.19302	0.08955	-0.44604	-0.13277	-0.41049	0.03373	0.00444
28	-0.17211	-0.35779	-0.16439	-0.34245	-0.17151	0.09205	-0.28628	-0.06098	-0.27815	0.03360	0.02126
36	-0.63154	-1.18707	-0.62719	-1.17782	-0.04150	0.03564	-0.47505		-0.44909	0.02350	0.08489
Alcohols (CN):	$k_{a,ij}$	$l_{a,ij}$	$k_{a,ij}$	$l_{a,ij}$	$k_{a,ij}$	$l_{a,ij}$	$k_{a,ij}$	$k_{b,ij}$	$l_{a,ij}$	$k_{a,ij}$	$k_{b,ij}$
10	-0.05409	-0.18517	-0.05467	-0.18313	0.03207	0.02156	1.61813	0.90762	1.18924	0.03678	0.03887
12	-0.14865	-0.32957	-0.14822	-0.32609	-0.03844	0.05342	1.38041	0.70348	1.05082	0.02977	0.06692
14	-0.11295	-0.27403	-0.11324	-0.27199	-0.03557	0.05428	0.36029	0.19818	0.26358	0.03548	0.05959
16	-0.12283	-0.29426	-0.12317	-0.29254	-0.05761	0.06985	0.07680	0.06916	0.03464	0.03852	0.06090
18	-0.18718	-0.39799	-0.18694	-0.39553	-0.19505	0.13441	0.36174	0.18518	0.27271	0.03707	0.07830
Acids (CN):	$k_{a,ij}$	$l_{a,ij}$	$k_{a,ij}$	$l_{a,ij}$	$k_{a,ij}$	$l_{a,ij}$	$k_{a,ij}$	$k_{b,ij}$	$l_{a,ij}$	$k_{a,ij}$	$k_{b,ij}$
10	0.04085	0.05210	0.04417	0.06052	-0.13716	0.05502	-0.32050	-0.21352	-0.25045	-0.00636	-0.05844
12	0.00743	-0.01645	0.01023	-0.00921	-0.21062	0.08704	-0.26139	-0.15949	-0.21082	0.00279	-0.03410
14	-0.05921	-0.14615	-0.05754	-0.14094	-0.32701	0.18330	0.02232		0.01145	0.01260	0.00563
16	-0.11692	-0.25343	-0.11553	-0.24885	-0.25130	0.15348	-0.15170	-0.04285	-0.13738	0.01653	0.02644
18	-0.11430	-0.25845	-0.11347	-0.25520	-0.60058	0.29191	1.08342	0.36943	0.89047	0.02438	0.02609
Meth. Est. (CN):	$k_{a,ij}$	$l_{a,ij}$	$k_{a,ij}$	$l_{a,ij}$	$k_{a,ij}$	$l_{a,ij}$	$k_{a,ij}$	$k_{b,ij}$	$l_{a,ij}$	$k_{a,ij}$	$k_{b,ij}$
10	0.06102	0.07842	0.06757	0.09283	-0.03223	0.00861	-0.61235	-0.34601	-0.48789	0.01451	-0.03721
12	-0.06941	-0.14074	-0.06500	-0.12947		0.00416	-0.27357	-0.10952	-0.22975	0.01249	0.01480
14	-0.09535	-0.19503	-0.09144	-0.18493	0.03980	-0.00647	0.42048	0.18533	0.32571	0.01835	0.02858
16	-0.08626	-0.20978	-0.08013	-0.19678	0.04240	-0.00183	-0.31504	-0.10041	-0.29403	0.03532	0.01109
18	-0.24787	-0.50328	-0.24177	-0.49045	0.05539	0.00197	0.20587	0.12825	0.13312	0.03929	0.05140

Stellenbosch University https://scholar.sun.ac.za

Table E. 3 BIPs for best regression case for each model – Propane systems

Solvent:	Propane										
Model:	PR		PR-BM		SRK		SR-POLAR			RK-ASPEN	
Solute	BIP's:		BIP's:		BIP's:		BIP's:			BIP's:	
Alkanes (CN):	$k_{a,ij}$	$l_{a,ij}$	$k_{a,ij}$	$l_{a,ij}$	$k_{a,ij}$	$l_{a,ij}$	$k_{a,ij}$	$k_{b,ij}$	$l_{a,ij}$	$k_{a,ij}$	$k_{b,ij}$
14	-0.04425	-0.10901	-0.04076	-0.10010	-0.03378	0.00887	-6.60909	-2.96890	-5.32856	0.03407	0.01283
16		-0.05509		-0.05221	0.01611	0.00258	-5.12155	-2.19084	-4.15632	0.04687	-0.03919
24	-0.06181	-0.14316	-0.05300	-0.12785		-0.00244	-1.54344	-0.50449	-1.29802	0.03308	0.00204
28	-0.16028	-0.30372	-0.15128	-0.28785		0.00164	-1.36516	-0.37121	-1.17107	0.02736	0.01823
36	-0.46939	-0.83524	-0.45946	-0.81725	-0.22814	0.07535	-2.81974	-0.53069	-2.48578	0.01514	0.04840
Alcohols (CN):	$k_{a,ij}$	$l_{a,ij}$	$k_{a,ij}$	$l_{a,ij}$	$k_{a,ij}$	$l_{a,ij}$	$k_{a,ij}$	$k_{b,ij}$	$l_{a,ij}$	$k_{a,ij}$	$k_{b,ij}$
10	-0.04735	-0.11542	-0.05009	-0.10977		0.00317	-2.22036	-1.29888	-1.65724	0.02295	0.01159
12	-0.01343	-0.06357	-0.01343	-0.06357		0.00433			-0.01502	0.02138	
14	0.02629		0.02506		0.04883	-0.00479	-0.55231	-0.35680	-0.43561	0.02660	-0.05278
16		-0.05649		-0.05649	0.02101		-1.36255	-0.72991	-1.08810	0.03295	
18		-0.02477		-0.02477	0.02567	-0.00431	-0.82279	-0.39606	-0.66333	0.01249	
Acids (CN):	$k_{a,ij}$	$l_{a,ij}$	$k_{a,ij}$	$l_{a,ij}$	$k_{a,ij}$	$l_{a,ij}$	$k_{a,ij}$	$k_{b,ij}$	$l_{a,ij}$	$k_{a,ij}$	$k_{b,ij}$
10	0.02344	0.01340	0.02738	0.02104	-0.00061		-0.86512	-0.56421	-0.64899	0.00777	-0.04400
11	-0.02514	-0.05161	-0.02171	-0.04470		-0.00025			-0.00056	-0.00284	
12	-0.03840	-0.06640	-0.03417	-0.05829		-0.00080	-0.43720	-0.24721	-0.32853	-0.00586	
16	-0.05640	-0.12456	-0.05237	-0.11684		0.00398	0.49879	0.21507	0.37655	0.01392	-0.00459
18	-0.08640	-0.19311	-0.08384	-0.18777		0.00924	-0.07881	-0.02779	-0.08067	0.02302	0.01757

Stellenbosch University https://scholar.sun.ac.za

E.3 Pure components

E.3.1 n-Alkanes

PT:

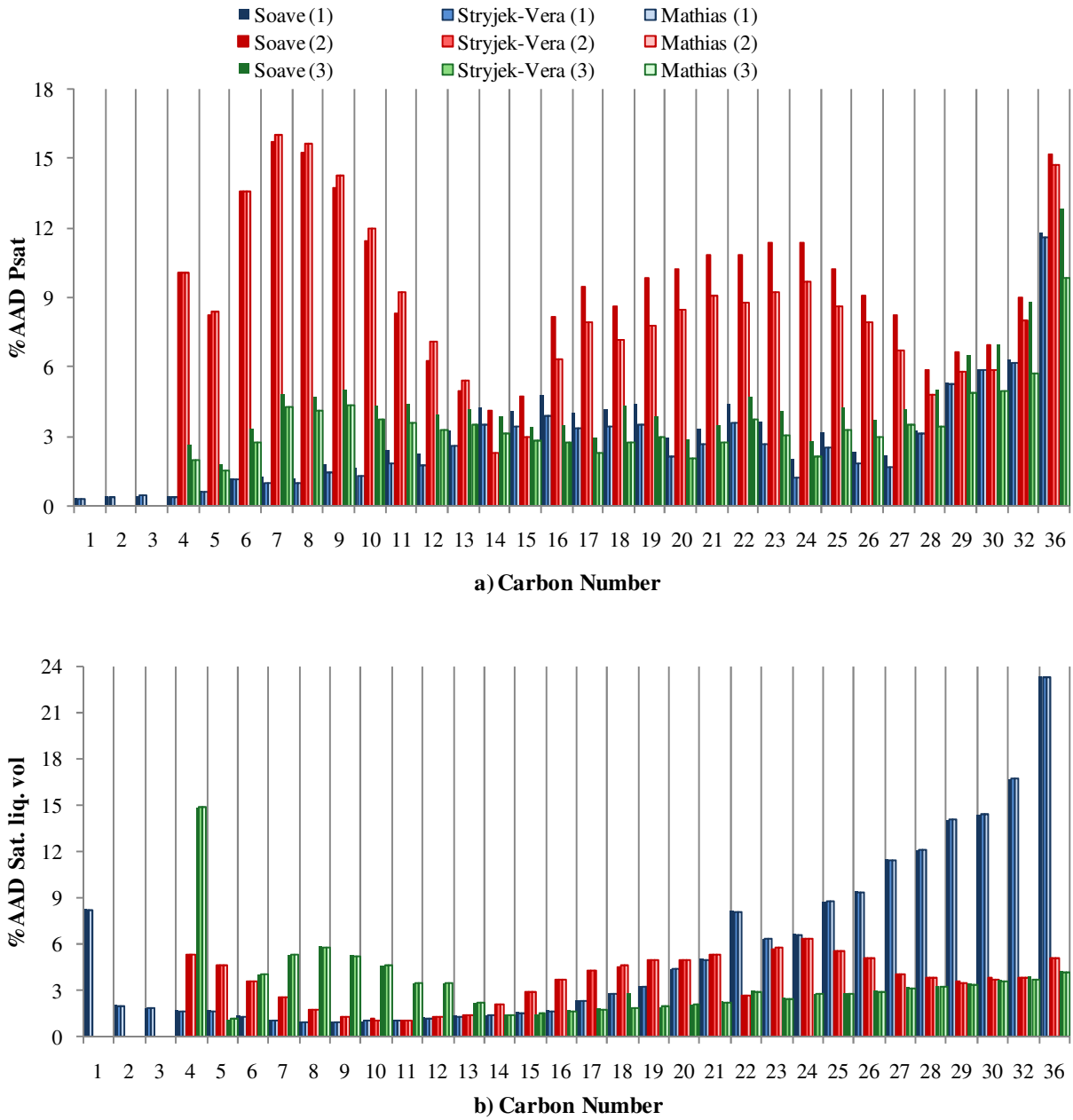

Figure E. 36 %AAD in avapour pressure and b) saturated liquid volume for the n-alkane series with the PT EOS using the Soave, Stryjek-Vera and Mathias alpha function for cases 1 (blue) ,2 (red) and 3 (green) as given in Table 6-4

Stellenbosch University https://scholar.sun.ac.za

SRK:

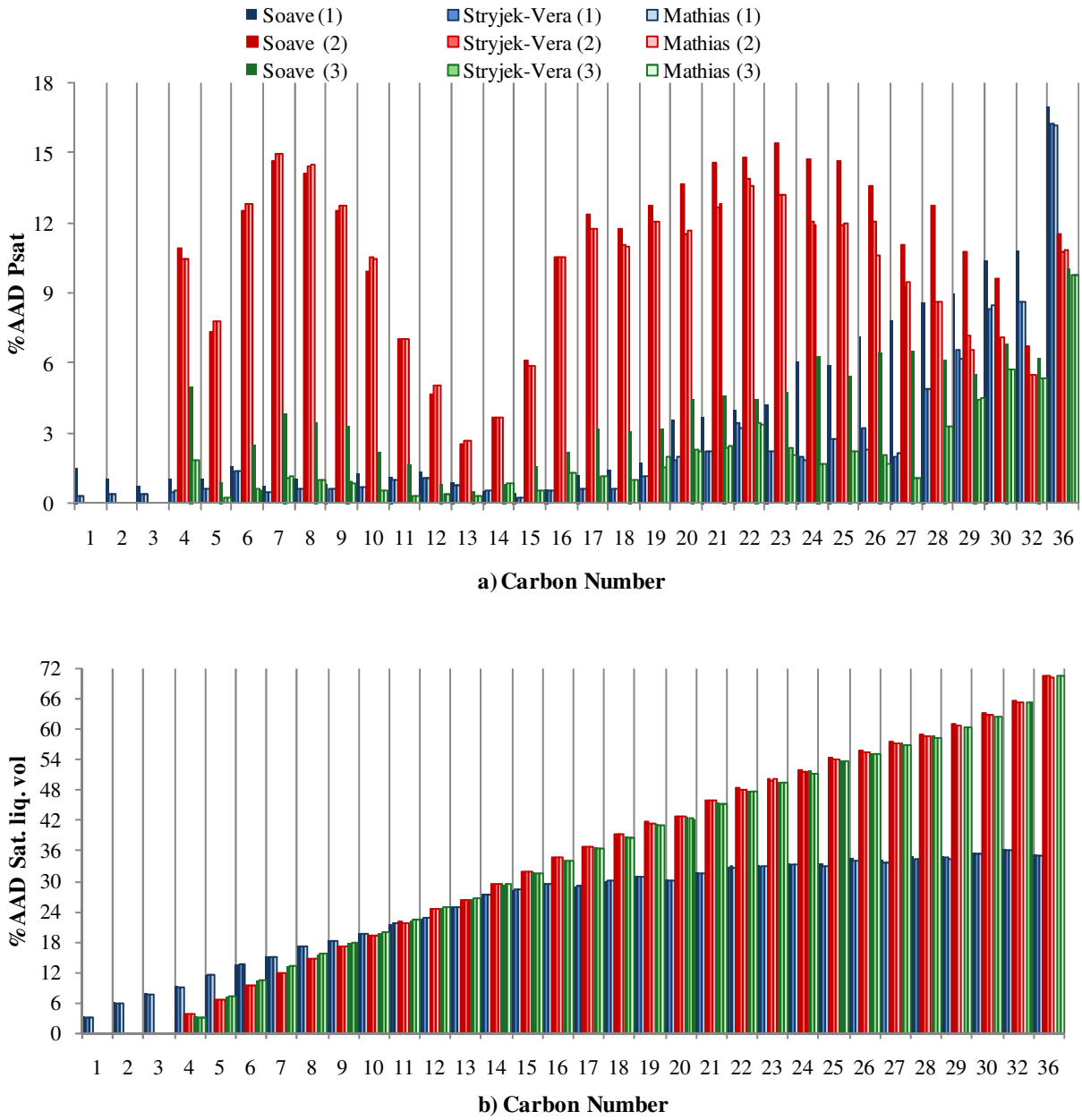

Figure E. 37 %AAD in a) vapour pressure and b) saturated liquid volume for the n-alkane series with the SRK EOS using the Soave, Stryjek-Vera and Mathias alpha function for cases 1 (blue) ,2 (red) and 3 (green) as given in Table 6-4

Stellenbosch University https://scholar.sun.ac.za

E.3.2-Alcohols

PR:

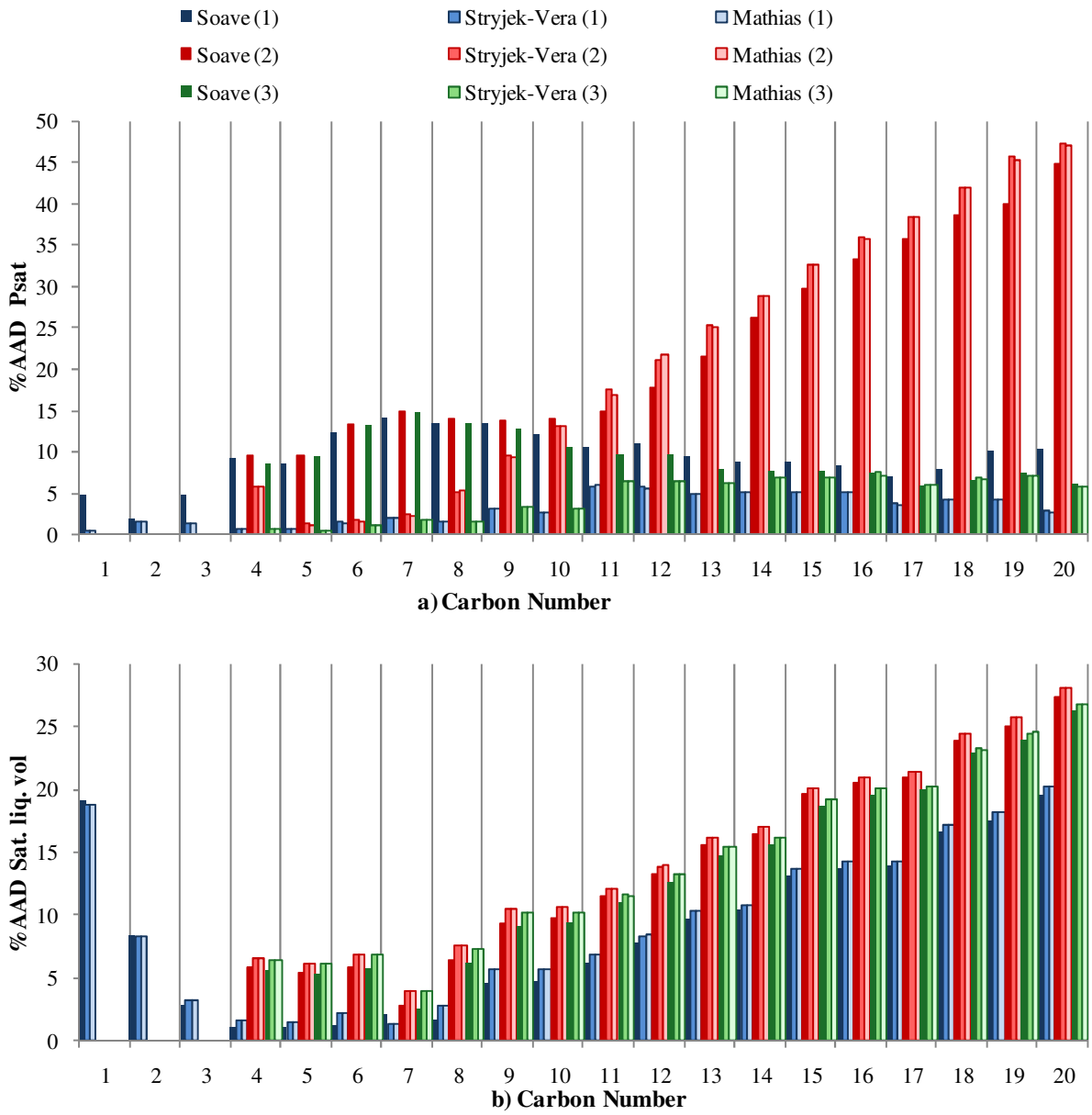

Figure E. 38 %AAD in a) vapour pressure and b) saturated liquid volume for the 1-alcohol series with the PR EOS using the Soave, Stryjek-Vera and Mathias alpha function for cases 1 (blue) ,2 (red) and 3 (green) as given inTable 6-4

Stellenbosch University https://scholar.sun.ac.za

PT:

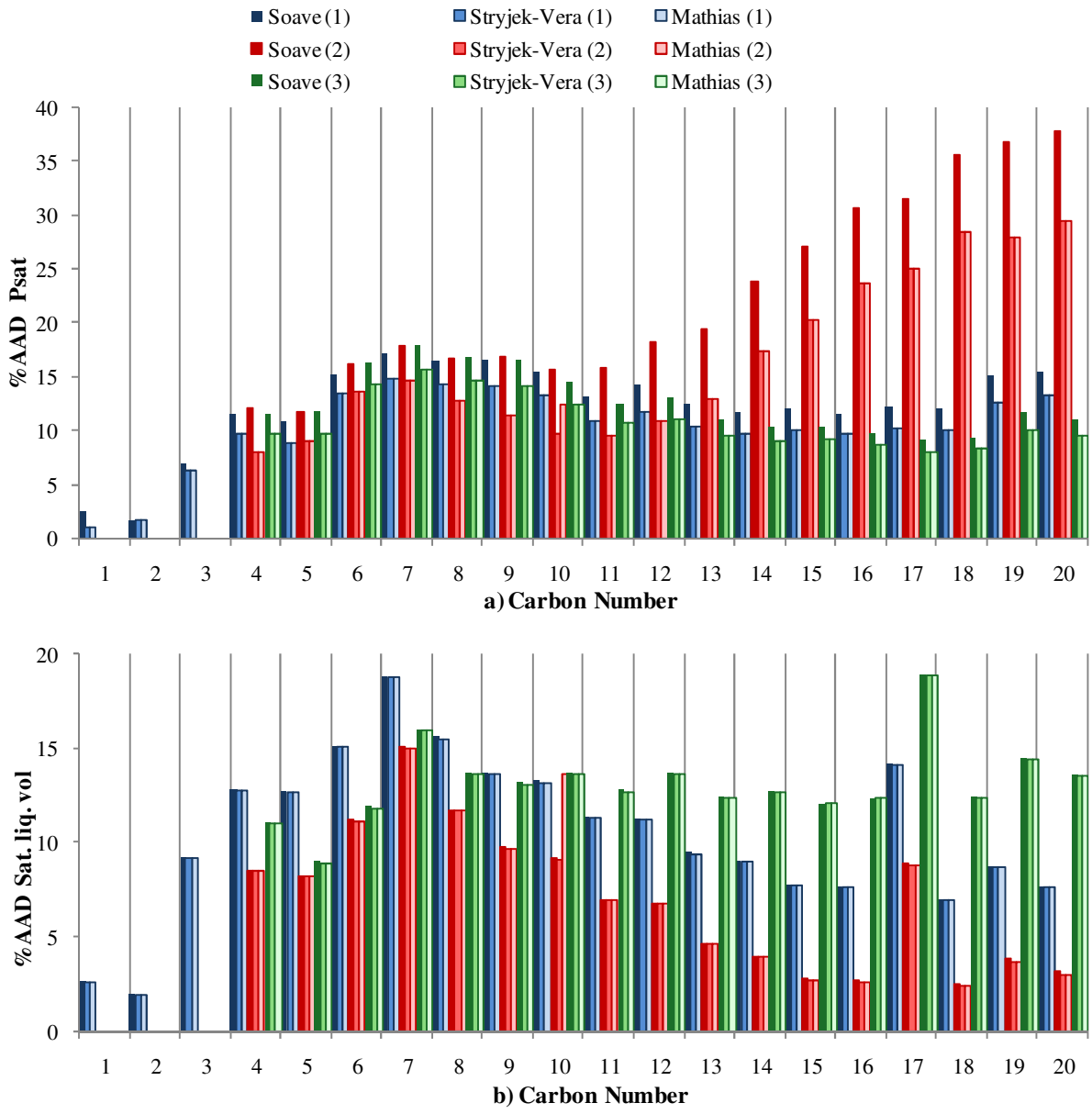

Figure E. 39 %AAD in a) vapour pressure and b) saturated liquid volume for the 1-alcohol series with the PT EOS using the Soave, Stryjek-Vera and Mathias alpha function for cases 1 (blue) ,2 (red) and 3 (green) as given inTable 6-4

Stellenbosch University https://scholar.sun.ac.za

SRK:

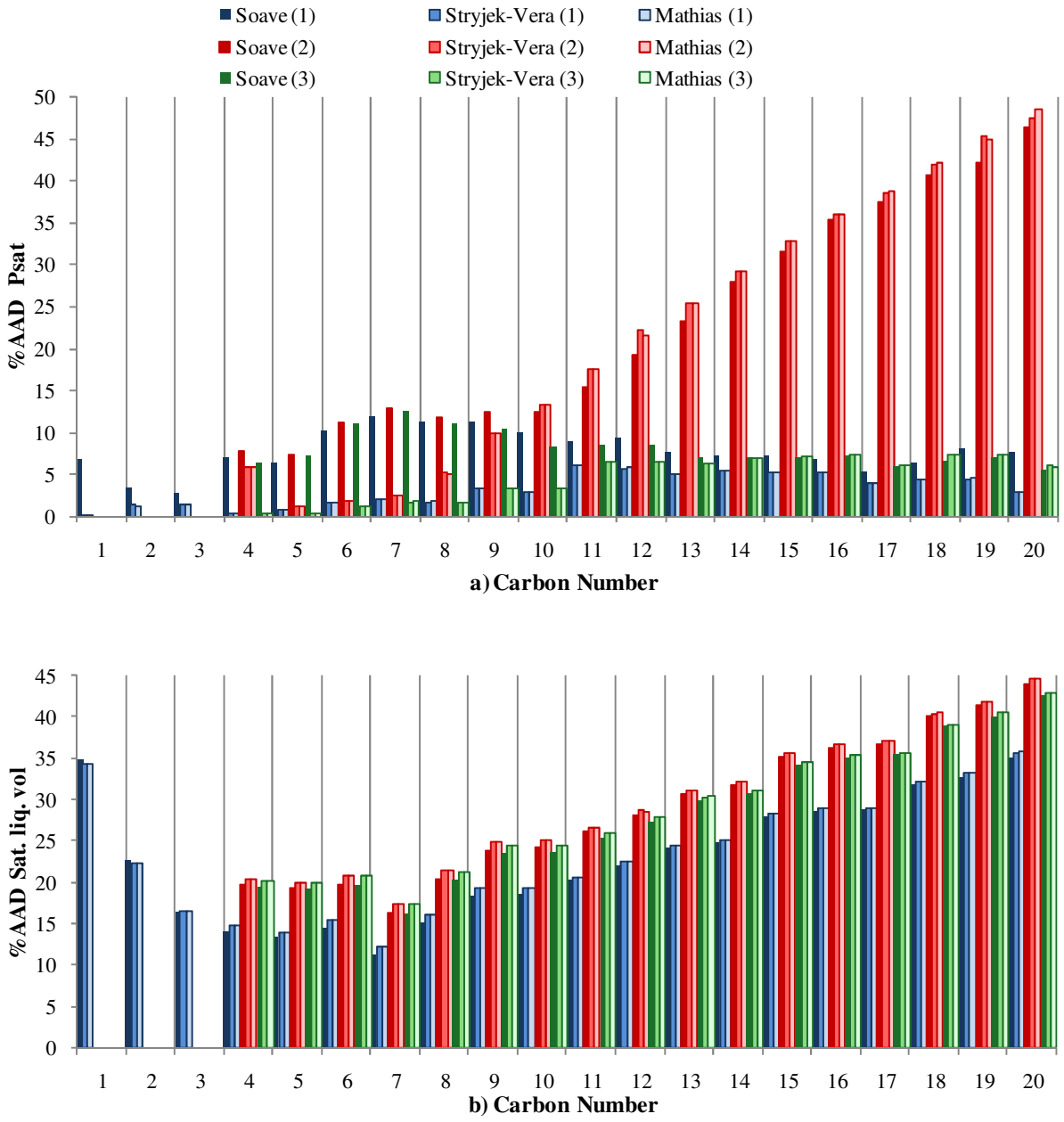

Figure E. 40 %AAD in a) vapour pressure and b) saturated liquid volume for the 1-alcohol series with the SRK EOS using the Soave, Stryjek-Vera and Mathias alpha function for cases 1 (blue) ,2 (red) and 3 (green) as given inTable 6-4

Stellenbosch University https://scholar.sun.ac.za

E.3.3 Carboxylic Acids

PR:

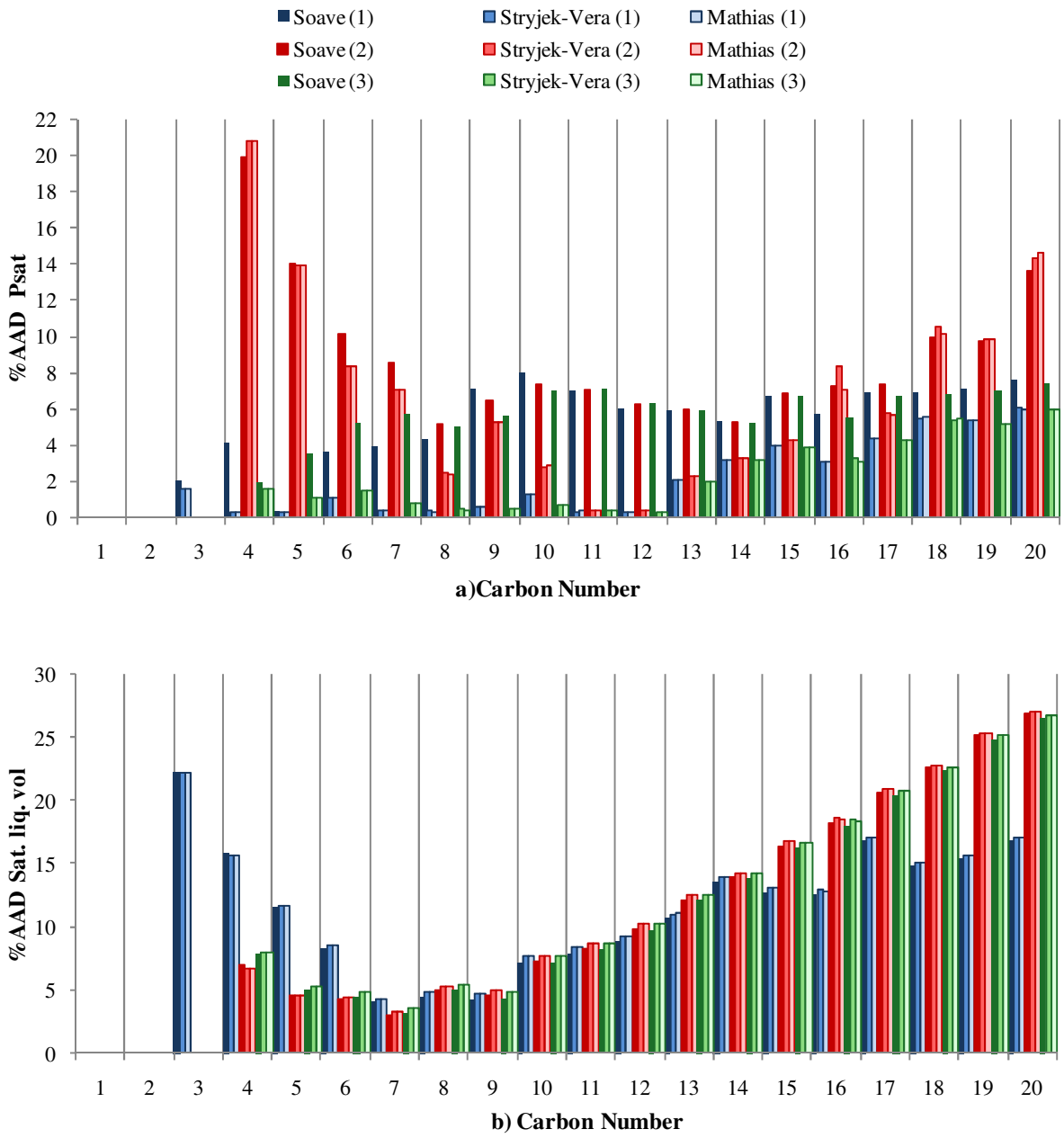

Figure E. 41 %AAD in a) vapour pressure and b) saturated liquid volume for the carboxylic acid series with the PR EOS using the Soave, Stryjek-Vera and Mathias alpha function for cases 1 (blue) ,2 (red) and 3 (green) as given inTable 6-4

Stellenbosch University https://scholar.sun.ac.za

PT:

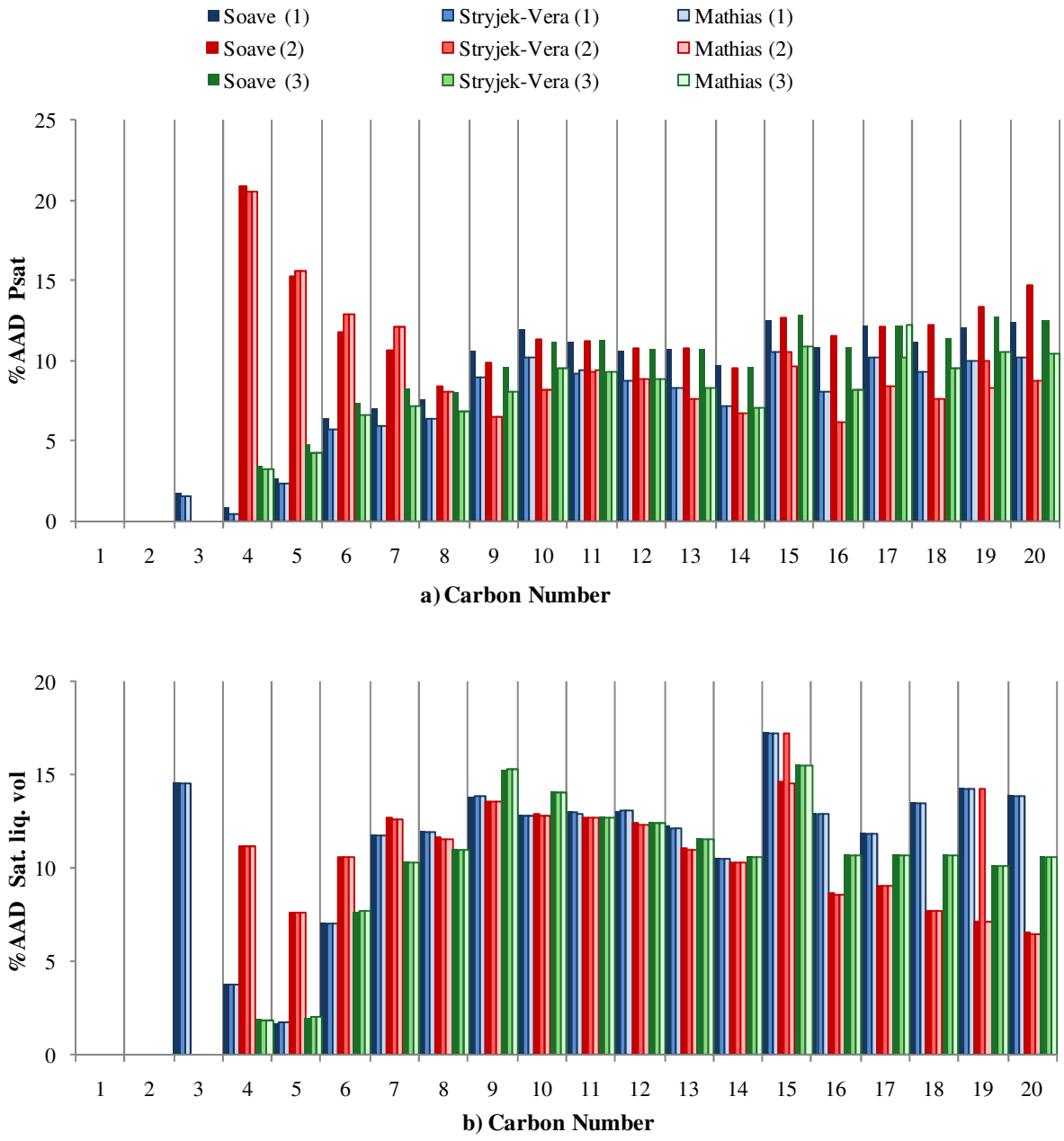

Figure E. 42 %AAD in a) vapour pressure and b) saturated liquid volume for the carboxylic acid series with the PT EOS using the Soave, Stryjek-Vera and Mathias alpha function for cases 1 (blue) ,2 (red) and 3 (green) as given inTable 6-4

Stellenbosch University https://scholar.sun.ac.za

SRK:

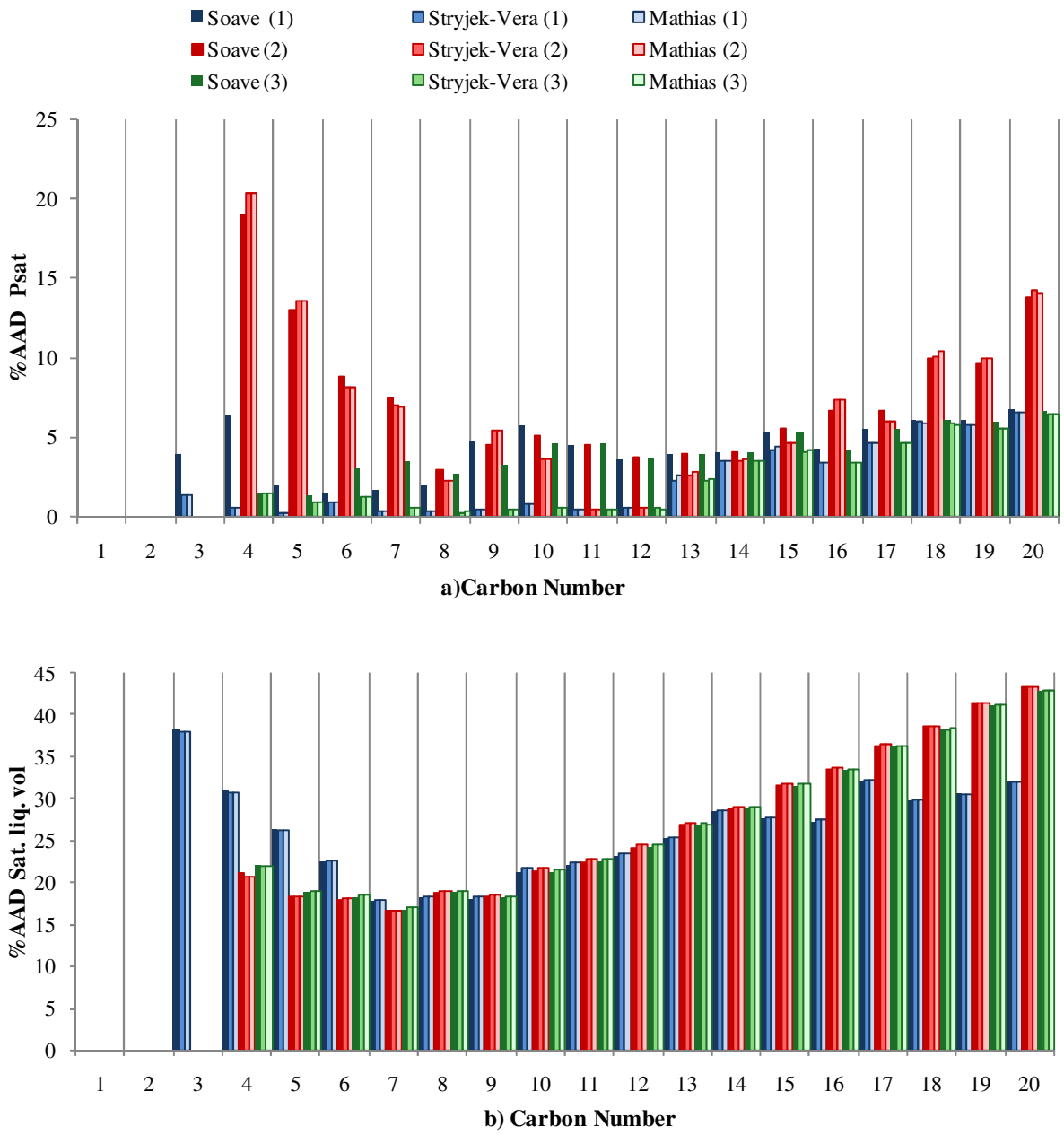

Figure E. 43 %AAD in a) vapour pressure and b) saturated liquid volume for the carboxylic acid series with the SRK EOS using the Soave, Stryjek-Vera and Mathias alpha function for cases 1 (blue) ,2 (red) and 3 (green) as given inTable 6-4

Stellenbosch University https://scholar.sun.ac.za

E.3.4 Methyl Esters

PR:

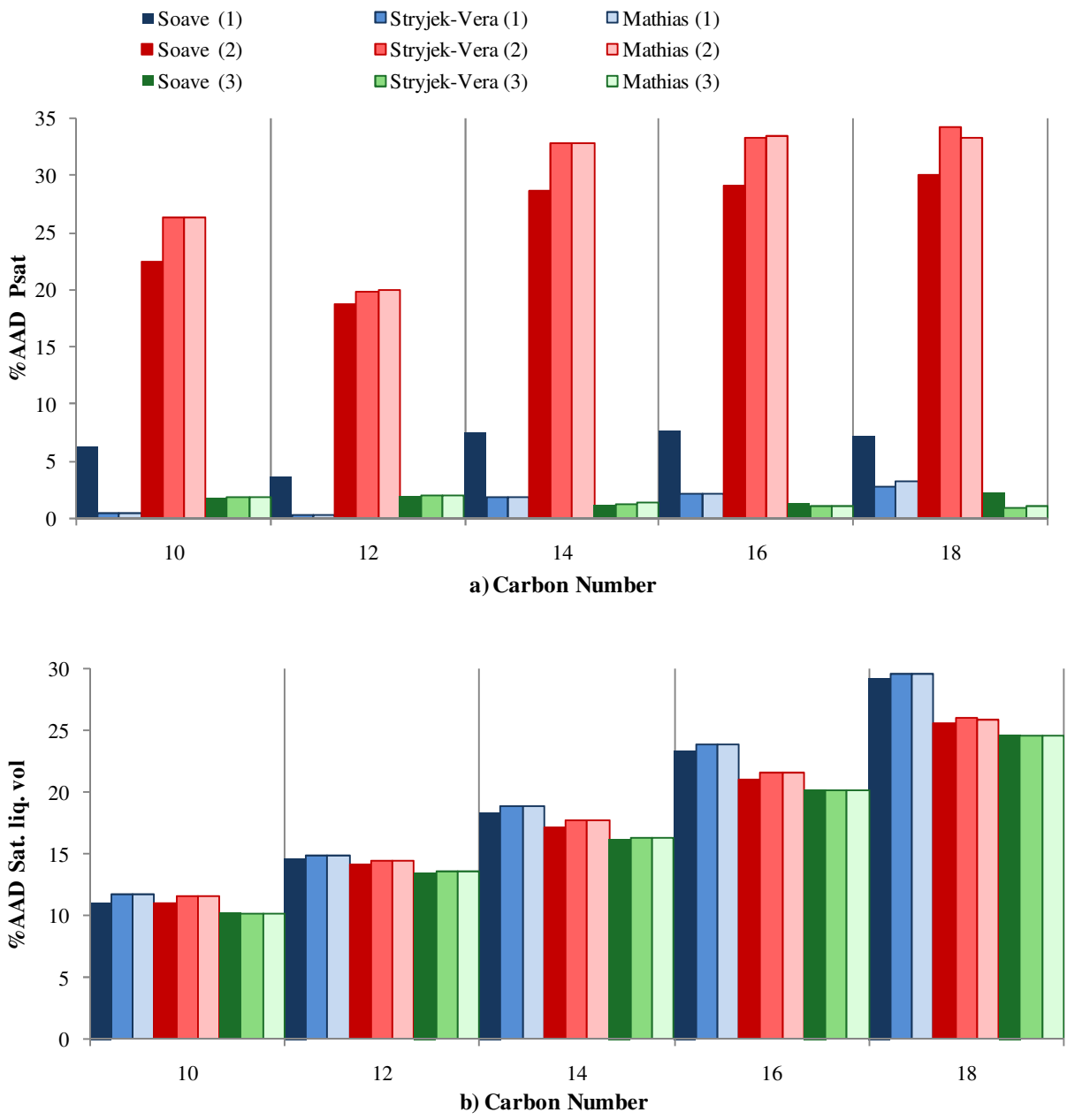

Figure E. 44 %AAD in a) pressure and b) saturated liquid volume for the methyl ester series with the PR EOS using the Soave, Stryjek-Vera and Mathias alpha function for cases 1 (blue) ,2 (red) and 3 (green) as given inTable 6-4

Stellenbosch University https://scholar.sun.ac.za

PT:

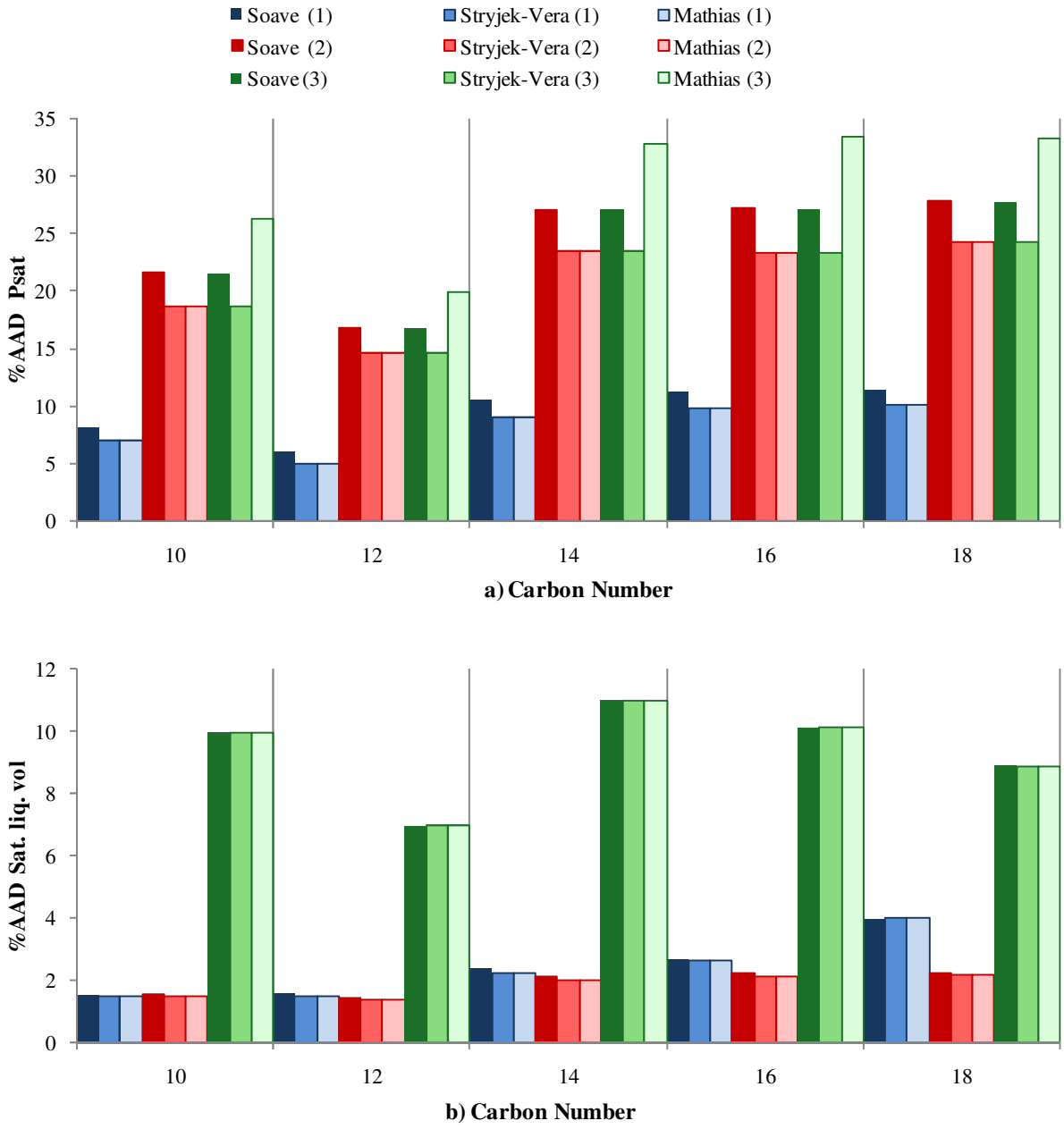

Figure E. 45 %AAD in a) pressure and b) saturated liquid volume for the methyl ester series with the PT EOS using the Soave, Stryjek-Vera and Mathias alpha function for cases 1 (blue) ,2 (red) and 3 (green) as given inTable 6-4

Stellenbosch University https://scholar.sun.ac.za

SRK:

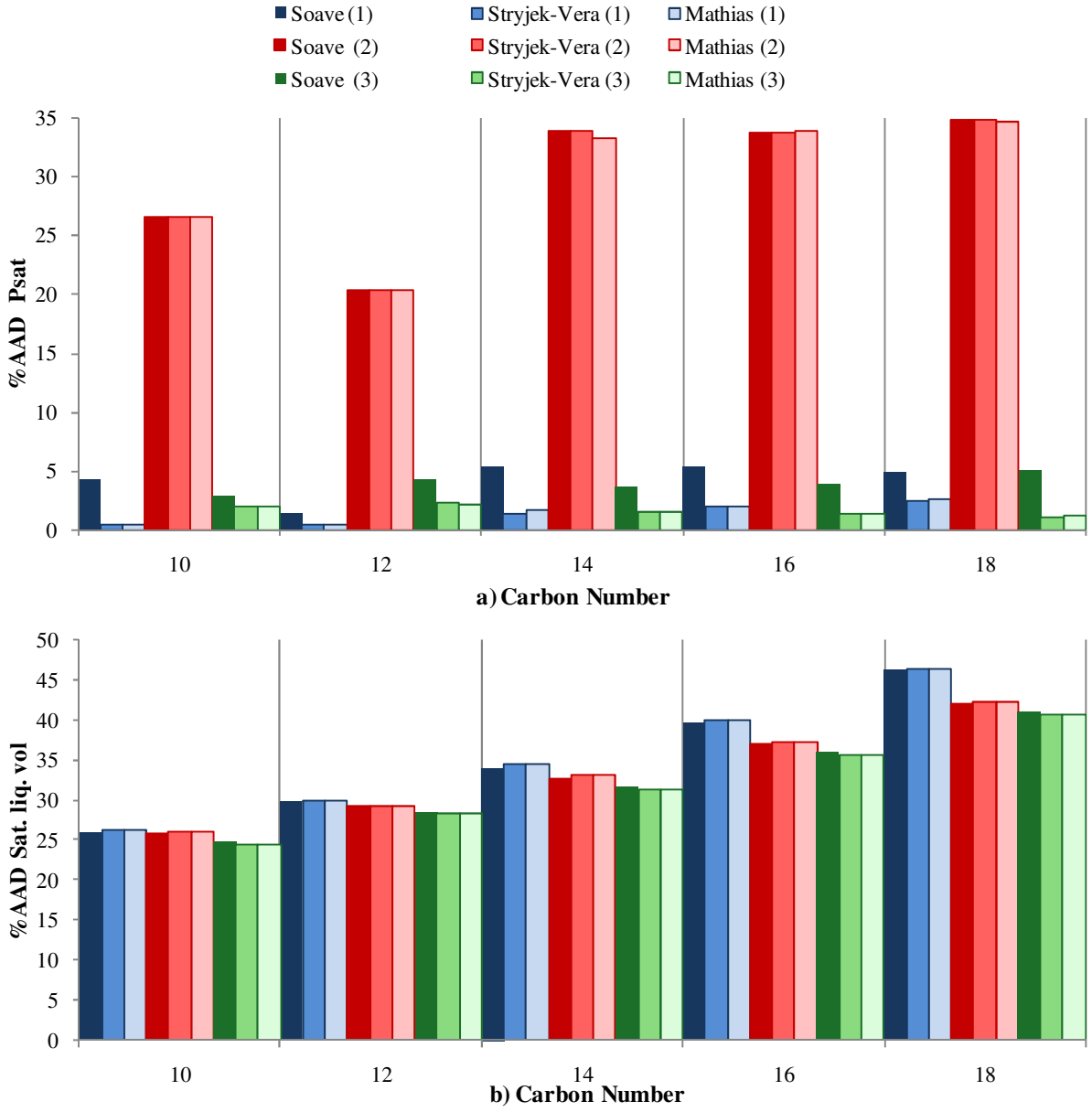

Figure E. 46 %AAD in a) pressure and b) saturated liquid volume for the methyl ester series with the SRK EOS using the Soave, Stryjek-Vera and Mathias alpha function for cases 1 (blue) ,2 (red) and 3 (green) as given inTable 6-4

Stellenbosch University https://scholar.sun.ac.za

E.3.5 Pure parameters

PRM

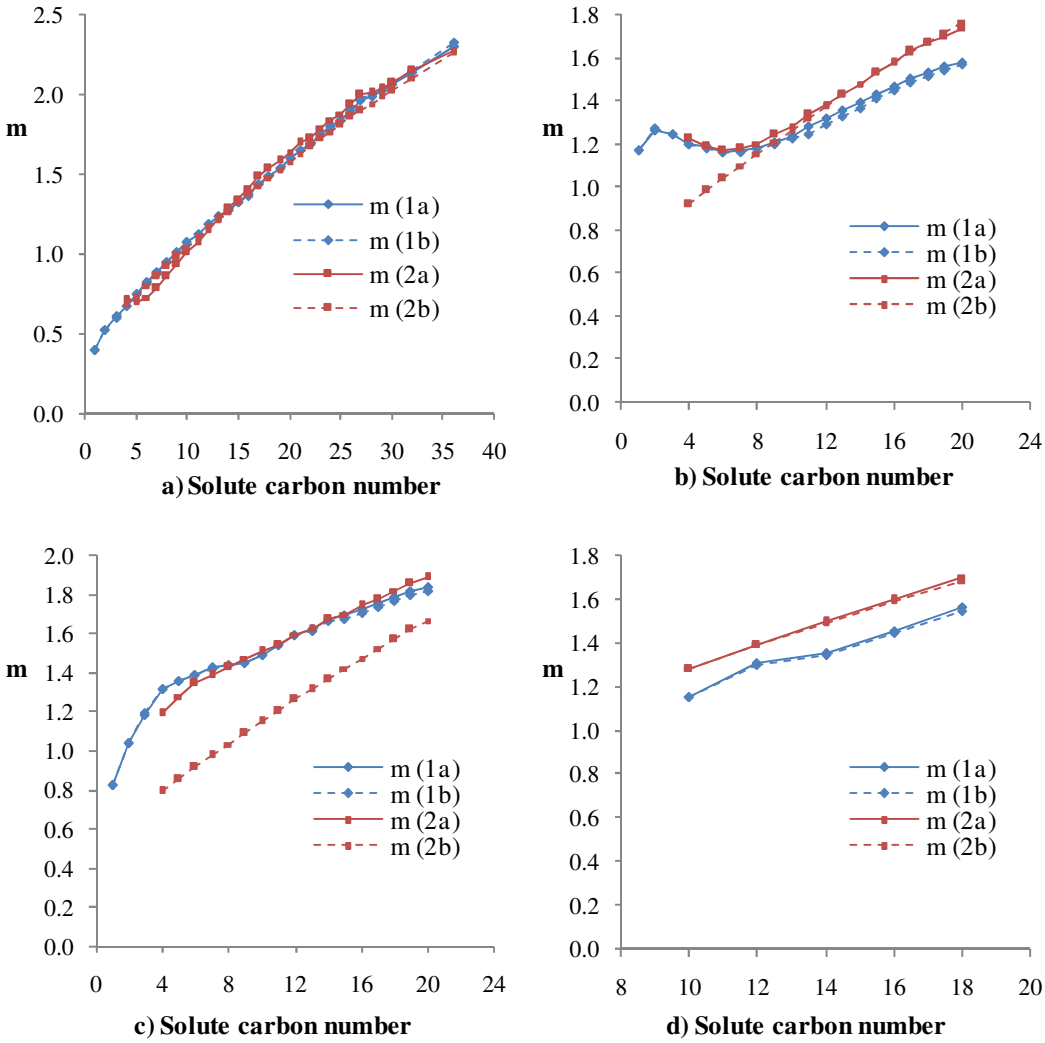

Figure E.47 Mathias alpha function parameter m vs. carbon number for the a) n-alkanes, b) 1-alcohols, c) carboxylic acid and d) methyl esters in the PR model for cases given in Table 6-3

Stellenbosch University https://scholar.sun.ac.za

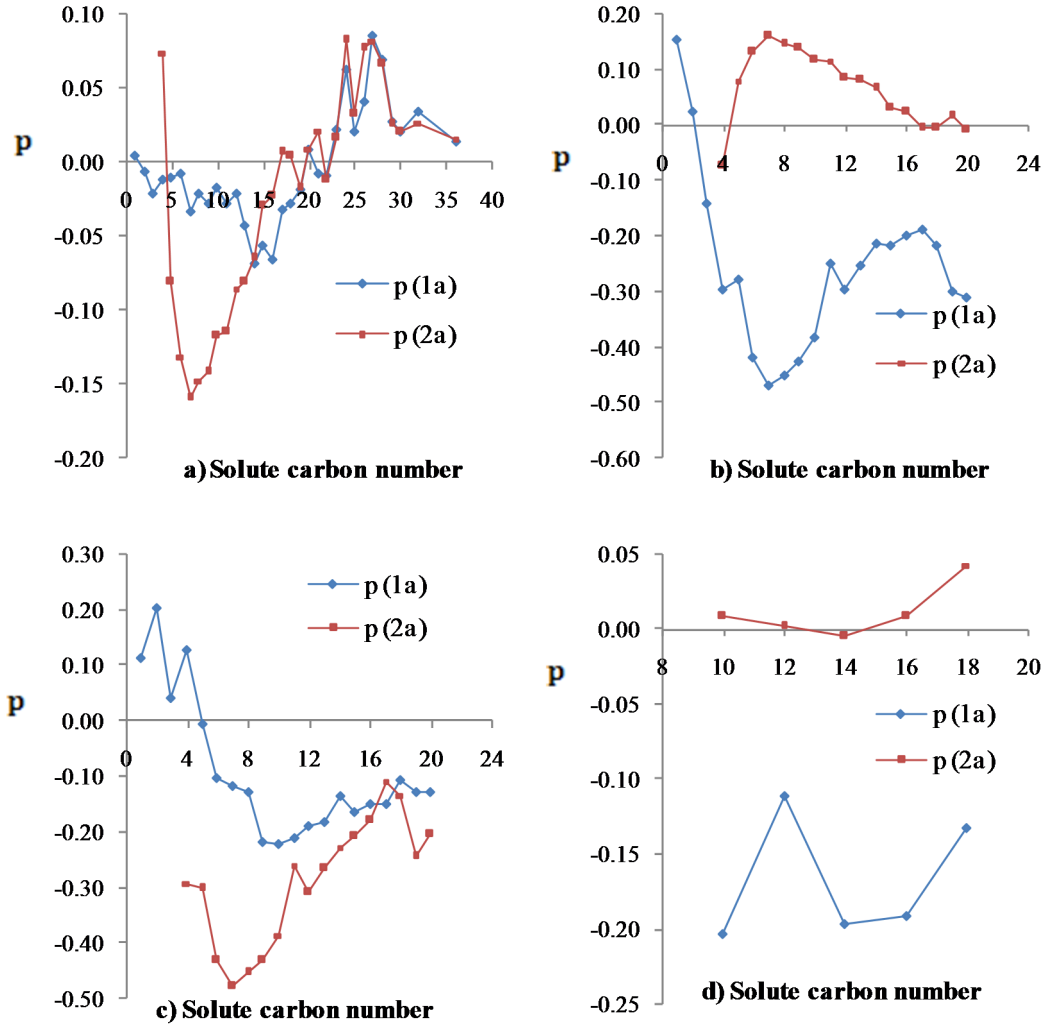

Figure E.48 Mathias alpha function parameter p vs. carbon number for the a) n-alkanes, b) 1-alcohols, c) carboxylic acid and d) methyl esters in the PR model for cases given in Table 6-3

Stellenbosch University https://scholar.sun.ac.za

SRK:

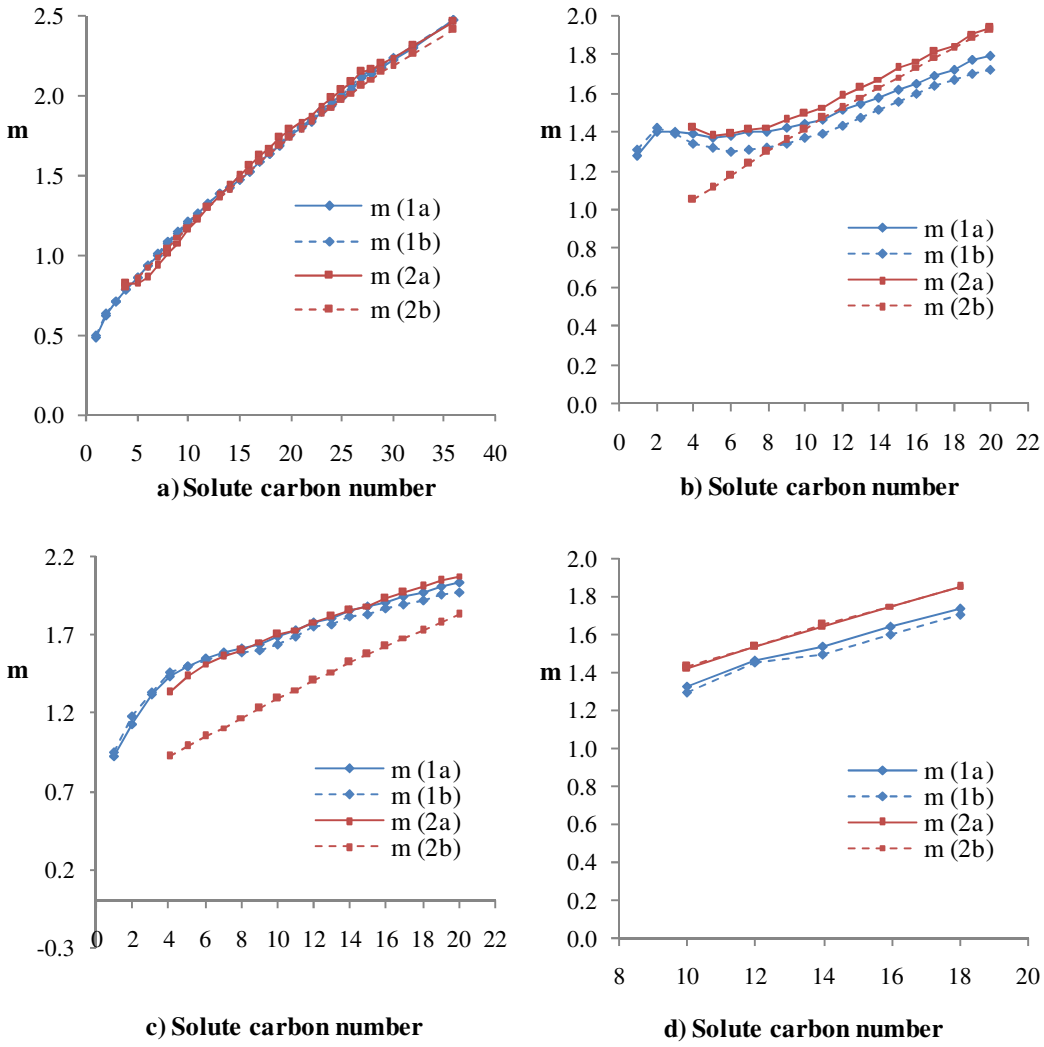

Figure E.49 Soave alpha-function parameter m vs. carbon number for the a) n-alkanes, b) 1-alcohols, c) carboxylic acid and d) methyl esters in the SRK model for cases given inTable 6-3

Stellenbosch University https://scholar.sun.ac.za

SRKSV

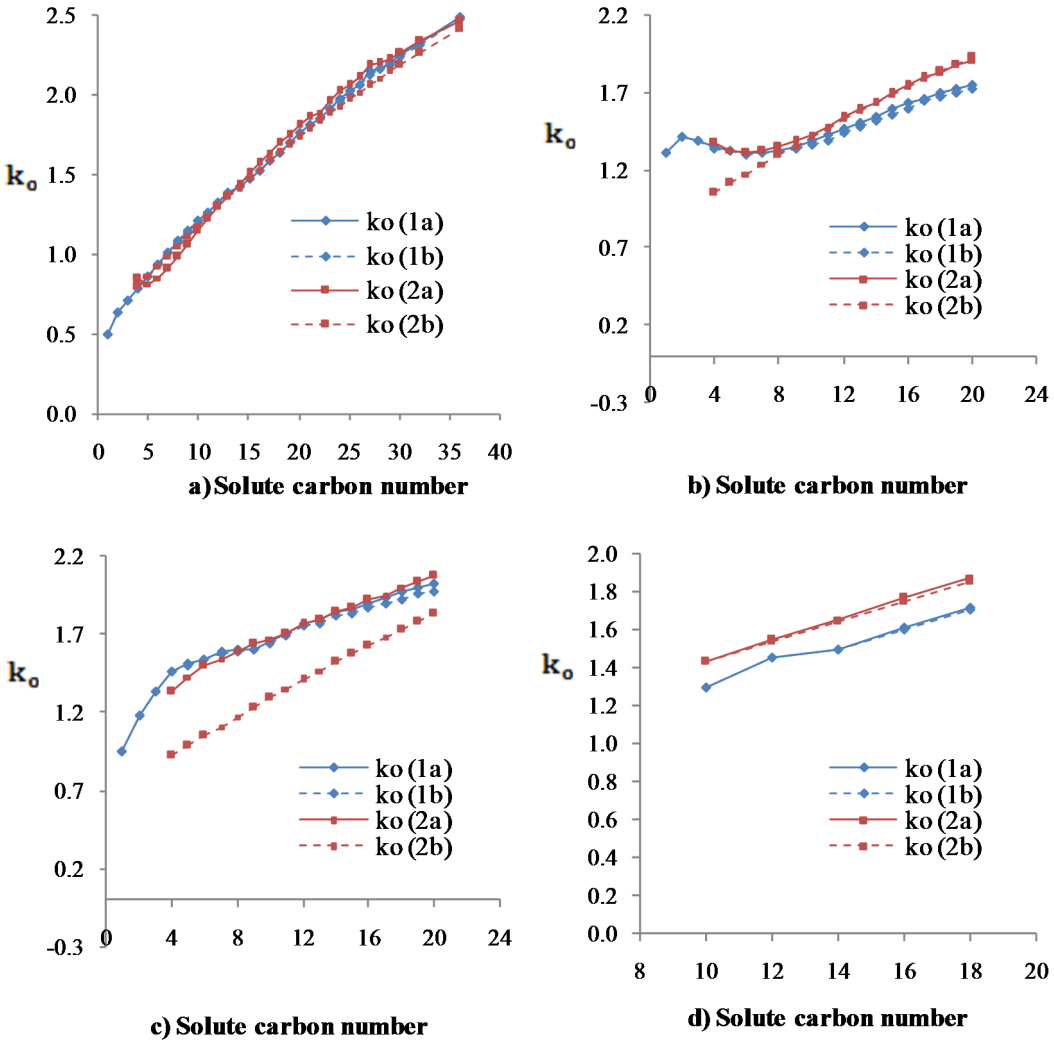

Figure E.50 Stryjek-Vera alpha function parameter k_0 vs. carbon number for the a) n-alkanes, b) 1-alcohols, c) carboxylic acid and d) methyl esters in the SRK model for cases given in Table 6-3

Stellenbosch University https://scholar.sun.ac.za

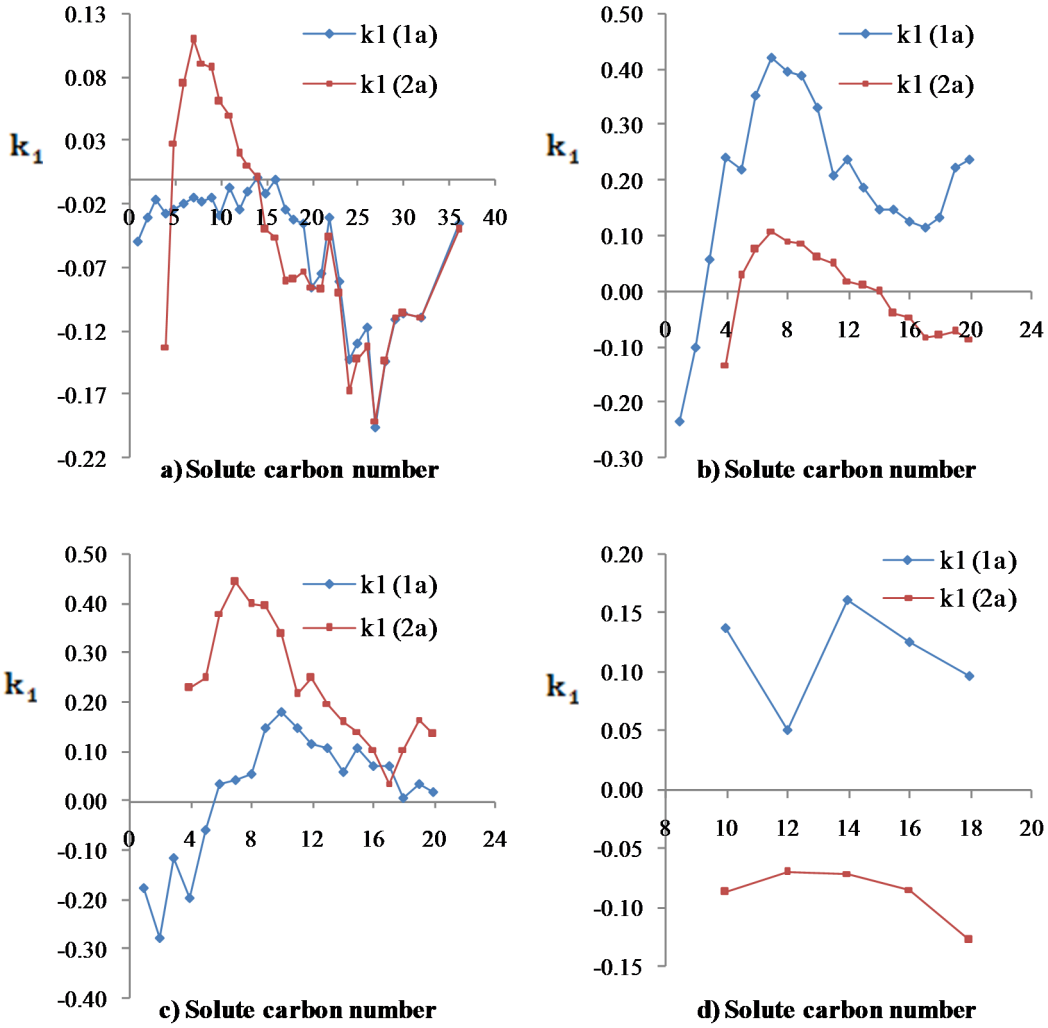

Figure E.51 Stryjek-Vera alpha function parameter k_1 vs. carbon number for the a) n-alkanes, b) 1-alcohols, c) carboxylic acid and d) methyl esters in the SRK model for cases given in Table 6-3

Stellenbosch University https://scholar.sun.ac.za

SRKM:

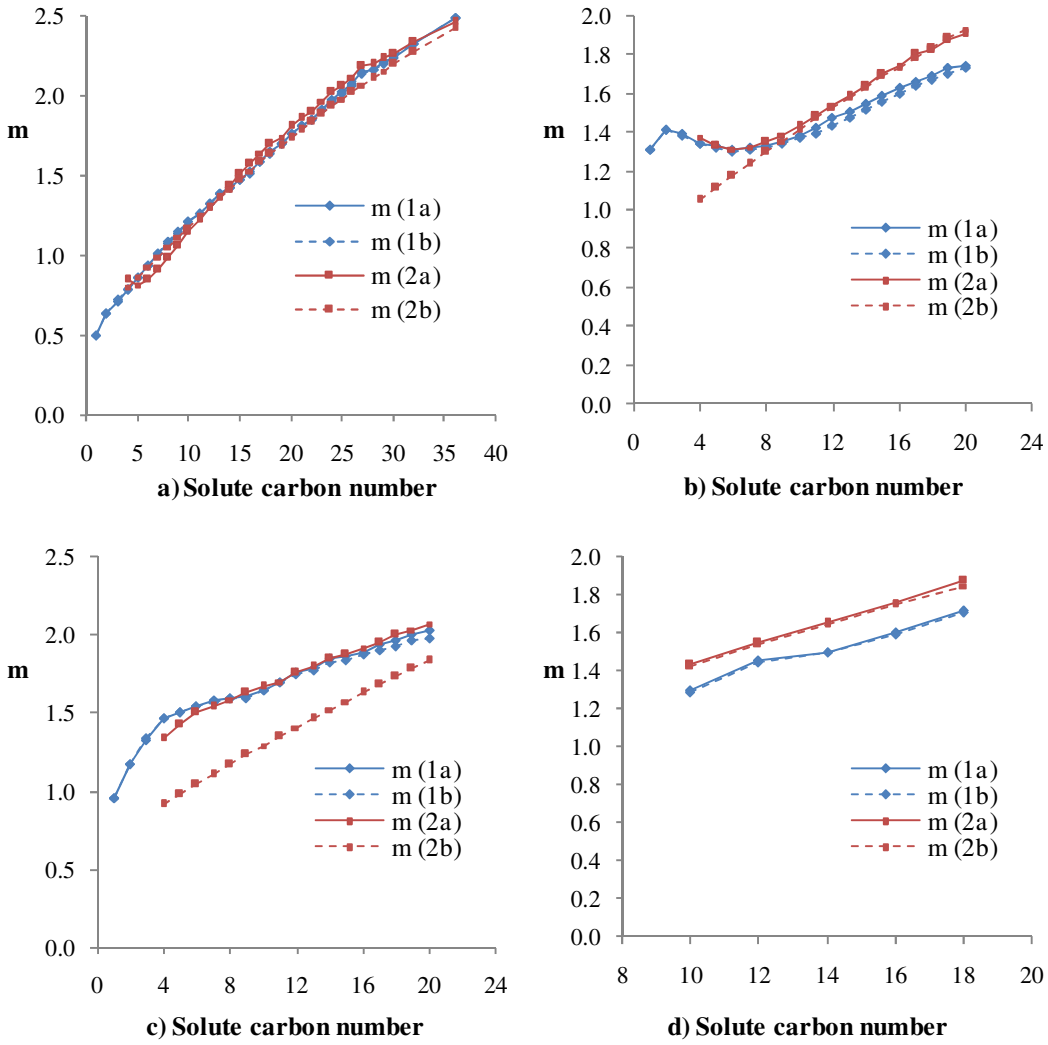

Figure E.52 Mathias alpha-function parameter m vs. carbon number for the a) n-alkanes, b) 1-alcohols, c) carboxylic acid and d) methyl esters in the SRK model for cases given inTable 6-3

Stellenbosch University https://scholar.sun.ac.za

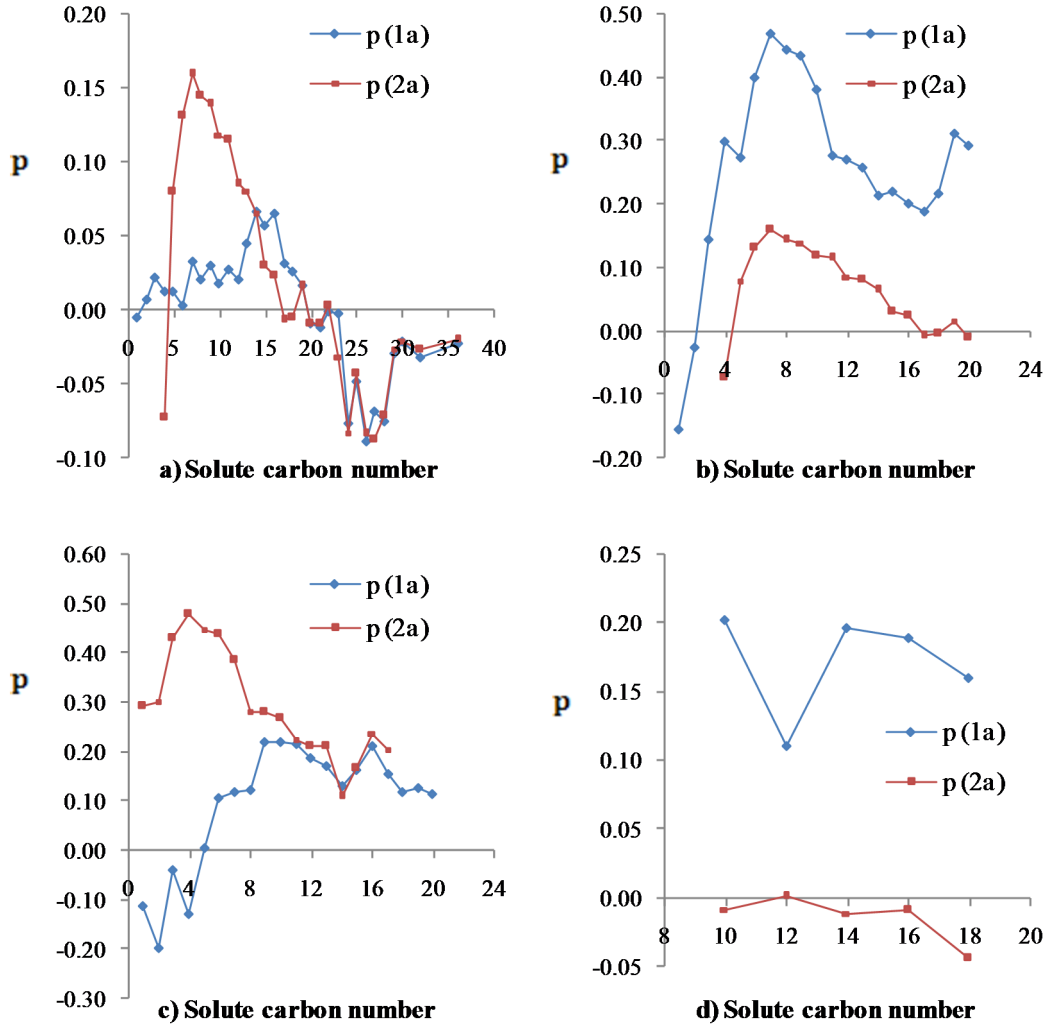

Figure E.53 Mathias alpha function parameter p vs. carbon number for the a) n-alkanes, b) 1-alcohols, c) carboxylic acid and d) methyl esters in the SRK model for cases given in Table 6-3

Stellenbosch University https://scholar.sun.ac.za

PT:

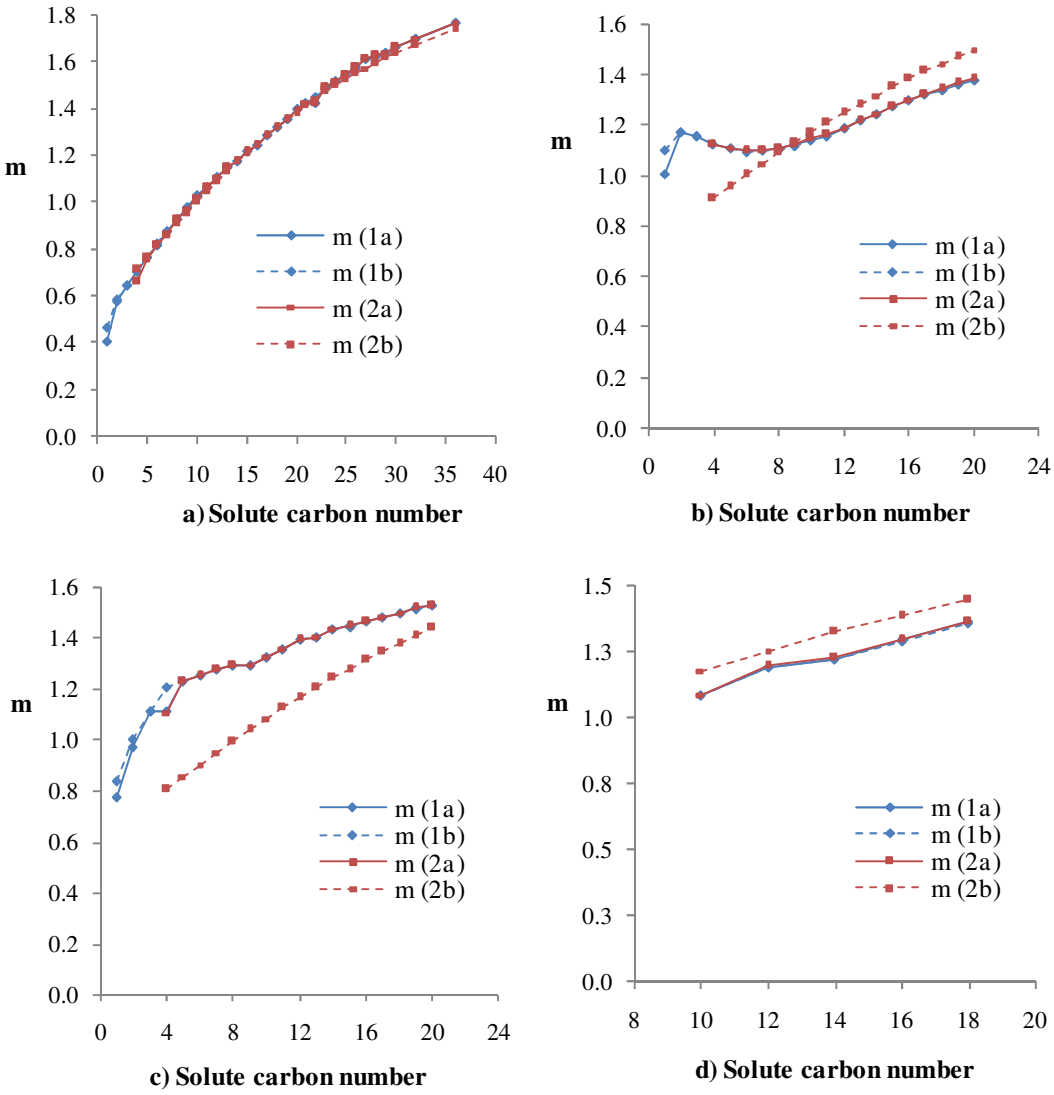

Figure E.54 Soave alpha-function parameter F (m) vs. carbon number for the a) n-alkanes, b) 1-alcohols, c) carboxylic acid and d) methyl esters in the PT model for cases given in Table 6-3

Stellenbosch University https://scholar.sun.ac.za

PRSV

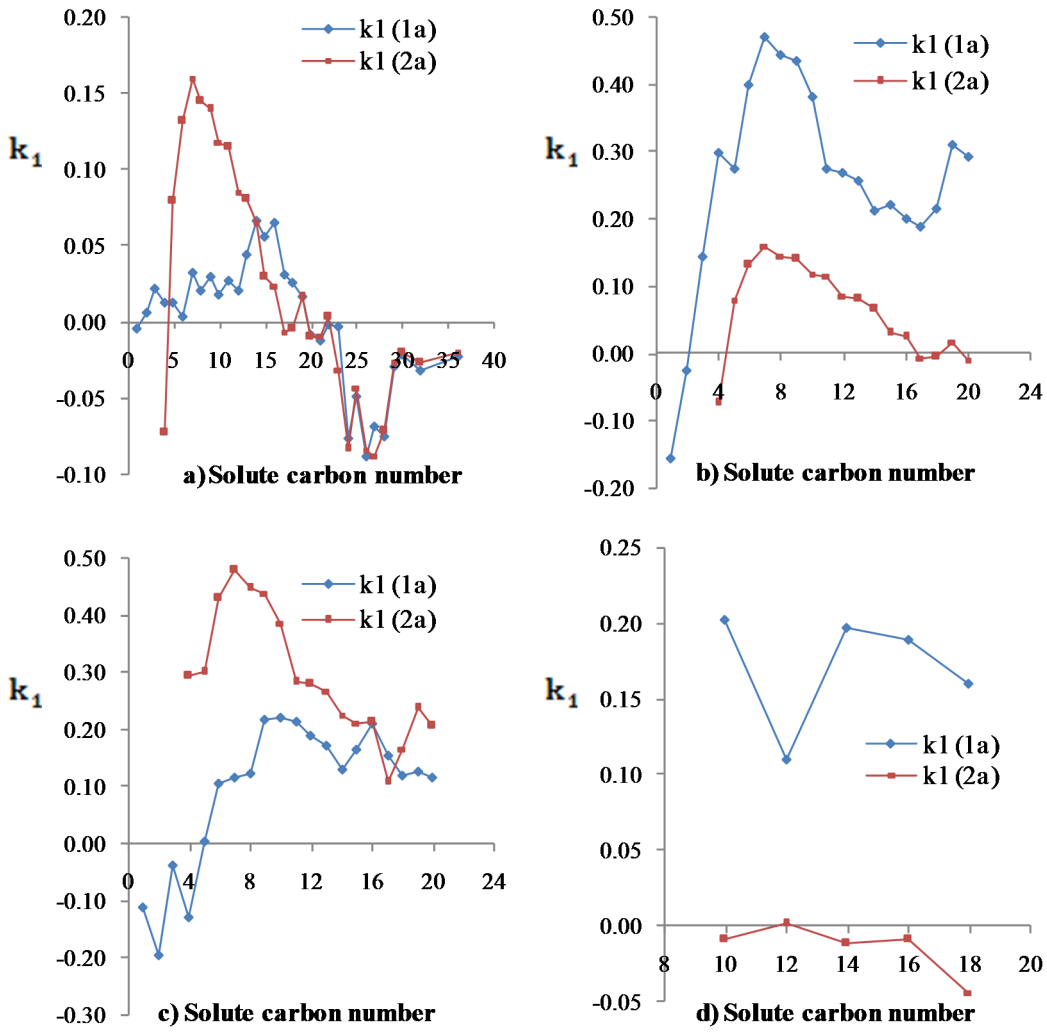

Figure E.55 Stryjek-Vera alpha function parameter k_1 vs. carbon number for the a) n-alkanes, b) 1-alcohols, c) carboxylic acid and d) methyl esters in the PR model for cases given in Table 6-3

Stellenbosch University https://scholar.sun.ac.za

PTSV

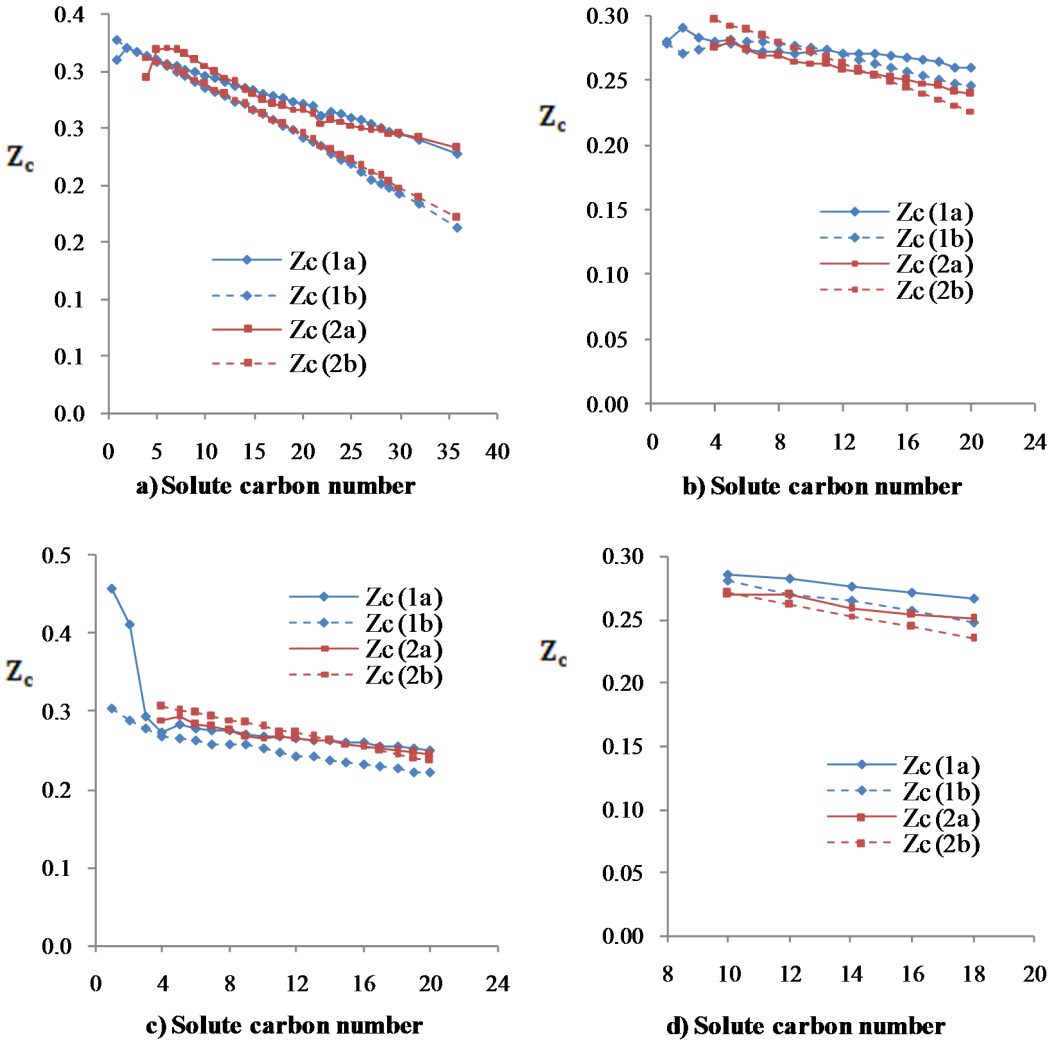

Figure E.56 Critical compressibility (Z_c) vs. carbon number for the a) n-alkanes, b) 1-alcohols, c) carboxylic acid and d) methyl esters in the PTSV model for cases given in Table 6-3

Stellenbosch University https://scholar.sun.ac.za

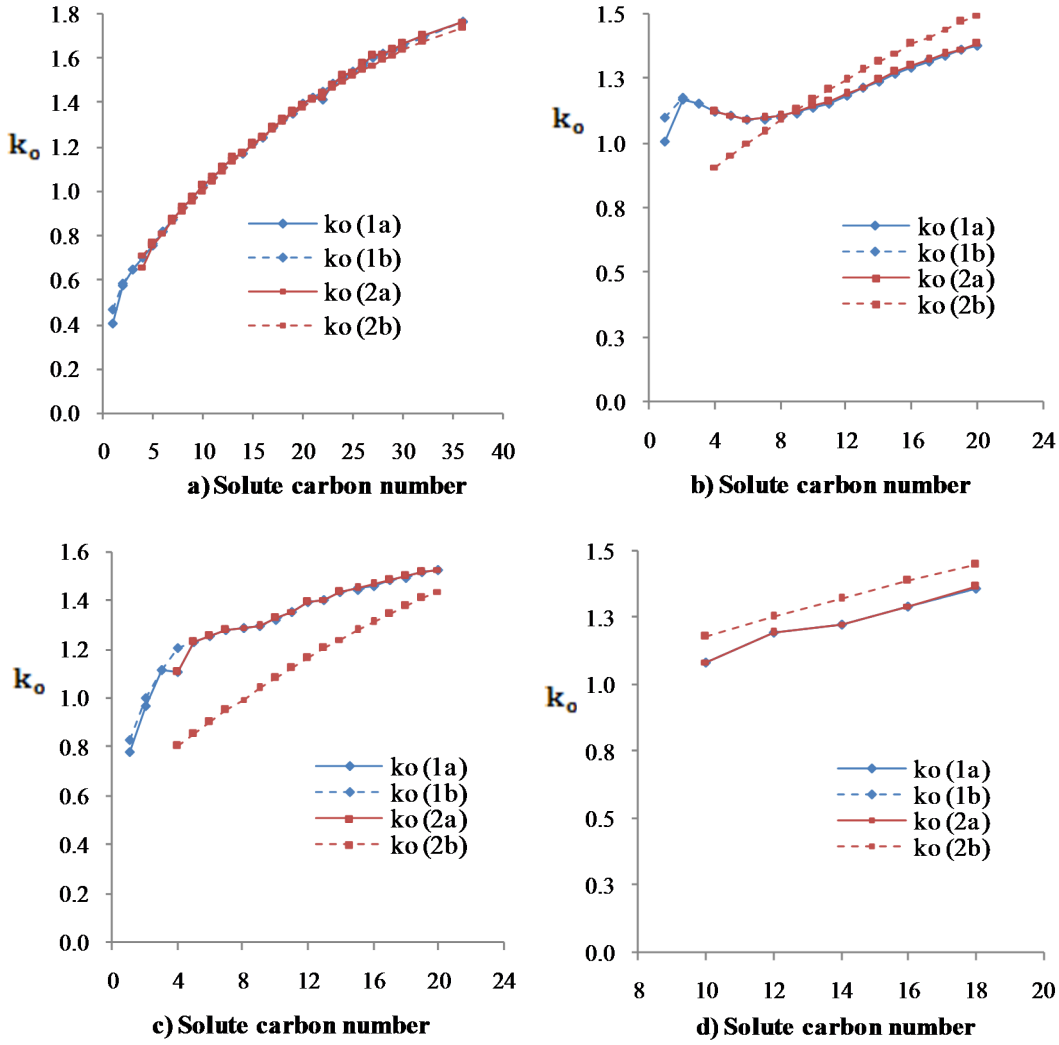

Figure E.57 Stryjek-Vera alpha function parameter k_0 vs. carbon number for the a) n-alkanes, b) 1-alcohols, c) carboxylic acid and d) methyl esters in the PT model for cases given in Table 6-3

Stellenbosch University https://scholar.sun.ac.za

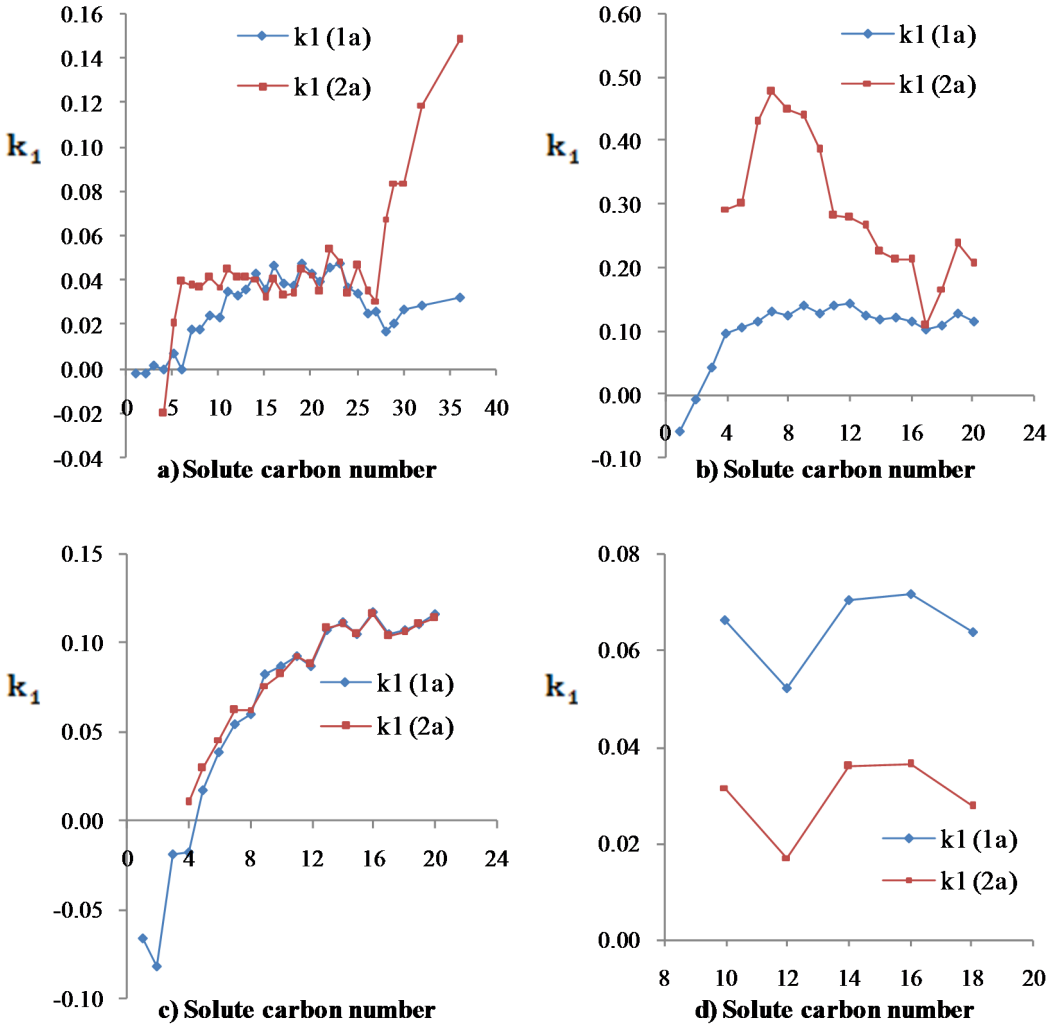

Figure E.58 Stryjek-Vera alpha function parameter k_1 vs. carbon number for the a) n-alkanes, b) 1-alcohols, c) carboxylic acid and d) methyl esters in the PT model for cases given in Table 6-3

Stellenbosch University https://scholar.sun.ac.za

PTM

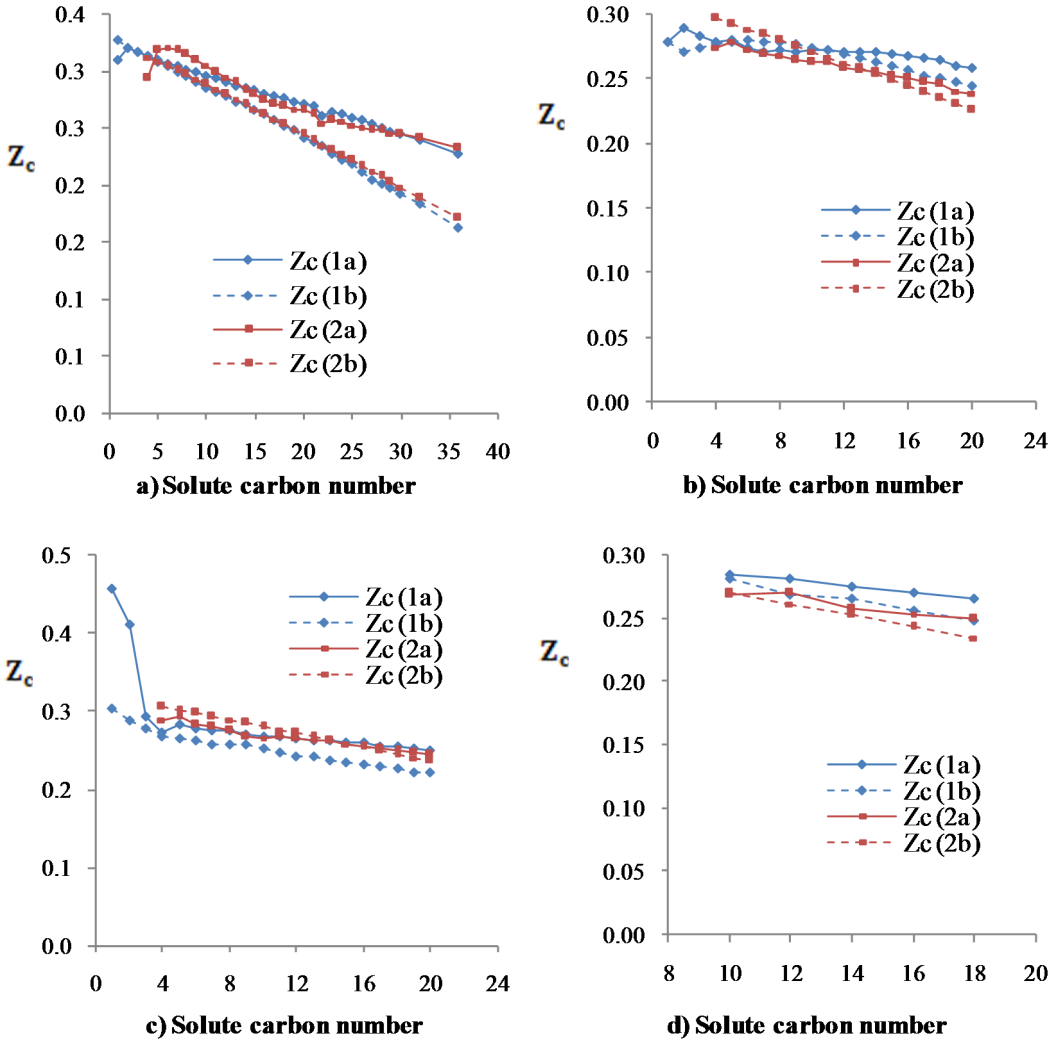

Figure E.59 Critical compressibility (Z_c) vs. carbon number for the a) n-alkanes, b) 1-alcohols, c) carboxylic acid and d) methyl esters in the PTM model for cases given in Table 6-3

Stellenbosch University https://scholar.sun.ac.za

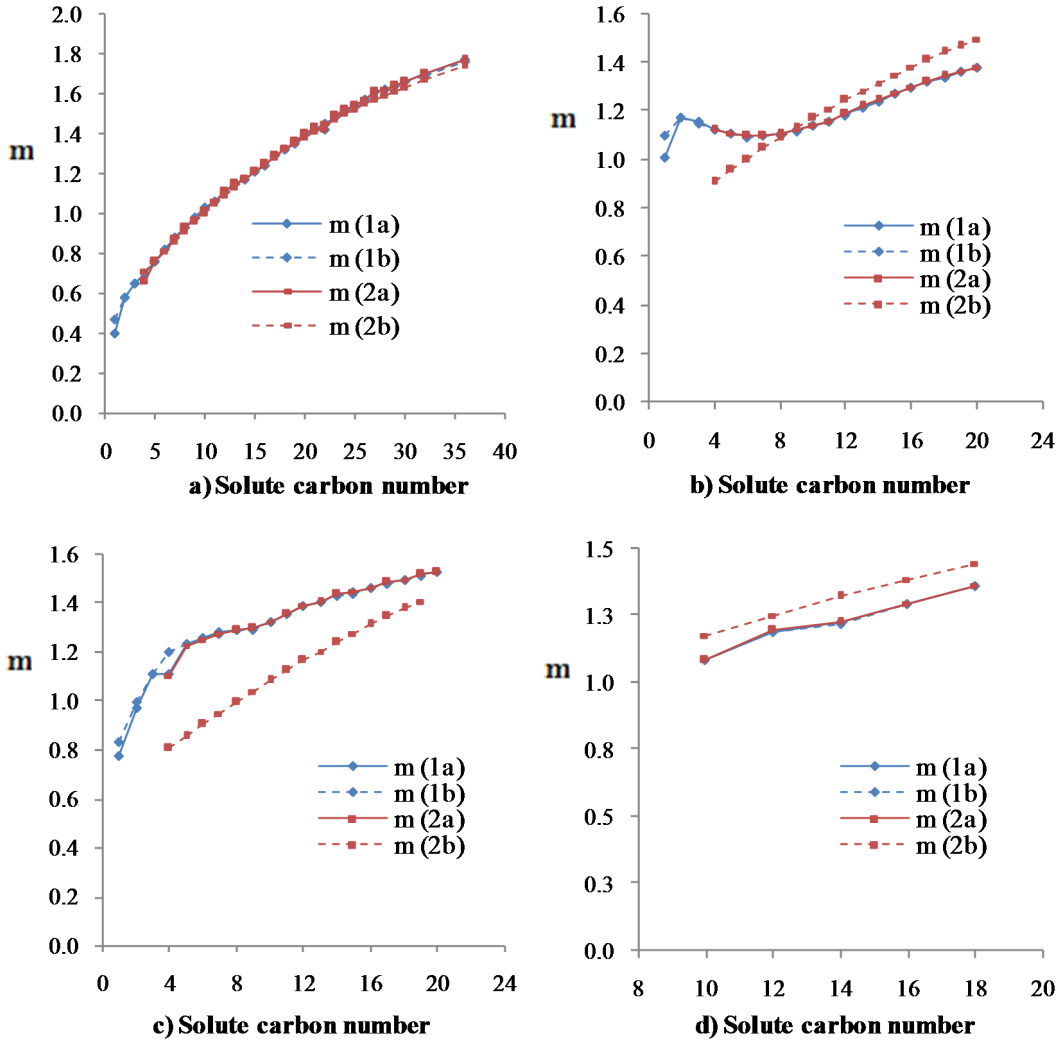

Figure E.60 Mathias alpha function parameter m vs. carbon number for the a) n-alkanes, b) 1-alcohols, c) carboxylic acid and d) methyl esters in the PT model for cases given in Table 6-3

Stellenbosch University https://scholar.sun.ac.za

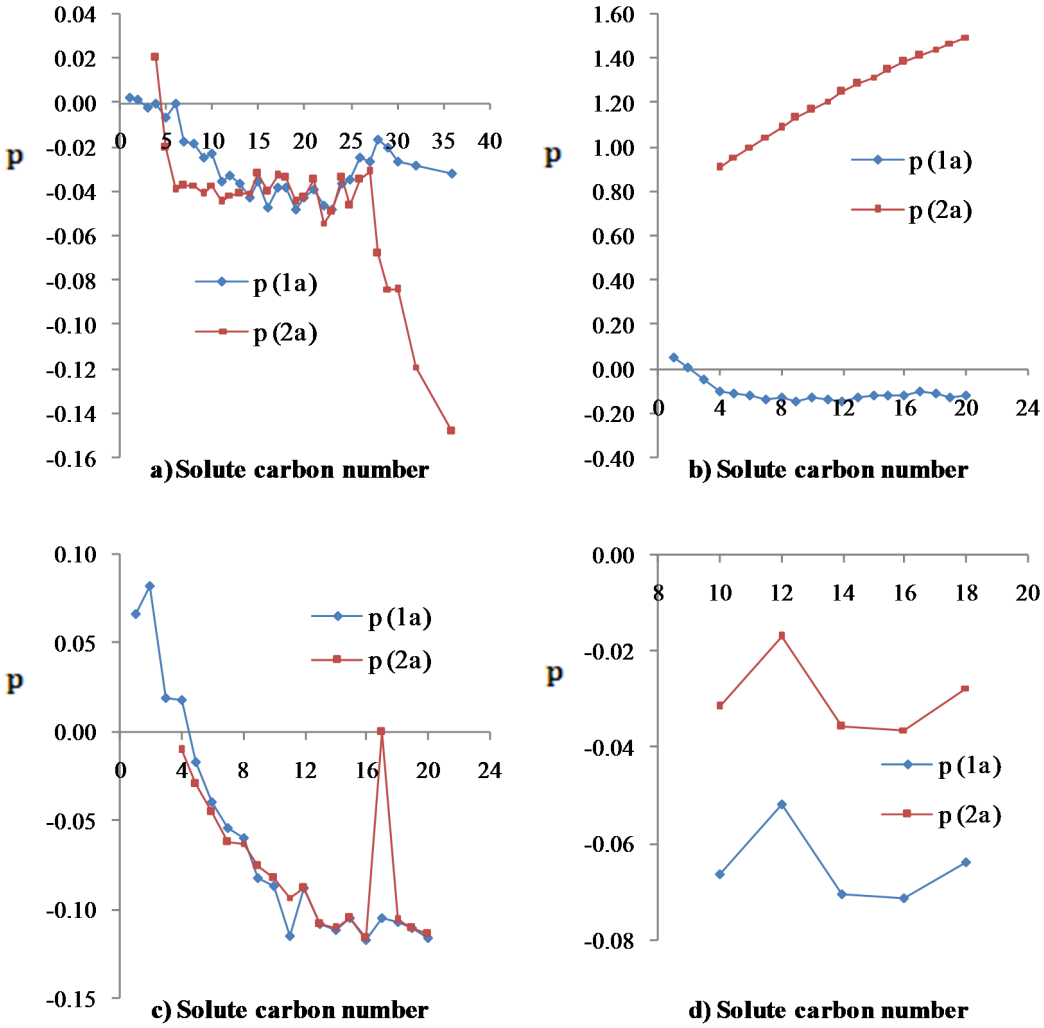

Figure E.61 Mathias alpha function parameter p vs. carbon number for the a) n-alkanes, b) 1-alcohols, c) carboxylic acid and d) methyl esters in the PT model for cases given in Table 6-3